CORA Cork Open Research Archive
Cartlann Taighde Oscailte Chorcaí

Title	Dairy powder breakage: mechanisms, impact factors, and influences on powder properties
Authors	Han, Jie
Publication date	2022-05
Original Citation	Han, J. 2022. Dairy powder breakage: mechanisms, impact factors, and influences on powder properties. PhD Thesis, University College Cork.
Type of publication	Doctoral thesis
Rights	© 2022, Jie Han. - https://creativecommons.org/licenses/by/4.0/
Download date	2026-11-04 03:14:41
Item downloaded from	https://hdl.handle.net/10468/13251



UCC
University College Cork, Ireland
Coláiste na hOllscoile Corcaigh

Teagasc Agriculture and Food Development Authority



and

Ollscoil na hÉireann, Corcaigh

National University of Ireland, Cork



Dairy Powder Breakage: Mechanisms, Impact Factors, and Influences on Powder Properties

Thesis presented by

Jie Han, MEng, BEng.

for the degree of

Doctor of Philosophy

University College Cork

Process and Chemical Engineering School

Head of School: Prof. Edmond Byrne

Supervisor(s): Prof. Song Miao (Teagasc), Dr. John Fitzpatrick (UCC), and Dr. Kevin Cronin (UCC)

May 2022

TABLE OF CONTENTS

DECLARATION I
DEDICATION II
ACKNOWLEDGEMENTS III
ABSTRACT V
SCHEMATIC OVERVIEW OF THESIS VIII
LIST OF PUBLICATIONS IX
LIST OF ABBREVIATIONS XI
INTRODUCTION 1
CHAPTER ONE 6
Literature Review 6
Abstract 7
1.1. Introduction 7
1.2. Particle breakage mechanisms 10
1.2.1. Continuum solids 10
1.2.2. Agglomerates 10
1.2.3. Crystalline particles 13
1.3. Dairy powder breakage characterization methods 13
1.3.1. Single-particle breakage tests 13
1.3.2. Multi-particle breakage tests 16
1.3.3. Other indirect methods 21
1.4. Influence of dairy powder breakage on powder physical properties and functionalities 22
1.4.1. Physical properties 22
1.4.2. Functionalities 24
1.5. Influencing factors - processing conditions 27
1.5.1. Breakage during dry-mixing 28
1.5.2. Breakage during in-plant transportation 29
1.5.3. Breakage during vibration 33
1.6. Influencing factors - particle characteristics 40
1.6.1. Powder physical properties 40
1.6.2. Powder composition 45
1.7. Conclusion 49
References 50
CHAPTER TWO 58

Particle size, powder properties and the breakage behaviour of infant milk formula 58
Abstract 59
2.1. Introduction 59
2.2. Materials and methods 62
2.2.1. Materials 62
2.2.2. Measurement of powder properties 64
2.2.3. Sample breakage in a powder venturi feeder 65
2.2.4. Sample breakage in the dilute-phase pneumatic conveying 68
2.2.5. Sample breakage in the high-speed mixing 69
2.2.6. Index of powder strength - breakage percentage 69
2.2.7. Scanning electron microscopy (SEM) and Light microscope 70
2.2.8. Statistical analysis 70
2.3. Results and discussion 71
2.3.1. Powder physical properties 71
2.3.2. Index of powder strength – breakage percentage 74
2.3.3. Breakage behaviour of four sieved fractions 76
2.3.4. Breakage behaviour of whole samples 86
2.4. Conclusion 87
References 90
CHAPTER THREE 94
Effects of different breakage mechanisms on the physical, water sorption, and mechanical characteristics of infant milk formula 94
Abstract 95
3.1. Introduction 95
3.2. Material and methods 97
3.2.1. Material 97
3.2.2. Sample preparation 97
3.2.3. Breakage mechanisms determination 99
3.2.4. Determination of powder physical properties 99
3.2.5. Powder surface composition 100
3.2.6. Morphological characteristics 101
3.2.7. Water sorption behaviour 101
3.2.8. Glass transition, initial crystallization and α-relaxation 103
3.2.9. Experimental design and statistical analysis 104
3.3. Result and discussion 104
3.3.1. Breakage mechanisms determination 104

3.3.2. Powder characterization 108
3.3.3. Water sorption behaviour 113
3.3.4. Glass transition and instant crystallization 121
3.3.5. Mechanical properties 122
3.4. Conclusion 123
Reference 125
Supplementary materials 128
CHAPTER FOUR 130
Breakage of infant milk formula through three different processing methods and its influence on powder properties 130
Abstract 131
4.1. Introduction 131
4.2. Material and methods 132
4.2.1. Materials 132
4.2.2. Equipment and powder breakage sample preparation 133
4.2.3. Particle size distribution and specific surface area 134
4.2.4. Bulk density, particle density, and porosity 134
4.2.5. Scanning electron microscopy (SEM) 134
4.2.6. Surface free fat content 134
4.2.7. Rehydration properties 134
4.2.8. Powder flowability - flow function test 135
4.2.9. Bulk density under consolidation 136
4.2.10. Statistical analysis 136
4.3. Results and discussion 136
4.3.1. Powder physical properties 136
4.3.2. Rehydration properties 143
4.3.3. Flow properties 145
4.3.4. Specific bulk volume and powder compressibility 147
4.4. Conclusion 149
Reference 149
CHAPTER FIVE 152
Investigation of the influence of powder characteristics on the breakage of dairy powders 152
Abstract 153
5.1. Introduction 153
5.2. Material and methods 155

5.2.1. Material 155
5.2.2. The main bulk and surface composition of samples 156
5.2.3. Sauter mean particle size of samples 156
5.2.4. Particle density, bulk density, and interparticle porosity 157
5.2.5. Friability 157
5.2.6. Powder structural properties 157
5.2.7. Powder breakage in the powder venturi feeder 157
5.2.8. Experimental design and statistical analysis 157
5.3. Result and discussion 158
5.3.1. Composition and physical properties of powders 158
5.3.2. Structural properties of powders 166
5.3.3. Powder breakage in the venturi feeder 167
5.4. Conclusion 175
Reference 176
CHAPTER SIX 179
Investigation of breakage behaviour and its influence on spray-dried agglomerated whey protein/lactose powders: Effect of protein and lactose content 179
Abstract 180
6.1. Introduction 181
6.2. Materials and methods 182
6.2.1. Materials 182
6.2.2. Model agglomerated powder preparation 182
6.2.3. Powder characterization 183
6.2.4. Breakage behaviour of model samples 184
6.2.5. Influence of breakage on functionalities of model samples 185
6.2.6. Statistical analysis 186
6.3. Results and discussion 186
6.3.1. Powder characterization 188
6.3.2. Dynamic breakage under different mechanical stresses 192
6.3.3. Breakage under repeated mechanical stresses - the influence of fatigue 195
6.3.4. Rehydration properties of model samples after breakage 197
6.3.5. Water adsorption, glass transition, and lactose crystallization 200
6.4. Conclusion 203
6.5. Reference 204
Supplementary materials 206
CHAPTER SEVEN 208

Breakage behaviour and functionality of spray-dried agglomerated model infant milk formula: Effect of proteins and carbohydrates content 208
Abstract 209
7.1. Introduction 209
7.2. Material and methods 211
7.2.1. Materials 211
7.2.2. Model IMF preparation 211
7.2.3. Powder characterisation 213
7.2.4. Breakage behaviour of model powders 214
7.2.5. Powder functionality and the influence of breakage 214
7.2.6. Statistical analysis 215
7.3. Result and discussion 215
7.3.1. Powder characterisation 215
7.3.2. The influence of formulation on breakage behaviour of model powders 224
7.3.3. Functionality and the impact of breakage of powders with different composition 228
7.4. Conclusion 237
Reference 238
CHAPTER EIGHT 241
General Discussion and Conclusions 241
8.1. Overview and summary 242
8.1.1. Dairy powder breakage mechanisms 242
8.1.2. The influence of dairy powder breakage on powder properties 243
8.1.3. The impact of dairy powder characteristics on breakage 248
8.2. Overall conclusions 250
8.3. Potential applications and future work 253
8.3.1. Potential applications 253
8.3.2. Future work directions 253
Reference 256
APPENDIX 259
Publications 259

DECLARATION

This is to certify that the work I am submitting is my own and has not been submitted for another degree, either at University College Cork or elsewhere. All external references and sources are clearly acknowledged and identified within the contents. I have read and understood the regulations of University College Cork concerning plagiarism and intellectual property.

_____

Jie Han

May 2022

DEDICATION

Dedicated with love, respect, and gratitude to

My mother Xie zhang

My father Xingzhu Han

My sisters Dandan Han & Ye Han

My brother Jinlai Han

Teachers and close friends

All people who love me

ACKNOWLEDGEMENTS

Undertaking this PhD in Ireland has been a truly precious life experience for me and this journey would not have been possible without the support and guidance that I received from many people.

Firstly, I would like to express my sincere and warm gratitude to my chief supervisor Professor Song Miao in Teagasc Food Researcher Centre, Moorepark, for giving me the precious opportunity to study in Ireland and for his suggestions, support, encouragement, and guidance throughout the whole programme. I am also very grateful to my academic supervisors Dr. John Fitzpatrick and Dr. Kevin Cronin in University College Cork, for their valuable advice and suggestions on my project to indicate the way forward and generate new ideas, and also for their encouragement on my English. My supervisors never stopped inspiring me, and I know I would not be the researcher and the person I am today without them.

Many thanks to Teagasc - Agriculture and Food Development Authority whose financial support has made it possible for me to study in Ireland and complete the research. I am also thankful to the colleagues and staff in Teagasc, Moorepark for their help and advice on my research and assistance to access some instruments: Dr. Valentyn Maidannyk, Dr. Kamrul Haque, Dr. Prabin Lamichhane, Dr. Sean Hogan, Dr. André Brodkorb, Ms. Helen Slattery, Dr. Deirdre Kennedy, Dr. Yonas Alemu, Dr. Norah O'Shea, Ms. Martina O'Brien, and Mr. Bernard Corrigan.

My gratitude must be extended to my sisters in Ireland, Min Yap, Runjing Li, and Taís Kuniyoshi, and I am so lucky to have them on the whole journey. Thank you for listening, sharing, supporting, cooking, tolerance, selfless help, and constructive suggestions on my research, which made my PhD life wonderful and enjoyable and I will never forget. Wish my best Min enjoys her final year PhD journey and everything goes well with her. Big thanks also go out to all my friends, who brought me lots of happiness and help over the past few years: Yihong, Fabiana, Fang, Yunna, Xilong, Alin, Maria, Elena, Meng, Qingsong, Yuanyuan, Guangya, Ning, and Archana.

I am very grateful to my groupmates, Wei Lu, Shaozong Wu, and Duanquan Lin, who kindly gave me many supports and help on my life and my project since the first day in Ireland. My thanks also to other group members, Xiaobin Ma, Tianjiao Chen, Qi Tang, Yichen Lin, Lili Tian, Yanjun Sun, Shuyang Wang, Jialing He, Marc, Lena, Chengdeng Chi, Zhili Ji, and Na Liu, for their contributions to my wonderful life here.

Finally, I extend my deepest thanks to my parents, sisters, brother, brothers-in-law, sister-in-law, and nephews, for their unwavering love and support throughout my entire journey. Love you all forever and wish you good health and happiness.

Thank you all for always being there!

Jie

Fermoy, Ireland

November 2021

ABSTRACT

Dairy powders provide a good form for convenient and stable preservation and transportation of milk ingredients, and most commercial dairy powders are agglomerated to improve powder functionalities. However, particle breakage during production and transportation is an important issue for agglomerates and only a few studies on dairy powder breakage have been published. Therefore, there is limited information to understand this phenomenon and find ways to decrease it. The present study investigated the breakage mechanisms of dairy powders, the influence of dairy powder breakage on powder properties, and the impact of powder characteristics on dairy powder breakage. This provides more information to better understand and control dairy powder breakage in an effort to improve the functionalities of dairy powders.

The main breakage mechanisms of agglomerated infant milk formula (IMF) during transportation and mixing included dispersion, chipping (surface breakage), and fragmentation (body breakage, which includes both disintegration and splitting), which correspond to an increasing extent of breakage. The breakage mechanism of whole samples was one or a combination of breakage mechanisms because the breakage behaviour of samples with different particle sizes at the same process condition was different.

Dairy powder breakage significantly decreased the particle size and porosity of powders and increased the specific surface area, particle density, and bulk density of samples. It also changed the shapes and surface composition of particles as seen with the increase in lactose content and the decrease in protein and fat contents for most samples. These changes in physical properties significantly deteriorated the rehydration properties of dairy powders, including the wettability and dispersibility, while it had only a small influence on powder flowability. In addition, body breakage had greater influences on powder physical properties than surface breakage. Thus, surface breakage had no influence on water sorption and mechanical

properties of powders but body breakage significantly deteriorated these properties as seen with the increase in water sorption rates and final water contents, the acceleration in the crystallization, and the decrease in the overall molecular mobility.

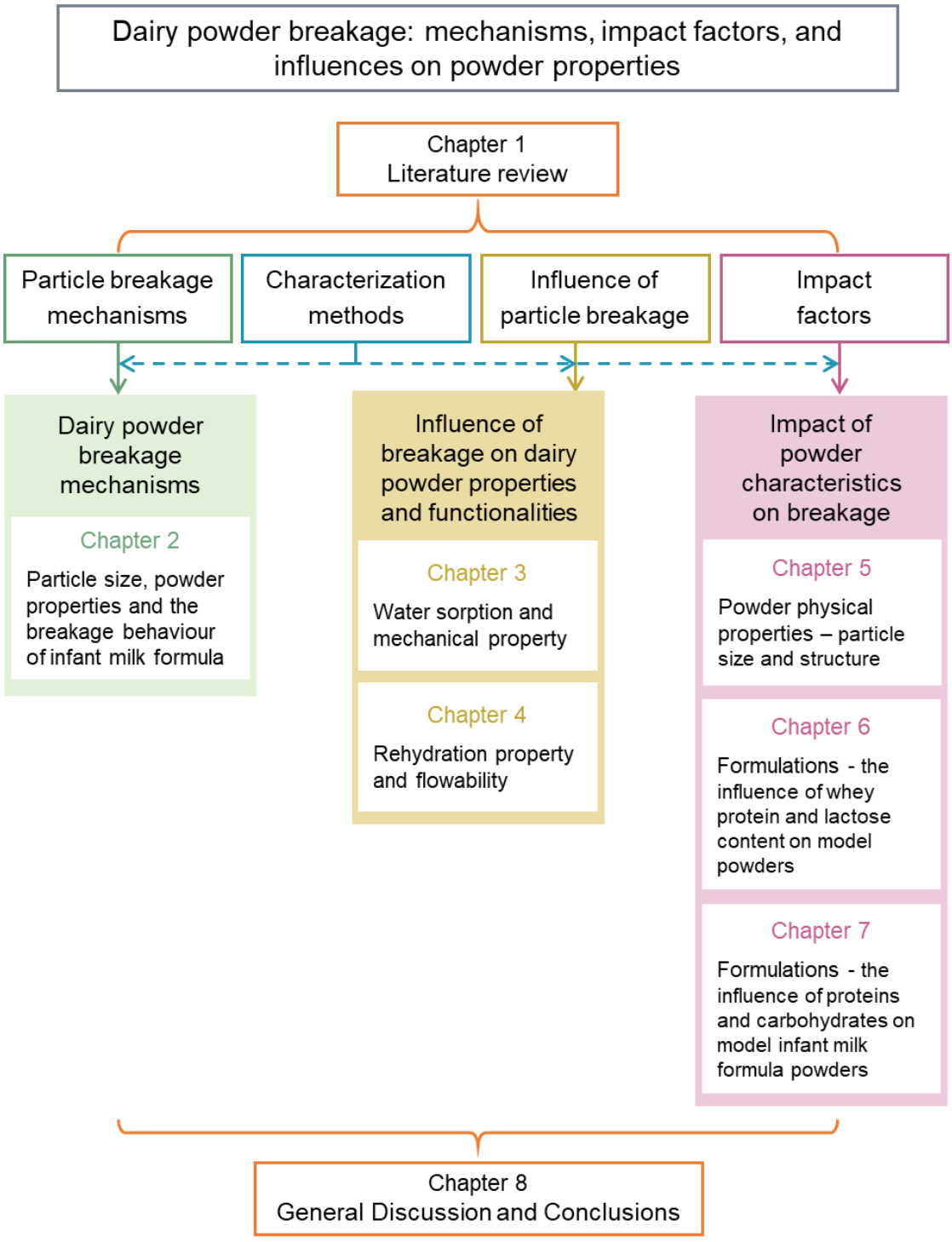
Dairy powder breakage degree or mechanisms was determined by the process conditions and particle characteristics. Breakage increased with increasing intensity of processing conditions, such as the transportation velocity and air pressures. In addition, fatigue affected the breakage of agglomerates dairy powders. For powder characteristics, the breakage degree of dairy powders increased with increasing particle size and decreasing particle structural strength. Considering particle structure, the strength of crystals and continuum solids were the highest, followed by particles with numerous holes throughout the particle, followed by the hollow sphere particle with a very thin shell. Under the same spray drying conditions, the formulation of dairy powders significantly affects dairy powder breakage by influencing the physical properties of powder particles, especially for particle size and particle structure. For whey protein/lactose model agglomerated powders, the two higher whey-protein powders were smaller in particle size, were less irregular in shape and had higher particle densities, which resulted in less breakage in comparison to the two lower whey-protein powders. For agglomerated model IMF powders that contained different protein and carbohydrates, whey protein powders were bigger in particle size, weaker in structural strength, and more irregular in shape in comparison to pure casein powders. This resulted in the better rehydration properties of whey protein powders but more breakage. Similarly, sucrose IMF samples had better rehydration properties but suffered more breakage than maltodextrin and pure lactose powders because of their bigger particle size.

Findings in this study indicate that body breakage significantly deteriorates powder properties, so breakage should be limited to surface breakage. Since powder breakage cannot be avoided, changes to processing conditions (using lower conveying speeds or air pressures) and powder physical

properties (mainly particle size and particle structure by changing production conditions or formulations) should be done to reduce breakage intensity.

.

SCHEMATIC OVERVIEW OF THESIS



LIST OF PUBLICATIONS

Peer Reviewed Journals

1. Han, J., Fitzpatrick, J., Cronin, K., & Miao, S. (2021). Dairy powder breakage: Mechanisms, characterization methods, impacted properties and influencing factors. *Trends in Food Science & Technology 114*, 608-624.

2. Han, J., Fitzpatrick, J., Cronin, K., Maidannyk, V., & Miao, S. (2021). Particle size, powder properties and the breakage behaviour of infant milk formula. *Journal of Food Engineering 292*, 110367.

3. Han, J., Fitzpatrick, J., Cronin, K., & Miao, S. (2022). Effects of different breakage mechanisms on the physical, water sorption, and mechanical characteristics of infant milk formula. *Journal of Food Engineering*, 110939.

4. Han, J., Fitzpatrick, J., Cronin, K., Maidannyk, V., & Miao, S. (2020). Breakage of infant milk formula through three different processing methods and its influence on powder properties. *Journal of Food Engineering 282*, 109997.

5. Han, J., Fitzpatrick, J., Cronin, K., & Miao, S. (2021). Investigation of the influence of powder characteristics on the breakage of dairy powders. *Food Research International*, 110775.

6. Han, J., Fitzpatrick, J., Cronin, K., Maidannyk, V., & Miao, S. Investigation of breakage behavior and its influence on spray-dried agglomerated whey protein/lactose powders: Effect of protein and lactose content. (Submitted to *Journal of Dairy Science*)

7. Han, J., Fitzpatrick, J., Cronin, K., Maidannyk, V., & Miao, S. Breakage behaviour and functionality of spray-dried agglomerated model infant milk formula: Effect of proteins and carbohydrates content. (Submitted to *Food Chemistry*)

Conference Presentations

1. **Han, J.**, Fitzpatrick, J., Cronin, K., & Miao, S. Structural changes of infant formula through three different processing methods and its influence on powder physical properties and functionalities. *4th Food Structure and Functionality Symposium*, October 19-20, 2021, Ireland (Poster presentation).

2. **Han, J.**, Fitzpatrick, J., Cronin, K., & Miao, S. Breakage behaviour of infant milk formula during production. *49th Annual Food Science and Technology Conference*, December 15th, 2020, (Poster presentation).

LIST OF ABBREVIATIONS

IMF	Infant milk formula
WPI	Whey protein isolate
WPC	Whey protein concentrate
SMP	Skim milk powder
LFMP	Low-fat milk powder
MPI	Milk protein isolate
WMP	Whole milk powder
INFP	Instant non-fat milk powder
IWMP	Instant whole milk powder
FFMP	Fat-filled milk powder/Full fat milk powder
LAC	α-Lactose Monohydrate
NWP	nutritional whey protein
MCC	Micellar casein concentrate
EMP	Enriched milk powder
PS	Particle size
PSD	Particle size distribution
V-PSD	Volume particle size distribution
N-PSD	Number particle size distribution
D_{10}	10% size value below the particle size distribution
D_{50}	50% size value below the particle size distribution
D_{90}	90% size value below the particle size distribution
$D_{3,2}$	Sauter mean value
$D_{4,3}$	Volume mean diameter
BP	Breakage percentage

B_r	Relative breakage
B_p	Breakage potential
B_t	Total breakage
BE	Extent of breakage
FI	Friability index
AI	Attrition index
DAI	Differential attrition index
SI	Shattering index
CI	Compression index
AP	Threshold air pressure
ρ_0	Initial bulk density
ρ_{tapped}	Tapped (100 taps) bulk density
ρ_b	Loose bulk density
ρ_p	Particle density
ε	Porosity
DI	Dispersibility index
DMA	Dynamic Mechanical Analyser
DSC	Differential scanning calorimeter
PFT	Powder flow tester
SEM	Scanning electron microscopy
XPS	X-ray photoelectron spectroscopy measurements
SFF	surface free fat content
SSA	Specific surface area
a_W	Water Activity
RVP	Relative water vapor pressure
m_m	Monolayer moisture content

GAB	Guggenheim-Anderson de Boer isotherm model
m_i	Experimental moisture content
m_i^*	Calculated moisture content
c_d	Density of sorbed water
N_{am}	Number of adsorbed monolayers
A	Surface area of adsorbent
φ	Spreading pressure
T_g	Glass transition temperature
T_{ic}	Initial crystalized temperatures
T_α	α-relaxation temperatures
RMS	Relative percentage Root Mean Square
w/w	Weight/ weight

INTRODUCTION

Dairy powders provide a good form for convenient and stable preservation and transportation of milk ingredients. Currently, most commercial dairy powders are agglomerated powders as agglomeration results in the formation of large particles which provides improved powder functionalities such as flowability and rehydration properties (Ji et al., 2017). However, particle breakage, where one particle breaks into a few fragments, is an important issue for many industries involving operations that include crystallization, agglomeration, transportation and storage of particulate materials, such as the pharmaceutical, mining, catalysts, chemical, agricultural, and fertilizer (Deng and Davé, 2017; Gupta et al., 2017; Gupta, 2017; Norazirah et al., 2016; Reynolds et al., 2005; Salman et al., 2003; Shan et al., 2018).

Particle breakage is caused by mechanical loads (such as impact, shear, and compression/crushing) imposed on the particle, which is the result of particle-particle and particle-equipment interactions (such as collisions and frictions) (Kotzur et al., 2018). It is very common for particles to be subjected to mechanical loads in many processes throughout dairy powder production, transportation, storage, and handling. For example, dry mixing is a special process during the production of infant milk formula (IMF) to achieve the uniform blend of macro- and micronutrients necessary for a complete product. It is accomplished by the movement of particles between various parts of a whole particulate mass to reach the desired uniform distribution. Also, pneumatic conveying is a widely used method for dairy powder in-plant transportation but the collisions and frictions between particles and particle to wall always happen, especially at the bends. Meanwhile, there is a long-distance for dairy powders from the production factories to customers, and once the product leaves the factory, particles may still suffer mechanical loads due to handling and transportation. Therefore, dairy powder breakage easily occurs in many processes during production and transportation. Boiarkina et al. (2016) reported the breakage of instant whole milk powder in two different industrial plants with different transport systems, a pneumatic

conveying system and a bucket elevator. Hanley (2011) described the disintegration of IMF during pneumatic conveying. Yan et al. (2001b) also reported the breakage of instant non-fat milk powders during vibration. However, there was no study on the breakage behaviour or mechanisms of dairy powders or even other food powders, which would be useful to better understand this phenomenon.

Based on the research in other industries, if the breakage is excessive, it can lead to a number of serious consequences including but not limited to a loss in functionality and product performance (Bemrose and Bridgwater, 1987; Boiarkina et al., 2016; Zumaeta et al., 2005) and increase in dust generation (Kalman and Goder, 1998; Oveisi et al., 2013; Salman et al., 2002; Wu and Wu, 2017). In addition, fine dust produced may lead to air pollution and plugging of processing equipment, increased possibility of dust explosions, and loss of product through the production of undersized particles. Meanwhile, dairy powder breakage may cause changes in powder density, which can result in errors in the dosage consumed, especially for IMF. Nevertheless, only a few studies about dairy powder breakage have been published so there is limited information to understand the influence and its mechanisms of breakage on dairy powder properties.

On the other hand, controlling or reducing unwanted breakage to maintain the properties of dairy powders is more important. The research on undesirable or intentional particle breakage in other industries demonstrated that the applied stress from processing conditions and together with the particle characteristics dictate the response of particles for given loading conditions and they are the two main factors that influence particle breakage (Kotzur et al., 2018; Lu et al., 2014; Petukhov and Kalman, 2004; Yan and Barbosa-Cánovas, 2001a). Hanley (2011) found that compared with dense-phase pneumatic conveying, dilute-phase pneumatic conveying resulted in high breakage of IMF and the extent of breakage increased with increasing air velocities. Besides, the number and the radius of bends in the pneumatic conveyor also influenced the breakage of IMF. During the tapping test of instant non-fat milk powders, it was found that powder breakage increased

with increasing tapping number (Yan & Barbosa-Cánovas, 2001b). However, sometimes it is not easy to change the equipment or parameters during production and transportation in factories. Thus, the influence of powder characteristics on dairy powder breakage would be useful to fully understand dairy powder breakage and find suitable ways to decrease it but it has not been investigated yet.

Considering the above, the overall objective of the present study is to provide more information to better understand dairy powder breakage. Firstly, the breakage behaviour and breakage mechanisms of dairy powders were investigated. Then the influence of dairy powder breakage on powder physical and functional properties was studied. Finally, the impact of powder characteristics on dairy powder breakage was explored. The specific objectives were:

(i) To investigate the breakage behaviour and breakage mechanisms of agglomerated dairy powders during the handling and processing of commercial IMF powder (Chapter 2);

(ii) To understand the influence of dairy powder breakage on powder properties and functionalities. These included the physical, structural, and surface properties, water adsorption behaviour and its impact on mechanical properties (Chapter 3), powder flowability and rehydration properties (Chapter 4);

(iii) To investigate the impact of dairy powder properties on powder breakage. This involved firstly comparing fifteen commercial or lab-scale agglomerated or non-agglomerated dairy powder samples to study the influence of powder physical properties on breakage (Chapter 5). Then model samples were produced at the same drying conditions but with different components to explore the influence of powder composition on breakage, including the influence of protein and lactose content on whey protein/lactose model powder (Chapter 6) and the influence of different protein and carbohydrates on the IMF model powder (Chapter 7).

Reference

Bemrose, C.R., & Bridgwater, J. (1987). A review of attrition and attrition test methods. *Powder Technology* 49(2), 97-126. https://doi.org/10.1016/0032-5910(87)80054-2.

Boiarkina, I., Sang, C., Depree, N., Prince-Pike, A., Yu, W., Wilson, D.I., & Young, B.R. (2016). The significance of powder breakdown during conveying within industrial milk powder plants. *Advanced Powder Technology* 27(6), 2363-2369. https://doi.org/10.1016/j.apt.2016.10.019.

Deng, X., & Davé, R.N. (2017). Breakage of fractal agglomerates. *Chemical Engineering Science* 161, 117-126. https://doi.org/10.1016/j.ces.2016.12.018.

Gupta, V., Sun, X., Xu, W., Sarv, H., & Farzan, H. (2017). A discrete element method-based approach to predict the breakage of coal. *Advanced Powder Technology* 28(10), 2665-2677. https://doi.org/10.1016/j.apt.2017.07.019.

Gupta, V.K. (2017). Effect of size distribution of the particulate material on the specific breakage rate of particles in dry ball milling. *Powder Technology* 305, 714-722. https://doi.org/10.1016/j.powtec.2016.10.075.

Hanley, K.J., 2011. Experimental quantification and modelling of attrition of infant formulae, Department of Process and Chemical Engineering. University College Cork, Cork, Ireland.

Ji, J., Cronin, K., Fitzpatrick, J., & Miao, S. (2017). Enhanced wetting behaviours of whey protein isolate powder: The different effects of lecithin addition by fluidised bed agglomeration and coating processes. *Food Hydrocolloids* 71, 94-101. https://doi.org/10.1016/j.foodhyd.2017.05.005.

Kalman, H., & Goder, D. (1998). Design criteria for particle attrition. *Advanced Powder Technology* 9(2), 153-167. https://doi.org/10.1016/S0921-8831(08)60584-1.

Kotzur, B.A., Berry, R.J., Zigan, S., García-Triñanes, P., & Bradley, M.S.A. (2018). Particle attrition mechanisms, their characterisation, and application to horizontal lean phase pneumatic conveying systems: A review. *Powder Technology* 334, 76-105. https://doi.org/10.1016/j.powtec.2018.04.047.

Lu, X., Liu, C., Zhu, L., & Qu, X. (2014). Influence of process parameters on the characteristics of TiAl alloyed powders by fluidized bed jet milling. *Powder Technology* 254, 235-240. https://doi.org/10.1016/j.powtec.2013.11.013.

Norazirah, A., Fuad, S.H.S., & Hazizan, M.H.M. (2016). The effect of size and shape on breakage characteristic of mineral. *Procedia Chemistry* 19, 702-708. https://doi.org/10.1016/j.proche.2016.03.073.

Oveisi, E., Lau, A., Sokhansanj, S., Lim, C.J., Bi, X., Larsson, S.H., & Melin, S. (2013). Breakage behaviour of wood pellets due to free fall. *Powder Technology* 235, 493-499. https://doi.org/10.1016/j.powtec.2012.10.022.

Petukhov, Y., & Kalman, H. (2004). Empirical breakage ratio of particles due to impact. *Powder Technology* 143-144, 160-169. https://doi.org/10.1016/j.powtec.2004.04.009.

Reynolds, G.K., Fu, J.S., Cheong, Y.S., Hounslow, M.J., & Salman, A.D. (2005). Breakage in granulation: A review. *Chemical Engineering Science* 60(14), 3969-3992. https://doi.org/10.1016/j.ces.2005.02.029.

Salman, A.D., Fu, J., Gorham, D.A., & Hounslow, M.J. (2003). Impact breakage of fertiliser granules. *Powder Technology* 130(1), 359-366. https://doi.org/10.1016/S0032-5910(02)00237-1.

Salman, A.D., Hounslow, M.J., & Verba, A. (2002). Particle fragmentation in dilute phase pneumatic conveying. *Powder Technology* 126(2), 109-115. https://doi.org/10.1016/S0032-5910(02)00048-7.

Shan, J., Xu, S., Liu, Y., Zhou, L., & Wang, P. (2018). Dynamic breakage of glass sphere subjected to impact loading. *Powder Technology* 330, 317-329. https://doi.org/10.1016/j.powtec.2018.02.009.

Wu, F., & Wu, D. (2017). Attrition resistances and mechanisms of three types of FCC catalysts. *Powder Technology* 305, 289-296. https://doi.org/10.1016/j.powtec.2016.09.077.

Yan, H., & Barbosa-Cánovas, G.V. (2001a). Attrition evaluation for selected agglomerated food powders: the effect of agglomerate size and water activity. *Journal of Food Process Engineering* 24(1), 37-49. https://doi.org/ 10.1111/j.1745-4530.2001.tb00530.x.

Yan, H., & Barbosa-Cánovas, G.V. (2001b). The effect of padding foam on the compression characteristics of some agglomerated food powders. *Food Science and Technology International* 7(5), 417-423. https://doi.org/ 10.1106/wc69-qfnv-vn6e-lh00.

Zumaeta, N., Cartland-Glover, G.M., Heffernan, S.P., Byrne, E.P., & Fitzpatrick, J.J. (2005). Breakage model development and application with CFD for predicting breakage of whey protein precipitate particles. *Chemical Engineering Science* 60(13), 3443-3452. https://doi.org/10.1016/j.ces.2005.02.016.

CHAPTER ONE

Literature Review

Chapter 1 was published in:

Han, J., Fitzpatrick, J., Cronin, K., & Miao, S. (2021). Dairy powder breakage: Mechanisms, characterization methods, impacted properties and influencing factors. *Trends in Food Science & Technology 114*, 608-624.

The work contained in this chapter was undertaken and written solely by myself with specific contributions from each co-author:

Jie Han: Conceptualization, Writing - original draft.

John Fitzpatrick: Supervision, Writing - review & editing.

Kevin Cronin: Supervision, Writing - review & editing.

Song Miao: Supervision, Conceptualization, Writing - review & editing, Funding acquisition, Project administration.

Abstract

Particle breakage deteriorates dairy powder properties and it easily takes place in many processes. However, there currently is a lack of research on dairy powder breakage for understanding and controlling it. The research on particle breakage in other industries is very extensive and thorough, and could act as good reference knowledge for dairy powder breakage research, but at this time there is no review of this useful information. Based on the research done in dairy powder breakage and findings of particle breakage studies of other industries relevant to dairy powder particle properties, this chapter includes the breakage mechanisms of dairy powders, methods suitable for studying dairy powder breakage, the influence of breakage on powder properties, and influencing factors of dairy powder breakage which also can be considered as controlling factors. Powder breakage significantly affects dairy powder physical properties which in turn influence powder functionalities, especially the rehydration properties. The extent of breakage in agglomerates corresponds to different breakage mechanisms which result in different final particle sizes and particle size distributions. The processing conditions (such as the parameters during dry-mixing, vibration, and pneumatic conveying) and the characteristics of particles (including physical properties and composition) are two main influencing factors that can be considered to control dairy powder breakage. However, there are currently not enough studies showing which factors are more effective in controlling breakage. Some single-particle or multi-particle tests can be used to investigate dairy powder breakage and further research on the effectiveness of those controlling factors should be done.

Keywords: Dairy powder breakage; Breakage mechanisms; Processing parameters; Powder properties

1.1. Introduction

The production of dairy powders is growing rapidly worldwide because it provides a good way to preserve and transport milk ingredients in a stable

and convenient form (Yildirim and Genc, 2017). Currently, most commercial dairy powders are agglomerated powders as agglomeration results in the formation of large particles which improved powder functionality such as the flowability and rehydration properties (Ji et al., 2017). However, particle breakage is an important issue for many industries involving operations that include crystallization, agglomeration, transportation and storage of particulate materials (Salman et al., 2007a). Food agglomerates are normally less robust and have lower mechanical strength than inorganic or polymeric particles, and they are also usually fragile and brittle (Yan and Barbosa-Cánovas, 1997; Yan and Barbosa-Cánovas, 2001a). Thus, unwanted particle breakage in agglomerated dairy powders easily happens when powders are exposed to mechanical loads, such as impact, shear, vibration, and static pressure (Han et al., 2020; Yan and Barbosa-Cánovas, 2001b).

Powder breakage takes place in many processes throughout dairy powder production wherever there is relative movement between powder particles in contact with each other or against the container wall, such as agglomeration in the fluidized bed, in-plant transportation in pneumatic conveying, or dry blending in a mixer (Boiarkina et al., 2016; Hazlett et al., 2020; Ortega-Rivas et al., 2006; Reynolds et al., 2005). It is also not rare to encounter the problem where a product leaves the manufacturing site meeting its specifications for size distribution, but exhibits severe problems such as dustiness when it reaches the hands of the customer (Ghadiri et al., 1991). In general, for some industries dealing with particulate solids, the notable and serious consequences of unwanted particle breakage include an increase in dust generation, dust explosions, hazardous problems to plant operator, loss of product because of undersized particles produced, and plugging of processing equipment (Kotzur et al., 2018). Moreover, dairy powder breakage significantly deteriorates the rehydration properties of infant milk formula (IMF), whey protein isolate powder (WPI), instant whole milk powder, agglomerated whey protein concentrate (WPC), and granulated fat-filled milk powder (Barletta and Barbosa-Cánovas, 1993a, b; Boiarkina et al., 2016; Han et al., 2020; Hanley et al., 2011a; Hazlett et al., 2020; Yan and Barbosa-Cánovas, 2001b; Zhang et al., 2020). Also, breakage could affect the bulk

density of IMF, which affects nutrient serving on volume basis. Thus, particle breakage is a problem that cannot be ignored in dairy powder production. However, only a few studies about dairy powder breakage have been published and they mainly focused on the influence of breakage on powder properties or the influence of transportation parameters on breakage. There is currently not enough research on breakage behaviours and the influencing factors of breakage that are very important for understanding and controlling dairy powder breakage.

The research on undesirable or intentional particle breakage in other industries, such as the pharmaceutical, agricultural, mineral, granulation, and catalysts chemical industry, is very extensive and thorough, and could act as good reference knowledge for the study of dairy powder breakage, as some of the processes are necessary for dairy powder production (Deng and Davé, 2017; Gupta et al., 2017; Gupta, 2017; Norazirah et al., 2016; Reynolds et al., 2005; Salman et al., 2003; Shan et al., 2018). Numerical modelling combined with different types of tests were used for investigating the breakage patterns, influencing factors, breakage forecast, and characterization methods (Bonakdar et al., 2016; Bridgwater et al., 2003; Deng and Davé, 2017; Gupta et al., 2017; Liu et al., 2010; Salman et al., 2002; Shan et al., 2018). Some investigation methods or results are very useful for the study of dairy powder breakage, but there is currently no review of this useful information. On the other hand, the property and structure of dairy powder particles are different from other industry particles or model particles with regular shapes, so it is important to review relevant information combined with dairy powder characteristics.

Therefore, instead of only summarising the research done in dairy powder breakage, this chapter mainly focuses on reviewing findings and principles of particle breakage studies of other industries that could be applied to dairy powder particles. Based on the combination of these two aspects, it provides an overview of the current status of knowledge about the breakage mechanisms of particles, methods suitable for characterizing dairy powder breakage, the influence of breakage on dairy powder properties, and the

factors influencing breakage which can be used to control dairy powder breakage.

1.2. Particle breakage mechanisms

1.2.1. Continuum solids

The breakage of continuum solids has traditionally been classified into three modes of failure: brittle, semi-brittle, and ductile (Reynolds et al., 2005; Subero and Ghadiri, 2001). Brittle fracture takes place without noticeable plastic deformation in the material. Plastic deformation is the permanent distortion that occurs when a material is subjected to stresses that exceed its yield strength. In contrast, the ductile mode describes fractures with considerable plastic deformation in the solid. The semi-brittle fracture is an intermediate case where the brittle fracture occurs at the boundaries of a region of limited plastic deformation. While this form of breakage mechanism is not expected to have direct relevance to commercial dairy powders as most of them are agglomerates, it is included here for completeness.

1.2.2. Agglomerates

In contrast to continuum solids, agglomerates consist of several primary particles, which adhere together by adhesion force at their randomly distributed contacts. Depending on the agglomeration process, the internal adhesive forces are influenced by the superposition of different interactions forming material bridges, such as liquid or solid bridges or sinter necks[1] or even interlocking of primary particles (Bika et al., 2005; Salman. et al., 2015). Thus, it has been argued that those three modes of failure of continuum solids cannot be extended to describe structure materials, such as agglomerates and non-agglomerated porous solids (Reynolds et al., 2005;

[1] A sinter neck is a kind of bridge between two particles produced during sintering. Sintering is a processing technique employed to produce density-controlled materials and components from metal and/or ceramic powders by applying thermal energy. Sintering acts to bond particles together into strong, useful shapes. This process involves the atoms in materials diffusing across the particle boundaries and fusing together into one piece. The initial stage of sintering corresponds to neck growth between contacting particles.

Subero and Ghadiri, 2001). In order to characterize the mechanisms governing the failure of agglomerates, some experimental and numerical studies have been done and three breakage patterns were found: surface abrasion, chipping, and fragmentation (Aarseth, 2004; Kotzur et al., 2018; Little et al., 2016; Van Laarhoven et al., 2012; Zhang and Ghadiri, 2002). Abrasion is generally associated with limited particle damage, while fragmentation can drastically change the particle morphology (Papadopoulos and Ghadiri, 1996). Considering the cohesiveness of dairy powders, dispersion may occur (Han et al., 2021, Chapter 2). Three possible breakage mechanisms and their typical volume particle size distribution (PSD) plots (plotted on logarithmic scale x-axis) are summarized in Figure 1-1 (Bayham et al., 2016; Han et al., 2021; Materic et al., 2014; Scala et al., 2013).

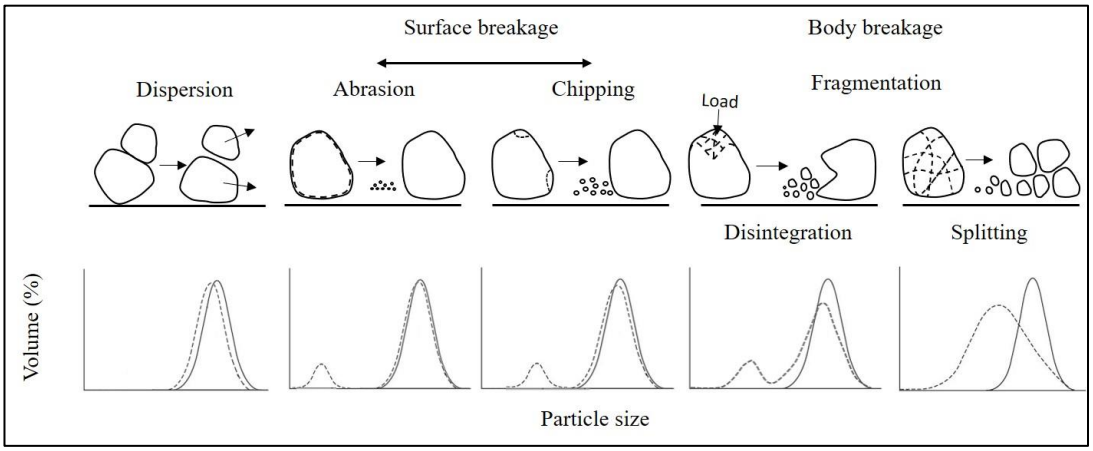


Figure 1-1. Outline of agglomerated particle breakage patterns and their typical particle size distribution curves (plotted on a logarithmic scale x-axis) before (solid line) and after (dotted line) breakage, recreated based on Scala et al. (2013), King (2012), and Han et al. (2021, Chapter 2).

Dispersion: At low processing conditions, dispersion of particles that exist as clusters held together by cohesive attractions may occur during many processes throughout production and transportation. These clusters are susceptible to breakage, thus small stresses can break the clusters and disperse them into their original particles. When the processing conditions are not gentle, the mechanical force acting on the particle can disperse clusters and the breakage of initial particles can happen. The clusters exist in the larger sizes of the PSD and when they are broken, the particles are

liberated causing the PSD shift to the left, with no production of fines (Han et al., 2021, Chapter 2).

Surface breakage: This includes abrasion and chipping. When particles are subject to low-level external mechanical stress, the main mechanism of breakage is the surface breakage, leading to the production of minuscule particles whilst still retaining the identity of the original particles. Hence the original volume PSD is still evident and moves a little to the smaller particle size with the appearance of the peak for the newly formed small particles and well separated from the original peak by a range of sizes that contains no particles (King, 2012). With the production of fine particles, the uniformity level of powders decreases, and the main volume of samples are big size particles but the main number of samples is small size particles. Based on this, surface breakage can be determined according to the birth of bimodal PSD (Bonakdar et al., 2016; Paluszny et al., 2016; Salman et al., 2003; Scala et al., 2013; Wu and Wu, 2017). The difference between abrasion and chipping is where the small peak occurs. The particle size of the small peak of chipping is bigger than that of the abrasion so the small peak of abrasion is at the smaller value compared with the chipping, as illustrated in Figure 1-1.

Body breakage: This includes disintegration and splitting, and both are sometimes collectively termed fragmentation. In principle, fragmentation is the large-scale breakage where the cracks are generated in the areas with high-level stresses and then develop within part of or through the whole volume of the particle, corresponding to disintegration and splitting, respectively (Ghadiri and Zhang, 2002). As shown in Figure 1-1, the PSD of disintegration particles is relatively narrow but will often be bimodal or even multimodal (King, 2012). Splitting results in the generation of a small number of coarse fragments, all significantly smaller than the parent, as illustrated in Figure 1-1. Splitting has the effect of translating the original PSD to the left but retaining its fundamental shape with a broad spectrum of particle sizes. In the breakage study of IMF, the initial sample had a single-peak PSD (plotted on a logarithmic scale x-axis) with a range from 127.0 μm to 586.0

μm. After disintegration, samples had bimodal PSD and a range of the main peak was still narrow which was 76.0 μm to 516.0 μm with the child particle peak from 7.64 μm to 66.9 μm. After splitting, the sample had a broader single-peak PSD, from 4.58 μm to 516.0 μm (Han et al., 2021, Chapter 2).

1.2.3. Crystalline particles

Lactose is an important ingredient for dairy powders and is sometimes in the crystalline form. For crystalline particles, the breakage mechanism is dependent on the distribution of loading forces across the topography of the particle. If crystalline material is semi-brittle, it will typically break via the previously described, abrasion or chipping mechanisms. If via a pure brittle mechanism, rupture along fracture planes[2] is expected. In the case where a particle is composed of two or more crystals, cleavage may occur at the interface, and child particles are relatively undamaged (Cleaver et al., 1993; Ghadiri et al., 1991).

1.3. Dairy powder breakage characterization methods

Currently, two main types of experimental tests have been designed to study the breakage of particulate systems: single-particle and multi-particle breakage tests (Bonakdar et al., 2016; Ortega-Rivas et al., 2006; Salman et al., 2007b). Both types of experimental tests are important for the study of dairy powder breakage. Depending on the mode of loading, each type of test can be divided into impact or dropping, static compression, and shear. The first two are commonly used to analyse the breakage behaviour or strength of particles.

1.3.1. Single-particle breakage tests

Single-particle test methods, including impact, crushing, dropping, and compression, have the advantage of applying a well-characterized load on

[2] A fracture plane is a two-dimensional plane of weakness along which a crystal or other solids will break when under stress.

the particle, providing fundamental information about particle properties, and enhancing the understanding of particle breakage (Bonakdar et al., 2016; Salman et al., 2002; Shan et al., 2018; Subero and Ghadiri, 2001). However, they are not fully representative of industrial conditions, and results are difficult to compare with attrition observed in practice because of the variations among particles in a certain bulk. For dairy powder breakage investigation, the particle size of dairy powders is usually too small for use in the single-particle methods. Some studies were performed on large-sized (710-850 μm) IMF agglomerates using single-particle compression and dropping tests by a texture analyser and a stainless steel plate combined with a high-speed camera, respectively (Hanley, 2011).

In single-particle tests, particle breakage is mainly due to crack propagation. Combined with the photography from a high-speed camera (Antonyuk et al., 2005; Papadopoulos and Ghadiri, 1996), single-particle tests can be used to investigate the breakage behaviour and how cracks develop in particles. In addition, single-particle breakage tests can be used to measure the strength of particles. Particle strength would be influenced by both material and structure strengths, which is an integrated mechanical property. For discussion, particle strength was defined as the minimum amount of stress that might be applied to a particle to cause macroscopic damage to the particle structure, which represented fracture toughness, hardness, yield stress, and breaking stress-related strength for different loading conditions (Bika et al., 2001; Kotzur et al., 2018).

For static compression tests, either single-particle or multi-particle, the force-deformation curves can be used to analyse the breakage behaviour and strength of particles (Hanley, 2011; Shan et al., 2018; Yan and Barbosa-Cánovas, 1997). For the single-particle compression test, the strength of agglomerates and the normal force and strain at the point of breakage can be obtained from the force-deformation curves. The deformation behaviour of most agglomerates lies between the extremes of brittle failure and plastic failure. For brittle failure, the compaction goes through three stages: elastic loading (the applied force increases with increasing deformation), breakage

(where the maximum applied force is and it can be clearly identified), and then further development of the cracks. For plastic failure, the particle deforms plastically and does not show a definite point of breakage and then the formation of a large contact area is followed. In some studies, the maximum applied force at breakage was taken as the particle strength (Beekman et al., 2003). In addition to the maximum applied force, Tavares et al. used the specific fracture energy when they studied the breakage of iron ore pellets (Tavares et al., 2018; Tavares and de Almeida, 2020). The specific fracture energy was obtained by dividing the absorbed energy by the mass of the particle and the absorbed energy was given by numerical integration from the force-deformation curve. However, each curve of agglomerated dairy powder particles had several peaks and troughs because they were irregular. Some peaks represented surface breakage, while others represented body breakage. An algorithm was developed to identify the first body breakage point (Hanley, 2011). Besides, even with the identical production process, the strength of the individual agglomerates differs in the microstructure because of the distribution and orientation of bonds, defects, and pore size distribution (Antonyuk et al., 2005). Thus, dairy powder particles are different so the force-deformation curves of different particles in the same sample could be different.

In impact or dropping tests, the coefficient of restitution was used in the single-particle test to show the particle strength (Hanley, 2011). It was defined that the magnitude of the normal velocity after impact divided by the normal velocity before impact. Every collision was recorded using a high-speed camera. Each file was analysed using software to track the position of each agglomerate over time, and thus provided the normal velocity of particles before and after the collision. Where coefficients of restitution were low, this implied that extensive breakage of either bonds or primary particles occurred which absorbed energy.

It is worth mentioning that the results of single-particle tests are difficult to compare with breakage in practice but they can be used in process simulations using the appropriate tools, such as the Discrete Element

Method (DEM) and DEM coupled with Computational Fluid Dynamics (CFD), to predict particle breakage. DEM simulations have been widely used to investigate the breakage of agglomerates, particularly breakage induced by impact with a focus on the effect of impact velocity, impact angle, and surface energy. Han et al. (2003) applied a 2D CFD-DEM model to simulate particle breakage behaviour in a dilute-phase pneumatic conveying system. The simulated results were comparable to experimental data. However, under-prediction of particle breakage was observed with increasing numbers of passes through the system, which was attributed to the disregard of fatigue. Uzi et al. (2016) presented a model of particle breakage within pneumatic conveying systems. Empirical comminution functions (strength, equivalence, fatigue, and breakage) for particle characteristics and machine functions (collision velocity and collision frequency) were developed from CFD-DEM simulations to inform the model. The model predictions of particle breakage were in good agreement with the breakage results obtained in pneumatic conveying experiments. This means that the single-particle tests of dairy powders can be used in the simulations of production processes, which will assist efforts in understanding breakage and reducing the associated problems in industrial systems.

1.3.2. Multi-particle breakage tests

Unlike the single-particle tests, multi-particle test methods, using shear cells, compression cells, vibrations, and fluidized beds, are close to real life industrial situations, even though the loading conditions experienced by each particle are not known (Wu and Wu, 2017; Yan and Barbosa-Cánovas, 1997; Yan and Barbosa-Cánovas, 2001a). Vertical vibration tests using a tap density tester were applied to investigate breakage and its influencing factors (particle size and water activity) of instant coffee powder and milk powders (Barletta and Barbosa-Cánovas, 1993a, b; Yan and Barbosa-Cánovas, 2001a). Samples were sieved into different fractions with different particle sizes before being confined to a graduated cylinder at a certain fixed height and exposed to a certain number of vertical vibrations on a tap density tester. After the test, the total sample weight was recorded. For each sample with a

different particle size range, a corresponding sieve was used to gently sieve the sample to determine the weight fraction of the agglomerates that maintained their original size. The recorded amounts of particles retained on the sieve and passed through it were used for calculating the attrition index. The multi-particle compression test using a TA texture analyser was used to analyse the effect of padding foam on reducing breakage in instant coffee and milk powders (Yan and Barbosa-Cánovas, 1997; Yan and Barbosa-Cánovas, 2001b). Some studies used laboratory-scale equipment, such as a pneumatic conveyor, a simulated pneumatic conveying rig, or a dry mixer to analyse the breakage of different kinds of agglomerated dairy powders (Han et al., 2020; Hanley, 2011; Hazlett et al., 2020; Zhang et al., 2020). In these treatments, the following different assessment methods were used to evaluate the breakage or breakage behaviour.

1.3.2.1. Characterization of breakage behaviour

For the multi-particle compression tests, the force-deformation curves are smooth and can illustrate the whole compression process of samples. It is generally believed that the compression of agglomerates occurs in three stages, rearrangement of agglomerates, breakdown of agglomerates, and rearrangement of primary particles. Thus, particle breakage behaviour can be analysed according to the changes of force-deformation curves (Yan and Barbosa-Cánovas, 1997). For some impact or dropping tests, the changes of PSD before and after breakage can indicate the breakage mechanisms (as shown in Figure 1-1) and has been used in some areas, such as lactose crystals, catalysts, limestone, calcium looping sorbents, and model porous powders (Agrawal et al., 2011; Bonakdar et al., 2016; Materic et al., 2014; Ortega-Rivas et al., 2006; Scala et al., 2007; Wu and Wu, 2017; Zhao et al., 1999). In addition, the loss of at least 10% of the mass of the original particles in a given stressing event has been defined as the threshold between surface breakage and body breakage, which has been used in some studies including single-particle breakage tests (Tavares et al., 2018).

1.3.2.2. Characterization of powder strength

Some breakage indices were proposed to describe the extent of breakage or indirect powder strength (Agrawal et al., 2011; Barletta and Barbosa-Cánovas, 1993a; Yan and Barbosa-Cánovas, 1997).

1.3.2.2.1. Static compression tests

For the multi-particle compression tests, the ease of breakage can be analysed according to the changes of force-deformation curves. The compression index (*CI*), presented in Eq. (1-1), was used to indicate the compressibility and ease of breakage. The higher the *CI*, the easier it is for agglomerates to be broken. Eq. (1-1) was successfully applied to describe the sigmoid compressive stress-strain relationships (Swyngedau et al., 1991). Besides, some researchers used the percentage of bulk density change to indicate the compressibility (Fu et al., 2012)

$$\frac{\rho(\sigma)-\rho_0}{\rho_0} = C + CI \cdot log\sigma \qquad \text{Eq. (1-1)}$$

where $\rho(\sigma)$ is the bulk density under compression stress σ, ρ_0 is the initial bulk density, and C is constant.

1.3.2.2.2. Impact or dropping tests

In impact or dropping tests, the indication of strength or the extent of breakage is based on the changes in particle size or PSD, or the production of child particles, depending on the methods used and the characteristics of original particles (Bonakdar et al., 2016).

(1) The changes in particle size

Friability refers to the ability of powder particles to fragment into smaller particles, which can be used to represent particle strength, and the bigger the friability index (*FI*), the easier it is for particles to be broken. The *FI* of samples is deduced from the changes of particle size which is measured by laser light scattering analysers with dry dispersion modes at two dispersion air pressures. For instance, *FI* can be calculated as Eq. (1-2) (Schuck et al., 2012) when the particle size is measured by laser diffraction analysers

$$FI = \left(\frac{D50_{\ 0.5\ bar} - D50_{\ 4.0\ bar}}{D50_{\ 0.5\ bar}}\right) \times 100\% \quad \text{Eq. (1-2)}$$

where $D50_{0.5\ bar}$ and $D50_{4.0\ bar}$ are the particle size (D_{50}, taken from the volume PSD) measured with compressed air at 0.5 and 4.0 bar, respectively. *FI* is suitable for distributions that are both monomodal and do not change their shape after breakage. Also, because the D_{50} is calculated from the volume-weighted PSD, it is insensitive to changes at the fine end of the distribution. Dairy powder breakage results in the production of fine particles so instead of using D_{50}, the Sauter mean diameter ($D_{3,2}$) should be used in Eq. (1-2) because it is more sensitive to the presence of fine particulates in the size distribution than the volume mean diameter ($D_{4,3}$) (Hu et al., 2014; Mun et al., 2011).

(2) The changes in PSD

The attrition index (*AI*) has been used to compare the extent of breakage and it is the ratio of the volume of fine particles and other particles after breakage. In Figure 1-2A, the particle size of fines is most simply defined as the lower limit size of the initial PSD. *AI* can be calculated with Eq. (1-3) (Agrawal et al., 2011). A differential attrition index (*DAI*) was defined as the sum of the volume fraction of particles that appear or disappear within size classes across the distribution divided by 2. It signifies the net volumetric movement of particles from larger to smaller size groups. Disappearance from one size class means appearance at another size class. Based on the difference of the PSDs before and after breakage as shown in Figure 1-2B, *DAI* can be calculated in Eq. (1-4) (Agrawal et al., 2011)

$$AI = \frac{a}{b+d} \quad \text{Eq. (1-3)}$$

$$DAI = \frac{m+n}{2} \quad \text{Eq. (1-4)}$$

where a, b, d, m, and n are the areas of the corresponding enclosed area in Figure 1-2. Compared with *AI*, *DAI* is equal to area *a*+*b* or area *c*. *AI* excludes the newly generated particles represented by area *b* so *DAI* is more sensitive to changes in shifting PSDs, and *DAI* is more suitable when PSD changes are minor.

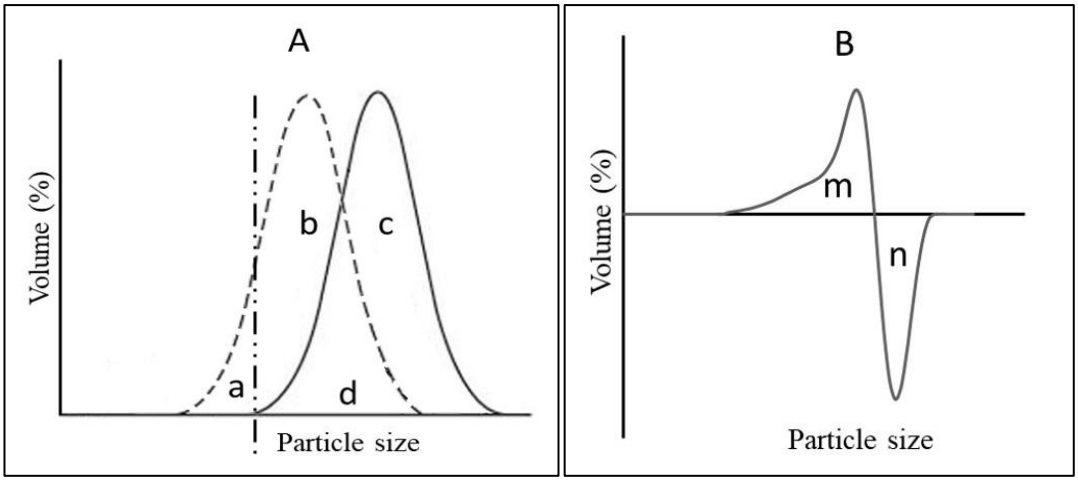


Figure 1-2. The particle size distribution curves before (solid line) and after (dotted line) breakage (A), and the difference of them (B), recreated based on Agrawal et al. (2011).

Rather than using the PSD with percentages of the particles contained in each size category shown on a linear vertical axis, as shown in Figure 1-2A, cumulative particle size distributions, shown in Figure 1-3, can be used to get the relative breakage (B_r) (Einav, 2007). Before calculating the B_r, a baseline particle size must be selected, depending on the properties of samples. For example, 20 μm was chosen as the baseline particle size when analysing the breakage of IMF because measured changes in the particle size distributions of IMF below this threshold were negligible (Hanley, 2011). The breakage potential (B_p) is defined as the area enclosed between the particle size distribution before breakage and the baseline size, as shown in Figure 1-3A, and it quantifies the breakage if all particles have final sizes below the baseline size. The total breakage (B_t), is the area enclosed between the particle size distributions before and after breakage for particle diameters greater than the baseline particle size, as shown in Figure 1-3B, which is a measure of the actual breakage. B_r can be calculated from the Eq. (1-5).

$$B_r = \frac{B_t}{B_p} \qquad \text{Eq. (1-5)}$$

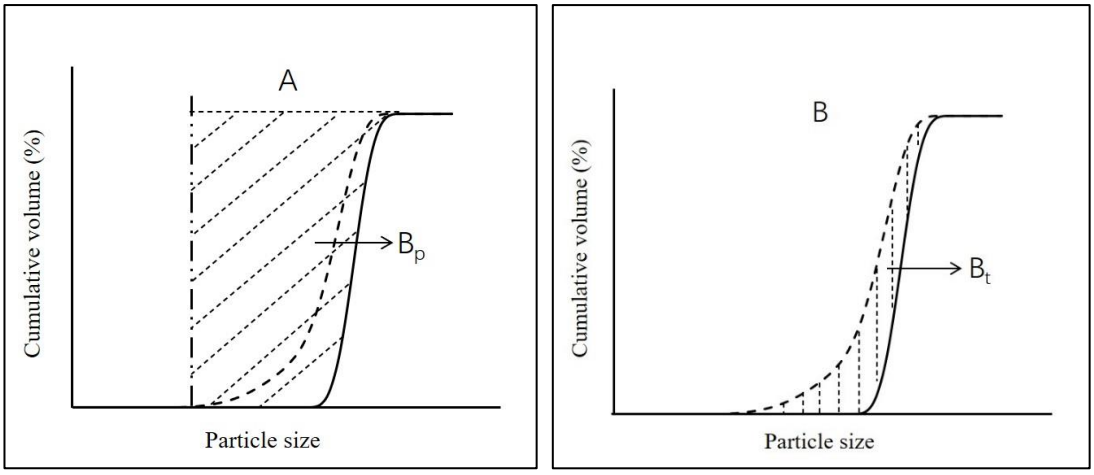


Figure 1-3. Cumulative particle size distributions before (solid line) and after (dotted line) breakage with shaded areas indicating the breakage potential B_p (A), and the total breakage B_t (B), recreated based on Hanley (2011). B_p: breakage potential. B_t: total breakage.

(3) The production of child particles

In this type of experiment, a narrow PSD should be used. Particles were collected after breakage, even the single-particle test methods, and sieved into child particles and mother particles. The results are expressed in terms of the extent of breakage (*BE*) using Eq. (1-6) (Bonakdar et al., 2016)

$$BE = \frac{M_D}{M_0 + M_D} \times 100\% \qquad \text{Eq. (1-6)}$$

where M_D and M_0 are mass of child and mother particles, respectively.

1.3.3. Other indirect methods

Besides the two types of methods above, some researchers have developed other indirect methods where the load did not directly act on the powder or the object of loading was not the original powder.

Agrawal et al. (2011) investigated lactose powder breakage inside the liquid mixing cell (called the small volume liquid sample presentation unit) of a laser diffraction particle sizer (Malvern Mastersizer) where the stirring time and rate of the propeller inside the cell could be controlled to break lactose particles. This approach provided an on-line particle size measurement that prevented experimental losses and errors during filtration, drying, weighing, and sieving. However, samples needed to be dispersed in non-solvent media

liquids. Methanol was chosen as the non-solvent medium by Agrawal et al. for the lactose crystals attrition study. The shattering index (*SI*), quite similar to the *FI*, was used to represent lactose strength in this study. *SI* was calculated with Eq. (1-7) when the breakage degree was controlled by dispersing at different times

$$SI = \left(\frac{D50_{\,0} - D50_{\,t}}{D50_{\,0}}\right) \times 100\% \qquad \text{Eq. (1-7)}$$

where $D50_0$ and $D50_t$ are the particle size (D_{50}, taken from the volume PSD) after breakage treatment for 0 and t time, respectively. As the description in 1.3.2.2.2- (1), instead of using D_{50}, $D_{3,2}$ should be used in Eq. (1-7).

A KQ-3 particle strength tester was used to measure mechanical strength of three fluid-bed catalytic cracking catalyst samples with mean particle diameters around 100 μm (Wu and Wu, 2017). Since it is impossible to measure the mechanical strength of a single particle in this device, flakes of pressed particles were employed. All flakes were also made of catalyst particles of the same mass. The pressing time and pressure were also the same. The test results of flakes were used to reflect some extent of the bond strength of the original samples.

1.4. Influence of dairy powder breakage on powder physical properties and functionalities

Different breakage mechanisms result in different particle sizes and PSDs of the final samples, which then can influence powder properties. The influence of breakage on dairy powder properties is an important issue for the dairy powder industry. This section will summarize the effects into two categories: physical properties and functionalities.

1.4.1. Physical properties

Dairy powder breakage significantly reduces the particle size which is an essential and important property for dairy powders (Li et al., 2016). The particle size of IMF fell from 143 μm progressively to 65.4 μm after the laboratory-scale high-speed mixing for 7 min (Han et al., 2020, Chapter 4).

After in-plant transportation using pneumatic conveying or a bucket elevator, the average particle size of instant whole milk powder decreased and the PSD shifted to a smaller value (Boiarkina et al., 2016). The particle size of WPC, fat-filled milk powder and WPI decreased during the pneumatic conveying (Hazlett et al., 2020; Zhang et al., 2020). The specific surface area (SSA) increases with the decreasing particle size because SSA is typically inferred from the particle's size. The bulk density and porosity also relate to particle size so the bulk density of powders significantly increases and porosity decreases after breakage (Boiarkina et al., 2016; Han et al., 2020; Hanley, 2011). There were a lot of pores inside dairy powder particles and after breakage, some internal stomata were exposed, which led to the increase of particle density. Thus, the breakage does not only break solid bridges within agglomerated particles resulting in the decrease of particle size and increase of bulk density but also breaks primary particles leading to the increase of particle density (Han et al., 2020, Chapter 4).

Dairy powder breakage influences the surface composition of particles. Murrieta-Pazos et al. (2012) using X-ray Photoelectron Spectroscopy coupled with Energy Dispersive X-ray analyses investigated the first 5 nm and the first micrometre of the dairy powder particle surface respectively. They proposed that the distribution of milk components (lactose, lipids, proteins, and minerals) from the particle surface to the core was different. This means the distribution of each component in the particle is not uniform, so breakage can influence the surface composition. There was higher surface free fat content for broken dairy powder samples, including IMF and fat-filled milk powder, and the higher the extent of breakage, the higher the surface free fat content (Han et al., 2020; Hanley et al., 2011b; Hazlett et al., 2020). As these powders contained much higher concentrations of fat, homogenisation steps were used before spray drying to stabilise the fat that dispersed through the particle's bulk structure after spray drying. Particle breakage produced more surface area and exposed fat that hidden within the interior of the powder particles, leading to increases in the concentrations of free fat on particle surfaces. There is currently no research presented on the effect of breakage on the other components.

The changes in physical properties seriously affect the use of dairy powder. For example, bulk density is functionally an important characteristic as it is for calculating the capacity of packing materials, especially for IMFs as they are usually dispensed on a volume basis using a scoop. It is also important that changes in physical properties lead to a decline in functional properties.

1.4.2. Functionalities

1.4.2.1. Rehydration properties

Rehydration properties are considered an important benchmark to determine the overall quality of powder products and regarded as critical issues in the dairy industry. The rehydration process mainly consists of three sequential stages, which are wetting, dispersing, and solubilization (Ji et al., 2016).

Wettability is the ability of particles to imbibe a liquid and overcome the surface tension between them based on the capillary force (Forny et al., 2011; Richard et al., 2013). There are two steps for the wetting process of powders (Yuan and Lee, 2013). The first step is the replacement of gas by water so the interface of powders-gas is replaced by the interface of powder-water. Secondly, inward diffusion of the liquid through the capillary structures of the porous powder particle. It is usually believed that wettability depends on the powder particle size, density, porosity, surface charge, surface area, the presence of amphipathic substances, and the surface activity of the particles (Hogekamp and Schubert, 2003; Sharma et al., 2012). High extent powder breakage results in the significant decrease of porosity, and the increase of the surface free fat content. Lower porosity reduces the capillary radius between particles, and higher surface free fat content makes the particle surface more hydrophobic, which both inhibit water penetration into powders, thus slowing down the wetting process. Han et al. (2020, Chapter 4) showed that the wetting time of IMF before breakage was around 1 s using the contact angle measurement while 5 min was needed for samples with a high extent of breakage. Agglomerated WPC and fat-filled milk powder

also displayed significant impairment in their wettability on breakage during pneumatic conveying, with reductions in the levels of wettability (the mass percentage of the wetted particles to the initial sample) from 68.7% and 65.9% to 39.2% and 34.9%, respectively (Hazlett et al., 2020). Similarly, the wettability of WPI decreased after transported by the dilute-phase pneumatic conveying due to the greater breakage (Zhang et al., 2020).

Dispersibility is the ease with which lumps and agglomerates of powder separate into individual particles in water, and it is influenced by particle size, porosity, and density (Goalard et al., 2006; Sharma et al., 2012). It was found that breakage decreased the dispersibility of IMF, agglomerated WPC, and fat-filled milk powder, and decreased gradually with the increase of the extent of breakage (Han et al., 2020; Hazlett et al., 2020). The substantial decrease of particle size and porosity and the increase of surface free fat content may be the reason for the deterioration of the dispersibility of broken samples by slowing down the penetration of water into the powder.

Solubility is a measure of the final condition to which the constituents of the powder can be brought into solution or stable suspension, depending mainly on the chemical composition and physical state of the powder, such as the fat content in milk (Pugliese et al., 2017; Sharma et al., 2012). Pugliese et al. (2017) found that the solubility of skim milk powder was higher than whole milk powder because of the lower water dispersion of fats in water. The mechanism proposed to explain milk powder insolubility involves the unfolding of the β-lactoglobulin and its aggregation with casein, and also the fouling of heating equipment which is associated with the drying conditions (Thomas et al., 2004). Currently, no research has found that dairy powder breakage affects powder solubility. Hazlett et al. (2020) found that there was no significant difference in the solubility of some dairy powders before and after breakage, including IMF, agglomerated WPC, and fat-filled milk powder.

1.4.2.2. Flowability

Powder flowability is important in handling and processing operations and it depends on the powder properties and storage conditions as they influence the cohesiveness of powders. After breakage, the particle size and porosity decrease, which acts to bring the powder particles into closer arrangement, resulting in a greater number and strength of interparticle interactions, such as van der Waals and electrostatic interactions, reducing powder flowability through increased cohesiveness (Zafar et al., 2017). Additionally, the SSA and surface free fat content increase after breakage, and fat has the propensity to form liquid bridges between neighboring particles, which also increases the cohesiveness of powders, thus decreasing the flowability. It was found that with increasing breakage, the flowability of instant coffee and some agglomerated dairy powders decreased (Hanley, 2011; Hazlett et al., 2020). On the contrary, the breakage of some IMF, WPI and granulated fat-filled milk powder did not significantly influence their flowability (Han et al., 2020; Hazlett et al., 2020; Zhang et al., 2020). Moreover, the improvement of the flowability of some sieved big-sized IMF samples after breakage was found by Hanley (2011). Thus, no clear trends have been observed for the influence of powder breakage on the flowability of dairy powders. This might be because breakage degree and powders' initial properties influenced the effect of breakage on flowability.

1.4.2.3. Water sorption, glass transition, and mechanical properties

Water strongly affects glass transition and structures of amorphous food solids, and it is an important factor determining their chemical and physical stability (Li et al., 2019). The increasing water content induces the formation of liquid bridges between particles, which may result in caking and sticking problems of food powders. Furthermore, the mechanical properties of dairy powders, including the storage modulus, loss modulus, and α-relaxation, are influenced by the glass transition as they are related to molecular mobility (Li et al., 2016; Maidannyk et al., 2020). However, there is currently no research on the influence of breakage on these properties of dairy powders. Previous studies have shown that the SSA of powders increased after breakage,

which means more surface area is potentially available for water sorption, thus breakage may increase the water sorption speed. Besides, breakage significantly decreases the particle size of powders. Water sorption properties of lactose/milk protein isolate solids systems with different particle sizes were analysed (Li et al., 2016). It was found that the water content of large particle samples (the D_{50} was around 25-50 μm) was lower than the small-sized samples (the D_{50} was around 6.7-7.5 μm) with the same composition at 0.54 a_W at 25°C for 168 h. On the other hand, the decrease of porosity can slow down the water sorption because of the small capillary radius between particles.

In general, breakage significantly deteriorates powder properties. It is necessary to control the unwanted breakage during the production and transportation of dairy powders. However, there is currently not enough research on it. Based on the literature on the breakage of other materials, the applied stress from processing conditions and the characteristics of particles are two main effects that influence particle breakage (Petukhov and Kalman, 2004). Thus, the control of dairy powder breakage can be considered from these two aspects. In the next two sections, these two influencing factors on dairy powder breakage are reviewed.

1.5. Influencing factors - processing conditions

Dairy powders are produced by dehydrating water in raw milk during several processes and the main steps are categorized as pre-treatment (standardization, homogenization, and pasteurization), concentration, and drying (Moejes and van Boxtel, 2017; Yildirim and Genc, 2017). Spray drying is a common practice in dairy powder production where liquid state feed is turned into a solid-state product by spraying the liquid into a hot air environment (Yildirim and Genc, 2017). Combining spray drying (with fines return) with fluidized bed processing is mostly used for drying and particle granulation. Breakage very easily occurs in the fluidized bed but breakage and agglomeration occur simultaneously in the fluidized bed (Reynolds et al., 2005). After agglomeration and cooling down the temperature, powders are

transported to packaging or storing in a silo using pneumatic conveying or bucket elevator (Boiarkina et al., 2016; Walstra et al., 2005). After packaging, vibration is unavoidable before products are consumed. There is a special process during the production of the IMF called the 'dry blending' process. Ingredients in powdered form are mixed, using either a ribbon blender or other large-scale blending equipment, to achieve the uniform blend of macro- and micronutrients necessary for a complete IMF product (Jiang and Guo, 2014; Kent et al., 2015). In the context of particle attrition, it has been demonstrated that the collisions among agglomerates and against static container walls due to mechanical impact, shear, or compression provide the kinetic energy that causes the breakage of agglomerated particles (Kotzur et al., 2018). Unwanted breakage is the breakage that happens after agglomeration, which mainly occurs during in-plant transportation (pneumatic conveying or bucket elevator), dry blending, and vibration.

1.5.1. Breakage during dry-mixing

Dry mixing requires the motion of ingredients to reach the desired homogeneity or a uniform distribution. It is accomplished by the movement of particles between various parts of a whole particulate mass (Lindley, 1991b). Particle breakage occurs during movement, especially for surface breakage or dust generation (Bridgwater, 2010; Lindley, 1991a). Forces acting on particles during mixing include gravity, vessel walls, and the motion of mixing blades (Lindley, 1991b). Three mixing mechanisms have been recognized in solids mixing: convection, diffusion, and shear (Kuakpetoon et al., 2001; Lindley, 1991a, b; Pernenkil and Cooney, 2006). Shear mixing is sometimes considered as part of the convective mechanism. Three mechanisms take place simultaneously in powder mixing processes (Kotzur et al., 2018). In convective mixing, a circulating flow of powders is caused by the rotational motion of a mixer vessel, an agitating impeller (such as a ribbon or a paddle), or gas flow. The impeller provides great shear so large portions are moved at relatively high rates which causes changes at a microscopic scale and produces fine particles (Niranjan et al., 1994; Ortega-Rivas et al., 2006). The rate of mixing by diffusion is low compared with convective mixing so it can

cause less breakage but pure diffusion mixing is exceedingly slow. Shear mixing is induced by the momentum exchange of powder particles having different velocities. Mixing due to shear force occurs and is developed by the formation of slipping planes in the bulk material (Lindley, 1991b; Rhodes, 2008). The originally coherent particle groups are compressed and extended then gradually broken along these planes.

Dry-mixing is a basic and important process for a range of industries including pharmaceutical, chemical, agriculture, material, and food (Pernenkil and Cooney, 2006). For example, the slightest changes in ingredient properties or process operating conditions for manufacturing of a drug can have a huge impact on its quality (Bertrand et al., 2005). In flour milling, dust generation is a primary concern (Bemrose and Bridgwater, 1987). Duraccio et al. (2019) used three different dry-mixing techniques followed by a compression molding step to prepare medical composites and found that the dry-mixing techniques affected the structural and morphological features of the composites that, in turn, influenced the mechanical behaviour. Portillo et al. (2008) also mentioned that in cases where the sample was agglomerated, increasing the intensity of the mixing mechanism could reduce the size of agglomerates when they characterized the continuous convective powder mixing processes.

1.5.2. Breakage during in-plant transportation

Agglomerated dairy powders must be transported from the fluidized bed via an intermediate silo to a filling line or a storage silo. The conveying distances involved are typically 50-200 m in the horizontal direction, and 10-20 m in the vertical direction (Hanley, 2011). Mechanical transfer systems are needed for powder transportation from a low level to a higher level of the silo entrance. There are many different mechanical transfer systems for dry particulate materials, such as transport screws, bucket elevators, and belts (Go Yanko, 2007). Boiarkina et al. (2016) found that the breakage of instant whole milk powder occurred during transportation using a bucket elevator. However, these conveyors have rarely been selected for dairy powder transportation because of the distances, hygienic operations, and cleaning

(Go Yanko, 2007). Pneumatic conveying is a widely used method for dairy powder transportation because it has several advantages such as hygiene, the flexibility of routing, and it can be easily automated (Boiarkina et al., 2016; Go Yanko, 2007; Kotzur et al., 2018). Thus, this section will mainly focus on the breakage during pneumatic conveying. For the same particles, parameters affecting the extent of breakage during the pneumatic conveying can be divided practically into operation parameters (velocity and particle concentration) and pipeline structure (bend radius and number of bends).

1.5.2.1. Operation parameters

There are two major pneumatic conveying regimes, dilute phase, and dense phase. Dilute-phase pneumatic conveying is defined as the condition where all particles are suspended in the airflow, and it requires high superficial air velocities and low particle concentrations within the pipeline. Dense phase pneumatic conveying is characterized by particles populating the entire cross-section of the pipeline, and particles moving through the pipe in batches separated by air pockets. This form of conveying generally needs low superficial air velocities and high particle concentrations.

The dilute phase has been linked with high particle breakage due to the requirement of high superficial air velocities which results in high-energy impacts against the walls and bends (Kalman, 1999). Some research on IMF and WPI breakage in dilute-phase pneumatic conveying found that the extent of breakage increased with increasing air velocities (Han et al., 2020; Hanley, 2011; Zhang et al., 2020). The same results were found in some studies on the breakage of general-purpose fertilizers in impact experiments or dilute-phase pneumatic conveying (Salman et al., 2003; Salman et al., 2002). Salman et al. (2002) found that a threshold velocity existed in the single-particle impact studies, and below the threshold velocity, no breakage occurred. Another reason for the dilute phase resulting in high breakage is the low particle concentration in the pipeline. Based on some studies on particle breakage in dilute-phase pneumatic conveying with different powder materials (such as IMF with large particle sizes between 710 μm and 850 μm, wood dust, Silica flour, Olivine sand, and sea salt), particle breakage

decreases with increasing particle concentration (Han et al., 2003; Hanley, 2011; Macchini et al., 2013; McKee et al., 1995). This phenomenon is always explained by the shielding effect where high-velocity particle-pipeline impacts are partially mitigated by inter-particle contacts, thus only a fraction of the conveyed particles come into direct contact with the pipeline (Kotzur et al., 2018; Macchini et al., 2013).

1.5.2.2. Pipeline structure

Particle to particle interactions and impacts against pipeline walls and bends are thought to be the predominant causes of particle breakage in pneumatic conveying (Brosh et al., 2010; Kotzur et al., 2018). Among them, particles experience extensive impact loads mainly at the bends because the flow direction is changing. In addition, the mean inter-particle collision velocity is generally much lower than the normal impact velocity at pipeline bends, thus, some researchers mainly considered the impact between particles and bends (Hanley et al., 2013). Particle breakage due to impact at bends depends on the balance between the resulting impact forces and is influenced by bend radius and numbers.

Breakage occurs if the impact force between the particle and bend exceeds the intrinsic strength of the particle (Hanley et al., 2013). The collision velocity, angle, and elasticity of the collision significantly affect the impact force (Kalman, 2000). When particles collide with a wall at some slope, the impact can be divided into two components, normal and tangential (Kalman, 2000). The tangential component causes a slight slide and shear loads. The impact force is proportional to the normal impact velocity that causes the main breakage (Hanley et al., 2013). The normal component decreases with decreasing collision angles and at 90° when the particle collides with the wall perpendicular it becomes maximum. Single-particle impact research (Salman et al., 2003) showed that the breakage probability of a fertilizer particle at a given speed varied slowly with impact angle from 90° down to about 50°, but then decreased rapidly below 50°. At 10° only a limited amount of damage occurred. Similar results were found during the pneumatic conveying of feed pellets for livestock, showing that the fraction of

broken particles was fairly similar for impact angles between 50° and 90° while for lower impact angles (<50°), the particle fracture decreased with the decreasing impact angle (Aarseth, 2004). Additional results in the literature that support the findings have been presented on the effect of impact angle by simulation, demonstrating that the energy dissipated in the collision remains relatively constant from 90 to about 50-60 degrees, dropping significantly below that (Tavares et al., 2018). The radius of bends is an important factor affecting the impact angle, and the collision angle will decrease with increasing radius. At the same time, the radius also influences the elasticity of the collision, and particles are expected to be subjected to a few impacts in long radius bends (Kalman, 1999). Thus, short radius bends produce more breakage because of the high impact angle and the elasticity of the collision. In a study on the breakage of IMF in pneumatic conveying, it was found that the radius of bends significantly influenced the breakage, which then influenced the bulk density of powders (Hanley, 2011). Aarseth (2004) investigated the effects of bend radius on the breakage of commercial feeds during pneumatic conveying and found that a shorter bend radius resulted in more breakage for all conveying velocities (20-50 m/s) relative to bends of the longer radius.

Particles can also be broken due to lower impact loads than their strength when the collision occurs many times, which is known as fatigue (Goder et al., 2002; Kalman, 1999, 2000). In actual factories, powders are transported repeatedly through processes for receiving, storage, re-processing, and packing (Konami et al., 2002). Thus, the breakage that results from repetitive transport should be taken into account. The number of impacts is affected by the number of bends in the system and the elasticity of collision. Breakage is more sensitive to the number of impacts when the extent of breakage at the first impact is low (Samimi et al., 2003). In the research on the relationship between the number of impacts and breakage of fertilizer particles, it was found that the number of impacts showed no effect on the breakage at three experimental impact velocities, while similar tests with polystyrene particles found a linear increase in the breakage with increasing impact number

(Salman et al., 2002). Therefore, whether the breakage is affected by the number of impacts is dependent on the material of the particles.

1.5.3. Breakage during vibration

There is a long-distance from the production factories to customers, and once the dairy powder products leave the factory, breakage may still occur due to handling and transportation. Surface transportation by rail or road particularly imposes multiple strains to the particulate material, and vibration is inevitable. Breakage can be caused by relative movement between particles induced by vibration in a bed of particles by using either a form of resonance or a simple mechanical motion transmitted from a container to the particles (Ortega-Rivas et al., 2006). When a container of powder is subject to vibration, in most cases, particles are rearranged and fine particles percolate through the coarse particles and fill the voids, so powder settles and the bulk density of powders increases (Ortega-Rivas et al., 2006).

Vibration tests in a container or on a sieve have been used to study the breakage tendency of particulate systems and determine agglomerated powders' friability which is defined as the tendency of particles to break down during storage and handling (Ortega-Rivas et al., 2006). The vibration intensity of particles depends on particle size and density, vibration frequency and amplitude, and the depth of the bed of particles (Barletta et al., 1993; Bemrose and Bridgwater, 1987). A commercial tapping density tester was used to study the breakage tendency of instant coffee and milk powders (Barletta and Barbosa-Cánovas, 1993a, b; Yan and Barbosa-Cánovas, 2001a). Remarkable bulk density changes were noticed for all tapping tests, especially at high tapping numbers. Gerhard et al. (2004) presented a vibration test that could be performed on any laboratory sieving machine to measure the breakage of agglomerated cocoa beverage powders and the particle size of powders significantly decreased. The breakage of ferric oxide granules during a tapping test showed that the mechanism of breakage was mainly the interaction of granules themselves in the whole granule layer (Utsumi et al., 2001). The tapping of agglomerated instant coffee confined in a cylindrical container generated significant breakage

where the particle size distribution shifted from a unimodal to a bimodal distribution and a lot of small-sized particles were produced (Barletta et al., 1993). From the perspective of packaging, adding padding foam might be a strategy to reduce attrition during vibration in agglomerated food powders. It was found that the padding thickness and positions significantly affect the breakage of instant coffee and instant milk. The padding effect was more obvious when the foam was put at the top of the powder bed than put at the middle or bottom (Yan and Barbosa-Cánovas, 2001b).

The process conditions (summarized in Table 1-1) play a fundamental role in the determination of dairy powders breakage and that, together with particle characteristics, dictates the response of a particle for a given loading condition (Antonyuk et al., 2005; Lu et al., 2014).

Table 1-1. Summary of the influence of processing conditions on the breakage of powders or particles.

Processing methods	Processing conditions	Trends or key points	Industries or powder materials	References
Dry-mixing	**Mixing mechanisms or rates**	• In convective mixing, large portions are moved at relatively high rates which causes a high extent of breakage. • The rate of mixing by diffusive is low compared with convective mixing so it could cause less breakage.	• Flour milling; • Manufacturing of drugs; • Preparing medical composites; • Blending pharmaceutical formulation;	(Bertrand et al., 2005; Duraccio et al., 2019; Niranjan et al., 1994; Ortega-Rivas et al., 2006; Portillo et al., 2008)
Transportation using bucket elevators	–	• Broken agglomerated powder.	• Dairy powders (IMP);	(Boiarkina et al., 2016)
Pneumatic conveying	**Air velocity**	• Particle breakage increases with increasing air velocity which results in high-energy impacts against the walls and bends. • A threshold velocity existed in the single-particle impact studies, and below the	• Dairy powders (IMF and WPI); • Fertilizer granules;	(Han et al., 2020; Hanley, 2011; Kalman, 1999; Salman et al., 2003; Salman et al., 2002; Zhang et al., 2020)

		threshold velocity, no breakage occurred.		
	Particle concentration	• Particle breakage decreases with increasing particle concentration, which may be caused by the shielding effect. • The increasing particle concentration increases inter-particle collisions leading to a wider distribution of impact velocities and impact angles.	• Dairy powders (IMF); • Wood dust; • Silica flour; • Olivine sand; • Sea salt;	(Han et al., 2003; Hanley, 2011; Macchini et al., 2013; McKee et al., 1995)
	Bend radius	• Particle breakage decreases with increasing pipe bend radius which decreases the collision angles and the number of collisions.	• Dairy powders (IMF); • Feed pellets for livestock; • Fertilizer granules;	(Aarseth, 2004; Hanley, 2011; Kalman, 1999; Salman et al., 2003, Tavares et al., 2018)
	Number of bends or collisions	• Particle breakage increases with increasing number of bends. • Particles can also be broken due to lower impact loads than their strength when the collision occurs many times (fatigue).	• Fertilizer granules; • Polystyrene particles; • Tungsten-carbide tablets;	(Goder et al., 2002; Kalman, 1999, 2000; Konami et al., 2002; Salman et al., 2002; Samimi et al., 2003)
Vibration	**Vibration frequency, amplitude, and numbers**	• Particles are rearranged and fine particles percolate through the coarse particles and fill the voids so powder settle and the bulk density of powders increases. • High tapping numbers causes a high extent of breakage.	• Instant coffee; • Ferric oxide granules; • Agglomerated cocoa beverage powders; • Dairy powders (IMP);	(Barletta and Barbosa-Cánovas, 1993a, 1993b; Barletta et al., 1993; Gerhards et al., 2004; Ortega-Rivas et al., 2006; Utsumi et al., 2001; Yan and Barbosa-CÁNovas, 2001a)

1. - Not applicable. IMP: instant milk powder. IMF: infant milk formula. WPI: whey protein isolate powder.

Table 1-2. Summary of the influence of particle characteristics on the breakage of powders or particles.

The characteristics of particles		Trends or key points	Industries or sample materials	References
Physical properties	**Particle size and porosity**	• Particle breakage increases with increasing particle size due to the likelihood of a greater number of imperfections in larger particles. • Particle breakage increases with increasing porosity because pores are analogous to imperfections and the number of contact points of primary particles decreases with increasing porosity. • The highest local tensile stress is generated at imperfections so that the fracture initiates from these zones. • Small particles are more difficult to break owing to the few flaws, the stronger interparticle forces, and the lowering of the collision energy.	• Dairy powders (IMF, WPI, SMP, LFMP, and lactose crystals); • Food powders (Instant coffee, salt crystals, and cocoa beverage powders); • Industrial agglomerates (γ-Al_2O_3, the synthetic zeolite, and sodium benzoate); • Pegmatite; • Burkeite particles; • Single crystals of MgO, NaCl, and KCl; • Detergent particles;	(Agrawal et al., 2011; Antonyuk et al., 2005; Bonakdar et al., 2016; Fu et al., 2012; Gerhards et al., 2004; Ghadiri et al., 1991; Han et al., 2021; Norazirah et al., 2016; Samimi et al., 2003; Yan & Barbosa-Cánovas, 1997; Yan and Barbosa-CÁNovas, 2001a; Zhang et al., 2020; Zhang and Ghadiri, 2002)
	PSD	• Particle breakage decreases with increasing the fine particle ratio (mass fraction) due to the cushioning action of fines. • Particles enclose the coarse granules and thereby act as a cushioning medium.	• Dairy powders (IMF); • Cement clinkers; • Coals; • Tungsten-carbide tablets;	(Gupta, 2017; Han et al., 2021; Konami et al., 2002)
	Morphology	• The more alike to the sphere, the higher the particle strength. • For non-spherical agglomerates, breakage depends	• Dairy powders (crystalline α-lactose monohydrate); • DEM model agglomerates	(Deng and Davé, 2017; Fu et al., 2012; Golchert et al., 2004;

		not only on the impact speed, impact angle, and interface energy but also on agglomerate orientation. • Spherical particles can break down along one or more fracture planes, producing a small number of large fragments, while irregular particles exhibit much more non-uniform loading, causing the forces to permeate through the particle, rather than along a particular plane or axis.	(spherical, cuboidal, cylindrical, or different fractal dimensions); • Pegmatite;	Liu et al., 2010; Norazirah et al., 2016)
	Particle size and PSD of primary particles	• A decreasing primary particle size increases the agglomerates' strength and large primary particles result in a loose agglomerate structure and weak agglomerates. • A narrowing of the PSD of primary particles corresponds to a reduction in the agglomerate strength because of the limitation of the layering mechanism.	• Dairy powders (agglomerated lactose); • Agglomerated calcium carbonates;	(Johansen and Schæfer, 2001; Keningley et al., 1997; van den Dries et al., 2003)
Powder composition	**Protein**	• In some situations, the higher the protein content or protein to fat ratio, the higher the particle strength.	• Dairy powders (IMF);	(Hanley, 2011; Hanley, Cronin, et al., 2011)
	Fat	• Fat reduces the strength of dairy powders. •Fat liquefaction can soften the powder.	• Dairy powders (SMP, high-fat milk powder, WMP, and LFMP);	(Rennie et al., 1999; Yan and Barbosa-Cánovas, 1997)
	Lactose	• Increasing the percentage of carbohydrates increases the stiffness of infant milk formula. • When lactose is in solid-state, it can be in a crystalline state or an amorphous state:	• Dairy powders (IMF); • Food powders (lactose-sugars systems, including in glucose, maltose, sucrose,	(Hanley, 2011; Li et al., 2019; Li et al., 2017)

	•Compared to tightly packed molecules in the crystalline state, lactose molecules in the amorphous state are disordered, forming a more open and porous structure, which makes powders more easily deformed and compacted. •Crystalline materials exhibit elasticity and brittleness upon exposure to external stress, while molecules in the amorphous state tend to exhibit varying degrees of viscoelasticity. •The mechanical strength of amorphous solids is brittle or fragile, while that of crystalline solids is strong.	trehalose, and corn syrup solids);	
Binders	• The strength or particle size of agglomerates obtained using different kinds of binders is different. •Sucrose or glucose usually produces hard and brittle bridges while gelatin and acacia gum provide slow disintegration and high hardness to the agglomerates. •Using water as a binder creates more irregular agglomerated MPI than using lactose and sucrose and the larger agglomerate size fraction is produced with the lactose binder. • A high viscosity binder increases the strength of agglomerates. • The dynamic yield strength of agglomerates decreases with decreasing binder surface tension.	• Agglomerates of microcrystalline; • Dairy powders (agglomerated MPI, lactose monohydrate); • Cylindrical pellets (glass ballotini with a range of binders); • Agglomerated calcium carbonates; • Agglomerates (lactose and hydroxypropylcellulose);	(Eliasen et al., 1998; Ji et al., 2015; Johansen & Schæfer, 2001; Iveson and Litster, 1998; van den Dries et al., 2003; Zajic and Buckton, 1990)
Moisture	• Drying strengthens the agglomerates presumably due to the solidification of bridges while humidifying	• Dairy powders (SMP and WMP);	(Rennie et al., 1999; Samimi et al., 2003;

	the granules decreases their strength. • Increased moisture content can soften the powder material, resulting in the deformation of the powder. • There is lower yield stress and larger plastic deformation during the breakage of the humidified samples when compared to the dry samples. • The particle surface is altered by solubilization, liquid layer formation, or local plasticization, which influences the properties of binders thus influences the particle strength.	• Detergent granules;	Yan and Barbosa-CÁNovas, 2001a)

1. IMF: infant milk formula. WPI: whey protein isolate powder. SMP: skim milk powder. LFMP: low-fat (2%) milk powder. PSD: particle size distribution. WMP: whole milk powder. MPI: milk protein isolate powder.

1.6. Influencing factors - particle characteristics

In addition to the applied stress, powder breakage depends on the powder strength, which is influenced by powder physical properties (particle size and PSD, powder porosity, and morphology) and composition (ingredients and moisture content). The powder properties (summarized in Table 1-2) influencing dairy powder breakage could be manipulated to control breakage.

1.6.1. Powder physical properties

1.6.1.1. Particle size and porosity

It has been repeatedly demonstrated that particle strength decreases with increasing particle size (Bonakdar et al., 2016; Gerhards et al., 2004; Norazirah et al., 2016; Zhang and Ghadiri, 2002). This is attributed to the likelihood of a greater number of imperfections in larger particles, which in turn provides a greater number of cracks which may propagate as a result of an imposed load (Antonyuk et al., 2005; Norazirah et al., 2016). Large particle size and porous structure can be obtained after agglomeration, which is necessary for sufficient rehydration properties and flowability. The porosity and its shape, orientation, and size distribution have a large effect on the breakage of agglomerates. The pore can be regarded as a crack release zone (Antonyuk et al., 2005). The pores and structural defects in agglomerates are analogous to imperfections, inhomogeneities, or microcracks in material science. The highest local tensile stress is generated at these defective zones in agglomerates so that the fracture initiates from this zone. The number of contact points of a primary particle can be decreased with larger porosities, by which the strength of agglomerates decreases (Antonyuk et al., 2005). Besides the few flaws and low porosity, small particles are more difficult to break owing to the stronger interparticle forces that bind particles together including van der Waals forces, electrostatics, and liquid bonds (Reynolds et al., 2005). From an energy perspective, the probability of breakage is related to the amount of energy that is absorbed by the particle during impact (if breakage is caused by the

impact). The particle is able to absorb a certain amount of energy before it breaks during a collision. When a particle is subject to impact stress, it initially deforms elastically, absorbing impact energy as stored elastic strain. The internal stresses in the particle increase until a crack occurs at the most sensitive part. The stored elastic strain energy in the particle drives the growing crack and any remaining stored elastic energy is dissipated as the kinetic energy of the child particles. The energy that is absorbed and stored represents the minimum energy that is required to break the particle under the particular external loading and stress pattern that the particle experiences. This energy is called the particle fracture energy and it is a material property that is influenced by its particle size, shape, orientation that the particle presents to the impact stress, and the presence of flaws in the particle. For particles of the same material, the smaller the particles, the higher the fracture energy, and hence the less likely the particle will break (King, 2012).

It was found that the breakage of IMF and WPI was very sensitive to the particle size of powders during the pneumatic conveying (Han et al., 2021; Zhang et al., 2020). The breakage of IMF increased with increasing particle size at the same processing conditions, and for WPI, there appeared to be a threshold size below which breakage was almost negligible. Three industrial spherical agglomerates, γ-Al_2O_3, synthetic zeolite, and sodium benzoate, were used as model materials in a single-particle compression test to study the mechanical behaviour of agglomerates from elastic to the plastic range during breakage (Antonyuk et al., 2005). It was shown that more mass-related breakage energy was needed to break off smaller agglomerates than bigger ones. Compression tests were used to characterize the breakage of agglomerated skim milk powder, low-fat milk powder, and instant coffee powder (Yan and Barbosa-Cánovas, 1997). Particle size played a significant role in compression tests in that the greater the particle size, the greater the volume reduction. The same results were found in the compression test of crystalline α-lactose monohydrate (Fu et al., 2012). The big particle-sized sample was more compressible than the small-sized one. In tapping tests, the larger the agglomerates, the higher the breakage index which was

defined as the ratio of the weight fraction of fines generated in the breakage test to that of the agglomerates retaining their original particle size (Yan and Barbosa-Cánovas, 2001a). Ghadiri et al. (1991) investigated the breakage of salt crystals using a single-particle impact test and micro-indentation. It was found that big-sized particles suffered more breakage than the smaller sized particles at all velocities, irrespective of which basis was used for breakage. During the breakage of lactose crystals, the particle size markedly affected breakage and the attrition index of the big-sized crystal (250-300 μm) was much higher than that of small-sized lactose (150-180 μm) (Agrawal et al., 2011).

1.6.1.2. Particle size distribution

It has been found that the PSD of particulate material significantly influenced the breakage of particles. The extent of breakage is reduced with an increasing fine particle ratio (mass fraction). Presumably, that is because the particles enclose the coarse granules and thereby act as a cushioning medium that reduces the granule stress and levels of attrition, which is attributed to the cushioning action of fines (Konami et al., 2002). In the case of two types of cement clinkers and two types of coals, the breakage of all sizes slowed down significantly when the number of fines exceeded a certain limit in individual cases (Gupta, 2017). For IMF samples with the same median particle size (D_{50}, taken from the volume PSD), a narrowing of the PSD corresponded to a reduction of powder strength (Han et al., 2021 Chapter 2).

1.6.1.3. Particle size and distribution of primary particles

It is generally assumed that high granule strength is associated with small primary particle size. It was found that the formulation parameters, viscosity and primary particle size, determined the eventual particle strength during the production of agglomerated lactose in a high shear mixer (van den Dries et al., 2003). A decreasing primary particle size increases the strength of agglomerates, which eventually leads to a clear reduction of breakage. The large particle size results in a loose agglomerate structure and weak

agglomerates that can easily be broken down (other agglomeration conditions are consistent) because smaller primary particles have a higher affinity for the layering agglomeration than coarser primary particles (Johansen and Schæfer, 2001; Keningley et al., 1997; van den Dries et al., 2003). The layering mechanism is a way of agglomeration where small particles become layered on larger particles, combined with coalescence between the smallest particles. During the agglomeration of calcium carbonates, it was found that a narrowing of the PSD of primary particles corresponded to a reduction in the agglomerate strength because of the limitation of the layering mechanism (Johansen and Schæfer, 2001). The size of powder primary particles depends on the type of atomization and drying conditions (Moejes and van Boxtel, 2017).

1.6.1.4. Morphology

There is a heavy dependence upon the agglomerate shape and structure as to the type and extent of breakage (Golchert et al., 2004; Norazirah et al., 2016). Different particle shapes have been the subject of different particles breakage studies, such as spherical particles, cubic crystalline particles, flaky particles, equidimensional shape, and irregular agglomerates (Golchert et al., 2004; Norazirah et al., 2016; Samimi et al., 2003). DEM simulation results show that the breakage behaviour of spherical, cuboidal, and cylindrical agglomerates differ from each other because for non-spherical agglomerates, the degree of breakage depends not only on the impact speed, impact angle, and interface energy but also on agglomerate orientation (Liu et al., 2010). The spherical particles follow classical tensile fracture behaviour by breaking along a fracture plane through the middle of the particle, with a limited number of contacts broken within the particle. In contrast, the load on the irregular particles until a sharp critical value causes the particle to shatter. The results of numerical compression studies on the breakage of spheres or irregular particles with DEM showed that spherical particles could break down at low impact energies along one or more fracture planes, producing a small number of large fragments and only 3% of contacts were broken (Golchert et al., 2004). The resistance to breakage at

low compression distance could be due to the external spherical shape of the agglomerate. The irregular particles exhibited much more non-uniform loading than the spherical particles, causing the forces to permeate through the particle, rather than along a particular plane or axis and 14.2% of the total contacts were broken.

The more alike to the sphere, the higher the particle strength. DEM simulations were conducted to investigate the breakage of fractal agglomerates with fractal dimensions ranging from about 2.0 to 2.8 (Deng and Davé, 2017). The fractal dimension can vary from 1 to 3, corresponding respectively to a chain-like structure and spherical agglomerate. Simulation results showed that the damage ratio decreased with increasing fractal dimension in the range between 2.0 and 2.6. With the further increase of the fractal dimension, the damage ratio showed an asymptotic behaviour. Two crystalline α-lactose monohydrate samples with the same particle size but different shapes were used to analyse the effect of particle shape on the compressibility (Fu et al., 2012). It was found that the sample with irregular shape was more compressible than the sample that was more spherical. Samimi et al. (2003) studied the impact breakage of two types of detergent particles from different processes and exhibiting different structures. One type was denser and more spherical, and the other type had a more cauliflower-type structure and was more porous. It was found that the former exhibited less breakage than the latter. In terms of application, this means that the morphology of agglomerates may be an important part of controlling unwanted breakage.

Primary dairy powder particles are usually spherical whereas agglomerated particles are irregular (Kim et al., 2005). Three parameters were generally used to quantify and indicate the morphology of powders, circularity, convexity, and elongation (Ji et al., 2015). The bigger circularity value means that the particles are more spherical. The maximum theoretical convexity is 1 that means the surface of the particle is very smooth. Elongation stands for aspect ratio of particles and a needle shape has a high value which is close to 1. The circularity, convexity, and elongation of un-

agglomerated milk protein isolate were around 0.85, 0.95, and 0.2, respectively (Ji et al., 2015). After agglomeration using a laboratory fluidized bed, those three measures changed to 0.65, 0.75, and 0.28, respectively. However, there is currently no research on the influence of morphology on dairy powder breakage or strength.

1.6.2. Powder composition

1.6.2.1. Protein

In some situations, the higher the protein content or protein to fat ratio, the higher the particle strength. Four typical IMFs with different protein to fat ratios but the same particle size range (710 - 850 μm) were used to investigate the influence of protein and fat content on the breakage of IMF during the compression test and laboratory-scale dilute-phase pneumatic conveying (Hanley, 2011; Hanley et al., 2011b). As conveying velocity increased, the increases of the bulk density for those two samples containing the least protein were considerably greater than others, indicating that more breakage occurred for two IMFs with lower protein contents. The possible reason was as the percentage of protein increased, the bulk densities of samples increased accordingly before conveying, which increased powder strength. The results of the compression test showed that the force at breakage generally increased with increasing protein to fat ratio. As the description in 1.3.1, the maximum applied force can be taken as the particle strength in the single-particle compression test. Increasing the protein content caused an increase in the mean force and a decrease in the mean strain at breakage. This also explained why these samples showed the least variation in bulk density during pneumatic conveying. However, more research on the influence of protein content and different kinds of milk proteins on breakage is needed.

1.6.2.2. Fat

Current results suggest that fat reduces the strength of dairy powders. Compression characteristics of agglomerated instant non-fat milk and low-fat

milk powder with the same particle size range were analysed using a texture analyser (Yan and Barbosa-Cánovas, 1997). The force-deformation data showed that compared with the non-fat milk powder, it was easier to compress low-fat milk powder, especially for samples with particle sizes of 212, 300, and 425 μm. This might be because fat liquefaction could soften powders, resulting in the easy deformation of powder particles during compression (Rennie et al., 1999).

1.6.2.3. Lactose

According to the research on the breakage of IMF, increasing the percentage of carbohydrates increased agglomerate stiffness (Hanley, 2011). Lactose is an important source of carbohydrate for infant milk formula. Hazlett et al. (2020) investigated the breakage of IMF (initial particle size: 252 μm; protein: 8.52% and fat: 25.6%; the decrease of particle size after breakage: 23%) and agglomerated WPC (initial particle size: 209 μm; protein: 80.0% and fat: 8.5%; the decrease of particle size after breakage: 26%) during a simulated pneumatic conveying. It was found that the particle size of IMF was bigger than that of WPC while the breakage of IMF was lower so the high concentration of lactose in IMF might increase its strength. But more studies are needed to analyse if the increase in lactose content is positively correlated with the increase in powder strength.

When lactose is in solid-state, it can be in a crystalline state or an amorphous state. Amorphous powders show good compressibility, low density, and high internal porosity, which makes powders more easily deformed and compacted. This is because compared to tightly packed molecules in the crystalline state, lactose molecules in the amorphous state are disordered, forming a more open and porous structure (Li et al., 2017). Compared with amorphous solids, the mechanical strength of crystalline solids is strong but also more brittle or fragile. This depends on the degree of crystallinity, with higher crystallinity resulting in a harder but also more brittle material. Typically, most crystalline materials tend to exhibit high levels of brittleness upon exposure to external stress and may fracture along cleavage

planes. By contrast, molecules in the amorphous state tend to exhibit varying degrees of viscoelasticity.

1.6.2.4. Binders

Fluidized bed agglomeration, as one of the most used agglomeration methods during dairy powder production, is a process by which agglomerated particles are obtained by spraying a binder as a solution, suspension, or melting onto a fluidized powder bed and then coalescing and agglomerating together by creating solid bridges between primary particles (Ji et al., 2015). Thus, binders are one of the important factors which influence particle properties including particle size, density, morphology, and strength (Iveson and Litster, 1998; Keningley et al., 1997). In food systems, aqueous solutions of lactose and sucrose are the most used binders in fluid bed agglomeration and a lot of other binders have been studied, such as dextrose, gelatin, and starch (Onwulata, 2005). Binders have different effects due to varied chemical composition, mechanical properties, concentration, viscosity, and inter-particular interactions between the particles and the binders.

Firstly, the strength or particle size of agglomerates obtained using different kinds of binders is different. For example, sucrose or glucose usually produces hard and brittle bridges while gelatin and acacia gum provide slow disintegration and high hardness to the agglomerates (Ji et al., 2015). Agglomerates of microcrystalline cellulose were made using hydroxypropylmethylcellulose (HPMC), polyvinylpyrrolidone, and water as binding agents (Zajic and Buckton, 1990). Agglomerates made with HPMC were less friable and larger particle size than most of the other particles that were produced with the other two binders. Three different binders, water, lactose, and sucrose solution (15% *w/v*) were used to agglomerate milk protein isolate powder in a laboratory-scale fluidized bed (Ji et al., 2015). It was found that using water as a binder created more irregular particles than using the other two sugar binders while the larger agglomerate size fraction was produced with the lactose binder. In addition, it is also generally found that the strength of agglomerates shows strong viscosity effects and a high

viscosity binder increases the strength of agglomerates (Iveson and Litster, 1998; Johansen and Schæfer, 2001; van den Dries et al., 2003). During the agglomeration of lactose monohydrate in a high shear mixer, a lower binder viscosity caused high porosity and decreased the strength of agglomerates (Eliasen et al., 1998). Increasing binder viscosity increases the agglomerates' dynamic yield stress, and for high viscosity binders, increasing binder content increases this yield stress (Iveson and Litster, 1998). During the agglomeration of calcium carbonates in a high shear mixer with a larger primary powder particle size, a high binder viscosity was necessary to achieve an agglomerate strength sufficient to avoid breakage (Johansen and Schæfer, 2001). At the same time, to produce spherical agglomerates, a low viscosity binder had to be chosen when agglomerating a powder with small particle size, and a high viscosity binder must be applied for large particles. Furthermore, binder surface tension plays a role in determining granule strength by causing capillary force between primary particles (Iveson and Litster, 1998). Decreases in binder surface tension decrease the dynamic yield strength of agglomerates.

It should be noted that the mechanical characteristics of primary particles and bonding agents are randomly distributed within agglomerates. Even with the identical production process, the strength of the individual agglomerates differs in the microstructure because of the distribution and orientation of bonds, defects, and pore size distribution (Antonyuk et al., 2005).

1.6.2.5. Moisture content

Generally, the increase in moisture content within a certain range can reduce powder strength. All powders tend to absorb moisture from the air and then have two kinds of changes (Yan and Barbosa-Cánovas, 2001a). The first is that the solid material softens and becomes plasticized. Increased moisture content can soften the powder material, especially the water-soluble constituents, which would result in the deformation of powders and the decrease of strength (Kim et al., 2005; Rennie et al., 1999). The second is that the particle surface is altered by solubilization, liquid layer formation, or local plasticization, which influences the properties of binders and thus

influences the particle strength. Solid bridge formation is the dominant agglomeration mechanism for materials in the agglomerated state and is mainly due to the crystallization of binders (lactose for example). Drying strengthens the agglomerates presumably due to the solidification of bridges while humidifying the granules decreases their strength (Samimi et al., 2003). There are lower yield stress and larger plastic deformation during the breakage of the humidified samples compared to the dry samples. For humidified agglomerates, a larger portion of the kinetic energy is dissipated during impact as plastic deformation or ductile failure (shown as stretching and the rupture of interparticle bonds) (Samimi et al., 2003). For agglomerated skim milk powder, the higher the water activity, the greater the breakage during the vibration test (Yan and Barbosa-Cánovas, 2001a).

1.7. Conclusion

Agglomerated dairy powder breakage usually occurs during production and transportation and may significantly impact dairy powder physical properties and functionalities. The influence of breakage on powder properties depends on the extent of breakage caused by different breakage mechanisms. The characteristics of particles and processing conditions are two main factors that influence breakage and can be considered to control dairy powder breakage. The processing conditions include the parameters during dry-mixing, vibration, and pneumatic conveying. The physical properties and the composition of powders can also dictate the response of powders for a given loading condition by influencing the powder strength. Further research on the factors that control dairy powder breakage and their effectiveness is required. The methods suitable for investigating dairy powder breakage include single-particle or multi-particle tests. Both types of tests complement each other, single-particle tests providing fundamental information about particle breakage and multi-particle methods mimicking real industrial situations.

References

Aarseth, K.A. (2004). Attrition of feed pellets during pneumatic conveying: the influence of velocity and bend radius. *Biosystems Engineering* 89(2), 197-213. https://doi.org/10.1016/j.biosystemseng.2004.06.008.

Agrawal, S.G., Balandier, A., Paterson, A.H.J., & Jones, J.R. (2011). Study on lactose attrition inside the mixing cell of a laser diffraction particle sizer using a novel attrition index. *Powder Technology* 208(3), 669-675. https://doi.org/10.1016/j.powtec.2011.01.007.

Antonyuk, S., Tomas, J., Heinrich, S., & Mörl, L. (2005). Breakage behaviour of spherical granulates by compression. *Chemical Engineering Science* 60(14), 4031-4044. https://doi.org/10.1016/j.ces.2005.02.038.

Barletta, B.J., & Barbosa-Cánovas, G.V. (1993a). An attrition index to assess fines formation and particle size reduction in tapped agglomerated food powders. *Powder Technology* 77(1), 89-93. https://doi.org/10.1016/0032-5910(93)85011-W.

Barletta, B.J., & Barbosa-Cánovas, G.V. (1993b). Fractal analysis to characterize ruggedness changes in tapped agglomerated food powders. *Journal of Food Science* 58(5), 1030-1035. https://doi.org/ 10.1111/j.1365-2621.1993.tb06105.x.

Barletta, B.J., Kinight, K.M., & Barbosa-Cánovas, G.V. (1993). Compaction characteristics of agglomerated coffee during tapping. *Journal of Texture Studies* 24(3), 253-268. https://doi.org/ 10.1111/j.1745-4603.1993.tb01283.x.

Bayham, S.C., Breault, R., & Monazam, E. (2016). Particulate solid attrition in CFB systems – An assessment for emerging technologies. *Powder Technology* 302, 42-62. https://doi.org/10.1016/j.powtec.2016.08.016.

Beekman, W.J., Meesters, G.M.H., Becker, T., Gaertner, A., Gebert, M., & Scarlett, B. (2003). Failure mechanism determination for industrial granules using a repeated compression test. *Powder Technology* 130(1), 367-376. https://doi.org/10.1016/S0032-5910(02)00238-3.

Bemrose, C.R., & Bridgwater, J. (1987). A review of attrition and attrition test methods. *Powder Technology* 49(2), 97-126. https://doi.org/10.1016/0032-5910(87)80054-2.

Bertrand, F., Leclaire, L.A., & Levecque, G. (2005). DEM-based models for the mixing of granular materials. *Chemical Engineering Science* 60(8), 2517-2531. https://doi.org/10.1016/j.ces.2004.11.048.

Bika, D., Tardos, G.I., Panmai, S., Farber, L., & Michaels, J. (2005). Strength and morphology of solid bridges in dry granules of pharmaceutical powders. *Powder Technology* 150(2), 104-116. https://doi.org/10.1016/j.powtec.2004.11.024.

Bika, D.G., Gentzler, M., & Michaels, J.N. (2001). Mechanical properties of agglomerates. *Powder Technology* 117(1), 98-112. https://doi.org/10.1016/S0032-5910(01)00318-7.

Boiarkina, I., Sang, C., Depree, N., Prince-Pike, A., Yu, W., Wilson, D.I., & Young, B.R. (2016). The significance of powder breakdown during conveying within industrial milk powder plants. *Advanced Powder Technology* 27(6), 2363-2369. https://doi.org/10.1016/j.apt.2016.10.019.

Bonakdar, T., Ghadiri, M., Ahmadian, H., Martin de Juan, L., Xu, D., Tantawy, H., & Smith, D. (2016). Impact attrition of spray-dried burkeite particles. *Powder Technology* 304, 2-7. https://doi.org/10.1016/j.powtec.2016.08.024.

Bridgwater, J. (2010). Mixing of particles and powders: Where next? *Particuology* 8(6), 563-567. https://doi.org/10.1016/j.partic.2010.07.001.

Bridgwater, J., Utsumi, R., Zhang, Z., & Tuladhar, T. (2003). Particle attrition due to shearing-the effects of stress, strain and particle shape. *Chemical Engineering Science* 58(20), 4649-4665. https://doi.org/10.1016/j.ces.2003.07.007.

Brosh, T., Kalman, H., & Levy, A. (2010). DEM simulation of particle attrition in dilute-phase pneumatic conveying. *Granular Matter* 13(2), 175-181. https://doi.org/ 10.1007/s10035-010-0201-z.

Cleaver, J.A.S., Ghadiri, M., & Rolfe, N. (1993). Impact attrition of sodium carbonate monohydrate crystals. *Powder Technology* 76(1), 15-22. https://doi.org/10.1016/0032-5910(93)80036-A.

Deng, X., & Davé, R.N. (2017). Breakage of fractal agglomerates. *Chemical Engineering Science* 161, 117-126. https://doi.org/10.1016/j.ces.2016.12.018.

Duraccio, D., Strongone, V., Faga, M.G., Auriemma, F., Mussano, F.D., Genova, T., & Malucelli, G. (2019). The role of different dry-mixing techniques on the mechanical and biological behaviour of UHMWPE/alumina-zirconia composites for biomedical applications. *European Polymer Journal* 120, 109274. https://doi.org/10.1016/j.eurpolymj.2019.109274.

Einav, I. (2007). Breakage mechanics - Part I: Theory. *Journal of the Mechanics and Physics of Solids* 55(6), 1274-1297. https://doi.org/10.1016/j.jmps.2006.11.003.

Eliasen, H., Schæfer, T., & Gjelstrup Kristensen, H. (1998). Effects of binder rheology on melt agglomeration in a high shear mixer. *International Journal of Pharmaceutics* 176(1), 73-83. https://doi.org/10.1016/S0378-5173(98)00306-8.

Forny, L., Marabi, A., & Palzer, S. (2011). Wetting, disintegration and dissolution of agglomerated water soluble powders. *Powder Technology* 206(1), 72-78. https://doi.org/10.1016/j.powtec.2010.07.022.

Fu, X., Huck, D., Makein, L., Armstrong, B., Willen, U., & Freeman, T. (2012). Effect of particle shape and size on flow properties of lactose powders. *Particuology* 10(2), 203-208. https://doi.org/10.1016/j.partic.2011.11.003.

Gerhards, C., Kaell, C., & Schubert, H. (2004). Measurement of attrition of agglomerated cocoa beverage powders: a comparison of Friabilator and vibration tests. *Journal of Food Engineering* 65(1), 101-108. https://doi.org/10.1016/j.jfoodeng.2004.01.002.

Ghadiri, M., Yuregir, K.R., Pollock, H.M., Ross, J.D.J., & Rolfe, N. (1991). Influence of processing conditions on attrition of NaCl crystals. *Powder Technology* 65(1), 311-320. https://doi.org/10.1016/0032-5910(91)80195-O.

Ghadiri, M., & Zhang, Z. (2002). Impact attrition of particulate solids. Part 1: A theoretical model of chipping. *Chemical Engineering Science* 57(17), 3659-3669. https://doi.org/10.1016/S0009-2509(02)00240-3.

Go Yanko, E. (2007). Hygienic engineering of transfer systems for dry particulate materials. *Trends in Food Science & Technology* 18(12), 626-631. https://doi.org/10.1016/j.tifs.2007.08.005.

Goalard, C., Samimi, A., Galet, L., Dodds, J.A., & Ghadiri, M. (2006). Characterization of the dispersion behaviour of powders in liquids. *Particle & Particle Systems Characterization* 23(2), 154-158. https://doi.org/ 10.1002/ppsc.200601024.

Goder, D., Kalman, H., & Ullmann, A. (2002). Fatigue characteristics of granular materials. *Powder Technology* 122(1), 19-25. https://doi.org/10.1016/S0032-5910(01)00390-4.

Golchert, D., Moreno, R., Ghadiri, M., & Litster, J. (2004). Effect of granule morphology on breakage behaviour during compression. *Powder Technology* 143-144, 84-96. https://doi.org/10.1016/j.powtec.2004.04.032.

Gupta, V., Sun, X., Xu, W., Sarv, H., & Farzan, H. (2017). A discrete element method-based approach to predict the breakage of coal. *Advanced Powder Technology* 28(10), 2665-2677. https://doi.org/10.1016/j.apt.2017.07.019.

Gupta, V.K. (2017). Effect of size distribution of the particulate material on the specific breakage rate of particles in dry ball milling. *Powder Technology* 305, 714-722. https://doi.org/10.1016/j.powtec.2016.10.075.

Han, Fitzpatrick, J., Cronin, K., Maidannyk, V., & Miao, S. (2020). Breakage of infant milk formula through three different processing methods and its influence on

powder properties. *Journal of Food Engineering* 282, 109997. https://doi.org/10.1016/j.jfoodeng.2020.109997.
Han, Fitzpatrick, J., Cronin, K., Maidannyk, V., & Miao, S. (2021). Particle size, powder properties and the breakage behaviour of infant milk formula. *Journal of Food Engineering* 292, 110367. https://doi.org/10.1016/j.jfoodeng.2020.110367.
Han, T., Levy, A., & Kalman, H. (2003). DEM simulation for attrition of salt during dilute-phase pneumatic conveying. *Powder Technology* 129(1), 92-100. https://doi.org/10.1016/S0032-5910(02)00252-8.
Hanley, K.J., 2011. Experimental quantification and modelling of attrition of infant formulae, Department of Process and Chemical Engineering. University College Cork, Cork, Ireland.
Hanley, K.J., Byrne, E.P., & Cronin, K. (2013). Probabilistic analysis of particle impact at a pipe bend in pneumatic conveying. *Powder Technology* 233, 176-185. https://doi.org/10.1016/j.powtec.2012.08.018.
Hanley, K.J., Byrne, E.P., Cronin, K., Oliveira, J.C., O'Mahony, J.A., & Fenelon, M.A. (2011a). Effect of pneumatic conveying parameters on physical quality characteristics of infant formula. *Journal of Food Engineering* 106(3), 236-244. https://doi.org/10.1016/j.jfoodeng.2011.04.029.
Hanley, K.J., Cronin, K., O'Sullivan, C., Fenelon, M.A., O'Mahony, J.A., & Byrne, E.P. (2011b). Effect of composition on the mechanical response of agglomerates of infant formulae. *Journal of Food Engineering* 107(1), 71-79. https://doi.org/10.1016/j.jfoodeng.2011.05.042.
Hazlett, R., Schmidmeier, C., & O'Mahony, J.A. (2020). Influence of mechanical integrity during pneumatic conveying on the bulk handling and rehydration properties of agglomerated dairy powders. *Journal of Food Engineering*, 110103. https://doi.org/10.1016/j.jfoodeng.2020.110103.
Hogekamp, S., & Schubert, H. (2003). Rehydration of Food Powders. *Food Science and Technology International* 9(3), 223-235. https://doi.org/10.1177/1082013203034938.
Hu, X., Zhao, M., Li, L., Yang, B., Yang, X., Wang, H., & Ren, J. (2014). Emulsifying Properties of Cross-Linking Between Proteins Extracted from Cold/Hot Pressed Peanut Meal and Hydrolysed Fish (Decapterus Maruadsi) Proteins. *International Journal of Food Properties* 17(8), 1750-1762. https://doi.org/10.1080/10942912.2012.724755.
Iveson, S.M., & Litster, J.D. (1998). Liquid-bound granule impact deformation and coefficient of restitution. *Powder Technology* 99(3), 234-242. https://doi.org/10.1016/S0032-5910(98)00115-6.
Ji, J., Cronin, K., Fitzpatrick, J., Fenelon, M., & Miao, S. (2015). Effects of fluid bed agglomeration on the structure modification and reconstitution behaviour of milk protein isolate powders. *Journal of Food Engineering* 167, 175-182. https://doi.org/10.1016/j.jfoodeng.2015.01.012.
Ji, J., Cronin, K., Fitzpatrick, J., & Miao, S. (2017). Enhanced wetting behaviours of whey protein isolate powder: The different effects of lecithin addition by fluidised bed agglomeration and coating processes. *Food Hydrocolloids* 71, 94-101. https://doi.org/10.1016/j.foodhyd.2017.05.005.
Ji, J., Fitzpatrick, J., Cronin, K., Maguire, P., Zhang, H., & Miao, S. (2016). Rehydration behaviours of high protein dairy powders: The influence of agglomeration on wettability, dispersibility and solubility. *Food Hydrocolloids* 58, 194-203. https://doi.org/10.1016/j.foodhyd.2016.02.030.
Jiang, Y.J., & Guo, M. (2014). 8 - Processing technology for infant formula. In M. Guo (Ed.), *Human Milk Biochemistry and Infant Formula Manufacturing Technology* (pp. 211-229). Woodhead Publishing, https://doi.org/10.1533/9780857099150.2.211.
Johansen, A., & Schæfer, T. (2001). Effects of interactions between powder particle size and binder viscosity on agglomerate growth mechanisms in a high shear

mixer. *European Journal of Pharmaceutical Sciences* 12(3), 297-309. https://doi.org/10.1016/S0928-0987(00)00182-2.
Kalman, H. (1999). Attrition control by pneumatic conveying. *Powder Technology* 104(3), 214-220. https://doi.org/10.1016/S0032-5910(99)00097-2.
Kalman, H. (2000). Attrition of powders and granules at various bends during pneumatic conveying. *Powder Technology* 112(3), 244-250. https://doi.org/10.1016/S0032-5910(00)00298-9.
Keningley, S.T., Knight, P.C., & Marson, A.D. (1997). An investigation into the effects of binder viscosity on agglomeration behaviour. *Powder Technology* 91(2), 95-103. https://doi.org/10.1016/S0032-5910(96)03230-5.
Kent, R.M., Fitzgerald, G.F., Hill, C., Stanton, C., & Ross, R.P. (2015). Novel approaches to improve the intrinsic microbiological safety of powdered infant milk formula. *Nutrients* 7(2), 1217-1244. https://doi.org/ 10.3390/nu7021217.
Kim, E.H.J., Chen, X., & Pearce, D. (2005). Effect of surface composition on the flowability of industrial spray-dried dairy powders. *Colloids and Surfaces B: Biointerfaces* 46(3), 182-187. https://doi.org/10.1016/j.colsurfb.2005.11.005.
King, R.P. (2012). Modeling and simulation of mineral processing systems. (pp. 153-252). Society for Mining, Metallurgy, and Exploration (SME).
Konami, M., Tanaka, S., & Matsumoto, K. (2002). Attrition of granules during repeated pneumatic transport. *Powder Technology* 125(1), 82-88. https://doi.org/10.1016/S0032-5910(02)00002-5.
Kotzur, B.A., Berry, R.J., Zigan, S., García-Triñanes, P., & Bradley, M.S.A. (2018). Particle attrition mechanisms, their characterisation, and application to horizontal lean phase pneumatic conveying systems: A review. *Powder Technology* 334, 76-105. https://doi.org/10.1016/j.powtec.2018.04.047.
Kuakpetoon, D., Flores, R.A., & Milliken, G.A. (2001). Dry mixing of wheat fours: effect of particle properties and blending ratio. *LWT - Food Science and Technology* 34(3), 183-193. https://doi.org/10.1006/fstl.2001.0756.
Li, R., Lin, D., Roos, Y.H., & Miao, S. (2019). Glass transition, structural relaxation and stability of spray-dried amorphous food solids: A review. *Drying Technology* 37(3), 287-300. https://doi.org/ 10.1080/07373937.2018.1459680.
Li, R., Roos, Y.H., & Miao, S. (2016). Roles of particle size on physical and mechanical properties of dairy model solids. *Journal of Food Engineering* 173, 69-75. https://doi.org/10.1016/j.jfoodeng.2015.10.041.
Li, R., Roos, Y.H., & Miao, S. (2017). Characterization of physical and mechanical properties of miscible lactose-sugars systems. *Journal of Food Science* 82(9), 2105-2112. https://doi.org/ 10.1111/1750-3841.13831.
Lindley, J.A. (1991a). Mixing processes for agricultural and food materials: 1. Fundamentals of mixing. *Journal of Agricultural Engineering Research* 48, 153-170. https://doi.org/10.1016/0021-8634(91)80012-4.
Lindley, J.A. (1991b). Mixing processes for agricultural and food materials: 3. Powders and particulates. *Journal of Agricultural Engineering Research* 49, 1-19. https://doi.org/10.1016/0021-8634(91)80025-A.
Little, L., Mainza, A.N., Becker, M., & Wiese, J.G. (2016). Using mineralogical and particle shape analysis to investigate enhanced mineral liberation through phase boundary fracture. *Powder Technology* 301, 794-804. https://doi.org/10.1016/j.powtec.2016.06.052.
Liu, L., Kafui, K.D., & Thornton, C. (2010). Impact breakage of spherical, cuboidal and cylindrical agglomerates. *Powder Technology* 199(2), 189-196. https://doi.org/10.1016/j.powtec.2010.01.007.
Lu, X., Liu, C., Zhu, L., & Qu, X. (2014). Influence of process parameters on the characteristics of TiAl alloyed powders by fluidized bed jet milling. *Powder Technology* 254, 235-240. https://doi.org/10.1016/j.powtec.2013.11.013.

Macchini, R., Bradley, M.S.A., & Deng, T. (2013). Influence of particle size, density, particle concentration on bend erosive wear in pneumatic conveyors. *Wear* 303(1), 21-29. https://doi.org/10.1016/j.wear.2013.02.014.

Maidannyk, V., McSweeney, D.J., Hogan, S.A., Miao, S., Montgomery, S., Auty, M.A.E., & McCarthy, N.A. (2020). Water sorption and hydration in spray-dried milk protein powders: Selected physicochemical properties. *Food Chemistry* 304, 125418. https://doi.org/10.1016/j.foodchem.2019.125418.

Materic, V., Holt, R., Hyland, M., & Jones, M.I. (2014). An internally circulating fluid bed for attrition testing of Ca looping sorbents. *Fuel* 127, 116-123. https://doi.org/10.1016/j.fuel.2013.10.071.

McKee, S.L., Dyakowski, T., Williams, R.A., Bell, T.A., & Allen, T. (1995). Solids flow imaging and attrition studies in a pneumatic conveyor. *Powder Technology* 82(1), 105-113. https://doi.org/10.1016/0032-5910(94)02894-T.

Moejes, S.N., & van Boxtel, A.J.B. (2017). Energy saving potential of emerging technologies in milk powder production. *Trends in Food Science & Technology* 60, 31-42. https://doi.org/10.1016/j.tifs.2016.10.023.

Mun, S., McClements, D.J., & Surh, J. (2011). Influence of maltodextrin addition on the freeze-dry stability of β-lactoglobulin-based emulsions with controlled electrostatic and/or steric interactions. *Food Science and Biotechnology* 20(4), 1143. https://doi.org/ 10.1007/s10068-011-0156-9.

Murrieta-Pazos, I., Gaiani, C., Galet, L., & Scher, J. (2012). Composition gradient from surface to core in dairy powders: Agglomeration effect. *Food Hydrocolloids* 26(1), 149-158. https://doi.org/10.1016/j.foodhyd.2011.05.003.

Niranjan, K., Smith, D.L.O., Rielly, C.D., Lindley, J.A., & Phillips, V.R. (1994). Mixing processes for agricultural and food materials: Part 5, Review of mixer types. *Journal of Agricultural Engineering Research* 59(3), 145-161. https://doi.org/10.1006/jaer.1994.1072.

Norazirah, A., Fuad, S.H.S., & Hazizan, M.H.M. (2016). The effect of size and shape on breakage characteristic of mineral. *Procedia Chemistry* 19, 702-708. https://doi.org/10.1016/j.proche.2016.03.073.

Onwulata, C. (2005). *Encapsulated and powdered foods*. Taylor & Francis Group. https://doi.org/10.1201/9781420028300.

Ortega-Rivas, E., Juliano, P., & Yan, H. (2006). *Food powders: physical properties, processing, and functionality*. Springer US.

Paluszny, A., Tang, X., Nejati, M., & Zimmerman, R.W. (2016). A direct fragmentation method with Weibull function distribution of sizes based on finite- and discrete element simulations. *International Journal of Solids and Structures* 80, 38-51. https://doi.org/10.1016/j.ijsolstr.2015.10.019.

Papadopoulos, D.G., & Ghadiri, M. (1996). Impact breakage of poly-methylmethacrylate (PMMA) extrudates: I. Chipping mechanism. *Advanced Powder Technology* 7(3), 183-197. https://doi.org/10.1016/S0921-8831(08)60495-1.

Pernenkil, L., & Cooney, C.L. (2006). A review on the continuous blending of powders. *Chemical Engineering Science* 61(2), 720-742. https://doi.org/10.1016/j.ces.2005.06.016.

Petukhov, Y., & Kalman, H. (2004). Empirical breakage ratio of particles due to impact. *Powder Technology* 143-144, 160-169. https://doi.org/10.1016/j.powtec.2004.04.009.

Portillo, P.M., Ierapetritou, M.G., & Muzzio, F.J. (2008). Characterization of continuous convective powder mixing processes. *Powder Technology* 182(3), 368-378. https://doi.org/10.1016/j.powtec.2007.06.024.

Pugliese, A., Cabassi, G., Chiavaro, E., Paciulli, M., Carini, E., & Mucchetti, G. (2017). Physical characterization of whole and skim dried milk powders. *Journal of Food Science and Technology* 54(11), 3433-3442. https://doi.org/ 10.1007/s13197-017-2795-1.

Rennie, P.R., Chen, X., Hargreaves, C., & Mackereth, A.R. (1999). A study of the cohesion of dairy powders. *Journal of Food Engineering* 39(3), 277-284. https://doi.org/10.1016/S0260-8774(98)00158-7.

Reynolds, G.K., Fu, J.S., Cheong, Y.S., Hounslow, M.J., & Salman, A.D. (2005). Breakage in granulation: A review. *Chemical Engineering Science* 60(14), 3969-3992. https://doi.org/10.1016/j.ces.2005.02.029.

Rhodes, M. (2008). Mixing and Segregation. In M. Rhodes (Ed.), *Introduction to Particle Technology-Second Edition* (pp. 293-310). John Wiley & Sons, Ltd., https://doi.org/ 10.1002/9780470727102.ch11.

Richard, B., Le Page, J.F., Schuck, P., Andre, C., Jeantet, R., & Delaplace, G. (2013). Towards a better control of dairy powder rehydration processes. *International Dairy Journal* 31(1), 18-28. https://doi.org/10.1016/j.idairyj.2012.07.007.

Salman, A.D., Fu, J., Gorham, D.A., & Hounslow, M.J. (2003). Impact breakage of fertiliser granules. *Powder Technology* 130(1), 359-366. https://doi.org/10.1016/S0032-5910(02)00237-1.

Salman, A.D., Ghadiri, M., & Hounslow, M.J. (2007a). *Handbook of powder technology-Volume 12-Particle breakage*. Elsevier.

Salman, A.D., Ghadiri, M., & Hounslow, M.J. (2007b). *Handbook of powder technology-Volume 12-Particle breakage*. 225). Elsevier.

Salman, A.D., Hounslow, M.J., & Verba, A. (2002). Particle fragmentation in dilute phase pneumatic conveying. *Powder Technology* 126(2), 109-115. https://doi.org/10.1016/S0032-5910(02)00048-7.

Salman., Russell, A., Aman, S., & Tomas, J. (2015). Breakage probability of granules during repeated loading. *Powder Technology* 269, 541-547. https://doi.org/10.1016/j.powtec.2014.09.044.

Samimi, A., Ghadiri, M., Boerefijn, R., Groot, A., & Kohlus, R. (2003). Effect of structural characteristics on impact breakage of agglomerates. *Powder Technology* 130(1), 428-435. https://doi.org/10.1016/S0032-5910(02)00246-2.

Scala, F., Chirone, R., & Salatino, P. (2013). 6 - Attrition phenomena relevant to fluidized bed combustion and gasification systems. In F. Scala (Ed.), *Fluidized Bed Technologies for Near-Zero Emission Combustion and Gasification* (pp. 254-315). Woodhead Publishing, https://doi.org/10.1533/9780857098801.1.254.

Scala, F., Montagnaro, F., & Salatino, P. (2007). Attrition of Limestone by Impact Loading in Fluidized Beds. *Energy & Fuels* 21(5), 2566-2572. https://doi.org/ 10.1021/ef0700580.

Schuck, P., Dolivet, A., & Jeantet, R. (2012). *Analytical methods for food and dairy powders*. Wiley-Blackwell.

Shan, J., Xu, S., Liu, Y., Zhou, L., & Wang, P. (2018). Dynamic breakage of glass sphere subjected to impact loading. *Powder Technology* 330, 317-329. https://doi.org/10.1016/j.powtec.2018.02.009.

Sharma, A., Jana, A.H., & Chavan, R.S. (2012). Functionality of milk powders and milk-based powders for end use applications - a review. *Comprehensive Reviews in Food Science and Food Safety* 11(5), 518-528. https://doi.org/ 10.1111/j.1541-4337.2012.00199.x.

Subero, J., & Ghadiri, M. (2001). Breakage patterns of agglomerates. *Powder Technology* 120(3), 232-243. https://doi.org/10.1016/S0032-5910(01)00276-5.

Swyngedau, S., Nussinovitch, A., Roy, I., Peleg, M., & Huang, V. (1991). Comparison of four models for the compressibility of breads and plastic foams. *Journal of Food Science* 56(3), 756-759. https://doi.org/ 10.1111/j.1365-2621.1991.tb05375.x.

Tavares, L.M., Cavalcanti, P.P., de Carvalho, R.M., da Silveira, M.W., Bianchi, M., & Otaviano, M. (2018). Fracture probability and fragment size distribution of fired Iron ore pellets by impact. *Powder Technology* 336, 546-554. https://doi.org/10.1016/j.powtec.2018.06.036.

Tavares, L.M., & de Almeida, R.F. (2020). Breakage of green iron ore pellets. *Powder Technology* 366, 497-507. https://doi.org/10.1016/j.powtec.2020.02.074.
Thomas, M.E.C., Scher, J., Desobry-Banon, S., & Desobry, S. (2004). Milk Powders ageing: effect on physical and functional properties. *Critical Reviews in Food Science and Nutrition* 44(5), 297-322. https://doi.org/10.1080/10408690490464041.
Utsumi, R., Hata, T., Hirano, T., Mori, H., Tsubaki, J., & Maeda, T. (2001). Attrition testing of granules with a tapping sieve. *Powder Technology* 119(2), 128-133. https://doi.org/10.1016/S0032-5910(00)00412-5.
Uzi, A., Kalman, H., & Levy, A. (2016). A novel particle attrition model for conveying systems. *Powder Technology* 298, 30-41. https://doi.org/10.1016/j.powtec.2016.05.014.
van den Dries, K., de Vegt, O.M., Girard, V., & Vromans, H. (2003). Granule breakage phenomena in a high shear mixer; influence of process and formulation variables and consequences on granule homogeneity. *Powder Technology* 133(1), 228-236. https://doi.org/10.1016/S0032-5910(03)00106-2.
Van Laarhoven, B., Schaafsma, S.H., & Meesters, G.M.H. (2012). Toward a desktop attrition tester; validation with dilute phase pneumatic conveying. *Chemical Engineering Science* 73, 321-328. https://doi.org/10.1016/j.ces.2011.08.038.
Walstra, P., Wouters, J.T., & Geurts, T.J. (2005). *Dairy science and technology*. CRC press.
Wu, F., & Wu, D. (2017). Attrition resistances and mechanisms of three types of FCC catalysts. *Powder Technology* 305, 289-296. https://doi.org/10.1016/j.powtec.2016.09.077.
Yan, H., & Barbosa-Cánovas, G.V. (1997). Compression characteristics of agglomerated food powders: Effect of agglomerate size and water activity Características de la compresión de alimentos en polvo: Efecto del tamaño del aglomerado y del contenido de humedad. *Food Science and Technology International* 3(5), 351-359. https://doi.org/ 10.1177/108201329700300506.
Yan, H., & Barbosa-Cánovas, G.V. (2001a). Attrition evaluation for selected agglomerated food powders: the effect of agglomerate size and water activity. *Journal of Food Process Engineering* 24(1), 37-49. https://doi.org/10.1111/j.1745-4530.2001.tb00530.x.
Yan, H., & Barbosa-Cánovas, G.V. (2001b). The effect of padding foam on the compression characteristics of some agglomerated food powders. *Food Science and Technology International* 7(5), 417-423. https://doi.org/ 10.1106/wc69-qfnv-vn6e-lh00.
Yildirim, N., & Genc, S. (2017). Energy and exergy analysis of a milk powder production system. *Energy Conversion and Management* 149, 698-705. https://doi.org/10.1016/j.enconman.2017.01.064.
Yuan, Y., & Lee, T.R. (2013). Contact angle and wetting properties. *Surface science techniques* (pp. 3-34). Springer.
Zafar, U., Vivacqua, V., Calvert, G., Ghadiri, M., & Cleaver, J.A.S. (2017). A review of bulk powder caking. *Powder Technology* 313, 389-401. https://doi.org/10.1016/j.powtec.2017.02.024.
Zajic, L., & Buckton, G. (1990). The use of surface energy values to predict optimum binder selection for granulations. *International Journal of Pharmaceutics* 59(2), 155-164. https://doi.org/10.1016/0378-5173(90)90090-Q.
Zhang, F., Olaleye, A.K., O'Mahony, J.A., Miao, S., & Cronin, K. (2020). Dilute phase pneumatic conveying of whey protein isolate powders: Particle breakage and its effects on bulk properties. *Advanced Powder Technology* 31(8), 3342-3350. https://doi.org/10.1016/j.apt.2020.06.019.

Zhang, Z., & Ghadiri, M. (2002). Impact attrition of particulate solids. Part 2: Experimental work. *Chemical Engineering Science* 57(17), 3671-3686. https://doi.org/10.1016/S0009-2509(02)00241-5.

Zhao, R., Goodwin, J.G., & Oukaci, R. (1999). Attrition assessment for slurry bubble column reactor catalysts. *Applied Catalysis A: General* 189(1), 99-116. https://doi.org/10.1016/S0926-860X(99)00261-6.

CHAPTER TWO

Particle size, powder properties and the breakage behaviour of infant milk formula

Chapter 2 was published in:

Han, J., Fitzpatrick, J., Cronin, K., Maidannyk, V., & Miao, S. (2021). Particle size, powder properties and the breakage behaviour of infant milk formula. *Journal of Food Engineering 292*, 110367.

The work contained in this chapter was undertaken and written solely by myself with specific contributions from each co-author:

Jie Han: Conceptualization, Formal analysis, Investigation, Methodology, Visualization, Writing - original draft, Data curation

John Fitzpatrick: Supervision, Writing - review & editing

Kevin Cronin: Supervision, Writing - review & editing

Valentyn Maidannyk: Investigation

Song Miao: Supervision, Conceptualization, Writing - review & editing, Funding acquisition, Project administration, Investigation.

Abstract

Dairy powder breakage occurs in many processes and causes deterioration in powder properties but there is currently no research presented in the literature on dairy powder breakage behaviour. The breakage behaviour and the effect of powder properties of an infant milk formula and its sieved size fractions were investigated during three processing methods (powder venturi feeder, lab-scale dilute phase pneumatic conveyor, and laboratory high-speed mixer) based on the changes of particle size distributions (PSD) before and after breakage. Particle size influenced other properties and the breakage behaviour of powders. Four breakage mechanisms were found, dispersion, chipping, disintegration, and splitting, corresponding to the increasing degree of breakage. More intense processing conditions were needed to cause the same breakage mechanism for smaller-sized particles because of their higher powder strength. The breakage of samples with wide PSD often displayed a combination of breakage mechanisms due to the influence of particle size on breakage behaviour.

Keywords: Infant milk formula; Breakage behaviour; Powder strength; Powder venturi feeder; Dilute-phase pneumatic conveying; High-speed mixing

2.1. Introduction

The production of dairy powders provides a good way to preserve and transport milk ingredients in a stable and convenient form. Currently, most of the commercial dairy powders are agglomerated powders as agglomeration results in the formation of large granules which improve some functional properties of powders. However, food agglomerates are normally less robust and have lower mechanical strength and aptitude for resisting loads than inorganic or polymeric particles, and they are also usually fragile, and brittle, thus unwanted particle breakage in agglomerated food powders easily happens when powders are exposed to mechanical impact or vibration

during processing or transportation (Yan, Hong and Barbosa-Cánovas, G. V., 2001; Yan, H. and Barbosa-Cánovas, G. V., 2001).

Breakage is one of the major and ubiquitous problems for some industries dealing with particulate solids, such as the pharmaceutical, agricultural, mineral, fertilizer, granulation and catalysts (Deng and Davé, 2017; Dosta et al., 2016; Gupta et al., 2017; Gupta, 2017; Norazirah et al., 2016; Salman et al., 2003; Shan et al., 2018). The most notable and serious consequences of unwanted particle breakage, include the dust generation, adverse effect on product properties and reduction of the product's functionalities (Kotzur et al., 2018; Salman et al., 2002; Wu and Wu, 2017). Based on limited published works on dairy powders breakage, particle attrition significantly decreased the particle size and increased the bulk density, reducing the rehydration properties and flowability of agglomerated dairy powders (Barleita and Barbosa-cáovas, 1993; Barletta and Barbosa-cánovas, 1993; Boiarkina et al., 2016; Han et al., 2020; Hanley et al., 2011; Hazlett et al., 2020; Yan, H. and Barbosa-Cánovas, G. V., 2001). Furthermore, for infant milk formula (IMF), breakage decreased the specific bulk volume, which influenced the size of product containers and the scoop volume requirement for the preparation of infant milk. Moreover, particle breakage takes place whenever there is relative movement between particles in contact with each other or against the container wall. In the context of particle attrition, it has been demonstrated that the collisions among agglomerates and against static container walls due to mechanical impact, shear, or compression provide the kinetic energy that causes the breakage of agglomerates (Kotzur et al., 2018). Unwanted dairy powder breakage occurs in many processes throughout production and transportation, such as in-plant transportation before packing (Boiarkina et al., 2016; Han et al., 2020; Hanley, 2011; Hazlett et al., 2020), dry mixing (Han et al., 2020, Chapter 4), and vibration during transportation (Barleita and Barbosa-cáovas, 1993; Barletta and Barbosa-cánovas, 1993; Ortega-Rivas et al., 2006). Thus, the investigation of dairy powder breakage is very important for the quality control of dairy powders.

As described in 1.3, two types of experimental tests have been designed to study the particle breakage of particulate systems: single-particle and multi-particle breakage tests (Bonakdar et al., 2016; Ortega-Rivas et al., 2006; Salman et al., 2007). Single-particle tests have the advantage of applying a well-characterized load on the particle, providing fundamental information about particle properties, and enhancing the understanding of particle breakage. However, they are not fully representative of industrial conditions and results are difficult to compare with attrition observed in practice because of the variations among particles in a certain bulk. On the contrary, multi-particle tests are close to the real industrial situations. To study dairy powder breakage behaviour, the latter is more applicable because dairy powder particles are too small to use most of the single-particle methods.

Based on particle breakage research in other industries, agglomerated particle breakage can be classified into surface breakage and body breakage, as shown in Figure 1-1 (Francioli, 2015; King, 2012). Breakage patterns depend on the characteristics of the material and the applied stress (Petukhov and Kalman, 2004). Of the various particulate materials, four breakage mechanisms have been reported to govern the breakage behaviour: abrasion (/erosion), chipping, disintegration, and splitting (Aarseth, 2004; Kotzur et al., 2018; Little et al., 2016; van Laarhoven et al., 2012; Zhang and Ghadiri, 2002). Abrasion and chipping are associated with low load levels on the particle, and disintegration and splitting with higher levels. Associated with each breakage mechanism is a characteristic change to the particle size distribution (PSD) (Figure 1-1) (Bayham et al., 2016; King, 2012; Materic et al., 2014; Scala et al., 2013). The changes of PSDs before and after breakage (as described in 1.2.2) can indicate the breakage mechanisms and has been used and confirmed in some areas, such as lactose, limestone, calcium looping sorbents, and model porous powders (Agrawal et al., 2011; Bonakdar et al., 2016; Materic et al., 2014; Ortega-Rivas et al., 2006; Scala et al., 2007; Wu and Wu, 2017; Zhao et al., 1999). However, there is currently no research on dairy powder breakage

mechanisms as well as how the powder properties influence their breakage behaviour.

The objective of this chapter is to investigate dairy powder breakage and how powder properties, especially the particle size, affect breakage behaviour. A commercial agglomerated IMF was selected because of its larger particles, wide PSD range, and comprehensive composition. Three separate devices were employed, a powder venturi feeder, a lab-scale dilute-phase pneumatic conveying pipeline and a laboratory high-speed mixer. These were selected to mimic the variety of processing conditions that powder experiences at the industrial scale, including the in-plant transportation in pneumatic conveying and dry mixing during the production of the IMF using the 'dry blending' process.

2.2. Materials and methods

2.2.1. Materials

A commercial agglomerated IMF, SMA PRO 'stage 2', was purchased from a local grocery store (Cork, Ireland). The IMF was sieved by a set of sieve screens to collect several fractions with narrow PSD. The opening sizes of the sieve screens used for size classification were 355, 250, and 180 μm, corresponding to four size fractions greater than 355 μm, from 355 to 250 μm, from 250 to 180 μm, and less than 180 μm, respectively (termed S>355, S355-250, S250-180, and S<180). The mass percentages of each component to the whole sample were 25.97%, 27.48%, 27.54%, and 19.01%, respectively. Four fractions were mixed gently in equal proportions as the whole sample (termed WS) used for analyzing the breakage behaviour of samples with a wider PSD. The composition of samples is shown in Table 2-1.

It should be noted that the commercial IMF had most likely already undergone breakage during its handling from spray drying through to packing as a commercial product as well as the sieving process for preparing samples. Thus, samples were more resistant to breakage than the original

spray-dried powder. Thus, the processing conditions described below are relatively severe and were selected to ensure breakage could be expected.

Table 2-1. The main composition of sieved infant milk formula samples *[1].

Ingredients	WS	S>355	S355-250	S250-180	S<180
Protein content (%)	10.36 ^{ab}±0.07	10.66 ^{a}±0.04	10.11 ^{b}±0.05	9.98 ^{c}±0.06	10.37 ^{ab}±0.04
Fat content *[2] (%)	23.82 ^{a}±0.11	23.47 ^{ab}±0.18	22.02 ^{c}±0.07	21.97 ^{c}±0.08	23.06 ^{b}±0.05
Lactose content (%)	37.21 ^{b}±0.06	38.21 ^{ab}±0.11	36.08 ^{c}±0.02	37.27 ^{b}±0.04	38.55 ^{a}±0.42
Galactose content (%)	0.203 ^{a}±0.002	0.179 ^{b}±0.004	0.194 ^{ab}±0.004	0.187 ^{ab}±0.001	0.205 ^{a}±0.007
Glucose content (%)	1.225 ^{a}±0.018	1.246 ^{a}±0.056	1.219 ^{a}±0.029	1.263 ^{a}±0.002	1.268 ^{a}±0.013

1. *[1]Total protein content was measured using the Kjeldahl method. Total fat contents were determined as per GEA Niro. The lactose, galactose, and glucose content were determined using high performance liquid chromatography (HPLC).
   Based on the commodity ingredient list, maltodextrin was present in this product. Therefore, the total content in the table would be lower than 100%.
2. Values are mean ± standard deviation (n=2).
3. *[2] The fat was a combination of a few kinds of vegetable oil (palm, rapeseed, coconut, and sunflower). The fat fusion temperature measured by DSC was from -22.64°C to 22.16°C.
4. $^{a-c}$ different values within rows in each ingredient are significantly different at $P<0.05$.

2.2.2. Measurement of powder properties

2.2.2.1. Particle size and specific surface area

The Sauter mean particle size ($D_{3,2}$, the surface-weighted average of the PSD), median particle size (D_{50}, the size that splits the PSD with half above and half below this diameter) of the volume PSD, specific surface area (SSA), and PSD of powders were measured using a Malvern Mastersizer 3000 (Malvern Instruments Ltd., Worcestershire, UK) with a standard stainless steel venturi feeder. Samples were added to the disperser, and compressed air at 0 bar was used to transport powders to minimise damage to the powder during measurement. The background measurement time was 20 s and the sample measurement was 10 s. The laser obscuration level was at 1-4%. Measurements were performed in triplicate.

2.2.2.2. Powder density and porosity

The particle density (ρ_p) and bulk density (loose bulk density (ρ_b) and tapped (100 taps) bulk density (ρ_{tapped})) of samples were measured as per GEA Niro (2006) using a Gas Pycnometer (Accupyc II 1340 Gas Pycnometer, Micromeritics Instrument Corporation, USA) and Jolting volumeter (Funke Gerber, Berlin, Germany), respectively. The interparticle porosity (ϵ) was evaluated from Eq. (2-1).

$$\epsilon = 1 - \frac{\rho_{tapped}}{\rho_p} \qquad \text{Eq. (2-1)}$$

2.2.2.3. Surface free fat content

The surface free fat (SFF) content of samples was measured as per GEA Niro (2006), which is based on the extraction of the fat on the surface of particles. Approximately 50 ml of petroleum ether was added into around 10 g of sample then agitated 15 min. The solution was filtered then 25 ml of the filtrate was pipetted into the aluminium dish. Most of the petroleum ether was evaporated then it was dried in the oven for one hour at 105 ± 1°C. Samples were cooled in a desiccator until at room temperature then weighed.

Measurements were carried out in duplicate. The content of surface free fat content was calculated as Eq. (2-2):

$$SFF(\%) = \frac{a \times 50 \times 100}{(ml - \frac{a}{0.94}) \times b} \quad \text{Eq. (2-2)}$$

where *ml* (ml) is the volume of filtrate, *a* (g) is the evaporation residue, *b* (g) is the weight of the sample, and 0.94 is the estimated value of the density of free fat.

2.2.2.4. Cohesiveness

The cohesion of powders was assessed by measuring the powder flow function by the powder flow tester (PFT) (Brookfield Engineering Laboratories, Inc., Middleboro, MA, USA) using the standard flow function test. Samples were filled into the aluminium trough (with the internal diameter 15.2 cm) of the annular shear cell at room temperature. The axial and torsional speeds for the PFT were 1.0 mm/s and 1 rev/h, respectively. The involved uniaxial normal stresses were between 0.2 and 4.8 kPa. The cohesion of samples under major principal consolidating stress around 4.4 kPa was used to represent powder cohesiveness.

2.2.3. Sample breakage in a powder venturi feeder

2.2.3.1. Powder venturi feeder

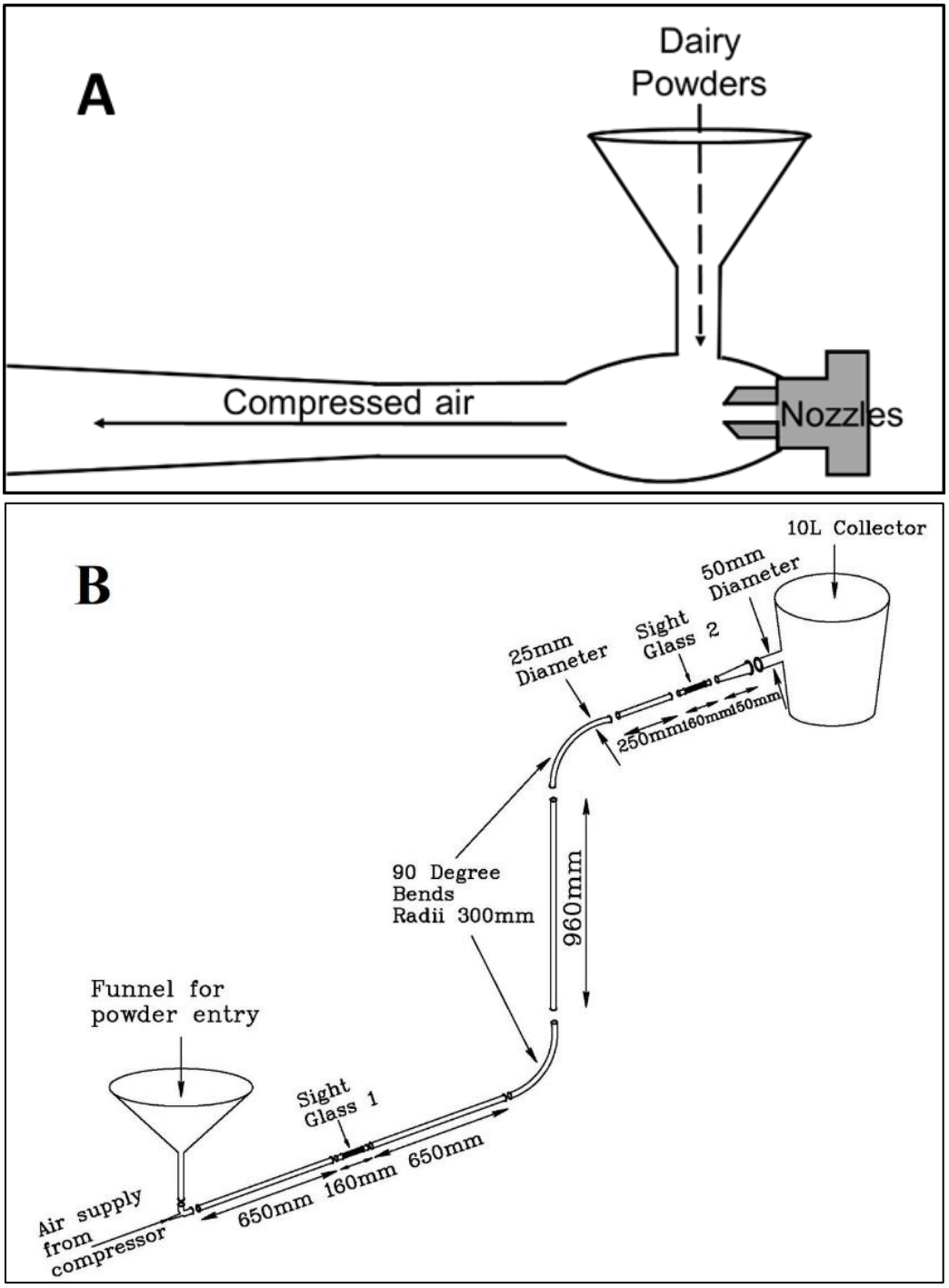
There is a powder venturi feeder or dispersion unit (diagram is shown in Figure 2-1A) in the Malvern Mastersizer 3000. It has been developed for particle size analysis and is used to disperse powders into individual particles within an airflow by the three mechanisms (velocity gradients caused by particle-to-particle impacts, shear stress, and particle-to-wall impacts) before entering the particle size measuring zone.

The compressed air (0 to 4.0 bar), coming out from the nozzle (Figure 2-1A), produces slight vacuum and a high-velocity airflow, which entrains particles into the airflow. Based on the modelling results, the maximum velocity of airflow inside the venturi feeder is at the tip of the nozzle and the velocity reduces as it moves downstream (Bonakdar et al., 2021). The

trajectories of particles inside the venturi feeder were predicted based on the numerical analysis of the fluid flow field by Computational Fluid Dynamic modelling and Lagrangian particle tracking (Bonakdar et al., 2021). Particles at low impact velocity collide with the surrounding walls at an oblique angle in the entrance and then accelerate along the pipe by the compressed air while also having impact or attrition with the wall or other particles, potentially causing breakage (Boiarkina et al., 2016). Compared to larger particles, smaller particles accelerate to higher velocities because of lower inertia. For example, at 2.5 bar, the velocities of particles before entrance into the airflow are around 5 m/s or 15 m/s for 250 μm or 50 μm particles, respectively. The velocities of these particles can be accelerated inside the entrance region until 20-35 m/s or 35-70 m/s, respectively. The speeds of particles conveying in the horizontal pipe before entering the measuring zone are around 30 m/s or 60 m/s, respectively. The slight decrease of the velocity is because of the decrease in kinetic energy during the mechanical impacts or attritions. The particle initially deforms elastically when it is subject to impact or attrition, absorbing impact energy as stored elastic strain (King, 2012). The internal stresses in the particle increase until a crack occurs at the most sensitive part. The stored elastic strain energy in the particle drives the growing crack and the remaining stored elastic energy is converted into the kinetic energy of the child particles. Then these child particles (or damaged particles) are conveyed immediately by the airflow to the laser diffraction zone for particle size analysis.

The dispersion efficiency is controlled by air pressure, sample feed rate, and venturi feeder geometry. There are many similarities in the trajectories and the collisions of particles during the dispersion and conveying by this venturi feeder and during the transportation by the pneumatic conveying that dairy powder experiences at the industrial scale for in-plant transportation or packaging (Hazlett et al., 2020). The feeder permits more conditions than pneumatic conveying, having a wide range of air pressure to control the different extents of breakage. Meanwhile, the particle size range measured by the Mastersizer 3000 is from 0.1 μm to 3500 μm which covers the agglomerated dairy powders and fragments. Also, particle velocities during

the dispersion and conveying in the venturi feeder are close to the speed used during the pneumatic conveying in the industrial scale. Therefore, the powder venturi feeder or dispersion unit in the Malvern Mastersizer 3000 was used to apply loading on powders and assess their breakability.



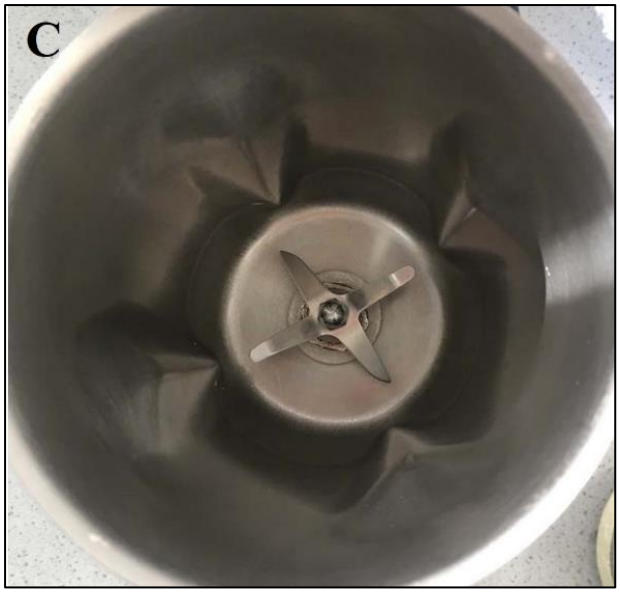


Figure 2-1. The diagram of the powder venturi feeder (A), the lab-scale pneumatic conveyor (B, adapted from Han et al. (2020)), and the inside of the laboratory high-speed mixer (C).

2.2.3.2. Sample breakage

Samples were fed to the powder venturi feeder, and the laser obscuration level was controlled at 1-4% by controlling the hopper gap and the feed speed. Low laser obscuration level ensured that most particles in the same fractions underwent similar conditions. For each sample, a series of air pressures (from 0 - 1.0 bar in 0.1 bar increments, and from 0.2 - 4.0 bar in 0.2 bar increments) were applied and the volume and number PSDs were measured. Measurements were performed in triplicate.

2.2.4. Sample breakage in the dilute-phase pneumatic conveying

Samples were blown through the lab-scale pneumatic conveyor (presented in Figure 2-1B which is adapted from Hanley (2011)) with an air velocity of 20, 30, and 40 m/s (termed PC20, PC30, and PC40) and a feeding rate of 3.0 g/s. Low feeding rate ensured that most particles in the same fractions underwent similar conditions. The diameter of the conveyor was constant at 25 mm, except for a 50 mm diameter terminal section (length was 150 mm). There were two horizontal sections linked to a vertical section (length was 960 mm) by two 90º bends (bend radii was 300 mm). The pressure of the compressed air was controlled to provide different air

velocities which were measured with an airflow meter (Nixon NL/MIN AIR @ 7 bar'G 1.293kg/m3 20 ºC) after the vertical section. Samples were poured into the air stream using a funnel and collected into a 10 L powder capture with a filter on the top of the capture in order to let the compressed air come out. The dominant source of powder breakage during the dilute-phase pneumatic conveying is caused by particle-wall impacts, particularly at the bends (Kotzur et al., 2018). The particle size and PSD of samples were measured using the method described in section 2.2.2.1 above.

2.2.5. Sample breakage in the high-speed mixing

Powders (50 g) were placed in the laboratory high-speed mixer (Waring, USA) (presented in Figure 2-1C) operated at 22,000 rpm for four different durations of 10, 30, 60, and 180 s (termed HM10, HM30, HM60, and HM180). Samples just covered the blade of the mixer. During mixing, powders move from the bottom of the mixer out towards the wall, then up the wall, and then cascade down towards the centre of the mixer (Tran, 2015). Momentum is transferred from the blade to the powder through a combination of impact, centrifugal, frictional, shear, gravity and inertial forces (Tran, 2015). The general perception in literature is that particles are more likely to break on impact during mixing (Iveson et al., 2001; van den Dries et al., 2003). The particle size and PSD of samples were measured using the method described in section 2.2.2.1 above.

2.2.6. Index of powder strength - breakage percentage

Particle strength can be defined as the minimum amount of stress that may be applied to a particle to cause macroscopic damage to the particle structure (Kotzur et al., 2018; Ortega-Rivas et al., 2006; Walton and Mumford, 1999). The physical strength of a single spray-dried dairy powder particle is very difficult to determine because of its small physical size. Thus, indirect approaches were employed to measure powder strength. The breakage percentage (*BP*) was the percentage decrease in particle size under different processing conditions compared with the initial particle size (Agrawal et al., 2011; Hazlett et al., 2020). Dairy powder breakage results in

the production of fine particles so the Sauter mean diameter ($D_{3,2}$) was used because it is more sensitive to the presence of fine particulates in the size distribution than the volume mean diameter ($D_{4,3}$) (Hu et al., 2014; Mun et al., 2011). It was calculated as Eq. (2-3), where $D3,2_b$ and $D3,2_i$ were the $D_{3,2}$ of broken samples and initial samples, respectively. The $D_{3,2}$ of powders before and after breakage was measured by a Malvern Mastersizer 3000 at 0 bar using the method described in section 2.2.2.1 (the $D_{3,2}$ of broken samples in the powder venturi feeder was measured at their corresponding pressures, as described in section 2.2.3.2). Measurements were performed in triplicate.

$$BP = \left(\frac{D3,2_{\ i} - D3,2_{\ b}}{D3,2_{\ i}}\right) \times 100\% \qquad \text{Eq. (2-3)}$$

2.2.7. Scanning electron microscopy (SEM) and Light microscope

The SEM (Zeiss-Supra 40 VP/Gemini Column, Carl Zeiss, Germany) and the polarised light microscope with a build-in camera (Instruction BX51, Olympus, Tokyo, Japan) were employed to observe the morphology of some broken samples (S355-250). Samples were mounted on carbon adhesive discs attached to SEM specimen stubs and coated with gold ions in a sputter coater (K575X Sputter Coater, Quorum Technologies, UK). Samples were dropped on a microscope slide, covered with a glass coverslip, and observed using a 10 × objective lens and 10 × eyepiece of the optical microscopy.

2.2.8. Statistical analysis

Results were expressed as mean ± standard deviation (SD). One-way analysis of variance (ANOVA), followed by Tukey's test, was used to determine the significant differences (SPSS, IBM, USA). A significance level of $P < 0.05$ was used throughout the study.

2.3. Results and discussion

2.3.1. Powder physical properties

2.3.1.1. Particle size and distribution

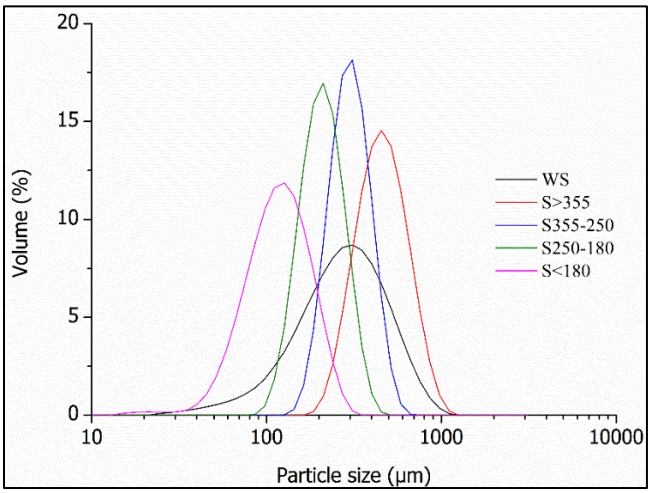


Figure 2-2. The particle size volume distributions of samples. WS: whole sample.

The particle size and volume PSDs of samples are shown in Table 2-2 and Figure 2-2, respectively. The $D_{3,2}$ of four fractions, S>355, S355-250, S250-180, and S<180 were 443, 295, 207, and 107 μm, respectively. Figure 2-2 shows that the PSDs of all samples without S<180 appeared as Log-normal distribution. There was a small peak in S<180, from 14.5 μm to 30 μm which might be the fractions produced during handling or the sieving process. Almost 80% of sieved samples fell within the range of the opening sizes of the sieve screens. The $D_{3,2}$ of WS, 214 μm, was significantly different from other samples (P<0.05) but closer to S250-180. The PSD of WS was wider than the four fractions, as expected, and the peak of the PSD plot was close to that of S355-250, which is consistent with the results of D_{50}.

Table 2-2. Properties of sieved infant milk formula samples.

Properties	WS	S>355	S355-250	S250-180	S<180
$D_{3,2}$ (μm)	214.7^{c}±2.5	443.7^{a}±4.1	295.3^{b}±0.5	207.0^{d}	107.0^{e}
D_{50} (μm)	284^{c}±5.1	473^{a}±4.9	308^{b}±0.8	216.7^{d}±0.5	123.0^{e}
Particle density (kg/L)	1.288^{b}±0.004	1.285^{c}±0.001	1.288^{b}±0.001	1.296^{a}±0.001	1.296^{a}±0.003
Bulk density (kg/L)	0.546^{b}±0.002	0.438^{d}±0.001	0.488^{c}±0.007	0.526^{b}±0.001	0.617^{a}±0.01
Porosity (%)	57.63^{c}±0.09	65.93^{a}±0.05	62.15^{b}±0.26	59.17^{bc}±0.01	52.41^{d}±0.55
Cohesion (kPa)	0.163^{b}±0.006	0.050^{d}±0.003	0.061^{c}±0.004	0.103^{bc}±0.003	0.311^{a}±0.005
SSA (m^2/kg)	26.6^{c}±0.3	12.9^{e}±0.1	20.3^{d}±0.1	29.0^{b}±0.1	56.1^{a}±0.1
SFF (%)	0.93^{c}±0.01	0.66^{d}±0.01	0.67^{d}±0.01	1.10^{b}±0.02	1.42^{a}±0.04

1. WS: whole sample. $D_{3,2}$: mean particle size. D_{50}: median particle size. SSA: specific surface area. SFF: surface free fat content.
2. Values are mean ± standard deviation (n=3).
3. $^{a-e}$ different values within rows in each property are significantly different at $P<0.05$.

2.3.1.2. Powder density and porosity

Particle density, bulk density, and porosity of samples are presented in Table 2-2. Particle density is the mass per unit volume of a particle, including the closed pores but excluding the open pores or cracks so it is also related to the particle structure properties. The particle density of all samples was around 1.29 or 1.30 kg/L and small particles had slightly higher particle density than large ones. This difference might be because big particles had more chance to have closed pores inside of the particle or the slight difference in composition. It was reported that, with the same parameters of spray drying, the composition of powders with different particle sizes was slightly different (O'Donoghue et al., 2019). The bulk density of powders depends on the PSD and particle shapes. The results show that the larger the particle size, the smaller the bulk density and the bigger the porosity as the larger particles are more agglomerated, and agglomerates tend to have more porous structures. The bulk density and porosity of WS were similar to those of S250-180 (P >0.05).

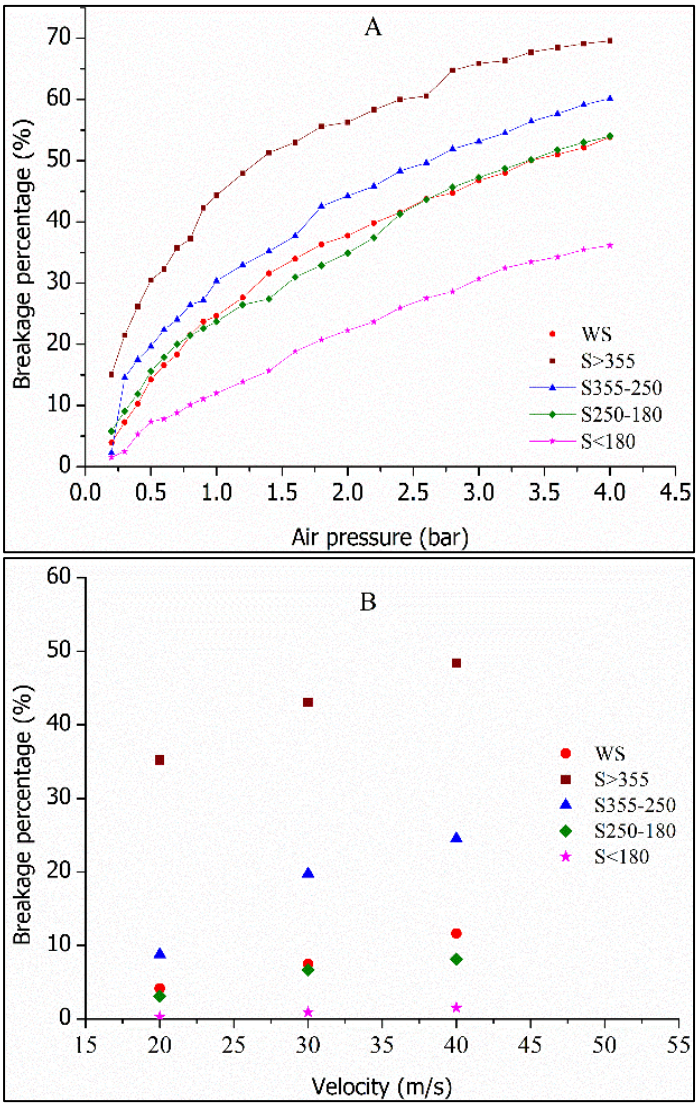
2.3.1.3. Cohesiveness

Some of the dairy powders are cohesive and particles may exist as clusters held together by cohesive attractions. Small stresses could break the clusters and dispersed them into their original particles. SFF has a major influence on powder cohesiveness (Fitzpatrick et al., 2007). Cohesion increases with increased SFF, especially at higher temperatures with greater fat liquefaction and liquid bridge formation causing the particles to adhere to one another or agglomerate (Fitzpatrick et al., 2007). Meanwhile, the large SSA meant more surface area is available for cohesive forces, and SSA can also be correlated with the energy required to cause breakage (Bemrose and Bridgwater, 1987). The cohesion, SSA, and SFF of samples are presented in Table 2-2. The significant differences in SSA and SFF were found in most samples (P<0.05), and both increased as particle size decreased. SSA and SFF of WS were similar to those of S250-180. The cohesiveness was increased with decreasing particle size and increasing SFF and SAA, which

is consistent with other research (Fitzpatrick et al., 2004). There was no significant difference between the cohesion of WS and S250-180.

2.3.2. Index of powder strength – breakage percentage

BP was used as an index of powder strength that was applied to compare the strengths of the powder size fractions based on the changes of particle size before and after breakage at specific operating conditions. The lower the *BP*, the more resistant the powder is to breakage, thus the stronger the powder is. Figure 2-3 displays the *BP* for each of the five IMF samples for each of the three processing methods as a function of process conditions. For any sample, the *BP* increased with increasing processing conditions in each method. Comparing different samples, results of the three processing methods show the same trends.



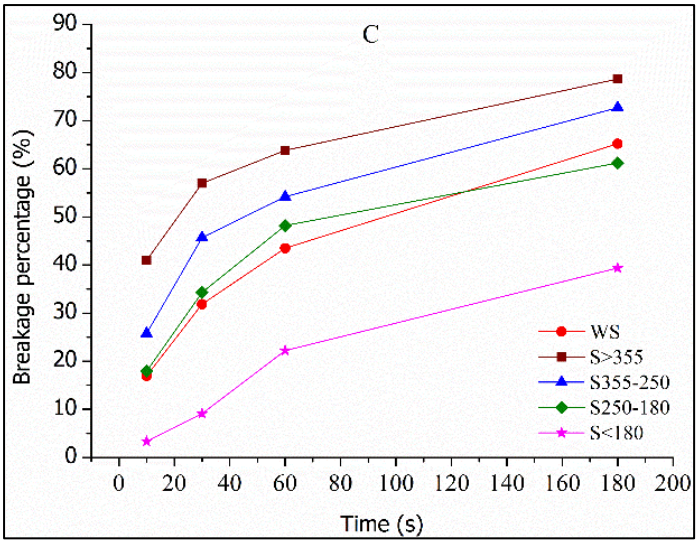


Figure 2-3. The percentage decrease in particle size ($D_{3,2}$) of samples before and after breakage during three processing methods. A: Powder venturi feeder at different air pressures. B: Dilute-phase pneumatic conveying under the air velocity of 20, 30, and 40 m/s. C: Laboratory high-speed mixing for 10, 30, 60, and 180 s. WS: whole sample.

Firstly, for the four sieved fractions, under the same processing conditions, *BP* increased with increasing initial particle size, which shows that powder strength increased with decreasing initial particle size and porosity. This finding is in agreement with results of some research on the extent of breakage of agglomerated dairy powders (Boiarkina et al., 2016; Hazlett et al., 2020). It has been reported that particle size is one of the most important influencing factors for particle breakage and that particle strength decreases with increasing particle size (Fu et al., 2005; Ghadiri et al., 1991; Zhang and Ghadiri, 2002). It has been attributed to the likelihood of a greater number of imperfections in larger particles, which in turn provides a greater number of cracks. The highest local tensile stress is generated at these defective zones so that the fracture initiates from this zone and propagates (Antonyuk et al., 2005). This may also be the reason that porosity and density could influence particle strength because the pores and the structural defects in agglomerates are analogous to imperfections, inhomogeneities, or microcracks in material science (Antonyuk et al., 2005). In addition, the number of contact points of a primary particle can be decreased with larger porosities, by which the strength of agglomerates decreases. Besides the few flaws and low porosity, small particles are more difficult to break owing to

the stronger interparticle forces that bind particles together including van der Waals forces, electrostatics, and liquid bonds (Reynolds et al., 2005). From an energy perspective, the more energy that can be absorbed, the lower the collision energy (if the breakage is caused by the impact), and the less likely the particle will break. Small particles can absorb a larger amount of energy than big particles (Agrawal et al., 2011; King, 2012), which results in the lowering of the breakage extent.

Moreover, WS and S355-250 have similar D_{50} values (Table 2-2), however, the strength of WS was higher than that of S355-250 and similar to S250-180, which means that the much broader PSD of WS corresponds to an increase in powder strength. This might be because the decrease of particle uniformity increased the cushioning action of fines. It has been found that the fine particles enclosed the coarse granules and thereby acted as a cushioning medium that reduced the granule stress and levels of attrition (Konami et al., 2002).

2.3.3. Breakage behaviour of four sieved fractions

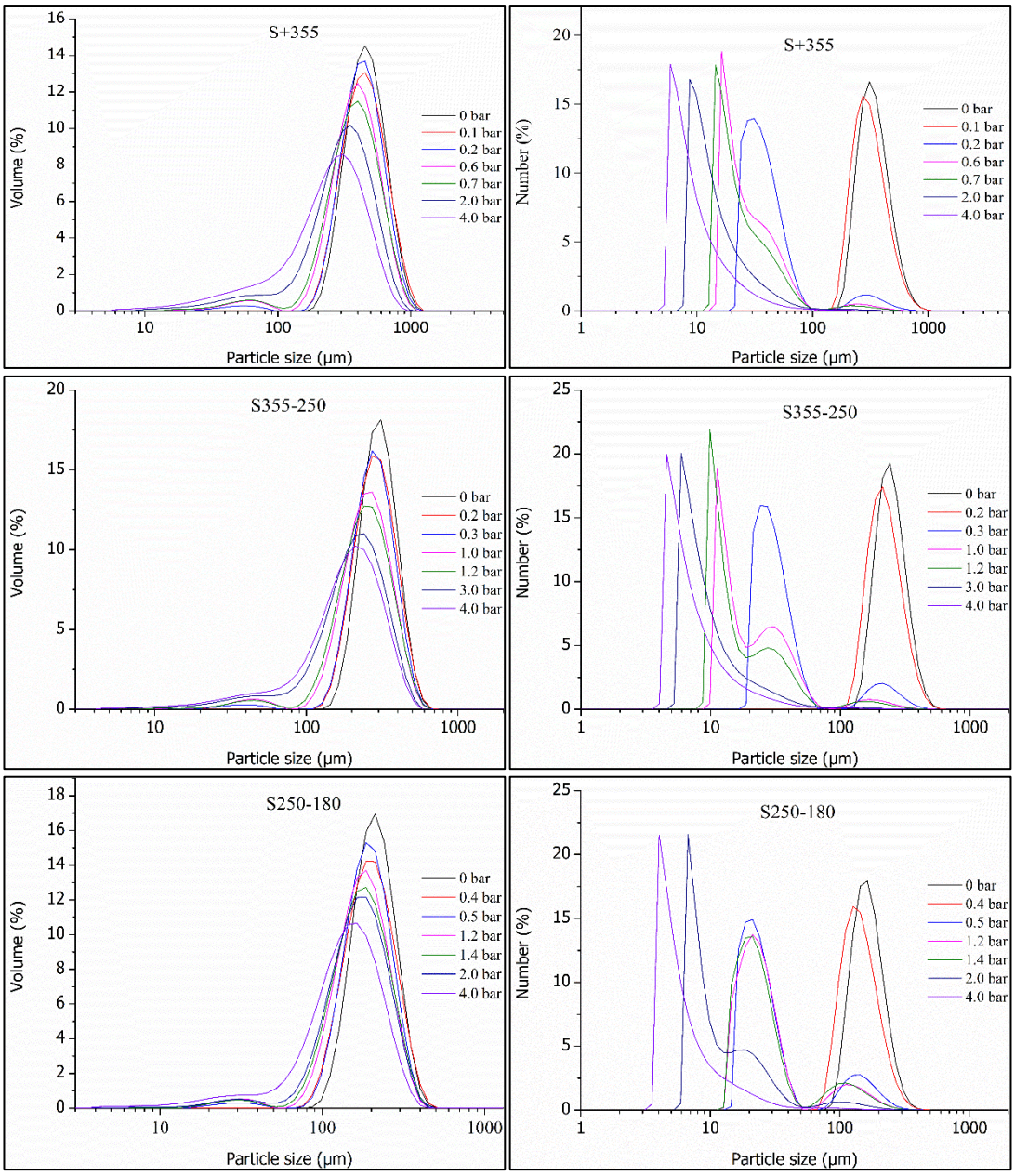
The changes of PSDs were used to identify the breakage behaviour of four sieved fractions, S>355, S355-250, S250-180, and S<180, during three processing methods. It should be mentioned that in order to facilitate analysis, different mechanisms were distinguished here according to their descriptions in the Introduction (2.1) and particle size distributions (illustrated in Figure 1-1). The mechanisms identified here were the primary mechanisms leading to breakage, not necessarily the sole mechanism. Moreover, the main breakage behaviour was not based on single impact or shear but compared the changes of particles before and after the entire processes where the stresses might act on the initial particles and their child particles.

2.3.3.1. Powder venturi feeder

The evolution of particle size volume (V-PSD) and number (N-PSD) distributions of four samples at different air pressures in the powder venturi

feeder are shown in Figure 2-4. The air pressures had a great impact on the PSD of all samples. Furthermore, the larger the particle size, the more sensitive the powder was to increasing air pressure, and the more breakage occurred, which is consistent with the data presented in Figure 2-3.

In Figure 2-4, the PSD of S>355, S355-250, and S250-180 control samples (0 bar) were narrow and showed symmetric unimodal with the logarithm of particle size. The changes in the PSDs of these three samples at different air pressures were quite similar and there were four breakage patterns.



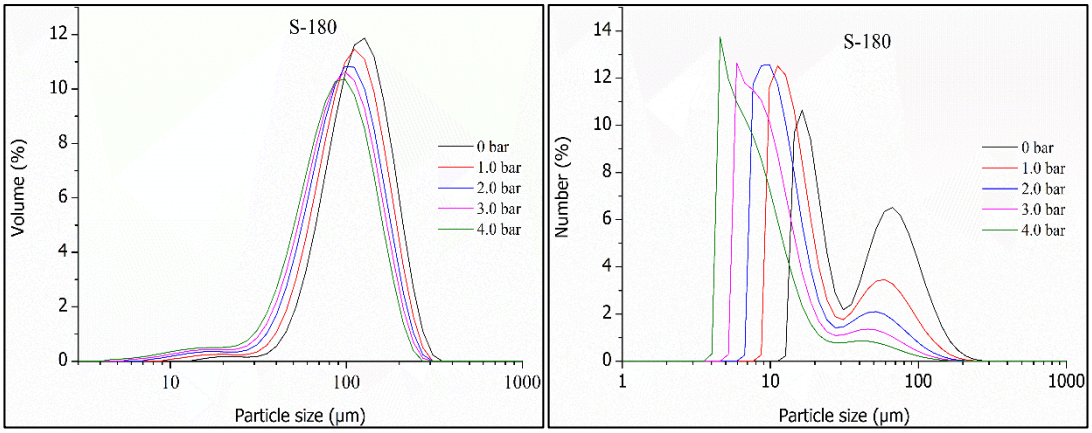


Figure 2-4. The particle size volume and number distribution of samples broken by powder venturi feeder at different air pressures.

(1) For these three samples, the PSD plots gradually shifted left as the air pressure increased from 0 to 0.1, 0.2, and 0.4 bar, respectively. This implies that the particle size decreased but there were no small particles produced and all particles were still big (N-PSDs). Thus, the reason for this decrease in particle size was most likely due to the dispersion of clusters that were particles held together by cohesive attractions. The clusters existed in the larger sizes of the PSD and when they were broken, the particles were liberated causing the PSD shift to the left, with no occurrence of a fine's peak.

(2) With the further increase of air pressure, chipping most likely occurred according to the appearance of bimodal PSDs and the two peaks were well separated by a range of sizes that contained no particles. There were lots of small particles produced (N-PSDs) and showed up as a distinct peak at the small sizes in V-PSDs but the main volume of samples were big-sized particles (V-PSDs). The produced small particles for S>355, S355-250, and S250-180 were around 50, 35, and 30 μm, respectively. They were big enough to decrease the particle size of mother particles implying that the main mechanism was not surface abrasion, that may have happened during the handling from spray drying through to packing or sieving process (the particle size of the whole sample decreased 2.3% for $D_{3,2}$ and 2.8% for $D50$ after sieving, data not shown). There was a threshold air pressure for chipping (AP_c) where the small-sized peaks in V-PSDs or the middle peaks in N-PSDs appeared. The AP_c for S>355, S355-250, and S250-180 were

0.2, 0.3 and 0.5 bar, respectively, which increased with decreasing particle size because smaller particles were more resistant to breakage, thus higher pressures were required to initiate chipping. Salman et al. (2002) also found that a threshold velocity existed in the single-particle impact studies, and below the threshold velocity, no breakage occurred. In this pattern, the proportion of small particles continued to increase and the V-PSDs shifted left and were always with two well-separated peaks which gradually got closer as air pressure increased.

(3) Disintegration most likely became the primary breakage mechanism with two V-PSDs' peaks merging when the threshold air pressures (AP_d) were reached. The AP_d for S>355, S355-250, and S250-180 were 0.7, 1.2, and 1.4 bar, respectively, which increased with decreasing particle size. In this pattern, stress propagates through part of the particle from the point of application of the stress and causes a portion of it to fail as many small particles(Scala et al., 2013). The two peaks of V-PSD merged gradually, and the middle peaks of N-PSD lowered as air pressure increased.

(4) When the air pressure further increased, particles travel at higher speed and higher energy, which resulted in the breakage mainly by splitting with the disappearance of small-sized peaks in V-PSDs or the middle peaks in N-PSDs. Initial particles were broken into lots of fines (N-PSD) and mid-sized particles (V-PSD) with a broad spectrum of particle sizes. Same as AP_c and AP_d, for S>355, S355-250, and S250-180, the threshold air pressures for splitting (AP_s) were 2.0, 3.0 and 3.6 bar, respectively.

Differing from the three samples above, the PSDs of S<180 were bimodal and there were a lot of small particles in the control sample (N-PSD), which might be produced by abrasion during handling or sieving. Thus, the application of the analysis presented above for the other fractions could not be used as a basis for judgment. However, it was clear that the volume and population of fine particles continued to grow, and those of the big-sized particles were gradually lowered as air pressure increased, although there were still some big-sized particles even at high breakage intensities. Moreover, the above threshold air pressures increased with decreasing initial

particle size, so the threshold air pressures of S<180 should be higher than those of S250-180. Thus, it could be concluded that chipping and disintegration most likely played an important role in the breakage of S<180. The mechanism at lower air pressure (at least lower than 0.5 bar which was the AP_c for S250-180) might be dispersion because the strength of S<180 was higher than that of S250-180.

In summary, during powder venturi feeder at different air pressures, the breakage behaviour of four fractions with different particle sizes was different. Four breakage mechanisms were found, dispersion, chipping, disintegration, and splitting, corresponding to the increasing extent of breakage. For S<180, chipping and disintegration might play leading roles at high air pressures. For the other three samples, the breakage was progressive with increasing air pressure: particle size decreased due to the dispersion when the air pressure was low, but when the air pressure was higher than AP_c, AP_d, and AP_s, the main mechanism was chipping, disintegration, and splitting, respectively. These threshold air pressures increased with decreasing particle size because of the increase of powder strength. The threshold air pressures were defined to facilitate analysis, however in reality, the mechanism around AP_d or AP_s might be a combination of disintegration and chipping or splitting, respectively.

2.3.3.2. Lab-scale dilute-phase pneumatic conveying

The evolution of PSDs of samples during the dilute-phase pneumatic conveying at different air velocities are shown in Figure 2-5. The air velocity affected the PSD evolution of S>355 and S355-250, especially for the former. For S>355, disintegration most likely occurred at all air velocities and when the velocity increased, the breakage gradually increased. For S355-250, dispersion most likely occurred up to at least 20 m/s conveying and chipping mainly happened at the higher velocities. There was no significant breakage for S250-180 during conveying under 20 m/s. The decrease of particle size for S250-180 after 30 or 40 m/s conveying might be because of dispersion. There was no significant breakage for S<180 at all speeds. These results indicate that disintegration and chipping in pneumatic

conveying mainly occurred in S>355 and S355-250 respectively while dispersion most likely occurred in S250-180 under high velocities.

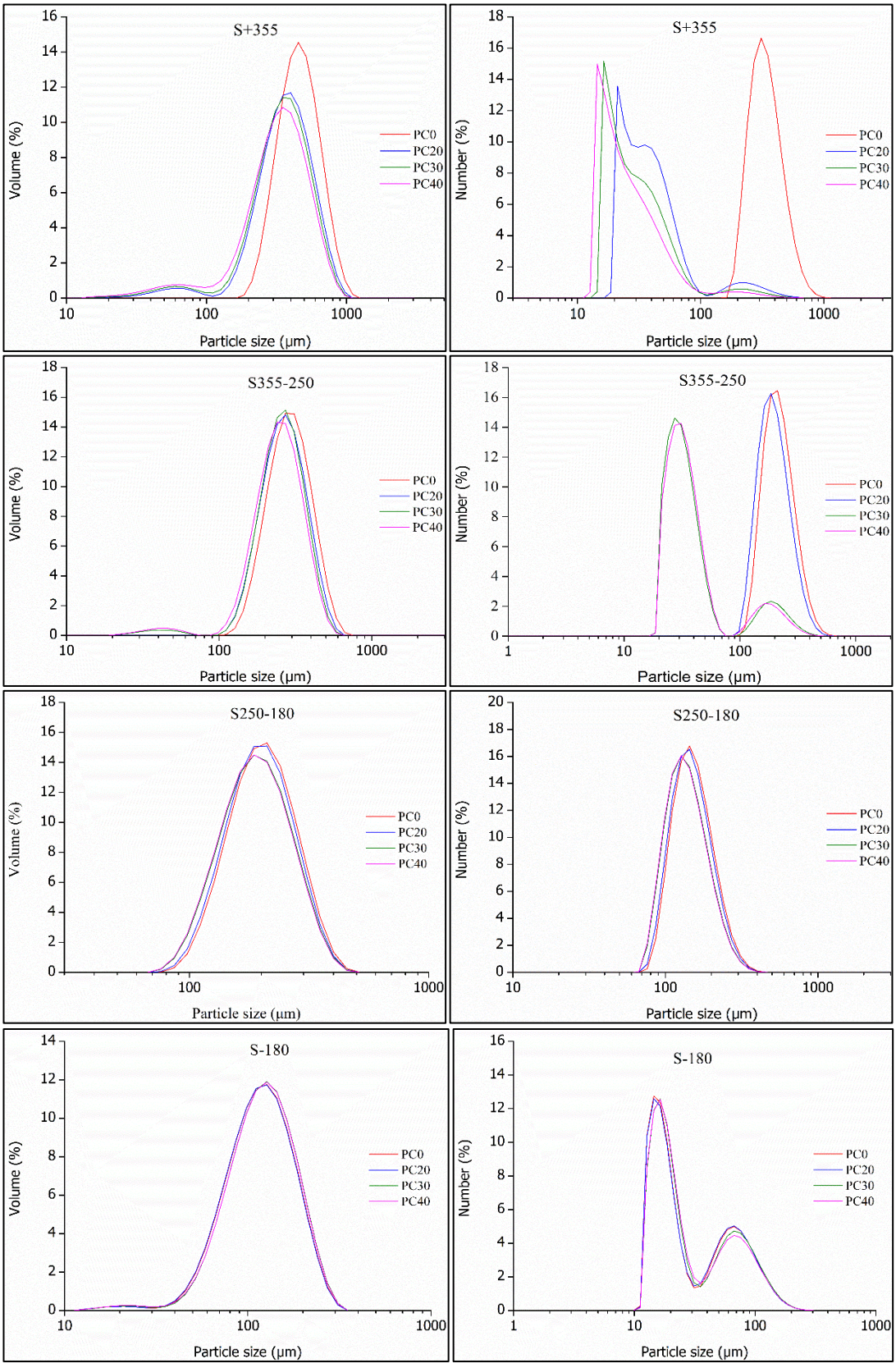


Figure 2-5. The particle size volume and number distribution of samples broken by

dilute-phase pneumatic conveying under the air velocity of 20 m/s (PC20), 30 m/s (PC30), and 40 m/s (PC40).

2.3.3.3. Laboratory high-speed mixing

The changes of PSDs of samples during the high-speed mixing for different times are shown in Figure 2-6. In some processes, the breakage evolves with repeated loads, such as with time spent in fluidized beds (Materic et al., 2014), ultrasonic systems (Raman and Abbas, 2008; Zhao et al., 1999), attrition tests (Wu and Wu, 2017), and mixing in this study. On the one hand, in some tests, breakage during the process can be analyzed and divided into primary and secondary breakage (Materic et al., 2014). The stress levels should not vary much over time during mixing because the mixing speed was constant. However, the stresses may act on the child particles rather than the initial particles due to the continuous formation of child particles over time. For example, disintegration appeared to be the main mechanism for S>355 at 10 s mixing, and the small-sized peak grew over time and its distinctiveness disappeared that was likely to be due to a progressive breakage of child particles by either chipping or disintegration (assuming that only the initial particles were broken in the first 10 seconds). It was not applicable to analyse breakage during mixing in this way as it did not easily distinguish between primary and secondary breakage. On the other hand, the breakage of the whole process can be analyzed, such as the comparison of PSDs (Zhao et al., 1999) or attrition rates (Raman and Abbas, 2008) of catalysts before and after breakage in ultrasonic systems for certain times and energy outputs. This can obtain meaningful breakage information for the industrial processing conditions. From Figure 2-6, fragmentation most likely occurred in all S>355 and S355-250 samples, with disintegration occurring at 10 s mixing and splitting occurring at the other higher mixing times. The main breakage mechanisms for S250-180 were most likely chipping for 10 s, disintegration at 30 s, and splitting for the longer times. The changes of PSD in S<180 during mixing was similar to that in the powder venturi feeder, so chipping and disintegration most likely played an important role in the breakage of S<180. Consequently, during mixing for different

times, the main breakage behaviour was chipping and two kinds of fragmentation.

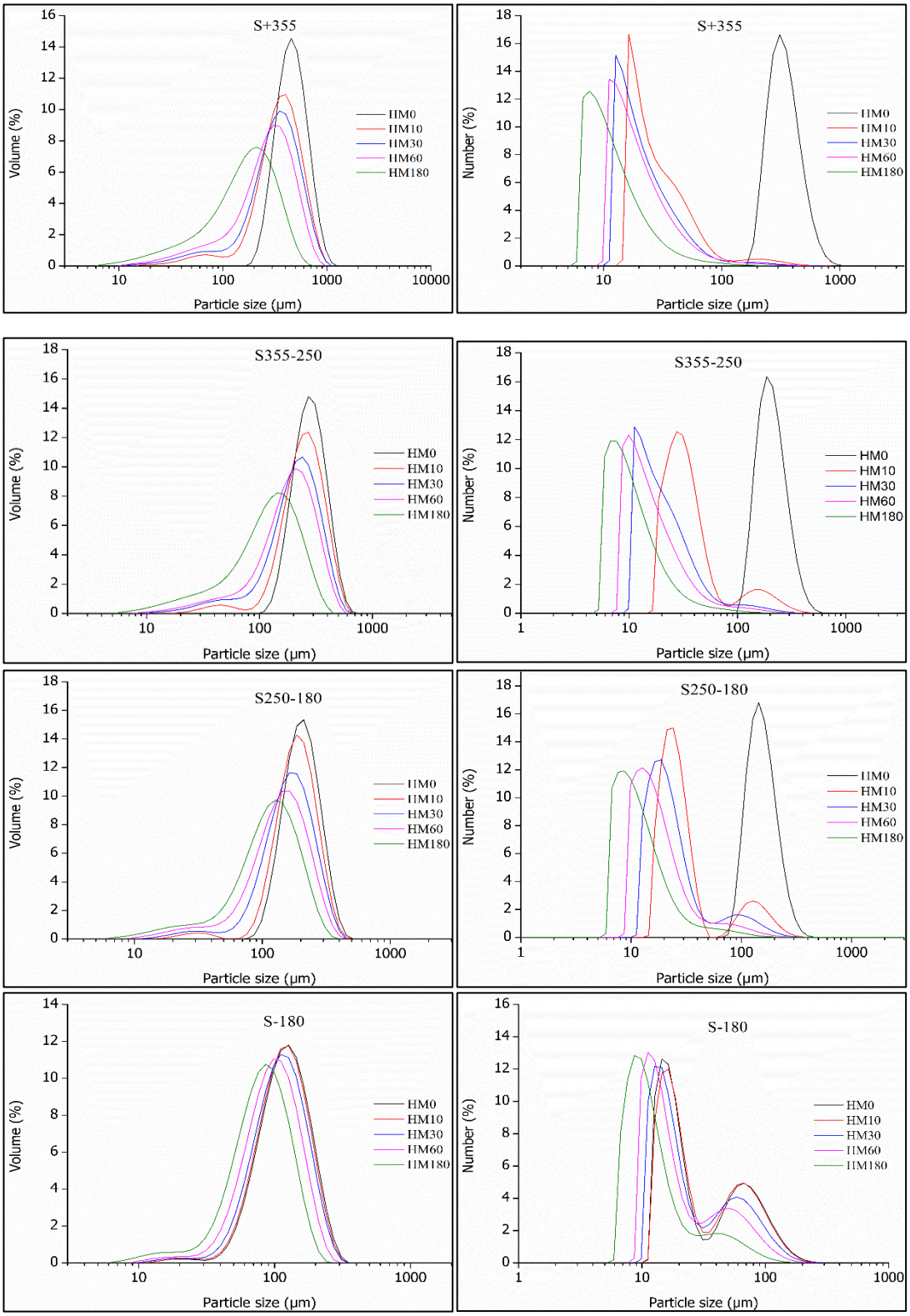


Figure 2-6. The particle size volume and number distribution of samples broken by the laboratory high-speed mixing for 10 s (HM10), 30 s (HM30), 60 s (HM60), and 180 s (HM180).

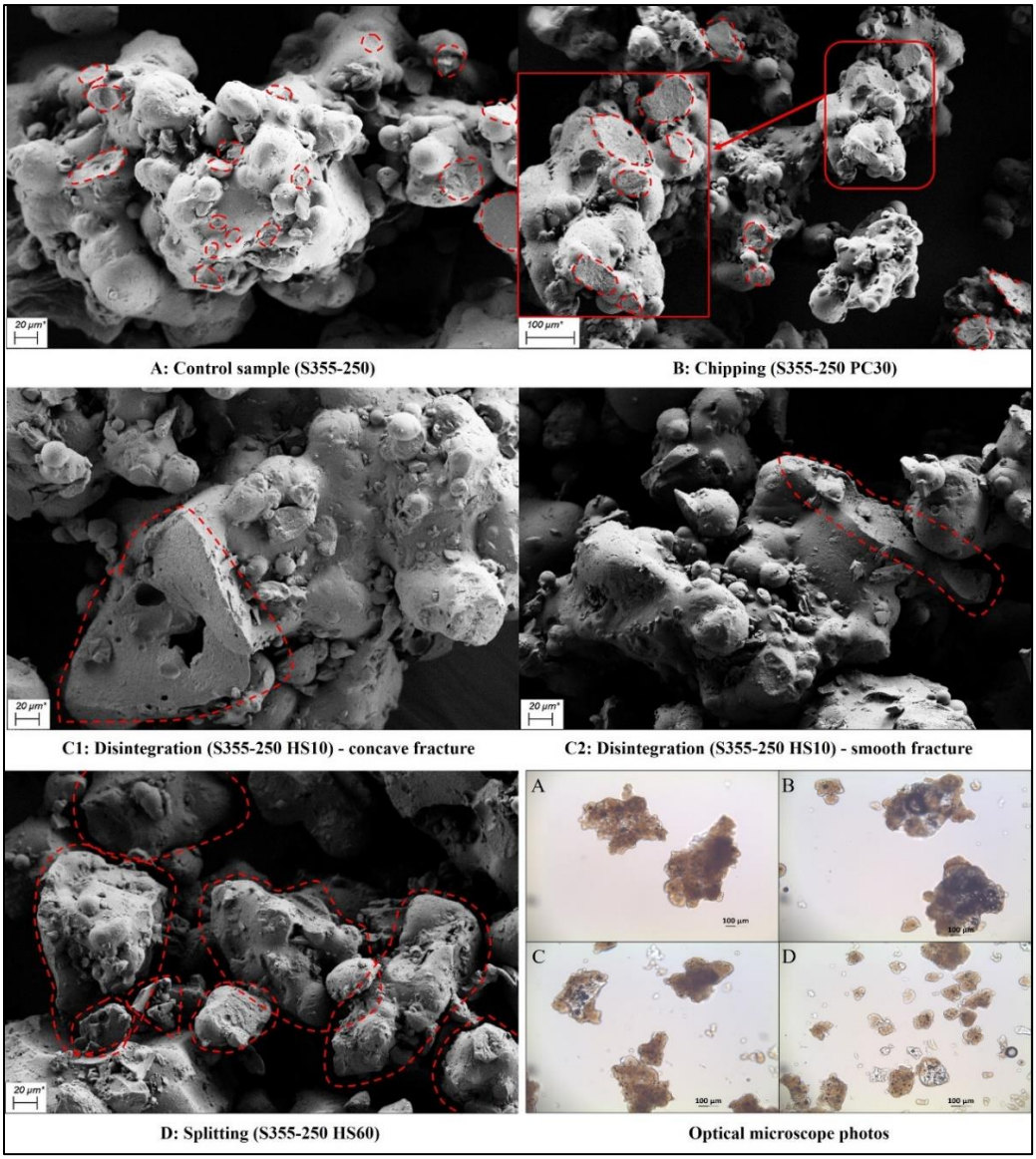


Figure 2-7. The SEM and optical micrographs of some broken samples (S355-250). Control powder sample (A), and broken samples by chipping (B), disintegration (C) with a concave (C1) or a smooth fracture (C2), and splitting (D).

According to the analysis of Figures 2-4, 2-5, and 2-6, the breakage behaviour of the four sieved IMF fractions during three processing methods was similar and there were four breakage mechanisms (dispersion, chipping, disintegration, and splitting) resulted in the increasing extent of breakage. The SEM and optical micrographs of some S355-250 samples, corresponding to the last three mechanisms, are shown in Figure 2-7. Particles of the control sample (Figure 2-7A) were irregular and there were some small defects (less than 20 μm) on the surface, which represents surface abrasion. Defects became bigger when chipping occurred (Figure 2-7B) while the main particle body was not damaged. The body was partly

broken when disintegration happened and left a concave (Figure 2-7C1) or smooth (Figure 2-7C2) fracture, and was completely crushed by splitting (Figure 2-7D). Surface breakage likely occurred on the raised part of agglomerates, and this kind of structure was influenced by the spray drying and agglomerated parameters, and the composition of particles. The body breakage was influenced by the location of the applied stress and the structure of agglomerates. Dairy powder particles are heterogeneous in composition (Murrieta-Pazos et al., 2012), thus the location of a crack might also be affected by the composition. Figure 2-8 outlines the typical V- and N-PSDs of these four patterns of breakage. The typical N-PSDs of chipping and disintegration was not unique and they depended on the initial particle size and the processing conditions. At the same condition, the breakage behaviour of different samples was different, depending on the powder strength. The combined results show that when the main breakage behaviour of S250-180 was dispersion, the bigger-sized sieved fractions mainly underwent chipping and disintegration. When the main breakage behaviour of S250-180 was disintegration, the bigger-sized sieved fractions were broken by splitting.

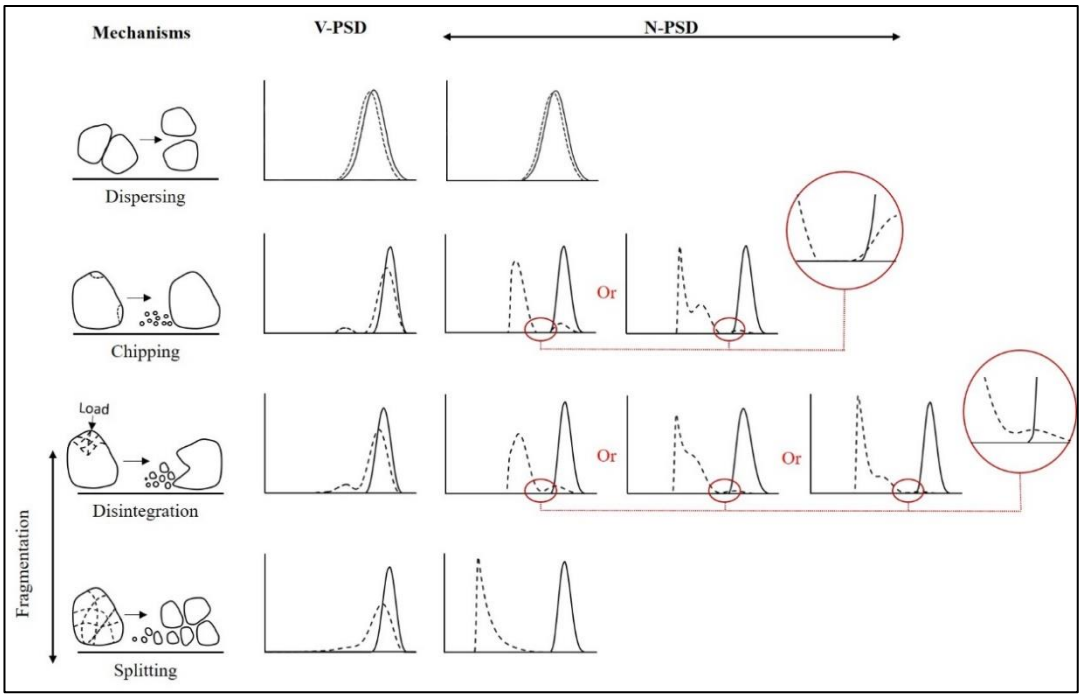


Figure 2-8. Sieved infant milk formula breakage typical volume- (V-PSD) and number-particle size distribution (N-PSD) curves before (solid line) and after (dotted line) breakage.

2.3.4. Breakage behaviour of whole samples

In order to easily observe the breakage behaviour, IMF was sieved into different fractions with narrow distributions, while the study of breakage behaviour of whole samples would provide more practical knowledge. The evolution of PSDs of WS during powder venturi feeder (PF), dilute-phase pneumatic conveying (PC), and high-speed mixing (HM) are shown in Figure 2-9. It was shown that varying extent of breakage occurred for WS during three processing methods with different conditions. Most breakages happened after HM for 180 s, and the least occurred during PC, which is consistent with the degree of breakage of four fractions during three processes.

For the breakage behaviour of WS during PF and HM, it was clear that V-PSDs of WS gradually became shorter and shifted left, and the population of fine particles continued to increase with increasing process conditions. There was not enough evidence to easily identify the main breakage mechanisms only based on the changes in PSDs because there was no bimodal PSDs or other features. This was due to the wide range of PSD of WS which was from tens to hundreds of microns, and the child particles were still in that range. Moreover, according to the analysis of four fractions, different sized particles had different breakage behaviours at the same process condition. Thus, the breakage of WS was a mixture of all particles' breakage and the breakage behaviour could be one or a combination of dispersion, chipping, and fragmentation. Splitting might be identified based on the changes of PSDs because almost all particles experienced splitting when the processing conditions were high enough, for example, the HM for 180 s or PF at 3.0 to 4.0 bar. Therefore, the breakage behaviour of WS was one or a combination of breakage mechanisms because particles with different particle size in WS underwent different breakage patterns at the same condition. Mechanisms without splitting could not be identified for WS based on the changes in PSDs because of the wide range of PSD.

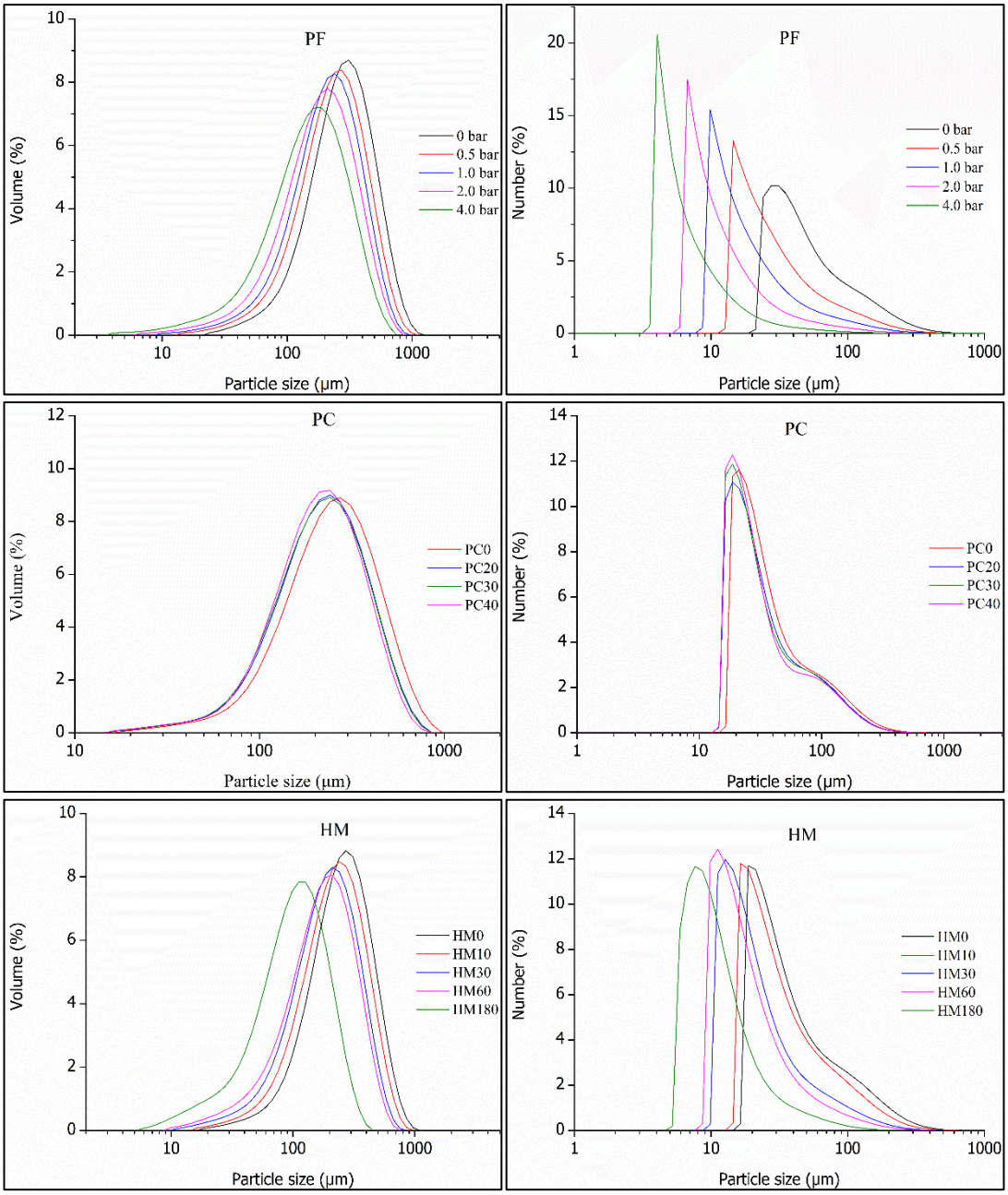


Figure 2-9. The particle size volume and number distribution of whole samples (WS) broken by powder venturi feeder (PF) at different air pressures, by dilute-phase pneumatic conveying (PC) under the air velocity of 20 m/s, 30 m/s, and 40 m/s, and by the laboratory high-speed mixing (HM) for 10 s, 30 s, 60 s, and 180 s.

2.4. Conclusion

This chapter was performed on the particle breakage behaviour and the effect of powder properties of sieved IMF samples during three different processing methods (powder venturi feeder, lab-scale pneumatic conveyor, and laboratory high-speed mixer) which mimic the industrial-scale processing

conditions. Powder properties and breakage behaviours of samples were summarized in Table 2-3.

Powder strength influenced the breakage behaviour, and it increased with the decrease of particle size and porosity, and the expansion of the PSD range. The main breakage mechanisms for IMF samples included dispersion, chipping, and fragmentation (disintegration and splitting), corresponding to the increasing extent of breakage and depending on the breakage process conditions and particle characteristics. The breakage behaviour of S>355, S355-250, and S250-180 could be determined according to the changes of PSDs. Their main breakage mechanisms during powder venturi feeder changed gradually from dispersion until splitting with increasing air pressures. Smaller sized particles were more resistant to breakage and higher air pressures were needed to cause the same breakage mechanism for smaller sized particles. For dilute-phase pneumatic conveying, disintegration, chipping, and dispersion occurred for three samples respectively. Mixing caused the greatest breakage and two kinds of fragmentations most likely happened during mixing. For S<180, no breakage happened during dilute-phase pneumatic conveying. Chipping and disintegration were the main mechanisms during the other two methods. The breakage behaviour of whole samples was one or a combination of breakage mechanisms because the breakage behaviour of samples with different particle size at the same process condition was different. Overall, a better understanding of the breakage behaviour of dairy powders and the impact of powder properties will assist efforts in trying to reduce powder breakage and the problems associated with it.

Table 2-3. Summary of the properties and main breakage mechanisms a of infant milk formula.

Sample	Properties	Main breakage mechanisms		
		Powder venturi feeder	**Dilute-phase pneumatic conveying**	**High-speed mixing** [b]
S>355	**With PS↓** Particle density ↑ Bulk density ↑ Porosity ↓ SSA ↑ SFF ↑ **These changes resulted in:** Cohesiveness ↑ Powder strength ↓(BP↑)	Dispersion: 0.1 bar Chipping: 0.2-0.6 bar Disintegration: 0.7-1.8 bar Splitting: 2.0-4.0 bar	Disintegration for all speeds.	Disintegration: 10 s Splitting: 30 s, 60 s, 180 s
S355-250		Dispersion: 0.1-0.2 bar Chipping: 0.3-1.0 bar Disintegration: 1.2-2.8 bar Splitting: 3.0-4.0 bar	Dispersion: 20 m/s Chipping: 30 m/s, 40 m/s	Disintegration: 10 s Splitting: 30 s, 60 s, 180 s
S250-180		Dispersion: 0.1-0.4 bar Chipping: 0.5-1.2 bar Disintegration: 1.4-3.4 bar Splitting: 3.6-4.0 bar	No breakage: 20 m/s Dispersion: 30 m/s, 40 m/s	Chipping: 10 s Disintegration: 30 s Splitting: 60 s, 180 s
S<180		Chipping and disintegration	No breakage	Chipping and disintegration
WS	Similar to S250-180	• Particles with different particle sizes underwent different breakage mechanisms at the same condition. • The breakage of WS displayed a combination of breakage mechanisms.		

1. [a]: Different mechanisms were distinguished according to their descriptions and particle size distributions. The mechanisms identified were the primary mechanisms leading to breakage, not necessarily the sole mechanism.
2. [b]: The main breakage mechanisms considered the effect of the whole process on the powders rather than the changes in the process.
3. WS: whole sample. PS: particle size ($D_{3,2}$). SSA: specific surface area. SFF: surface free fat content. BP: breakage percentage.

References

Aarseth, K.A. (2004). Attrition of feed pellets during pneumatic conveying: the influence of velocity and bend radius. *Biosystems Engineering* 89(2), 197-213. https://doi.org/10.1016/j.biosystemseng.2004.06.008.

Agrawal, S.G., Balandier, A., Paterson, A.H.J., & Jones, J.R. (2011). Study on lactose attrition inside the mixing cell of a laser diffraction particle sizer using a novel attrition index. *Powder Technology* 208(3), 669-675. https://doi.org/10.1016/j.powtec.2011.01.007.

Antonyuk, S., Tomas, J., Heinrich, S., & Mörl, L. (2005). Breakage behaviour of spherical granulates by compression. *Chemical Engineering Science* 60(14), 4031-4044. https://doi.org/10.1016/j.ces.2005.02.038.

Barleita, B.J., & Barbosa-cáovas, G.V. (1993). Fractal analysis to characterize ruggedness changes in tapped agglomerated food powders. *Journal of Food Science* 58(5), 1030-1035. https://doi.org/ 10.1111/j.1365-2621.1993.tb06105.x.

Barletta, B.J., & Barbosa-cánovas, G.V. (1993). An attrition index to assess fines formation and particle size reduction in tapped agglomerated food powders. *Powder Technology* 77(1), 89-93. https://doi.org/10.1016/0032-5910(93)85011-W.

Bayham, S.C., Breault, R., & Monazam, E. (2016). Particulate solid attrition in CFB systems - An assessment for emerging technologies. *Powder Technology* 302, 42-62. https://doi.org/10.1016/j.powtec.2016.08.016.

Bemrose, C.R., & Bridgwater, J. (1987). A review of attrition and attrition test methods. *Powder Technology* 49(2), 97-126. https://doi.org/10.1016/0032-5910(87)80054-2.

Boiarkina, I., Sang, C., Depree, N., Prince-Pike, A., Yu, W., Wilson, D.I., & Young, B.R. (2016). The significance of powder breakdown during conveying within industrial milk powder plants. *Advanced Powder Technology* 27(6), 2363-2369. https://doi.org/10.1016/j.apt.2016.10.019.

Bonakdar, T., Ali, M., & Ghadiri, M. (2021). Particle breakability assessment using an Aero S disperser. *International Journal of Pharmaceutics* 597, 120365. https://doi.org/10.1016/j.ijpharm.2021.120365.

Bonakdar, T., Ghadiri, M., Ahmadian, H., Martin de Juan, L., Xu, D., Tantawy, H., & Smith, D. (2016). Impact attrition of spray-dried burkeite particles. *Powder Technology* 304, 2-7. https://doi.org/10.1016/j.powtec.2016.08.024.

Deng, X., & Davé, R.N. (2017). Breakage of fractal agglomerates. *Chemical Engineering Science* 161, 117-126. https://doi.org/10.1016/j.ces.2016.12.018.

Dosta, M., Dale, S., Antonyuk, S., Wassgren, C., Heinrich, S., & Litster, J.D. (2016). Numerical and experimental analysis of influence of granule microstructure on its compression breakage. *Powder Technology* 299, 87-97. https://doi.org/10.1016/j.powtec.2016.05.005.

Fitzpatrick, J.J., Barry, K., Cerqueira, P.S.M., Iqbal, T., O'Neill, J., & Roos, Y.H. (2007). Effect of composition and storage conditions on the flowability of dairy powders. *International Dairy Journal* 17(4), 383-392. https://doi.org/10.1016/j.idairyj.2006.04.010.

Fitzpatrick, J.J., Iqbal, T., Delaney, C., Twomey, T., & Keogh, M.K. (2004). Effect of powder properties and storage conditions on the flowability of milk powders with different fat contents. *Journal of Food Engineering* 64(4), 435-444. https://doi.org/10.1016/j.jfoodeng.2003.11.011.

Francioli, D.M., 2015. Effect of operational variables on ball milling, Universidade Federal do Rio de Janeiro, Brazil.

Fu, J., Reynolds, G.K., Adams, M.J., Hounslow, M.J., & Salman, A.D. (2005). An experimental study of the impact breakage of wet granules. *Chemical*

Engineering Science 60(14), 4005-4018. https://doi.org/10.1016/j.ces.2005.02.037.
Ghadiri, M., Yuregir, K.R., Pollock, H.M., Ross, J.D.J., & Rolfe, N. (1991). Influence of processing conditions on attrition of NaCl crystals. *Powder Technology* 65(1), 311-320. https://doi.org/10.1016/0032-5910(91)80195-O.
Ghadiri, M., & Zhang, Z. (2002). Impact attrition of particulate solids. Part 1: A theoretical model of chipping. *Chemical Engineering Science* 57(17), 3659-3669. https://doi.org/10.1016/S0009-2509(02)00240-3.
Gupta, V., Sun, X., Xu, W., Sarv, H., & Farzan, H. (2017). A discrete element method-based approach to predict the breakage of coal. *Advanced Powder Technology* 28(10), 2665-2677. https://doi.org/10.1016/j.apt.2017.07.019.
Gupta, V.K. (2017). Effect of size distribution of the particulate material on the specific breakage rate of particles in dry ball milling. *Powder Technology* 305, 714-722. https://doi.org/10.1016/j.powtec.2016.10.075.
Han, J., Fitzpatrick, J., Cronin, K., Maidannyk, V., & Miao, S. (2020). Breakage of infant milk formula through three different processing methods and its influence on powder properties. *Journal of Food Engineering* 282, 109997. https://doi.org/10.1016/j.jfoodeng.2020.109997.
Hanley, K.J., 2011. Experimental quantification and modelling of attrition of infant formulae, Department of Process and Chemical Engineering. University College Cork, Cork, Ireland.
Hanley, K.J., Byrne, E.P., Cronin, K., Oliveira, J.C., O'Mahony, J.A., & Fenelon, M.A. (2011). Effect of pneumatic conveying parameters on physical quality characteristics of infant formula. *Journal of Food Engineering* 106(3), 236-244. https://doi.org/10.1016/j.jfoodeng.2011.04.029.
Hazlett, R., Schmidmeier, C., & O'Mahony, J.A. (2020). Influence of mechanical integrity during pneumatic conveying on the bulk handling and rehydration properties of agglomerated dairy powders. *Journal of Food Engineering*, 110103. https://doi.org/10.1016/j.jfoodeng.2020.110103.
Hu, X., Zhao, M., Li, L., Yang, B., Yang, X., Wang, H., & Ren, J. (2014). Emulsifying properties of cross-linking between proteins extracted from cold/hot pressed peanut meal and hydrolysed fish (Decapterus maruadsi) proteins. *International Journal of Food Properties* 17(8), 1750-1762. https://doi.org/ 10.1080/10942912.2012.724755.
Iveson, S.M., Litster, J.D., Hapgood, K., & Ennis, B.J. (2001). Nucleation, growth and breakage phenomena in agitated wet granulation processes: a review. *Powder Technology* 117(1), 3-39. https://doi.org/10.1016/S0032-5910(01)00313-8.
King, R.P. (2012). *Modeling and simulation of mineral processing systems*. Society for Mining, Metallurgy, and Exploration (SME).
Konami, M., Tanaka, S., & Matsumoto, K. (2002). Attrition of granules during repeated pneumatic transport. *Powder Technology* 125(1), 82-88. https://doi.org/10.1016/S0032-5910(02)00002-5.
Kotzur, B.A., Berry, R.J., Zigan, S., García-Triñanes, P., & Bradley, M.S.A. (2018). Particle attrition mechanisms, their characterisation, and application to horizontal lean phase pneumatic conveying systems: A review. *Powder Technology* 334, 76-105. https://doi.org/10.1016/j.powtec.2018.04.047.
Little, L., Mainza, A.N., Becker, M., & Wiese, J.G. (2016). Using mineralogical and particle shape analysis to investigate enhanced mineral liberation through phase boundary fracture. *Powder Technology* 301, 794-804. https://doi.org/10.1016/j.powtec.2016.06.052.
Materic, V., Holt, R., Hyland, M., & Jones, M.I. (2014). An internally circulating fluid bed for attrition testing of Ca looping sorbents. *Fuel* 127, 116-123. https://doi.org/10.1016/j.fuel.2013.10.071.

Mun, S., McClements, D.J., & Surh, J. (2011). Influence of maltodextrin addition on the freeze-dry stability of β-lactoglobulin-based emulsions with controlled electrostatic and/or steric interactions. *Food Science and Biotechnology* 20(4), 1143. https://doi.org/ 10.1007/s10068-011-0156-9.

Murrieta-Pazos, I., Gaiani, C., Galet, L., & Scher, J. (2012). Composition gradient from surface to core in dairy powders: Agglomeration effect. *Food Hydrocolloids* 26(1), 149-158. https://doi.org/10.1016/j.foodhyd.2011.05.003.

Niro, G. (2006). GEA Niro analytical methods dry products. *GEA Process Engineering A/S, Gladsaxevej, Denmark,*.

Norazirah, A., Fuad, S.H.S., & Hazizan, M.H.M. (2016). The effect of size and shape on breakage characteristic of mineral. *Procedia Chemistry* 19, 702-708. https://doi.org/10.1016/j.proche.2016.03.073.

O'Donoghue, L.T., Haque, M.K., Kennedy, D., Laffir, F.R., Hogan, S.A., O'Mahony, J.A., & Murphy, E.G. (2019). Influence of particle size on the physicochemical properties and stickiness of dairy powders. *International Dairy Journal* 98, 54-63. https://doi.org/10.1016/j.idairyj.2019.07.002.

Ortega-Rivas, E., Juliano, P., & Yan, H. (2006). *Food Powders: Physical Properties, Processing, and Functionality*. Springer US.

Petukhov, Y., & Kalman, H. (2004). Empirical breakage ratio of particles due to impact. *Powder Technology* 143-144, 160-169. https://doi.org/10.1016/j.powtec.2004.04.009.

Raman, V., & Abbas, A. (2008). Experimental investigations on ultrasound mediated particle breakage. *Ultrasonics Sonochemistry* 15(1), 55-64. https://doi.org/10.1016/j.ultsonch.2006.11.009.

Reynolds, G.K., Fu, J.S., Cheong, Y.S., Hounslow, M.J., & Salman, A.D. (2005). Breakage in granulation: A review. *Chemical Engineering Science* 60(14), 3969-3992. https://doi.org/10.1016/j.ces.2005.02.029.

Salman, A.D., Fu, J., Gorham, D.A., & Hounslow, M.J. (2003). Impact breakage of fertiliser granules. *Powder Technology* 130(1), 359-366. https://doi.org/10.1016/S0032-5910(02)00237-1.

Salman, A.D., Ghadiri, M., & Hounslow, M.J. (2007). *Handbook of technology--particle breakage*.

Salman, A.D., Hounslow, M.J., & Verba, A. (2002). Particle fragmentation in dilute phase pneumatic conveying. *Powder Technology* 126(2), 109-115. https://doi.org/10.1016/S0032-5910(02)00048-7.

Scala, F., Chirone, R., & Salatino, P. (2013). 6 - Attrition phenomena relevant to fluidized bed combustion and gasification systems. In F. Scala (Ed.), *Fluidized Bed Technologies for Near-Zero Emission Combustion and Gasification* (pp. 254-315). Woodhead Publishing, https://doi.org/10.1533/9780857098801.1.254.

Scala, F., Montagnaro, F., & Salatino, P. (2007). Attrition of limestone by impact loading in fluidized beds. *Energy & Fuels* 21(5), 2566-2572. https://doi.org/ 10.1021/ef0700580.

Shan, J., Xu, S., Liu, Y., Zhou, L., & Wang, P. (2018). Dynamic breakage of glass sphere subjected to impact loading. *Powder Technology* 330, 317-329. https://doi.org/10.1016/j.powtec.2018.02.009.

Tran, A.L.H., 2015. Powder flow in vertical high shear mixer granulators, School of Chemical Engineering. The University of Queensland.

van den Dries, K., de Vegt, O.M., Girard, V., & Vromans, H. (2003). Granule breakage phenomena in a high shear mixer; influence of process and formulation variables and consequences on granule homogeneity. *Powder Technology* 133(1), 228-236. https://doi.org/10.1016/S0032-5910(03)00106-2.

van Laarhoven, B., Schaafsma, S.H., & Meesters, G.M.H. (2012). Toward a desktop attrition tester; validation with dilute phase pneumatic conveying. *Chemical Engineering Science* 73, 321-328. https://doi.org/10.1016/j.ces.2011.08.038.

Walton, D.E., & Mumford, C.J. (1999). Spray dried products-characterization of particle morphology. *Chemical Engineering Research and Design* 77(1), 21-38. https://doi.org/10.1205/026387699525846.

Wu, F., & Wu, D. (2017). Attrition resistances and mechanisms of three types of FCC catalysts. *Powder Technology* 305, 289-296. https://doi.org/10.1016/j.powtec.2016.09.077.

Yan, H., & Barbosa-Cánovas, G.V. (2001). Attrition evaluation for selected agglomerated food powders: the effect of agglomerate size and water activity. *Journal of Food Process Engineering* 24(1), 37-49. https://doi.org/ 10.1111/j.1745-4530.2001.tb00530.x.

Yan, H., & Barbosa-Cánovas, G.V. (2001). The effect of padding foam on the compression characteristics of some agglomerated food powders. *Food Science and Technology International* 7(5), 417-423. https://doi.org/ 10.1106/wc69-qfnv-vn6e-lh00.

Zhang, Z., & Ghadiri, M. (2002). Impact attrition of particulate solids. Part 2: Experimental work. *Chemical Engineering Science* 57(17), 3671-3686. https://doi.org/10.1016/S0009-2509(02)00241-5.

Zhao, R., Goodwin, J.G., & Oukaci, R. (1999). Attrition assessment for slurry bubble column reactor catalysts. *Applied Catalysis A: General* 189(1), 99-116. https://doi.org/10.1016/S0926-860X(99)00261-6.

CHAPTER THREE

Effects of different breakage mechanisms on the physical, water sorption, and mechanical characteristics of infant milk formula

Chapter 3 was published in:

Han, J., Fitzpatrick, J., Cronin, K., & Miao, S. (2022). Effects of different breakage mechanisms on the physical, water sorption, and mechanical characteristics of infant milk formula. *Journal of Food Engineering*, 110939.

The work contained in this chapter was undertaken and written solely by myself with specific contributions from each co-author:

Jie Han: Conceptualization, Methodology, Formal analysis, Investigation, Data curation, Writing – original draft, Visualization

John Fitzpatrick: Supervision, Writing – review & editing

Kevin Cronin: Supervision, Writing – review & editing

Song Miao: Supervision, Conceptualization, Writing – review & editing, Funding acquisition, Project administration

Abstract

Two main breakage mechanisms, surface breakage and body breakage, were both found during laboratory dilute-phase pneumatic conveying and high-speed mixing of infant milk formula, respectively. Body breakage had a greater influence on powder physical properties, particle shapes, and surface composition than surface breakage. In particular, the particle size of samples decreased by only 10% after surface breakage but by 60% after body breakage. For samples where body breakage predominated, significant changes to both water sorption and mechanical properties of the powder were seen while surface breakage had very little effect on them. Body breakage significantly increased the water sorption rate of samples, at around 10% to 126% higher than the other samples for the first 3 h, which accelerated the time-dependent crystallization. Moreover, at a_w 0.11 to 0.33, the final water contents of body breakage samples were 3.5% to 22% higher than control samples. This decreased the crystallization temperature, by between 2°C to 10°C, and the overall molecular mobility of samples. These changes were due to the increase in the number of adsorbed monolayers, sorption surface area, and monolayer value of samples after body breakage.

Keywords: Infant milk formula; Surface breakage; Body breakage; Physical properties; Water sorption behaviour; Mechanical characteristics

3.1. Introduction

In Chapter 2, three possible breakage mechanisms have been found for agglomerated infant milk formula (IMF), that are dispersion, surface breakage, and body breakage (Han et al., 2021a). Studies have shown that the changes in powder particle size distributions (PSD) indicate the breakage mechanisms (Han et al., 2021a; Materic et al., 2014; Scala et al., 2007; Wu and Wu, 2017). When the processing condition is very gentle, dispersion may occur on clusters that are particles attracted together by cohesiveness. The mechanical force can disperse clusters into their individual component particles, which shifts the PSD to a smaller value with no production of fines

(Han et al., 2021a). When powders are exposed to low-level external mechanical stress, surface breakage produces tiny particles while the main body of the original particle still retains its integrity. Body breakage tends to produce a few coarse fragments or many smaller particles. Different breakage mechanisms result in different PSDs and particle sizes of the final samples, which then can influence powder properties.

It has been reported that powder breakage significantly increased densities and reduced the particle size of several agglomerated milk powders (Boiarkina et al., 2016; Han et al., 2020; Hanley, 2011; Hazlett et al., 2020). Furthermore, the changes in physical properties seriously led to a decline in the flowability and rehydration properties of powders (Han et al., 2020; Hazlett et al., 2020). In addition to these properties, water sorption and plasticization behaviour are also important for the physicochemical properties of dairy powders containing amorphous lactose. Spray-drying processes often produce amorphous lactose that is a nonequilibrium state with limited molecular mobility and high viscosity (Haque and Roos, 2006). The amorphous lactose tends to absorb moisture resulting in plasticization and is very sensitive to relative humidity and temperature (Saxena et al., 2019). When lactose is plasticized by moisture, or the environmental temperature higher than the glass transition temperature (T_g), the molecular mobility increases, which subsequently results in lactose rearranging into the highly ordered crystalline state (Saxena et al., 2019). This causes some further water liberation which enhances many deteriorative changes of dairy powders, such as stickiness, caking, non-enzymatic browning and significantly decreases storage stability and quality (Haque and Roos, 2004). Besides, the mechanical properties of dairy powders, including the storage modulus, loss modulus and α-relaxation are influenced by the molecular mobility which significantly changes at and above the T_g (Li et al., 2016c; Maidannyk et al., 2020). However, there is currently no published data on the influence of different breakage mechanisms on the water sorption behaviour and mechanical characteristics (such as the glass transition, crystallization, α-relaxation, storage modulus, and loss modulus) of dairy powders. Such

research is essential to increase the knowledge of dairy powder breakage and will assist efforts in the quality control of powders.

This chapter aims to fill this gap. Commercial agglomerated IMF was chosen due to its comprehensive composition and large particles. A laboratory dilute-phase pneumatic conveyor and high-speed mixer were used to mimic the industrial-scale processes that cause particle breakage, including in-plant pneumatic conveying transportation and dry mixing in the 'dry blending' process during IMF production. The main breakage mechanisms during different processing methods were determined, followed by the investigation of physical, water sorption and mechanical properties of broken samples caused by different mechanisms.

3.2. Material and methods

3.2.1. Material

Two commercial agglomerated IMF, purchased from a local grocery store (Cork, Ireland), Aptamil Profutura (termed A, composition: 9.57% protein, 22.34% fat and 47.23% lactose) and HIPP organic combiotic (termed B, composition: 8.57% protein, 17.76% fat and 51.43% lactose) follow on milk 'stage 2', were selected because of their significant differences in physical properties, especially for the particle size and PSD. Figure 3-1 shows their PSDs and light microscopy photos.

3.2.2. Sample preparation

Powders (50 g) were transported by the laboratory pneumatic conveyor (presented in Figure 2-1B) with a feeding rate of 3.0 g/s and an air velocity of 30 or 40 m/s (called PC30 and PC40, respectively). Samples (50 g) were fed to the lab-scale high-speed mixer (presented in Figure 2-1C) operated for two different durations of 2 and 6 mins (called HM2 and HM6, respectively). For each process method, 250 g of each sample was broken and mixed for the following measurement. The particle size of each batch was compared

before mixing and there were no significant differences between the batches (data not shown).

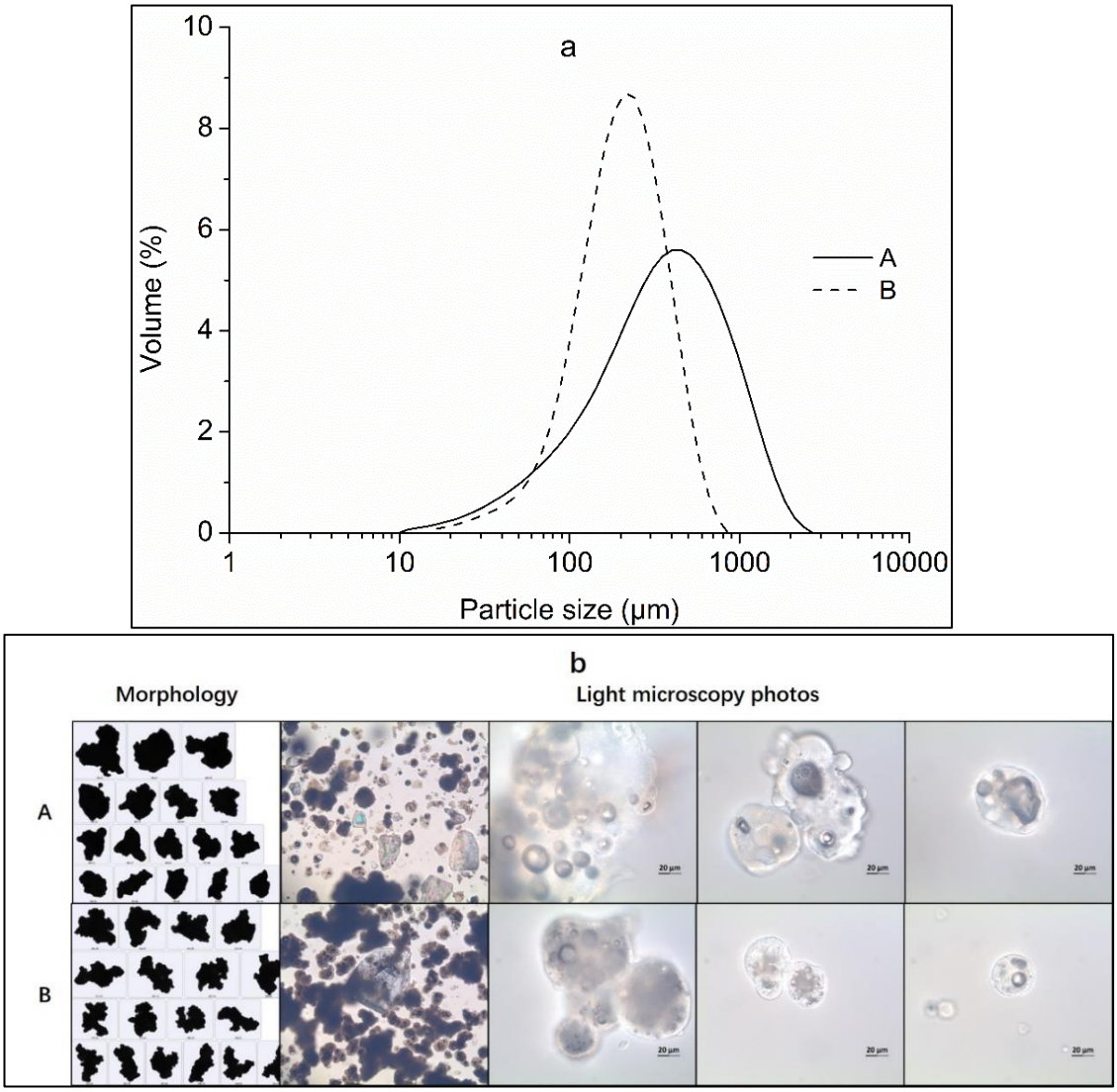


Figure 3-1. Particle size distribution (a) and microscopy photos (b) of samples. A: Apt Pro stage 2 infant milk formula. B: Hipp stage 2 infant milk formula.

The processing conditions used above were selected based on the result of Chapter 2 (Han et al., 2021a) and the aim of this chapter. In Chapter 2, it was found that the main breakage mechanism during high-speed mixing was body breakage and during pneumatic conveying was surface breakage. Pneumatic conveying and high-speed mixing were chosen for this chapter because samples after transportation by powder venturi feeder could not be collected and also this chapter aims to investigate the influence of different breakage mechanisms on powder properties. The main breakage mechanisms during these two treatments were different, which met the

objectives of this study. In addition, in order to control the number of samples, two levels of flow velocity and treatment time were used to ensure different breakage mechanisms could be expected.

3.2.3. Breakage mechanisms determination

The dominant breakage mechanisms were determined according to the changes in PSD of samples before and after breakage, following the method described in Chapter 2. A Malvern Mastersizer 3000 (Malvern Instruments Ltd., Worcestershire, UK) was used to measure the volume- and number-PSD of powders, according to the method described in 2.2.2.1.

The breakage mechanisms of samples broken in the higher-speed mixing were clear (and will be described in 3.3.1). In order to identify the primary breakage mechanisms of whole samples broken in the pneumatic conveying, samples were sieved into five size fractions, greater than 355 μm, from 355 to 250 μm, from 250 to 180 μm, from 180 to 125 μm, and less than 125 μm (called >355, 355-250, 250-180, 180-125, and <125, respectively). The mass percentages of each component (>355, 355-250, 250-180, 180-125, and <125) to the whole sample were 42.41%, 13.57%, 12.94%, 10.18%, and 20.90% for sample A, respectively, and were 9.88%, 16.58%, 27.43%, 24.73%, and 21.39% for sample B, respectively. Fractions were transported using the dilute-phase pneumatic conveyor, as described in 3.2.2, and then measured the PSD.

3.2.4. Determination of powder physical properties

3.2.4.1. Specific surface area and particle size

The specific surface area (SSA) and Sauter mean particle size ($D_{3,2}$) of the volume PSD of powders were measured using the Mastersizer 3000 with the transportation air pressure at 0.2 bar, as described in 2.2.2.1.

3.2.4.2. Friability

Friability assesses the susceptibility to the loss of component particles due to abrasion, friction, or mechanical shock. In food powders, friability refers to

the tendency of particulates to break down in size during handling or storage under the influence of physical forces (Ortega-Rivas et al., 2006), shown as friability indices (*FI*), which can be used to represent particle strength. Friability can be commonly determined using the shear, impact, compression, and vibration tests either on a bulk of particles or on a single particle, and different methods used different friability indices, such as the production of fragments and the changes in particle size. In this study, the friability index of powders was deduced from the results of particle size which was measured by the Mastersizer 3000 with different compressed air pressures, as described in 2.2.2.1. *FI* can be calculated as Eq. (3-1) (Schuck et al., 2012) and the bigger the *FI*, the easier it is for particles to be broken

$$FI = \left(\frac{D32_{\,0.5} - D32_{\,4.0}}{D32_{\,0.5}}\right) \times 100\% \qquad \text{Eq. (3-1)}$$

where $D32_{0.5}$ and $D32_{4.0}$ were the $D_{3,2}$ measured with compressed air at 0.5 and 4.0 bar, respectively.

3.2.4.3. Densities and porosity

Bulk densities (tapped (100 taps) bulk density (ρ_{tapped}) and loose bulk density (ρ_b)), particle density (ρ_p), and porosity (ε) of samples were measured according to the method as described in 2.2.2.2.

3.2.5. Powder surface composition

The relative amounts of C1s, N1s, and O1s at the surface of milk powder particles were determined by X-ray photoelectron spectroscopy measurements (XPS) using a Kratos AXIS Ultra spectrometer (Kratos Analytical Ltd., Manchester, UK). Any elements not detected may be absent or below the detection limit of the XPS (< 0.1 atomic %). From C, N, and O percentages, the relative amount of fat, lactose and protein (other components were neglected) of some dairy powders have been calculated with a matrix formula created from the elemental composition of the pure milk components (the relative atomic %: lactose - C, 61.6, O, 38.4; milk fat - C, 88.4, O, 11.6; whey proteins - C, 68.0, O, 17.6, N, 13.8) (Faldt et al., 1993; Murrieta-Pazos et al., 2012a). However, fat in IMF samples was mixed

vegetable oil so the relative content of fat, lactose and protein could not be calculated without the standard relative amount of C, N, and O of the mixed vegetable oil. Nevertheless, the N content can represent the relative protein content because only protein contains nitrogen.

3.2.6. Morphological characteristics

Three shape factors, convexity, elongation, and circularity, were used to indicate how similar the shape of a particle is to a perfect circle with values ranging from 0 to 1 (Ji et al., 2015). Convexity indicates particle surface roughness and the convexity of a smooth shape is 1. Elongation is calculated from [1-aspect ratio], where the value of shapes symmetrical in all axes, such as a circle or square, is 0. The circularity of a perfect circle is 1. The morphology of powders was determined via scanning and analyzing thousands of individual particles using a Malvern Morphologi G3 (Malvern Instruments Ltd.). Powders were dispersed into a single uniform layer and particles were well separated. Then all the particles were gradually scanned by the microscope and the average values were given.

3.2.7. Water sorption behaviour

3.2.7.1. Water sorption and time-dependent lactose crystallization

The static gravimetric method was used to determine the water sorption behaviour of IMF samples and the decrease in the sorbed water was a result of time-dependent lactose crystallization. Samples (1 g) were dried at 45°C in a vacuum oven (OV-12, Lab Companion, Daejeon, Korea) for 48 h. Powders were then equilibrated at 25 ºC for 168 h at different relative water vapor pressures (RVP) provided by different saturated salt solutions. They were NaCl, $NaNO_2$, $Mg(NO_3)_2$, K_2CO_3, $MgCl_2$, CH_3COOK, and LiCl which gave RVP of 76.1%, 65.6%, 54.5%, 44.1%, 33.2%, 23.1%, and 11.4%, respectively. Samples were weighed at 0, 3, 6, 9, 12, 24 h and then at 24 h intervals. The result was presented as the equilibrated water content of 100 g dry matter (based on non-fat solids as fat cannot absorb moisture (Kelly et

al., 2015; Maidannyk et al., 2019)). The average was calculated from triplicate samples.

According to the water contents at different time points, the average water sorption rate of every 3 h in the first 48 h was calculated as Eq. (3-2) (Li et al., 2016b). It is hypothesized that the sorption rate during the calculated 3 h was constant.

$$Sorption\ rate\ = \frac{Absorbed\ water}{time}\ (\%h^{-1}) \quad \text{Eq. (3-2)}$$

The experimental sorption data at RVP ≤44.1% was analyzed and correlated by the GAB (Guggenheim-Anderson de Boer) isotherm model that was given by Eq. (3-3). The constant α, β, and γ of its second-order polynomial (Eq. (3-4)) were calculated by plotting a_w/m against a_w where a_w was the water activity, and m (g/100g non-fat dry solid) was the equilibrium water content. The monolayer moisture content m_m (g/100g non-fat dry solid) and the constant K and C were calculated from Eq. (3-5) to (3-7), respectively.

$$\frac{m}{m_m} = \frac{CKa_w}{(1-Ka_w)(1-Ka_w+CKa_w)} \quad \text{Eq. (3-3)}$$

$$\frac{a_w}{m} = \alpha {a_w}^2 + \beta a_w + \gamma \quad \text{Eq. (3-4)}$$

$${m_m}^2 = -\frac{1}{4\alpha\gamma-\beta^2} \quad \text{Eq. (3-5)}$$

$$K = \frac{\beta-\frac{1}{m_m}}{-2\gamma} \quad \text{Eq. (3-6)}$$

$$C = \frac{1}{m_m\gamma K} \quad \text{Eq. (3-7)}$$

An indication of the fit of the GAB model, RMS (relative percentage Root Mean Square), was calculated from Eq. (3-8)

$$\%RMS = \sqrt{\frac{\sum_i^N\left[\frac{m_i-{m_i}^*}{m_i}\right]^2}{N}} \times 100 \quad \text{Eq. (3-8)}$$

where N was the number of experimental points, and m_i and m_i* were the experimental and the calculated moisture content, respectively.

3.2.7.2. Sorbed water properties

Some properties of sorbed water were analyzed using the linear form of Caurie's equation (Mazza and LeMaguer, 1978) (Eq. (3-9)), where c_d was the density of sorbed water (g/ml), and m and m_c were the equilibrium and monolayer moisture contents (g/100g non-fat dry solid), respectively. The number of adsorbed monolayers (N_{am}) and the surface area of adsorbent (A, m^2/g) were calculated from Eq. (3-10) and (3-11), respectively, where S was the slope of Eq. (3-9) (Červenka et al., 2015).

$$ln\left(\frac{1}{m}\right) = -ln(c_d m_c) + \frac{2c_d}{m_c} ln\frac{1-a_w}{a_w} \quad \text{Eq. (3-9)}$$

$$N_{am} = 2/S \quad \text{Eq. (3-10)}$$

$$S = 54.45/A \quad \text{Eq. (3-11)}$$

3.2.7.3. Spreading pressure

Spreading pressure (φ, J/m^2) is one of the thermodynamic properties which can be used to analyze the sorption phenomena. It is also known as surface potential, representing the excess free energy on the surface and has been used as the diffusion driving force in porous solids (Polatoğlu et al., 2011). φ is an indicator of the increase in surface tension in the free sorption sites because of the adsorption of molecules (Simón et al., 2016). High φ values indicate the high affinity of water molecules to active sites (Torres et al., 2012). φ was determined from Eq. (3-12)

$$\varphi = \frac{K_B T}{A_m} ln\left[\frac{1+CKa_w-Ka_w}{1-Ka_w}\right]_{0.05}^{a_w} \quad \text{Eq. (3-12)}$$

where the Boltzmann constant K_B was 1.380×10^{-23} J/K, T was the temperature (K), A_m was the surface area of a water molecule (1.06×10^{-19} m^2), and C and K were the constants in the GAB isotherm model (Lago et al., 2013). 0.05 was used as the lowest limit of Eq. (3-12) because the integral value of a_w=0 is indeterminate (Iglesias et al., 1976).

3.2.8. Glass transition, initial crystallization and α-relaxation

A differential scanning calorimeter (DSC Q2000, TA Instruments, Crawley, UK) was used to determine T_g (onset) and initial crystalized temperatures

(T_{ic}) of samples equilibrated for 168 h at different RVP (11.4%, 23.1%, 33.2%, and 44.1%). Besides, a Dynamic Mechanical Analyzer (DMA Q800, TA Instruments) was used to measure the dynamic mechanical properties of those equilibrated samples, including storage modulus, loss modulus and *α*-relaxation with multiple frequencies (0.5, 1, 2, 5 and 10 Hz). The temperatures of loss modulus peak values were taken as *α*-relaxation temperatures (T_{α}). Measurements followed the methods described by Li et al. (2016a).

3.2.9. Experimental design and statistical analysis

Measurements of powder surface composition, T_g, T_{ic}, T_{α}, and modulus changes were carried out in duplicate, and all other measurements were performed in triplicate. Results were shown as mean ± standard deviation (SD). One-way ANOVA with Tukey's test (IBM SPSS Statistics version 24, IBM, USA) was used to determine significant differences with a confidence level of P <0.05.

3.3. Result and discussion

3.3.1. Breakage mechanisms determination

The dominant breakage mechanisms (not necessarily the sole one) of IMF samples were determined according to the PSDs changes before and after breakage. The volume- and number-PSD of whole powders are given in Figure 3-2. At the same processing conditions, the changes in PSD of the two whole samples were similar and compared with sample B (Figure 3-2c&d), more breakage occurred for sample A (Figure 3-2a&b) during mixing.

It was shown that after mixing for 2 or 6 mins, the PSDs of the two samples significantly moved to the smaller value and most of the initial big-sized mother particles were broken into many small-sized child particles. This observation was supported by the movement of the number-PSD to the smaller value and most of the particles were small-sized particles. These

results suggest that the main breakage mechanism after mixing for two IMF samples was body breakage.

Compared with mixing samples, there was not enough evidence to easily identify the main breakage mechanisms of the pneumatic conveying samples based only on the changes in PSDs of whole samples because there was no bimodal PSDs or other features. Thus, the volume PSD of sieved fractions of the two samples before and after transportation are given in Figure 3-3. For sample A (Figure 3-3a-c), transportation impacted the PSD of particles bigger than 250 μm. The larger the particles, the more sensitive they were to transportation, and the greater the PSD changed. It has been attributed to the likelihood of a greater number of imperfections in larger particles (Antonyuk et al., 2005; Norazirah et al., 2016). The highest local tensile stress is generated at these defective zones so that the fracture initiates from this zone and propagates. Besides the few flaws, small particles are more difficult to break owing to the stronger interparticle forces that bind particles together including van der Waals forces, electrostatics, and liquid bonds (Reynolds et al., 2005). From an energy perspective, the smaller the particles, the higher the fracture energy, and hence the less likely the particle will break (King, 2012). For samples A>355 and A355-250, the main particles were still big-sized particles but large numbers of small particles were produced and appeared as a well-separated peak on the left in PSDs. This means that surface breakage most likely occurred for these particles. For the other three small-sized fractions of sample A, the PSD slightly shifted to the smaller value for A250-180 and A180-125 without the production of small particles, and the PSD curves of A<125 were similar. This means that the slight decrease of particle size for A250-180 and A180-125 might be because of dispersion. These results indicate that the breakage of sample A during pneumatic conveying mostly occurred on particles bigger than 250 μm. Besides, the mass percentage of A>355 and A355-250 to the whole sample was around 56%. Thus, it can be concluded that surface breakage occurred on around 56% of particles of sample A after pneumatic conveying. Similarly, for sample B (Figure 3-3d-g), surface breakage most likely occurred at all air velocities transportation for B355-250 and 40 m/s

conveying for B250-180 while dispersion was the main breakage mechanism for B180-125. Unlike A>355, low-degree body breakage most likely occurred for B>355 after transportation but its mass percentage to the whole sample was only 10%. Thus, the breakage of sample B during pneumatic conveying mostly occurred on particles bigger than 180 μm and the dominant mechanism was surface breakage.

Overall, for the two samples, particle breakage after high-speed mixing was mainly due to body breakage, while breakage after the dilute-phase pneumatic conveying was mainly caused by surface breakage which occurred on big-sized particles. Different breakage mechanisms showed different effects on powder physical properties and subsequently on water sorption and mechanical properties, which will be discussed in the next few sections.

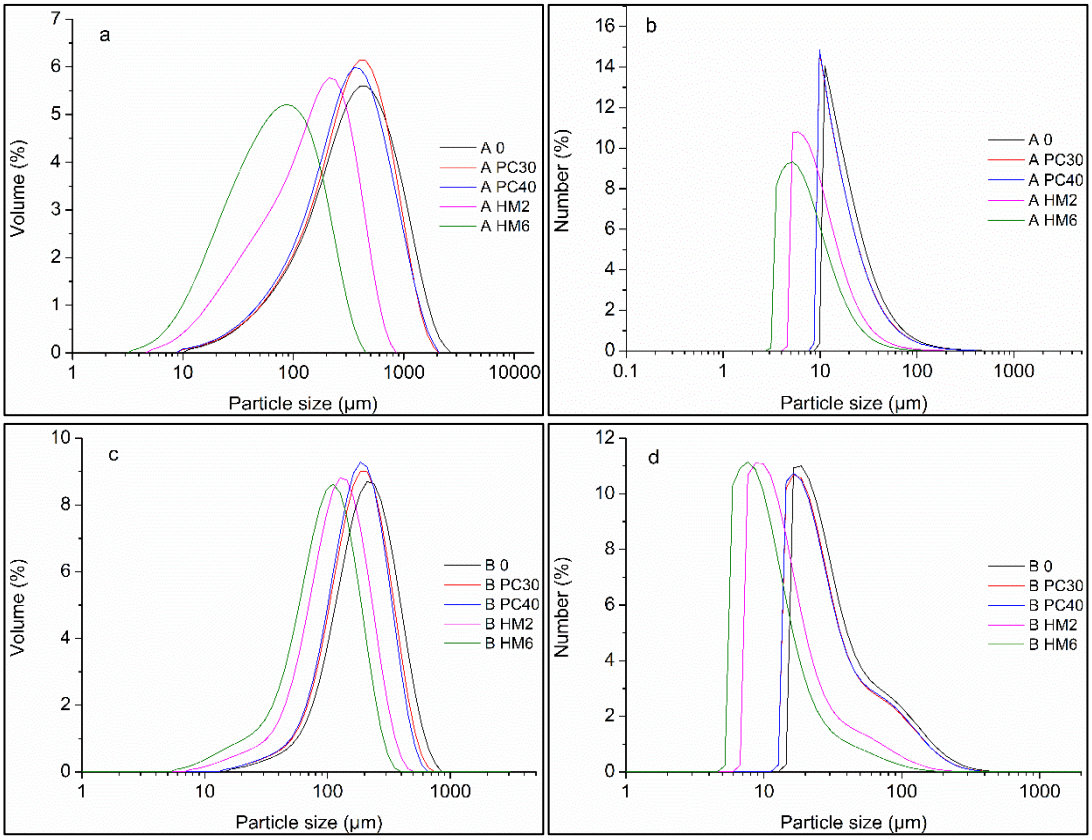


Figure 3-2. Volume- (a and c) and number-particle size distributions (b and d) of whole infant milk samples. A: Apt Pro stage 2 infant milk formula. B: Hipp stage 2 infant milk formula. 0: control samples. PC: broken by pneumatic conveying under the air velocity of 30 m/s and 40 m/s. HM: broken by the laboratory high-speed mixer for 2 min and 6 min.

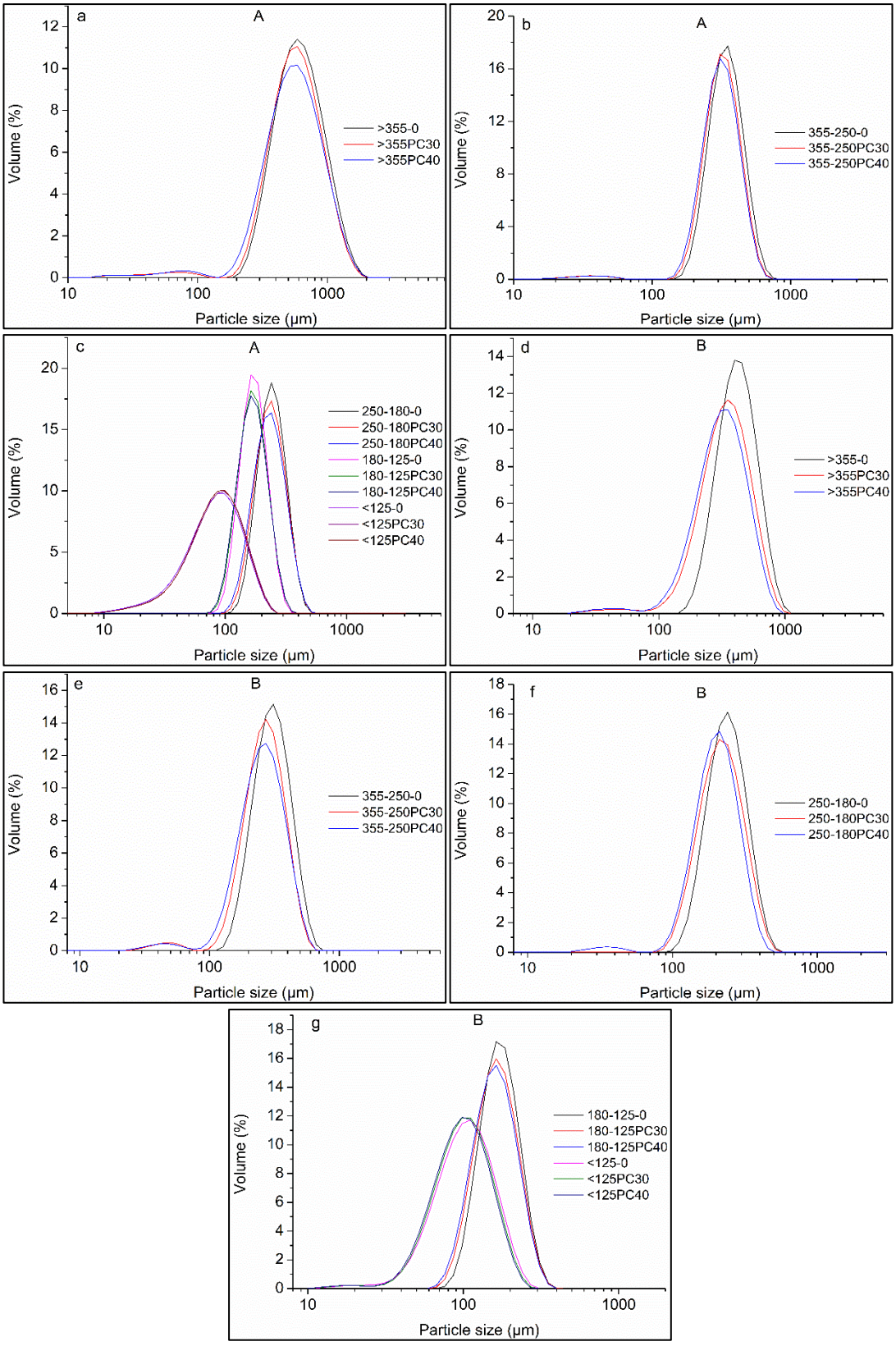


Figure 3-3. Particle size distributions of sieved fractions of infant milk samples (a-c: sample A; d-g: sample B). A: Apt Pro stage 2 infant milk formula. B: Hipp stage 2 infant milk formula. 0: control samples. PC: broken by pneumatic conveying under the air velocity of 30 m/s and 40 m/s. HM: broken by the laboratory high-speed mixer for 2 min and 6 min.

3.3.2. Powder characterization

3.3.2.1. Particle size and friability

The $D_{3,2}$ and its percentage change compared with control samples are shown in Table 3-1. The $D_{3,2}$ of broken powders was significantly lower (P<0.05) than those of control powders and body breakage had a greater effect on the decrease of $D_{3,2}$ than surface breakage. This is consistent with the results of PSD changes. From Table 3-1, the $D_{3,2}$ decreased by around 10% after surface breakage but body breakage decreased it considerably more with reductions of 45 to 80%. Compared with sample A, the particle size of sample B decreased more after surface breakage while decreased less after body breakage. It has been reported that the strength of agglomerates decreased with increasing particle size (Fu et al., 2005; Han et al., 2021b). This is consistent with the results of *FI* that was decreased with decreasing particle size or the increasing breakage degree (Table 3-1). Thus, the reason for the higher $D_{3,2}$ decreases of sample A after body breakage might be because the initial particle size of sample A was bigger than that of sample B. This also explained why the *FI* of A samples were higher than those of B samples. However, this contradicted with the result that the $D_{3,2}$ of sample B decreased more after surface breakage. This might be because there were more big-sized crystalline particles in sample A (Figure 3-1b). For crystalline particles, the breakage may occur at the interface of crystals instead of on the surface (Cleaver et al., 1993; Ghadiri et al., 1991). This means, at low processing conditions, compared with crystalline particles, the normal agglomerated dairy particles may be more sensitive to the mechanical force. This was supported by the analysis in 3.3.1 that at the same transportation condition, B>355 suffered body breakage while surface breakage occurred for A>355.

Table 3-1. Physical properties of infant milk formula samples.

Samples	Particle size $D_{3,2}$ (μm)	Percentage change in $D_{3,2}$ (%)	Friability index (%)	Particle density (Kg/L)	Loose bulk density (Kg/L)	Tapped bulk density (Kg/L)	Porosity (%)	SSA (m^2/kg)
IMF-A								
0	200.0^{a}±2.4	/	53.0^{b}±2.3	0.984^{e}±0.001	0.438^{a}±0.001	0.587^{e}±0.002	40.4^{e}±0.2	30.5^{e}±0.4
PC30	187.3^{b}±2.6	6.3^{d}±1.4	52.4^{b}±0.6	0.997^{d}±0.001	0.444^{a}±0.002	0.608^{d}±0.002	39.1^{d}±0.2	32.1^{d}±0.5
PC40	178.0^{c}±2.2	11.0^{c}±1.1	55.9^{a}±0.2	0.992^{c}±0.002	0.442^{a}±0.001	0.616^{c}±0.001	37.9^{c}±0.1	34.0^{c}±0.4
HM2	74.4^{d}±0.7	62.8^{b}±0.4	37.4^{c}±1.0	1.172^{b}±0.001	0.446^{a}±0.001	0.637^{b}±0.001	45.7^{b}±0.1	68.8^{b}±0.7
HM6	44.0^{e}±0.1	78.0^{a}	28.8^{b}±0.1	1.276^{a}±0.002	0.445^{a}±0.004	0.647^{a}±0.002	49.3^{a}±0.1	107.0^{a}±0.1
IMF-B								
0	165.0^{A}	/	45.7^{A}±0.6	1.214^{E}±0.001	0.465^{C}±0.002	0.571^{D}±0.001	52.9^{A}±0.1	30.0^{C}±0.1
PC30	148.0^{B}±0.8	10.3^{D}±1.3	41.5^{B}	1.217^{D}±0.001	0.491^{B}±0.003	0.593^{CD}±0.010	51.3^{AB}±0.8	33.4^{C}±0.3
PC40	143.3^{C}±1.2	13.1^{C}±1.1	40.6^{B}±1.1	1.219^{C}±0.001	0.499^{B}±0.013	0.611^{BC}±0.009	49.8^{BC}±0.7	34.4^{C}±0.3
HM2	91.4^{D}±0.6	44.6^{B}±0.4	31.3^{C}±0.4	1.234^{B}±0.001	0.527^{A}±0.003	0.640^{AB}±0.001	48.2^{CD}±0.1	56.1^{B}±4.2
HM6	68.5^{E}±0.2	58.5^{A}	26.3^{D}±0.2	1.251^{A}±0.001	0.543^{A}±0.003	0.663^{A}±0.007	47.0^{D}±0.6	70.1^{A}±0.3

1. IMF-A: Apt Pro stage 2 infant milk formula. IMF-B: Hipp stage 2 infant milk formula. 0: control samples. PC: broken by pneumatic conveying under the air velocity of 30 m/s and 40 m/s. HM: broken by the laboratory high-speed mixer for 2 min and 6 min. SSA: specific surface area.
2. Values are mean ± standard deviation (n=3).
3. $^{a-e}$ and $^{A-E}$ different values within columns in IMF-A and IMF-B groups are significantly different at P <0.05, respectively.

3.3.2.2. Powder densities and porosity

The changes in densities and porosity may influence the water sorption behaviour of samples through affecting the number of liquid bridges (Carpin et al., 2017). Besides, the bulk density of powders is used to calculate the volumetric capacity of packing materials. It is an important property for IMF as they are dispensed on a volume basis using a scoop. From Table 3-1, as expected, the particle density of sample B, around 1.2 kg/L, did not change a lot even after body breakage, which has been found in previous research (Han et al., 2020, Chapter 4). However, the particle density of body breakage sample A significantly increased from 0.98 kg/L to around 1.2 kg/L. After breakage, particularly for body breakage, the bulk densities of sample B significantly increased and the porosity decreased. This corresponded with several studies on agglomerated milk powder breakage (Han et al., 2020; Hanley, 2011; Hazlett et al., 2020). Similarly, the tapped bulk density of sample A significantly increased after breakage, while no significant difference was observed for its loose bulk density. Besides, the porosity of sample A was significantly increased after body breakage because its particle density substantially increased.

3.3.2.3. Powder surface properties

Dairy powder breakage may influence the surface area and the surface composition of particles because of the production of more particles and the uneven distribution of ingredients throughout the particles. The changes in the surface properties might affect their water sorption behaviour (Li et al., 2016c). The SSA and the relative amounts of elements (C1s, O1s, N1s) on particles' surfaces are given in Table 3-1 and Figure 3-4, respectively. The SSA of the two initial samples were similar, around 30 m^2/kg, and it slightly increased after surface breakage but significantly increased to 60 to 100 m^2/kg after body breakage because of the production of more particles.

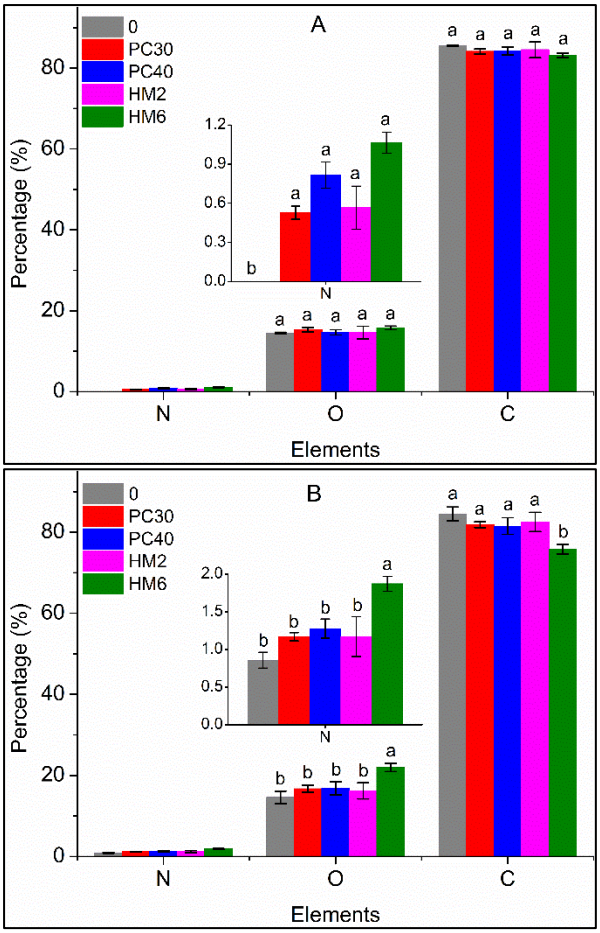


Figure 3-4. Relative elements (C, O, and N) on the surface of particles. A: Apt Pro stage 2 infant milk formula. B: Hipp stage 2 infant milk formula. 0: control samples. PC: broken by pneumatic conveying under the air velocity of 30 m/s and 40 m/s. HM: broken by the laboratory high-speed mixer for 2 min and 6 min. Different a-b values between samples in each group (A and B) within each element (C, O, and N) are significantly different at P <0.05.

From Figure 3-4, the amount of N was increased after breakage, which means that powder breakage increased the protein proportion on the surface of particles. Besides, around 80% of the element on the surface of IMF particles was C. It has been reported that the standard relative amounts of C and O on the surface of lactose were very close, 52.2% and 47.8%, respectively, but for fat and protein, the relative content of C was much higher than O (milk fat: 89.1% C and 10.9% O; casein: 65% C, 19% O, and 16% N) (Kim et al., 2002). This means that most of the particle surface was fat, consistent with previous research (O'Donoghue et al., 2019; O'Neill et al., 2019). In addition, after breakage, the relative amount of C and O slightly decreased and increased, respectively (Figure 3-4). These results suggest that powder breakage slightly decreased the fat and increased the lactose

proportions on the surface of particles, which could decrease particle hydrophobicity. This could be explained by the results of previous studies regarding the surface to core composition of agglomerated milk powder particles (Murrieta-Pazos et al., 2012b). For particles containing fat, the fat content significantly decreased from the surface to the core, and opposite behaviours were observed for proteins and lactose.

3.3.2.4. Morphological characteristics

Table 3-2. Morphological characteristics of infant milk formula samples.

Samples	Elongation	Circularity	Convexity
IMF-A			
0	$0.295^{a}\pm0.021$	$0.774^{b}\pm0.027$	$0.977^{b}\pm0.003$
PC30	$0.272^{ab}\pm0.007$	$0.804^{ab}\pm0.018$	$0.981^{b}\pm0.005$
PC40	$0.270^{b}\pm0.001$	$0.802^{ab}\pm0.010$	$0.979^{b}\pm0.005$
HM2	$0.284^{ab}\pm0.003$	$0.792^{ab}\pm0.012$	$0.980^{b}\pm0.004$
HM6	$0.276^{ab}\pm0.003$	$0.836^{a}\pm0.08$	$0.993^{a}\pm0.002$
IMF-B			
0	$0.240^{BC}\pm0.008$	$0.812^{D}\pm0.010$	$0.975^{D}\pm0.002$
PC30	$0.226^{CD}\pm0.002$	$0.836^{C}\pm0.004$	$0.981^{C}\pm0.001$
PC40	$0.225^{D}\pm0.004$	$0.838^{BC}\pm0.004$	$0.980^{C}\pm0.000$
HM2	$0.253^{AB}\pm0.001$	$0.855^{AB}\pm0.001$	$0.992^{B}\pm0.000$
HM6	$0.258^{A}\pm0.004$	$0.860^{A}\pm0.003$	0.995^{A}

1. IMF-A: Apt Pro stage 2 infant milk formula. IMF-B: Hipp stage 2 infant milk formula. 0: control samples. PC: broken by pneumatic conveying under the air velocity of 30 m/s and 40 m/s. HM: broken by the laboratory high-speed mixer for 2 min and 6 min
2. Values are mean ± standard deviation (n=3).
3. $^{a-b}$ and $^{A-D}$ different values within columns in IMF-A and IMF-B groups are significantly different at P <0.05, respectively.

The shape of particles can influence powder bulk density and porosity, which subsequently affects the water sorption property of powders. The morphological characteristics (circularity, convexity, and elongation) of samples are shown in Table 3-2. The elongation of samples largely remained unchanged before and after breakage, but the elongation of samples used in this study was higher than other non-agglomerated dairy powders (Li et al., 2017). This might be because granulated particles were more irregular. Compared with surface breakage particles, the circularity and convexity of most body breakage particles were significantly higher than those of their control samples. These results indicate that body breakage particles had more rounded shapes and smoother surfaces and surface breakage did not

significantly change particle shapes. This also can be observed from photos of some particles scanned by the Morphologi G3 (Figure 3-5).

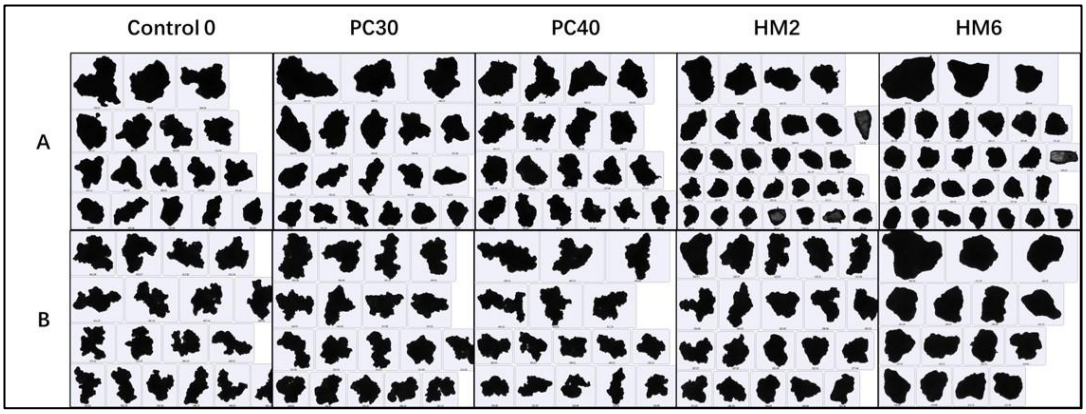
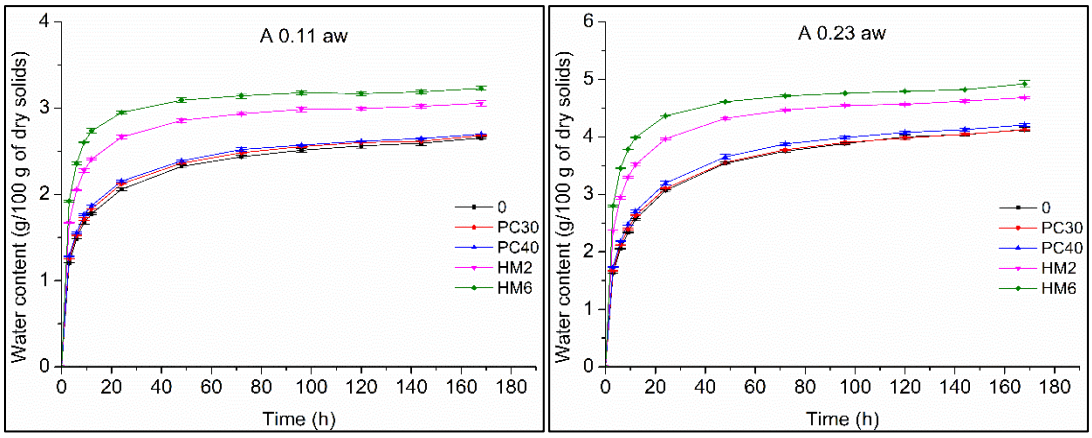


Figure 3-5. Photos of some particles in samples scanned by the Morphologi G3. A: Apt Pro stage 2 infant milk formula. B: Hipp stage 2 infant milk formula. 0: control samples. PC: broken by pneumatic conveying under the air velocity of 30 m/s and 40 m/s. HM: broken by the laboratory high-speed mixer for 2 min and 6 min.

3.3.3. Water sorption behaviour

3.3.3.1. Water sorption and time-dependent lactose crystallization

The influence of breakage on the water sorption behaviour of the two IMF samples was similar, thus the following discussion is mainly based on sample A. Water contents of A samples at several a_w (0.11-0.76) were plotted as a function of time and shown in Figure 3-6 (the data of B samples are shown in Supplementary Figure 3-S1). Table 3-3 shows the experimental water contents of samples equilibrated for 168 h at different a_w.



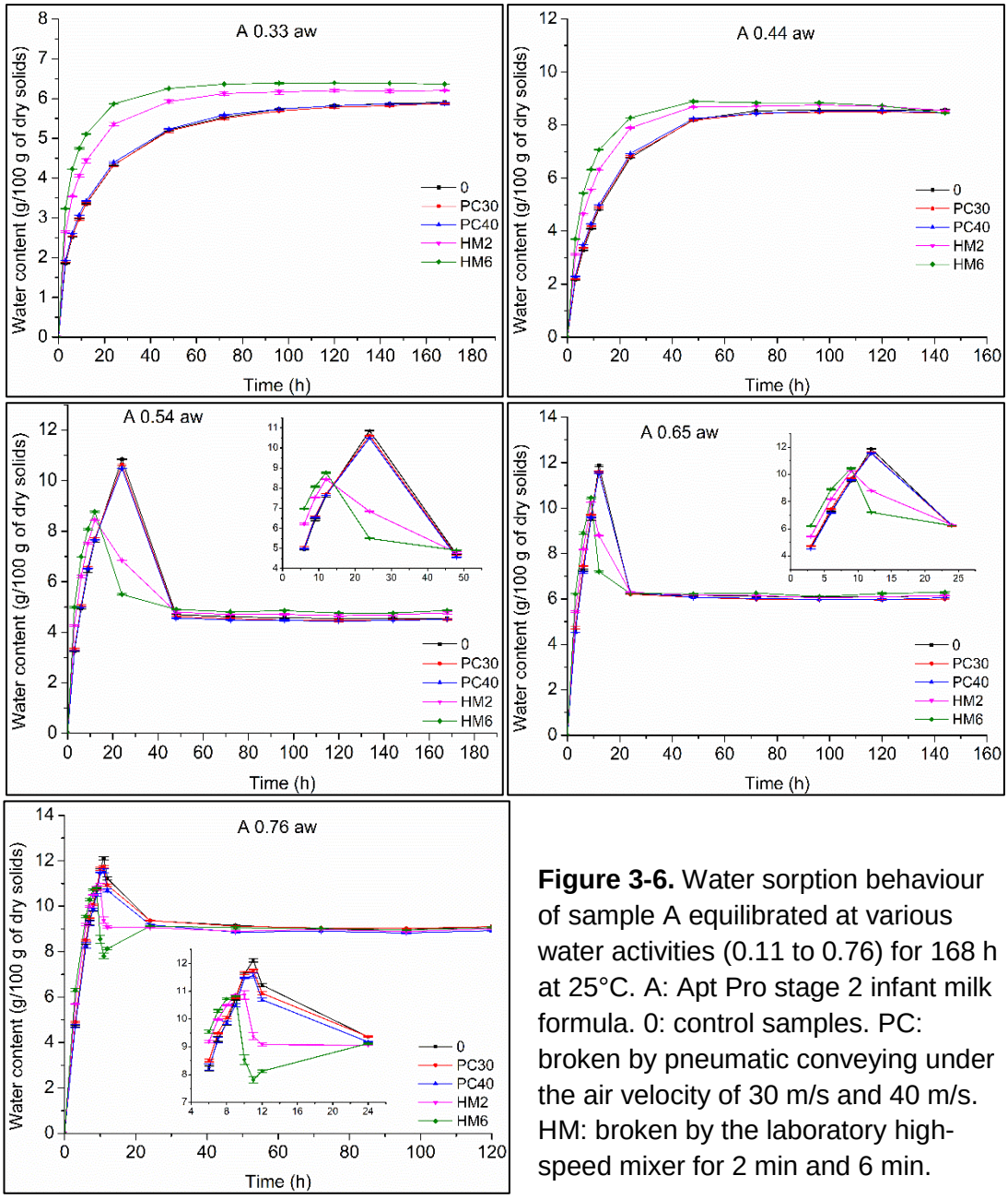


Figure 3-6. Water sorption behaviour of sample A equilibrated at various water activities (0.11 to 0.76) for 168 h at 25°C. A: Apt Pro stage 2 infant milk formula. 0: control samples. PC: broken by pneumatic conveying under the air velocity of 30 m/s and 40 m/s. HM: broken by the laboratory high-speed mixer for 2 min and 6 min.

Surface breakage did not significantly influence the water sorption behaviour of IMF samples at most of the corresponding RVP even though the particle size decreased around 10%. In contrast, body breakage samples sorbed 4-22% larger amount of water than those of control samples at RVP ≤33.2% and the difference decreased with increasing RVP. Besides, at the same RVP, the water content increased as the body breakage degree increased. The large SSA value and small particle size of body breakage samples might be reasons that they sorbed larger amounts of water. Water is mainly absorbed on the surface of particles, thus the larger SSA means more

area for sorption of water molecules (Li et al., 2016c; McCarthy et al., 2013). Besides, hydrophilic groups bind moisture molecules via formatting hydrogen bonds, thus the amount of adsorbed water depends on the presence of compounds with hydrophilic groups (Červenka et al., 2015). Moreover, hydrogen bonds between molecules depend on the size of particles (Haque and Roos, 2004). Similar results were found where coarse powders sorbed less water than fine powders for lactose/different protein powder systems at PVR ≤33.2% (Haque and Roos, 2004). Li et al. (2016c) and Carpin et al. (2017) also had similar findings for lactose/MPI samples at PVR ≤44.1% and lactose at PVR ≤95%. It is also possible that the internal hydrophilic groups were exposed after body breakage, and samples had higher amounts of hydrogen bonding sites for sorption of moisture molecules. However, the same trend was not observed for skim milk powder, and the authors suggested that the difference in hygroscopicity between different size particles might be primarily due to the differences in composition (O'Donoghue et al., 2019). Thus, the changes in surface composition might be another reason for different water content between body breakage samples and other samples. After body breakage, the surface fat proportion slightly decreased and lactose proportion increased, which could decrease particle hydrophobicity.

These reasons also caused significantly higher water absorption rates of body breakage samples than other samples. The sorption rates of samples equilibrated at different a_w (0.11-0.76) in the first 3 h are shown in Figure 3-7a&b. For all samples, the sorption rates increased with increasing a_w. Body breakage samples sorbed water significantly faster (at around 35% to 126% higher for IMF-A and 10% to 85% higher for IMF-B) than other samples at same storage conditions and this difference increased as a_w increased. Besides, the water sorption rate decreased with increasing equilibration time and it decreased faster for body breakage samples. The sorption rates of sample A equilibrated at 0.23 a_w at 3-hour intervals in the first 48 h are shown in Figure 3-7c, where the rates of body breakage samples were lower than those of other samples after equilibration around 10 h.

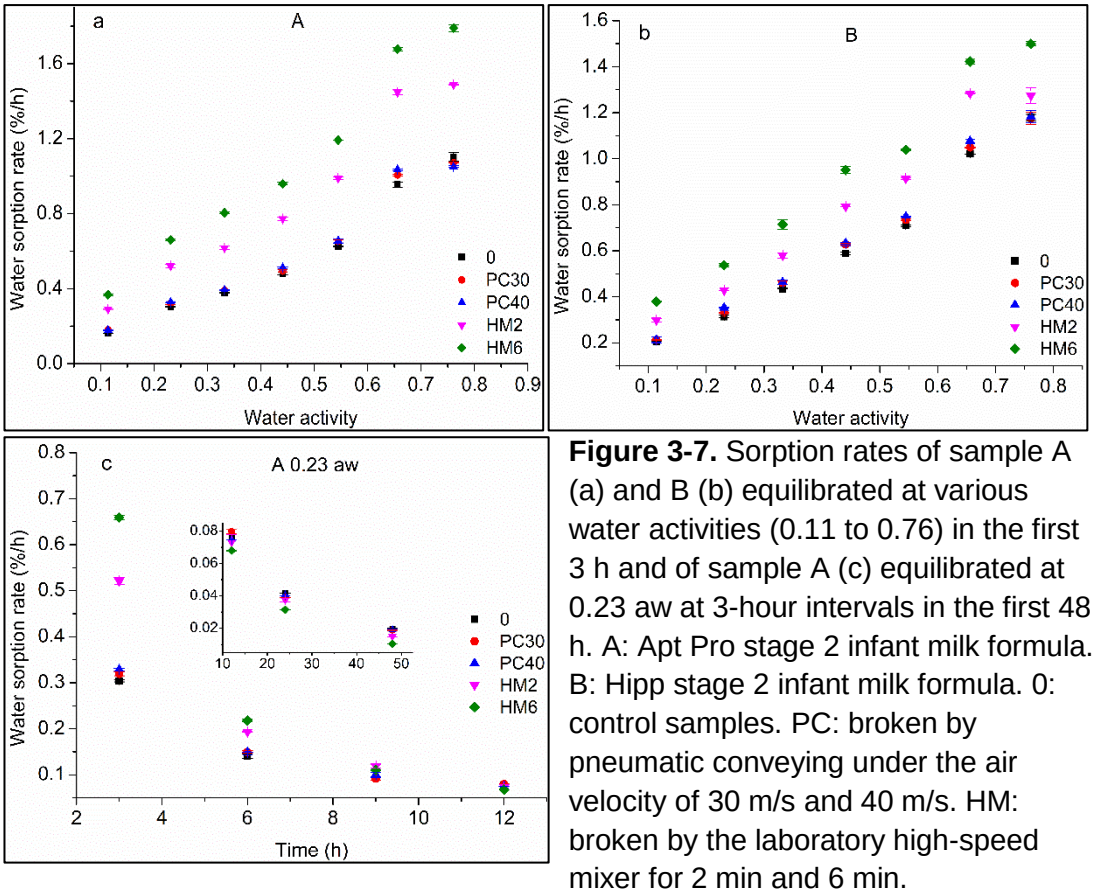


Figure 3-7. Sorption rates of sample A (a) and B (b) equilibrated at various water activities (0.11 to 0.76) in the first 3 h and of sample A (c) equilibrated at 0.23 aw at 3-hour intervals in the first 48 h. A: Apt Pro stage 2 infant milk formula. B: Hipp stage 2 infant milk formula. 0: control samples. PC: broken by pneumatic conveying under the air velocity of 30 m/s and 40 m/s. HM: broken by the laboratory high-speed mixer for 2 min and 6 min.

Due to time-dependent lactose crystallization, part of sorbed water bound by amorphous lactose was released within 24 or 48 h at RVP ≥54.5%. This is consistent with the result obtained by McCarthy et al. (2013) who found the discontinuity in the isotherm at 54.5% RVP for a model IMF sample. From Figure 3-6, body breakage significantly influenced lactose crystallization during storage. Loss of sorbed water in body breakage samples appeared after 9 or 10, 9 and 12 h of storage and in other samples appeared after 11, 12 and 24 h of storage at 76.1%, 65.6% and 54.5% of RVP, respectively. Besides, body breakage samples sorbed less water before crystallization. These results mean that body breakage accelerated the time-dependent lactose crystallization and samples crystallized at lower moisture contents. In addition, the water content of HM6 increased after the loss of sorbed water at 76.1% RVP, which might be because of the recrystallization of lactose. It has been reported that unstable anhydrous *β*-lactose could recrystallize into stable *α*-lactose monohydrate by further absorbing water during storage. Likewise, at the same storage considerations, loss of sorbed water levelled off at nearly the same time with similar water contents (Table 3-3) in body

breakage samples and other samples. These results mean breakage might not affect final crystallization but might influence recrystallization during the crystal formation.

At 44.1% RVP, particle breakage did not influence the water content and there was no time-dependent lactose crystallization occurred. There was a rapid increase in the water content of samples in 33.2%-44.1% RVP (Table 3-3), indicative of water migrating into powders as it approached the glass transition region, before crystallization (Kelly et al., 2016).

Table 3-3. Water contents of samples equilibrated for 168 h at various water activities (0 to 0.76) at 25°C.

Samples	Water activity						
	0.11	0.23	0.33	0.44	0.54	0.65	0.76
IMF-A							
0	2.65^{c}±0.01	4.12^{c}±0.03	5.91^{c}±0.01	8.57^{a}±0.02	3.82^{a}±0.00	5.46^{a}±0.01	9.11^{a}±0.00
PC30	2.68^{c}±0.01	4.12^{c}±0.00	5.88^{c}±0.01	8.47^{b}±0.01	3.79^{ab}±0.03	5.54^{a}±0.00	9.10^{a}±0.01
PC40	2.70^{c}±0.00	4.20^{c}±0.02	5.88^{c}±0.03	8.47^{b}±0.01	3.68^{bc}±0.01	5.44^{a}±0.01	8.92^{b}±0.01
HM2	3.05^{b}±0.04	4.68^{b}±0.01	6.20^{b}±0.01	8.55^{a}±0.01	3.61^{c}±0.04	5.34^{b}±0.02	9.01^{ab}±0.03
HM6	3.23^{a}±0.02	4.92^{a}±0.06	6.36^{a}±0.00	8.45^{b}±0.00	3.78^{ab}±0.02	5.46^{a}±0.04	9.06^{a}±0.04
IMF-B							
0	2.70^{C}±0.00	3.82^{D}±0.03	5.90^{B}±0.03	8.53^{B}±0.02	4.44^{A}±0.00	6.74^{A}±0.05	9.79^{B}±0.01
PC30	2.73^{C}±0.00	3.92^{C}±0.01	6.00^{B}±0.01	8.62^{AB}±0.00	4.24^{BC}±0.03	6.52^{B}±0.05	9.82^{B}±0.03
PC40	2.76^{C}±0.05	3.95^{C}±0.03	5.96^{B}±0.05	8.60^{AB}±0.01	4.16^{BC}±0.03	6.52^{B}±0.00	9.80^{B}±0.03
HM2	2.94^{B}±0.02	4.06^{B}±0.02	6.10^{AB}±0.05	8.68^{A}±0.01	4.08^{C}±0.01	6.38^{C}±0.03	9.99^{A}±0.03
HM6	3.11^{A}±0.01	4.29^{A}±0.01	6.25^{A}±0.12	8.67^{A}±0.07	3.86^{D}±0.03	5.96^{D}±0.03	9.88^{B}±0.04

1. IMF-A: Apt Pro stage 2 infant milk formula. IMF-B: Hipp stage 2 infant milk formula. 0: control samples. PC: broken by pneumatic conveying under the air velocity of 30 m/s and 40 m/s. HM: broken by the laboratory high-speed mixer for 2 min and 6 min.
2. Values are mean ± standard deviation (n=3).
3. $^{a-e}$ and $^{A-E}$ different values within columns in IMF-A and IMF-B groups are significantly different at P <0.05, respectively.

Table 3-4. Monolayer values (m_m, g/100g dry solid), constants *K* and *C* for the GAB isotherms and monolayer values (m_c, g/100g dry solid), number of adsorbed monolayers (N_{am}), surface area of adsorbent (*A*, m^2/g) and density of sorbed water (c_d, g/ml) of Caurie's equations.

Samples	GAB					Caurie's equations			
	m_m	*K*	*C*	R^2	%RMS	m_c	N_{am}	*A*	c_d
IMF-A									
0	3.45^{c}±0.05	1.41^{a}±0.01	9.2^{a}±0.1	0.9822	1.30	5.44^{c}±0.01	3.12^{c}±0.02	84.8^{c}±0.6	1.75^{a}±0.01
PC30	3.43^{c}±0.03	1.41^{a}±0.01	9.7^{a}±0.2	0.9813	1.39	5.45^{c}±0.00	3.17^{c}±0.00	86.4^{c}±0.1	1.72^{a}±0.00
PC40	3.54^{c}±0.00	1.38^{a}±0.00	9.5^{a}±0.1	0.9933	0.75	5.48^{c}±0.00	3.20^{c}±0.01	87.1^{c}±0.4	1.71^{a}±0.01
HM2	4.07^{b}±0.12	1.26^{b}±0.02	10.8^{a}±0.9	1.0000	0.02	5.80^{b}±0.02	3.56^{b}±0.04	97.0^{b}±1.1	1.63^{b}±0.01
HM6	4.53^{a}±0.17	1.15^{c}±0.03	10.9^{a}±0.8	0.9988	0.15	5.97^{a}±0.00	3.80^{a}±0.02	103.5^{a}±0.6	1.57^{c}±0.01
IMF-B									
0	2.97^{B}±0.01	1.52^{A}±0.00	13.3^{A}±0.1	0.8890	3.95	5.41^{C}±0.00	3.15^{C}±0.00	85.8^{C}±0.0	1.72^{A}±0.00
PC30	3.11^{B}±0.01	1.50^{A}±0.00	12.2^{A}±0.1	0.8963	3.70	5.45^{C}±0.00	3.15^{C}±0.00	85.8^{C}±0.1	1.73^{A}±0.00
PC40	3.10^{B}±0.13	1.50^{A}±0.02	13.5^{A}±0.5	0.9188	3.33	5.47^{C}±0.02	3.20^{C}±0.05	87.0^{C}±1.4	1.71^{A}±0.02
HM2	3.11^{B}±0.03	1.50^{A}±0.01	16.2^{A}±0.1	0.9178	3.68	5.60^{B}±0.02	3.34^{B}±0.02	91.0^{B}±0.4	1.67^{AB}±0.00
HM6	3.37^{A}±0.06	1.43^{B}±0.00	16.1^{A}±0.4	0.9430	3.11	5.76^{A}±0.00	3.53^{A}±0.05	96.1^{A}±1.4	1.63^{B}±0.02

1. IMF-A: Apt Pro stage 2 infant milk formula. IMF-B: Hipp stage 2 infant milk formula. 0: control samples. PC: broken by pneumatic conveying under the air velocity of 30 m/s and 40 m/s. HM: broken by the laboratory high-speed mixer for 2 min and 6 min.
2. Values are mean ± standard deviation (n=3).
3. $^{a-c}$ and $^{A-C}$ different values within columns in IMF-A and IMF-B groups are significantly different at P <0.05, respectively.

3.3.3.2. Sorption isotherm

The GAB model was used to model the experimental water content of samples equilibrated at a_w ≤0.441 (Figure 3-8) and the parameters are given in Table 3-4. From Figure 3-8, equilibrium water content increased as a_w increased and moisture adsorption isotherms of all samples were sigmoid shape. Meanwhile, isotherms were similar for both control and surface breakage samples but different from body breakage samples. According to the low RMS values, the GAB model fitted well with the experimental water sorption data at a_w ≤0.441 where the water contents of body breakage samples were higher or similar to those of other samples. In contrast, the predicted water contents of body breakage samples were lower than those of other samples at higher a_w (>0.441). This is consistent with the results that body breakage samples sorbed less water before crystallization at a_w ≥0.545.

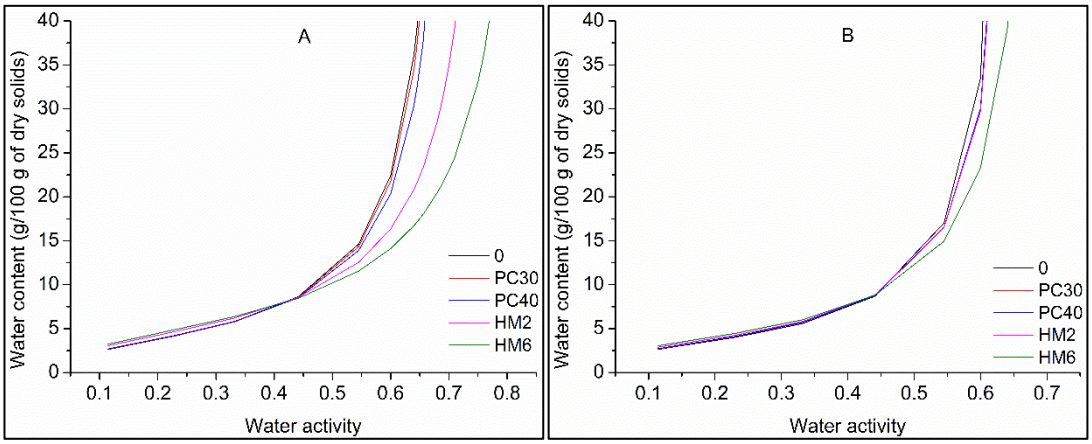


Figure 3-8. Water sorption isotherms of samples stored for 168 h at 25°C predicted with the GAB model using experimental data. A: Apt Pro stage 2 infant milk formula. B: Hipp stage 2 infant milk formula. 0: control samples. PC: broken by pneumatic conveying under the air velocity of 30 m/s and 40 m/s. HM: broken by the laboratory high-speed mixer for 2 min and 6 min.

From Table 3-4, the m_m of body breakage powders were significantly higher than other powders, and it increased from around 3.4 to 4.5 g/100 g dry solids for sample A and from around 3 to 3.4 g/100 g dry solids for sample B. The m_m represents the moisture content when each polar group in a molecule binds with one moisture molecule (McCarthy et al., 2013). Thus, the higher m_m of body breakage samples corresponded to their higher water

contents. Besides, after body breakage, *K* and *C* of samples were decreased and increased, respectively. *K* was used to correct the properties of the multilayer molecules relative to the bulk liquid. *C* represents the strength of binding of water to the primary binding sites (Lazou and Krokida, 2011). Thus, water bounded stronger in the monolayer in body breakage samples than in other samples.

3.3.3.3. Sorbed water properties

Several properties of sorbed water derived from Caurie's equations are shown in Table 3-4. The monolayer values obtained from Caurie's equation (m_c) were higher than those derived from the GAB model (m_m). This is consistent with the previous reports that the monolayer values obtained using GAB and BET models were lower than those obtained using Caurie model (Dalgıç et al., 2012). Nevertheless, m_c showed the same trend as m_m, where the m_c significantly increased after the body breakage and surface breakage had no significant influence on it. Besides, body breakage samples had higher *A* compared with other samples, corresponding to the higher SSA, which confirmed that there were more effective areas for body breakage samples to adsorb water. This resulted in the higher N_{am}, corresponding to the higher final water contents.

3.3.3.4. Spreading pressure

Figure 3-9 illustrates the spreading pressures of samples at various a_W. As already shown for starch powders, the spreading pressure of samples increased as a_W increased (Al-Muhtaseb et al., 2004). Besides, breakage decreased the spreading pressure of powders especially for sample A whose spreading pressure decreased with increasing degree of breakage at a given a_W, and the effects of breakage increased with increasing a_W. These results mean, from the perspective of spreading pressure, breakage decreased the affinity of water molecules to active sites thus broken samples were easier to absorb water.

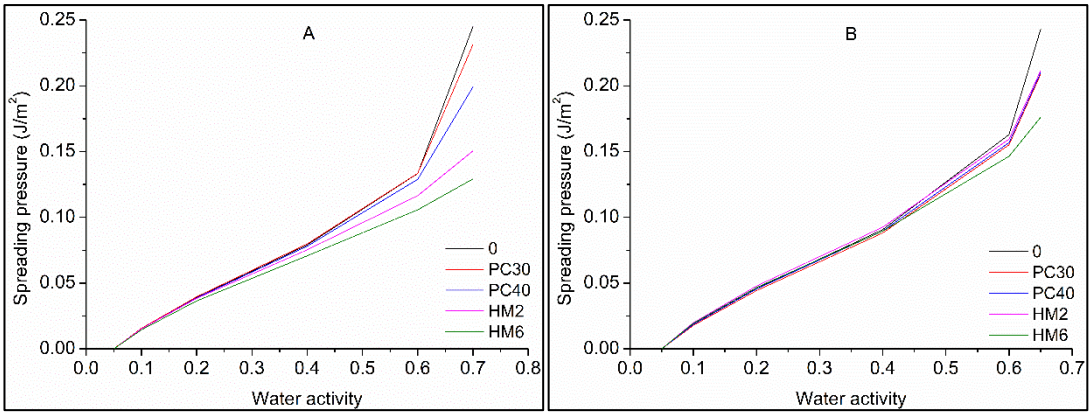


Figure 3-9. Spreading pressure isotherms at different water activities of samples. A: Apt Pro stage 2 infant milk formula. B: Hipp stage 2 infant milk formula. 0: control samples. PC: broken by pneumatic conveying under the air velocity of 30 m/s and 40 m/s. HM: broken by the laboratory high-speed mixer for 2 min and 6 min.

3.3.4. Glass transition and instant crystallization

The T_g (onset) and T_{ic} of samples over the a_w range of 0 to 0.441 are shown in Table 3-5.T_g represents the overall stability of powders to changes caused by moisture and temperature and lower T_g is indicative of problems more easily occurring during storage (Kelly et al., 2015). From Table 3-5, T_g decreased drastically with increasing a_w because of the water plasticization (Haque and Roos, 2004; Haque and Roos, 2006; Saxena et al., 2020; Zouari et al., 2020). Breakage did not influence the T_g of anhydrous samples, around 105°C or 107°C for A or B samples, respectively. This value was similar to the T_g of anhydrous freeze-dried lactose, around 105°C (Haque and Roos, 2006). A significant difference in T_g was found between body breakage samples and other samples at a_w from 0.114 to 0.332, which was due to the higher water content of body breakage samples. It was shown that T_{ic} decreased as a_w and water content increased and surface breakage did not influence the T_{ic} while the T_{ic} of body breakage samples were significantly lower than those of other samples. This is similar to the effect of breakage on T_g but the influence on T_{ic} was greater. Thus, the temperature differences between glass transition and crystallization (T_{ic} - T_g) of body breakage samples were lower than those of other samples. All these results suggest that lower temperature or a_w is required for body breakage samples when stored.

Table 3-5. Glass transition temperature (T_g), initial crystallization temperature (T_{ic}) and α-relaxation temperature (T_α at 1 Hz) of infant formula samples stored for 168 h at various water activities (0 to 0.44) at 25°C.

Samples		Water activity				
		0	0.11	0.23	0.33	0.44
IMF-A						
0	T_g	105.1±0.2	66.3±0.7	48.9±0.3	32.0±0.0	16.2±0.1
	T_{ic}	/	120.9±0.0	101.0±0.7	83.7±0.3	64.2±0.0
	T_α	115.5±0.6	87.3±0.7	72.7±1.1	54.7±0.0	35.2±0.2
PC30	T_g	104.4±0.5	66.1±0.4	48.4±0.2	32.3±0.1	15.9±0.2
	T_{ic}	/	120.8±0.8	100.4±0.1	84.9±0.5	64.0±0.1
	T_α	114.0±1.0	84.0±0.8	69.7±1.0	52.2±0.2	33.8±0.2
PC40	T_g	102.7	65.9±0.0	48.7±0.2	32.6±0.1	16.1±0.1
	T_{ic}	/	120.0±0.4	100.5±0.4	83.6±0.1	63.9±0.0
	T_α	115.6±0.6	86.7±0.9	70.6±0.4	50.9±0.0	35.0±0.5
HM2	T_g	105.7±0.0	64.8±0.1	46.7±0.1	31.7±0.4	15.2±0.3
	T_{ic}	/	114.2±0.1	94.0±0.1	78.8±0.4	59.1±0.6
	T_α	114.0±0.1	83.9±0.2	68.0±0.6	51.1±0.4	36.6±0.4
HM6	T_g	105.9±0.1	63.5±0.5	46.0±0.4	31.1±0.1	14.84±0.8
	T_{ic}	/	110.4±0.8	91.6±0.8	77.0±0.0	58.4±0.1
	T_α	115.7±1.0	78.9±0.2	67.0±0.6	50.9±0.2	34.8±0.1
IMF-B						
0	T_g	107.5±0.1	63.9±0.4	49.0±0.2	32.8±0.1	15.9±0.1
	T_{ic}	/	116.2±0.3	98.9±0.0	84.3±0.2	64.3±0.2
	T_α	117.6±0.6	84.3±0.1	70.9±0.4	58.1±0.0	36.5±0.0
PC30	T_g	107.5±0.1	63.2±0.3	49.2±0.1	32.8±0.0	16.1±0.1
	T_{ic}	/	115.3±0.2	98.3±0.0	83.5±0.2	63.5±0.0
	T_α	119.4±1.6	87.8±0.3	70.3±0.6	55.6±0.4	34.7±0.1
PC40	T_g	107.3±0.2	62.4±0.5	48.7±0.2	32.5±0.1	15.7±0.1
	T_{ic}	/	113.8±0.4	98.5±0.2	83.4±0.1	63.2±0.6
	T_α	119.6±1.9	83.2±1.2	71.2±0.3	56.2±0.0	34.6±0.2
HM2	T_g	107.2±0.2	62.5±0.3	48.7±0.1	32.5±0.1	16.0±0.5
	T_{ic}	/	112.3±0.2	96.4±0.4	81.1±0.3	61.5±0.8
	T_α	124.0±1.9	85.0±0.6	70.1±0.4	57.9±0.9	36.0±1.1
HM6	T_g	107.7±0.0	62.2±0.4	48.1±0.0	32.0±0.1	15.1±0.0
	T_{ic}	/	110.5±0.6	99.9±0.3	79.2±0.0	59.3±0.3
	T_α	121.2±0.3	79.7±1.0	67.6±0.5	55.4±0.1	36.7±0.2

1. IMF-A: Apt Pro stage 2 infant milk formula. IMF-B: Hipp stage 2 infant milk formula. 0: control samples. PC: broken by pneumatic conveying under the air velocity of 30 m/s and 40 m/s. HM: broken by the laboratory high-speed mixer for 2 min and 6 min.
2. Values are mean ± standard deviation (n=2).

3.3.5. Mechanical properties

For amorphous materials, the physical properties often change around T_g, which may result in an α-relaxation related to molecular mobility (Silalai and Roos, 2011a, b). The α-relaxation shows a peak in loss modulus and a

decrease in storage modulus around T_g. T_α decreased with increasing frequency (data not shown) and a_W (Table 3-5), which agrees with previous research (Li et al., 2016b; Silalai and Roos, 2011b). From Table 3-5, breakage almost did not influence the T_α and only a few body breakage samples had significantly lower T_α than other samples. Nevertheless, it was found that body breakage significantly affected mechanical α-relaxation behaviour that was the changes of storage modulus and loss modulus (Figure 3-10). From Figure 3-10a, compared with other samples, the storage modulus of body breakage samples showed smaller decreases and remained at higher levels for the rubbery plateau. For loss modulus (Figure 3-10b), α-relaxation peaks of control and surface breakage samples were more pronounced, and the peak size of body breakage samples decreased with increasing breakage degree. The small magnitudes of modulus changes mean that body breakage decreased the overall molecular mobility of powders.

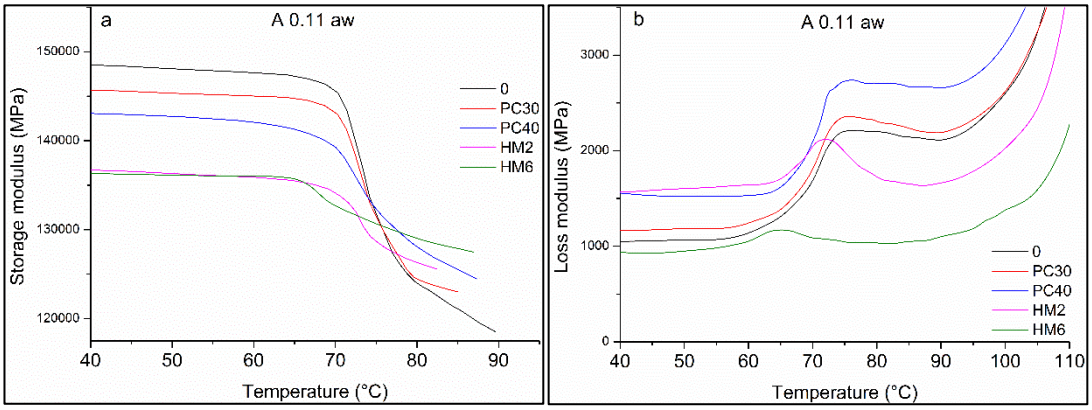


Figure 3-10. Storage modulus (a) and loss modulus (b) of sample A equilibrated at 0.11 a_W for 168 h at 25°C. A: Apt Pro stage 2 infant milk formula. 0: control samples. PC: broken by pneumatic conveying under the air velocity of 30 m/s and 40 m/s. HM: broken by the laboratory high-speed mixer for 2 min and 6 min.

3.4. Conclusion

This chapter was performed on the influence of two different breakage mechanisms on the physical, water sorption and mechanical properties of commercial agglomerated IMF. Two different processing methods (laboratory dilute-phase pneumatic conveying and high-speed mixing) were used to mimic the breakage of IMF samples during industrial-scale processing

conditions. The dominant breakage mechanism during high-speed mixing was body breakage while surface breakage occurred on most particles during pneumatic conveying. Compared with surface breakage, body breakage had greater impact on the properties of samples.

Breakage significantly increased the SSA and bulk densities and decreased the particle size of samples. The effect of breakage on porosity and particle density was influenced by the particle size of initial samples. After breakage, the surface compositions slightly changed, protein and lactose proportions increased and fat decreased. In addition, body breakage particles had more rounded shapes and smoother surfaces while surface breakage did not significantly change particle morphology. Body breakage had a greater influence on powder physical properties, which subsequently affected the water sorption and mechanical properties. In contrast, surface breakage only slightly affected physical properties and not other characteristics. Body breakage increased the water sorption rate and water content of samples and accelerated the time-dependent crystallization. The experimental water sorption data at $a_W \leq 0.441$ fitted well with the GAB model. The number of adsorbed monolayers, sorption surface area, and monolayer moisture content of body breakage powders were significantly higher than other powders and their spreading pressures were lower. Higher water contents of body breakage samples significantly decreased T_{ic} but slightly decreased T_g and T_α. Besides, body breakage decreased the overall molecular mobility of powders and resulted in smaller magnitudes of modulus changes than other samples.

Overall, surface breakage affected powder physical properties but not water sorption and mechanical properties, while body breakage significantly impacted those characteristics. This finding also has industrial importance. If powder breakage during production and transportation cannot be avoided, it should be limited to the surface breakage. However, this would still influence some functionalities such as bulk density that is important for IMF. On the other hand, sorption of moisture by dairy powders can have a whole range of serious chemical, physical and microbial consequences. Therefore, further

research on the effect of breakage mechanisms on these properties will be useful.

Reference

Al-Muhtaseb, A.H., McMinn, W.A.M., & Magee, T.R.A. (2004). Water sorption isotherms of starch powders. Part 2: Thermodynamic characteristics. *Journal of Food Engineering* 62(2), 135-142. https://doi.org/10.1016/S0260-8774(03)00202-4.

Antonyuk, S., Tomas, J., Heinrich, S., & Mörl, L. (2005). Breakage behaviour of spherical granulates by compression. *Chemical Engineering Science* 60(14), 4031-4044. https://doi.org/10.1016/j.ces.2005.02.038.

Boiarkina, I., Sang, C., Depree, N., Prince-Pike, A., Yu, W., Wilson, D.I., & Young, B.R. (2016). The significance of powder breakdown during conveying within industrial milk powder plants. *Advanced Powder Technology* 27(6), 2363-2369. https://doi.org/10.1016/j.apt.2016.10.019.

Carpin, M., Bertelsen, H., Dalberg, A., Bech, J.K., Risbo, J., Schuck, P., & Jeantet, R. (2017). How does particle size influence caking in lactose powder? *Journal of Food Engineering* 209, 61-67. https://doi.org/10.1016/j.jfoodeng.2017.04.006.

Červenka, L., Hloušková, L., & Žabčíková, S. (2015). Moisture adsorption isotherms and thermodynamic properties of green and roasted Yerba mate (Ilex paraguariensis). *Food Bioscience* 12, 122-127. https://doi.org/10.1016/j.fbio.2015.10.001.

Cleaver, J.A.S., Ghadiri, M., & Rolfe, N. (1993). Impact attrition of sodium carbonate monohydrate crystals. *Powder Technology* 76(1), 15-22. https://doi.org/10.1016/0032-5910(93)80036-A.

Dalgıç, A.C., Pekmez, H., & Belibağlı, K.B. (2012). Effect of drying methods on the moisture sorption isotherms and thermodynamic properties of mint leaves. *Journal of Food Science and Technology* 49(4), 439-449. https://doi.org/10.1007/s13197-011-0302-7.

Faldt, P., Bergenstahl, B., & Carlsson, G. (1993). The surface coverage of fat on food powders analyzed by ESCA (electron spectroscopy for chemical analysis). *Food Structure* 12(2), 10.

Fu, J., Reynolds, G.K., Adams, M.J., Hounslow, M.J., & Salman, A.D. (2005). An experimental study of the impact breakage of wet granules. *Chemical Engineering Science* 60(14), 4005-4018. https://doi.org/10.1016/j.ces.2005.02.037.

Ghadiri, M., Yuregir, K.R., Pollock, H.M., Ross, J.D.J., & Rolfe, N. (1991). Influence of processing conditions on attrition of NaCl crystals. *Powder Technology* 65(1), 311-320. https://doi.org/10.1016/0032-5910(91)80195-O.

Han, J., Fitzpatrick, J., Cronin, K., Maidannyk, V., & Miao, S. (2020). Breakage of infant milk formula through three different processing methods and its influence on powder properties. *Journal of Food Engineering* 282, 109997. https://doi.org/10.1016/j.jfoodeng.2020.109997.

Han, J., Fitzpatrick, J., Cronin, K., Maidannyk, V., & Miao, S. (2021a). Particle size, powder properties and the breakage behaviour of infant milk formula. *Journal of Food Engineering* 292, 110367. https://doi.org/10.1016/j.jfoodeng.2020.110367.

Han, J., Fitzpatrick, J., Cronin, K., & Miao, S. (2021b). Dairy powder breakage: Mechanisms, characterization methods, impacted properties and influencing factors. *Trends in Food Science & Technology* 114, 608-624. https://doi.org/10.1016/j.tifs.2021.05.043.

Hanley, K.J., 2011. Experimental quantification and modelling of attrition of infant formulae, Department of Process and Chemical Engineering. University College Cork, Cork, Ireland.
Haque, M.K., & Roos, Y.H. (2004). Water Sorption and Plasticization Behaviour of Spray-dried Lactose/Protein Mixtures. *Journal of Food Science* 69(8), E384-E391. https://doi.org/ 10.1111/j.1365-2621.2004.tb09900.x.
Haque, M.K., & Roos, Y.H. (2006). Differences in the physical state and thermal behaviour of spray-dried and freeze-dried lactose and lactose/protein mixtures. *Innovative Food Science & Emerging Technologies* 7(1), 62-73. https://doi.org/10.1016/j.ifset.2004.12.004.
Hazlett, R., Schmidmeier, C., & O'Mahony, J.A. (2020). Influence of mechanical integrity during pneumatic conveying on the bulk handling and rehydration properties of agglomerated dairy powders. *Journal of Food Engineering*, 110103. https://doi.org/10.1016/j.jfoodeng.2020.110103.
Iglesias, H.A., Chirife, J., & Viollaz, P. (1976). Thermodynamics of water vapour sorption by sugar beet root. *International Journal of Food Science & Technology* 11(1), 91-101. https://doi.org/10.1111/j.1365-2621.1976.tb00705.x.
Ji, J., Cronin, K., Fitzpatrick, J., Fenelon, M., & Miao, S. (2015). Effects of fluid bed agglomeration on the structure modification and reconstitution behaviour of milk protein isolate powders. *Journal of Food Engineering* 167, 175-182. https://doi.org/10.1016/j.jfoodeng.2015.01.012.
Kelly, G.M., O'Mahony, J.A., Kelly, A.L., Huppertz, T., Kennedy, D., & O'Callaghan, D.J. (2015). Influence of protein concentration on surface composition and physico-chemical properties of spray-dried milk protein concentrate powders. *International Dairy Journal* 51, 34-40. https://doi.org/10.1016/j.idairyj.2015.07.001.
Kelly, G.M., O'Mahony, J.A., Kelly, A.L., & O'Callaghan, D.J. (2016). Water sorption and diffusion properties of spray-dried dairy powders containing intact and hydrolysed whey protein. *LWT - Food Science and Technology* 68, 119-126. https://doi.org/10.1016/j.lwt.2015.11.056.
Kim, E.H.J., Chen, X.D., & Pearce, D. (2002). Surface characterization of four industrial spray-dried dairy powders in relation to chemical composition, structure and wetting property. *Colloids and Surfaces B: Biointerfaces* 26(3), 197-212. https://doi.org/10.1016/S0927-7765(01)00334-4.
King, R.P. (2012). Modeling and simulation of mineral processing systems. (pp. 153-252). Society for Mining, Metallurgy, and Exploration (SME).
Lago, C.C., Liendo-Cárdenas, M., & Noreña, C.P.Z. (2013). Thermodynamic sorption properties of potato and sweet potato flakes. *Food and Bioproducts Processing* 91(4), 389-395. https://doi.org/10.1016/j.fbp.2013.02.005.
Lazou, A., & Krokida, M. (2011). Thermal characterisation of corn–lentil extruded snacks. *Food Chemistry* 127(4), 1625-1633. https://doi.org/10.1016/j.foodchem.2011.02.029.
Li, R., Roos, Y.H., & Miao, S. (2016a). Flavor release from spray-dried amorphous matrix: Effect of lactose content and water plasticization. *Food Research International* 86, 147-155. https://doi.org/10.1016/j.foodres.2016.06.003.
Li, R., Roos, Y.H., & Miao, S. (2016b). Physical and mechanical properties of lactose/WPI mixtures: Effect of pre-crystallisation. *International Dairy Journal* 56, 55-63. https://doi.org/10.1016/j.idairyj.2015.12.014.
Li, R., Roos, Y.H., & Miao, S. (2016c). Roles of particle size on physical and mechanical properties of dairy model solids. *Journal of Food Engineering* 173, 69-75. https://doi.org/10.1016/j.jfoodeng.2015.10.041.
Li, R., Roos, Y.H., & Miao, S. (2017). Characterization of mechanical and encapsulation properties of lactose/maltodextrin/WPI matrix. *Food Hydrocolloids* 63, 149-159. https://doi.org/10.1016/j.foodhyd.2016.08.033.

Maidannyk, V., McSweeney, D.J., Hogan, S.A., Miao, S., Montgomery, S., Auty, M.A.E., & McCarthy, N.A. (2020). Water sorption and hydration in spray-dried milk protein powders: Selected physicochemical properties. *Food Chemistry* 304, 125418. https://doi.org/10.1016/j.foodchem.2019.125418.

Maidannyk, V.A., Lim, A.S.L., Auty, M.A.E., & Roos, Y.H. (2019). Effects of lipids on the water sorption, glass transition and structural strength of carbohydrate-protein systems. *Food Research International* 116, 1212-1222. https://doi.org/10.1016/j.foodres.2018.10.008.

Materic, V., Holt, R., Hyland, M., & Jones, M.I. (2014). An internally circulating fluid bed for attrition testing of Ca looping sorbents. *Fuel* 127, 116-123. https://doi.org/10.1016/j.fuel.2013.10.071.

Mazza, G., & LeMaguer, M. (1978). Water Sorption Properties of Yellow Globe Onion (Allium cepa L.). *Canadian Institute of Food Science and Technology Journal* 11(4), 189-193. https://doi.org/10.1016/S0315-5463(78)73269-4.

McCarthy, N.A., Gee, V.L., Hickey, D.K., Kelly, A.L., O'Mahony, J.A., & Fenelon, M.A. (2013). Effect of protein content on the physical stability and microstructure of a model infant formula. *International Dairy Journal* 29(1), 53-59. https://doi.org/10.1016/j.idairyj.2012.10.004.

Murrieta-Pazos, I., Gaiani, C., Galet, L., Calvet, R., Cuq, B., & Scher, J. (2012a). Food powders: Surface and form characterization revisited. *Journal of Food Engineering* 112(1), 1-21. https://doi.org/10.1016/j.jfoodeng.2012.03.002.

Murrieta-Pazos, I., Gaiani, C., Galet, L., & Scher, J. (2012b). Composition gradient from surface to core in dairy powders: Agglomeration effect. *Food Hydrocolloids* 26(1), 149-158. https://doi.org/10.1016/j.foodhyd.2011.05.003.

O'Donoghue, L.T., Haque, M.K., Kennedy, D., Laffir, F.R., Hogan, S.A., O'Mahony, J.A., & Murphy, E.G. (2019). Influence of particle size on the physicochemical properties and stickiness of dairy powders. *International Dairy Journal* 98, 54-63. https://doi.org/10.1016/j.idairyj.2019.07.002.

Ortega-Rivas, E., Juliano, P., & Yan, H. (2006). *Food powders: physical properties, processing, and functionality*. Springer US.

O'Neill, G.J., Hollingsworth, A., Harbourne, N., & O'Riordan, E.D. (2019). Reducing stickiness in spray dried dairy emulsions. *Food Hydrocolloids* 90, 330-340. https://doi.org/10.1016/j.foodhyd.2018.12.033.

Polatoğlu, B., Beşe, A.V., Kaya, M., & Aktaş, N. (2011). Moisture adsorption isotherms and thermodynamics properties of sucuk (Turkish dry-fermented sausage). *Food and Bioproducts Processing* 89(4), 449-456. https://doi.org/10.1016/j.fbp.2010.06.003.

Reynolds, G.K., Fu, J.S., Cheong, Y.S., Hounslow, M.J., & Salman, A.D. (2005). Breakage in granulation: A review. *Chemical Engineering Science* 60(14), 3969-3992. https://doi.org/10.1016/j.ces.2005.02.029.

Saxena, J., Adhikari, B., Brkljaca, R., Huppertz, T., Chandrapala, J., & Zisu, B. (2019). Physicochemical properties and surface composition of infant formula powders. *Food Chemistry* 297, 124967. https://doi.org/10.1016/j.foodchem.2019.124967.

Saxena, J., Adhikari, B., Brkljaca, R., Huppertz, T., Chandrapala, J., & Zisu, B. (2020). Inter-relationship between lactose crystallization and surface free fat during storage of infant formula. *Food Chemistry* 322, 126636. https://doi.org/10.1016/j.foodchem.2020.126636.

Scala, F., Montagnaro, F., & Salatino, P. (2007). Attrition of Limestone by Impact Loading in Fluidized Beds. *Energy & Fuels* 21(5), 2566-2572. https://doi.org/10.1021/ef0700580.

Schuck, P., Dolivet, A., & Jeantet, R. (2012). *Analytical methods for food and dairy powders*.

Silalai, N., & Roos, Y.H. (2011a). Coupling of dielectric and mechanical relaxations with glass transition and stickiness of milk solids. *Journal of Food Engineering* 104(3), 445-454. https://doi.org/10.1016/j.jfoodeng.2011.01.009.

Silalai, N., & Roos, Y.H. (2011b). Mechanical relaxation times as indicators of stickiness in skim milk–maltodextrin solids systems. *Journal of Food Engineering* 106(4), 306-317. https://doi.org/10.1016/j.jfoodeng.2011.05.018.

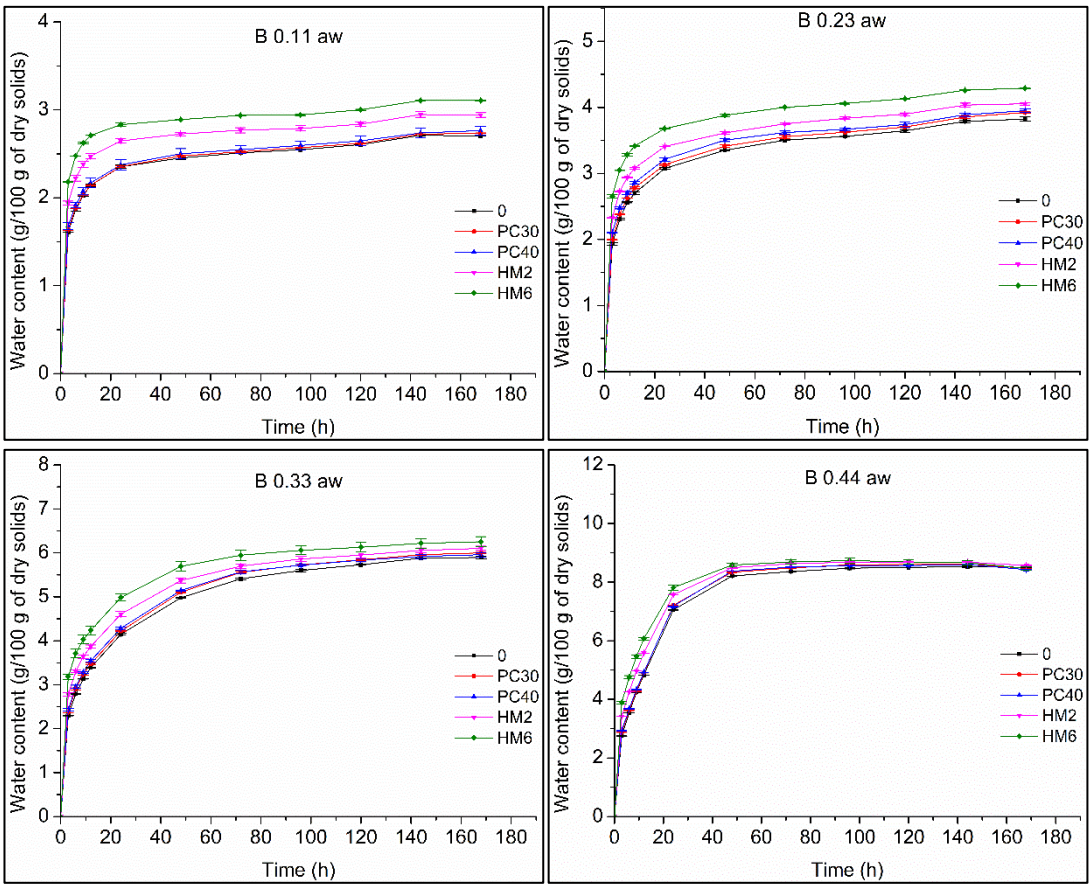
Simón, C., Esteban, L.G., de Palacios, P., Fernández, F.G., & García-Iruela, A. (2016). Thermodynamic properties of the water sorption isotherms of wood of limba (Terminalia superba Engl. & Diels), obeche (Triplochiton scleroxylon K. Schum.), radiata pine (Pinus radiata D. Don) and chestnut (Castanea sativa Mill.). *Industrial Crops and Products* 94, 122-131. https://doi.org/10.1016/j.indcrop.2016.08.008.

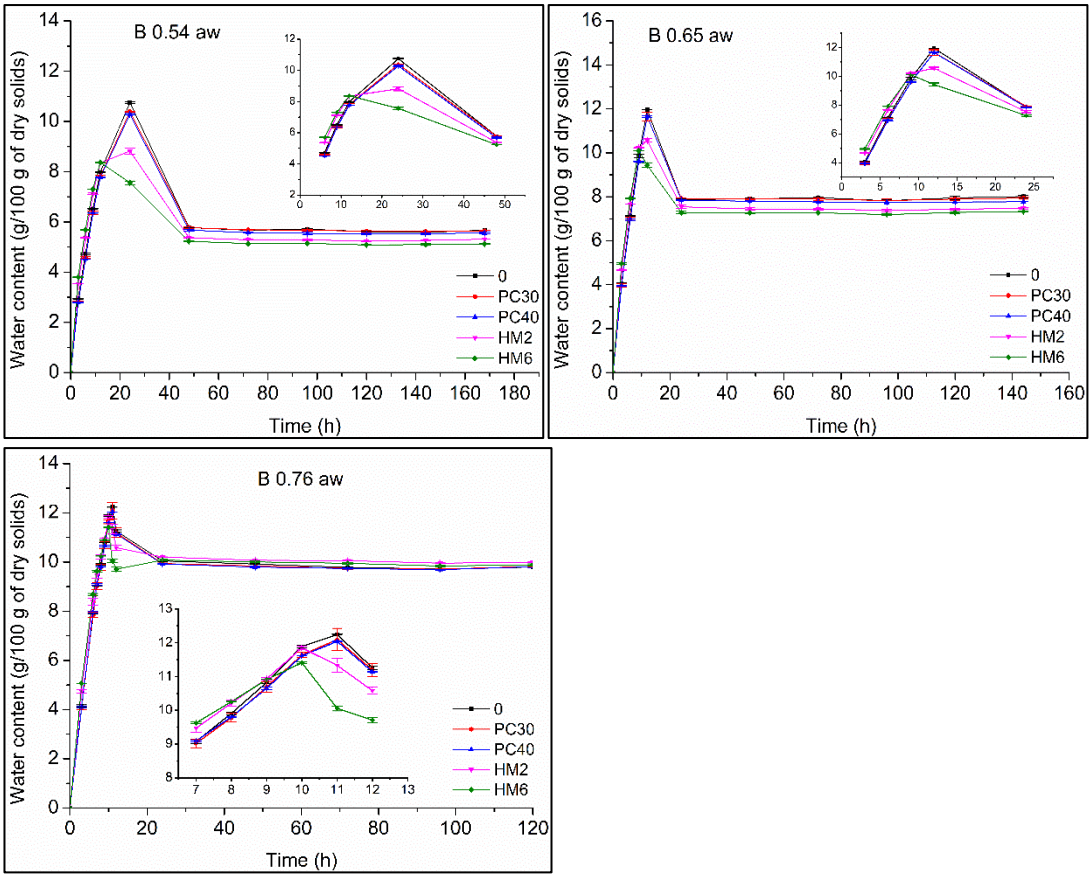
Torres, M.D., Moreira, R., Chenlo, F., & Vázquez, M.J. (2012). Water adsorption isotherms of carboxymethyl cellulose, guar, locust bean, tragacanth and xanthan gums. *Carbohydrate Polymers* 89(2), 592-598. https://doi.org/10.1016/j.carbpol.2012.03.055.

Wu, F., & Wu, D. (2017). Attrition resistances and mechanisms of three types of FCC catalysts. *Powder Technology* 305, 289-296. https://doi.org/10.1016/j.powtec.2016.09.077.

Zouari, A., Briard-Bion, V., Gaucheron, F., Schuck, P., Gaiani, C., Triki, M., Attia, H., & Ali Ayadi, M. (2020). Effect of pH on the physicochemical characteristics and the surface chemical composition of camel and bovine whey protein's powders. *Food Chemistry*, 127514. https://doi.org/10.1016/j.foodchem.2020.127514.

Supplementary materials





Supplementary Figure 3-S1. Water sorption of infant milk formula sample B equilibrated at various water activity (0.11 to 0.76) for 168 h at 25°C. B: Hipp stage 2 infant milk formula. 0: control samples. PC: broken by pneumatic conveying under the air velocity of 30 m/s and 40 m/s. HM: broken by the laboratory high-speed mixer for 2 min and 6 min.

CHAPTER FOUR

Breakage of infant milk formula through three different processing methods and its influence on powder properties

Chapter 4 was published in:

Han, J., Fitzpatrick, J., Cronin, K., Maidannyk, V., & Miao, S. (2020). Breakage of infant milk formula through three different processing methods and its influence on powder properties. *Journal of Food Engineering 282*, 109997.

The work contained in this chapter was undertaken and written solely by myself with specific contributions from each co-author:

Jie Han: Conceptualization, Methodology, Writing - original draft, Data curation

John Fitzpatrick: Supervision, Writing - review & editing

Kevin Cronin: Supervision, Writing - review & editing

Valentyn Maidannyk: Investigation

Song Miao: Supervision, Conceptualization, Writing - review & editing, Funding acquisition, Project administration, Investigation

Abstract

Dairy powder breakage has always occurred during production and transportation though few studies on it have been published. This chapter examines the breakage of infant milk formula using three different processing methods (laboratory high-speed mixing, lab-scale dilute-phase pneumatic conveying, and factory-scale blending) and the effect of breakage on powder properties. In both mixing and high-velocity pneumatic conveying, particles were broken into smaller entities and the particle size of samples significantly decreased. Particle breakage was accompanied by a significant decrease in porosity and increase in density and surface free fat. This in-turn decreased the rehydration properties of samples, especially for high-speed mixing, while breakage had only a small influence on powder flowability. By contrast, some agglomeration occurred during blending for short time in the blender and the particle size did not decrease (P >0.05) even for blending at longer time, thus, there were only minor impacts on physical and functional properties of powders.

Keywords: Dairy powder breakage; Physical characteristics; Rehydration properties; Flowability; Specific bulk volume; Powder compressibility

4.1. Introduction

Several physical characteristics, including particle size, density, porosity, morphology, surface, and adsorption properties, are important to powder functionalities (Bronlund and Paterson, 2004; Fitzpatrick et al., 2004; Fu et al., 2012). There are many factors influencing these properties, from composition, production processes, transportation, to storage conditions (Finney et al., 2002; Ji et al., 2016b; Langrish et al., 2006; Sharma et al., 2012). Currently, most studies on factors influencing dairy powder characteristics have mainly focused on the ingredients, the parameters during homogenization and spray drying, but ignored powder changes caused by mechanical forces. Particle breakage will occur after spray drying

due to mechanical forces imposed on powder particles during the post-drying and transportation processes.

In Chapter 3, it was found that breakage significantly increased the surface area and bulk densities, and decreased the particle size of powders. After breakage, the surface composition slightly changed, protein and lactose proportions increased and fat decreased. In addition, particle morphology might be changed after breakage due to body breakage. This in-turn affected the water sorption and mechanical properties of samples, especially for body breakage. In addition to these two functionalities, rehydration is considered an important benchmark in the dairy industry to determine the overall quality of powder products. In addition, for spray-dried dairy powders, the flow properties are very important in handling and processing operations (Kim et al., 2005; Peleg, 1977). However, there are very few published works on the influence of breakage on these functionalities.

The objective of this chapter is to investigate the breakage of commercial agglomerated infant milk formula (IMF) using three processing methods, lab-scale dilute-phase pneumatic conveying, laboratory high-speed mixing and factory-scale blending. At the same time, the influences of breakage on rehydration properties, powder flowability, and specific storage volume of IMF were investigated. The aim is to build a better understanding of dairy powder breakage and its influence.

4.2. Material and methods

4.2.1. Materials

Two batches of Cow and Gate “follow on milk stage 2” IMF products were purchased from a local pharmacy (Cork, Ireland) to complete all the experiments. The nominal composition was 56.4% lactose, 20.4% fat, and 9.5% protein in this sample.

4.2.2. Equipment and powder breakage sample preparation



Figure 4-1. An isometric view of the inside of the Forberg blender.

An isometric view of the lab-scale pneumatic conveyor (presented in Figure 2-1B) and photos of the inside of the factory-scale blender (Forberg, F-20, Norway; presented in Figure 4-1) and laboratory high-speed mixer (presented in Figure 2-1C) were used to break samples. Powders were placed in the mixer operated at 22,000 rpm for three different durations of 1 min, 2 min, and 7 min (termed HM1, HM2, and HM7). Other samples were placed in the Forberg blender for the duration of 15 min, 30 min, and 70 min (termed FB15, FB30, and FB70). The processing capacities for mixer and blender were 100 g and 1,600 g, respectively. Samples just covered the blade of the mixer and the level of the powder was in the middle of the blade in the blender. The second batch of samples was blown through the pneumatic conveyor with an air velocity of 40 m/s and 50 m/s (termed PC40 and PC50) and feeding rate of 3.0 g/s.

As mentioned in 2.2.1, the samples used in this study were a packaged product that had most likely already undergone breakage during its handling from spray drying through to packing and thus this powder was more resistant to breakage than the original spray-dried powder. Therefore, the

processing conditions described above are relatively severe and were selected to ensure breakage could be expected.

4.2.3. Particle size distribution and specific surface area

The particle size ($D_{3,2}$), specific surface area (SSA), and particle size distribution (PSD) of samples were measured using a Malvern Mastersizer 3000 (Malvern Instruments Ltd., Worcestershire, UK) with a compressed air at 0.2 bar, following the method as described in 2.2.2.1. Measurements were performed in triplicate.

4.2.4. Bulk density, particle density, and porosity

Loose bulk density (ρ_b), tapped (100 taps) bulk density (ρ_{tapped}), particle density (ρ_p), and interparticle porosity (ε) of all samples were measured according to the method as described in 2.2.2.2.

4.2.5. Scanning electron microscopy (SEM)

The SEM (Zeiss-Supra 40 VP/Gemini Column, Carl Zeiss, Germany) was employed to observe the morphology of the samples according to the method as described in 2.2.7.

4.2.6. Surface free fat content

The surface free fat (SFF) content of milk powder was measured as per 2.2.2.3.

4.2.7. Rehydration properties

4.2.7.1. Wettability - contact angle

Dynamic contact angle was used to quantify the wetting process. This was monitored by an optical Tensiometer (Attention Theta, Biolin Scientific Ltd., Espoo, Finland) using the sessile drop spread wetting procedure (Ji et al., 2016a). A powder bed with a smooth surface was formed by passing a leveler across the surface. A set volume of 10 mL deionized water droplet

was gently dropped onto the surface of the powder bed at room temperature. The contact angle was recorded as a function of penetrating time using the sessile drop spread wetting procedure. The penetrating time taken for the contact angle to become zero was used to represent the wettability. All the measurements were conducted five times.

4.2.7.2. Dispersibility – dispersibility index

The dispersibility index (*DI*) of samples was measured as per GEA (2006). The use of *DI* is the traditional standard method to measure the percentage of dry matter that passes through a sieve (180 μm) after mixing for a short time. 25 g sample was added into a 600 mL beaker with 250 mL deionized water at 37ºC and then mixed vigorously with a spatula for exactly 20 s making 20 full strokes along the diameter of the beaker in both directions. The reconstituted samples were then poured onto the 180 μm sieve and the samples that passed through the sieve were collected for further measurement of dry matter content. The *DI* was calculated as Eq. (4-1):

$$DI = \frac{W_d \times (100+W)}{w \times \frac{100-W_m}{100}} \qquad \text{Eq. (4-1)}$$

where w is the weight of the sample, W_d (%, w/w) is the dry matter, W_m (%, w/w) is the free moisture content of the powder. All the measurements were repeated three times.

4.2.8. Powder flowability - flow function test

The flowability and flow index (Jenike index, ff_c) of samples was assessed by measuring their standard flow function with a powder flow tester (PFT), following the method as described in 2.2.2.4. The flow index was quantified by constructing the plot of the failure strength versus the consolidation stress. The standard classification of the flow index is if ff_c <1, powders are non-flowing; if 1< ff_c <2, powders are very cohesive; if 2< ff_c <4, powders are cohesive; if 4< ff_c <10, powders are easy to flow; and if ff_c >10, powders are very free-flowing.

4.2.9. Bulk density under consolidation

Bulk density and its variation under consolidation load is an important property of a powder. The PFT was used to measure the bulk density of the powders at the consolidation stresses used in section 4.2.8 above. The compressibility index (*CI*) indicates the extent to which the volume of a powder sample changes under a compressive load and it is used for analyzing the compressibility of powders during storage (Bhandari et al., 2013; Ji et al., 2017). The *CI* was calculated from Eq. (4-2):

$$CI(\%) = \frac{\rho_c - \rho_b}{\rho_c} \times 100 \qquad \text{Eq. (4-2)}$$

where ρ_b is the loose bulk density without compressing; ρ_c is the compressed bulk density at 4.838 kPa major principle consolidation stress. All the measurements were repeated in triplicate.

4.2.10. Statistical analysis

Results were expressed as mean ± standard deviation (SD). One-way analysis of variance (ANOVA), followed by Turkey's test, was used to determine the significant differences (SPSS, IBM, USA). A significance level of P <0.05 was used throughout the study.

4.3. Results and discussion

Breakage directly affects powder particle size and other physical properties, and as a consequence, may influence its functional properties, such as the ability to rehydrate, flow properties and specific storage volume.

4.3.1. Powder physical properties

4.3.1.1. Particle size and specific surface area

The particle size and SSA of samples are shown in Figure 4-2 and Table 4-1, respectively. After breakage, the particle size of PC and HM samples was significantly smaller than that of control samples (P <0.05). Meanwhile, with the increase of treatment time (in the HM group) or air velocities (in the

PC group), the particle size decreased gradually. For the pneumatic conveyor, particle size fell from 126 μm to 117.3 μm (at a conveying speed of 40 m/s) and to 109.3 μm for a speed of 50 m/s. For the high-speed mixer, breakage was significant too with particle size falling from 143 μm progressively to 65.4 μm for lengthening mixing times. The significant differences in SSA were also found in those two groups (P <0.05) and SSA increased with the decrease of particle size. The SSA was doubled after mixing for 7 min by the high-speed mixer. By contrast, powder in the Forberg blender was relatively unaffected by breakage with marginal changes in mean size for different blending times (P >0.05); particle size increased slightly for short blending times but then fell back at longer times.

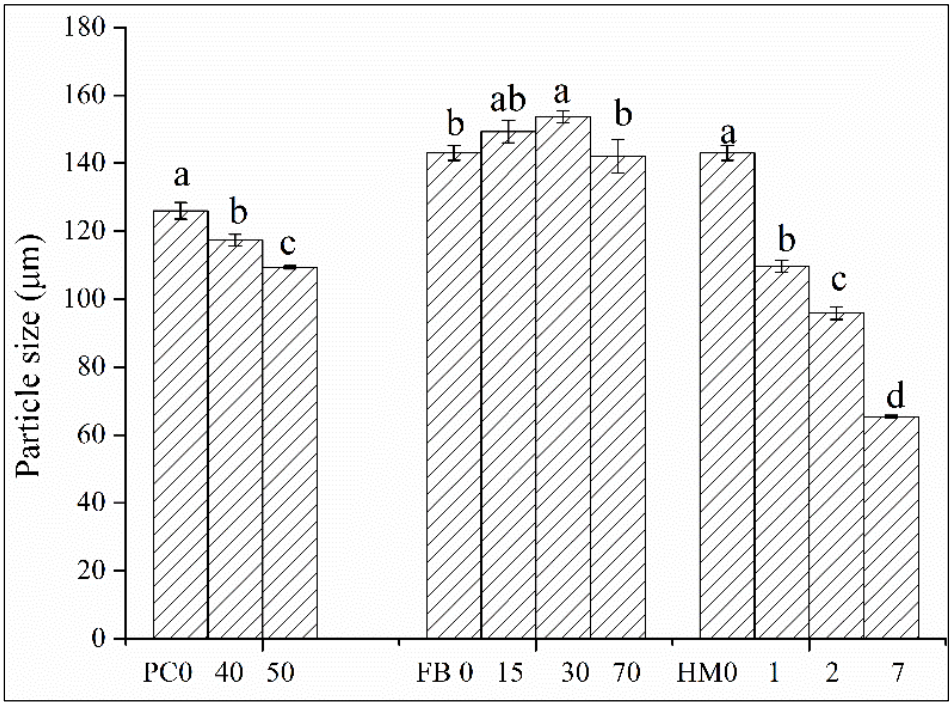


Figure 4-2. The particle size ($D_{3,2}$) of powder samples. PC: broken by pneumatic conveying under the air velocity of 40 m/s and 50 m/s. FB: broken by the Forberg blender for 15 min, 30 min, and 70 min. HM: broken by the laboratory high-speed mixer for 1 min, 2 min, and 7 min. Different a-d values within each group (PC, FB and HM) are significantly different at P <0.05.

Table 4-1. Properties of infant milk formula samples.

Samples	SSA (m^2/kg)	Bulk density (kg/L)	Particle density (kg/L)	Porosity (%)	SFF(%)
PC0	$47.6^{c}\pm0.8$	$0.492^{c}\pm0.003$	$1.2571^{b}\pm0.0008$	$55.80^{a}\pm0.08$	$1.183^{b}\pm0.012$
PC40	$51.2^{b}\pm0.8$	$0.506^{b}\pm0.001$	$1.2619^{a}\pm0.0008$	$53.47^{b}\pm0.03$	$1.238^{ab}\pm0.029$
PC50	$55.0^{a}\pm0.3$	$0.517^{a}\pm0.001$	$1.2627^{a}\pm0.0053$	$52.50^{c}\pm0.02$	$1.308^{a}\pm0.001$
FB0	$42.0^{a}\pm0.7$	$0.532^{b}\pm0.003$	$1.2119^{c}\pm0.0004$	$50.89^{a}\pm0.03$	$0.460^{d}\pm0.018$
FB15	$40.2^{ab}\pm0.9$	$0.532^{b}\pm0.005$	$1.2199^{a}\pm0.0007$	$50.30^{b}\pm0.03$	$0.503^{c}\pm0.001$
FB30	$39.0^{b}\pm0.4$	$0.541^{ab}\pm0.009$	$1.2125^{c}\pm0.0002$	$50.87^{a}\pm0.11$	$0.569^{b}\pm0.004$
FB70	$42.3^{a}\pm1.5$	$0.555^{a}\pm0.006$	$1.2185^{b}\pm0.0005$	$48.81^{c}\pm0.12$	$0.645^{a}\pm0.003$
HM0	$42.0^{d}\pm0.7$	$0.532^{c}\pm0.003$	$1.2119^{d}\pm0.0004$	$50.89^{a}\pm0.03$	$0.460^{d}\pm0.018$
HM1	$54.8^{c}\pm0.8$	$0.580^{b}\pm0.007$	$1.2203^{c}\pm0.0003$	$45.64^{b}\pm0.15$	$0.947^{c}\pm0.019$
HM2	$62.6^{b}\pm1.3$	$0.586^{b}\pm0.006$	$1.2285^{b}\pm0.0005$	$45.15^{c}\pm0.06$	$1.233^{b}\pm0.039$
HM7	$91.8^{a}\pm0.6$	$0.600^{a}\pm0.005$	$1.2311^{a}\pm0.0004$	$44.88^{c}\pm0.14$	$1.884^{a}\pm0.041$

1. PC: broken by pneumatic conveying under the air velocity of 40 m/s and 50 m/s. FB: broken by the Forberg blender for 15 min, 30 min, and 70 min. HM: broken by the laboratory high-speed mixer for 1 min, 2 min, and 7 min.
2. Values are mean ± standard deviation (n=3).
3. $^{a-d}$ different values within columns in each group (PC, FB and HM) are significantly different at $P<0.05$.

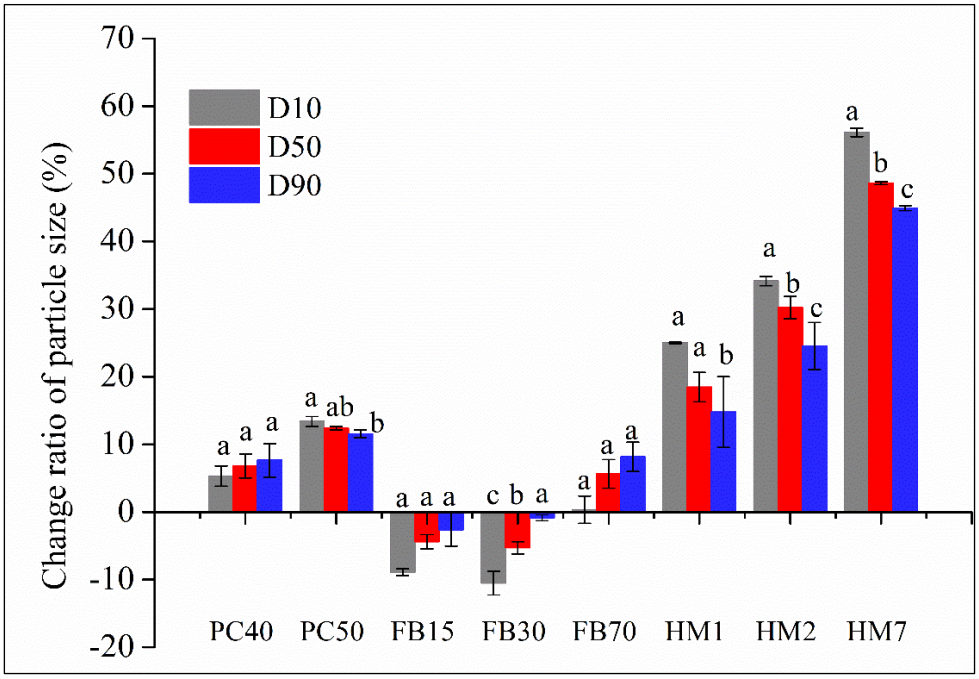


Figure 4-3. Percent decreases in different kinds of particle sizes (D_{10}, D_{50}, and D_{90}) of samples. D_{10}, D_{50}, and D_{90} mean 10%, 50%, and 90% of the sample are below this diameter, separately. PC: broken by pneumatic conveying under the air velocity of 40 m/s and 50 m/s. FB: broken by the Forberg blender for 15 min, 30 min, and 70 min. HM: broken by the laboratory high-speed mixer for 1 min, 2 min, and 7 min.

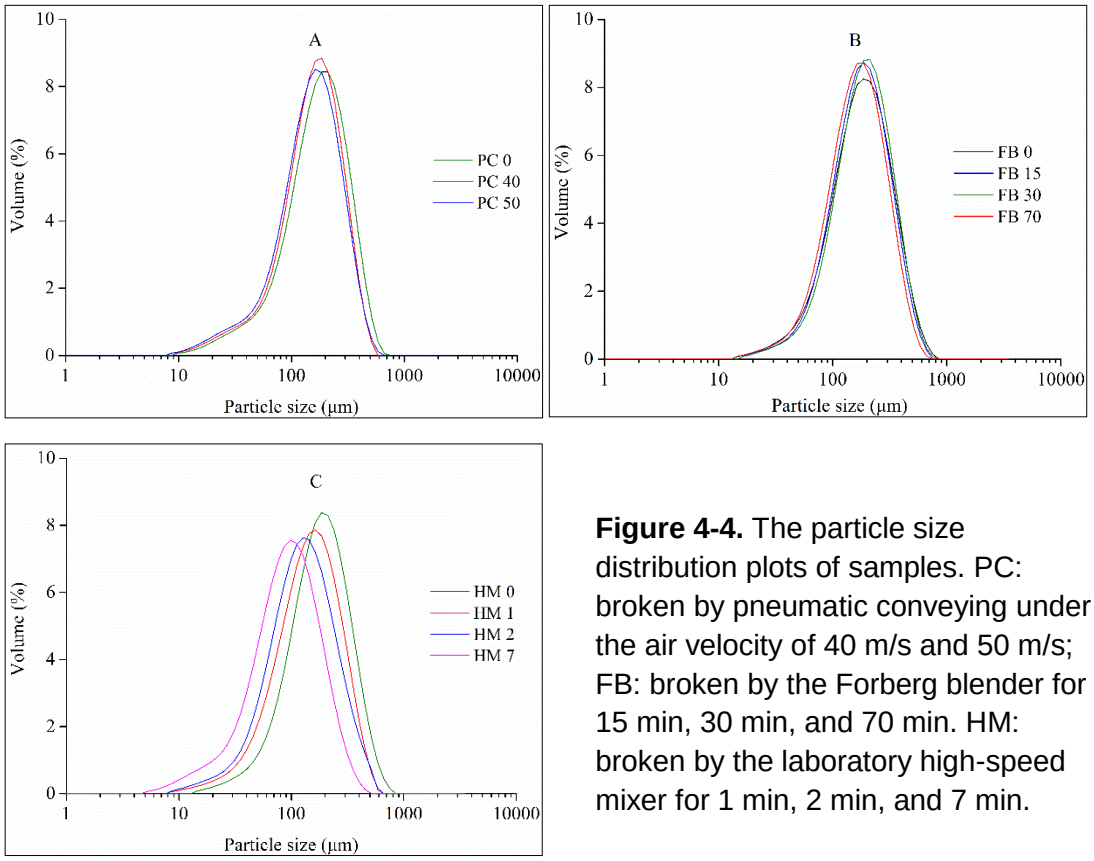


Figure 4-4. The particle size distribution plots of samples. PC: broken by pneumatic conveying under the air velocity of 40 m/s and 50 m/s; FB: broken by the Forberg blender for 15 min, 30 min, and 70 min. HM: broken by the laboratory high-speed mixer for 1 min, 2 min, and 7 min.

In order to further investigate the breakage patterns of samples during three processing methods, the percentage change in three different sizes, D_{10}, D_{50} and D_{90} for each system and condition and PSD plots were analyzed and shown in Figure 4-3 and Figure 4-4, respectively. The HM and PC group samples had much higher decreased ratios than FB group samples, which illustrates that particles of HM and PC group disintegrated much more than the FB group of particles. In pneumatic conveying, there was a similar decrease in all these sizes; a 5% decrease at 40 m/s and a 13% decrease at 50 m/s. This implies that all particles broke proportionally and the dispersion in size remained approximately the same. For the mixer, longer mixing times produced increasingly larger changes in these three size points ranging from 14% at the shortest time to over 45% at the longest time and their PSD plots shifted towards smaller values. Meanwhile, for this device, the D_{10} size always experienced a larger decrease than the D_{50} and D_{90} (P <0.05), which means all particles were broken with the production of more fine particles. The breakage during mixing and pneumatic conveying is typically associated with high-magnitude loading conditions, where the stresses applied to the particle exceed the particle strength and generate free surface area (Kotzur et al., 2018).

On the contrary for the Forberg blender, three kinds of particle sizes of FB15 and FB30 were slightly increased compared to their control sample, and from PSD plots the medium size increased. This result might be because some agglomeration occurred resulting in the decrease of fine particles and a slight increase of particle size. For FB70, the D_{50} and D_{90} slightly decreased compared to control samples and the volume fraction of medium size particles slightly increased. This result implies some of the corners and edges on the surface of original big particles might be separated and most particles after blending were the medium size that was the reason that the particle size of this sample had no significant difference with control samples.

Particle size is an important characteristic of dairy powder as it is closely related to many other characteristics, such as appearance, rehydration,

flowability, and density (Fitzpatrick et al., 2004; Sharma et al., 2012). The SSA values might affect the water sorption behaviours as the large surface area of particles meant more area for water molecules to attach.

4.3.1.2. Bulk density, particle density, and porosity

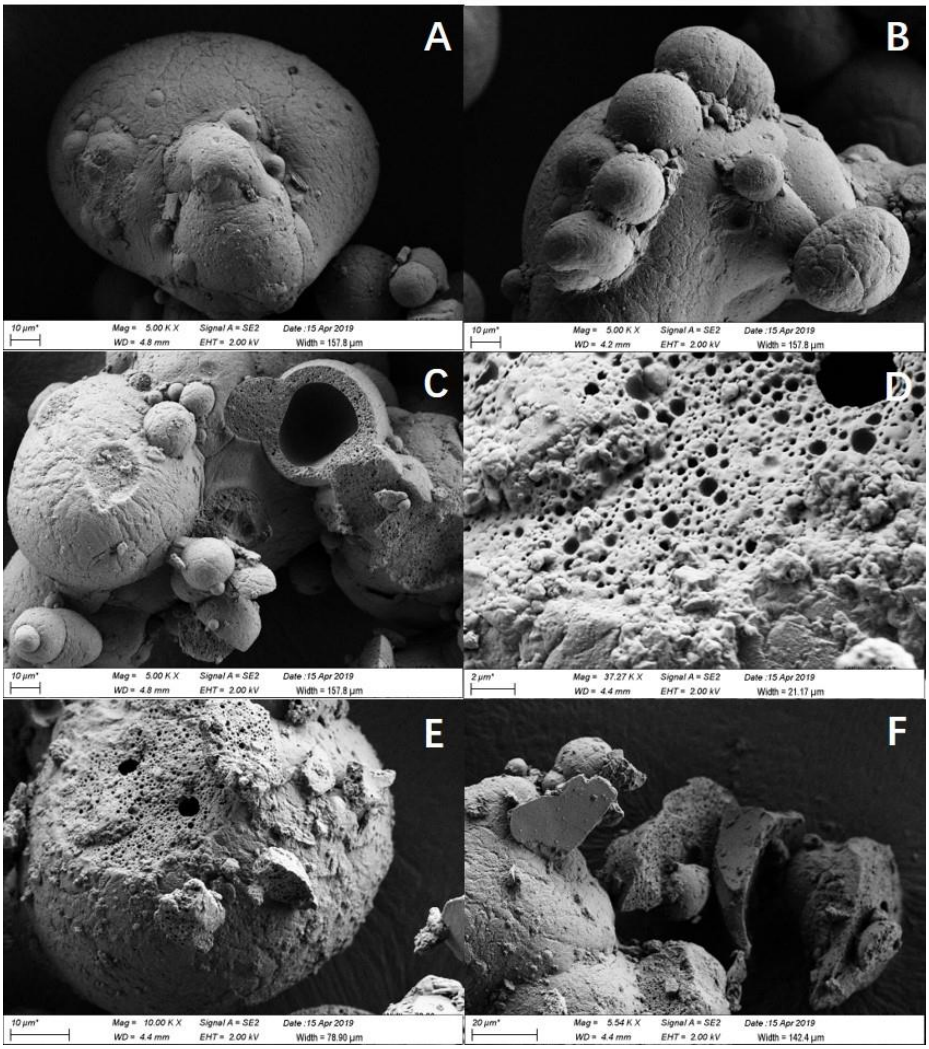


Figure 4-5. The SEM micrographs of control powder sample (A-B) and broken samples by the laboratory high-speed mixer for 7 min (C-F).

The density and porosity values of samples are shown in Table 4-1. It was shown that the bulk density of most broken samples significantly increased compared to control samples, and the porosity significantly decreased (P <0.05). After breakage, small particles that were broken from the original particles possibly filled void spaces between large particles, which caused the increase of the bulk density and the decrease of the porosity. The bulk density and porosity of some FB samples also changed (P <0.05), which

suggests that blending did influence structure even though the particle size did not decrease.

After breakage, the particle density of PC and HM group samples significantly increased (P <0.05). The SEM micrographs of some samples are shown in Figure 4-5. From micrographs, there were a lot of pores inside particles. Thus, the breakage did not only break solid bridges within agglomerated particles resulting in decreased particle size and increased bulk density, but also broke primary particles exposing internal pores leading to the increase of the particle density.

4.3.1.3. Surface free fat content

The surface free fat (SFF) content of samples is shown in Table 4-1. After breakage, the SFF of some samples were significantly increased (P <0.05), especially for HM samples, PC50 and FB70. Meanwhile, the SFF increased gradually with the increase of the processing time. HM7 had the highest SFF, 1.88±0.04%, which was four times more than the control sample. Powder particles generally consist of a continuous mass of amorphous lactose and other components in which fat globules and proteins are embedded (Sharma et al., 2012). The unprotected fat on particles covers the outermost surface and, beneath it fat bound to protein or proteins is present (Kim et al., 2003; Nijdam and Langrish, 2006). Particle breakage produced more surface area and liberated more free fat, which resulted in an increase of the SFF. The increase in SFF of the Forberg blender samples might be because the inter-particle contact was sufficient to break fat globules on the surface. At the same time, it might explain the small increases in particle size as the fat acts as a binder inducing some agglomeration. The increase of the SFF might affect the rehydration properties, especially for the wettability, as the SFF influences the surface hydrophobicity of powders.

4.3.2. Rehydration properties

4.3.2.1. Wettability - contact angles

Wettability is the ability of particles to imbibe a liquid and overcome the surface tension between them based on the capillary force (Forny et al., 2011; Ji et al., 2015; Ji et al., 2016a; Richard et al., 2013). The contact angle is usually used as a primary parameter to indicate the degree of the wetting process with a small contact angle ($\theta < 90^{o}$) representing good wettability and a large angle ($\theta > 90^{o}$) corresponding to poor wettability (Yuan and Lee, 2013). It is important to monitor the change of contact angle until reaching an equilibrium angle to quantify the wettability of powders as wetting behaviour is a dynamic procedure (Crowley et al., 2015). The penetrating time for water droplets to disappear and curves of contact angle as a function of penetrating time are shown in Figure 4-6. There was no significant difference in the penetrating time between FB samples, and water droplets were absorbed in 0.75 s. For PC40 and PC50 samples, droplets took 1.94 and 2.95 s to disappear, respectively; while the PC0 sample took around 0.94 s. These significant differences (P <0.05) mean when the air velocity is high enough, pneumatic conveying samples have poorer wettability compared to the control sample. The HM samples exhibited extremely poor wetting behaviours with penetration times of 4 s, 35 s, and 5 min for HM1, HM2, and HM7, respectively. Figure 4-6B also showed that the changes in contact angles of PC and HM samples were significantly slower than that of control samples. Thus, broken samples had poor wettability compared to control samples and as the degree of breakage increased, the wettability became worse.

There are two steps for the wetting process of powders. The first step is the replacement of gas by water so the interface of powders-gas is replaced by the interface of powder-water. Secondly, inward diffusion of the liquid through the capillary structures of the porous powder particle (Yuan and Lee, 2013). It is usually believed that wettability improves with larger particle size with higher bed porosity (Hogekamp and Schubert, 2003). The significant decrease of the particle size and porosity, as well as the increase of the SFF,

especially for the HM samples, is most likely the main reason for the poor wettability. Lower porosity with a small capillary radius between particles and greater surface hydrophobicity due to higher SFF inhibited water penetration into the powders, thus slowing down the wetting process.

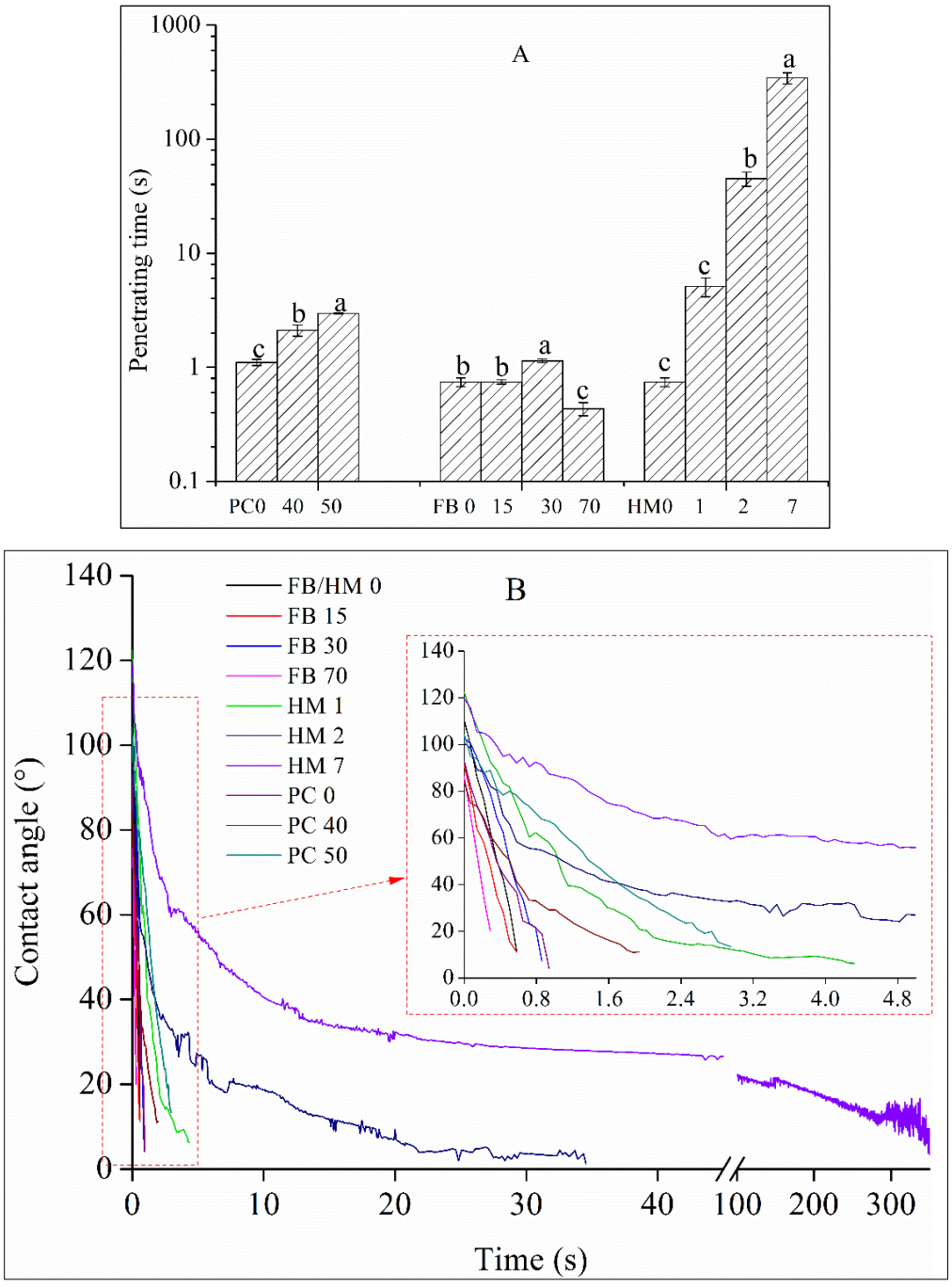


Figure 4-6. A: The penetrating time takes for water droplets to be absorbed. B: The change of contact angle as a function of penetrating time in approx. 20ºC temperature. PC: broken by pneumatic conveying under the air velocity of 40 m/s and 50 m/s. FB: broken by the Forberg blender for 15 min, 30 min, and 70 min. HM: broken by the laboratory high-speed mixer for 1 min, 2 min, and 7 min. Different a-c values within each group (PC, FB and HM) are significantly different at P <0.05.

4.3.2.2. Dispersibility - dispersibility index

Dispersibility is also an important step in the rehydration process, as it is necessary for particles to be dispersed into the liquid before dissolving (Galet et al., 2004; Goalard et al., 2006). Figure 4-7 illustrates the influence of breakage on the *DI* of samples. For PC and HM group samples, the *DI* significantly decreased compared to control samples and decreased gradually with the increase of treatment time. While, for FB samples, there was no significant difference between the *DI*. The substantial decrease of particle size and porosity, and increased SFF might be the reason for the deterioration of the dispersibility of broken samples by slowing down the penetration of water into the powder.

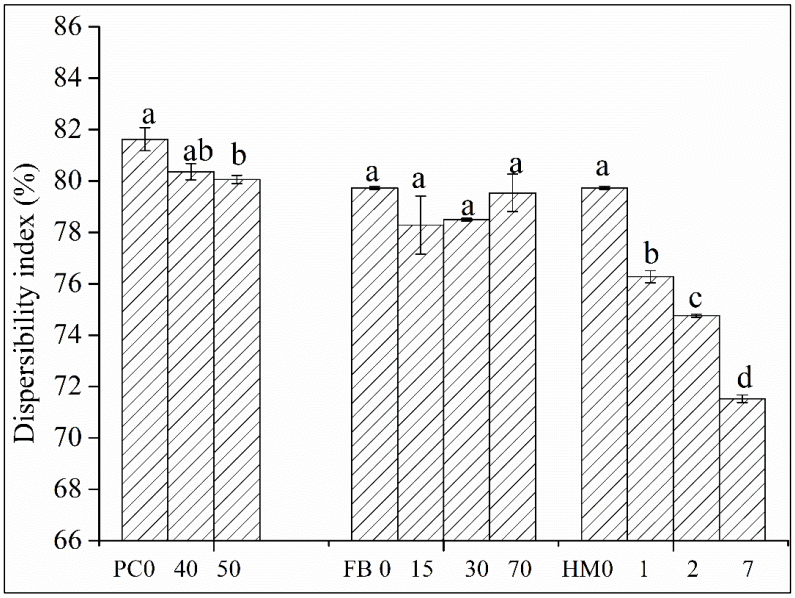


Figure 4-7. Dispersibility index for samples. PC: broken by pneumatic conveying under the air velocity of 40 m/s and 50 m/s. FB: broken by the Forberg blender for 15 min, 30 min, and 70 min. HM: broken by the laboratory high-speed mixer for 1 min, 2 min, and 7 min. Different a-d values within each group (PC, FB and HM) are significantly different at P <0.05.

4.3.3. Flow properties

The measured powder flow functions and flow indices (ff_c) are presented in Figure 4-8 and Table 4-2, respectively. It was shown that all powders were essentially easy-flowing and breakage had only a small influence on the flow functions and had no significant influence on the ff_c of powders. For PC and

HM group samples, it shows that breakage resulted in a small reduction in powder flowability. However, the FB powders displayed the poorest flowability relative to the others, even though there was little or no breakage.

Flow properties of dairy powders depend on their composition, in particular surface composition and physical characteristics, such as PSD, porosity, particle shape, surface properties, and water content (Crowley et al., 2014; Janjatović et al., 2012; Kim et al., 2005). The SFF of powders increased after breakage, which could be one of the reasons for the small decrease in powder flowability. SFF influences powder stickiness and liquid fat can form liquid bridges between individual particles reducing flowability (Kim et al., 2005; Peleg, 1977; Sharma et al., 2012). Furthermore, particle size decreased and bulk density increased after breakage, which meant more particle surface area was available for cohesive and frictional forces to resist flow. Thus powder flowability was reduced. However, overall, Figure 4-8 showed that the powder breakage observed did not have a major impact on powder flowability.

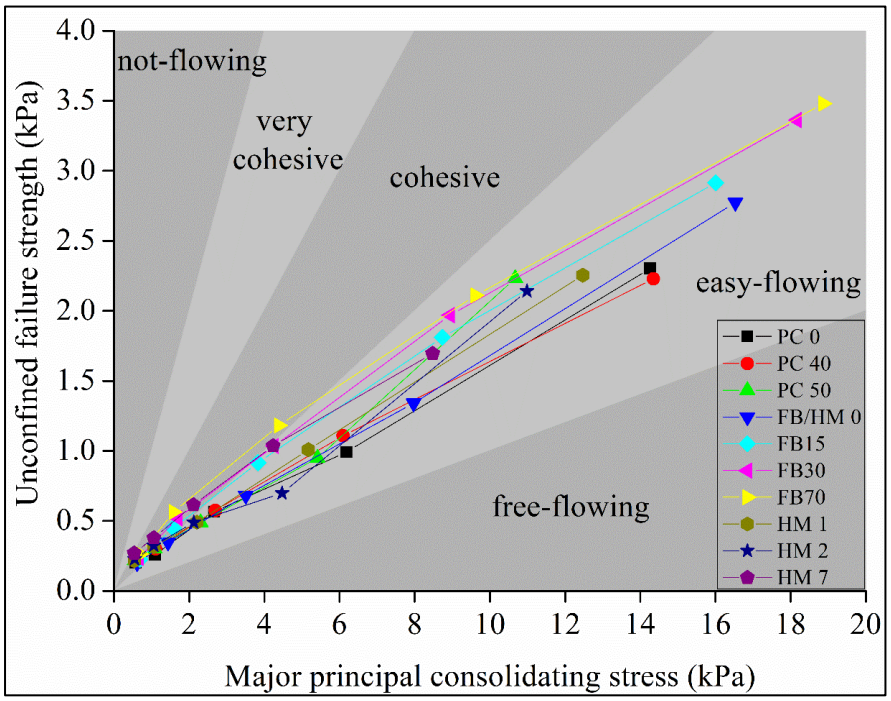


Figure 4-8. Unconfined strength as a function of major principal consolidating stress for infant milk formula samples. PC: broken by pneumatic conveying under the air velocity of 40 m/s and 50 m/s. FB: broken by the Forberg blender for 15 min, 30 min, and 70 min. HM: broken by the laboratory high-speed mixer for 1 min, 2 min, and 7 min.

Table 4-2. Loose specific bulk volume, compressibility index (*CI*), and flow index (ff_c)* of infant milk formula samples.

Samples	Loose specific bulk volume (L/kg)	*CI* (%)	ff_c
PC0	2.031^{a}±0.001	25.8^{a}±0.7	6.49^{a}±0.25
PC40	1.976^{b}±0.003	27.6^{a}±0.4	5.74^{a}±1.13
PC50	1.934^{c}±0.005	26.5^{a}±0.1	5.51^{a}±0.43
FB0	1.88^{a}±0.01	26.5^{a}±0.8	5.61^{a}±0.97
FB15	1.88^{a}±0.02	28.3^{a}±2.9	5.59^{a}±1.09
FB30	1.85^{a}±0.03	28.4^{a}±2.1	5.77^{a}±0.10
FB70	1.80^{b}±0.02	28.9^{a}±0.3	5.91^{a}±0.26
HM0	1.88^{a}±0.01	26.5^{a}±0.8	5.61^{a}±0.97
HM1	1.72^{b}±0.02	25.6^{a}±0.1	5.86^{a}±0.32
HM2	1.71^{bc}±0.02	29.3^{a}±0.2	5.50^{a}±0.19
HM7	1.67^{c}±0.01	24.7^{a}±0.3	5.58^{a}±0.31

1. PC: broken by pneumatic conveying under the air velocity of 40 m/s and 50 m/s. FB: broken by the Forberg blender for 15 min, 30 min, and 70 min. HM: broken by the laboratory high-speed mixer for 1 min, 2 min, and 7 min.
2. Values are mean ± standard deviation (n=3).
3. * The standard classification of the flow index is if ff_c <1, powders are non-flowing; if 1< ff_c <2, powders are very cohesive; if 2< ff_c <4, powders are cohesive; if 4< ff_c <10, powders are easy to flow; and if ff_c >10, powders are very free-flowing.
4. $^{a\text{-}c}$ different values within columns in each group (PC, FB and HM) are significantly different at P <0.05.

4.3.4. Specific bulk volume and powder compressibility

The specific bulk volume and how it is influenced by consolidation is an important powder functionality, as it influences the storage volume required to store a given mass of powder. Furthermore, for IMF, the specific bulk volume influences the size of product containers and the scoop volume requirement for the preparation of infant milk (Hanley, 2011; Li et al., 2016). The loose specific bulk volume is presented in Table 4-2 (this is the inverse of loose bulk density). It shows that the breakage occurring during pneumatic conveying and high-speed mixing significantly reduced the specific bulk volume requirement by about 3 to 11%. It also shows little or no reduction in specific bulk volume for the Forberg blender, as there was little or no breakage.

Figure 4-9 shows how bulk density varies for the different powder samples under consolidation. As expected, consolidation resulted in higher bulk

densities for all the samples. Like the loose powder case, Figure 4-9 shows that breakage resulted in higher bulk densities for all consolidations. This shows that breakage resulted in reduced specific bulk volume requirements under consolidations tested.

CI was calculated using the bulk density data (at 4.838 kPa major principle consolidation stress) and a high *CI* indicates the potential for high compressibility of powders during storage or transportation (Crowley et al., 2014). Table 4-2 presents the *CI* of different powder samples, which shows values mainly in the range of 26% to 29%, due to increases in bulk density during consolidation. Table 4-2 also shows that there was no significant relationship between breakage and the *CI*, which means that breakage had no influence on the compressibility of samples, even with the significant decrease in particle size and porosity. This is in-part due to the definition of *CI* in Eq. (4-2). Even though the compressed bulk density (ρ_c) is higher with greater breakage, the loose bulk density (ρ_b) is also higher, resulting in no clear relationship between breakage and *CI*.

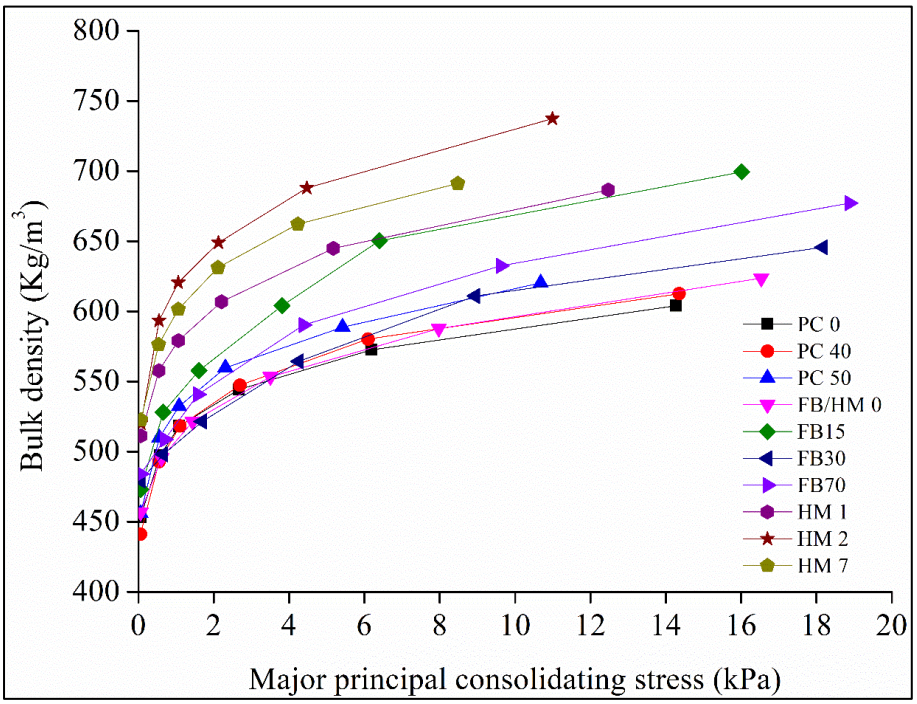


Figure 4-9. Bulk density as a function of major principal consolidating stress for infant milk formula samples. PC: broken by pneumatic conveying under the air velocity of 40 m/s and 50 m/s. FB: broken by the Forberg blender for 15 min, 30 min, and 70 min. HM: broken by the laboratory high-speed mixer for 1 min, 2 min, and 7 min.

4.4. Conclusion

This chapter was performed on the particle breakage of commercial IMF during three different processing methods (lab-scale pneumatic conveyor, laboratory high-speed mixer and Forberg blender), and how the breakage influenced the powder physical properties and functional properties (rehydration, flowability, and storage volume). The Forberg blender had a relatively small effect on particle size, even for very long blending times, but it did cause a gradual increase in SFF content, which may explain the small increases in average particle size observed. There were only minor impacts on the physical and functional properties of powder blended in the Forberg blender due to the minor changes in particle size.

Significant particle breakage occurred in the pneumatic conveyor and the high-speed laboratory mixer, and the longer or the more intense the processing, the greater the breakage. Particle breakage increased bulk density, which in-turn reduced specific bulk storage volume by about 3 to 11%. Powder breakage was accompanied by a significant decrease in particle size and increases in SFF content and bulk density. This in-turn impacted on powder rehydration in particular. Particle breakage caused a major reduction in powder wettability, especially for the high-speed mixer at longer times where much breakage occurred. These results emphasize the importance of controlling breakage levels in processing to maintain rehydration properties. Breakage in the high-speed mixer and pneumatic conveyor did not have a major impact on powder flowability, where there was only a minor negative impact observed.

Reference

Bhandari, B.R., Bansal, N., Zhang, M., & Schuck, P. (2013). *Handbook of food powders: Processes and properties* pp. 441-442). Elsevier.

Bronlund, J., & Paterson, T. (2004). Moisture sorption isotherms for crystalline, amorphous and predominantly crystalline lactose powders. *International Dairy Journal* 14(3), 247-254. https://doi.org/10.1016/S0958-6946(03)00176-6.

Crowley, S.V., Desautel, B., Gazi, I., Kelly, A.L., Huppertz, T., & O'Mahony, J.A. (2015). Rehydration characteristics of milk protein concentrate powders. *Journal*

of Food Engineering 149, 105-113. https://doi.org/10.1016/j.jfoodeng.2014.09.033.
Crowley, S.V., Gazi, I., Kelly, A.L., Huppertz, T., & O'Mahony, J.A. (2014). Influence of protein concentration on the physical characteristics and flow properties of milk protein concentrate powders. *Journal of Food Engineering* 135, 31-38. https://doi.org/10.1016/j.jfoodeng.2014.03.005.
Finney, J., Buffo, R., & Reineccius, G.A. (2002). Effects of Type of Atomization and Processing Temperatures on the Physical Properties and Stability of Spray-Dried Flavors. *Journal of Food Science* 67(3), 1108-1114. https://doi.org/10.1111/j.1365-2621.2002.tb09461.x.
Fitzpatrick, J.J., Iqbal, T., Delaney, C., Twomey, T., & Keogh, M.K. (2004). Effect of powder properties and storage conditions on the flowability of milk powders with different fat contents. *Journal of Food Engineering* 64(4), 435-444. https://doi.org/10.1016/j.jfoodeng.2003.11.011.
Forny, L., Marabi, A., & Palzer, S. (2011). Wetting, disintegration and dissolution of agglomerated water soluble powders. *Powder Technology* 206(1), 72-78. https://doi.org/10.1016/j.powtec.2010.07.022.
Fu, X., Huck, D., Makein, L., Armstrong, B., Willen, U., & Freeman, T. (2012). Effect of particle shape and size on flow properties of lactose powders. *Particuology* 10(2), 203-208. https://doi.org/10.1016/j.partic.2011.11.003.
Galet, L., Vu, T.O., Oulahna, D., & Fages, J. (2004). The Wetting Behaviour and Dispersion Rate of Cocoa Powder in Water. *Food and Bioproducts Processing* 82(4), 298-303. https://doi.org/10.1205/fbio.82.4.298.56399.
Goalard, C., Samimi, A., Galet, L., Dodds, J.A., & Ghadiri, M. (2006). Characterization of the Dispersion Behaviour of Powders in Liquids. *Particle & Particle Systems Characterization* 23(2), 154-158. https://doi.org/10.1002/ppsc.200601024.
Hanley, K.J., 2011. Experimental quantification and modelling of attrition of infant formulae, Department of Process and Chemical Engineering. University College Cork, Cork, Ireland.
Hogekamp, S., & Schubert, H. (2003). Rehydration of Food Powders. *Food Science and Technology International* 9(3), 223-235. https://doi.org/10.1177/1082013203034938.
Janjatović, D., Benković, M., Srečec, S., Ježek, D., Špoljarić, I., & Bauman, I. (2012). Assessment of powder flow characteristics in incoherent soup concentrates. *Advanced Powder Technology* 23(5), 620-631. https://doi.org/10.1016/j.apt.2011.07.003.
Ji, J., Cronin, K., Fitzpatrick, J., Fenelon, M., & Miao, S. (2015). Effects of fluid bed agglomeration on the structure modification and reconstitution behaviour of milk protein isolate powders. *Journal of Food Engineering* 167, 175-182. https://doi.org/10.1016/j.jfoodeng.2015.01.012.
Ji, J., Fitzpatrick, J., Cronin, K., Crean, A., & Miao, S. (2016a). Assessment of measurement characteristics for rehydration of milk protein based powders. *Food Hydrocolloids* 54, 151-161. https://doi.org/10.1016/j.foodhyd.2015.09.027.
Ji, J., Fitzpatrick, J., Cronin, K., Fenelon, M.A., & Miao, S. (2017). The effects of fluidised bed and high shear mixer granulation processes on water adsorption and flow properties of milk protein isolate powder. *Journal of Food Engineering* 192, 19-27. https://doi.org/10.1016/j.jfoodeng.2016.07.018.
Ji, J., Fitzpatrick, J., Cronin, K., Maguire, P., Zhang, H., & Miao, S. (2016b). Rehydration behaviours of high protein dairy powders: The influence of agglomeration on wettability, dispersibility and solubility. *Food Hydrocolloids* 58, 194-203. https://doi.org/10.1016/j.foodhyd.2016.02.030.
Kim, E.H.J., Chen, X.D., & Pearce, D. (2005). Effect of surface composition on the flowability of industrial spray-dried dairy powders. *Colloids and Surfaces B: Biointerfaces* 46(3), 182-187. https://doi.org/10.1016/j.colsurfb.2005.11.005.

Kim, E.H.J., Dong Chen, X., & Pearce, D. (2003). On the Mechanisms of Surface Formation and the Surface Compositions of Industrial Milk Powders. *Drying Technology* 21(2), 265-278. https://doi.org/ 10.1081/DRT-120017747.

Kotzur, B.A., Berry, R.J., Zigan, S., García-Triñanes, P., & Bradley, M.S.A. (2018). Particle attrition mechanisms, their characterisation, and application to horizontal lean phase pneumatic conveying systems: A review. *Powder Technology* 334, 76-105. https://doi.org/10.1016/j.powtec.2018.04.047.

Langrish, T.A.G., Marquez, N., & Kota, K. (2006). An Investigation and Quantitative Assessment of Particle Shape in Milk Powders from a Laboratory-Scale Spray Dryer. *Drying Technology* 24(12), 1619-1630. https://doi.org/ 10.1080/07373930601031133.

Li, R., Roos, Y.H., & Miao, S. (2016). Influence of pre-crystallisation and water plasticization on flow properties of lactose/WPI solids systems. *Powder Technology* 294, 365-372. https://doi.org/10.1016/j.powtec.2016.02.047.

Nijdam, J.J., & Langrish, T.A.G. (2006). The effect of surface composition on the functional properties of milk powders. *Journal of Food Engineering* 77(4), 919-925. https://doi.org/10.1016/j.jfoodeng.2005.08.020.

Niro, G. (2006). GEA Niro analytical methods dry products. *GEA Process Engineering A/S, Gladsaxevej, Denmark,*.

Oveisi, E., Lau, A., Sokhansanj, S., Lim, C.J., Bi, X., Larsson, S.H., & Melin, S. (2013). Breakage behaviour of wood pellets due to free fall. *Powder Technology* 235, 493-499. https://doi.org/10.1016/j.powtec.2012.10.022.

Peleg, M. (1977). FLOWABILITY OF FOOD POWDERS AND METHODS FOR ITS EVALUATION — A REVIEW. *Journal of Food Process Engineering* 1(4), 303-328. https://doi.org/ 10.1111/j.1745-4530.1977.tb00188.x.

Richard, B., Le Page, J.F., Schuck, P., Andre, C., Jeantet, R., & Delaplace, G. (2013). Towards a better control of dairy powder rehydration processes. *International Dairy Journal* 31(1), 18-28. https://doi.org/10.1016/j.idairyj.2012.07.007.

Sharma, A., Jana, A.H., & Chavan, R.S. (2012). Functionality of Milk Powders and Milk-Based Powders for End Use Applications—A Review. *Comprehensive Reviews in Food Science and Food Safety* 11(5), 518-528. https://doi.org/ 10.1111/j.1541-4337.2012.00199.x.

Yuan, Y., & Lee, T.R. (2013). Contact angle and wetting properties. *Surface science techniques* (pp. 3-34). Springer.

CHAPTER FIVE

Investigation of the influence of powder characteristics on the breakage of dairy powders

Chapter 5 was published in:

Han, J., Fitzpatrick, J., Cronin, K., & Miao, S. (2021). Investigation of the influence of powder characteristics on the breakage of dairy powders. *Food Research International*, 110775.

The work contained in this chapter was undertaken and written solely by myself with specific contributions from each co-author:

Jie Han: Conceptualization, Methodology, Formal analysis, Investigation, Data curation, Writing – original draft, Visualization

John Fitzpatrick: Supervision, Writing – review & editing

Kevin Cronin: Supervision, Writing – review & editing

Song Miao: Supervision, Conceptualization, Writing – review & editing, Funding acquisition, Project administration

Abstract

Dairy powder breakage occurs in many processes and deteriorates powder properties and functionalities. This chapter investigated the influence of powder and particle characteristics on the dynamic breakage of dairy powders during the dispersion and conveying in a powder venturi feeder to provide information on assessing and reducing powder breakage during production and transportation. Four kinds of dairy powders (fifteen samples) were analysed: lactose crystals, agglomerates, commercial and lab-scale non-agglomerates. During the dispersion and conveying, breakage degree increased with increasing particle size and decreasing particle structural strength. Considering particle structure, the strength of crystals was the highest, followed by the continuum solids, followed by particles with numerous small holes throughout the particle, followed by particles with a small number of randomly distributed internal holes, followed by the hollow sphere particle with a very thin shell. The breakage behaviour of crystals during conveying was different from the other powders due to the difference in particle structures.

Keywords: Dairy powder breakage; Powder venturi feeder; Powder dispersion and conveying process; Breakage percentage; Particle size; Particle structure

5.1. Introduction

Previous chapters and other recent research showed that powder breakage significantly increased densities and surface free fat contents, and reduced the particle size and porosities of agglomerated dairy powders, including infant milk formula (IMF), instant whole milk powder, fat-filled milk powder, and whey protein concentrate powder (Boiarkina et al., 2016; Han et al., 2020; Han et al., 2022; Hazlett et al., 2020). In addition, powder breakage changed the surface area and surface composition of dairy powders, as well as the particle shapes. The changes in these physical properties of dairy powders led to a decline in the flowability and rehydration properties (Han et

al., 2020; Hazlett et al., 2020). Among these, the rehydration properties were more affected, especially for the wetting and dispersing stages of reconstitution (Chapter 4). In addition, in Chapter 3 it was found that body breakage increased the water sorption rate and final water content, and then accelerated the time-dependent crystallization of IMF (Han et al., 2022). As the higher water contents of body breakage samples, their glass transition and *α*-relaxation temperatures slightly decreased. This indicates that broken samples have more strict requirements on the storage environment, such as lower storage temperature and water activity.

These properties are important for the use and storage of dairy powders, therefore, in order to keep the functionalities of dairy powders, it is necessary to control the unwanted breakage during the production, storage, and transportation of powders. Based on the particle breakage studies of other materials, the applied stress from processing conditions and the characteristics of particles are two main effects that influence particle breakage (Petukhov and Kalman, 2004). The process conditions (including the parameters during dry-mixing, vibration, and pneumatic conveying) play a fundamental role in the determination of particle breakage and that, together with particle characteristics, dictates the response of particles for given loading conditions (Kotzur et al., 2018; Lu et al., 2014; Petukhov and Kalman, 2004; Yan and Barbosa-Cánovas, 2001). Thus, the control of dairy powder breakage can be considered from these two aspects. For the former, Hanley (2011) investigated the breakage of agglomerated IMF during the pneumatic conveying. It was found that, compared with dense-phase pneumatic conveying, dilute-phase pneumatic conveying resulted in high breakage and the extent of breakage increased with increasing air velocities. Besides, the number and the radius of bends in the pneumatic conveyor also influenced the breakage of IMF. During the tapping test of instant non-fat milk powders, it was found that powder breakage increased with increasing tapping number (Yan and Barbosa-Cánovas, 2001). However, there is currently not enough research on the influence of particle characteristics on dairy powder breakage when particles are subjected to mechanical loads.

This chapter mainly considered the influence of powder and particle characteristics on dairy powder breakability during the dispersion and conveying in a powder venturi feeder (the Aero S disperser of Malvern Mastersizer 3000). The powder venturi feeder is commonly used to disperse fine and cohesive particles but it also could break particles during the dispersion and conveying. There are many similarities in the conditions that dairy powder experiences in this device and during the pneumatic conveying at the industrial scale for in-plant transportation or packaging (Han et al., 2021a; Hazlett et al., 2020). Fifteen commercial or lab-scale dairy powders with different physical properties and ingredients were studied to provide as comprehensive situations as possible. The aim is to provide information on reducing or controlling dairy powder breakage from the aspect of powder characteristics rather than the process parameters.

5.2. Material and methods

5.2.1. Material

Fifteen different dairy powders were studied including ten commercial samples, *α*-Lactose Monohydrate (LAC, Arla Food Ingredients, Sønderhøj 10-12 8260 DK-Viby J, Denmark), nutritional whey protein (NWP, Volac International Limited, Hertfordshire, UK), sodium caseinate (SC, protein content around 90%, Kerry Ingredients, County Kerry, Ireland), micellar casein concentrate (MCC, Molkereigesellschaft Lauingen mbH, Lauingen, Germany), IMF (IMF1 and IMF2 were Aptamil Profutura follow on milk ‘stage 1’ and ‘stage 2’, respectively), skim milk powder (SMP1: Kerry Ingredients, County Kerry, Ireland; SMP2: Glanbia plc, Kilkenny, Ireland), enriched milk powder (EMP, Glanbia plc, Kilkenny, Ireland), and full-fat milk powder (FFMP, Lakelands dairies, Bailieborough, Cavan, Ireland), and five lab-scale model samples with different percentages of whey protein isolate (WPI) and lactose (WPI: LAC were around 1:1, 2:1, 4:1, 1:2, and 1:4) produced with the same process by a single-stage spray dryer, termed as WL11, WL21, WL41, WL12, and WL14, respectively.

As the particle size distributions of LAC, IMF, SMP, FFMP, and EMP were wide, samples were also sieved into four size fractions, from 125 to 75 μm, from 180 to 125 μm, from 250 to 180 μm, from 355 to 250 μm (termed 125-75, 180-125, 250-180, and 355-250, respectively) to investigate the influence of particle size on breakage. Due to the high cohesiveness of powders, FFMP and EMP were only sieved into the last two size fractions and the other particles were not separated.

5.2.2. The main bulk and surface composition of samples

The lactose content of samples was determined using high performance liquid chromatography (HPLC) with an Aminex HPX 87C fixed ion resin column. Samples were diluted in water and then analysed for quantification of lactose. The eluent was run at 0.5 ml/min and the lactose was detected using a refractive index detector with a sensitivity set at 512, an internal temperature set at 35℃ and a positive polarity. Total protein content was measured using the Kjeldahl method to measure total nitrogen and calculated using a nitrogen-to-protein conversion factor of 6.38. Total fat contents of samples were determined using the CEM SMART Trac 2 (CEM Corporation, Matthews, USA).

The surface composition of samples was determined based on the method as described in 3.2.5. It should be mentioned that the surface fat content in IMF1 and IMF2 was calculated based on the elemental composition of milk fat because the fat in infant milk formula was mixed vegetable fat.

5.2.3. Sauter mean particle size of samples

The Sauter mean particle size ($D_{3,2}$) of samples samples was measured by a Malvern Mastersizer 3000 (Malvern Instruments Ltd., Worcestershire, UK), following the method as described in 2.2.2.1.

5.2.4. Particle density, bulk density, and interparticle porosity

Particle density (ρ_p), bulk density (tapped (100 taps) bulk density (ρ_{tapped}) and loose bulk density (ρ_b)), and interparticle porosity (ε) of samples were measured according to the method as described in 2.2.2.2.

5.2.5. Friability

Friability refers to the ability of particles to break into smaller particles and can be used to represent powder strength. The friability index (*FI*) of powders was measured according to the method as described in 3.2.4.2.

5.2.6. Powder structural properties

A polarised light microscope (Instruction BX51, Olympus Optical Co. Ltd., Tokyo, Japan) was employed to observe the samples with a 10× objective or a 60× oil objective, following the method as described in 2.2.7.

5.2.7. Powder breakage in the powder venturi feeder

Powders were fed to the powder venturi feeder (diagram is shown in Figure 2-1A) of the Mastersizer 3000, and the $D_{3,2}$ of samples was measured at a series of air pressures (from 0 to 4.0 bar in 0.5 bar increments), following the method as described in 2.2.3.2.

The degree of breakage was shown as the breakage percentage (*BP*) that was evaluated as Eq. (2-3), according to the method as described in 2.2.6. The *BP* under a series of air pressures represents the breakage of powders under different loads, which is different from the *FI*, although the calculation of *BP* under 4 bar (difference between $D3,2_0$ and $D3,2_{4.0}$) is similar to the *FI* (difference between of $D3,2_{0.5}$ and $D3,2_{4.0}$).

5.2.8. Experimental design and statistical analysis

The experimental design was completely randomized. Measurements of bulk density and porosity were carried out in duplicate, and all other measurements were performed in triplicate. Results were expressed as

mean ± standard deviation (SD). Student's t-test with a 95% confidence interval was used to determine the significant differences in particle size and friability between two size fractions (355-250 and 250-180) in each sample (EMP and FFMP). One-way ANOVA with Tukey's test (IBM SPSS Statistics version 24, IBM, USA) was used to determine significant differences in other results with a confidence level of P <0.05.

5.3. Result and discussion

The physical and structural characteristics of samples were firstly determined and then samples were divided into several groups for breakage discussion based on the differences in characteristics.

5.3.1. Composition and physical properties of powders

5.3.1.1. The bulk and surface composition

The main bulk and surface composition (fat, protein, and lactose) of fifteen samples are shown in Table 5-1.

As expected, the purity of commercial ingredients (LAC, MCC, SC, and NWP) were relatively high where the bulk lactose content of LAC was higher than 99%, and the bulk protein contents of MCC, SC, and NWP were around 85%. For other commercial powders (SMP, IMF, EMP, and FFMP), SMP had the highest bulk protein contents, around 35%, and the lowest bulk fat contents, around 1%. The bulk fat contents of the other four samples were around 20% or 30%, and those of EMP and FFMP were higher than those of IMF who had the highest bulk lactose content. The ratio of bulk protein to lactose of lab-scale non-agglomerated WPI/lactose model powders met the expectation where the bulk protein content ranged from 18 to 71%, and lactose contents were from 19 to 70% with around 0.5% fat.

From Table 5-1, the most component on the surface of particles from LAC and commercial protein ingredients (NWP, MCC, and SC) are lactose and protein, respectively. For other commercial agglomerated powders, the composition on the surfaces of sample particles was very different from their

Table 5-1. The main bulk and surface composition of different dairy powders.

Group	Sample	Bulk composition (%)			Surface composition (%)		
		Fat	Protein	Lactose	Fat	Protein	Lactose
A	LAC	0^{i}	0.15^{j}±0.02	99.57^{a}±0.12	0^{e}	4.6^{d}±2.7	95.4^{a}±2.7
	IMF1	26.02^{c}±0.01	11.05^{h}±0.01	62.08^{c}±0.05	87.2^{a}±2.4	4.2^{d}±0.5	8.6^{de}±1.8
	IMF2	20.98^{d}±0.14	9.91^{i}±0.03	67.85^{b}±0.04	88.5^{a}±2.3	4.1^{d}±0.8	7.4^{def}±1.5
	EMP	33.33^{a}±0.01	21.14^{g}±0.03	39.37^{f}±0.04	78.6^{b}±0.6	7.0^{d}±0.3	13.5^{d}±0.3
	FFMP	28.14^{b}±0.07	26.75^{f}±0.21	40.02^{f}±0.05	84.9^{a}±1.0	5.5^{d}±2.5	9.0^{de}±1.5
	SMP1	0.82^{g}±0.01	37.59^{d}±0.05	51.92^{e}±0.04	15.3^{d}±1.0	44.9^{c}±0.4	38.0^{c}±0.8
	SMP2	1.05^{f}	34.71^{e}±0.09	55.64^{d}±0.06	26.7^{c}±0.6	11.5^{d}±1.1	60.5^{b}±0.3
	NWP	0.59^{h}±0.01	86.00^{b}±0.01	2.45^{gh}±0.26	3.1^{e}±0.7	91.8^{a}±1.0	3.9^{ef}±0.3
	MCC	1.27^{f}±0.02	87.24^{a}±0.01	3.07^{g}±0.05	20.1^{d}±4.4	76.9^{b}±5.0	0^{f}
	SC	1.53^{e}±0.02	82.48^{c}±0.05	2.65^{g}±0.14	18.6^{d}±0.8	76.9^{b}±3.9	3.4^{ef}±2.9
B	WL11	0.58^{A}±0.01	44.93^{C}±0.09	40.02^{C}±0.05	12.2^{A}±2.5	59.2^{C}±2.5	28.2^{B}±0.1
	WL21	0.55^{A}±0.01	58.73^{B}±0.19	23.06^{D}±0.02	9.7^{A}±2.6	69.4^{B}±4.2	20.3^{C}±1.8
	WL41	0.55^{A}	70.23^{A}±0.12	18.03^{E}±0.06	6.3^{A}±1.5	81.3^{A}±1.2	11.4^{D}±0.1
	WL12	0.57^{A}±0.01	30.34^{D}±0.01	58.60^{B}±0.06	8.1^{A}±1.7	53.2^{CD}±0.5	38.2^{A}±2.1
	WL14	0.57^{A}±0.01	18.86^{E}±0.06	71.24^{A}±0.06	8.4^{A}±2.5	49.3^{D}±1.0	41.8^{A}±1.7

1. LAC: α-Lactose Monohydrate; IMF: infant milk formula; EMP: enriched milk powder; FFMP: full-fat milk powder; SMP: skim milk powder; NWP: nutritional whey protein; MCC: micellar casein concentrate; SC: sodium casein; WL: model samples with different percentage of whey protein and lactose.
2. Values are mean ± standard deviation (n=2).
3. $^{a\text{-}j}$ and $^{A\text{-}E}$ different values within columns in each group, A and B, respectively, are significantly different at P <0.05.

bulk composition and the fat contents on the surface of particles were remarkably higher than their bulk fat contents. This was not surprising and similar results were found in some commercial milk particles, such as milk protein concentrate, low-fat milk powder, and whole milk powder (Foerster et al., 2016; Kim et al., 2009). This might because of the different migration properties of milk components toward the interior or surface of the droplet during the atomization stage and the subsequent drying stage resulted in the redistribution of the components within the particles (Shrestha et al., 2007). Based on the Stoke-Einstein equation, free fat particle or fat globules, casein micelles, whey protein, lactose, and salts are descending in size, while their diffusivities are inverse (Kim et al., 2003). Therefore, during drying after atomization, lactose very quickly diffuses toward the center of the droplet, followed by whey protein and free fat or fat globules. However, some researchers demonstrated that fat globules were ruptured and spread homogeneously over the droplet surface, creating a thin fat film during the atomization stage and resulting in a higher surface fat content than bulk fat content (Foerster et al., 2016). For lab-scale non-agglomerated WPI/lactose model powders, the highest content on particle surfaces was whey protein, from 49.3% to 81.3%, even for WL12 and WL14 whose bulk whey protein content was lower than 50%. The distribution of components on the surface of particles is driven by the bulk composition of powders and also the drying approach and parameters.

5.3.1.2. Particle size

The particle sizes of initial whole samples and sieved fractions are given in Table 5-2 and Table 5-3, respectively. It has been demonstrated that particle size is one of the most important factors affecting particle breakage and particle strength decreases as the particle size increases (Bonakdar et al., 2016; Gerhards et al., 2004; Norazirah et al., 2016; Zhang and Ghadiri, 2002). This is attributed to the likelihood of a greater number of imperfections in larger particles. The structural defects in particles are analogous to microcracks, imperfections, or inhomogeneities in material science. The highest local tensile stress is generated at these defective zones in the

agglomerates so that the fracture initiates from this zone. Besides lesser flaws, small particles are more difficult to break because of the stronger interparticle forces (including van der Waals forces, electrostatics, and liquid bonds) that bind particles together (Reynolds et al., 2005). From an energy perspective, the probability of breakage is related to the amount of energy that is absorbed by the particle during the breakage. The particle can absorb a certain amount of energy as stored elastic strain before it breaks. The energy that is absorbed and stored represents the minimum energy that is required to break the particle under the particular external loading and stress pattern that the particle experiences. This energy is called the particle fracture energy and it is a material property that is influenced by its particle size, shape, the orientation that the particle presents to the impact stress, and the presence of flaws in the particle. For particles of the same material, the smaller the particles, the higher the fracture energy, and hence the less likely particles will break (King, 2012).

5.3.1.3. Powder densities and interparticle porosities

The particle densities, bulk densities, and porosities of the initial whole samples are shown in Table 5-2. Particle density is the mass per unit volume of particles, including the closed pores but excluding the cracks or open pores so it is related to particle structure characteristics that may affect the breakage behaviour of particles. From Table 5-2, the particle density of IMF was the smallest, at around 1.0 kg/L, and LAC had the highest particle density that was around 1.9 kg/L. Besides, SC and WPI/lactose model samples had a similar particle density, around 1.3 kg/L, which was slightly lower than that of SMP2 but higher than those of other samples. The bulk density of powders is also influenced by particle structure and shapes. Similar to the particle density, LAC had the highest tapped bulk density and loose bulk density and they were significantly higher than those of other samples. However, instead of the IMF, the bulk densities of WPI/lactose model samples were the smallest. This is because these small particles were much lighter and had much higher specific surface areas and thus trapped air much more easily in a bed of powder, which reduced the bulk density and

increased the porosity. The bulk densities of other samples were in between those of LAC and model samples, where those of IMF, SMP, and SC were higher than those of NWP, FFMP, EMP, and MCC. By definition, interparticle porosity is affected by the particle density and tapped bulk density of powders and it may influence the multi-particles behaviour of dairy powders. From Table 5-2, the porosity of IMF was the smallest, at around 40% or 45%, while WPI/lactose model samples had the highest porosities, at around 75% to 78%. The porosities of other samples were in between of them, where those of LAC, SMP1, and SC were around 50%, those of EMP, FFMP, SMP2, and NWP were around 60%, and that of MCC was around 70%.

5.3.1.4. Friability

Friability index is the most used index to indicate the strength of food powders or the sensitivity of particles to the breakage when particles are subjected to mechanical loads. The *FI* of the initial whole samples and sieved fractions are given in Table 5-2 and Table 5-3, respectively. For the initial whole sample, it was shown that the *FI* of samples was different, ranging from 10% to 54%. IMF, NWP, and WL41 particles were the easiest to break while SC and MCC particles were the most difficult to break. For sieved fractions of most samples, the *FI* increased with increasing particle size, except for the sieved fractions of LAC 125-75 and IMF1 180-125. This means the bigger the particles, the easier it is for them to be broken, which is consistent with previous studies (Han et al., 2021a). However, this trend was not suitable for comparing some powders with different composition or production conditions. For example, for the same sieved size fraction of 250-180, the particle size of SMP1, FFMP, and LAC were 229, 240.5, and 247.0 μm, respectively while their *FI* were 44%, 39%, and 20%, respectively. Besides, the particle size of model samples was much smaller than those of other samples while their FI was not the smallest, especially for WL21 and WL41. These results show that although particle size has a major influence on powder breakage, there are other powder characteristics that influence breakage, including composition and the structure of the particles and the powder.

Table 5-2. Physical properties of different dairy powders.

Group	Sample	Particle size $D_{3,2}$ (μm)	Particle density (kg/L)	Loose bulk density (kg/L)	Tapped bulk density (kg/L)	Porosity (%)	Friability Index (%)
A	LAC	160.3^{e}±1.2	1.543^{a}±0.029	0.743^{a}±0.003	0.917^{a}±0.008	50.5^{f}±0.4	23.6^{h}±0.5
	IMF1	203.7^{b}±1.9	1.053^{g}±0.002	0.446^{c}±0.003	0.577^{e}±0.001	45.2^{g}±0.1	48.9^{b}±1.1
	IMF2	224^{a}±3.6	1.023^{h}±0.001	0.441^{cd}±0.006	0.602^{d}±0.002	41.1^{h}±0.2	53.8^{a}±1.8
	EMP	184^{d}	1.197^{f}±0.001	0.364^{f}±0.001	0.507^{g}±0.002	57.6^{c}±0.1	39.3^{e}±0.4
	FFMP	191^{c}±2.4	1.244^{d}±0.001	0.384^{e}±0.001	0.547^{f}±0.001	56.0^{d}±0.1	36.3^{f}±0.2
	SMP1	117.3^{g}±0.5	1.219^{e}±0.001	0.460^{b}±0.002	0.576^{e}±0.001	52.7^{e}±0.1	31.2^{g}±0.8
	SMP2	130^{f}	1.402^{b}±0.001	0.433^{d}±0.001	0.617^{c}±0.001	56.0^{d}±0.1	41.2^{d}±0.4
	NWP	87.9^{h}±1.2	1.195^{f}±0.001	0.376^{e}±0.002	0.485^{h}±0.002	59.4^{b}±0.1	44.7^{c}±0.6
	MCC	33.9^{j}±0.1	1.230^{de}±0.002	0.295^{g}±0.004	0.373^{i}±0.001	69.6^{a}±0.1	16.2^{i}±0.4
	SC	60.1^{i}±1.0	1.312^{c}±0.001	0.436^{d}±0.002	0.627^{b}±0.001	52.2^{e}±0.1	10.1^{j}±0.1
B	WL11	7.0^{A}±0.1	1.315^{D}±0.001	0.229^{C}±0.003	0.289^{B}±0.003	78.0^{A}±0.2	32.3^{D}±0.2
	WL21	6.7^{B}±0.1	1.320^{C}±0.002	0.273^{A}±0.002	0.316^{A}±0.001	76.1^{B}±0.1	42.9^{B}±0.4
	WL41	6.6^{B}±0.1	1.300^{E}±0.001	0.267^{A}±0.002	0.314^{A}±0.005	75.9^{C}±0.4	46.4^{A}±0.1
	WL12	6.3^{C}±0.1	1.343^{A}±0.002	0.257^{B}	0.292^{B}	78.3^{A}	35.8^{C}±0.2
	WL14	6.1^{D}±0.1	1.333^{B}±0.002	0.272^{A}±0.004	0.309^{A}±0.001	76.9^{BC}±0.1	30.4^{E}±0.2

1. LAC: α-Lactose Monohydrate; IMF: infant milk formula; EMP: enriched milk powder; FFMP: full-fat milk powder; SMP: skim milk powder; NWP: nutritional whey protein; MCC: micellar casein concentrate; SC: sodium casein; WL: model samples with different percentage of whey protein and lactose.
2. Values are mean ± standard deviation (n≥2). $^{a\text{-}j}$ and $^{A\text{-}E}$ different values within columns in each group, A and B, respectively, are significantly different at P <0.05.

Table 5-3. Particle size and friability index of sieved fractions of several agglomerated dairy powders.

Sample	Size range	Particle size $D_{3,2}$ (μm)	Friability Index (%)	Sample	Size range	Particle size $D_{3,2}$ (μm)	Friability Index (%)
LAC	355-250	334.7^{a}±1.2	30.1^{a}±0.2	IMF1	355-250	329.3^{a}±1.9	53.9^{a}±0.2
	250-180	247.0^{b}±1.4	20.1^{b}±0.2		250-180	244.5^{b}±0.5	51.3^{c}
	180-125	182.3^{c}±0.5	15.9^{d}±0.1		180-125	174.5^{c}±0.5	53.0^{b}±0.1
	125-75	117.7^{d}±0.5	17.1^{c}±0.3		125-75	113.0^{d}±1.0	46.8^{d}
IMF2	355-250	344.3^{a}±0.5	57.5^{a}±0.1	SMP1	355-250	302.0^{a}±1.4	47.8^{a}±1.0
	250-180	249.7^{b}±0.5	56.3^{b}±0.1		250-180	229.0^{b}	44.2^{b}±0.2
	180-125	177.0^{c}	52.2^{c}±0.2		180-125	158.0^{c}	34.2^{c}±0.2
	125-75	109.0^{d}	49.3^{d}±0.1		125-75	107.3^{d}±0.5	30.3^{d}±0.1
EMP	355-250	309.5^{a}±0.5	51.3^{a}±0.2	FFMP	355-250	332.0^{a}±0.8	49.8^{a}±0.2
	250-180	235.0^{b}	46.7^{b}		250-180	240.5^{b}±0.5	39.2^{b}±0.5

1. LAC: α-Lactose Monohydrate; IMF: infant milk formula; EMP: enriched milk powder; FFMP: full-fat milk powder; SMP: skim milk powder; NWP: nutritional whey protein.
2. Values are mean ± standard deviation (n=3).
3. $^{a-d}$ different values within columns in each powder (LAC, IMF1, IMF2, SMP1, EMP and FFMP) are significantly different at P <0.05.

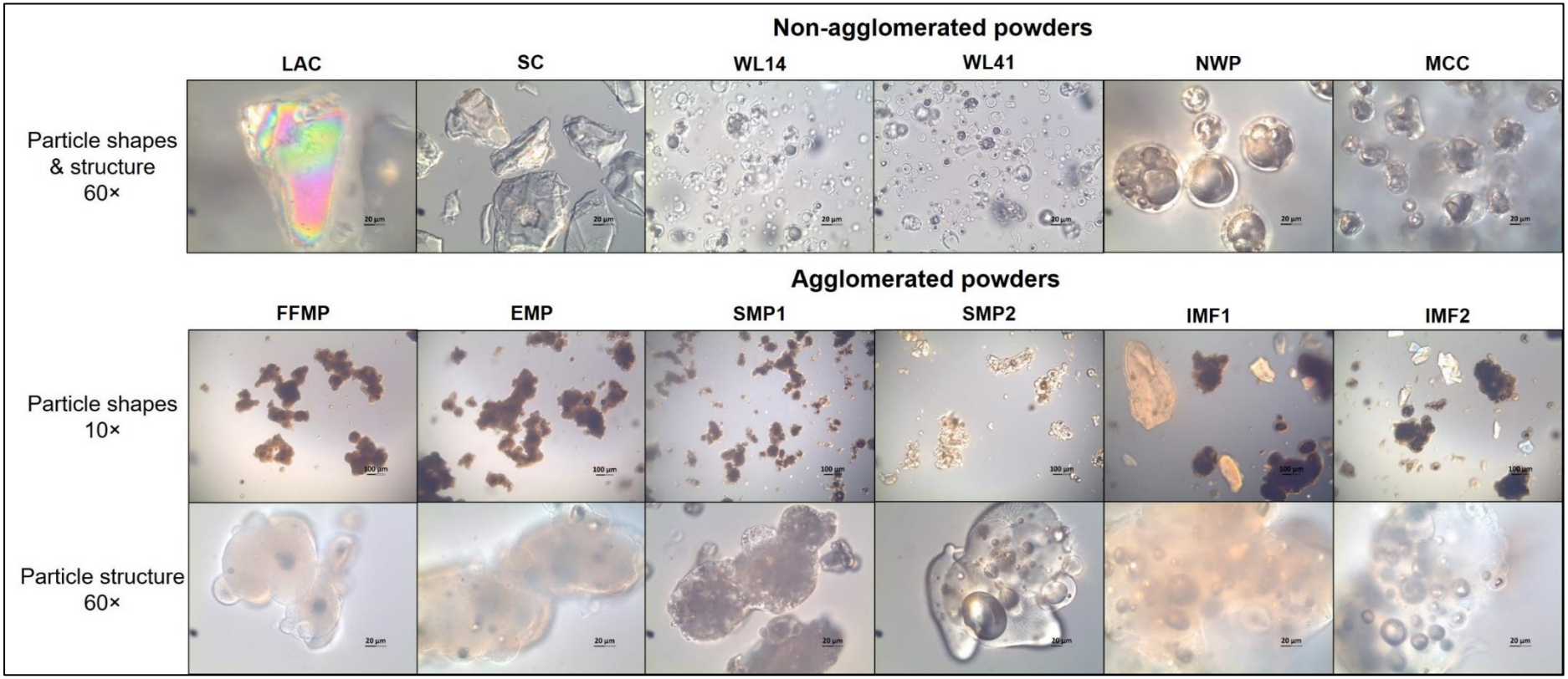


Figure 5-2. Microscopy photos of dairy powders with different scales (60× oil objective: 20 µm; 10× objective: 100 µm) for showing particle shapes and structures. LAC: α-Lactose Monohydrate; SC: sodium casein; WL: whey protein and lactose model samples (WL14: WPI: lactose was 1:4; WL41: WPI: lactose is 4:1); NWP: nutritional whey protein; MCC: micellar casein concentrate; FFMP: full-fat milk powder; EMP: enriched milk powder; SMP: skim milk powder; IMF: infant milk formula.

5.3.2. Structural properties of powders

Light microscopy photos from initial whole powders are presented in Figure 5-2 and it shows a few different microstructures of powders. Particle microstructure is influenced by the parameters of the powder drying process and powder composition.

5.3.2.1. Crystal and irregular continuum solid structure

From Figure 5-2, the characteristic tomahawk-like shape for *α*-lactose monohydrate crystal was observed (LAC). The *α*-lactose crystals are monoclinic sphenoidal and have only 1 axis of symmetry. They have trapezoidal side faces, rhombic tops and bottoms, and bevelled faces at the base and apex, giving the crystal a distinct tomahawk appearance (Hunziker and Nissen, 1927). The shapes of lactose crystals depend on the types and conditions of crystallization (Wong and Hartel, 2014). Compared with amorphous lactose, lactose crystals are very hard and brittle (Li et al., 2016b). This may result in different breakage behaviour of lactose crystals and other samples. Compared with other samples, the microstructure of SC particles was most similar to that of LAC. From Figure 5-2, the particles of SC were irregular continuum solid without internal holes and their surface was unsmooth.

5.3.2.2. Hollow sphere structure

The structure of particles in WPI/lactose model samples was similar so only two samples' microscopy photos are shown in Figure 5-2 (WL14 and WL41). These particles separated from each other and had spherical shapes with large internal holes and thin outer covering. Besides, some fragments were observed, which means some particles were broken. This could also be used to explain why particle densities of WPI/lactose model samples were much higher than most of the other samples even though their particles were hollow. For some of the particles, there were multiple bubbles inside before the droplets were dried. From Figure 5-2, particles from NWP and MCC were also non-agglomerated and they had hollow sphere structures similar to

WPI/lactose model sample particles. Compared with MCC particles, NWP particles were more spherical and their outer walls were thinner. A similar structure was observed in previous researches on milk protein concentrate particles (Bouvier et al., 2013). This structure is generated during the final stage of spray drying when there is no more wet area on the particle surface. The air that is trapped inside the particle expands as the particle temperature increased, which leads to particles with a hollow interior. This structure might be the reason that the particle densities of NWP and MCC were significantly smaller than that of SC. Besides, the internal holes may reduce the strength of particles because the pores inside particles can be regarded as imperfections and crack release zones (Antonyuk et al., 2005).

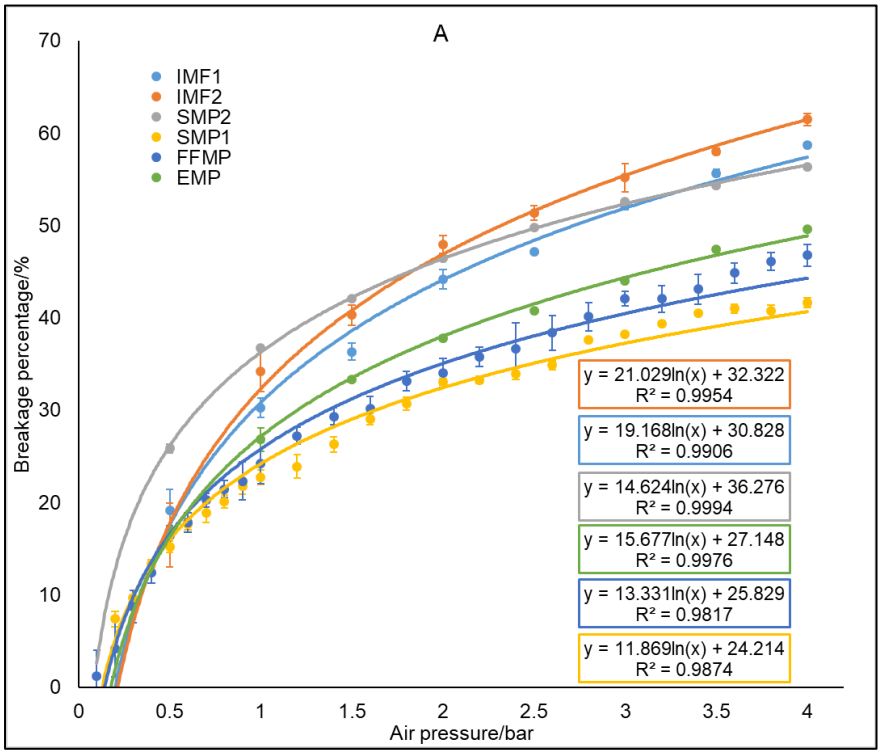
5.3.2.3. Irregular agglomerated particle structure with internal holes

From Figure 5-2, the particle shapes of FFMP, EMP, and SMP2 particles were similar and they were irregular agglomerated particles with a small number of randomly distributed small internal holes. SMP1 particles were agglomerated and irregular, similar to the other agglomerated particles but had highly porous matrices with numerous small holes distributed throughout the particle. Besides, the diameters of most internal holes in SMP1 particles (around 2.5 μm) were much smaller than those in other agglomerated samples (≥ 8 μm). This might result in a stronger structure of SMP1 particles than other agglomerated particles as the particle was more homogenous. The structure of SMP1 and SMP2 were different but their composition (fat, protein, and lactose) were similar, which might be because of the different drying parameters. For IMF, samples were mixtures of lactose crystals and agglomerated particles (Figure 5-2 IMF1 and IMF2). Some of the lactose crystals were tomahawk shape and some were irregular fragments. The shapes of agglomerated particles were similar to those of FFMP, EMP, and SMP2 but the internal holes were more and larger.

5.3.3. Powder breakage in the venturi feeder

The dynamic breakage of dairy powders under different loads during the dispersion and conveying in the venturi feeder was represented by a series

of *BP*. The *BP* of all initial whole samples and the sieved size fractions at different air pressures are given in Figure 5-3 and Figure 5-4, respectively. The *BP* increased with increasing air pressures, which was because increasing the air pressure increased the airspeed which in turn increased the particle speed. Hence higher air pressures mean more severe particle collisions and higher kinetic energy and this caused more breakage. It was clear that the changes in *BP* of LAC and other dairy powders were different, where the *BP* of LAC increased linearly with increasing air pressure while those of other samples increased logarithmically (Figure 5-3). Besides, based on the analyses in the physical and structural properties, other dairy powders could be divided into three groups: agglomerated powders (A group, including IMF, SMP, FFMP, and EMP), non-agglomerated powders (B group, including NWP, MCC, and SC), and model samples (C group, including WL11, WL21, WL41, WL12, and WL14). The breakage behaviour of different group powders and the influence of powder characteristics on the breakage is discussed in the following parts.



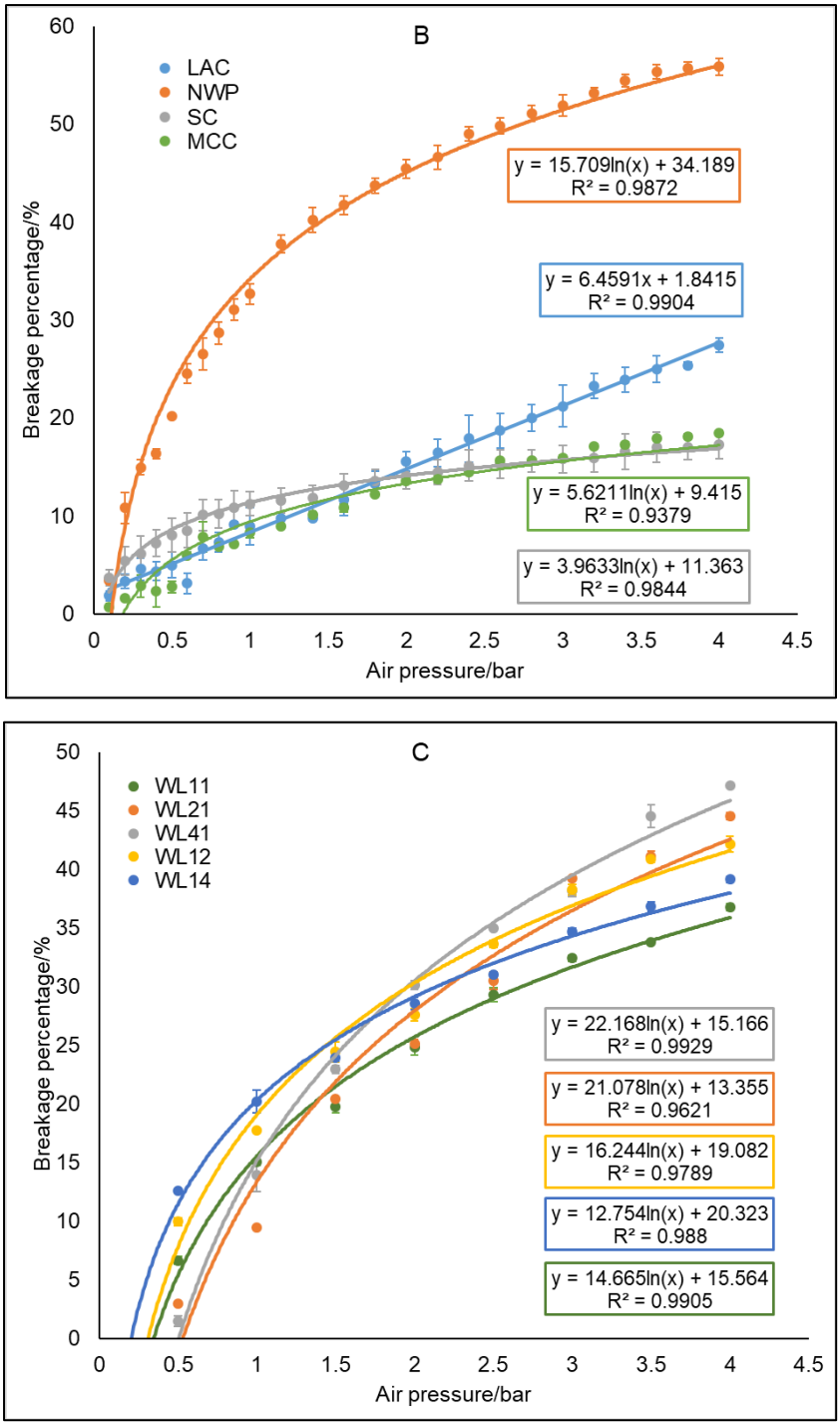
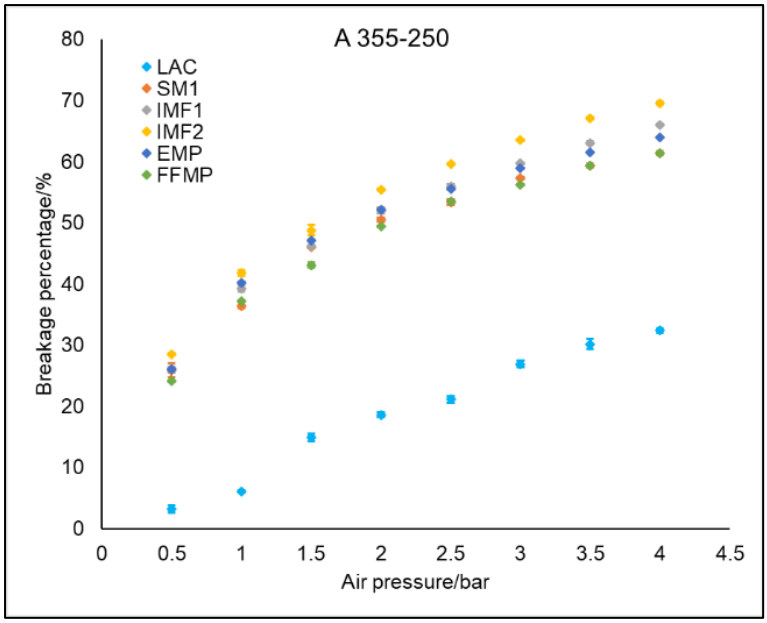
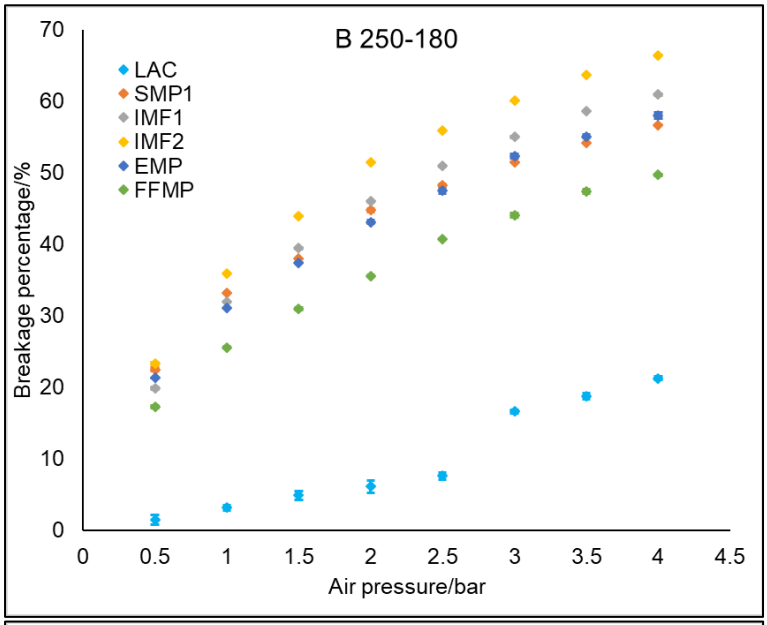
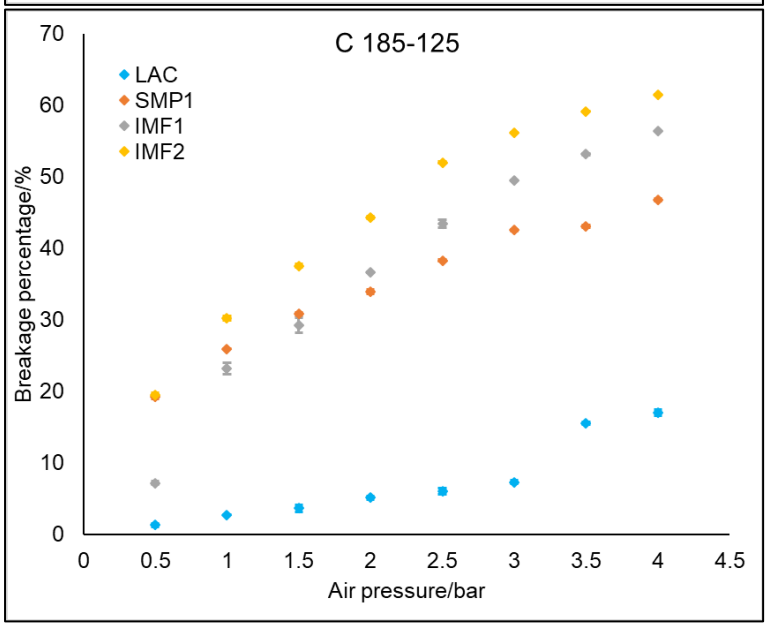


Figure 5-3. Breakage percentages of dairy powders during the transportation by the powder venturi feeder at different air pressures. Its trendlines and the corresponding mathematical functions are presented in the boxes by colour. A: commercial agglomerated powders (IMF: infant milk formula; SMP: skim milk powder; FFMP: full-fat milk powder; EMP: enriched milk powder). B: commercial non-agglomerated powders and α-Lactose Monohydrate (LAC: α-Lactose Monohydrate; NWP: nutritional whey protein; SC: sodium casein; MCC: micellar casein concentrate). C: lab-scale model samples (WL: model samples with different percentages of whey protein and lactose).


A 355-250
LAC
SM1
IMF1
IMF2
EMP
FFMP
Breakage percentage/%
Air pressure/bar
0
10
20
30
40
50
60
70
80
0
0.5
1
1.5
2
2.5
3
3.5
4
4.5


B 250-180
LAC
SMP1
IMF1
IMF2
EMP
FFMP
Breakage percentage/%
Air pressure/bar
0
10
20
30
40
50
60
70
0
0.5
1
1.5
2
2.5
3
3.5
4
4.5


C 185-125
LAC
SMP1
IMF1
IMF2
Breakage percentage/%
Air pressure/bar
0
10
20
30
40
50
60
70
0
0.5
1
1.5
2
2.5
3
3.5
4
4.5

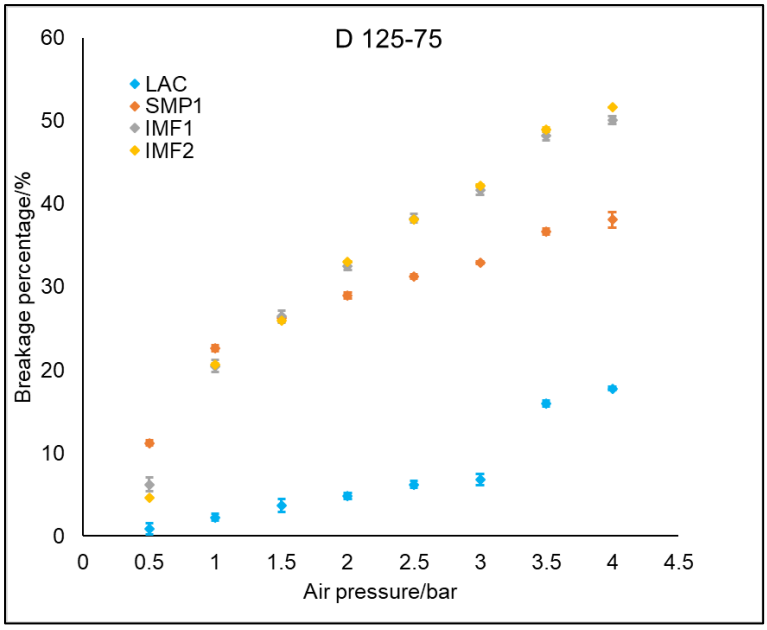


Figure 5-4. Breakage percentages of sieved sized fractions of several agglomerated samples during the transportation by the powder venturi feeder at different air pressures. A, B, C and D: particle size from 355 to 250 μm, from 250 to 180 μm, from 180 to 125 μm, from 125 to 75 μm, respectively.

From the perspective of powder characteristics, breakage is influenced by powder composition and powder physical properties, such as particle size, shape, density, and particle structure (Han et al., 2021b). The physical properties of powders are determined by several factors with the composition and drying conditions being the most prominent. Therefore, powder composition and drying conditions influence the breakage properties of powders through affecting powder physical properties. The fifteen samples used in this chapter covered a whole variety of composition (Table 5-1). However, the drying conditions of the 10 commercial powders were not known and different dairy companies may use different drying conditions for different products. Thus, in this study, there was a limitation to establish a clear relationship between powder composition and breakage without drying information. Nevertheless, the composition and the drying parameters determine the physical properties of powders. Therefore, the discussion of the influence of powder characteristics on the breakage in this study was mainly focused on the physical properties of the dairy powders.

5.3.3.1. Breakage of agglomerated powders

From Figure 5-3A, as expected, the *BP* of IMF were higher than those of most other samples because their particle sizes were the biggest. Besides, the particle sizes of FFMP and EMP were similar to that of IMF but their *BP* was smaller than those of IMF. This might be because IMF had lower particle density and there were more internal holes in IMF particles, resulting in the relatively weaker particle structure. In addition, the *BP* of SMP1 were much smaller than those of SMP2, which might be because the particle size of SMP2 was slightly bigger but this was more likely due to the difference in the particle structure. The more homogeneous porous structure with numerous smaller holes (SMP1) was stronger than the structure with several randomly distributed bigger internal holes (SMP2).

On the other hand, if the impact of particle size on breakage was considered, the *BP* of SMP should be much smaller than those of other agglomerated powders. However, the *BP* of SMP were similar or higher than those of other agglomerates. Besides, for 355-250 and 250-180 sieved fractions, the particle size of FFMP was bigger than those of the corresponding SMP1 while the particle structure of SMP1 was stronger than that of FFMP. Thus, the breakage degree of FFMP should be higher than that of the corresponding SMP1. In contrast, the *BP* of SMP1 fractions were higher than those of corresponding FFMP (Figure 5-4A&B). This might be because the fat in FFMP and other agglomerated powders (Table 5-1) could soften powders, resulting in the easy plastic deformation of particles during the dispersion and conveying instead of brittle fracture. Also, the *FI* of LAC 125-75 was bigger than that of LAC 180-125 but their *BP* at different air pressures were similar and smaller than those of the other two bigger-sized fractions. The *FI* of IMF1 180-125 was bigger than that of IMF1 250-180 but its *BP* were always smaller than those of IMF1 250-180. This indicates that sometimes it is inaccurate to predict the strength of different powders only by their *FI* because the *FI* only compared the size of particles under two specific mechanical stresses (0.5 bar and 4.0 bar) instead of comparing with the initial particle.

5.3.3.2. Breakage of commercial non-agglomerated powders

From microscopy photos, particles in NWP, SC, and MCC were non-agglomerated particles. From Figure 5-3, the *BP* of NWP were similar or higher than those of agglomerated powders but the particle sizes of most agglomerates were around 200 μm and that of NWP was only 88 μm. This might be because the particle structure of NWP, like a hollow ball, was weaker than the normal agglomerated particle structure. It was shown in Figure 5-3B that the *BP* of NWP were much higher than those of SC and MCC, which is consistent with the result of friability. This means that the particles of NWP were weaker than the other two samples, which might be because of its bigger particle size and weaker particle structure. This also caused the particles from NWP to be more sensitive to the increase in force compared to particles from SC and MCC. Therefore, the *BP* of SC and MCC were more stable with increasing air pressures compared with that of NWP.

Besides, MCC had a similar particle structure to NWP while the structure of SC particles was continuum solids and the particle size of SC was nearly twice that of MCC. From Figure 5-3B, compared with MCC, SC broke more when the air pressure was lower than 2.8 bar but broke slightly less at higher air pressures. The bigger particle size of SC might be the reason for the higher degree of breakage at low air pressures. When particles were subjected to higher-level external mechanical stress, compared with continuum solid structure, the weaker particle structure of MCC might result in more breakage. This means that the particle structural strength of continuum solid particles might be higher than spherical particles with a hollow interior surrounded by a highly compacted shell. On the other hand, it could be considered that for some dairy powders, the breakage might be mainly affected by the particle size when particles subjected to low-level external mechanical stress while the particle structure mainly affected the breakage when the stress was high. This also resulted in the inconsistent friability and *BP* of SC and MCC. The friability of SC was significantly lower than that of MCC while the changes in *BP* of SC were not always lower than those of MCC. This indicates that sometimes it is inaccurate to predict the

breakage degree of different powders only by their friability. The accuracy will depend on the difference between the actual force exerted during the production and the force during the transportation in the venturi feeder at 4.0 bar.

5.3.3.3. Breakage of non-agglomerated lab-scale WPI/lactose model solids

From Figure 5-3, the *BP* of model samples were between those of agglomerated and non-agglomerated powders. This implies the degree of breakage was very high even though the particle size of the model powders was very small, which might be because the particle structure, hollow sphere with a very thin shell, was weak. From Figure 5-3C, at low air pressures, the *BP* increased with increasing lactose content but not much difference. At high air pressures, WL11 had the lowest degree of breakage, and the *BP* of other model samples increased as the protein content increased, which is consistent with the result of particle size. From Figure 5-2, particle structures of model samples were similar. These results confirm that, with the same production conditions, the composition of powder affects the particle size of samples, which then influences the breakage during transportation.

5.3.3.4. Breakage of lactose crystals

The particle size of whole LAC (160 μm) was closer to those of group A samples while its *BP* at different air pressures were much lower than these samples even though for SMP whose particle size (120 or 130 μm) were smaller than that of LAC (Figure 3). From Figure 5-4, the *BP* of lactose fractions were lower than other samples. Besides, the *BP* of whole LAC were similar to those of MCC and SC while their particle sizes were 34 and 60 μm, respectively, much smaller than LAC particles. These results mean that the strength of the crystalline structure is much higher than those of other dairy powder particle structures thus lactose crystals had less breakage than other samples even if its particles were larger.

On the other hand, the changes in *BP* at different air pressures of LAC sieved fractions were different from those of other samples (Figure 5-4). The *BP* of other fractions increased logarithmically with increasing air pressure

while those of LAC fractions increased steadily then sharply when the air pressure reached a particular threshold. This might be because the breakage behaviour of normal particles and crystals was different. It has been established that different from continuum solids or agglomerates, the breakage mechanism of crystalline particles is due to the distribution of loading forces across the topography of the particle. It will typically break via the surface breakage mechanism if crystalline material is semi-brittle. When particles are subject to low-level external mechanical stress, the main mechanism of breakage is the surface breakage, leading to the production of minuscule particles whilst still retaining the identity of the original particles. These minuscule child particles originate at the points of the surface of the initial particle where the stress is applied. If crystalline material breaks via a pure brittle mechanism, rupture along preferred fracture planes is expected. When a particle is composed of two or more crystals, cleavage may occur at the interface, and child particles are relatively undamaged (Cleaver et al., 1993; Ghadiri et al., 1991). Thus, the slight increase of the *BP* might be because of the surface breakage while the sharp increase was caused by the cleavage that happened at the interface. Besides, the threshold air pressures increased as the particle size decreased (Figure 5-4, 1.5 bar for LAC355-250, 2.5 bar LAC 250-180, and 3 bar for LAC185-75), which also documented that the larger the particles, the easier it is for them to be broken.

5.4. Conclusion

This chapter was performed on the influence of particle characteristics on dairy powder breakage during the dispersion and conveying in a powder venturi feeder. The physical and structural characteristics and the breakage behaviour of dairy powders were analysed. Four kinds of dairy powders (fifteen samples) were considered: lactose crystals, agglomerated powders (including IMF, SMP, FFMP, and EMP), commercial non-agglomerated powders (NWP, SC, and MCC), and lab-scale non-agglomerated powders (model samples with different percentages of WPI and lactose).

During the dispersion and conveying, the breakage of powders was mainly influenced by the particle size and structures. The degree of breakage increased with increasing particle size and decreasing particle structural strength. For particle structure response, the strength of crystals was the highest, followed by continuums solids, followed by the highly porous matrices with numerous small holes distributed throughout the particle, followed by the particles with a small number of randomly distributed internal holes, followed by the hollow sphere particle with a very thin shell. Sometimes the breakage degree of small particles (model samples with a particle size around 7 μm) was higher than that of big particles (SC with particle size 60 μm) because of the weaker particle structure. Also, due to the difference in particle structures, the breakage behaviour of lactose crystals was different from other dairy powder particles. Overall, this chapter provides a better understanding of the influence of powder characteristics on dairy powder breakage and this can be used to assess and reduce powder breakage and related problems during the production and transportation of dairy powders.

Reference

Antonyuk, S., Tomas, J., Heinrich, S., & Mörl, L. (2005). Breakage behaviour of spherical granulates by compression. *Chemical Engineering Science* 60(14), 4031-4044. https://doi.org/10.1016/j.ces.2005.02.038.

Boiarkina, I., Sang, C., Depree, N., Prince-Pike, A., Yu, W., Wilson, D.I., & Young, B.R. (2016). The significance of powder breakdown during conveying within industrial milk powder plants. *Advanced Powder Technology* 27(6), 2363-2369. https://doi.org/10.1016/j.apt.2016.10.019.

Bonakdar, T., Ghadiri, M., Ahmadian, H., Martin de Juan, L., Xu, D., Tantawy, H., & Smith, D. (2016). Impact attrition of spray-dried burkeite particles. *Powder Technology* 304, 2-7. https://doi.org/10.1016/j.powtec.2016.08.024.

Bouvier, J.-M., Collado, M., Gardiner, D., Scott, M., & Schuck, P. (2013). Physical and rehydration properties of milk protein concentrates: comparison of spray-dried and extrusion-porosified powders. *Dairy Science & Technology* 93(4), 387-399. https://doi.org/ 10.1007/s13594-012-0100-7.

Cleaver, J.A.S., Ghadiri, M., & Rolfe, N. (1993). Impact attrition of sodium carbonate monohydrate crystals. *Powder Technology* 76(1), 15-22. https://doi.org/10.1016/0032-5910(93)80036-A.

Foerster, M., Gengenbach, T., Woo, M.W., & Selomulya, C. (2016). The impact of atomization on the surface composition of spray-dried milk droplets. *Colloids and Surfaces B: Biointerfaces* 140, 460-471. https://doi.org/10.1016/j.colsurfb.2016.01.012.

Gerhards, C., Kaell, C., & Schubert, H. (2004). Measurement of attrition of agglomerated cocoa beverage powders: a comparison of Friabilator and vibration tests. *Journal of Food Engineering* 65(1), 101-108. https://doi.org/10.1016/j.jfoodeng.2004.01.002.

Ghadiri, M., Yuregir, K.R., Pollock, H.M., Ross, J.D.J., & Rolfe, N. (1991). Influence of processing conditions on attrition of NaCl crystals. *Powder Technology* 65(1), 311-320. https://doi.org/10.1016/0032-5910(91)80195-O.

Han, J., Fitzpatrick, J., Cronin, K., Maidannyk, V., & Miao, S. (2020). Breakage of infant milk formula through three different processing methods and its influence on powder properties. *Journal of Food Engineering* 282, 109997. https://doi.org/10.1016/j.jfoodeng.2020.109997.

Han, J., Fitzpatrick, J., Cronin, K., Maidannyk, V., & Miao, S. (2021a). Particle size, powder properties and the breakage behaviour of infant milk formula. *Journal of Food Engineering* 292, 110367. https://doi.org/10.1016/j.jfoodeng.2020.110367.

Han, J., Fitzpatrick, J., Cronin, K., & Miao, S. (2021b). Dairy powder breakage: Mechanisms, characterization methods, impacted properties and influencing factors. *Trends in Food Science & Technology* 114, 608-624. https://doi.org/10.1016/j.tifs.2021.05.043.

Han, J., Fitzpatrick, J., Cronin, K., & Miao, S. (2022). Effects of different breakage mechanisms on the physical, water sorption, and mechanical characteristics of infant milk formula. *Journal of Food Engineering*, 110939. https://doi.org/10.1016/j.jfoodeng.2022.110939.

Hanley, K.J., 2011. Experimental quantification and modelling of attrition of infant formulae, Department of Process and Chemical Engineering. University College Cork, Cork, Ireland.

Hazlett, R., Schmidmeier, C., & O'Mahony, J.A. (2020). Influence of mechanical integrity during pneumatic conveying on the bulk handling and rehydration properties of agglomerated dairy powders. *Journal of Food Engineering*, 110103. https://doi.org/10.1016/j.jfoodeng.2020.110103.

Hunziker, O.F., & Nissen, B.H. (1927). Lactose Solubility and Lactose Crystal Formation: II. Lactose Crystal Formation. *Journal of Dairy Science* 10(2), 139-154. https://doi.org/10.3168/jds.S0022-0302(27)93825-9.

Kim, E.H.J., Chen, X.D., & Pearce, D. (2009). Surface composition of industrial spray-dried milk powders. 2. Effects of spray drying conditions on the surface composition. *Journal of Food Engineering* 94(2), 169-181. https://doi.org/10.1016/j.jfoodeng.2008.10.020.

Kim, E.H.J., Dong Chen, X., & Pearce, D. (2003). On the Mechanisms of Surface Formation and the Surface Compositions of Industrial Milk Powders. Drying Technology 21(2), 265-278. https://doi.org/10.1081/DRT-120017747.

King, R.P. (2012). Modeling and simulation of mineral processing systems. (pp. 153-252). Society for Mining, Metallurgy, and Exploration (SME).

Kotzur, B.A., Berry, R.J., Zigan, S., García-Triñanes, P., & Bradley, M.S.A. (2018). Particle attrition mechanisms, their characterisation, and application to horizontal lean phase pneumatic conveying systems: A review. *Powder Technology* 334, 76-105. https://doi.org/10.1016/j.powtec.2018.04.047.

Li, R., Roos, Y.H., & Miao, S. (2016a). The effect of water plasticization and lactose content on flow properties of dairy model solids. *Journal of Food Engineering* 170, 50-57. https://doi.org/10.1016/j.jfoodeng.2015.09.014.

Li, R., Roos, Y.H., & Miao, S. (2016b). Physical and mechanical properties of lactose/WPI mixtures: Effect of pre-crystallisation. *International Dairy Journal* 56, 55-63. https://doi.org/10.1016/j.idairyj.2015.12.014.

Lu, X., Liu, C., Zhu, L., & Qu, X. (2014). Influence of process parameters on the characteristics of TiAl alloyed powders by fluidized bed jet milling. *Powder Technology* 254, 235-240. https://doi.org/10.1016/j.powtec.2013.11.013.

Norazirah, A., Fuad, S.H.S., & Hazizan, M.H.M. (2016). The effect of size and shape on breakage characteristic of mineral. *Procedia Chemistry* 19, 702-708. https://doi.org/10.1016/j.proche.2016.03.073.

Petukhov, Y., & Kalman, H. (2004). Empirical breakage ratio of particles due to impact. *Powder Technology* 143-144, 160-169. https://doi.org/10.1016/j.powtec.2004.04.009.

Reynolds, G.K., Fu, J.S., Cheong, Y.S., Hounslow, M.J., & Salman, A.D. (2005). Breakage in granulation: A review. *Chemical Engineering Science* 60(14), 3969-3992. https://doi.org/10.1016/j.ces.2005.02.029.

Shrestha, A.K., Howes, T., Adhikari, B.P., Wood, B.J., & Bhandari, B.R. (2007). Effect of protein concentration on the surface composition, water sorption and glass transition temperature of spray-dried skim milk powders. Food Chemistry 104(4), 1436-1444. https://doi.org/10.1016/j.foodchem.2007.02.015.

Wong, S.Y., & Hartel, R.W. (2014). Crystallization in Lactose Refining—A Review. *Journal of Food Science* 79(3), R257-R272. https://doi.org/10.1111/1750-3841.12349.

Yan, H., & Barbosa-Cánovas, G.V. (2001). Attrition evaluation for selected agglomerated food powders: the effect of agglomerate size and water activity. *Journal of Food Process Engineering* 24(1), 37-49. https://doi.org/10.1111/j.1745-4530.2001.tb00530.x.

Zhang, Z., & Ghadiri, M. (2002). Impact attrition of particulate solids. Part 2: Experimental work. *Chemical Engineering Science* 57(17), 3671-3686. https://doi.org/10.1016/S0009-2509(02)00241-5.

CHAPTER SIX

Investigation of breakage behaviour and its influence on spray-dried agglomerated whey protein/lactose powders: Effect of protein and lactose content

Chapter 6 has been submitted:

Han, J., Fitzpatrick, J., Cronin, K., Maidannyk, V., & Miao, S. Investigation of breakage behaviour and its influence on spray-dried agglomerated whey protein/lactose powders: Effect of protein and lactose content (submitted to *Journal of Dairy Science*).

The work contained in this chapter was undertaken and written solely by myself with specific contributions from each co-author:

Jie Han: Conceptualization, Methodology, Formal analysis, Investigation, Data curation, Writing - original draft, Visualization

John Fitzpatrick: Supervision, Writing - review & editing

Kevin Cronin: Supervision, Writing - review & editing

Valentyn Maidannyk: Investigation

Song Miao: Supervision, Conceptualization, Writing - review & editing, Funding acquisition, Project administration

Abstract

This chapter explored the effect of whey protein and lactose content on dynamic breakage and its relevant properties on agglomerated whey protein/lactose powders to provide useful information from the perspective of particle characteristics in controlling unwanted dairy powder breakage. A series of model agglomerates with different whey protein and lactose ratios were produced through a pilot plant trial with the same spray-drying conditions. The particle size and irregularity of agglomerates that contained more lactose was significantly higher than those that contained more protein. This resulted in higher particle breakage during the dynamic breakage for samples that contain more lactose. Also, removing the initial moisture did not influence the breakage of powders but increasing the moisture content could increase the breakage. This was because drying did not change the particle structure and texture but the particle size of powders increased at higher water activity. In addition, increased water content can soften powder material and bridges (lactose for example) in agglomerates. Fatigue affected the breakage of agglomerates, especially for the two higher lactose powders. Breakage changed the morphology and surface composition of particles and decreased particle size. It decreased the dispersibility of powders and increased the wetting time of wettable samples but decreased the wetting time of powders with poor wettability. Also, breakage accelerated the time-dependent crystallization and decreased the crystallization temperatures but did not influence the glass transition temperatures of samples. Thus, under the same drying conditions, the formulation significantly affected model powder breakage mainly by influencing the physical properties of powder particles and then deteriorated powder functionalities.

Keywords: Spray-dried agglomerated whey protein/lactose powders; Particle size; Particle structure; Dynamic breakage; Rehydration properties

6.1. Introduction

Particle breakage of dairy powders significantly causes deterioration in the properties and functionalities of dairy powders. From particle breakage research in other industries, the characteristics of particles and the force applied on particles from processing conditions were two main factors that determine the response of particles for the given loading condition (Kotzur et al., 2018; Lu et al., 2014; Petukhov and Kalman, 2004; Yan and Barbosa-Cánovas, 2001). Therefore, these two factors could be manipulated to reduce the unwanted dairy powder breakage.

The processing condition plays a fundamental role in determining dairy powder breakage. Besides the applied force from the processing conditions, powder breakage relies on the powder characteristics, which includes powder physical properties (morphology, particle size, particle size distribution, powder porosity, and densities) and powder composition (Han et al., 2021b, c). In Chapter 5, it was found that particle size, porosity, and particle structure were the most important particle physical properties which influenced the breakage. Regarding the influence of powder composition, limited research on comparing different commercial dairy powders has been done. It was found that fat might increase the compressibility of dairy powders as fat liquefaction could soften powders, resulting in the easy deformation of particles (Rennie et al., 1999; Yan and Barbosa-Cánovas, 1997). Hanley et al. (2011) explored the breakage of four types of IMF with the same particle size range but different protein to fat ratios during the pneumatic conveying and more breakage was found for two lower protein IMF. However, the differences in spray drying parameters between these compared samples were not considered and these parameters would influence the physical properties of particles which would impact their breakage behaviour. Moreover, as protein and lactose are the basic ingredients in milk powders, the investigation on the influence of the relative content of these two components on the breakage of dairy powders will provide useful information for controlling the breakage.

In this chapter, a series of agglomerated WPI/lactose model powders were prepared by a three-stage spray dryer at the same spray drying conditions to investigate the influence of whey protein and lactose content on the breakage of model powders and the impact of breakage on powder properties. Two kinds of breakage were considered, dynamic breakage under different mechanical stresses in a venturi feeder which mimics pneumatic conveying, and the breakage under repeated lab-scale dilute-phase pneumatic conveying - to investigate the influence of fatigue. Then the influence of breakage on the rehydration and water adsorption properties of model powders were investigated as these two functionalities dis-improved the most in IMF after breakage.

6.2. Materials and methods

6.2.1. Materials

WPI (PROVON 295, protein content was 88.59%; ash content was 2.66%; moisture content was 4.59%) and lactose (LAFB VEGETARIAN LACTOSE, lactose content was 99.69%; ash content was 0.15%; moisture content was 0.03%) were obtained from Glanbia (Glanbia plc).

6.2.2. Model agglomerated powder preparation

WPI was dispersed at around 60℃ for 15 min in deionized water (30%, w/w) with a high shear disperser (Bart Whelan Elec Ltd) and then was reconstituted for 2 h in a 200 L stainless steel mixing tank with an agitator (BS550, Teagasc Food Research Centre) with agitation (1200 rpm) followed by overnight storage at 4℃ with gentle agitation (500 rpm). Lactose solution (30%, w/w) was prepared in deionized water at 70℃ for 2 h. WPI-lactose mixture (30%, w/w) with different WPI to lactose ratios (100:0, 75:25, 50:50, and 25:75) were produced and labeled as WL10, WL31, WL11, and WL13, respectively. Then mixtures (50 kg, which was determined based on the minimum capability of the spray dryer) were warmed up until 80℃ and subsequently spray-dried using a pilot scale three-stage spray dryer

(Anhydro Micraspray 750, Teagasc Food Research Centre) that contains an integrated fluid bed in the main drying chamber and an external fluid bed. Also, there is a fines return system to inject fines into the product stream at the atomizer (a two-fluid nozzle atomization system) to agglomerate particles. The feeding rate of the mixture was controlled by a pump and was automatically adjusted according to the outlet temperature. Inlet and outlet temperatures of the spray dryer were set at 180℃ and 80℃, respectively. For each sample, the first 3-4 kg of powder was discarded to make sure the spray drying conditions were stable and the following powder (8-10 kg) was sampled at different times. There was no significant difference in particle size of samples from different time points thus all batches were manufactured at once. All chemical analysis of powders was completed immediately after spray drying and the other analysis was performed within 2 months.

6.2.3. Powder characterization

6.2.3.1. Bulk composition of WPI/lactose powders

The lactose content and total protein content of samples were determined following the method as described in 5.2.2. Total fat contents and the surface-free fat contents of samples were determined as per GEA Niro (2006). The moisture content of powders was determined using the HR83 Hologen Moisture Analyzer (Mettler Toledo International Inc.). The a_W of samples were measured using a water activity meter (Novasina LabMaster AW, Novatron Scientific Ltd.).

6.2.3.2. Surface composition of WPI/lactose powders

The surface composition of samples was determined by XPS measurements based on the method as described in 3.2.5.

6.2.3.3. Particle size and specific surface area

The specific surface area (SSA), and Sauter mean particle size ($D_{3,2}$) of model samples were measured using a Malvern Mastersizer 3000 (Malvern Instruments Ltd.), following the method as described in 2.2.2.1.

6.2.3.4. Particle density, bulk densities and porosity

Bulk density (tapped (100 taps) bulk density (ρ_{tapped}) and loose bulk density (ρ_b)), particle density (ρ_p), and interparticle porosity (ε) of samples were measured according to the method as described in 2.2.2.2.

6.2.3.5. Powder structural properties

A Malvern Morphologi G3 (Malvern Instruments Ltd.) was used to determine the morphology of model powders, following the method as described in 3.2.6.

The SEM (Zeiss-Supra 40 VP/Gemini Column) and a polarized light microscope (Instruction BX51, Olympus Optical Co. Ltd.) with a 10× objective or a 60× oil objective were used to observe the structure and morphology of particles from model powders, following the methods as described in 2.2.7.

6.2.4. Breakage behaviour of model samples

6.2.4.1. Dynamic breakage under different mechanical stresses

Model samples with three different a_W (at around 0.01, 0.2, and 0.4) were prepared. The a_W of the initial powders was around 0.2 so the other two a_W samples were prepared based on the initial powders. Samples were dried in a vacuum oven at 45°C for 48 h and then were transferred immediately to desiccators over P_2O_5 until the a_W of powder decreased around 0.01. For samples with a_W around 0.4, initial samples were kept in desiccators with saturated K_2CO_3 solutions which gave a relative water vapor pressure (RVP) of 44.1% until the a_W of powders increased around 0.4. The water content and a_W of samples were determined after sample preparation following the methods described in 6.2.3.1.

The dynamic breakage of samples under different mechanical stresses was investigated using the Malvern Mastersizer 3000. Samples were added to the venturi feeder (diagram is shown in Figure 2-1A), and the $D_{3,2}$ of samples was measured at a range of air pressures (from 0 - 1.0 bar in 0.2 bar increments, 1.2, 1.4, 1.6, 1.8, 2.0, 2.5, 3.0, 3.5, and 4.0 bar), following

the method as described in 2.2.3.2. The degree of breakage was shown as the breakage percentage (*BP*) that was evaluated as Eq. (2-3), according to the method as described in 2.2.6.

6.2.4.2. Breakage during repeated lab-scale pneumatic conveying

Particle breakage occurs when the mechanical load exceeds the intrinsic strength of the particle. Breakage could also happen when mechanical loads, lower than the strength of particles, occur multiple times, which is defined as fatigue (Goder et al., 2002; Kalman, 1999, 2000). The susceptibility of model samples to fatigue was investigated by repeated dilute-phase pneumatic conveying tests using a lab-scale pneumatic conveyor (diagram as shown in Figure 2-1B). Seven samples from each model powders were performed on the pneumatic conveying test 1 to 7 times with an air velocity of 40 m/s (according to the method as described in 2.2.4), termed PC1 to PC7, respectively. The particle size of samples was measured after the pneumatic conveying tests following the method described in 6.2.3.2.

6.2.5. Influence of breakage on functionalities of model samples

PC4 samples from 6.2.4.2 and the initial model powders were used to study the effect of breakage on the functionalities of model powders.

6.2.5.1. Rehydration properties – wettability and dispersibility

The wettability of powders was quantified by measuring the wetting time of samples. The wetting time was the time needed to achieve complete wetting of a given quantity of powder without any agitation and it was measured by a modified method described by Ji et al. (2016). Distilled water (300 g at 40℃) was filled into an 800 mL beaker and then powders (4 g) were gently dropped on the surface of the water. The wetting time was the time it took for the immersion of powders in the water.

The dispersibility of samples, represented by the dispersibility index (*DI*), was the proportion of dry matter that passes through a sieve after mixing with water for a short time. Samples (25 g) were filled into a 600 mL beaker with

deionized water (100 g at 40ºC) and then vigorously mixed with a spatula for 20 s as per GEA Niro (2006). The reconstituted samples were poured onto the 180 µm sieve and samples that passed through were collected for dry matter content measurement. *DI* was calculated with Eq. (4-2).

6.2.5.2. Water adsorption, glass transition, and lactose crystallization properties

The water adsorption property and time-dependent lactose crystallization of initial and broken model samples at different RVP were measured using the static gravimetric method, as described in 3.2.7.1. Then the glass transition temperature (T_g, inflection point) and initial crystalized temperature (T_{ic}, peak) of samples (equilibrated at different RVP: 11.4%, 23.1%, 33.2%, and 44.1%) were determined, following the method described in 3.2.8.

6.2.6. Statistical analysis

The experimental design was completely randomized. Measurements of moisture content, particle size, SSA, dynamic breakage under different mechanical stress, rehydration and water adsorption properties were performed in triplicate, and all other measurements were carried out in duplicate. Results were expressed as mean ± standard deviation (SD). Student's *t*-test with a 95% confidence interval was used to determine the significant differences between samples before and after the breakage in each model powder. One-way ANOVA with Tukey's test (IBM SPSS Statistics version 24) was used to determine significant differences between each initial model sample with a confidence level of $P < 0.05$.

6.3. Results and discussion

The physical characteristics, composition, and structure of model powders were measured, and then the dynamic breakage under different mechanical stresses was analyzed, followed by the investigation of the influence of fatigue on model samples. Finally, the rehydration and water adsorption properties of model powders before and after breakage were compared.

Table 6-1. Bulk and surface composition of initial WPI/lactose model powders.

Samples	Bulk samples					Surface composition of particles		
	Moisture content (%)	Total fat content (%)	Total protein content (%)	Lactose content (%)	Surface free fat contents (%)	Fat (%)	Whey protein (%)	Lactose (%)
WL10	5.98^{a}±0.07	0.98^{a}±0.02	86.47^{a}±0.23	1.91^{d}±0.01	0.07^{a}±0.01	23.6^{ab}±0.9	75.6^{a}±1.1	0.0^{d}
WL31	4.09^{b}±0.11	0.89^{b}±0.02	68.94^{b}±0.04	22.56^{c}±0.09	0.04^{b}±0.01	24.5^{a}±5.7	66.1^{b}±3.3	8.8^{c}±2.5
WL11	3.58^{c}±0.03	0.76^{c}	45.38^{c}±0.32	48.50^{b}±0.01	0.03^{b}±0.01	7.1^{bc}±0.9	63.2^{b}±0.3	29.2^{b}±1.2
WL13	4.29^{b}±0.02	0.65^{d}±0.01	23.48^{d}±0.04	71.66^{a}±0.10	0.00^{c}	0.5^{c}±0.5	50.3^{c}±2.1	48.5^{a}±1.9

1. $^{a-d}$ Means different values within columns are significantly different at P <0.05, respectively.
2. Values are mean ± standard deviation (n ≥2).
3. WL10: WPI to lactose ratio is 100:0. WL31: WPI to lactose ratio is 75:25. WL11: WPI to lactose ratio is 50:50. WL13: WPI to lactose ratio is 25:75.

Table 6-2. Physical properties of initial WPI/lactose model powders.

Samples	Particle size $D_{3,2}$ (μm)	SSA (m²/kg)	Particle density (kg/L)	Loose bulk density (kg/L)	Tapped bulk density (kg/L)	Porosity (%)
WL10	47.5^{c}±0.2	120.4^{b}±0.5	1.008^{a}±0.002	0.217^{b}±0.007	0.329^{a}±0.002	67.32^{a}±0.02
WL31	43.5^{d}±0.2	131.6^{a}±0.7	0.938^{b}±0.007	0.217^{b}±0.006	0.316^{a}±0.011	66.27^{b}±0.24
WL11	72.8^{b}±0.2	78.5^{c}±0.2	0.850^{c}±0.001	0.228^{b}±0.001	0.316^{a}±0.002	62.80^{c}±0.06
WL13	86.6^{a}±0.1	66.0^{d}±0.1	0.851^{c}±0.001	0.247^{a}±0.004	0.331^{a}±0.005	61.15^{d}±0.03

1. $^{a-d}$ Means different values within columns are significantly different at P <0.05, respectively.
2. Values are mean ± standard deviation (n=3).
3. WL10: WPI to lactose ratio is 100:0. WL31: WPI to lactose ratio is 75:25. WL11: WPI to lactose ratio is 50:50. WL13: WPI to lactose ratio is 25:75. SSA: specific surface area.

6.3.1. Powder characterization

6.3.1.1. Powder bulk and surface composition

The bulk and surface composition of four initial model samples are presented in Table 6-1. Whey protein content ranged from 86.5 to 23.5%, and lactose contents were from 1.9 to 71.7% for agglomerated WPI/lactose powders. The moisture contents of samples were different and WL10 had the highest moisture content. The total fat contents and surface-free fat contents of samples were decreased with decreasing whey protein content. This was because the fat in the model samples came from the ingredient WPI instead of lactose.

From the result of XPS, the lactose contents on the surface of particles increased and whey protein and fat contents decreased with decreasing bulk protein content of model samples, which is consistent with the changing trend of their bulk composition. However, the composition on the surfaces of model sample particles were very different from their bulk composition. The fat contents on the surface of particles from WL10 and WL31 were around 24%, which is remarkably higher than their bulk fat contents. Also, the highest content on the surface of particles was whey protein, from 50% to 76%, even for WL11 and WL13 whose bulk lactose contents were not lower than 50%. Unlike fat and protein, the lactose concentration on the particle surfaces was lower than that of the bulk. Similar results were found in some commercial milk particles, such as low-fat model powder, skim milk powder (SMP), whole milk powder, SMP/lactose mixtures, milk protein concentrate, and demineralized whey powder (Foerster et al., 2016; Kim et al., 2009; Shrestha et al., 2007). This might be because of the different migration properties of components toward the interior or surface of the particle during the drying, as described in 5.3.1.1. In addition, some researchers demonstrated that fat globules were ruptured and spread homogeneously over the droplet surface, creating a thin fat film during the atomization stage and resulting in a higher surface fat content than bulk fat content (Foerster et al., 2016). The difference in surface composition of model samples may affect the breakage by influencing the cohesiveness of powders because fat

on the surface increases the cohesiveness of bulk samples. Also, uneven distribution of ingredients throughout the particles may lead to the difference in the functionalities and properties of powders before and after breakage.

6.3.1.2. Powder physical properties

Some physical properties of four initial model samples are shown in Table 6-2. The physical properties of spray-dried agglomerates are determined by powder composition and the spray-drying parameters. Thus, the physical properties of WPI/lactose powders were different because of the difference in ingredients. It was found that the $D_{3,2}$ of WL13 and WL11 were significantly higher (P <0.05) than those of WL31 and WL10, which is different from the un-agglomerated MPI/lactose model powders where the higher the protein content, the bigger the particles (Li et al., 2016a,b). This might be because the higher content of lactose made the mixture liquid stickier and the lactose worked as the binder during the agglomeration. This increased the efficiency of the agglomeration and produced bigger particles. It should be mentioned that, β-lactoglobulin exists naturally as a dimer, which unfolds with heat at temperatures above 65℃ and exposes a free sulphydryl group that is normally buried. This activated form of β-lactoglobulin can then react with other molecules of itself, other whey proteins such as α-lactalbumin or cow's serum albumin via disulphide linkages. The heat-induced denaturation of β-lactoglobulin and the subsequent protein-protein interactions would form whey protein aggregates and increase the particle size of the mixture liquid, which may influence the particle size of the final particles.

Previous research showed that particle size was an important factor that influences dairy powder breakage and at the same processing conditions, the degree of breakage amplified as the particle size increased when the particle structure was similar (Han et al., 2021a). This is due to the possibility of more imperfections in bigger particles, like internal holes and cracks where the highest local tensile stress will generate, leading to the initiation and propagation of fractures (Antonyuk et al., 2005). Besides lesser flaws, small particles are harder to break because the inter-particle forces (such as liquid bonds, electrostatics, and van der Waals forces) that bind particles together

are stronger (Reynolds et al., 2005). This may result in higher degrees of breakage for WL13 and WL11 than for WL31 and WL10 under the same mechanical stress. As WL31 and WL10 had smaller particle sizes, they showed larger SSA values.

The particle densities of WL31 and WL11 were similar, at around 0.85 kg/L, and significantly lower than those of high protein model powders, at around 1.0 kg/L. The particle densities of these model powders were much lower than those of un-agglomerated WPI/lactose model powders, at around 1.3 kg/L. Particle density is the mass per unit volume of particles, that includes closed internal holes but not cracks or open holes so it is associated with particle structure characteristics that are another important factor influencing the dynamic breakage of dairy powder particles. Instead of individual particles, porosity would influence the properties of bulk particles. The porosity of model powders decreased with increasing lactose content and the porosities of WL13 and WL11 were similar while those of WL13 and wl10 were similar. Compared with their loose bulk density, their tapped bulk densities were more similar, at around 0.32 kg/L. The loose bulk density of WL10 and WL 31 were smaller, which might be because their particle size were small and these small particles were lighter and had higher specific surface areas and thus trapped air more easily in a bed of powder. Also, their flowability was very poor that resulted in the large packing irregularities and scraped level during the sample filling.

6.3.1.3. Powder morphology and structure

Three morphological characteristics (circularity, convexity, and elongation) (Table 6-3) and SEM and light microscopy photos (Figure 6-1) of particles from model powders were used to identify the particle shapes and microstructures of samples. Previous research shows that the extent and type of breakage were heavily dependent on the structure and shape of agglomerates (Golchert et al., 2004; Norazirah et al., 2016), and the more alike a sphere, the greater the particle strength (Deng and Davé, 2017). Also, Discrete Element Model simulation results showed differences in non-spherical and spherical agglomerate breakage because the degree of

breakage in non-spherical agglomerates depended not only on the interface energy, impact angle, and impact speed but also on the orientation (Liu et al., 2010). Considering particle structure, the strength of crystals and continuum solids was higher than particles with internal holes because the internal holes were the defective zones. The number, distribution, and size of internal holes also influence the strength of particles. Particle shape and structure are influenced by the parameters of the powder drying process and powder composition.

Table 6-3. Morphological characteristics of initial WPI/lactose model powders.

Samples	Elongation	Circularity	Convexity
WL10	0.199^{d}±0.004	0.861^{a}±0.007	0.987^{a}±0.003
WL31	0.205^{c}±0.001	0.851^{b}±0.014	0.986^{b}±0.004
WL11	0.243^{b}±0.001	0.822^{c}±0.001	0.983^{c}±0.002
WL13	0.249^{a}±0.004	0.805^{d}±0.003	0.977^{d}±0.001

1. $^{a-d}$ Means different values within columns are significantly different at P <0.05, respectively.
2. Values are mean ± standard deviation (n=2).
3. WL10: WPI to lactose ratio is 100:0. WL31: WPI to lactose ratio is 75:25. WL11: WPI to lactose ratio is 50:50. WL13: WPI to lactose ratio is 25:75.

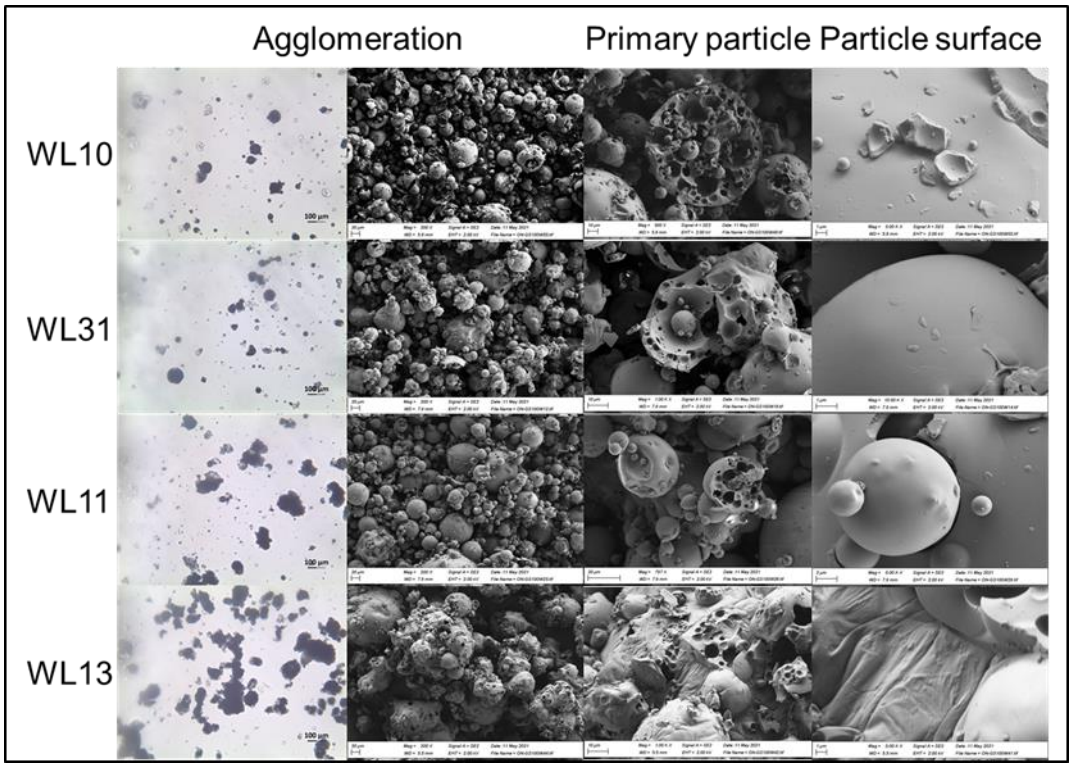


Figure 6-1. Microscopy photos of initial WPI/lactose model particles (WL10: WPI to lactose ratio is 100:0; WL31: WPI to lactose ratio is 75:25; WL11: WPI to lactose ratio is 50:50; WL13: WPI to lactose ratio is 25:75).

From Figure 6-1, it was clear that particles from model powders were agglomerated and there was no crystallized lactose. From SEM photos, the shape and the structure of the primary particles from the four samples were similar, which might be because the atomization stage and spray-drying parameters were the same. Most of the primary particles were hollow sphere particles with numerous different-sized holes throughout the particle. Compared with WL13 primary particles with a “shrivelled-like” surface, the surface of primary particles from the other three samples that contained less lactose was smoother. This has been reported in previous research on milk protein powders, SMP, and model IMF (Kim et al., 2009; Maidannyk et al., 2020; McCarthy et al., 2013; Murrieta-Pazos et al., 2011). It was shown from the light microscopy photos that the agglomeration degrees of WL13 and WL11 were higher than those of WL31 and WL10, which resulted in the difference in their particle size. After agglomeration, particles were irregular and the irregularity of particles increased with increasing lactose content, as shown in the decrease in circularity and convexity, and the increase in elongation (Table 6-3). Thus, the higher particle size and more irregular particle shapes might result in weaker particle strength and higher particle breakage for model samples that contain more lactose. Also, some of the primary particles on the surface of agglomerates were broken and the internal holes were exposed, especially for WL13 where the surface of particles was very rough. This was because agglomeration and breakage of particles occurred concurrently during the granulation (Reynolds et al., 2005). Breakage influenced the strength and homogeneity of agglomerates and was an important rate process during agglomeration. Also, the connection areas between primary particles in WL13 were bigger than the other three samples, which might make the structural strength of particles from WL13 higher than other particles.

6.3.2. Dynamic breakage under different mechanical stresses

The dynamic breakage of initial agglomerated WPI/lactose model powders (with a_W 0.2) under different mechanical stresses in the venturi feeder was represented by a series of *BP* (Figure 6-2). It was shown that for each

sample, the *BP* increased with increasing air pressures. This was because increasing the air pressure increased the air velocity which in turn increased the particle speed. Hence higher air pressures mean more severe particle collisions and this caused more breakage. On the other hand, the *BP* of each model powder increased logarithmically with increasing air pressure, which is consistent with previous studies on the breakage of some agglomerated or non-agglomerated dairy powders, such as SMP, IMF, WPI, and so on. From Figure 6-2, it was shown that there was no significant difference in *BP* between initial WL31 and WL10, which was because their particle size and structure were similar. The *BP* of WL13 and WL11 was higher than that of the other two samples, which could also be explained by their bigger particle size, higher elongation, and lower convexity and circularity. For the same reason, the *BP* of WL13 was higher than that of WL11. These results mean that, for WPI/lactose agglomerates, the degree of breakage increased with increasing lactose content of powders at the same processing conditions because of the increase in the particle size and the more irregular particle shapes but the breakage of WPI and agglomerates contained 25% lactose was similar. This was not observed in non-agglomerated WPI/lactose powders (Chapter 5, whey protein content ranged from 80% to 20%, and lactose contents were from 20% to 80%) and their BP was similar, which could be because of their comparable particle size (from 6.1 µm to 7 µm).

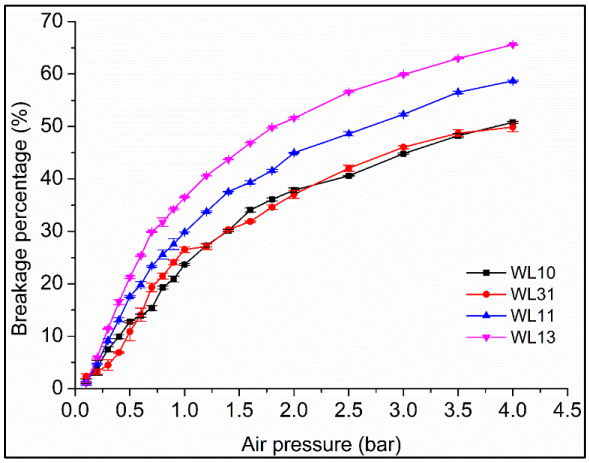


Figure 6-2. Breakage percentages of initial WPI/lactose model powders (with water activities 0.2) during the transportation by the powder venturi feeder at different air pressures. WL10: WPI to lactose ratio is 100:0. WL31: WPI to lactose ratio is 75:25. WL11: WPI to lactose ratio is 50:50. WL13: WPI to lactose ratio is 25:75. Error bars represent the SD.

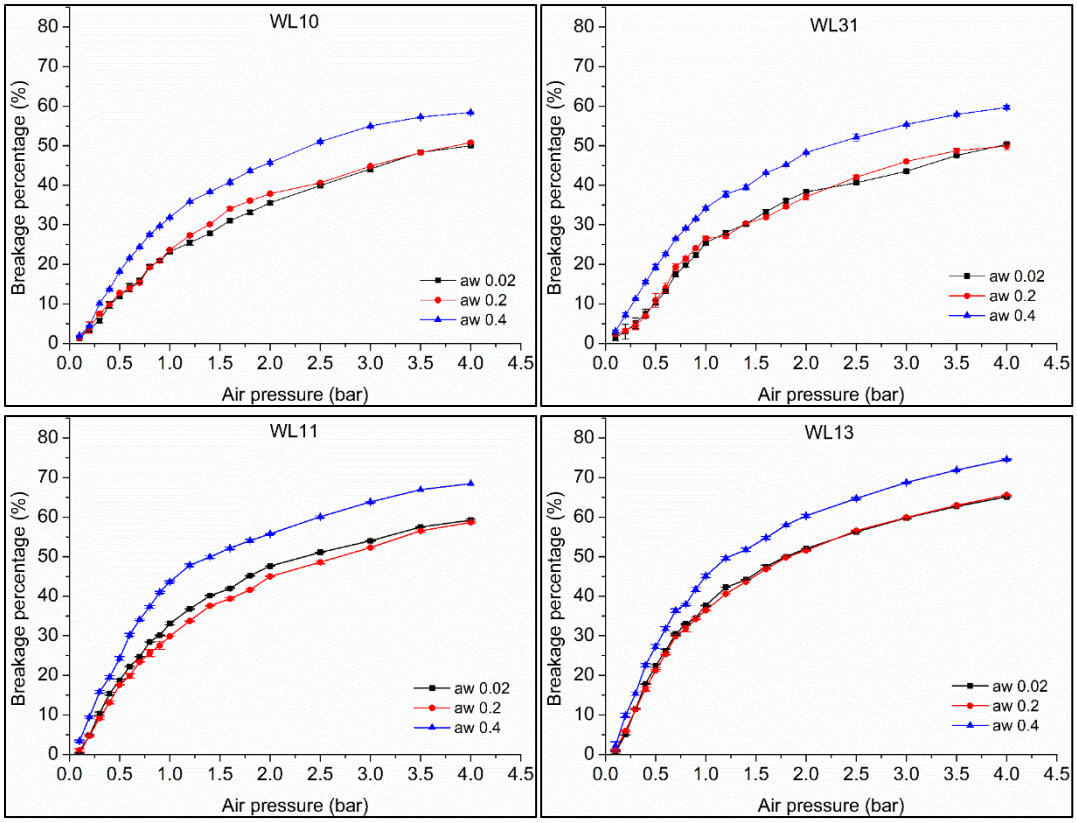


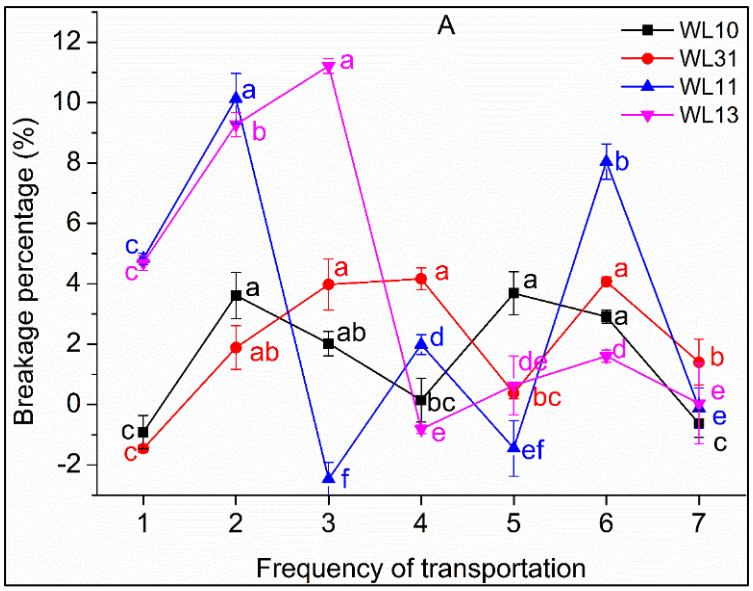
Figure 6-3. Breakage percentages of WPI/lactose model powders with different water activities (0.02, 0.2, and 0.4) during the transportation by the powder venturi feeder at different air pressures. WL10: WPI to lactose ratio is 100:0. WL31: WPI to lactose ratio is 75:25. WL11: WPI to lactose ratio is 50:50. WL13: WPI to lactose ratio is 25:75. Error bars represent the SD.

The *BP* of four powders with three different a_w at different air pressures are given in Figure 6-3. For each sample, the *BP* of dried powders (a_w 0.02) was similar to their initial powders (a_w 0.2) but that of high water content powders (a_w 0.4) was much higher than initial powders. Previous studies have also reported that during the vibration test of agglomerated SMP, greater breakage occurred on samples with a higher a_w (0.44) than samples with a lower a_w (0.2) (Yan and Barbosa-Cánovas, 2001). These results mean that removing the initial moisture did not influence the breakage of model powders but increase the moisture content within a certain range at the base of initial powders could reduce the strength of powders. This might be because the drying process only removed the moisture inside particles but did not change the particle structure and texture, and the particle size between samples at a_w 0.02 and 0.2 were not significantly different (P >0.05, data was not shown). In contrast, the particle size of samples at a_w 0.4 was

bigger than their initial samples, for example, the particle size of WL13 increased from 86.6 μm to 93.0 μm when its a_w increased from 02 to 0.4. Also, increased water content can soften the material of powders, particularly the water-soluble components, which would deform powders and decrease their strength (Kim et al., 2005; Rennie et al., 1999). In addition, the main agglomeration mechanism for materials in the agglomerated state is the formation of powder bridges using binders (lactose for example). Humidifying the agglomerates can change particle surfaces by local plasticization, liquid layer formation, or solubilization, which may decrease the strength of bridges or affect the other properties of binders (Samimi et al., 2003).

6.3.3. Breakage under repeated mechanical stresses - the influence of fatigue

Particles could break in a single collision during pneumatic conveying when the impact load is greater than its strength. Additionally, repeated lower impact loads can cause breakage, which is known as fatigue. Under these circumstances, although the first impact did not break particles, it might lead to cracks, which made particles more sensitive to the next impact. In actual factories, there are many bends in the pneumatic conveying system and during processes such as receiving, packing, re-processing, and storage, powders are repeatedly transported (Konami et al., 2002). Therefore, the breakage caused by repetitive transport should be considered.



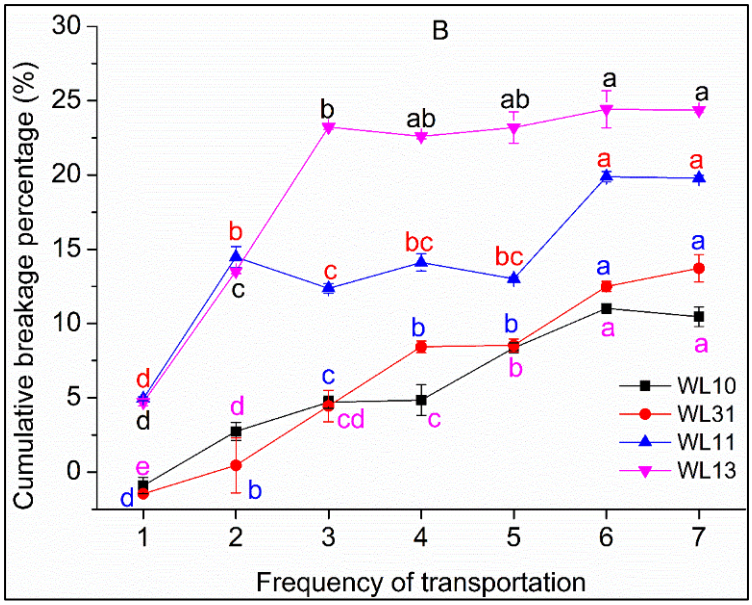


Figure 6-4. Breakage percentages of WPI/lactose model powders after each time of transportation by lab-scale dilute-phase pneumatic conveying at 40 m/s compared with the previously transported powders (A) or with initial powders (B). WL10: WPI to lactose ratio is 100:0. WL31: WPI to lactose ratio is 75:25. WL11: WPI to lactose ratio is 50:50. WL13: WPI to lactose ratio is 25:75. Error bars represent the SD.

The influence of fatigue on WPI/lactose agglomerates was shown as the changes in particle size after each time of lab-scale dilute-phase pneumatic conveying with an air velocity of 40 m/s, shown in Figure 6-4A. It was clear that, for all samples, the changes in particle size after different time pneumatic conveying were different. Based on previous research, at the same processing conditions, the degree of breakage reduced with decreasing particle size. With increasing the times of pneumatic conveying tests, the particle size of samples gradually decreased but the breakage degrees were not decreased gradually, which means cracks were produced and decreased the strength of particles and led to the high degree of breakage for some smaller particles. These results imply that fatigue did influence the breakage of WPI/lactose agglomerates, especially for high lactose contained powders, which might be because of their bigger particle size and more irregular particle shapes. These findings also mean that increasing the particle size or particle irregularity might enhance the influence of fatigue on the degree of breakage, which is consistent with the results obtained from research on the impact breakage of detergent agglomerates (Samimi et al., 2003). Also, the cumulative breakage of WL13

and WL11 were much bigger than those of the other samples (Figure 6-4B), which was consistent with the results of *BP* under different mechanical stresses (Figure 6-2) and confirmed that breakage was greater for the higher lactose powders.

6.3.4. Rehydration properties of model samples after breakage

The impact of breakage on the wettability and dispersibility of WPI/lactose model agglomerates was investigated by comparing properties of initial samples and broken samples produced by four times of dilute-phase pneumatic conveying (PC4). The scanning electron micrographs and some properties of broken powders are shown in Figure 6-5 and Supplementary Table 6-S1, respectively, and the changes in physical and structural properties before and after breakage could influence the functionalities of model powders.

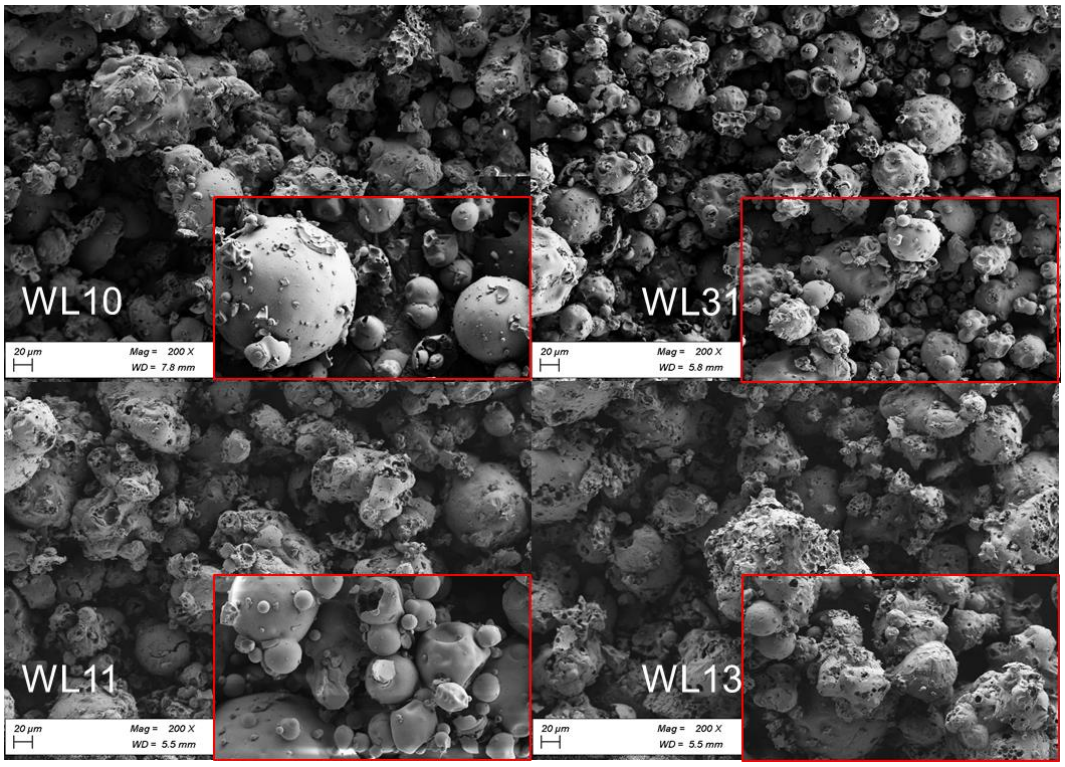


Figure 6-5. Microscopy photos of broken WPI/lactose model particles after four times transportation by lab-scale dilute-phase pneumatic conveying at 40 m/s. WL10: WPI to lactose ratio is 100:0. WL31: WPI to lactose ratio is 75:25. WL11: WPI to lactose ratio is 50:50. WL13: WPI to lactose ratio is 25:75.

From the SEM photos, breakage changed the morphology of particles, primary particles on agglomerate surfaces were broken and particle surfaces became very rough, especially for WL13 and WL11. These changes decreased the particle size (their $D_{3,2}$ decreased 5% to 22% for different samples) and increased the SSA and particle density, which is consistent with previous research (Boiarkina et al., 2016; Han et al., 2020; Hazlett et al., 2020; Zhang et al., 2020). Also, the bigger the particles, the greater the changes occurred. Furthermore, the surface composition also changed after breakage because of the exposure of the interior of the particles as seen with the increase in lactose content and the slight decrease in whey protein and fat contents on most samples.

The wetting process is the first step of rehydration and is the ability of particles to overcome the surface tension between them and imbibe a liquid based on the capillary force (Ji et al., 2016). The wetting time of model powders before and after breakage is shown in Figure 6-6. It should be mentioned that for this method, powders are considered non-wettable if the wetting time is longer than 2 min (Niro, 2006). As shown in Figure 6-6, only WL13 was wettable with a wetting time of 1.6 min. In this study, the wetting time of the other three samples was still compared to show the influence of breakage on the wettability even though they were not-wettable. From Figure 6, the wettability significantly decreased (P <0.05) after breakage for WL13 and WL11, especially for WL13 where the wetting time increased 38%. This is not surprising because their particle size decreased and this is consistent with previous research on IMF, fat-filled milk powder, and whey protein concentrate powders (Han et al., 2020; Han et al., 2022; Hazlett et al., 2020). In contrast, the wetting time of WL31 and WL10 was significantly decreased (P <0.05), especially for WL10. This might be because they contained high contents of protein that had poor wettability when particles were in small size, while breakage roughed the surface of particles and more internal holes exposed, which might improve the water penetrate into the particles. This could also be because of the changes in the particles' surface composition (Supplementary Table 6-S1). Both samples have shown a reduction in surface fat content, and W31 also showed an increase in surface lactose

content, which could reduce wetting time. These results imply that breakage could increase the wetting time of wettable samples but decrease the wetting time of powders with poor wettability which was caused by higher protein content.

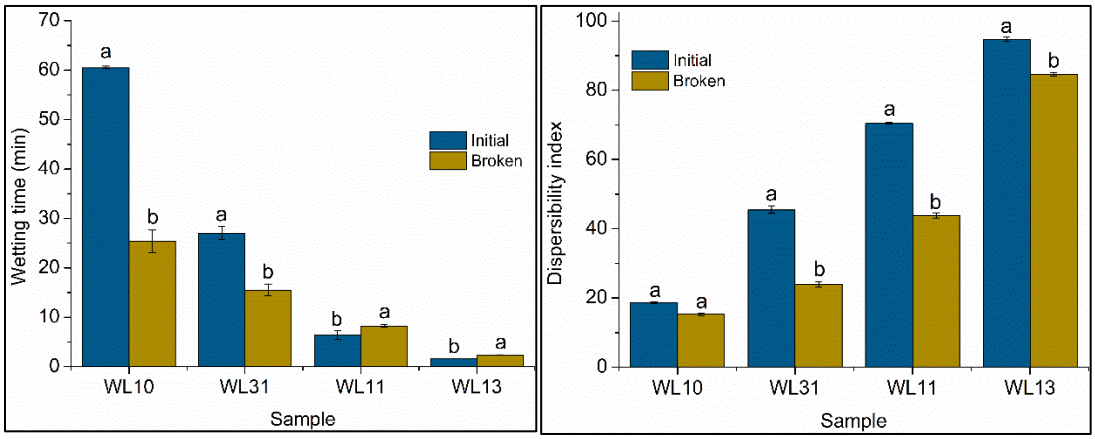


Figure 6-6. The wetting time and dispersibility index of initial and broken (after four times transportation by lab-scale dilute-phase pneumatic conveying at 40 m/s) WPI/lactose model powders. a-b means different values within samples are significantly different at P <0.05, respectively. WL10: WPI to lactose ratio is 100:0. WL31: WPI to lactose ratio is 75:25. WL11: WPI to lactose ratio is 50:50. WL13: WPI to lactose ratio is 25:75. Error bars represent the SD.

After the wetting process, particles need to be dispersed into the water before dissolving (Goalard et al., 2006). Figure 6-6 shows the effect of breakage on the *DI* of four WPI/lactose model powders. It was shown that dispersibility increased with increasing lactose content because lactose disperses much more easily than whey protein. Also, breakage reduced the dispersibility of all powder samples because of the decrease in particle size, which makes it harder for water to penetrate into the powder bulk. Similar findings were observed on IMF, fat-filled milk powder, and whey protein concentrate powders (Han et al., 2020; Hazlett et al., 2020). Besides, the *DI* of WL11 and WL31 were more influenced compared with those of the other two samples. This might be because the dispersibility of WL13 and WL10 was more influenced by their composition. For example, the dispersibility of WL13 was very good as it contained a large amount of hydrophilic lactose that makes it easy for water to penetrate into the agglomerates and thereby sinking and dispersing quickly in the water. The dispersibility was still good even with a 20% decrease in particle size while the opposite was true for

WL10. These results imply that breakage decreased the dispersibility of model samples, especially for samples with moderate dispersibility (the *DI* was around 50%).

6.3.5. Water adsorption, glass transition, and lactose crystallization

The water adsorption behaviour at several a_W (0.11-0.76) of model powders before and after breakage was plotted as a function of time (Figure 6-7). The water adsorption behaviour at all a_W and the final water contents of WL10 were not influenced by breakage. For the other three samples that contained lactose, breakage did not influence their water adsorption rate and final water contents at 0.11-0.44 a_W but accelerated their time-dependent crystallization at $a_W \geq 0.54$ and the higher the lactose content, the greater the impact. It was shown that only WL13 was influenced by breakage on time-dependent crystallization at 0.54 a_W, and the water content decreased earlier and faster for break samples. Similarly, the time-dependent crystallization of WL11 and WL31 start to be accelerated by breakage at 0.66 a_W and 0.76 a_W, respectively. This must be because protein interferes with lactose crystallization, where proteins in the system would absorb more water faster and more easily than amorphous lactose, which could delay the time-dependent crystallization of lactose (Shrestha et al., 2007). Besides, the final water contents after crystallization of breakage samples were slightly higher than their initial samples for WL13 and WL11 at $a_W \geq 0.65$. This is different from the finding of a previous study (Chapter 3) on the effect of breakage mechanisms on the water adsorption behaviour of IMF where the final water content of samples after crystallization was not influenced by breakage. This difference might be because of the difference in the composition of the two kinds of samples. In addition, at all a_W, the final water contents of powders increased with increasing protein content. These results mean that breakage would not influence the water adsorption rate and final water content of WPI/lactose agglomerates at low a_W but accelerated the time-dependent crystallization and slightly increased the final water content after the crystallization.

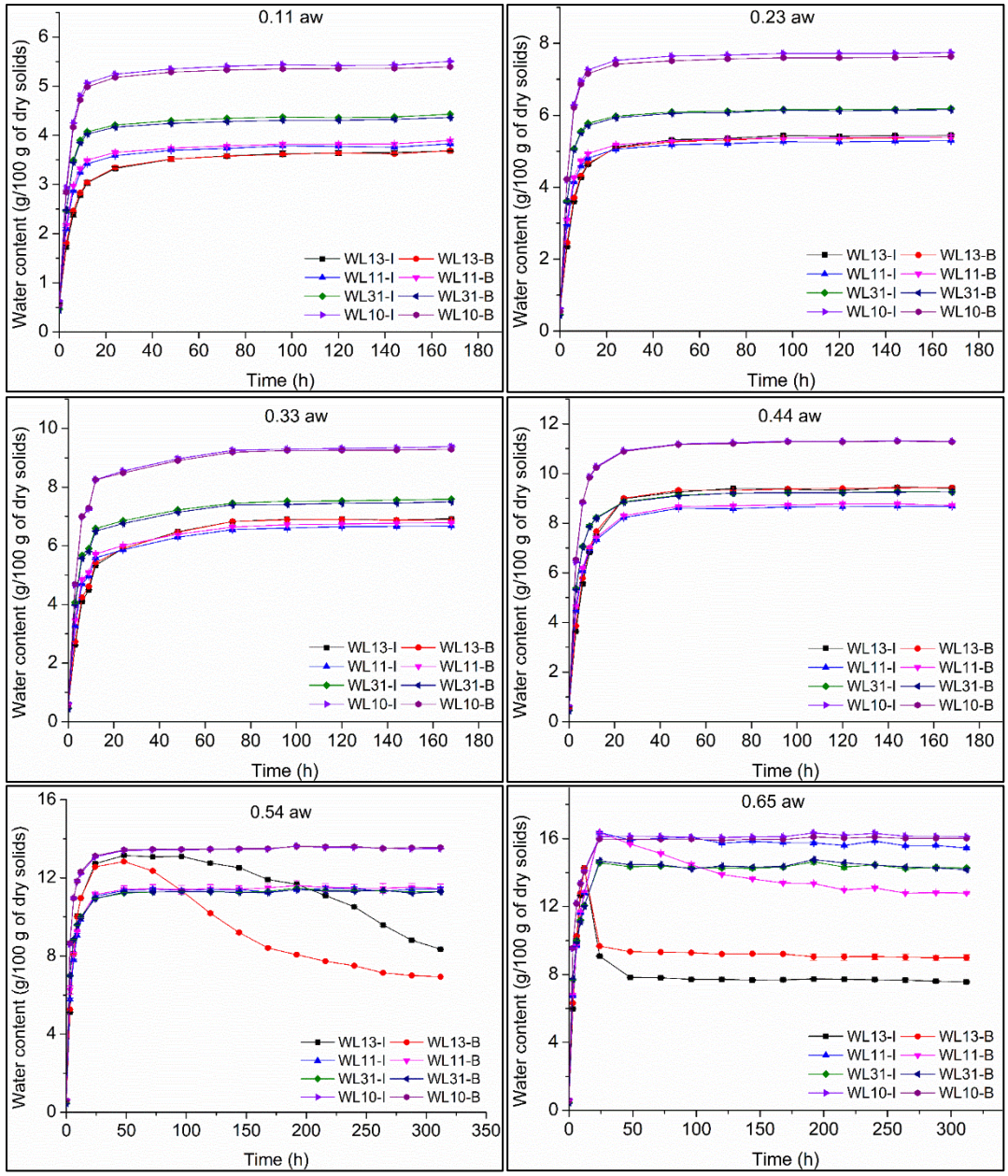


Figure 6-7. Water sorption behaviour of initial and broken (after four times transportation by lab-scale dilute-phase pneumatic conveying at 40 m/s) WPI/lactose model powders equilibrated at various water activities (0.11 to 0.76) for 168 or 312 h at 25°C. WL10: WPI to lactose ratio is 100:0. WL31: WPI to lactose ratio is 75:25. WL11: WPI to lactose ratio is 50:50. WL13: WPI to lactose ratio is 25:75.

Table 6-4. Glass transition temperature (T_g, inflection point) and initial crystallization temperature (T_{ic}, peak) of WPI/lactose model powders stored for 168 h at various water activities (0 to 0.44) at 25°C.

Samples[2]			Water activity				
			0	0.11	0.23	0.33	0.44
WL10	T_g	Initial	/	/	/	/	/
		PC4[3]	/	/	/	/	/
	T_{ic}	Initial	/	145.6±1.2	143.3±0.1	138.9±0.3	142.7±0.6
		PC4	/	147.4±0.5	142.9±0.5	138.9±0.3	141.2±0.6
WL31	T_g	Initial	/	86.1±0.1	66.8±1.3	55.4±1.0	42.1±0.1
		PC4	/	87.2	67.8±0.3	58.2±0.7	42.4±1.0
	T_{ic}	Initial	/	149.1±0.1	147.2±0.3	144.4±0.9	146.0±0.4
		PC4	/	148.5±0.2	146.6±0.1	145.9±0.3	144.5±0.6
WL11	T_g	Initial	121.8±0.4	74.1±0.3	60.1±0.3	48.5±0.2	32.6±0.2
		PC4	122.0±0.3	73.8±0.2	60.0±0.2	48.3±0.3	33.7±0.3
	T_{ic}	Initial	/	152.7±0.2	151.5±0.1	148.2±0.1	148.1±0.4
		PC4	/	152.7±0.1	149.6±0.1	145.3±0.3	137.7±0.2
WI13	T_g	Initial	115.7±0.4	69.6±0.3	53.8±0.5	42.7±0.6	26.4±0.9
		PC4	115.6±0.1	69.8±1.0	53.4±0.1	42.3±0.2	25.7±0.1
	T_{ic}	Initial	/	144.0±0.2	129.1±0.2	117.0±0.1	95.2±0.2
		PC4	/	134.7±0.6	118.6±0.1	105.8±0.1	86.0±0.1

1. Values are mean ± standard deviation (n=2).
2. WL10: WPI to lactose ratio is 100:0. WL31: WPI to lactose ratio is 75:25. WL11: WPI to lactose ratio is 50:50. WL13: WPI to lactose ratio is 25:75.
3. PC4: four times transportation by lab-scale dilute-phase pneumatic conveying at 40 m/s.

The T_g (inflection point) and T_{ic} (peak) of samples over the a_W range of 0 to 0.44 are shown in Table 6-4. It was found that at the same a_W, T_g increased with decreasing lactose content and increasing protein content, which was because protein absorbed most of the water, leaving less water available for lactose plasticization and subsequent crystallization. This has been reported by Shrestha et al. (2007). For the same sample, T_g decreased with increasing a_W because of the higher water contents. For each sample at all a_W, no significant differences in T_g were found between the initial and break samples because of their similar final water contents. Different from T_g, the initial crystalized temperatures were decreased by breakage, especially for samples that contained high content lactose, and the higher the lactose content, the greater the influence. The T_{ic} of WL13 was decreased around 10℃ after breakage at $a_W \leq 0.44$, even there was no difference in the final water content of initial and breakage samples. Overall, breakage did not influence the T_g of WPI/lactose agglomerates but decreased the T_{ic} of powders that contained lactose.

6.4. Conclusion

This chapter was performed on the influence of protein and lactose content on whey protein/lactose model powders' breakage behaviour. It was found that, the whey-protein/lactose composition influenced breakage by influencing the particle size and structure of the agglomerates formed during the same drying conditions. The two higher protein powders were smaller in particle size, were less irregular in shape, and had higher particle densities, which resulted in less breakage in comparison to the two higher lactose powders. Also, removing the initial moisture did not influence the breakage of powders but increasing the moisture content within a certain range could increase the breakage. Fatigue affected the breakage of WPI/lactose agglomerates, especially for the two higher lactose powders. Breakage changed the morphology and surface composition of particles, decreasing the particle size and increasing the SSA and particle density. These changes decreased the dispersibility of samples and increased the wetting time of wettable samples but decreased the wetting time of powders with poor

wettability. Also, breakage accelerated the time-dependent crystallization and decreased the T_{ic} of powders that contained lactose. Overall, this chapter confirms that under the same drying conditions, the formulation significantly affects dairy powder breakage by influencing the physical properties of powder particles. Further research on the effect of other milk powder ingredients in more complex powders on breakage will be useful.

6.5. Reference

Antonyuk, S., Tomas, J., Heinrich, S., & Mörl, L. (2005). Breakage behaviour of spherical granulates by compression. Chemical Engineering Science 60(14), 4031-4044. https://doi.org/10.1016/j.ces.2005.02.038.

Boiarkina, I., Sang, C., Depree, N., Prince-Pike, A., Yu, W., Wilson, D.I., & Young, B.R. (2016). The significance of powder breakdown during conveying within industrial milk powder plants. Advanced Powder Technology 27(6), 2363-2369. https://doi.org/10.1016/j.apt.2016.10.019.

Deng, X., & Davé, R.N. (2017). Breakage of fractal agglomerates. Chemical Engineering Science 161, 117-126. https://doi.org/10.1016/j.ces.2016.12.018.

Foerster, M., Gengenbach, T., Woo, M.W., & Selomulya, C. (2016). The impact of atomization on the surface composition of spray-dried milk droplets. Colloids and Surfaces B: Biointerfaces 140, 460-471. https://doi.org/10.1016/j.colsurfb.2016.01.012.

Goalard, C., Samimi, A., Galet, L., Dodds, J.A., & Ghadiri, M. (2006). Characterization of the dispersion behaviour of powders in liquids. Particle & Particle Systems Characterization 23(2), 154-158. https://doi.org/10.1002/ppsc.200601024.

Goder, D., Kalman, H., & Ullmann, A. (2002). Fatigue characteristics of granular materials. Powder Technology 122(1), 19-25. https://doi.org/10.1016/S0032-5910(01)00390-4.

Golchert, D., Moreno, R., Ghadiri, M., & Litster, J. (2004). Effect of granule morphology on breakage behaviour during compression. Powder Technology 143-144, 84-96. https://doi.org/10.1016/j.powtec.2004.04.032.

Han, J., Fitzpatrick, J., Cronin, K., Maidannyk, V., & Miao, S. (2020). Breakage of infant milk formula through three different processing methods and its influence on powder properties. Journal of Food Engineering 282, 109997. https://doi.org/10.1016/j.jfoodeng.2020.109997.

Han, J., Fitzpatrick, J., Cronin, K., Maidannyk, V., & Miao, S. (2021a). Particle size, powder properties and the breakage behaviour of infant milk formula. Journal of Food Engineering 292, 110367. https://doi.org/10.1016/j.jfoodeng.2020.110367.

Han, J., Fitzpatrick, J., Cronin, K., & Miao, S. (2021b). Dairy powder breakage: Mechanisms, characterization methods, impacted properties and influencing factors. Trends in Food Science & Technology 114, 608-624. https://doi.org/10.1016/j.tifs.2021.05.043.

Han, J., Fitzpatrick, J., Cronin, K., & Miao, S. (2021c). Investigation of the influence of powder characteristics on the breakage of dairy powders. Food Research International, 110775. https://doi.org/10.1016/j.foodres.2021.110775.

Han, J., Fitzpatrick, J., Cronin, K., & Miao, S. (2022). Effects of different breakage mechanisms on the physical, water sorption, and mechanical characteristics of

infant milk formula. Journal of Food Engineering, 110939. https://doi.org/10.1016/j.jfoodeng.2022.110939.
Hanley, K.J., 2011. Experimental quantification and modelling of attrition of infant formulae. PhD Thesis, Department of Process and Chemical Engineering. University College Cork, Ireland.
Hanley, K.J., Cronin, K., O'Sullivan, C., Fenelon, M.A., O'Mahony, J.A., & Byrne, E.P. (2011). Effect of composition on the mechanical response of agglomerates of infant formulae. Journal of Food Engineering 107(1), 71-79. https://doi.org/10.1016/j.jfoodeng.2011.05.042.
Hazlett, R., Schmidmeier, C., & O'Mahony, J.A. (2020). Influence of mechanical integrity during pneumatic conveying on the bulk handling and rehydration properties of agglomerated dairy powders. Journal of Food Engineering, 110103. https://doi.org/10.1016/j.jfoodeng.2020.110103.
Ji, J., Fitzpatrick, J., Cronin, K., Crean, A., & Miao, S. (2016). Assessment of measurement characteristics for rehydration of milk protein based powders. Food Hydrocolloids 54, 151-161. https://doi.org/10.1016/j.foodhyd.2015.09.027.
Kalman, H. (1999). Attrition control by pneumatic conveying. Powder Technology 104(3), 214-220. https://doi.org/10.1016/S0032-5910(99)00097-2.
Kalman, H. (2000). Attrition of powders and granules at various bends during pneumatic conveying. Powder Technology 112(3), 244-250. https://doi.org/10.1016/S0032-5910(00)00298-9.
Kim, E.H.J., Chen, X., & Pearce, D. (2005). Effect of surface composition on the flowability of industrial spray-dried dairy powders. Colloids and Surfaces B: Biointerfaces 46(3), 182-187. https://doi.org/10.1016/j.colsurfb.2005.11.005.
Kim, E.H.J., Chen, X.D., & Pearce, D. (2009). Surface composition of industrial spray-dried milk powders. 2. Effects of spray drying conditions on the surface composition. Journal of Food Engineering 94(2), 169-181. https://doi.org/10.1016/j.jfoodeng.2008.10.020.
Konami, M., Tanaka, S., & Matsumoto, K. (2002). Attrition of granules during repeated pneumatic transport. Powder Technology 125(1), 82-88. https://doi.org/10.1016/S0032-5910(02)00002-5.
Kotzur, B.A., Berry, R.J., Zigan, S., García-Triñanes, P., & Bradley, M.S.A. (2018). Particle attrition mechanisms, their characterisation, and application to horizontal lean phase pneumatic conveying systems: A review. Powder Technology 334, 76-105. https://doi.org/10.1016/j.powtec.2018.04.047.
Li, R., Roos, Y.H., & Miao, S. (2016a). The effect of water plasticization and lactose content on flow properties of dairy model solids. Journal of Food Engineering 170, 50-57. https://doi.org/10.1016/j.jfoodeng.2015.09.014.
Li, R., Roos, Y.H., & Miao, S. (2016b). Roles of particle size on physical and mechanical properties of dairy model solids. Journal of Food Engineering 173, 69-75. https://doi.org/10.1016/j.jfoodeng.2015.10.041.
Liu, L., Kafui, K.D., & Thornton, C. (2010). Impact breakage of spherical, cuboidal and cylindrical agglomerates. Powder Technology 199(2), 189-196. https://doi.org/10.1016/j.powtec.2010.01.007.
Lu, X., Liu, C., Zhu, L., & Qu, X. (2014). Influence of process parameters on the characteristics of TiAl alloyed powders by fluidized bed jet milling. Powder Technology 254, 235-240. https://doi.org/10.1016/j.powtec.2013.11.013.
Maidannyk, V., McSweeney, D.J., Hogan, S.A., Miao, S., Montgomery, S., Auty, M.A.E., & McCarthy, N.A. (2020). Water sorption and hydration in spray-dried milk protein powders: Selected physicochemical properties. Food Chemistry 304, 125418. https://doi.org/10.1016/j.foodchem.2019.125418.
McCarthy, N.A., Gee, V.L., Hickey, D.K., Kelly, A.L., O'Mahony, J.A., & Fenelon, M.A. (2013). Effect of protein content on the physical stability and microstructure of a model infant formula. International Dairy Journal 29(1), 53-59. https://doi.org/10.1016/j.idairyj.2012.10.004.

Murrieta-Pazos, I., Gaiani, C., Galet, L., Cuq, B., Desobry, S., & Scher, J. (2011). Comparative study of particle structure evolution during water sorption: Skim and whole milk powders. Colloids and Surfaces B: Biointerfaces 87(1), 1-10. https://doi.org/10.1016/j.colsurfb.2011.05.001.
Niro, G. (2006). GEA Niro analytical methods dry products. GEA Process Engineering A/S, Gladsaxevej, Denmark,.
Norazirah, A., Fuad, S.H.S., & Hazizan, M.H.M. (2016). The effect of size and shape on breakage characteristic of mineral. Procedia Chemistry 19, 702-708. https://doi.org/10.1016/j.proche.2016.03.073.
Petukhov, Y., & Kalman, H. (2004). Empirical breakage ratio of particles due to impact. Powder Technology 143-144, 160-169. https://doi.org/10.1016/j.powtec.2004.04.009.
Rennie, P.R., Chen, X., Hargreaves, C., & Mackereth, A.R. (1999). A study of the cohesion of dairy powders. Journal of Food Engineering 39(3), 277-284. https://doi.org/10.1016/S0260-8774(98)00158-7.
Reynolds, G.K., Fu, J.S., Cheong, Y.S., Hounslow, M.J., & Salman, A.D. (2005). Breakage in granulation: A review. Chemical Engineering Science 60(14), 3969-3992. https://doi.org/10.1016/j.ces.2005.02.029.
Samimi, A., Ghadiri, M., Boerefijn, R., Groot, A., & Kohlus, R. (2003). Effect of structural characteristics on impact breakage of agglomerates. Powder Technology 130(1), 428-435. https://doi.org/10.1016/S0032-5910(02)00246-2.
Shrestha, A.K., Howes, T., Adhikari, B.P., Wood, B.J., & Bhandari, B.R. (2007). Effect of protein concentration on the surface composition, water sorption and glass transition temperature of spray-dried skim milk powders. Food Chemistry 104(4), 1436-1444. https://doi.org/10.1016/j.foodchem.2007.02.015.
Yan, H., & Barbosa-Cánovas, G.V. (1997). Compression characteristics of agglomerated food powders: Effect of agglomerate size and water activity Food Science and Technology International 3(5), 351-359. https://doi.org/10.1177/108201329700300506.
Yan, H., & Barbosa-Cánovas, G.V. (2001). Attrition evaluation for selected agglomerated food powders: the effect of agglomerate size and water activity. Journal of Food Process Engineering 24(1), 37-49. https://doi.org/10.1111/j.1745-4530.2001.tb00530.x.
Zhang, Olaleye, A.K., O'Mahony, J.A., Miao, S., & Cronin, K. (2020). Dilute phase pneumatic conveying of whey protein isolate powders: Particle breakage and its effects on bulk properties. Advanced Powder Technology 31(8), 3342-3350. https://doi.org/10.1016/j.apt.2020.06.019.

Supplementary materials

Supplementary Table 6-S1. Properties of broken WPI/lactose model powders during four times of pneumatic conveying transportation at 40 m/s.

Samples		Particle size $D_{3,2}$ (μm)	SSA (m^2/kg)	Morphological characteristics			Surface composition of particles		
				Elongation	Circularity	Convexity	Fat (%)	Whey protein (%)	Lactose (%)
WL10	Initial	47.5^{a}±0.2	120.4^{b}±0.5	0.199^{b}±0.004	0.861^{a}±0.007	0.987^{a}±0.003	23.6^{a}±0.9	75.6^{a}±1.1	0.0^{a}
	PC4	45.2^{b}±0.1	126.5^{a}±1.0	0.222^{a}±0.003	0.838^{b}±0.008	0.985^{a}±0.002	17.8^{a}±0.5	76.5^{a}±0.1	0.0^{a}
WL31	Initial	43.5^{a}±0.2	131.6^{b}±0.7	0.205^{b}±0.001	0.851^{a}±0.014	0.986^{a}±0.004	24.5^{a}±5.7	66.1^{a}±3.3	8.8^{a}±2.5
	PC4	41.5^{b}±0.3	143.6^{a}±0.3	0.228^{a}±0.008	0.832^{a}±0.010	0.986^{a}±0.002	17.8^{a}±0.5	67.4^{a}±0.9	14.2^{a}±0.1
WL11	Initial	72.8^{a}±0.2	78.5^{b}±0.2	0.243^{b}±0.001	0.822^{a}±0.001	0.983^{a}±0.002	7.1^{a}±0.9	63.2^{a}±0.3	29.2^{a}±1.2
	PC4	63.8^{b}±0.4	91.4^{a}±0.8	0.256^{a}±0.002	0.823^{a}±0.004	0.987^{a}±0.001	10.1^{a}±2.3	57.4^{a}±2.8	31.8^{a}±0.6
WL13	Initial	86.6^{a}±0.1	66.0^{b}±0.1	0.249^{b}±0.004	0.805^{a}±0.003	0.977^{b}±0.001	0.5^{a}±0.5	50.3^{a}±2.1	48.5^{a}±1.9
	PC4	66.0^{b}±0.2	86.6^{a}±0.3	0.267^{a}±0.004	0.824^{a}±0.004	0.996^{a}±0.001	0.01^{a}±0.01	45.4^{a}±0.3	53.1^{a}±0.4

1. WL10: WPI to lactose ratios is 100:0. WL31: WPI to lactose ratios is 75:25. WL11: WPI to lactose ratios is 50:50. WL13: WPI to lactose ratios is 25:75. SSA: specific surface area. PC4: four times transportation by lab-scale dilute-phase pneumatic conveying at 40 m/s.
2. Values are mean ± standard deviation (n=3).
3. $^{a-b}$ different values within columns in each samples are significantly different at P <0.05, respectively.

CHAPTER SEVEN

Breakage behaviour and functionality of spray-dried agglomerated model infant milk formula: Effect of proteins and carbohydrates content

Chapter 7 has been submitted:

Han, J., Fitzpatrick, J., Cronin, K., Maidannyk, V., & Miao, S. Breakage behaviour and functionality of spray-dried agglomerated model infant milk formula: Effect of proteins and carbohydrates content (submitted to *Food Chemistry*).

The work contained in this chapter was undertaken and written solely by myself with specific contributions from each co-author.

Jie Han: Conceptualization, Methodology, Formal analysis, Investigation, Data curation, Writing - original draft, Visualization

John Fitzpatrick: Supervision, Writing - review & editing

Kevin Cronin: Supervision, Writing - review & editing

Valentyn Maidannyk: Investigation

Song Miao: Supervision, Conceptualization, Writing - review & editing, Funding acquisition, Project administration

Abstract

This chapter explored the effect of protein content (whey protein and casein) and carbohydrate content (lactose, sucrose, and maltodextrin) on the breakage behaviour and its influence on spray-dried agglomerated model infant milk formula. Whey protein powders were bigger in particle size, weaker in structural strength, and marginally more irregular in shape, which resulted in better rehydration properties but more breakage than pure casein powders. Similarly, sucrose samples had better rehydration properties and higher glass transition temperatures but suffered more breakage than maltodextrin and pure lactose powders because of their bigger particle size. The influence of different proteins on powder properties and breakage was greater than that of the different combinations of carbohydrates. Breakage changed the physical and structural properties of powders, especially for whey protein and sucrose samples, which caused the deterioration of rehydration properties and the decrease in crystallization temperatures. From the perspective of particle breakage, unwanted dairy powder breakage could be controlled by changing powder formulations.

Keywords: Agglomerated dairy powders; Breakage behaviour; Protein; Carbohydrate; Powder functionality

7.1. Introduction

It has been demonstrated that particle characteristics (powder physical properties and powder composition) and the force applied on particles from processing conditions were two main factors that determine particles' response to the applied loading conditions (Han et al., 2021b; Kotzur et al., 2018; Lu et al., 2014; Petukhov and Kalman, 2004). Unwanted dairy powder breakage could be reduced by manipulating these two factors.

For physical properties, in Chapter 5, it was found that particle size and particle structure were the most important physical properties which influenced the dynamic breakage of dairy powders during pneumatic conveying (Han et al., 2021c). Regarding the influence of powder

composition, limited research on comparing different commercial dairy powders has been done and the differences in drying parameters between these samples were not considered and these parameters would influence powder physical properties and impact their breakage behaviour (Hanley, 2011). Therefore, Chapter 6 studied the effect of whey protein and lactose content on the breakage behaviour of whey-protein/lactose powders formed during the same drying conditions. It was found that protein and lactose composition influenced breakage by influencing the particle size and structure of the agglomerates. Powders with higher whey protein content were smaller in particle size, less irregular in shape, and had higher particle densities, which resulted in less breakage in comparison to powders with lower whey protein content. However, the formulation of dairy powder products is always more complex, for example, use of different kinds of dairy proteins or carbohydrates, and with or without fat. Thus, research on the effect of powder formulations in more complex model powders on powder breakage will be useful.

In this chapter, agglomerated model IMF were produced using the same spray drying conditions to investigate the effect of proteins (whey protein and casein) and carbohydrates (lactose, sucrose, and maltodextrin) content on the breakage behaviour and functionality of model powders and the changes in powder properties after breakage. Two kinds of breakage were considered, dynamic breakage under different mechanical stresses in a venturi feeder, and breakage under repeated lab-scale pneumatic conveying – to investigate the influence of fatigue. Then broken samples from the fatigue test were chosen to analyse the impact of breakage on the rehydration and water adsorption properties of model IMF with different composition.

7.2. Material and methods

7.2.1. Materials

Whey protein isolate (WPI, protein content was 88.59%) and lactose (lactose content was 99.69%) were obtained from Glanbia (Glanbia plc, Kilkenny, Ireland). Micellar casein MC85 (MC, protein content was 88.45%) was obtained from InLeit (InLeit New Nutrition, Curtis, A Coruña, Spain). Maltodextrin (Glucidex 19, DE value 18-20) was obtained from AnabioTechnologies Ltd (Cork, Ireland). Sunflower oil and granulated sucrose were purchased from a local supermarket.

7.2.2. Model IMF preparation

Eight model IMF powders were formulated with a target fat: protein: carbohydrate ration of 26:15: 59 (w/w) using sunflower oil, WPI, MC, lactose, sucrose, and maltodextrin. They were labelled as WLM, CLM, WLS, CLS, WL, CL, WC82L, and WC64L based on their formulations, as shown in Figure 7-1. The ratio of fat, protein, and carbohydrate was determined based on the commercial IMF products. For WC82L and WC64L, the whey protein to casein ratios were 80:20, and 60:40, respectively. This was designed according to the protein contents of the commercial first stage (for babies up to 6 months of age) and second or third stages (for babies older than 6 months) IMF products, respectively. In WLM, CLM, WLS, and CLS, 30% of lactose (17.7% of whole powders) was replaced by sucrose or maltodextrin, respectively, because based on the relevant regulation, maltodextrin can be added up to 30% of the total carbohydrate content in IMF (European Commission, 2006). Although sucrose can only be added up to 20% of the total carbohydrate content in IMF, it is a common ingredient in other dairy powder products. Therefore, the results of this study can be applied not only to IMF but to all dairy powder products. Also, for easier comparison, the content of sucrose was added to 30%, the same as the maltodextrin.

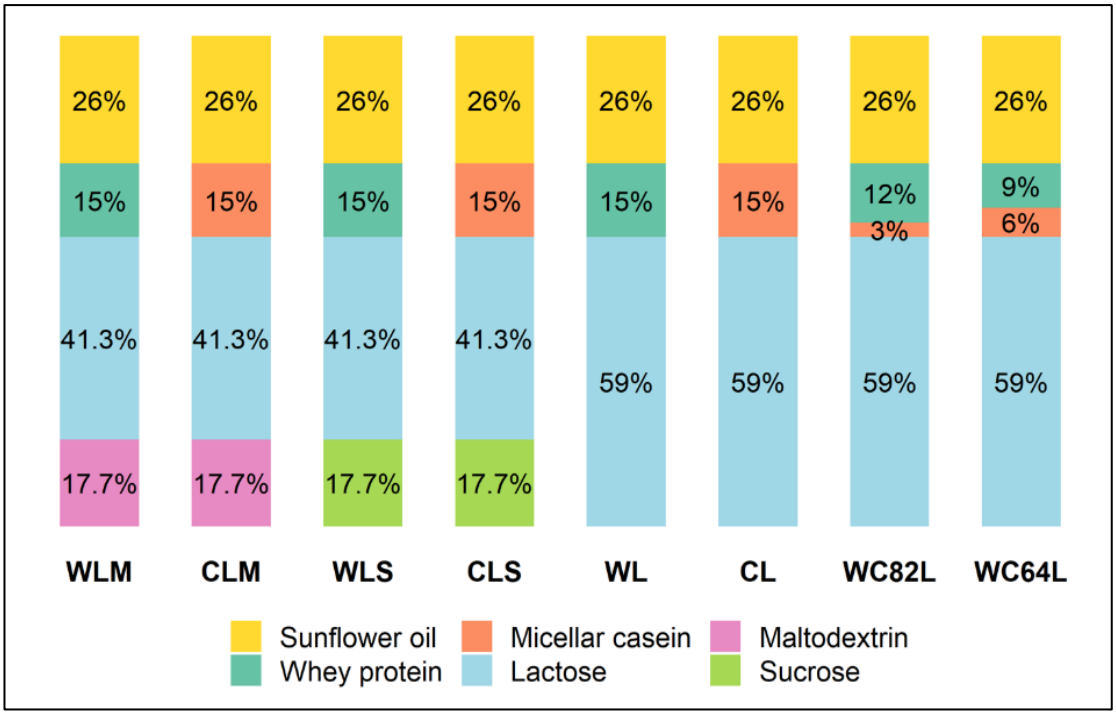


Figure 7-1. The formulations of initial model powders. W (whey protein), L (lactose), M (maltodextrin), C (micellar casein), S (sucrose).

WPI and MC were reconstituted separately in deionized water (15%, w/w) at around 45℃ for 2 h followed by overnight storage at 4℃ with gentle agitation. Lactose, sucrose, and maltodextrin solution (34%, w/w) were prepared separately in deionized water at 70℃ for 2 h. Emulsions (50 kg, 33% w/w) were prepared based on their formulations by reconstituting the relevant ingredients and mixing for 20 min before processing. After complete mixing, the pH of emulsions were adjusted to 6.8 using sodium hydroxide solution (10%, w/v). Emulsions were heated at 70℃ for 15 s using the MicroThermics Lab heat exchanger (MicroThermics, North Carolina, USA) and subsequently homogenized using the in-line two-stage valve homogenizer (NS2006H, Niro Soavi, Parma, Italy) with first and second stage pressures of 17.5 MPa and 3.0 MPa, respectively. Then mixtures (50 kg) were spray-dried using a three-stage spray dryer with inlet and outlet temperatures of 180℃ and 80℃, respectively, at the Teagasc Food Research Centre, Moorepark, Fermoy, Co. Cork, Ireland. For each sample, the first 4-5 kg powders were discarded to make sure the spray drying was operating stably and subsequent powders (around 10 kg) were sampled at

different times. All composition analysis of powders was performed directly after spray drying and the other analysis was carried out within 2 months.

7.2.3. Powder characterisation

7.2.3.1. Particle size and specific surface area

The specific surface area (SSA), and Sauter mean particle size ($D_{3,2}$) of model samples were measured using a Malvern Mastersizer 3000 (Malvern Instruments Ltd., Worcestershire, UK)), following the method as described in 2.2.2.1. The measurements were performed in triplicate.

7.2.3.2. Particle density, bulk densities, and porosity

Loose bulk density (ρ_b), tapped bulk density (100 taps, ρ_{tapped}), particle density (ρ_p), and interparticle porosity (ε) of samples were measured according to the method as described in 2.2.2.2.

7.2.3.3. Powder structure

A polarised light microscope (Instruction BX51, Olympus Optical Co. Ltd., Tokyo, Japan) with a 10× objective or a 60× oil objective and a scanning electron microscope (SEM, Zeiss-Supra 40 VP/Gemini Column, Carl Zeiss, Germany) were used to observe the structure of particles from model powders, following the methods as described in 2.2.7.

7.2.3.4. Powder morphology

A Malvern Morphologi G3 (Malvern Instruments Ltd.) was used to determine the morphology of model powders, following the method as described in 3.2.6. The measurements were performed in duplicate.

7.2.4. Breakage behaviour of model powders

7.2.4.1. Dynamic breakage during venturi feeder under different mechanical stresses

The dynamic breakage of powders under different mechanical stresses in powder venturi feeder (diagram is shown in Figure 2-1A) was investigated using the Mastersizer 3000, following the method as described in 2.2.3.2. The degree of breakage was shown as the breakage percentage (*BP*) that was evaluated as Eq. (2-3), according to the method as described in 2.2.6.

7.2.4.2. Breakage during repeated lab-scale pneumatic conveying

The susceptibility of model powders to fatigue was studied by repeated pneumatic conveying transportation. The diameter of the conveyor was 47 mm, and there were two horizontal sections (lengths were 3.1 m) connected to a vertical section (length was 430 mm) by two 90º bends (bend radii was 250 mm). Powders (800 g) were blown through the conveyor with an air pressure of 2.5 bar. Seven samples from each model IMF were performed on the pneumatic conveying transportation 1 to 7 times, termed PC1 to PC7, respectively. The particle size of samples after transportation was measured following the method described in 7.2.3.1.

7.2.5. Powder functionality and the influence of breakage

The rehydration and water adsorption properties of PC7 samples from 7.2.4.2 and initial powders were investigated. Powder characteristics of PC7 samples were determined following the method described in 7.2.3.

7.2.5.1. Rehydration properties – wettability and dispersibility

The wettability of powders was quantified by penetrating time, following the method as described in 4.2.7.1. All the measurements were conducted five times.

The dispersibility of samples, represented by the dispersibility index (*DI*), is the proportion of dry matter that passes through a sieve after mixing for a

short time. Samples (25 g) were filled into an 800 mL beaker with deionized water (250 g at 25ºC) and then mixed vigorously with a spatula for exactly 20 s as per GEA Niro (2006). The reconstituted samples were poured onto the 180 µm sieve and the samples that passed through the sieve were collected for solid content measurement. The *DI* was calculated as Eq. (4-2). All the measurements were carried out in duplicate.

7.2.5.2. Water adsorption, glass transition, and lactose crystallization properties

The water adsorption property and time-dependent lactose crystallization of powders at different water vapor pressure (RVP, 11.4%, 23.1%, 33.2%, 44.1%, 54.5%, and 65.6%) were measured using the static gravimetric method, as described in 3.2.7.1. Then the initial crystalized (T_{ic}, peak) and glass transition (T_g, inflection point) temperature of samples (equilibrated at 11.4%, 23.1%, 33.2%, and 44.1% RVP) were measured, following the method described in 3.2.8. All measurements were carried out in duplicate.

7.2.6. Statistical analysis

Results were expressed as mean ± standard deviation (SD). Significant differences between each initial model sample was determined using one-way ANOVA with Tukey's test (IBM SPSS Statistics, IBM, USA) with a confidence level of P <0.05. Student's *t*-test with a 95% confidence interval was used to determine the significant differences between samples before and after the breakage in each model sample. Data visualization was performed with R (v3.6.3) with tidyverse, ggplot2 and ggpubr packages, and with OriginPro 8.5 (OriginLab, Massachusetts, USA).

7.3. Result and discussion

7.3.1. Powder characterisation

For easier reference, powders that had only casein (CLM, CLS, and CL) or only whey protein (WLM, WLS, and WL) were referred to as pure casein powders or pure whey protein powders, respectively. Whey protein powders

were pure whey protein powders and whey protein and casein mixtures (WC82L and WC64L). Similarly, powders that had only lactose (WL, CL, WC82L, and WC64L) were referred to as pure lactose powders while those that contained lactose and maltodextrin mixtures (WLM and CLM) or sucrose mixtures (WLS and CLS) were called maltodextrin or sucrose powders, respectively.

7.3.1.1. Powder physical properties

The physical properties of powders are influenced by both the drying process and the formulation. As the drying conditions were the same for the eight model samples, the difference in physical properties between them should be because of the different formulations. The particle size and some other physical properties of initial model powders are shown in Figure 7-2 and Table 7-1, respectively.

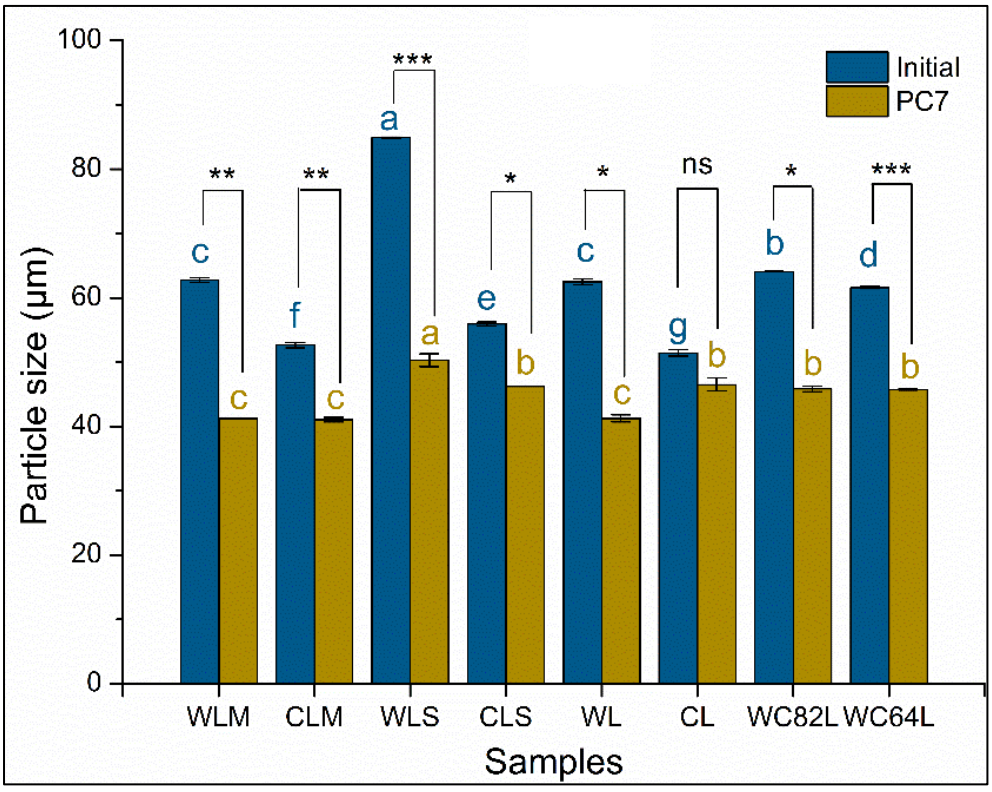


Figure 7-2. The particle size ($D_{3,2}$) of initial and broken (PC7) model powders. W (whey protein), L (lactose), M (maltodextrin), C (micellar casein), S (sucrose). PC7: seven times transportation by lab-scale pneumatic conveying.

From Figure 7-2, the $D_{3,2}$ of initial samples were from 51 to 85 μm and most of them were significantly different (P <0.05) from each other. It was shown that the $D_{3,2}$ of WLS was the biggest, 84.9 μm, and those of WLM, WL, and two WCL powders (WC82L and WC64L) were around 60 μm, while those of CLM, CLS, and CL were around 50 μm. This indicates that the particle size of the whey protein model IMF was significantly bigger than pure casein model powders, which is in accordance with previous research (Masum et al., 2020; Murphy et al., 2015). This might be because the casein used in this study mainly existed in the form of casein micelle and it was hard for them to adsorb at the oil-water interface to stabilize the fat globules, which resulted in the bigger particle size of emulsions that only contained casein (around 450 nm) than those that contained whey protein (around 300 nm, data not shown) after homogenization. The bigger particle size of emulsions means the smaller number of particles, which might contribute to the lower viscosity of emulsions and then resulted in the smaller particles during the atomisation stage of spray drying (Masum et al., 2020). From the perspective of different carbohydrates, the $D_{3,2}$ of WLS was significantly bigger than those of WLM and WL (P <0.05), which means that the particle size of sucrose powders was bigger than maltodextrin model IMF and pure lactose powders. This was also found for pure casein model powders where the $D_{3,2}$ of CLS was significantly bigger (P <0.05) than those of CLM and CL. The bigger particle size of WLS and CLS might be because the T_g of sucrose is lower than those of lactose and maltodextrin, which resulted in more stickiness during the spraying drying (Fang and Bhandari, 2012). The stickiness state of particles can cause inter-particle cohesion, which causes a higher degree of agglomeration. Previous research has shown that particle size is an important factor that influences particle breakage, and the degree of breakage is amplified as the particle size increases. This is because of the probability of more imperfections in bigger particles, like cracks and internal holes where the highest local tensile stress will generate, leading to the initiation and propagation of fractures (Antonyuk et al., 2005).

As the SSA was determined from the particle size, the significant differences in SSA (P <0.05) were also found between most of the initial

powders (Table 7-1). It was shown that pure casein model powders had the biggest SSA, at around 110 m²/kg, and WLS had the smallest SSA, at around 77 m²/kg, and those of the rest powders were around 95 m²/kg. The SSA of powders might impact the water sorption properties because water is mainly absorbed on the surface of particles and the larger SSA means more area for sorption of water molecules (Li et al., 2016; McCarthy et al., 2013).

Particle density is associated with particle structural characteristics because it is the mass per unit volume of particles that includes closed internal holes but not open holes or cracks. It was shown that the particle density of pure casein powders, at around 1.0 kg/L, was significantly higher than those of other model powders, at around 0.8 kg/L (Table 7-1). This indicates that there might be more internal pores within whey protein powder particles in comparison to pure casein IMF particles. When model powders had the same proteins but different carbohydrates, the particle density of sucrose model powders was slightly higher than maltodextrin or pure lactose powders. This might be because of the slight difference in particle internal structure or the density of the three carbohydrates. Powder bulk density is also affected by particle shapes and structures. Similar to the particle density, the loose bulk density of initial whey protein model powders, at around 0.29 kg/L, was significantly lower than those of pure casein model powders, at around 0.35 kg/L. Also, the bulk density of sucrose model powders was slightly higher than those of powders that contained the same protein but different carbohydrates. This might be because the particles that contained whey protein or sucrose were more irregular in comparison to relevant particles. In addition, the porosity of pure casein model powders was significantly lower than whey protein model samples (Table 7-1).

Table 7-1. Physical properties of initial and broken (PC7) model powders.

Samples	SSA (m^2/kg)		Particle density (kg/L)		Loose bulk density (kg/L)		Porosity (%)	
	Initial	PC7	Initial	PC7	Initial	PC7	Initial	PC7
WLM	$95.6^{e}\pm0.5^{B}$	$145.6^{a}\pm0.1^{A}$	$0.771^{f}\pm0.001^{B}$	$0.961^{f}\pm0.002^{A}$	$0.268^{f}\pm0.001^{B}$	$0.297^{f}\pm0.001^{A}$	$48.93^{a}\pm0.03^{B}$	$57.08^{a}\pm0.08^{A}$
CLM	$114.0^{b}\pm0.8^{B}$	$146.2^{a}\pm1.2^{A}$	$0.983^{c}\pm0.001^{B}$	$1.055^{b}\pm0.001^{A}$	$0.347^{b}\pm0.002^{B}$	$0.372^{c}\pm0.004^{A}$	$46.84^{f}\pm0.02^{B}$	$48.80^{f}\pm0.03^{A}$
WLS	$76.7^{g}\pm0.1^{B}$	$119.3^{d}\pm2.3^{A}$	$0843^{e}\pm0.001^{B}$	$1.001^{e}\pm0.001^{A}$	$0.308^{c}\pm0.002^{B}$	$0.376^{c}\pm0.002^{A}$	$47.30^{d}\pm0.05^{B}$	$51.29^{d}\pm0.02^{A}$
CLS	$107.3^{c}\pm0.5^{B}$	$129.9^{b}\pm0.1^{A}$	$1.048^{a}\pm0.001^{B}$	$1.086^{a}\pm0.001^{A}$	$0.366^{a}\pm0.005^{B}$	$0.409^{a}\pm0.004^{A}$	$45.99^{g}\pm0.05^{A}$	$46.54^{h}\pm0.06^{A}$
WL	$96.0^{e}\pm0.7^{B}$	$145.6^{a}\pm2.0^{A}$	$0.841^{e}\pm0.001^{B}$	$1.012^{d}\pm0.001^{A}$	$0.292^{de}\pm0.013^{B}$	$0.335^{e}\pm0.001^{A}$	$47.86^{b}\pm0.08^{B}$	$55.34^{b}\pm0.04^{A}$
CL	$116.7^{a}\pm1.2^{A}$	$124.2^{c}\pm2.0^{A}$	$1.001^{b}\pm0.001^{B}$	$1.057^{b}\pm0.002^{A}$	$0.358^{ab}\pm0.001^{B}$	$0.397^{b}\pm0.002^{A}$	$44.56^{h}\pm0.04^{B}$	$46.93^{g}\pm0.07^{A}$
WC82L	$93.6^{f}\pm0.1^{B}$	$131.0^{b}\pm1.3^{A}$	$0.840^{e}\pm0.001^{B}$	$0.998^{e}\pm0.002^{A}$	$0.283^{e}\pm0.002^{B}$	$0.348^{d}\pm0.002^{A}$	$47.15^{e}\pm0.03^{B}$	$53.38^{c}\pm0.06^{A}$
WC64L	$97.4^{d}\pm0.2^{B}$	$131.2^{b}\pm0.3^{A}$	$0.886^{d}\pm0.001^{B}$	$1.033^{c}\pm0.002^{A}$	$0.303^{cd}\pm0.004^{B}$	$0.370^{c}\pm0.003^{A}$	$47.45^{c}\pm0.01^{B}$	$49.16^{e}\pm0.09^{A}$

1. WLM (sunflower oil; WPI; lactose to maltodextrin ratio 70:30); CLM (sunflower oil; MC; lactose to maltodextrin ratio 70:30); WLS (sunflower oil; WPI; lactose to sucrose ratio 70:30); CLS (sunflower oil; MC; lactose to sucrose ratio 70:30); WL (sunflower oil; WPI; lactose); CL (sunflower oil; MC; lactose); WC82L (sunflower oil; WPI to MC ratio 80:20; lactose); WC64L (sunflower oil; WPI to MC ratio 60:40; lactose); with a target protein: fat: carbohydrate ration of 15:26:59 (w/w). PC7: seven times transportation by lab-scale pneumatic conveying.
2. Values are mean ± standard deviation (n=3). $^{a-h}$ different values within columns are significantly different at $P<0.05$. $^{A-B}$ different values within properties of each powder (initial and PC7) are significantly different at $P<0.05$.

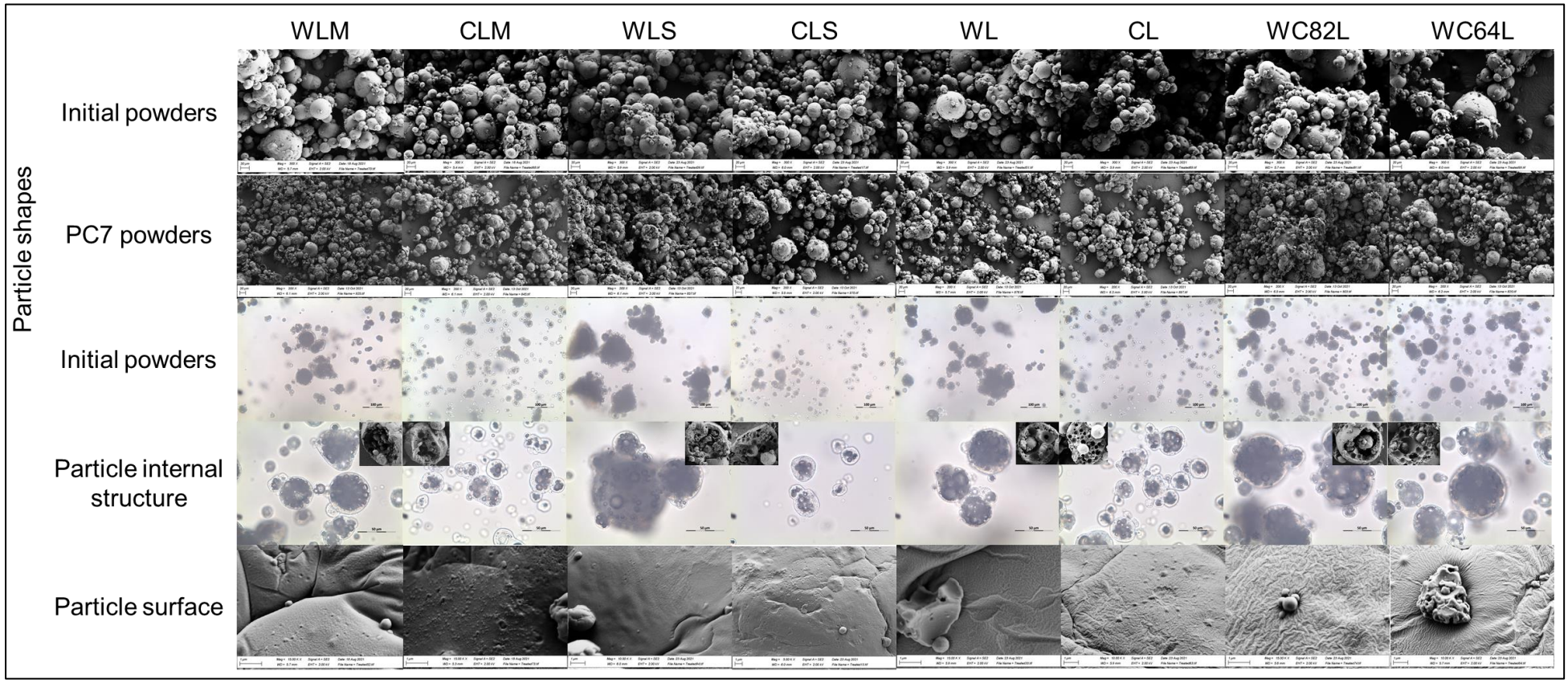


Figure 7-3. Microscopy photos of initial and broken (PC7) model powders. PC7: seven times transportation by lab-scale pneumatic conveying.

Table 7-2. Morphological characteristics of initial and broken model powders.

Samples	Elongation		Circularity		Convexity	
	Initial	PC7	Initial	PC7	Initial	PC7
WLM	$0.162^{abc}\pm0.005^{A}$	$0.196^{c}\pm0.001^{A}$	$0.912^{b}\pm0.007^{A}$	$0.893^{e}\pm0.001^{A}$	$0.993^{ab}\pm0.002^{A}$	$0.996^{a}\pm0.001^{A}$
CLM	$0.156^{bc}\pm0.006^{A}$	$0.166^{f}\pm0.001^{A}$	$0.923^{ab}\pm0.006^{A}$	$0.916^{b}\pm0.001^{A}$	$0.995^{a}\pm0.001^{A}$	$0.996^{a}\pm0.001^{A}$
WLS	$0.176^{a}\pm0.003^{B}$	$0.205^{b}\pm0.001^{A}$	$0.904^{b}\pm0.002^{A}$	$0.901^{d}\pm0.002^{A}$	$0.991^{b}\pm0.001^{A}$	0.996^{aA}
CLS	$0.168^{ab}\pm0.001^{A}$	$0.160^{g}\pm0.001^{B}$	$0.913^{b}\pm0.002^{B}$	$0.925^{a}\pm0.001^{A}$	$0.993^{ab}\pm0.001^{A}$	0.996^{aA}
WL	$0.169^{ab}\pm0.003^{A}$	$0.210^{a}\pm0.001^{A}$	$0.911^{b}\pm0.002^{A}$	0.823^{fB}	$0.993^{ab}\pm0.001^{A}$	$0.995^{a}\pm0.002^{A}$
CL	$0.158^{bc}\pm0.001^{B}$	$0.163^{g}\pm0.001^{A}$	$0.924^{ab}\pm0.003^{A}$	$0.892^{e}\pm0.001^{B}$	$0.995^{ab}\pm0.001^{A}$	$0.993^{a}\pm0.001^{A}$
WC82L	$0.152^{c}\pm0.002^{B}$	$0.181^{e}\pm0.001^{A}$	$0.921^{ab}\pm0.002^{A}$	$0.907^{c}\pm0.001^{A}$	$0.994^{ab}\pm0.001^{A}$	$0.994^{a}\pm0.002^{A}$
WC64L	$0.133^{d}\pm0.001^{B}$	$0.186^{d}\pm0.002^{A}$	$0.940^{a}\pm0.001^{A}$	$0.895^{e}\pm0.002^{B}$	0.996^{aA}	$0.991^{a}\pm0.001^{A}$

1. WLM (sunflower oil; WPI; lactose to maltodextrin ratio 70:30); CLM (sunflower oil; MC; lactose to maltodextrin ratio 70:30); WLS (sunflower oil; WPI; lactose to sucrose ratio 70:30); CLS (sunflower oil; MC; lactose to sucrose ratio 70:30); WL (sunflower oil; WPI; lactose); CL (sunflower oil; MC; lactose); WC82L (sunflower oil; WPI to MC ratio 80:20; lactose); WC64L (sunflower oil; WPI to MC ratio 60:40; lactose); with a target protein: fat: carbohydrate ration of 15:26:59 (w/w). PC7: seven times transportation by lab-scale pneumatic conveying.
2. Values are mean ± standard deviation (n=3). $^{a-d}$ different values within columns are significantly different at P <0.05. $^{A-B}$ different values within properties of each powder (initial and PC7) are significantly different at P <0.05.

7.3.1.2. Powder structure and morphology

Different formulations can cause varying powder structural properties that are also essential factors affecting the breakage behaviour of particles. SEM and light microscopy photos (Figure 7-3) and morphological characteristics (elongation, circularity, and convexity) (Table 7-2) of initial particles from model IMF were used to identify the shapes and structures of particles.

From Figure 7-3, particles were agglomerated and the agglomeration degrees of particles from initial pure casein model powders were lower than those of particles from other model powders, which resulted in the difference in their particle size. From SEM photos, the shape of primary particles from all model powders was spherical with different diameters. However, from the light microscopy photos and the SEM photos of the inside of broken particles, the internal structure of particles with different proteins was different. There were more bigger-sized internal pores in whey protein model IMF particles compared with pure casein model powder particles. This also could be supported by the particle density results where whey protein model powders had much smaller particle densities than pure casein model powders. In addition, the particle density of pure casein model powders decreased (4-7%) less than that of whey protein model powders (17-25%). This difference may cause different responses of particles to the mechanical stresses imposed on particles because the internal holes can be considered as crack release zones or imperfections and they could reduce particle strength (Antonyuk et al., 2005). Particle structure could be influenced by powder composition and production process conditions that include the drying method, spray drying and agglomeration conditions, atomization methods and parameters, homogenization, heat treatment parameters, solid content before spray drying, and the concentration methods (Masum et al., 2021; Zouari et al., 2019). The internal structure of particles with different carbohydrates was similar but their particle surface was different as shown by relatively smoother surfaces for sucrose and maltodextrin powder particles but “shrivelled-like” surfaces for pure lactose powder particles. Considering different proteins, some small bumps on the surface of pure

casein model powder particles were evident, which could be the casein micelles.

From Figure 7-3, agglomerates were irregular and the irregularity of particles was quantified with elongation, circularity, and convexity (Table 7-2). It was shown that the elongation and convexity of pure casein model powders were higher than most of the whey protein powders, and the circularity was the opposite. This means that particles from the pure casein model IMF were closer to spheres compared with whey protein model IMF particles. It has been demonstrated that particle breakage is impacted by the shape of the particle. The closer the particle shape is to a sphere, the stronger the particle and the less susceptible it is to breakage. This may be because the irregular particles exhibit much more non-uniform loading than the spherical particles when forces permeate through the particle. In irregular particles, loading can easily exceed the stress that the weakest part of the particle can withstand, causing breakage to originate from that point (Deng and Davé, 2017; Golchert et al., 2004; Norazirah et al., 2016).

From Figures 7-2, 7-3, Table 7-1, and 7-2, the differences in physical and structural properties of the initial model IMF were more sensitive to the types of protein used compared to carbohydrates. When the same carbohydrate was used, the particle size of whey protein IMF was significantly bigger than those of pure casein IMF, and there were more internal pores in the whey protein model powder particles, which resulted in their lower particle density. Also, the irregularity of pure whey protein IMF particles was marginally higher than pure casein particles, which contributed to higher porosity and lower loose bulk density. Meanwhile, replacing less than 40% whey protein with casein micelles showed no influence on the physical and structural characteristics of powders. Considering different carbohydrates, the particle size of sucrose model powders was bigger than those of maltodextrin and pure lactose model powders. The porosity, bulk density, and particle density of sucrose model powders were also different from the other two carbohydrate samples even though there was no significant difference in their particle shapes and structures.

7.3.2. The influence of formulation on breakage behaviour of model powders

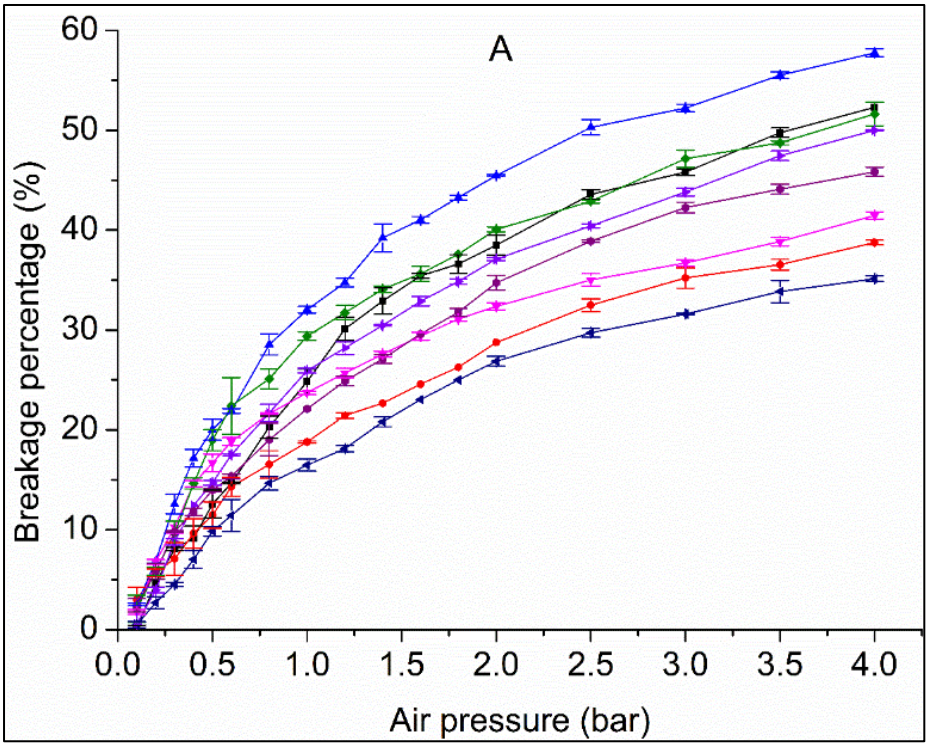
7.3.2.1. Dynamic breakage under different mechanical stresses

The dynamic breakage of model IMF under different mechanical stresses was represented by a series of *BP*, shown in Figure 7-4A. The *BP* of each IMF increased logarithmically with increasing air pressures, which corresponds with previous findings on many agglomerated commercial and lab-scale dairy powders (Chapter 5, Han et al., 2021a).

Considering the influence of protein, the *BP* of WLM was much higher than those of CLM where the *BP* of WLM and CLM at 3.0 bar were 45% and 35%, respectively. Similarly, the particle size of WLS and WL decreased more when they were exposed to the same level of mechanical stresses compared with CLS and CL, respectively. Also, more breakage happened on WC82L and WC64L particles than CL particles. These results indicate that whey protein model IMF particles were more sensitive to the mechanical stresses compared with casein model IMF particles and the difference in *BP* increased with increasing mechanical stresses. Also, replacing less than 40% whey protein with casein micelles slightly decreased the *BP* of model IMF. These results are mainly due to the bigger particles, the weaker particle structure, and marginally higher irregularity of whey protein model particles compared with pure casein model particles.

Considering the influence of carbohydrate, the *BP* of WLS and CLS were bigger than those of WLM and WL, CLM and CL, respectively, and these difference in *BP* was smaller than those between different protein model powder particles. This also can be explained by their different physical and structural properties where the particle size of sucrose powders was bigger than maltodextrin and pure lactose powders but their particle structure was similar. The material strength of different proteins or carbohydrates may be different, which could be another reason that they had different breakage behaviour. Meanwhile, based on these results, improving the particle structural strength would be a way to decrease the breakage.

The particle sizes of model powders measured at different air pressures are presented in Figure 7-4B. The particle size of WLS was always the biggest at all the air pressures even though its *BP* was the biggest. However, the initial particle size of WLM and WL (around 63 µm) were bigger than those of CLM, CLS, and CL (around 52 µm). Their particle size were similar at 2.5 bar, at around 35.7 µm, and when the air pressure higher than that, the particle size of WLM and WL were smaller than those of CLM, CLS, and CL. This is because the difference in their BP increased as air pressure increased. These results indicate that if the initial particle size is big enough, the final particles will remain big even after more breakage occurred. However, if not, the final particles may be even smaller than those particles with smaller initial particle sizes. This depends on the mechanical stresses imposed on the particles. Thus, besides improving the particle structural strength, increasing the initial particle size may be a good way to compensate for the particle breakage during the production of dairy powders when the imposed stress is low. However on the contrary, a smaller initial particle size may be more beneficial at higher imposed stresses because smaller particles are inherently more resistant to breakage.



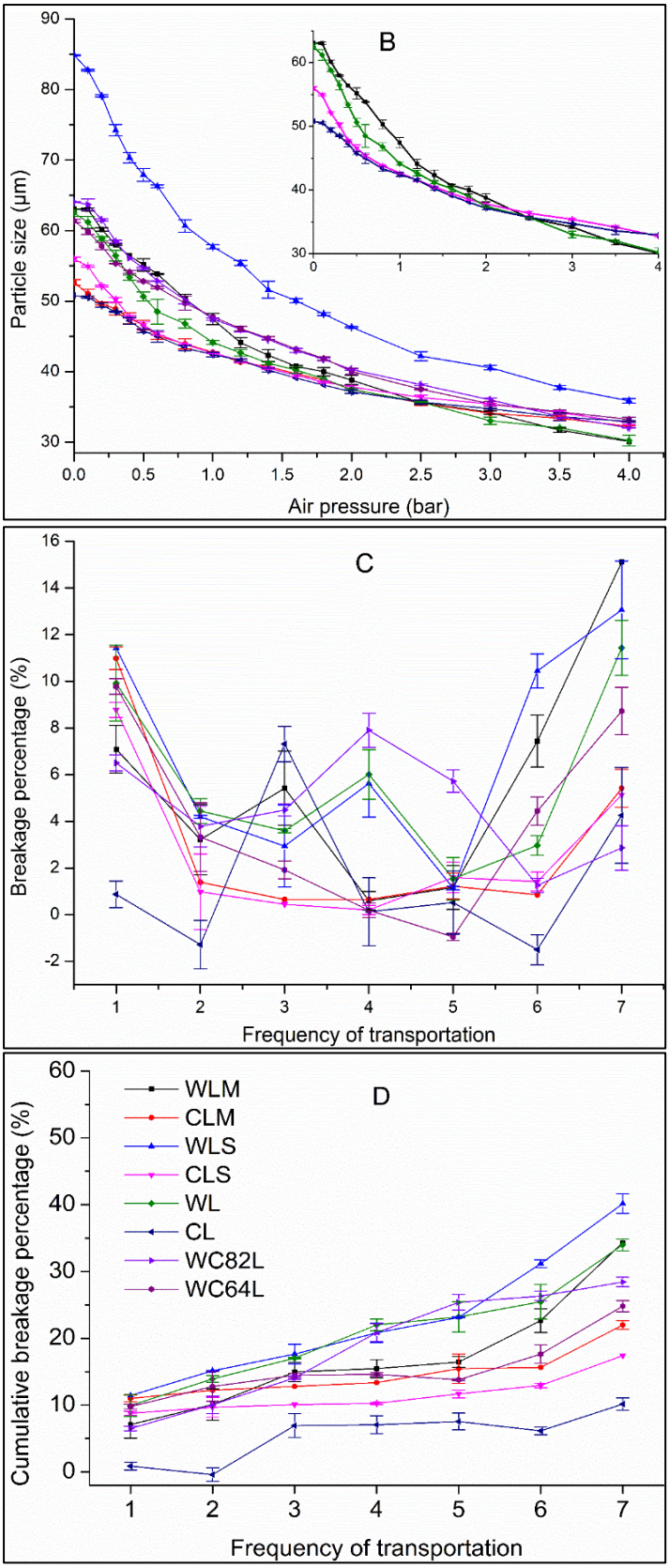


Figure 7-4. Breakage percentages (A) and particle size ($D_{3,2}$, B) of model powders during the transportation by the powder venturi feeder at different air pressures and breakage percentages after each cycle of transportation by pneumatic conveying compared with the previously cycle powders (C) or with the initial powders (D).

7.3.2.2. Breakage under repeated mechanical loads – the impact of fatigue

The influence of fatigue on model IMF was represented as the changes in $D_{3,2}$ after each cycle of pneumatic conveying compared with one cycle less transported samples (Figure 7-4C). It was shown that the changes in $D_{3,2}$ after different cycles were different. For most of the model powders, the greater breakage happened during the first and last cycles (P <0.05). There was almost no breakage during some cycles, such as the 2nd, 3rd, 4th, and 5th for CLS and CLM, the 5th and 6th for WLM and WC64L. It has been reported that from the perspective of particle size, under the same mechanical loads, the bigger the particle the greater the breakage. With increasing the cycles of transportation tests, the cumulative breakage (that was the changes in $D_{3,2}$ after each cycle of pneumatic conveying compared with initial samples) of samples gradually increased (Figure 7-4D) but the degree of breakage after each cycle did not decrease gradually. This indicates that cracks might be produced during some cycles where the particle size did not decrease a lot, which decreased the strength of particles and led to a higher degree of breakage at the next cycle. Thus, fatigue affected the breakage of model IMF and similar conclusions have also been found in some spray-dried agglomerated whey protein-lactose powders (Chapter 6). In addition, the cumulative breakage of model IMF (Figure 7-4D) was consistent with the *BP* results under different mechanical loads (Figure 7-4A). These results imply that for this model powder system, compared with carbohydrates, protein had a greater impact on the physical (7.3.1.1) and structural (7.3.1.2) properties of particles, which then influenced their breakage behaviour (7.3.2).

Normally, the particle size of dairy powders is directly proportional to the fat content within a certain range because fat can increase the viscosity of emulsions, leading to larger sprayed droplets (Felfoul et al., 2022). Also, fat could soften powders, resulting in easier plastic deformation of particles during dispersion and conveying instead of brittle fracture. Comparing one model powder (WL13: whey protein 25% and lactose 75%) in Chapter 6 and the IMF model powder WL (whey protein 15%, lactose 60%, and sunflower

oil 25%) in this chapter, the particle size and the *BP* of WL were smaller. This might be because the ratio of whey protein to lactose in these two powders and their production processes were slightly different where the emulsion of WL was homogenized before spray drying.

7.3.3. Functionality and the impact of breakage of powders with different composition

7.3.3.1. Changes in powder characteristics after breakage

In order to study the impact of breakage on powder functionality, the physical properties and morphology of broken powders were measured (Figures 7-2, 7-3, Table 7-1, and Table 7-2). From Figure 7-2, the particle size of most model powders significantly decreased (P <0.05, except CL), especially for whey protein powders. The $D_{3,2}$ of WLM decreased the most, at around 30 μm, and those of other whey protein or pure casein powders decreased around 20 μm or 10 μm, respectively. This resulted in that PC7-CLM and PC7-WLM had similar particle sizes, and the particle size of PC7-CL was bigger than that of PC7-WL. Also, the particle size of the two PC7-WCL powders was similar to those of PC7-CL instead of PC7-WL. From the SEM photos (Figure 7-3), breakage in pure casein powders was mainly of agglomerates where primary particles were separated because of the break in the connecting bridge between particles while primary particles remained intact. However, for whey protein powders, not only did the breakdown of agglomerates occur but some primary particles were also broken with many fragments produced and particle surfaces became rough after transportation. From Table 7-1, the SSA, bulk density, and particle density of PC7 powders were significantly higher than their initial powders, and the porosity of model powders significantly decreased after breakage. These results are in accordance with findings of commercial IMF, fat-filled milk powders, and whey protein concentrate (Hazlett et al., 2020; Zhang et al., 2020). Differing from previous research, the porosity of model powders significantly increased after breakage, which was because the changes in particle densities were greater than those of tapped bulk densities (data not shown).

For morphology characteristics, particle elongation increased (P <0.05) for most of the powders, and their circularity slightly decreased, which means that particles became more irregular after seven cycles of transportation. This is consistent with the results obtained with spray-dried agglomerated whey protein-lactose powders after four cycles of pneumatic conveying (Chapter 6). Furthermore, the surface composition could change after breakage because of the exposure of the interior of the particles. It has been reported that for powder particles containing fat, most of the fat stayed on particle surfaces and the fat content significantly decreased from the surface to the core, and opposite behaviours were observed for proteins and lactose (Murrieta-Pazos et al., 2012). These changes in surface, physical, and structural properties before and after breakage could influence the functionality of model IMF.

7.3.3.2. Rehydration properties

The wetting process is the first step of rehydration so the wettability of powders is important for their rehydration properties. The wetting time of initial and broken (PC7) model IMF is shown in Figure 7-5. For the initial powders, the wetting time of whey protein model IMF, less than 1.0 s, was lower than those of pure casein model IMF, at around 1.7 s. This might be explained by the difference in their physical properties where the whey protein model powders had bigger particle size and porosity than the pure casein model powders (Yuan and Lee, 2013). Also, compared with whey protein, the slow water transfer in micellar casein could be another reason for their lower wettability (Crowley et al., 2016; Schuck et al., 2007). Considering the influence of carbohydrates on powder wettability, WLM and WL had longer wetting times than WLS, which was because the particle size of WLS was much bigger than the other two powders. The wetting time of CLM and CLS, at around 1.65 s, was shorter than that of CL, 2.1 s, which was because of the smaller particle size and porosity of CL. This indicates that replacing 30% of lactose with sucrose could improve the wettability of model IMF.

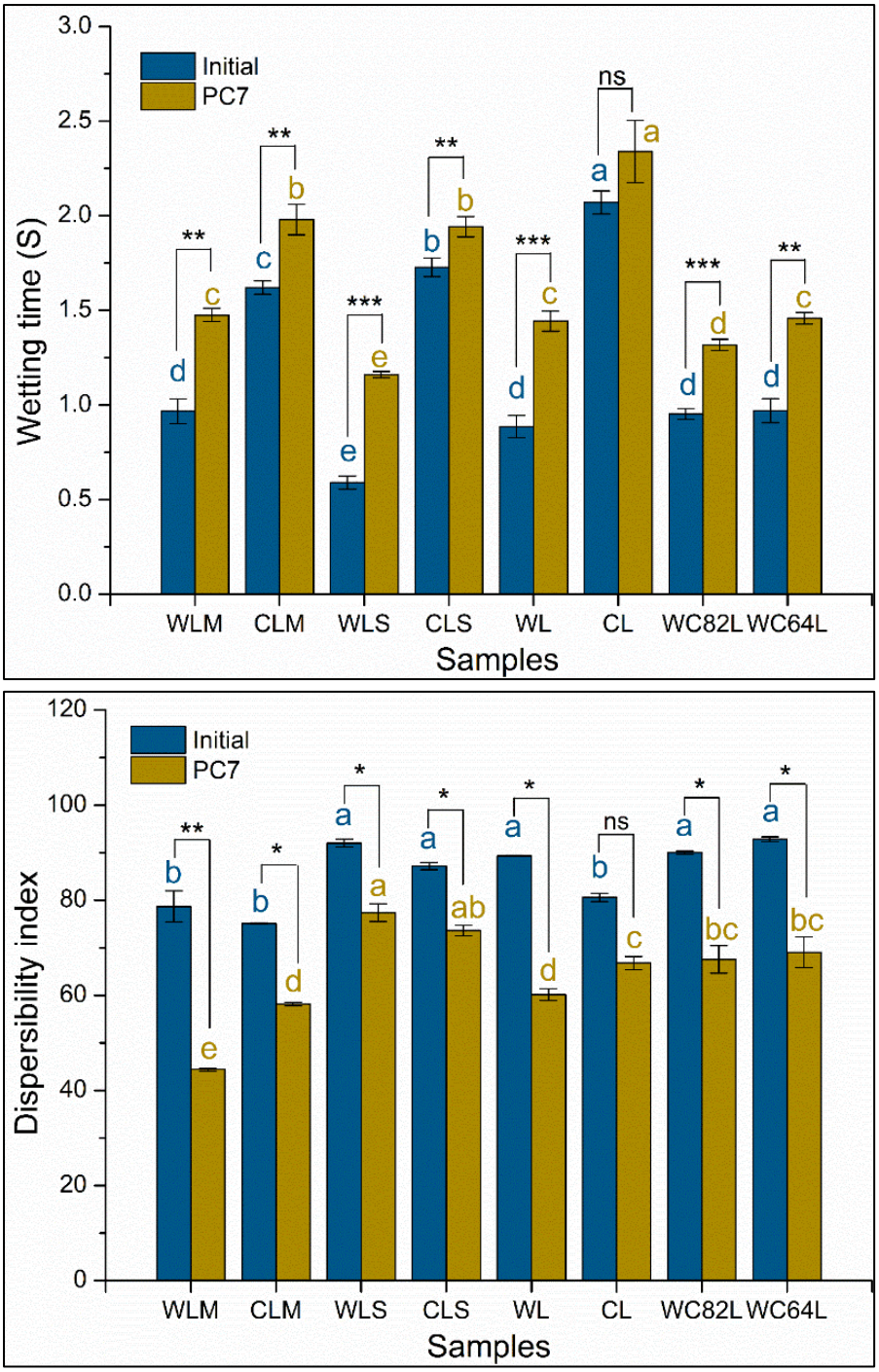


Figure 7-5. The wetting time and dispersibility index of initial and broken (PC7) model powders. PC7: seven times transportation by lab-scale pneumatic conveying.

After transportation by pneumatic conveying, the wetting time of powders significantly increased (P <0.05, except CL), especially for whey protein powders where the wetting time almost doubled for WLS and WL. This was caused by the decrease in their porosity and particle size after transportation. Lower porosity with a small capillary radius between particles could inhibit water penetration into powders and then slow down the wetting process

(Yuan and Lee, 2013). From the perspective of different carbohydrates, the wettability of sucrose powders was still better than those of maltodextrin and pure lactose powders. It should be noticed that the wettability of PC7 pure casein model powders was worse than that of PC7 whey protein powders even though some of their particle sizes were bigger. This was most likely because of the lower porosity of PC7 pure casein powders than those of PC7 whey protein powders, though it might be also due to the difference in protein contained in the powders. Thus, for this model IMF system, the influences of the type of protein and carbohydrate on powder wettability were greater than the influence of particle size.

After wetting, particles will disperse into the water, which is another important step in the rehydration process. The fragmentation of the wetted powder particles into component agglomerates, dispersion of agglomerated particles into primary particles, surface erosion of primary particles, and structural collapse of primary particles may all happen during this stage (Crowley et al., 2016). Figure 7-5 illustrates the *DI* of the initial and broken (PC7) model IMF. For the initial model IMF, the *DI* of whey protein model powders was significantly higher than those of the pure casein model samples with the same carbohydrates (P <0.05). This might be because the smaller particle size and lower porosity of pure casein powders slow down the inward diffusion of water to dissolve the bridges between the primary particles. Furthermore, compared with whey protein, casein micelles can form a network at the powder surface to prevent effective dispersion of particles, which has been reported in research on the rehydration properties of high protein milk powders (Crowley et al., 2016). Considering the influence of carbohydrates, sucrose powders had the best dispersibility, followed by pure lactose powders and maltodextrin powders (P <0.05). This indicates that replacing 30% of lactose with maltodextrin could decrease the dispersibility of IMF while sucrose could improve the dispersibility.

After transportation by pneumatic conveying, the dispersibility of powders significantly decreased (P <0.05), especially for whey protein powders, resulting in the higher *DI* of PC7-CLM and PC7-CL than those of PC7-WLM

and PC7-WL, respectively. This might be because the particle size of pure casein powders decreased less than whey protein powders. In terms of different carbohydrates, dispersibility results were similar to initial powders. This indicates that for this model IMF system, the influences of particle size or breakage on the dispersibility of powders were greater than the influence of the type of protein and carbohydrate.

7.3.3.3. Water adsorption, glass transition, and lactose crystallization

The water adsorption behaviour of the initial and broken (PC7) model IMF at several a_w (0.11-0.66) was investigated and some of them (0.44-0.66) were plotted as a function of time (Figure 7-6). The final water contents of powders equilibrated at different a_w are shown in Table 7-3.

For initial powders that contained the same carbohydrates, the final water contents of pure casein model samples were slightly higher than those of whey protein samples (P <0.05) but their water adsorption rates were similar (0.11-0.44). When the $a_w \geq 0.44$, the time-dependent crystallization of pure casein IMF happened earlier than whey protein model powders and the final water contents of casein powders were lower than those of whey protein powders (Figure 7-6). For example, at 0.54 a_w, the loss of sorbed water in CL and WL appeared after 12 and 24 h of storage with the final water contents around 3.6% and 6.2%, respectively. Considering the influence of carbohydrates, the time-dependent crystallization occurred earlier for pure lactose powders, followed by the sucrose and maltodextrin powders. The loss of sorbed water in CL, CLS, and CLM appeared after 12, 24, and 192 h of storage at 0.54 a_w, respectively, as seen in the results. This means that replacing 30% of lactose with sucrose or maltodextrin could delay the time-dependent crystallization of powders. According to previous studies, interactions between maltodextrin and lactose could reduce the rate of mobility or diffusion of lactose molecules, resulting in the delay of forming crystals and nucleation or crystal growth (Potes et al., 2012).

After transportation by pneumatic conveying, the water adsorption behaviour of powders at low a_w (0.11-0.44) was not influenced. Breakage

accelerated the time-dependent crystallization of whey protein model powders when $a_w \geq 0.44$. For example, at 0.54 a_w, the loss of sorbed water in WLS and PC7-WLS appeared after 168 and 24 h of storage, respectively. This might be because the breakage of whey protein powders was greater than pure casein powders after the transportation.

The T_g and T_{ic} of the initial and broken model IMF over the a_w range of 0 to 0.44 are shown in Table 7-4. For the initial model IMF, the T_g of powders with different carbohydrates were significantly different (P <0.05). For example, at 0.11 a_w, the T_g of maltodextrin powders, pure lactose powders, and sucrose powders were around 76, 71, and 64℃, respectively. This indicates that replacing 30% of lactose with maltodextrin would increase the T_g of powders while replacement with sucrose would cause the opposite, which is consistent with previous studies (Li et al., 2017). In terms of different proteins but the same carbohydrate, the T_g of whey protein powders were significantly higher than those of pure casein powders at the a_w range of 0.11 to 0.44 (P <0.05) and their T_g was similar at 0 a_w. This might be because pure casein powders adsorbed more water than whey protein powders. These results also indicate that the influences of carbohydrates were greater than proteins on the glass transition of powders. For the T_{ic} of initial powders that contained the same protein, maltodextrin and sucrose increased the T_{ic} compared to lactose. In terms of different proteins but the same carbohydrate, the T_{ic} of whey protein powders was higher than those of casein powders. These findings are in agreement with the time-dependent crystallization results.

After transportation by pneumatic conveying, the T_g of some powders slightly changed (P >0.05) but the T_{ic} significantly decreased (P <0.05) for all samples at the a_w range of 0.11 to 0.33 and whey protein powders at 0.44 a_w even though breakage did not significantly influence the final water contents (Figure 7-6). This is in accordance with the study on the breakage of spray-dried agglomerated whey protein-lactose powders after pneumatic conveying (Chapter 6).

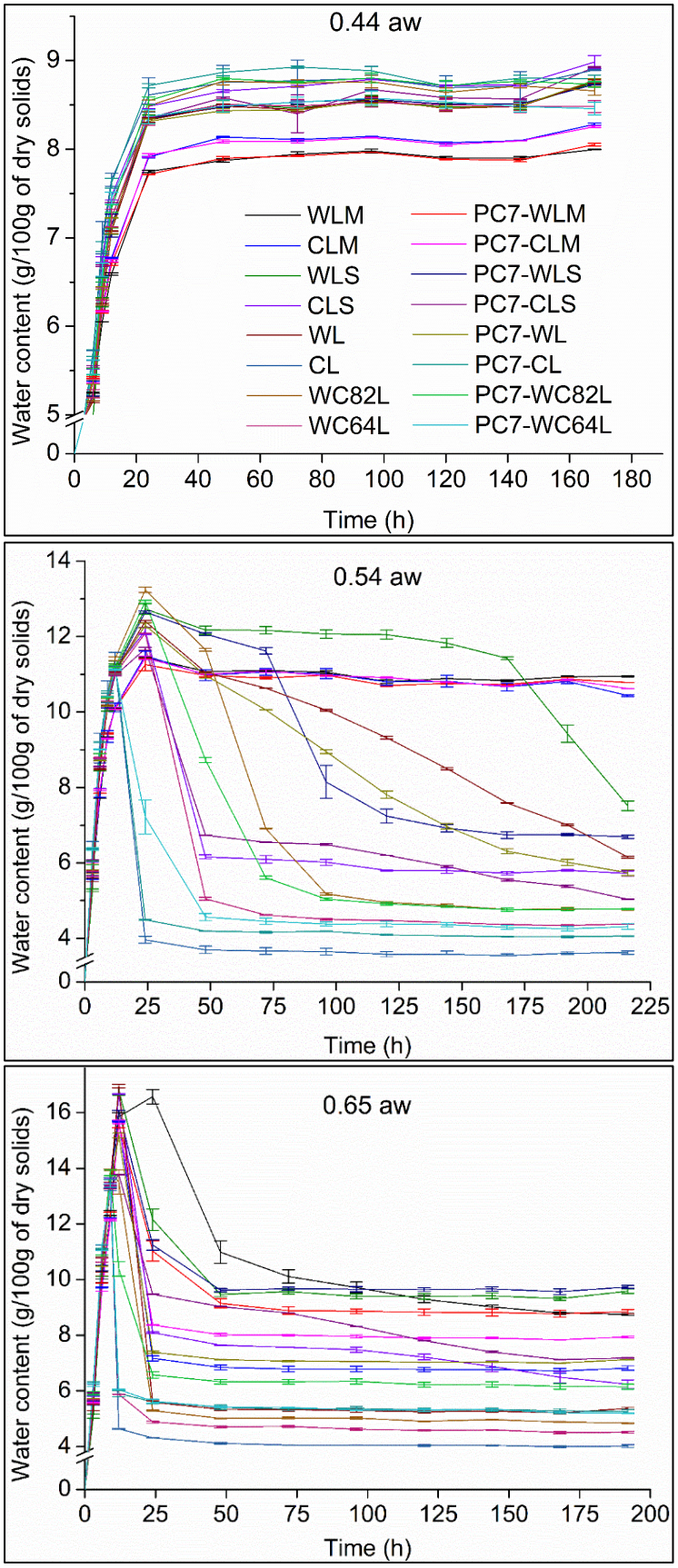


Figure 7-6. Water sorption behaviour of initial and broken (PC7) model powders equilibrated at various water activities (0.44 to 0.65) for at least 168 h at 25°C. PC7: seven times transportation by lab-scale pneumatic conveying.

Table 7-3. Water contents of samples equilibrated for 168 h at various water activities (0 to 0.76) at 25°C.

Samples	0.11		0.23		0.33		0.44	
	Initial	PC7	Initial	PC7	Initial	PC7	Initial	PC7
WLM	$2.80^{bc}\pm0.07^{A}$	$2.83^{bc}\pm0.02^{A}$	$4.63^{bc}\pm0.03^{A}$	$4.68^{b}\pm0.02^{A}$	$5.95^{c}\pm0.01^{A}$	$5.98^{d}\pm0.10^{A}$	$8.00^{f}\pm0.01^{A}$	$8.05^{e}\pm0.01^{A}$
CLM	$2.96^{a}\pm0.08^{A}$	$2.91^{a}\pm0.01^{A}$	$4.82^{ab}\pm0.02^{A}$	$4.75^{ab}\pm0.03^{A}$	$6.15^{b}\pm0.01^{A}$	$6.15^{bc}\pm0.03^{A}$	$8.28^{e}\pm0.01^{A}$	$8.25^{d}\pm0.01^{B}$
WLS	$2.52^{d}\pm0.04^{A}$	$2.53^{f}\pm0.02^{A}$	$4.43^{c}\pm0.07^{A}$	$4.48^{c}\pm0.01^{A}$	$5.88^{c}\pm0.08^{A}$	$5.99^{d}\pm0.05^{A}$	$8.75^{bc}\pm0.05^{A}$	$8.73^{b}\pm0.01^{A}$
CLS	$2.69^{c}\pm0.03^{A}$	$2.76^{de}\pm0.01^{A}$	$4.74^{ab}\pm0.02^{A}$	$4.76^{ab}\pm0.04^{A}$	$6.26^{b}\pm0.02^{A}$	$6.20^{ab}\pm0.01^{A}$	$8.98^{a}\pm0.07^{A}$	$8.93^{a}\pm0.01^{A}$
WL	$2.70^{c}\pm0.01^{A}$	$2.76^{de}\pm0.03^{A}$	$4.61^{bc}\pm0.01^{A}$	$4.65^{bc}\pm0.01^{A}$	$6.17^{b}\pm0.02^{A}$	$6.19^{ab}\pm0.01^{A}$	$8.76^{bc}\pm0.02^{A}$	$8.78^{b}\pm0.02^{A}$
CL	$2.88^{ab}\pm0.01^{A}$	$2.86^{ab}\pm0.02^{A}$	$4.89^{a}\pm0.04^{A}$	$4.88^{a}\pm0.01^{A}$	$6.48^{a}\pm0.08^{A}$	$6.34^{a}\pm0.05^{A}$	$8.89^{ab}\pm0.01^{A}$	$8.80^{b}\pm0.04^{A}$
WC82L	$2.67^{c}\pm0.02^{A}$	$2.71^{e}\pm0.01^{A}$	$4.76^{ab}\pm0.05^{A}$	$4.74^{ab}\pm0.01^{A}$	$6.23^{b}\pm0.03^{A}$	$6.16^{b}\pm0.01^{A}$	$8.66^{c}\pm0.05^{A}$	$8.73^{b}\pm0.03^{A}$
WC64L	$2.69^{c}\pm0.01^{A}$	$2.78^{cd}\pm0.03^{A}$	$4.66^{b}\pm0.05^{A}$	$4.81^{ab}\pm0.04^{A}$	$5.95^{c}\pm0.05^{A}$	$6.01^{cd}\pm0.02^{A}$	$8.48^{d}\pm0.07^{A}$	$8.46^{c}\pm0.07^{A}$

1. WLM (sunflower oil; WPI; lactose to maltodextrin ratio 70:30); CLM (sunflower oil; MC; lactose to maltodextrin ratio 70:30); WLS (sunflower oil; WPI; lactose to sucrose ratio 70:30); CLS (sunflower oil; MC; lactose to sucrose ratio 70:30); WL (sunflower oil; WPI; lactose); CL (sunflower oil; MC; lactose); WC82L (sunflower oil; WPI to MC ratio 80:20; lactose); WC64L (sunflower oil; WPI to MC ratio 60:40; lactose); with a target protein: fat: carbohydrate ration of 15:26:59 (w/w). PC7: seven times transportation by lab-scale pneumatic conveying.
2. Values are mean ± standard deviation (n=2). $^{a\text{-}f}$ different values within columns are significantly different at P <0.05. $^{A\text{-}B}$ different values within properties of each powder (initial and PC7) are significantly different at P <0.05.

Table 7-4. Glass transition temperature (T_g) and initial crystallization temperature (T_{ic}) of powders stored for 168 h at various water activities (0 to 0.44) at 25°C.

Samples		0		0.11		0.23		0.33		0.44	
		Initial	PC7	Initial	PC7	Initial	PC7	Initial	PC7	Initial	PC7
T_g	WLM	$130.4^{a}\pm2.9^{A}$	$132.7^{a}\pm0.1^{A}$	$78.0^{a}\pm0.1^{A}$	$75.8^{a}\pm2.0^{A}$	$62.4^{a}\pm0.6^{A}$	$61.5^{a}\pm0.4^{A}$	$47.0^{a}\pm0.8^{A}$	$46.6^{a}\pm0.1^{A}$	$33.4^{a}\pm0.8^{A}$	$33.2^{a}\pm1.9^{A}$
	CLM	$123.9^{b}\pm0.2^{A}$	$124.2^{b}\pm0.1^{A}$	$74.7^{b}\pm0.6^{A}$	$75.1^{a}\pm0.2^{A}$	$59.5^{b}\pm1.1^{A}$	$58.7^{b}\pm0.4^{A}$	$44.0^{b}\pm0.3^{A}$	$44.2^{b}\pm0.9^{A}$	$29.4^{b}\pm0.2^{A}$	$29.4^{ab}\pm0.1^{A}$
	WLS	$104.7^{d}\pm0.6^{A}$	$104.7^{f}\pm0.5^{A}$	$64.9^{e}\pm0.1^{A}$	$64.0^{c}\pm0.3^{A}$	$49.6^{e}\pm0.9^{A}$	$49.1^{f}\pm0.4^{A}$	$34.7^{e}\pm0.8^{A}$	$34.6^{e}\pm0.5^{A}$	$18.0^{d}\pm0.5^{A}$	$17.1^{d}\pm0.6^{A}$
	CLS	$101.7^{d}\pm0.3^{A}$	$102.1^{g}\pm0.1^{A}$	$62.9^{e}\pm0.3^{A}$	$62.0^{c}\pm0.2^{A}$	$46.7^{f}\pm0.1^{A}$	$46.4^{g}\pm0.3^{A}$	$31.4^{f}\pm0.2^{A}$	$30.9^{f}\pm0.9^{A}$	$15.5^{d}\pm1.4^{A}$	$15.1^{d}\pm0.5^{A}$
	WL	$119.4^{c}\pm0.2^{A}$	$119.3^{c}\pm0.3^{A}$	$73.7^{bc}\pm0.2^{A}$	$72.3^{b}\pm0.4^{A}$	$57.4^{c}\pm0.2^{A}$	$56.8^{c}\pm0.1^{A}$	$42.2^{c}\pm0.3^{A}$	$42.2^{bc}\pm0.1^{A}$	$24.9^{c}\pm0.7^{A}$	$27.2^{bc}\pm2.7^{A}$
	CL	$115.8^{c}\pm0.2^{A}$	$116.3^{e}\pm0.1^{A}$	$69.9^{d}\pm0.3^{A}$	$69.6^{b}\pm0.6^{A}$	$53.7^{d}\pm0.5^{A}$	$53.4^{e}\pm0.2^{A}$	$38.1^{d}\pm0.6^{A}$	$39.9^{d}\pm0.8^{A}$	$23.1^{c}\pm0.2^{A}$	$24.2^{c}\pm0.4^{A}$
	WC82L	$119.1^{c}\pm0.1^{A}$	$118.3^{cd}\pm0.2^{A}$	$69.8^{d}\pm1.0^{A}$	$71.1^{b}\pm0.1^{A}$	$56.6^{c}\pm0.5^{A}$	$56.2^{c}\pm0.1^{A}$	$41.9^{c}\pm0.2^{A}$	$41.5^{cd}\pm0.8^{A}$	$25.6^{c}\pm0.6^{A}$	$26.3^{bc}\pm1.6^{A}$
	WC64L	$117.3^{c}\pm0.2^{A}$	$117.5^{d}\pm0.3^{A}$	$71.5^{cd}\pm0.1^{A}$	$71.6^{b}\pm0.3^{A}$	$55.9^{c}\pm0.1^{A}$	$54.4^{d}\pm0.2^{A}$	$40.6^{c}\pm0.5^{A}$	$41.0^{cd}\pm0.5^{A}$	$24.4^{c}\pm0.9^{A}$	$23.6^{c}\pm0.4^{A}$
T_{ic}	WLM	-	-	-	-	-	-	-	$132.5^{a}\pm0.5$	-	$112.3^{a}\pm0.6$
	CLM	-	-	-	-	-	$139.8^{a}\pm0.1$	$129.6^{a}\pm0.4^{A}$	$119.4^{b}\pm0.8^{B}$	$99.3^{b}\pm0.2^{A}$	$98.8^{b}\pm0.1^{A}$
	WLS	-	-	-	-	-	$132.2^{b}\pm0.1$	-	$113.1^{c}\pm0.1$	$101.9^{d}\pm0.4^{A}$	$91.4^{c}\pm0.1^{B}$
	CLS	-	-	-	$146.0^{a}\pm0.7$	-	$123.5^{c}\pm0.1$	$115.4^{b}\pm0.2^{A}$	$104.3^{d}\pm0.5^{B}$	$74.6^{d}\pm0.4^{A}$	$74.8^{e}\pm0.9^{A}$
	WL	-	-	$149.7^{a}\pm0.2^{A}$	$136.6^{b}\pm0.4^{B}$	$134.2^{a}\pm0.2^{A}$	$120.8^{d}\pm0.2^{B}$	$115.4^{b}\pm0.7^{A}$	$103.4^{d}\pm0.4^{B}$	$85.8^{c}\pm0.7^{A}$	$82.8^{d}\pm0.2^{A}$
	CL	-	-	$130.4^{c}\pm0.3^{A}$	$120.7^{e}\pm0.2^{B}$	$111.6^{d}\pm0.3^{A}$	$102.2^{g}\pm0.3^{B}$	$94.2^{e}\pm0.9^{A}$	$88.1^{f}\pm0.2^{B}$	$70.5^{c}\pm0.3^{A}$	$70.4^{f}\pm0.1^{A}$
	WC82L	-	-	$143.8^{b}\pm0.4^{A}$	$132.0^{c}\pm0.2^{B}$	$130.2^{b}\pm0.3^{A}$	$115.4^{e}\pm0.1^{B}$	$111.1^{c}\pm0.2^{A}$	$98.8^{e}\pm0.1^{B}$	$83.2^{c}\pm0.2^{A}$	80.1^{dB}
	WC64L	-	-	$130.4^{c}\pm0.3^{A}$	$123.2^{d}\pm0.1^{B}$	$113.6^{c}\pm0.3^{A}$	$104.1^{f}\pm0.1^{B}$	$96.9^{d}\pm0.2^{A}$	$89.4^{f}\pm0.1^{B}$	$76.5^{c}\pm0.8^{A}$	$70.8^{f}\pm0.1^{A}$

1. WLM (sunflower oil; WPI; lactose to maltodextrin ratio 70:30); CLM (sunflower oil; MC; lactose to maltodextrin ratio 70:30); WLS (sunflower oil; WPI; lactose to sucrose ratio 70:30); CLS (sunflower oil; MC; lactose to sucrose ratio 70:30); WL (sunflower oil; WPI; lactose); CL (sunflower oil; MC; lactose); WC82L (sunflower oil; WPI to MC ratio 80:20; lactose); WC64L (sunflower oil; WPI to MC ratio 60:40; lactose); with a target protein: fat: carbohydrate ration of 15:26:59 (w/w). PC7: seven times transportation by lab-scale pneumatic conveying. - Not observed.
2. Values are mean ± standard deviation (n=2). $^{a-f}$ different values within columns are significantly different at P <0.05. $^{A-B}$ different values within properties of each powder (initial and PC7) are significantly different at P <0.05.

7.4. Conclusion

The physical and structural properties of the initial model IMF were different due to the difference in ingredients and the influence of proteins on these properties was greater than that of carbohydrates. From the perspective of different proteins, pure whey protein powders were bigger in particle size and had more bigger-sized internal holes and marginally higher irregularity of particle shapes than casein powders. Meanwhile, replacing less than 40% whey protein with casein micelles had little effect on powder properties. Considering the influence of carbohydrates, the particle size and particle density of sucrose powders were bigger than those of maltodextrin and pure lactose powders but their structural properties were similar. The difference in composition, physical and structural properties resulted in their different functionality. Whey protein and sucrose samples had better rehydration properties than casein and pure lactose or maltodextrin powders, respectively. The final water contents of casein samples were higher than those of whey protein samples, which resulted in the lower T_g, T_{ic}, and the earlier the time-dependent crystallization in casein samples. Sucrose and maltodextrin decreased final water contents of powders and then increased the T_g and T_{ic}, and delayed the time-dependent crystallization.

The composition of model IMF influenced breakage by influencing the particle size and structure of the agglomerates formed during the same drying conditions and the influence of proteins was greater than that of carbohydrates. Whey protein powders were bigger in particle size, weaker in structural strength, and marginally more irregular in shape, which resulted in more breakage in comparison to pure casein powders. Similarly, sucrose samples suffered more breakage than maltodextrin and pure lactose powders, which was mainly because of their bigger particle size. In addition, the material strength of different proteins or carbohydrates may be different, which could be another reason that they had different breakage behaviour. Meanwhile, fatigue affected the breakage of model powders, especially for big-sized samples. Breakage changed the morphology of particles, decreasing the particle size and increasing the SSA and particle density of

powders, especially for whey protein or sucrose samples. This resulted in the deterioration of rehydration properties and the decrease in T_{ic}.

From the perspective of particle breakage, unwanted dairy powder breakage can be controlled by changing the formulation of powders. This can be applied to improve particle structural strength, which is a way to decrease particle breakage. Also, increasing the initial particle size may be an alternative way to compensate for any particle breakage during the handling of dairy powders when the imposed stress is sufficiently low whereby the resultant particle size after breakage is still of acceptable size. On the other hand, smaller initial particle sizes may be more beneficial because they are inherently more resistant to particle breakage, especially at higher imposed stresses. Finally, it may not be feasible to alter the formulation of some products like IMF. Consequently, further study on the effect of spray drying parameters or other processes on milk powder breakage will be useful in trying to control powder particle breakage.

Reference

Antonyuk, S., Tomas, J., Heinrich, S., & Mörl, L. (2005). Breakage behaviour of spherical granulates by compression. Chemical Engineering Science 60(14), 4031-4044. https://doi.org/10.1016/j.ces.2005.02.038.

Crowley, S.V., Kelly, A.L., Schuck, P., Jeantet, R., & O'Mahony, J.A. (2016). Rehydration and Solubility Characteristics of High-Protein Dairy Powders. In P.L.H. McSweeney, J.A. O'Mahony (Eds.), Advanced Dairy Chemistry: Volume 1B: Proteins: Applied Aspects (pp. 99-131). Springer New York, New York, NY. https://doi.org/ 10.1007/978-1-4939-2800-2_4.

Deng, X., & Davé, R.N. (2017). Breakage of fractal agglomerates. Chemical Engineering Science 161, 117-126. https://doi.org/10.1016/j.ces.2016.12.018.

European Commission. (2006). Commission directive 2006/141/EC of 22 December 2006 on infant formulae and follow-on formulae and amending Directive 1999/21. EC.

Felfoul, I., Burgain, J., Perroud, C., Gaiani, C., Scher, J., Attia, H., & Petit, J. (2022). Impact of spray-drying conditions on physicochemical properties and rehydration ability of skim dromedary and cow's milk powders. Drying Technology, 40(3), 665-677. https://doi.org/10.1080/07373937.2020.1828448.

Fang, Z., & Bhandari, B. (2012). Comparing the efficiency of protein and maltodextrin on spray drying of bayberry juice. Food Research International 48(2), 478-483. https://doi.org/10.1016/j.foodres.2012.05.025.

Golchert, D., Moreno, R., Ghadiri, M., & Litster, J. (2004). Effect of granule morphology on breakage behaviour during compression. Powder Technology 143-144, 84-96. https://doi.org/10.1016/j.powtec.2004.04.032.

Han, J., Fitzpatrick, J., Cronin, K., Maidannyk, V., & Miao, S. (2021a). Particle size, powder properties and the breakage behaviour of infant milk formula. Journal of Food Engineering 292, 110367. https://doi.org/10.1016/j.jfoodeng.2020.110367.
Han, J., Fitzpatrick, J., Cronin, K., & Miao, S. (2021b). Dairy powder breakage: Mechanisms, characterization methods, impacted properties and influencing factors. Trends in Food Science & Technology 114, 608-624. https://doi.org/10.1016/j.tifs.2021.05.043.
Han, J., Fitzpatrick, J., Cronin, K., & Miao, S. (2021c). Investigation of the influence of powder characteristics on the breakage of dairy powders. Food Research International, 110775. https://doi.org/10.1016/j.foodres.2021.110775.
Hanley, K.J., 2011. Experimental quantification and modelling of attrition of infant formulae. PhD Thesis, Department of Process and Chemical Engineering. University College Cork, Ireland.
Hazlett, R., Schmidmeier, C., & O'Mahony, J.A. (2020). Influence of mechanical integrity during pneumatic conveying on the bulk handling and rehydration properties of agglomerated dairy powders. Journal of Food Engineering, 110103. https://doi.org/10.1016/j.jfoodeng.2020.110103.
Kotzur, B.A., Berry, R.J., Zigan, S., García-Triñanes, P., & Bradley, M.S.A. (2018). Particle attrition mechanisms, their characterisation, and application to horizontal lean phase pneumatic conveying systems: A review. Powder Technology 334, 76-105. https://doi.org/10.1016/j.powtec.2018.04.047.
Li, R., Roos, Y.H., & Miao, S. (2016). Roles of particle size on physical and mechanical properties of dairy model solids. Journal of Food Engineering 173, 69-75. https://doi.org/10.1016/j.jfoodeng.2015.10.041.
Li, R., Roos, Y.H., & Miao, S. (2017). Characterization of mechanical and encapsulation properties of lactose/maltodextrin/WPI matrix. Food Hydrocolloids 63, 149-159. https://doi.org/10.1016/j.foodhyd.2016.08.033.
Lu, X., Liu, C., Zhu, L., & Qu, X. (2014). Influence of process parameters on the characteristics of TiAl alloyed powders by fluidized bed jet milling. Powder Technology 254, 235-240. https://doi.org/10.1016/j.powtec.2013.11.013.
Masum, A. K. M., Chandrapala, J., Huppertz, T., Adhikari, B., & Zisu, B. (2021). Production and characterization of infant milk formula powders: A review. Drying Technology, 39(11), 1492-1512. https://doi.org/10.1080/07373937.2020.1767645.
Masum, A.K.M., Huppertz, T., Chandrapala, J., Adhikari, B., & Zisu, B. (2020). Physicochemical properties of spray-dried model infant milk formula powders: Influence of whey protein-to-casein ratio. International Dairy Journal 100, 104565. https://doi.org/10.1016/j.idairyj.2019.104565.
McCarthy, N.A., Gee, V.L., Hickey, D.K., Kelly, A.L., O'Mahony, J.A., & Fenelon, M.A. (2013). Effect of protein content on the physical stability and microstructure of a model infant formula. International Dairy Journal 29(1), 53-59. https://doi.org/10.1016/j.idairyj.2012.10.004.
Murphy, E.G., Roos, Y.H., Hogan, S.A., Maher, P.G., Flynn, C.G., & Fenelon, M.A. (2015). Physical stability of infant milk formula made with selectively hydrolysed whey proteins. International Dairy Journal 40, 39-46. https://doi.org/10.1016/j.idairyj.2014.08.012.
Murrieta-Pazos, I., Gaiani, C., Galet, L., & Scher, J. (2012). Composition gradient from surface to core in dairy powders: Agglomeration effect. Food Hydrocolloids 26(1), 149-158. https://doi.org/10.1016/j.foodhyd.2011.05.003.
Niro, G. (2006). GEA Niro analytical methods dry products. GEA Process Engineering A/S, Gladsaxevej, Denmark,.
Norazirah, A., Fuad, S.H.S., & Hazizan, M.H.M. (2016). The effect of size and shape on breakage characteristic of mineral. Procedia Chemistry 19, 702-708. https://doi.org/10.1016/j.proche.2016.03.073.

Petukhov, Y., & Kalman, H. (2004). Empirical breakage ratio of particles due to impact. Powder Technology 143-144, 160-169. https://doi.org/10.1016/j.powtec.2004.04.009.

Potes, N., Kerry, J.P., & Roos, Y.H. (2012). Additivity of water sorption, alpha-relaxations and crystallization inhibition in lactose–maltodextrin systems. Carbohydrate Polymers 89(4), 1050-1059. https://doi.org/10.1016/j.carbpol.2012.03.061.

Schuck, P., Mejean, S., Dolivet, A., Gaiani, C., Banon, S., Scher, J., & Jeantet, R. (2007). Water transfer during rehydration of micellar casein powders. Lait 87(4-5), 425-432.

Yuan, Y., & Lee, T.R. (2013). Contact angle and wetting properties. Surface science techniques (pp. 3-34). Springer.

Zhang, Olaleye, A.K., O'Mahony, J.A., Miao, S., & Cronin, K. (2020). Dilute phase pneumatic conveying of whey protein isolate powders: Particle breakage and its effects on bulk properties. Advanced Powder Technology 31(8), 3342-3350. https://doi.org/10.1016/j.apt.2020.06.019.

Zouari, A., Perrone, Í. T., Schuck, P., Gaucheron, F., Dolivet, A., Attia, H., & Ayadi, M. A. (2019). Effect of outlet drying temperature and milk fat content on the physicochemical characteristics of spray-dried camel milk powder. Drying Technology, 37(13), 1615-1624. https://doi.org/10.1080/07373937.2018.1526189.

CHAPTER EIGHT

General Discussion and Conclusions

8.1. Overview and summary

The present study investigated the breakage mechanisms and breakage behaviour of agglomerated dairy powders during the venturi feeder, lab-scale pneumatic conveying and high-speed mixing (**Chapter 2**), determined the influence of dairy powder breakage on powder physical properties, structure, and functionalities (**Chapter 3, 4**), and explored the impact of dairy powder characteristics on breakage, including the physical properties (**Chapter 5**) and powder formulations (**Chapter 6, 7**).

8.1.1. Dairy powder breakage mechanisms

Based on particle breakage research in other industries, of the various particulate materials, four breakage mechanisms have been reported to govern the breakage behaviour of particles and they can be classified into surface breakage (abrasion and chipping) and body breakage (disintegration and splitting) (Aarseth, 2004; Francioli, 2015; King, 2012, Kotzur et al., 2018; Little et al., 2016; van Laarhoven et al., 2012; Zhang and Ghadiri, 2002). The changes in particle size distribution (PSD) before and after breakage can indicate the breakage mechanisms and has been used and confirmed in some areas (Agrawal et al., 2011; Bonakdar et al., 2016; Materic et al., 2014; Ortega-Rivas et al., 2006; Scala et al., 2007; Wu and Wu, 2017; Zhao et al., 1999). However, there was no research on dairy powder breakage mechanisms.

Based on the changes in volume- and number-PSD, the breakage mechanisms and behaviour of agglomerated infant milk formula (IMF) during three different processing methods which were selected to mimic the variety of processing conditions that powder experiences at the industrial scale were investigated in **Chapter 2**. It was the first study on particle breakage mechanisms of food powders. Differing from the previous research on other particulate materials, surface abrasion was not observed in agglomerated dairy powders. It might happen during the agglomeration, handling from spray drying through to packing, and sample preparing process – sieving, because some small defects on initial particle surfaces were found. Similar to

previous research, chipping, disintegration and splitting were observed, corresponding to typical PSD movements and the increasing degree of breakage (**Figure 2-8**). Defects became bigger when chipping occurred while the main particle body was not damaged. The body was partly broken when disintegration happened and left a big fracture, and was completely crushed by splitting. Because of the cohesiveness of dairy powders, the dispersion of clusters that were particles held together by cohesive attractions might happen when particles suffered low-level mechanical loads. These four breakage mechanisms (dispersion, chipping, disintegration and splitting) reported in **Chapter 2** were also observed in **Chapter 3** for the other two commercial IMF samples. The breakage mechanism was determined by powder particle properties and the processing conditions that provided the mechanical load imposed on particles. The influence of powder particle properties will be discussed in 8.1.3. For the processing conditions, the more intense the processing conditions, the higher the breakage degree. In general, these four breakage mechanisms were present for powders in the three processing units used in this study (powder venturi feeder, lab-scale pneumatic conveying pipe, laboratory high-speed mixer) and as the intensity of processing increased, body breakage became more dominant.

The breakage mechanisms of crystallized lactose might be different from most of the agglomerated dairy powders **(Chapter 5)**. When crystalline particles subject to low-level external mechanical stress, the main mechanism of breakage is surface breakage, leading to the production of minuscule particles whilst still retaining the identity of the original particles. When a particle is composed of two or more crystals, cleavage may occur at the interface, and child particles are relatively undamaged (Cleaver et al., 1993; Ghadiri et al., 1991).

8.1.2. The influence of dairy powder breakage on powder properties

8.1.2.1. Powder physical properties

(1) Particle size and PSD

Particle breakage caused the decrease of particle size ($D_{3,2}$) and the changes in $D_{3,2}$ (breakage percentage, *BP*) was from 0 up to 80% depending on dairy powders and processing conditions (**Chapter 2-7**). The *BP* of most dairy powders was increased logarithmically with increasing processing conditions, while the *BP* of crystallized lactose increased steadily then sharply when the processing conditions reached a particular threshold. This is because of their different breakage mechanisms. The decrease in particle size was due to the generation of a large amount of small-sized child particles and the disappearance of big-sized mother particles. This was shown as the movement of the PSD to the smaller size (**Chapter 2, 3**).

(2) Powder density and porosity

The bulk density increased and the porosity correspondingly decreased after breakage (**Chapter 2-7**), which was consistent with previous research (Boiarkina et al., 2016; Hanley, 2011). In addition, there were a lot of pores inside dairy powder particles and after breakage, some internal stomata were exposed, which led to the increase of the particle density (**Chapter 2-7**). For example, the particle density of IMF increased around 30% after high-speed mixing for 6 mins (**Table 3-1**). Thus, breakage did not only break solid bridges within agglomerated particles resulting in the decrease of particle size and increase of bulk density but also broke primary particles leading to the increase of the particle density.

(3) Powder surface properties

Because of the generation of more particles after breakage, the specific surface area (SSA) of powders increased with the decreasing particle size (**Chapter 2-7**). The fat content significantly decreased from the surface to the core, and opposite behaviours were observed for proteins and lactose (Murrieta-Pazos et al., 2012b). Due to this uneven distribution of composition throughout dairy powder particles, the surface composition of particles was changed after breakage (**Chapter 3, 6**) as seen by an increase in lactose content and a slight decrease in protein and fat contents for most samples.

Nevertheless, the net extraction of the surface free fat content (SFF) of IMF increased after breakage because of the increase in SSA (**Chapter 4, 5**).

(4) Powder structure and morphology

From the SEM photos (**Chapter 2, 4, 6, 7**) and the morphology data (**Chapter 3, 6, 7**), breakage changed the structure of particles. When the breakage degree was low (surface breakage), some small defects on initial particle surfaces were generated and breakage was mainly of agglomerates where primary particles were separated because of the break in the connecting bridge between particles while primary particles remained intact. When the breakage degree was high (body breakage), not only did the breakdown of agglomerates occur but some primary particles were also broken with many fragments produced and particle surfaces became rough. For IMF samples, surface breakage did not significantly change particle morphology but body breakage particles had more rounded shapes after the high-speed mixing as shown by the higher circularity and convexity compared with their initial powders (**Chapter 3**). For plant pilot-scale IMF or whey protein/lactose model powders, their particles became more irregular after a number of passes through pneumatic conveying, as shown by the increase in elongation and slightly decrease in circularity (**Chapter 6, 7**).

8.1.2.2. Powder functionalities

The changes in physical properties deteriorated powder functionalities, especially for the water adsorption behaviour, crystallisation, and rehydration properties.

(1) Water adsorption

For commercial IMF (**Chapter 3**), surface breakage had no influence on the water sorption of powders but body breakage significantly influenced it. The number of adsorbed monolayers, sorption surface area and monolayer value of body breakage samples were significantly higher after high-speed mixing. This increased the water sorption rates and final water contents of powders and accelerated the time-dependent crystallization. The large SSA

and small particle size of body breakage samples might be reasons that they sorbed larger amounts of water. Water is mainly absorbed on the surface of particles, thus the larger SSA means more area for sorption of water molecules (Li et al., 2016; McCarthy et al., 2013). Besides, hydrophilic groups bind moisture molecules by forming hydrogen bonds, thus it is also possible that the internal hydrophilic groups were exposed after body breakage, and samples had higher amounts of hydrogen bonding sites for sorption of moisture molecules (Červenka et al., 2015). The changes in surface composition might be another reason for the different water content between body breakage samples and other samples.

For plant pilot-scale IMF or whey protein/lactose model powders (**Chapter 6, 7**), breakage did not influence the water adsorption rate and final water content of model powders at low water activities but accelerated the time-dependent crystallization of powders that contained lactose. The difference between commercial IMF and model samples might be because the commercial IMF (165 μm, 200 μm) was bigger than model powders (40- 90 μm) and the particle size of commercial IMF decreased 45-78% after body breakage but that of model powders decreased only 5-40%.

(2) Mechanical properties

During the water sorption, the moisture content increased and water acts as a plasticizer in amorphous powders. Increasing the water content of amorphous powder results in a rearrangement of molecules, which changes the mechanical properties of powders. Based on the changes in water adsorption behaviour, surface breakage did not impact the mechanical properties of commercial IMF while higher water contents of body breakage samples significantly decreased the initial crystalization temperature (T_{ic}) and slightly decreased the glass transition temperature (T_g) and α-relaxation temperature (T_α) (**Chapter 3**). For plant pilot scale model powders, breakage did not influence the T_g of samples but decreased the T_{ic} of powders that contained lactose (**Chapter 6, 7**). In addition, body breakage decreased the overall molecular mobility of powders and resulted in smaller magnitudes of modulus changes than other samples (**Chapter 3**).

(3) Rehydration properties

Rehydration is one of the most important properties of dairy powders. The wetting process is the first step of rehydration and is the ability of particles to overcome the surface tension between them and imbibe a liquid based on the capillary force (Ji et al., 2016). Broken samples had poor wettability compared to control samples and as the degree of breakage increased, the wettability became worse (**Chapter 4, 7**). This was caused by the decrease in particle size and porosity after breakage. Lower porosity with a small capillary radius between particles could inhibit water penetration into powders and then slow down the wetting process (Yuan et al., 2013). For IMF model samples, the influence of breakage on the wettability of whey protein powders was greater than that of casein powders (**Chapter 7**). Similarly, the impact of breakage on the wettability of maltodextrin and pure lactose powders was greater than that of sucrose powders (**Chapter 7**). For whey protein/lactose powder, breakage increased the wetting time of wettable samples but decreased the wetting time of powders with poor wettability (**Chapter 6**). After wetting, particles will disperse into the water, which is another important step in the rehydration process. Breakage reduced the dispersibility of all powder samples because of the decrease in particle size and porosity, which makes it harder for water to penetrate into the powder bulk (**Chapter 4, 6, 7**).

(4) Flowability

The flow properties are very important in handling and processing operations for dairy powders (Kim et al., 2005). Compared with the previous three functionalities, powder breakage did not have a major impact on the flowability of commercial IMF (**Chapter 4**). Breakage resulted in a small reduction in flowability because the SFF increased after breakage and liquid fat could form liquid bridges between individual particles reducing flowability (Kim et al., 2005; Peleg, 1977; Sharma et al., 2012) while powders were still essentially easy-flowing.

8.1.3. The impact of dairy powder characteristics on breakage

8.1.3.1. Powder physical properties

Based on the present study, the dynamic breakage of dairy powders was mainly influenced by the particle size and particle structure. Particle breakage research in other industries also demonstrated that the morphology of particles would impact the breakage of particles (Deng & Davé, 2017; Golchert et al., 2004; Norazirah et al., 2016) but most dairy powders were irregular agglomerated particles and their shapes were similar (**Chapter 3, 6, 7**).

(1) Particle size

Particle size was one of the most important factors that determined the response of particles to a certain mechanical load imposed on the particle. When particle structure was similar, bigger particles would suffer greater breakage than smaller particles under the same processing conditions (**Chapter 2, 3, 5, 6, 7**). For example, the particle size of IMF A (initial particle size was 200 μm) decreased around 70% after high-speed mixing but that of IMF B (initial particle size was 165 μm) decreased around 50% (**Chapter 3**). In addition, when the main breakage mechanism of powder whose particle size range was 250-180 μm was dispersion, the bigger-sized sieved fractions mainly underwent chipping and disintegration (**Chapter 2**). This was because of the probability of more imperfections in bigger particles, like cracks and internal holes where the highest local tensile stress will generate, leading to the initiation and propagation of fractures (Antonyuk, Tomas, Heinrich, & Mörl, 2005). From an energy perspective, for particles of the same material, the bigger the particles, the lower the fracture energy (particle is able to absorb a certain amount of energy before it breaks, 1.6.1.1). Furthermore, bigger particles have more momentum and more energy and thus collisions (if breakage is caused by the impact) lead to greater forces and more likely the particle will break.

(2) Powder structure and particle density

Differing from the particle structure of samples used in other industries, dairy powder particles were irregular and had different internal structures, like dense crystal structure, continuums solid structure, and porous structure. The degree of breakage increased with decreasing particle structural strength (**Chapter 5**). For particle structure response, the strength of crystals was the highest, followed by continuums solids, followed by the highly porous matrices with numerous small holes distributed throughout the particle, followed by the particles with a small number of randomly distributed internal holes, followed by the hollow sphere particle with a very thin shell. This was because the pores inside particles can be regarded as imperfections and crack release zones. Sometimes the breakage degree of small particles (**Chapter 5**, particle size around 7 μm) was higher than that of big particles (**Chapter 5**, SC with particle size 60 μm) because of the weaker particle structure.

Since the particle structure of some dairy powders was related to their particle densities especially when there were internal holes in particles, the particle density was another factor affecting dairy powder dynamic breakage (**Chapter 5, 7**).

8.1.3.2. Powder formulation

The present study shows that under the same spray drying conditions, dairy powder formulation affected dairy powder breakage mainly by influencing the physical properties of powder particles (**Chapter 6, 7**). Whey protein/lactose composition of the model powders influenced breakage by influencing the particle size and structure of the agglomerates where the two higher whey protein powders were smaller in particle size, were less irregular in shape and had higher particle densities, which resulted in less breakage in comparison to the two lower whey protein powders (**Chapter 6**). For model IMF powders, the protein/carbohydrate composition influenced breakage and the influence of proteins was greater than that of carbohydrates (**Chapter 7**). Whey protein powders were bigger in particle size, weaker in structural strength, and more irregular in shape, which resulted in more breakage in comparison to pure casein powders. Similarly, sucrose samples suffered

more breakage than maltodextrin and pure lactose powders, which was mainly because of their bigger particle size.

In addition, removing the initial moisture did not influence the breakage of model powders but increasing the moisture content within a certain range above initial powder moisture content could increase the breakage of the whey protein/lactose model powders (**Chapter 6**).

For the influence of fat on dairy powder dynamic breakage, the commercial dairy powder samples showed differently from plant pilot scale model powders (**Chapter 5-7**). The particle size of commercial dairy powers that contained fat was bigger than that of commercial dairy powders without fat but their breakage percentage was lower (**Chapter 5**). This might be because fat could act as a binder to increase agglomeration and it also could soften powders, resulting in easier plastic deformation of particles during dispersion and conveying instead of brittle fracture. However, the particle size of model samples WL13 (whey protein 25% and lactose 75%) from **Chapter 6** was bigger than that of WL (whey protein 15%, lactose 60%, and sunflower oil 25%) from **Chapter 7**, and the dynamic breakage percentage of WL13 was higher than that of WL through the powder venturi feeder with different air pressures. Thus, it was hard to say that fat in the IMF model samples decreased the breakage. These differences might be because the ratio of whey protein to lactose of these two powders and their production processes were slightly different where the solid content of mixtures before spray drying was 30% and 33%, respectively, and the emulsion of IMF model powders was homogenized.

8.2. Overall conclusions

Based on findings and discussion in this thesis, overall conclusions are outlined as follows:

- The changes in PSD of powders before and after breakage can be used to indicate the breakage mechanisms of agglomerated dairy powders. The main breakage mechanisms of IMF samples include dispersion,

surface breakage, and body breakage, corresponding to the increasing extent of breakage and depending on the breakage process conditions and particle characteristics (**Chapter 2**).

- The breakage behaviour of whole samples was one or a combination of breakage mechanisms because the breakage behaviour of samples with different particle sizes at the same process condition was different. More intense processing conditions were needed to cause the same breakage mechanism for smaller-sized particles (**Chapter 2**).

- Breakage significantly decreased the particle size and porosity of dairy powders and increased the specific surface area, particle density, and bulk density of samples. It also changed shapes and surface composition of particles as seen with the increase in lactose content and the decrease in protein and fat contents on most samples. Body breakage had greater influence on powder physical properties than surface breakage (**Chapter 3, 4, 6, 7**).

- Breakage significantly decreased the rehydration properties of dairy powders, including the wettability and dispersibility, while it had only a small influence on powder flowability (**Chapter 4, 6, 7**).

- Surface breakage had no influence on water sorption and mechanical properties of powders but body breakage significantly deteriorated them. The number of adsorbed monolayers, sorption surface area and monolayer value of body breakage samples were significantly higher than other samples. This increased the water sorption rates and water contents, accelerated the crystallization, and decreased the overall molecular mobility of samples (**Chapter 3, 6, 7**).

- Powder breakage degree increased with increasing particle size and decreasing particle structural strength. Considering particle structure, the strength of crystals was the highest, followed by the continuum solids, followed by particles with numerous small holes throughout the particle, followed by particles with a small number of randomly distributed internal

holes, followed by the hollow sphere particle with a very thin shell (**Chapter 5**).

- Removing the initial moisture did not influence the breakage of model powders but increasing the moisture content within a certain range above initial powder moisture content could increase the breakage of the powders (**Chapter 6**).

- Under the same spray drying conditions, the formulation significantly affects dairy powder breakage by influencing the physical properties of powder particles, especially for particle size and particle structure (**Chapter 6, 7**).

- For whey protein/lactose model agglomerated powders, the two higher whey-protein powders were smaller in particle size, were less irregular in shape and had higher particle densities, which resulted in less breakage in comparison to the two lower whey-protein powders (**Chapter 6**).

- For agglomerated model IMF powders that contained different protein (whey protein and casein) and carbohydrates (lactose, sucrose, and maltodextrin), whey protein powders were bigger in particle size, weaker in structural strength, and more irregular in shape, which resulted in better rehydration properties but more breakage in comparison to pure casein powders. Similarly, sucrose samples had better rehydration properties but suffered more breakage than maltodextrin and pure lactose powders because of their bigger particle size (**Chapter 7**).

- Fatigue affected the breakage of agglomerated dairy powders (**Chapter 6, 7**). This means that repeated lower mechanical stresses can cause dairy powder breakage even though the first mechanical load does not break particles but it may make particles more sensitive to the next load.

8.3. Potential applications and future work

8.3.1. Potential applications

This study provides useful information for industries to better understand dairy powder breakage and find ways to reduce it and improve the functionalities of their products. Firstly, dairy powder breakage should be limited to surface breakage to limit the deterioration of powder properties. Then, dairy powder breakage was determined by processing conditions and powder characteristics that included powder physical properties and formulation where the formulation impacted breakage by influencing powder physical properties. Therefore, using gentler processing conditions (for example, lower transportation speed to lower the mechanical loads) and modifying powder physical properties (mainly of particle size and particle structure or particle density) would be effective ways to reduce breakage. Improving the particle structure strength would be a way to decrease the breakage. Also, increasing the initial particle size may be an alternative way to compensate for the particle breakage during the production of dairy powders when the imposed stress is low. In contrast, a slight decrease in initial particle size may result in the bigger final particles after powder handling and processing because smaller particles are more resistant to breakage.

In addition, the present study could be used in other food powder breakage, such as granulated coffee, flour, nut powders, and so on.

8.3.2. Future work directions

Based on findings and discussion in this thesis, further studies on dairy powder breakage are still needed and recommended as follows:

(1) The influence of production process on powder physical properties

Based on the present study, from the perspective of particle characteristics, particle size and structure are two main physical properties influencing breakage. It would be useful to investigate the impact of

production processes on these properties, such as the spray-drying temperatures, the atomisation methods and parameters during the spray-drying, the solid content of emulsion before spray drying, and homogenization parameters, because compared with changing transportation conditions and formulations, changing these would be easier for factories.

(2) Exploring methods to determine the material strength of dairy powders

Based on previous research in other industries, particle breakage is also influenced by material strength (King, 2012). In the present study, the material strength was not considered separately because particle structure had greater influences on dairy powder breakage and most commercial dairy powders have similar composition. However, it would be interesting to find suitable methods to quantify the material strength of different dairy powder components and the relationship between the material strength of the formulation and the breakage behaviour of the particle. Masterson and Cao (2008) quantified the hardness of various pharmaceutical solids including sucrose, lactose, ascorbic acid, and ibuprofen using atomic force microscopy nanoindentation. This method could be a breakthrough to investigate the strength of milk powder ingredients, such as whey protein, casein, and lactose.

(3) Use of original spray-dried commercial powders

It would be interesting and useful if a similar study on breakage mechanisms and their influence on powder functionalities can be done on original spray-dried commercial powders to confirm if the same mechanisms apply to conditions that simulate the processes that powders undergo upon handling and transportation. Since samples used in Chapters 2 to 4 were commercial IMF, they had most likely already undergone breakage during their handling from spray drying through to packing as a commercial product. Samples used in Chapters 6 and 7 were original spray-dried powders but their particles were not big enough to accomplish this, because emulsions were not concentrated before spray drying.

In addition, some more specialised dryers have been designed and used to produce a more uniform particle size or shape of powder samples (Dai et al., 2013; You et al., 2014). It may be useful also to use this kind of device to study the influence of powder physical properties on breakage and delineate the effects of composition although it will not be reflective of actual spray drying but the combination of both would be beneficial.

(4) Improve some measurement methods

There are some limitations to the methods used in this study for measurements of some powder properties.

The specific surface area (SSA) is an important property for dairy powder functionalities, such as wettability and water sorption behaviour. The SAA of powders was measured with a laser diffraction particle sizer (Malvern Mastersizer 3000) and mathematically calculated from particle density data based on the assumption that the particles were both spherical and non-porous. However, dairy powder particles are always irregular and with internal pores. Therefore, some other methods can be designed or applied, such as the low-temperature gas adsorption method, to measure the SSA of dairy powders.

A typical industrial powder processing line will include several storage vessels, and feeding or handling steps. A major industrial problem is getting the powder to discharge reliably from storage into the next process step. Chapter 4 shows that breakage did not influence the flowability of commercial IMF. However, except for the flowability, a wall friction test could be useful to get the information on friction between the powder and a given wall surface for assessing mass-flow hopper half angles and gravity flow chute angles. This information may have industrial application for powder storage and transport.

The dynamic contact angle was used to quantify the wettability of some samples in this study with a water droplet gently dropped onto the smooth surface of the powder bed but in some other studies, the rough surface of powder beds was used. In addition, powder tablets that were produced by

compression using a press or other high-pressure devices were used in other publications. The changes in wettability before and after dairy powder breakage can be measured by the other two methods to get different pieces of information because surface features and roughness can result in large variations in measurements.

The distribution of components within dairy powder particles may influence the breakage behaviour of particles but no study has currently been done on this. In this study, the composition of the first 5 nm surface of dairy powder particles was measured using X-ray Photoelectron Spectroscopy (XPS). It is better suited for the compositional analysis of ultra-thin layers and thin microscale sample features. Energy Dispersive X-Ray Spectroscopy (EDS) has a typical analysis of the elemental composition of the depth of 1-3 µm surface. A combination of XPS, EDS, and free fat extractions has been used by Murrieta-Pazos et al. (2012) to study the repartition of components from the surface to the bulk of dairy powder particles. This could be a useful tool to study the influence of component distribution on dairy powder breakage.

Reference

Aarseth, K.A. (2004). Attrition of feed pellets during pneumatic conveying: the influence of velocity and bend radius. *Biosystems Engineering* 89(2), 197-213. https://doi.org/10.1016/j.biosystemseng.2004.06.008.

Agrawal, S.G., Balandier, A., Paterson, A.H.J., & Jones, J.R. (2011). Study on lactose attrition inside the mixing cell of a laser diffraction particle sizer using a novel attrition index. *Powder Technology* 208(3), 669-675. https://doi.org/10.1016/j.powtec.2011.01.007.

Antonyuk, S., Tomas, J., Heinrich, S., & Mörl, L. (2005). Breakage behaviour of spherical granulates by compression. *Chemical Engineering Science* 60(14), 4031-4044. https://doi.org/10.1016/j.ces.2005.02.038.

Bonakdar, T., Ghadiri, M., Ahmadian, H., Martin de Juan, L., Xu, D., Tantawy, H., & Smith, D. (2016). Impact attrition of spray-dried burkeite particles. *Powder Technology* 304, 2-7. https://doi.org/10.1016/j.powtec.2016.08.024.

Červenka, L., Hloušková, L., & Žabčíková, S. (2015). Moisture adsorption isotherms and thermodynamic properties of green and roasted Yerba mate (Ilex paraguariensis). *Food Bioscience* 12, 122-127. https://doi.org/10.1016/j.fbio.2015.10.001.

Cleaver, J.A.S., Ghadiri, M., & Rolfe, N. (1993). Impact attrition of sodium carbonate monohydrate crystals. *Powder Technology* 76(1), 15-22. https://doi.org/10.1016/0032-5910(93)80036-A.

Dai, Q., You, X., Che, L., Yu, F., Selomulya, C., & Chen, X.D. (2013). An Investigation in Microencapsulating Astaxanthin Using a Monodisperse Droplet

Spray Dryer. *Drying Technology* 31(13-14), 1562-1569. https://doi.org/10.1080/07373937.2013.800877.
Deng, X., & Davé, R.N. (2017). Breakage of fractal agglomerates. *Chemical Engineering Science* 161, 117-126. https://doi.org/10.1016/j.ces.2016.12.018.
Francioli, D.M., 2015. Effect of operational variables on ball milling, Universidade Federal do Rio de Janeiro, Brazil.
Golchert, D., Moreno, R., Ghadiri, M., & Litster, J. (2004). Effect of granule morphology on breakage behaviour during compression. *Powder Technology* 143-144, 84-96. https://doi.org/10.1016/j.powtec.2004.04.032.
Ghadiri, M., Yuregir, K.R., Pollock, H.M., Ross, J.D.J., & Rolfe, N. (1991). Influence of processing conditions on attrition of NaCl crystals. *Powder Technology* 65(1), 311-320. https://doi.org/10.1016/0032-5910(91)80195-O.
Ji, J., Fitzpatrick, J., Cronin, K., Maguire, P., Zhang, H., & Miao, S. (2016). Rehydration behaviours of high protein dairy powders: The influence of agglomeration on wettability, dispersibility and solubility. *Food Hydrocolloids* 58, 194-203. https://doi.org/10.1016/j.foodhyd.2016.02.030.
Kim, E.H.J., Chen, X.D., & Pearce, D. (2005). Effect of surface composition on the flowability of industrial spray-dried dairy powders. *Colloids and Surfaces B: Biointerfaces* 46(3), 182-187. https://doi.org/10.1016/j.colsurfb.2005.11.005.
King, R.P. (2012). *Modeling and simulation of mineral processing systems*. Society for Mining, Metallurgy, and Exploration (SME).
Kotzur, B.A., Berry, R.J., Zigan, S., García-Triñanes, P., & Bradley, M.S.A. (2018). Particle attrition mechanisms, their characterisation, and application to horizontal lean phase pneumatic conveying systems: A review. *Powder Technology* 334, 76-105. https://doi.org/10.1016/j.powtec.2018.04.047.
Li, R., Roos, Y.H., & Miao, S. (2016). Roles of particle size on physical and mechanical properties of dairy model solids. *Journal of Food Engineering* 173, 69-75. https://doi.org/10.1016/j.jfoodeng.2015.10.041.
Little, L., Mainza, A.N., Becker, M., & Wiese, J.G. (2016). Using mineralogical and particle shape analysis to investigate enhanced mineral liberation through phase boundary fracture. *Powder Technology* 301, 794-804. https://doi.org/10.1016/j.powtec.2016.06.052.
Materic, V., Holt, R., Hyland, M., & Jones, M.I. (2014). An internally circulating fluid bed for attrition testing of Ca looping sorbents. *Fuel* 127, 116-123. https://doi.org/10.1016/j.fuel.2013.10.071.
Masterson, V.M., & Cao, X. (2008). Evaluating particle hardness of pharmaceutical solids using AFM nanoindentation. International Journal of Pharmaceutics 362(1), 163-171. https://doi.org/10.1016/j.ijpharm.2008.06.015.
McCarthy, N.A., Gee, V.L., Hickey, D.K., Kelly, A.L., O'Mahony, J.A., & Fenelon, M.A. (2013). Effect of protein content on the physical stability and microstructure of a model infant formula. *International Dairy Journal* 29(1), 53-59. https://doi.org/10.1016/j.idairyj.2012.10.004.
Murrieta-Pazos, I., Gaiani, C., Galet, L., & Scher, J. (2012). Composition gradient from surface to core in dairy powders: Agglomeration effect. *Food Hydrocolloids* 26(1), 149-158. https://doi.org/10.1016/j.foodhyd.2011.05.003.
Norazirah, A., Fuad, S.H.S., & Hazizan, M.H.M. (2016). The effect of size and shape on breakage characteristic of mineral. *Procedia Chemistry* 19, 702-708. https://doi.org/10.1016/j.proche.2016.03.073.
Ortega-Rivas, E., Juliano, P., & Yan, H. (2006). *Food Powders: Physical Properties, Processing, and Functionality*. Springer US.
Peleg, M. (1977). FLOWABILITY OF FOOD POWDERS AND METHODS FOR ITS EVALUATION — A REVIEW. *Journal of Food Process Engineering* 1(4), 303-328. https://doi.org/ 10.1111/j.1745-4530.1977.tb00188.x.

Scala, F., Montagnaro, F., & Salatino, P. (2007). Attrition of limestone by impact loading in fluidized beds. *Energy & Fuels* 21(5), 2566-2572. https://doi.org/10.1021/ef0700580.

Sharma, A., Jana, A.H., & Chavan, R.S. (2012). Functionality of Milk Powders and Milk-Based Powders for End Use Applications—A Review. *Comprehensive Reviews in Food Science and Food Safety* 11(5), 518-528. https://doi.org/10.1111/j.1541-4337.2012.00199.x.

van Laarhoven, B., Schaafsma, S.H., & Meesters, G.M.H. (2012). Toward a desktop attrition tester; validation with dilute phase pneumatic conveying. *Chemical Engineering Science* 73, 321-328. https://doi.org/10.1016/j.ces.2011.08.038.

Wu, F., & Wu, D. (2017). Attrition resistances and mechanisms of three types of FCC catalysts. *Powder Technology* 305, 289-296. https://doi.org/10.1016/j.powtec.2016.09.077.

You, X., Zhou, Z., Liao, Z., Che, L., Chen, X.D., Wu, W.D., Woo, M., & Selomulya, C. (2014). Dairy Milk Particles Made with a Mono-Disperse Droplet Spray Dryer (MDDSD) Investigated for the Effect of Fat. *Drying Technology* 32(5), 528-542. https://doi.org/10.1080/07373937.2013.840650.

Yuan, Y., & Lee, T.R. (2013). Contact angle and wetting properties. *Surface science techniques* (pp. 3-34). Springer.

Zhang, Z., & Ghadiri, M. (2002). Impact attrition of particulate solids. Part 2: Experimental work. *Chemical Engineering Science* 57(17), 3671-3686. https://doi.org/10.1016/S0009-2509(02)00241-5.

Zhao, R., Goodwin, J.G., & Oukaci, R. (1999). Attrition assessment for slurry bubble column reactor catalysts. *Applied Catalysis A: General* 189(1), 99-116. https://doi.org/10.1016/S0926-860X(99)00261-6.

APPENDIX

Publications

Trends in Food Science & Technology 114 (2021) 608–624

Contents lists available at ScienceDirect

Trends in Food Science & Technology

journal homepage: www.elsevier.com/locate/tifs

Dairy powder breakage: Mechanisms, characterization methods, impacted properties and influencing factors

Jie Han [a,b], John Fitzpatrick [b], Kevin Cronin [b], Song Miao [a,c,*]

[a] Teagasc Food Research Centre, Moorepark, Fermoy, Co. Cork, Ireland
[b] Process & Chemical Engineering, School of Engineering, University College Cork, Cork, Ireland
[c] China-Ireland International Cooperation Centre for Food Material Sciences and Structure Design, Fujian Agriculture and Forestry University, Fuzhou, China

ARTICLE INFO

Keywords:
Dairy powder breakage
Breakage mechanisms
Processing parameters
Powder properties

ABSTRACT

Background: Particle breakage deteriorates dairy powder properties and it easily takes place in many processes. However, there currently is a lack of research on dairy powder breakage for understanding and controlling it. The research on particle breakage in other industries is very extensive and thorough, and could act as good reference knowledge for dairy powder breakage research, but at this time there is no review of this useful information.

Scope and approach: Based on the research done in dairy powder breakage and findings of particle breakage studies of other industries relevant to dairy powder particle properties, this review includes the breakage mechanisms of dairy powders, methods suitable for studying dairy powder breakage, the influence of breakage on powder properties, and influencing factors of dairy powder breakage which also can be considered as controlling factors.

Key findings and conclusions: Powder breakage significantly affects dairy powder physical properties which in-turn influence powder functionalities, especially the rehydration properties. The extent of agglomerates breakage corresponds to different breakage mechanisms which result in different final particle sizes and particle size distributions. The processing conditions (such as the parameters during dry-mixing, vibration, and pneumatic conveying) and the characteristics of particles (including physical properties and composition) are two main influencing factors that can be considered to control dairy powder breakage. However, there is currently not enough study showing which factors are more effective in controlling breakage. Some single-particle or multi-particle tests can be used to investigate dairy powder breakage and further research on the effectiveness of those controlling factors should be done.

1. Introduction

The production of dairy powders is growing rapidly worldwide because it provides a good way to preserve and transport milk ingredients in a stable and convenient form (Yildirim & Genc, 2017). Currently, most commercial dairy powders are agglomerated powders as agglomeration results in the formation of large particles which improved powder functionalities such as the flowability and rehydration properties (Ji, Cronin, Fitzpatrick, & Miao, 2017). However, particle breakage is an important issue for many industries involving operations that include crystallization, agglomeration, transportation and storage of particulate materials (Salman, Ghadiri, & Hounslow, 2007a, chap. 21, 25, 28). Meanwhile, food agglomerates are normally less robust and have lower mechanical strength than inorganic or polymeric particles, and they are also usually fragile and brittle (Yan & Barbosa-Cánovas, 1997, 2001a). Thus, unwanted particle breakage in agglomerated dairy powders easily happens when powders are exposed to mechanical loads, such as impact, shear, vibration, and static pressure (Han, Fitzpatrick, Cronin, Maidannyk, & Miao, 2020; Yan & Barbosa-Cánovas, 2001b).

Powder breakage takes place in many processes throughout dairy powder production wherever there is relative movement between powder particles in contact with each other or against the container wall, such as agglomeration in the fluidized bed, in-plant transportation in pneumatic conveying, and dry blending in a mixer (Boiarkina et al., 2016; Hazlett, Schmidmeier, & O'Mahony, 2020; Ortega-Rivas, Juliano, & Yan, 2006, chaps. 3, 6, 9, 12; Reynolds, Fu, Cheong, Hounslow, & Salman, 2005). It is also not rare to encounter the problem where a product leaves the manufacturing site meeting its specifications for size

* Corresponding author. Teagasc Food Research Centre, Moorepark, Fermoy, Co. Cork, Ireland.
E-mail address: Song.Miao@teagasc.ie (S. Miao).

https://doi.org/10.1016/j.tifs.2021.05.043
Received 31 August 2020; Received in revised form 5 May 2021; Accepted 28 May 2021
Available online 8 June 2021
0924-2244/© 2021 Elsevier Ltd. All rights reserved.

distribution, but when it reaches the hands of the customer, it exhibits severe problems such as dustiness (Ghadiri, Yuregir, Pollock, Ross, & Rolfe, 1991). In general, for some industries dealing with particulate solids, the notable and serious consequences of unwanted particle breakage is the increase in dust generation, which is associated with the possibility of dust explosions, hazardous problems to plant operator, loss of product because of undersize particles produced, and plugging of processing equipment (Kotzur, Berry, Zigan, García-Triñanes, & Bradley, 2018). Moreover, dairy powder breakage significantly deteriorated the rehydration properties of infant milk formula (IMF), whey protein isolate powder (WPI), instant whole milk powder, agglomerated whey protein concentrate (WPC), and granulated fat-filled milk powder (Barletta & Barbosa-Cánovas, 1993a, 1993b; Boiarkina et al., 2016; Han et al., 2020; Hanley, Byrne, et al., 2011; Hazlett et al., 2020; Yan & Barbosa-Cánovas, 2001b; Zhang, Olaleye, O'Mahony, Miao, & Cronin, 2020). Thus, particle breakage is a problem that cannot be ignored in dairy powder production. However, only a few studies about dairy powder breakage have been published (all of them are summarized in Table 1) and they mainly focused on the influence of breakage on powder properties or the influence of transportation parameters on breakage. There is currently not enough research on breakage behaviours and the influencing factors of breakage but they are very important for understanding and controlling dairy powder breakage.

The research on undesirable or intentional particle breakage in other industries, such as the pharmaceutical, agricultural, mineral, granulation, and catalysts chemical industry, is very extensive and thorough, and could act as good reference knowledge for the study of dairy powder breakage, as some of the processes are necessary for dairy powder production (Deng & Davé, 2017; Gupta, 2017; Gupta, Sun, Xu, Sarv, & Farzan, 2017; Norazirah, Fuad, & Hazizan, 2016; Reynolds et al., 2005; Salman, Fu, Gorham, & Hounslow, 2003; Shan, Xu, Liu, Zhou, & Wang, 2018). Numerical modelling combined with different types of tests were used for investigating the breakage patterns, influencing factors, breakage forecast, and characterization methods (Bonakdar et al., 2016; Bridgwater, Utsumi, Zhang, & Tuladhar, 2003; Deng & Davé, 2017; Gupta et al., 2017; Liu, Kafui, & Thornton, 2010; Salman, Hounslow, & Verba, 2002; Shan et al., 2018). Some investigation methods or results are very useful for the study of dairy powder breakage, but there is currently no review of this useful information. On the other hand, the property and structure of dairy powder particles are different from other industry particles or model particles with regular shapes, so it is important to review relevant information combined with dairy powder characteristics.

Therefore, instead of only summarising the research done in dairy powder breakage, this study mainly focuses on reviewing findings and principles of particle breakage studies of other industries that could be applied to dairy powder particles. Based on the combination of these two aspects, it provides an overview of the current status of knowledge about the breakage mechanisms of particles, methods suitable for characterizing dairy powder breakage, the influence of breakage on dairy powder properties, and the factors influencing breakage which can be used to control dairy powder breakage.

2. Particle breakage mechanisms

2.1. Continuum solids

The breakage of continuum solids has traditionally been classified into three modes of failure: brittle, semi-brittle, and ductile (Reynolds et al., 2005; Subero & Ghadiri, 2001). Brittle fracture takes place without noticeable plastic deformation in the material. In contrast, the ductile mode describes fractures with considerable plastic deformation in the solid. The semi-brittle fracture is an intermediate case where the brittle fracture occurs at the boundaries of a region of limited plastic deformation. While this form of breakage mechanism is not expected to find direct relevance to commercial dairy powders as most of them are agglomerates, it is included here for completeness.

2.2. Agglomerates

In contrast to continuum solids, agglomerates consist of several primary particles, which adhere together by adhesion force at their randomly distributed contacts. Depending on the agglomeration process, the internal adhesive forces are influenced by the superposition of different interactions forming material bridges, such as liquid or solid bridges or sinter necks or even interlocking of primary particles (Bika, Tardos, Panmai, Farber, & Michaels, 2005; Salman, Russell, Aman, & Tomas, 2015). Thus, it has been argued that those three modes of failure of continuum solids cannot be extended to describe structure materials, such as agglomerates and non-agglomerated porous solids (Reynolds et al., 2005; Subero & Ghadiri, 2001). In order to characterize the mechanisms governing the failure of agglomerates, some experimental and numerical studies have been done and three breakage patterns were found: surface abrasion, chipping, and fragmentation (Aarseth, 2004; Kotzur et al., 2018; Little, Mainza, Becker, & Wiese, 2016; Van Laarhoven, Schaafsma, & Meesters, 2012; Zhang & Ghadiri, 2002). Abrasion is generally associated with limited particle damage, while fragmentation can drastically change the particle morphology (Papadopoulos & Ghadiri, 1996). Considering the cohesiveness of dairy powders, dispersion may occur (Han, Fitzpatrick, Cronin, Maidannyk, & Miao, 2021). Three possible breakage mechanisms and their typical volume particle size distribution (PSD) plots (plotted on logarithmic scale x-axis) are summarized in Fig. 1 (Bayham, Breault, & Monazam, 2016; Han et al., 2021; Materic, Holt, Hyland, & Jones, 2014; Scala, Chirone, & Salatino, 2013).

Dispersion: At low processing conditions, dispersion of particles that exist as clusters held together by cohesive attractions may occur during many processes throughout the production and transportation. These clusters are susceptible to breakage, thus small stresses can break the clusters and disperse them into their original particles. When the processing conditions are not gentle, the mechanical force acting on the particle can disperse clusters and the breakage of initial particles can happen. The clusters exist in the larger sizes of the PSD and when they are broken, the particles are liberated causing the PSD shift to the left, with no production of fines (Han et al., 2021).

Surface breakage: This includes abrasion and chipping. When particles are subject to low-level external mechanical stress, the main mechanism of breakage is the surface breakage, leading to the production of minuscule particles whilst still retaining the identity of the original particles. Hence the original volume PSD is still evident and moves a little to the smaller particle size with the appearance of the peak for the newly formed small particles and well separated from the original peak by a range of sizes that contains no particles (King, 2012). With the production of fine particles, the uniformity level of powders decreases, and the main volume of samples are big size particles but the main number of samples is small size particles. Based on this, surface breakage can be determined according to the birth of bimodal PSD (Bonakdar et al., 2016; Paluszny, Tang, Nejati, & Zimmerman, 2016; Salman et al., 2003; Scala et al., 2013; Wu & Wu, 2017). The difference between abrasion and chipping is where the small peak occurs. The particle size of the small peak of chipping is bigger than that of the abrasion so the small peak of abrasion is at the smaller value compared with the chipping, as illustrated in Fig. 1.

Body breakage: This includes disintegration and splitting, and both are sometimes collectively termed fragmentation. In principle, fragmentation is the large-scale breakage where the cracks are generated in the areas with high-level stresses and then develop within part of or through the whole volume of the particle, corresponding to disintegration and splitting, respectively (Ghadiri & Zhang, 2002). As shown in Fig. 1, the PSD of disintegration particles is relatively narrow but will often be bimodal or even multimodal (King, 2012). Splitting results in the generation of a small number of coarse fragments, all significantly

Table 1
Summary of research done on the dairy powder breakage.

Reference	Type of dairy powders	The cause of breakage/The configuration caused breakage	Single- or multi-particle tests	Breakage evaluation	Key points
(Barletta & Barbosa-Cánovas, 1993a, 1993b)	• SMP	• Vibration	Multi-particle	• Attrition index (weight fraction of fine generation)	• The proposed attrition index was successful in describing the extent of attrition in a particulate material. • The effect of particle breakage was strongly dependent on the type of product and size of the agglomerates.
Yan and Barbosa-Cánovas (1997)	• INFP • LFMP	• Compression	Multi-particle	• Force-deformation relationships • Compressibility	• Particle size played a significant role in breakage and the greater the particle size, the greater the attrition. • The water activity (a_w) did not significantly affect attrition. • The force-deformation data showed that compared with the INFP, it was easier to compress LFMP.
Yan and Barbosa-Cánovas (2001a)	• INFP	• Vibration	Multi-particle	• Attrition index (weight fraction of fine generation)	• The larger the particle size and the higher the a_w the severer attrition they suffered. • The breakage could be minimized by properly controlling the particle size and a_w of products, and the environment relative humidity.
Agrawal et al. (2011)	• Lactose monohydrate (250–300 and 150–180 μm)	• Shear	Multi-particle	• Shattering index • Attrition index • Differential attrition index	• From the changes in PSD, three basic attrition mechanisms were recognizable: shattering, chipping, and abrasion. • Three mechanisms were differentiated by the collision energy intensity, which was a function of both crystal size and impact velocity. • Of the three variables studied, particle size and impeller speed significantly affected attrition while particle concentration least affected attrition.
Hanley, Byrne, et al. (2011)	• IMF	• Lab-scale modular pneumatic conveyor (dilute and dense-phase)	Multi-particle	• The percentage change in quality characteristics [a]*	• None of the factors [b]* had a significant influence on particle density. • Mode of conveying, air velocity and number of passes had a significant effect on bulk density. • For particle size and wettability, mode of conveying was the only significant factor. • Air velocity was significant for only dilute phase conveying, and not for dense phase.
Hanley, Cronin, et al. (2011)	• IMF	• Lab-scale pneumatic conveyor • Uniaxial compression • Drop test	Multi-particle [c]* Single-particle	• PSD changes • Forces and strains at failure • Stiffnesses • Coefficients of restitution	• The bulk density of IMF increased as conveying velocity increased. • Bulk densities before conveying and the force and the strain of individual particles at failure were increased with increasing the protein content of samples. • The force at failure and agglomerate stiffness were strongly correlated and generally increased with increasing protein to fat ratio while the strain at failure decreased.
Hanley et al. (2013)	• Macro-scale spherical model particles [d]* • IMF	• 90° bend during dilute-phase pneumatic conveying	Single-particle	• Failure force	• Breakage occurred when the impact force between the particle and pipe bend exceeded the intrinsic strength of the particle. • Impact force was proportional to normal impact velocity which in turn was the product of particle velocity and the sine of impact angle. • The results of the theoretical analysis were confirmed by Monte Carlo simulations.
Boiarkina et al. (2016)	• IWMP	• Industrial transport systems (pneumatic conveying and bucket elevator)	Multi-particle	• The changes in PSD of powders • The changes in bulk density of powders	• The powder with the larger final particle size had significantly larger particles before transport, which provided a larger buffer for breakage. • If the initial bulk density was sufficiently low, then this could compensate for the breakdown and the wettability remained good. • Optimising conveying systems is not the only way to compensate for breakdown, and the focus should equally be on producing powder

(*continued on next page*)

Table 1 (*continued*)

Reference	Type of dairy powders	The cause of breakage/The configuration caused breakage	Single- or multi-particle tests	Breakage evaluation	Key points
					of the right particle size and bulk density before transport.
Hazlett et al. (2020)	• WPC • FFMP • IMF	• A pressure dispersion rig (a simulated dilute-phase pneumatic conveying configuration)	Multi-particle	• Reducing particle size (D_{50}) • Increasing bulk density	• The initial size of agglomerates is a determinant of breakage and larger particles experienced a greater reduction in particle size. • The flowability of powders was impaired by agglomerate breakage via increased particle-particle interactions. • The initial stages of rehydration were impeded by breakage while powder solubility remained relatively unchanged.
Zhang et al. (2020)	• WPI	• A dilute-phase pneumatic conveying system	Multi-particle	• The changes in PSD • SEM micrograph of particles	• The conveying air velocity was the most important input variable [e]* and breakage rose rapidly at higher velocities. • Powder breakage was also very sensitive to particle size. • Bulk density of samples increased and wettability decreased due to the greater breakage while flowability was not significantly affected.
Han et al. (2020)	• IMF	• Lab-scale dilute-phase pneumatic conveyor • Laboratory high-speed mixer • Factory-scale blender	Multi-particle	• The changes in particle size ($D_{3,2}$)	• In both mixing and high-velocity pneumatic conveying, particles were broken into smaller entities while some agglomeration occurred during blending. • Particle breakage was accompanied by a significant decrease in porosity and increase in density and surface free fat. • Breakage decreased the rehydration properties of IMF while slightly influenced powder flowability.
Han et al. (2021)	• IMF	• Powder venturi feeder (simulated dilute-phase pneumatic conveyor) • Lab-scale dilute phase pneumatic conveyor • Laboratory high-speed mixer	Multi-particle	• Breakage percentage (the changes in particle size $D_{3,2}$)	• Four breakage mechanisms were firstly found in dairy powders, dispersion, chipping, disintegration, and splitting, depending on the breakage process conditions and powder strength. • Powder strength increased with the decrease of particle size and porosity, and the expansion of the PSD range. • The breakage behaviour of samples with different particle sizes at the same process condition was different.

1.SMP: instant skim milk powder. INFP: instant non-fat milk powder. LFMP: low fat (2%) milk powder. IWMP: instant whole milk powder. WPC: whey protein concentrate powder. FFMP: fat-filled milk powder. IMF: infant milk formula. WPI: whey protein isolate powder.

2. [a]* The quality characteristics included the bulk density, $D_{4,3}$ (volume mean diameter), particle density and wettability of IMF.

[b]* The factors that were tested included mode of conveying, air velocity, number of rig passes, bend radii and vertical rig section length.

[c]* The lab-scale pneumatic conveyor was a multi-particle test and the uniaxial compression and drop test were single-particle tests.

[d]* The other physical properties of spherical model particles were informed by experimental data obtained for IMF agglomerates.

[e]* The input variable considered included the conveying air velocity, solid loading rate, pipe bend radius and initial particle size of samples.

smaller than the parent, as illustrated in Fig. 1. Splitting has the effect of translating the original PSD to the left but retaining its fundamental shape with a broad spectrum of particle sizes. In the breakage study of IMF, the initial sample had a single-peak PSD (plotted on a logarithmic scale x-axis) with a range from 127.0 μm to 586.0 μm. After disintegration, samples had bimodal PSD and a range of the main peak was still narrow which was 76.0 μm to 516.0 μm with the child particle peak from 7.64 μm to 66.9 μm. After splitting, the sample had a broader single-peak PSD, from 4.58 μm to 516.0 μm (Han et al., 2021).

2.3. Crystalline particles

Lactose is an important ingredient for dairy powders and is sometimes in the crystalline form. For crystalline particles, the breakage mechanism is due to the distribution of loading forces across the topography of the particle. If crystalline material is semi-brittle, it will typically break via the previously described, abrasion or chipping mechanism. If via a pure brittle mechanism, rupture along preferred fracture planes is expected. In the case where a particle is composed of two or more crystals, cleavage may occur at the interface, and child particles are relatively undamaged (Cleaver, Ghadiri, & Rolfe, 1993; Ghadiri et al., 1991).

3. Dairy powder breakage characterization methods

Currently, two main types of experimental tests have been designed to study the breakage of particulate systems: single-particle and multi-particle breakage tests (Bonakdar et al., 2016; Ortega-Rivas et al., 2006, chaps. 3, 6, 9, 12; Salman, Ghadiri, & Hounslow, 2007b). Both types of experimental tests are important for the study of dairy powder breakage. Depending on the mode of loading, each type of test can be divided into impact or dropping, static compression, and shear. The first two are commonly used to analyse the breakage behaviour or strength of particles.

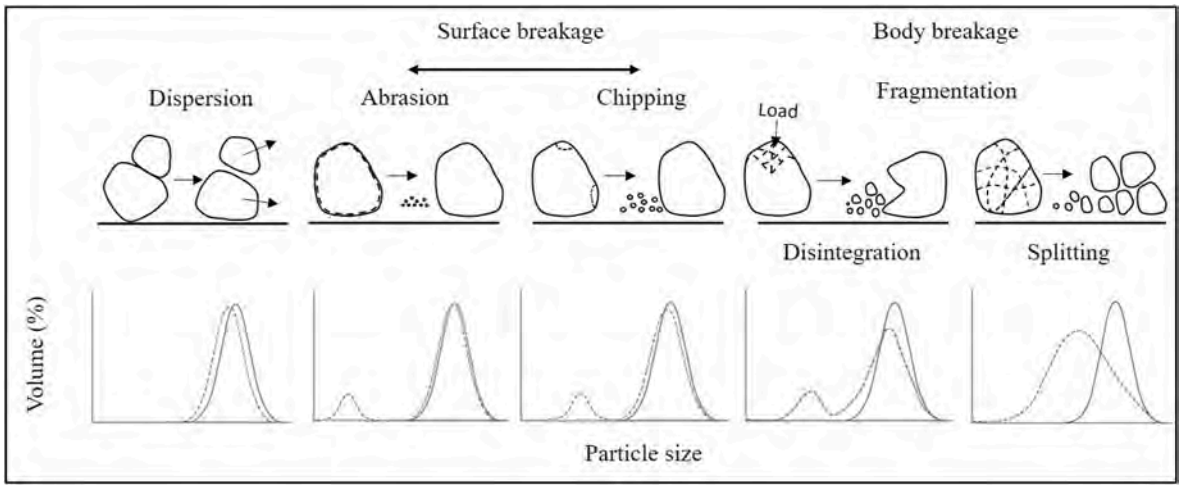


Fig. 1. Outline of agglomerated particle breakage patterns and their typical particle size distribution curves (plotted on a logarithmic scale x-axis) before (solid line) and after (dotted line) breakage, recreated based on Scala et al. (2013), King (2012), and Han et al. (2021).

3.1. *Single-particle breakage tests*

Single-particle test methods, including impact, crushing, dropping, and compression, have the advantage of applying a well-characterized load on the particle, providing fundamental information about particle properties, and enhancing the understanding of particle breakage (Bonakdar et al., 2016; Salman et al., 2002; Shan et al., 2018; Subero & Ghadiri, 2001). However, they are not fully representative of industrial conditions, and results are difficult to compare with attrition observed in practice because of the variations among particles in a certain bulk. For dairy powder breakage investigation, the particle size of dairy powders is usually too small for use in the single-particle methods. Some studies were performed on large-sized (710–850 μm) IMF agglomerates using single-particle compression and dropping tests by a texture analyser and a stainless steel plate combined with a high-speed camera, respectively (Hanley, 2011).

In single-particle tests, particle breakage is mainly due to crack propagation. Combined with the photography from the high-speed camera (Antonyuk, Tomas, Heinrich, & Mörl, 2005; Papadopoulos & Ghadiri, 1996), single-particle tests can be used to investigate the breakage behaviour and how cracks develop in particles. In addition, single-particle breakage tests can be used to measure the strength of particles. Particle strength would be influenced by both material and structure strengths, which is an integrated mechanical property. For discussion, particle strength was defined as the minimum amount of stress that might be applied to a particle to cause macroscopic damage to the particle structure, which represented fracture toughness, hardness, yield stress, and breaking stress-related strength for different loading conditions (Bika, Gentzler, & Michaels, 2001; Kotzur et al., 2018).

For static compression tests, either single-particle or multi-particle, the force-deformation curves can be used to analyse the breakage behaviour and strength of particles (Hanley, 2011; Shan et al., 2018; Yan & Barbosa-Cánovas, 1997). For the single-particle compression test, the strength of agglomerates and the normal force and strain at the point of breakage can be obtained from the force-deformation curves. The deformation behaviour of most agglomerates lies between the extremes of brittle failure and plastic failure. For brittle failure, the compaction goes through three stages: elastic loading (the applied force increases with increasing deformation), breakage (where the maximum applied force is and it can be clearly identified), and then further development of the cracks. For plastic failure, the particle deforms plastically and does not show a definite point of breakage and then the formation of a large contact area is followed. In some studies, the maximum applied force at breakage was taken as the particle strength (Beekman et al., 2003). In addition to the maximum applied force, Tavares et al. used the specific fracture energy when they studied the breakage of iron ore pellets (Tavares & de Almeida, 2020; Tavares et al., 2018). The specific fracture energy was obtained by dividing the absorbed energy by the mass of the particle and the absorbed energy was given by numerical integration from the force-deformation curve. However, each curve of agglomerated dairy powder particles had several peaks and troughs because they were irregular. Some peaks represented surface breakage, while others represented body breakage. An algorithm was developed to identify the first body breakage point (Hanley, 2011). Besides, even with the identical production process, the strength of the individual agglomerates differs in the microstructure because of the distribution and orientation of bonds, defects, and pore size distribution (Antonyuk et al., 2005). Thus, dairy powder particles are different so the force-deformation curves of different particles in the same sample could be different.

In impact or dropping tests, the coefficient of restitution was used in the single-particle test to show the particle strength (Hanley, 2011). It was defined that the magnitude of the normal velocity after impact divided by the normal velocity before impact. Every collision was recorded using a high-speed camera. Each file was analysed using software to track the position of each agglomerate over time, and thus provided the normal velocity of particles before and after the collision. Where coefficients of restitution were low, this implied that extensive breakage of either bonds or primary particles occurred which absorbed energy.

It is worth mentioning that the results of single-particle tests are difficult to compare with breakage in practice but they can be used in process simulations using the appropriate tools, such as the Discrete Element Method (DEM) and DEM coupled with Computational Fluid Dynamics (CFD), to predict the particle breakage. DEM simulations have been widely used to investigate the breakage of agglomerates, particularly the breakage induced by impact with the focus on the effect of impact velocity, impact angle, and surface energy. Han, Levy, and Kalman (2003) applied a 2D CFD-DEM model to simulate the particle breakage behaviour in a dilute-phase pneumatic conveying. The simulated results were comparable to the experimental data. However, under-prediction of particle breakage was observed with increasing numbers of passes through the system, which was attributed to the disregard of the fatigue. Uzi, Kalman, and Levy (2016) presented a model of particle breakage within pneumatic conveying systems. Empirical comminution functions (strength, equivalence, fatigue, and breakage) for the particle characteristics and machine functions (collision velocity and collision frequency) were developed from CFD-DEM simulations to inform the model. The model predictions of particle

breakage were in good agreement with the breakage results obtained in pneumatic conveying experiments. This means that the single-particle tests of dairy powders can be used in the simulations of production processes, which will assist efforts in understanding the breakage and reducing the associated problems in industrial systems.

3.2. Multi-particle breakage tests

Unlike the single-particle tests, multi-particle test methods, using shear cells, compression cells, vibration, and fluidized beds, are close to the real industrial situations, even though the loading conditions experienced by each particle are not known (Wu & Wu, 2017; Yan & Barbosa-Cánovas, 1997, 2001a). Vertical vibration tests using a tap density tester were used to investigate the breakage and its influencing factors (particle size and water activity) of instant coffee powder and milk powders (Barletta & Barbosa-Cánovas, 1993a, 1993b; Yan & Barbosa-Cánovas, 2001a). Samples were sieved into different fractions with different particle sizes before being confined to a graduated cylinder at a certain fixed height and exposed to a certain number of vertical vibrations on a tap density tester. After the test, the total sample weight was recorded. For each sample with a different particle size range, a corresponding sieve was used to gently sieve the sample to determine the weight fraction of the agglomerates that maintained their original size. The recorded amounts of particles retained on the sieve and passed through it were used for calculating the attrition index. The multi-particle compression test using a TA texture analyser was used to analyse the effect of padding foam on reducing breakage in instant coffee and milk powders (Yan & Barbosa-Cánovas, 1997, 2001b). Some studies used laboratory-scale equipment, such as a pneumatic conveyor, a simulated pneumatic conveying rig, or a dry mixer to analyse the breakage of different kinds of agglomerated dairy powders (Han et al., 2020; Hanley, 2011; Hazlett et al., 2020; Zhang et al., 2020). In these treatments, the following different assessment methods were used to evaluate the breakage or breakage behaviour.

3.2.1. Characterization of breakage behaviour

For the multi-particle compression tests, the force-deformation curves are smooth and can illustrate the whole compression process of samples. It is generally believed that the compression of agglomerates occurs in three stages, rearrangement of agglomerates, breakdown of agglomerates, and rearrangement of primary particles. Thus, particle breakage behaviour can be analysed according to the changes of force-deformation curves (Yan & Barbosa-Cánovas, 1997). For some impact or dropping tests, the changes of PSD before and after breakage can indicate the breakage mechanisms (as shown in Fig. 1) and has been used in some areas, such as lactose crystals, catalysts, limestone, calcium looping sorbents, and model porous powders (Agrawal, Balandier, Paterson, & Jones, 2011; Bonakdar et al., 2016; Materic et al., 2014; Ortega-Rivas et al., 2006, chaps. 3, 6, 9, 12; Scala, Montagnaro, & Salatino, 2007; Wu & Wu, 2017; Zhao, Goodwin, & Oukaci, 1999). In addition, the loss of at least 10% of the mass of the original particles in a given stressing event has been defined as the threshold between surface breakage and body breakage, which has been used in some studies including single-particle breakage tests (Tavares et al., 2018).

3.2.2. Characterization of powder strength

Some breakage indices were proposed to describe the extent of breakage or indirect powder strength (Agrawal et al., 2011; Barletta & Barbosa-Cánovas, 1993a; Yan & Barbosa-Cánovas, 1997).

3.2.2.1. Static compression tests. For the multi-particle compression tests, the ease of breakage can be analysed according to the changes of force-deformation curves. The compression index (*CI*), presented in Eq. (1), was used to indicate the compressibility and ease of breakage. The higher the *CI*, the easier it is for agglomerates to be broken. Eq. (1) was successfully applied to describe the sigmoid compressive stress-strain relationships (Swyngedau, Nussinovitch, Roy, Peleg, & Huang, 1991). Besides, some researchers used the percentage of bulk density change to indicate the compressibility (Fu et al., 2012)

$$\frac{\rho(\sigma)-\rho_0}{\rho_0} = C + CI \cdot log\sigma \tag{1}$$

where $\rho(\sigma)$ is the bulk density under compression stress σ, ρ_0 is the initial bulk density, and C is constant.

3.2.2.2. Impact or dropping tests. In impact or dropping tests, the indication of strength or the extent of breakage is based on the changes in particle size or PSD, or the production of child particles, depending on the methods used and the characteristics of original particles (Bonakdar et al., 2016).

(1) The changes in particle size

Friability refers to the ability of powder particles to fragment into smaller particles, which can be used to represent particle strength, and the bigger the friability index (*FI*), the easier it is for particles to be broken. The *FI* of samples is deduced from the changes of particle size which is measured by laser light scattering analysers with dry dispersion modes at two dispersion air pressures. For instance, *FI* can be calculated as Eq. (2) (Schuck, Dolivet, & Jeantet, 2012, p. 123) when the particle size is measured by laser diffraction analysers

$$FI = \left(\frac{D50_{\ 0.5\ bar} - D50_{\ 4.0\ bar}}{D50_{\ 0.5\ bar}}\right) \times 100\ \% \tag{2}$$

where $D50_{0.5\ bar}$ and $D50_{4.0\ bar}$ are the particle size (D_{50}, taken from the volume PSD) measured with compressed air at 0.5 and 4.0 bar, respectively. *FI* is suitable for distributions that are both monomodal and do not change their shape after breakage. Also, because the D_{50} is calculated from the volume-weighted PSD, it is insensitive to changes at the fine end of the distribution. Dairy powder breakage results in the production of fine particles so instead of using D_{50}, the Sauter mean diameter ($D_{3,2}$) should be used in Eq. (2) because it is more sensitive to the presence of fine particulates in the size distribution than the volume mean diameter ($D_{4,3}$) (Hu et al., 2014; Mun, McClements, & Surh, 2011).

(2) The changes in PSD

The attrition index (*AI*) has been defined for comparing the extent of breakage and it is the ratio of the volume of fine particles and other particles after breakage. In Fig. 2A, the particle size of fines is most simply defined as the lower limit size of the initial PSD. *AI* can be calculated as Eq. (3) (Agrawal et al., 2011). A differential attrition index (*DAI*) was defined as the sum of the volume fraction of particles that appear or disappear within size classes across the distribution divided by 2. It signifies the net volumetric movement of particles from larger to smaller size groups. Disappearance from one size class means appearance at another size class. Based on the difference of the PSDs before and after breakage as shown in Fig. 2B, *DAI* can be calculated as Eq. (4) (Agrawal et al., 2011)

$$AI = \frac{a}{b+d} \tag{3}$$

$$DAI = \frac{m+n}{2} \tag{4}$$

where a, b, d, m, and n are the areas of the corresponding enclosed area in Fig. 2.

Compared with *AI*, *DAI* is equal to area a+b or area c. *AI* excludes the newly generated particles represented by area b so *DAI* is more sensitive to changes in shifting PSDs, and *DAI* is more suitable when PSD changes

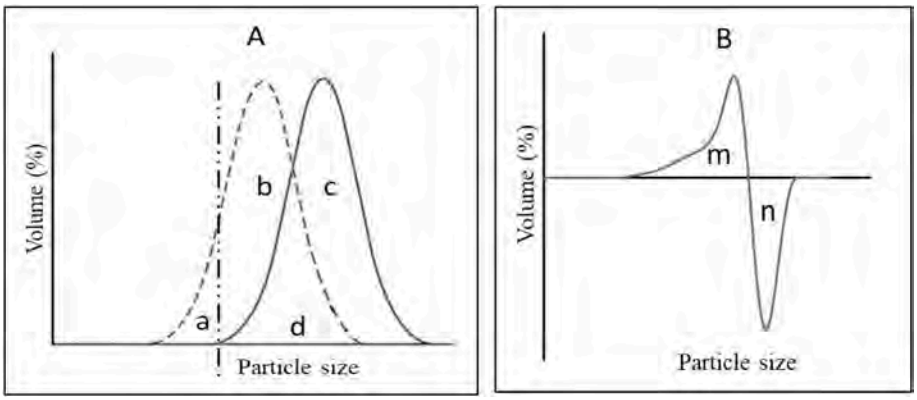


Fig. 2. The particle size distribution curves before (solid line) and after (dotted line) breakage (A), and the difference of them (B), recreated based on Agrawal et al. (2011).

are minor.

Rather than using the PSD with percentages of the particles contained in each size category shown on a linear vertical axis, as shown in Fig. 2A, cumulative particle size distributions, shown in Fig. 3, can be used to get the relative breakage (B_r) (Einav, 2007). Before calculating the B_r, a baseline particle size must be selected, depending on the properties of samples. For example, 20 μm was chosen as the baseline particle size when analysing the breakage of IMF because measured changes in the particle size distributions of IMF below this threshold were negligible (Hanley, 2011). The breakage potential (B_p) is defined as the area enclosed between the particle size distribution before breakage and the baseline size, as shown in Fig. 3A, and it quantifies the breakage if all the particles have final sizes below the baseline size. The total breakage (B_t), is the area enclosed between the particle size distributions before and after breakage for particle diameters greater than the baseline particle size, as shown in Fig. 3B, which is a measure of the actual breakage. B_r can be calculated from Eq. (5).

$$B_r = \frac{B_t}{B_p} \tag{5}$$

(3) The production of child particles

In this type of experiment, a narrow PSD should be used. Particles were collected after breakage, even the single-particle test methods, and sieved into child particles and mother particles. The results are expressed in terms of the extent of breakage (*BE*) using Eq. (6) (Bonakdar et al., 2016)

$$BE = \frac{M_D}{M_0 + M_D} \times 100\ \% \tag{6}$$

where M_D and M_0 are mass of child and mother particles, respectively.

3.3. Other indirect methods

Besides the two types of methods above, some researchers have developed other indirect methods where the loading did not directly act on the powder or the object of loading was not the original powder.

Agrawal et al. (2011) investigated lactose powder breakage inside the liquid mixing cell (called the small volume liquid sample presentation unit) of a laser diffraction particle sizer (Malvern Mastersizer) where the stirring time and rate of the propeller inside the cell could be controlled to break lactose particles. This approach provided an on-line particle size measurement that prevented experimental losses and errors during filtration, drying, weighing, and sieving. However, samples were needed to be dispersed in non-solvent media liquids. Methanol was chosen as the non-solvent medium by Agrawal et al. for the lactose crystals attrition study. The shattering index (*SI*), quite similar to the *FI*, was used to represent lactose strength in this study. *SI* was calculated as Eq. (7) when the breakage degree was controlled by dispersing at

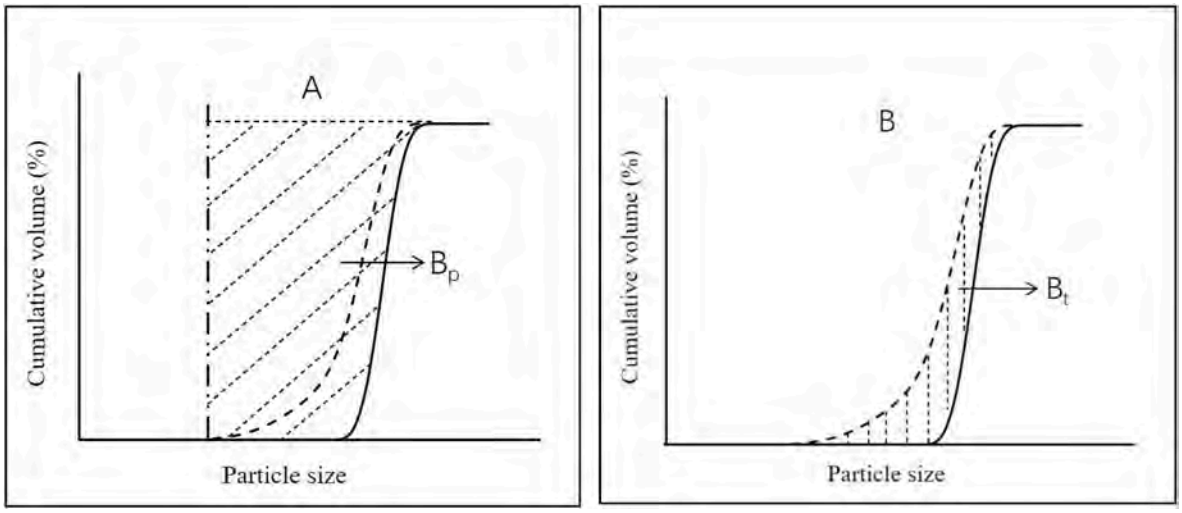


Fig. 3. Cumulative particle size distributions before (solid line) and after (dotted line) breakage with shaded areas indicating the breakage potential B_p (A), and the total breakage B_t (B), recreated based on Hanley (2011). B_p: breakage potential. B_t: total breakage.

different times

$$SI = \left(\frac{D50_{\,0} - D50_{\,t}}{D50_{\,0}}\right) \times 100\ \% \quad (7)$$

where $D50_0$ and $D50_t$ are the particle size (D_{50}, taken from the volume PSD) after breakage treatment for 0 and t time, respectively. As the description in 3.2.2.2- (1), instead of using D_{50}, $D_{3,2}$ should be used in Eq. (7).

A KQ-3 particle strength tester was used to measure the mechanical strength of three fluid-bed catalytic cracking catalyst samples with mean particle diameters around 100 μm (Wu & Wu, 2017). Since it is impossible to measure the mechanical strength of a single particle in this device, flakes of pressed particles were employed. All flakes were also made of catalyst particles of the same mass. The pressing time and pressure were also the same. The test results of flakes were used to reflect some extent of the bond strength of the original samples.

4. Influence of dairy powder breakage on powder physical properties and functionalities

Different breakage mechanisms result in different particle sizes and PSDs of the final samples, which then can influence powder properties. The influence of breakage on dairy powder properties is an important issue for the dairy powder industry. This section will summarize the effects into two categories: physical properties and functionalities.

4.1. Physical properties

Dairy powder breakage significantly reduces the particle size which is an essential and important property for dairy powders (Li, Roos, & Miao, 2016). The particle size of IMF fell from 143 μm progressively to 65.4 μm after the laboratory-scale high-speed mixing for 7 min (Han et al., 2020). After in-plant transportation using pneumatic conveying or a bucket elevator, the average particle size of instant whole milk powder decreased and the PSD shifted to a smaller value (Boiarkina et al., 2016). The particle size of WPC, fat-filled milk powder and WPI decreased during the pneumatic conveying (Hazlett et al., 2020; Zhang et al., 2020). The specific surface area (SSA) increases with the decreasing particle size because SSA is typically inferred from the particle size. The bulk density and porosity also relate to the particle size so the bulk density of powders significantly increases and porosity decreases after breakage (Boiarkina et al., 2016; Han et al., 2020; Hanley, 2011). There were a lot of pores inside dairy powder particles and after breakage, some internal stomata were exposed, which led to the increase of the particle density. Thus, the breakage does not only break solid bridges within agglomerated particles resulting in the decrease of particle size and increase of bulk density but also breaks primary particles leading to the increase of the particle density (Han et al., 2020).

Dairy powder breakage influences the surface composition of particles. Murrieta-Pazos, Gaiani, Galet, and Scher (2012) using X-ray Photoelectron Spectroscopy coupled with Energy Dispersive X-ray analyses investigated the first 5 nm and the first micrometre of the dairy powder particle surface respectively. They proposed that the distribution of milk components (lactose, lipids, proteins, and minerals) from the particle surface to the core was different. This means the distribution of each component in the particle is not uniform, so breakage can influence the surface composition. There was higher surface free fat content for broken dairy powder samples, including IMF and fat-filled milk powder, and the higher the extent of breakage, the higher the surface free fat content (Han et al., 2020; Hanley, Cronin, et al., 2011; Hazlett et al., 2020). As these powders contained much higher concentrations of fat, homogenization steps were used before spray drying to stabilise the fat that dispersed through the particle's bulk structure after spray drying. Particle breakage produced more surface area and exposed fat that hidden within the interior of the powder particles, leading to increases in the concentrations of free fat on particle surfaces. There is currently no research presented on the effect of breakage on the other components.

The changes in physical properties seriously affect the application of dairy powder. For example, bulk density is functionally an important characteristic as it is for calculating the capacity of packing materials, especially for IMFs as they are usually dispensed on a volume basis using a scoop. It is also important that changes in physical properties lead to a decline in functional properties.

4.2. Functionalities

4.2.1. Rehydration properties

Rehydration properties are considered an important benchmark to determine the overall quality of powder products and regarded as critical issues in the dairy industry. The rehydration process mainly consists of three sequential stages, which are wetting, dispersing, and solubilization (Ji et al., 2016).

Wettability is the ability of particles to imbibe a liquid and overcome the surface tension between them based on the capillary force (Forny, Marabi, & Palzer, 2011; Richard et al., 2013). There are two steps for the wetting process of powders (Yuan & Lee, 2013). The first step is the replacement of gas by water so the interface of powders-gas is replaced by the interface of powder-water. Secondly, inward diffusion of the liquid through the capillary structures of the porous powder particle. It is usually believed that wettability depends on the powder particle size, density, porosity, surface charge, surface area, the presence of amphipathic substances, and the surface activity of the particles (Hogekamp & Schubert, 2003; Sharma, Jana, & Chavan, 2012). High extent powder breakage results in the significant decrease of the porosity, and the increase of the surface free fat content. Lower porosity reduces the capillary radius between particles, and higher surface free fat content makes the particle surface more hydrophobic, which both inhibit water penetration into powders, thus slowing down the wetting process. Han et al. (2020) showed that the wetting time of IMF before breakage was around 1 s using the contact angle measurement while 5 min was needed for samples with a high extent of breakage. Agglomerated WPC and fat-filled milk powder also displayed significant impairment in their wettability on breakage during pneumatic conveying, with reductions in the levels of wettability (the mass percentage of the wetted particles to the initial sample) from 68.7% and 65.9% to 39.2% and 34.9%, respectively (Hazlett et al., 2020). Similarly, the wettability of WPI decreased after transported by the dilute phase pneumatic conveying due to the greater breakage (Zhang et al., 2020).

Dispersibility is the ease with which lumps and agglomerates of powder separate into individual particles in water, and is influenced by particle size, porosity, and density (Goalard, Samimi, Galet, Dodds, & Ghadiri, 2006; Sharma et al., 2012). It was found that breakage decreased the dispersibility of IMF, agglomerated WPC, and fat-filled milk powder, and decreased gradually with the increase of the extent of breakage (Han et al., 2020; Hazlett et al., 2020). The substantial decrease of particle size and porosity and the increase of surface free fat content may be the reason for the deterioration of the dispersibility of broken samples by slowing down the penetration of water into the powder.

Solubility is a measure of the final condition to which the constituents of the powder can be brought into solution or stable suspension, depending mainly on the chemical composition and physical state of the powder, such as the fat content in the milk (Pugliese et al., 2017; Sharma et al., 2012). Pugliese et al. (2017) found that the solubility of skim milk powder was higher than whole milk powder because of the lower water dispersion of fats in water. The mechanism proposed to explain milk powder insolubility involves the unfolding of the β-lactoglobulin and its aggregation with casein, and also the fouling of heating equipment which is associated with the drying conditions (Thomas, Scher, Desobry-Banon, & Desobry, 2004). Currently, no research has found that

dairy powder breakage affects powder solubility. Hazlett et al. (2020) found that there was no significant difference in the solubility of some dairy powders before and after breakage, including IMF, agglomerated WPC, and fat-filled milk powder.

4.2.2. Flowability

Powder flowability is important in handling and processing operations and it depends on the powder properties and storage conditions as they influence the cohesiveness of powders. After breakage, the particle size and porosity decrease, which acts to bring the powder particles into closer arrangement, resulting in a greater number and strength of interparticle interactions, such as van der Waals and electrostatic interactions, reducing powder flowability through increased cohesiveness (Zafar, Vivacqua, Calvert, Ghadiri, & Cleaver, 2017). Additionally, the SSA and surface free fat content increase after breakage, and fat has the propensity to form liquid bridges between neighboring particles, which also increases the cohesiveness of powders, thus decreasing the flowability. It was found that with increasing breakage, the flowability of instant coffee and some agglomerated dairy powders decreased (Hanley, 2011; Hazlett et al., 2020). On the contrary, the breakage of some IMF, WPI and granulated fat-filled milk powder did not significantly influence their flowability (Han et al., 2020; Hazlett et al., 2020; Zhang et al., 2020). Besides, the improvement of the flowability of some sieved big-sized IMF samples after breakage was found by Hanley (2011). Thus, no clear trends have been observed for the influence of powder breakage on the flowability of dairy powders. This might be because breakage degree and powders' initial properties influenced the effect of breakage on flowability.

4.2.3. Water sorption, glass transition, and mechanical properties

Water strongly affects glass transition and structures of amorphous food solids, and it is an important factor determining their chemical and physical stability (Li, Lin, Roos, & Miao, 2019). The increasing water content induces the formation of liquid bridges between particles, which may result in caking and sticking problems of food powders. Furthermore, the mechanical properties of dairy powders, including the storage modulus, loss modulus, and α-relaxation, are influenced by the glass transition as they are related to molecular mobility (Li et al., 2016; Maidannyk et al., 2020). However, there is currently no research on the influence of breakage on these properties of dairy powders. Previous studies have shown that the SSA of powders increased after breakage, which means more surface area is potentially available for water sorption, thus breakage may increase the water sorption speed. Besides, breakage significantly decreases the particle size of powders. Water sorption properties of lactose/milk protein isolate solids systems with different particle sizes were analysed (Li et al., 2016). It was found that the water content of large particle samples (the D_{50} was around 25–50 μm) was lower than the small-sized samples (the D_{50} was around 6.7–7.5 μm) with the same compositions at 0.54 a_W at 25 °C for 168 h. On the other hand, the decrease of porosity can slow down the water sorption because of the small capillary radius between particles.

In general, breakage significantly deteriorates powder properties. It is necessary to control the unwanted breakage during the production and transportation of dairy powders. However, there is currently not enough research on it. Based on the literature on the breakage of other materials, the applied stress from processing conditions and the characteristics of particles are two main effects that influence particle breakage (Petukhov & Kalman, 2004). Thus, the control of dairy powder breakage can be considered from these two aspects. In the next two sections, these two influencing factors on dairy powder breakage are reviewed.

5. Influencing factors - processing conditions

Dairy powders are produced by dehydrating water in raw milk during several processes and the main steps are categorized as pre-treatment (standardization, homogenization, and pasteurization), concentration, and drying (Moejes & van Boxtel, 2017; Yildirim & Genc, 2017). Spray drying is a common practice in dairy powder production where liquid state feed is turned into a solid-state product by spraying the liquid into a hot air environment (Yildirim & Genc, 2017). Combining spray drying (with fines return) with fluidized bed processing is mostly used for drying and particle granulation. Breakage very easily occurs in the fluidized bed but breakage and agglomeration occur simultaneously in the fluidized bed (Reynolds et al., 2005). After agglomeration and cooling down the temperature, powders are transported to packaging or storing in a silo using pneumatic conveying or bucket elevator (Boiarkina et al., 2016; Walstra, Wouters, & Geurts, 2005). After packaging, vibration is unavoidable before products are consumed. There is a special process during the production of the IMF called the 'dry blending' process. Ingredients in powdered form are mixed, using either a ribbon blender or other large-scale blending equipment, to achieve the uniform blend of macro- and micronutrients necessary for a complete IMF product (Jiang & Guo, 2014; Kent, Fitzgerald, Hill, Stanton, & Ross, 2015). In the context of particle attrition, it has been demonstrated that the collisions among agglomerates and against static container walls due to mechanical impact, shear, or compression provide the kinetic energy that causes the breakage of agglomerated particles (Kotzur et al., 2018). Unwanted breakage is the breakage that happens after agglomeration, which mainly occurs during in-plant transportation (pneumatic conveying or bucket elevator), dry blending, and vibration.

5.1. Breakage during dry-mixing

Dry mixing requires the motion of ingredients to reach the desired homogeneity or a uniform distribution. It is accomplished by the movement of particles between various parts of a whole particulate mass (Lindley, 1991b). Particle breakage occurs during the movement, especially for surface breakage or dust generation (Bridgwater, 2010; Lindley, 1991a). Forces acting on particles during mixing include gravity, vessel walls, and the motion of mixing blades (Lindley, 1991b). Three mixing mechanisms have been recognized in solids mixing: convection, diffusion, and shear (Kuakpetoon, Flores, & Milliken, 2001; Lindley, 1991a, 1991b; Pernenkil & Cooney, 2006). Shear mixing is sometimes considered as part of the convective mechanism. Three mechanisms take place simultaneously in powder mixing processes (Kotzur et al., 2018). In convective mixing, a circulating flow of powders is caused by the rotational motion of a mixer vessel, an agitating impeller (such as a ribbon or a paddle), or gas flow. The impeller provides great shear so large portions are moved at relatively high rates which causes changes at a microscopic scale and produces fine particles (Niranjan, Smith, Rielly, Lindley, & Phillips, 1994; Ortega-Rivas et al., 2006, chaps. 3, 6, 9, 12). The rate of mixing by diffusion is low compared with convective mixing so it can cause less breakage but pure diffusion mixing is exceedingly slow. Shear mixing is induced by the momentum exchange of powder particles having different velocities. Mixing due to shear force occurs and is developed by the formation of slipping planes in the bulk material (Lindley, 1991b; Rhodes, 2008). The originally coherent particle groups are compressed and extended then gradually broken along these planes.

Dry-mixing is a basic and important process for a range of industries that includes pharmaceutical, chemical, agriculture, material, and food (Pernenkil & Cooney, 2006). For example, the slightest changes in the ingredient properties or the process operating conditions for the manufacturing of a drug can have a huge impact on its quality (Bertrand, Leclaire, & Levecque, 2005). In flour milling, dust generation is a primary concern (Bemrose & Bridgwater, 1987). Duraccio et al. (2019) used three different dry-mixing techniques followed by a compression molding step to prepare medical composites and found that the dry-mixing techniques affected the structural and morphological features of the composites that, in turn, influenced the mechanical

behaviour. Portillo, Ierapetritou, and Muzzio (2008) also mentioned that in cases where the sample was agglomerated, increasing the intensity of the mixing mechanism could reduce the size of agglomerates when they characterized the continuous convective powder mixing processes.

5.2. Breakage during in-plant transportation

Agglomerated dairy powders must be transported from the fluidized bed via an intermediate silo to a filling line or a storage silo. The conveying distances involved are typically 50–200 m in the horizontal direction, and 10–20 m in the vertical direction (Hanley, 2011). Mechanical transfer systems are needed for powder transportation from a low level to a higher level of the silo entrance. There are many different mechanical transfer systems for dry particulate materials, such as transport screws, bucket elevators, and belts (Go Yanko, 2007). Boiarkina et al. (2016) found that the breakage of instant whole milk powder occurred during transportation using a bucket elevator. However, these conveyors have rarely been selected for dairy powder transportation because of the distances, hygienic operations, and cleaning (Go Yanko, 2007). Pneumatic conveying is a widely used method for dairy powder transportation because it has several advantages such as hygiene, the flexibility of routing, and easily automated (Boiarkina et al., 2016; Go Yanko, 2007; Kotzur et al., 2018). Thus, this section will mainly focus on the breakage during pneumatic conveying. For the same particles, parameters affecting the extent of breakage during the pneumatic conveying can be divided practically into operation parameters (velocity and particle concentration) and pipeline structure (bend radius and number of bends).

5.2.1. Operation parameters

There are two major pneumatic conveying regimes, dilute phase, and dense phase. Dilute phase pneumatic conveying is defined as the condition where all particles are suspended in the airflow, and it requires high superficial air velocities and low particle concentrations within the pipeline. Dense phase pneumatic conveying is characterized by particles populating the entire cross-section of the pipeline, and particles moving through the pipe in batches separated by air pockets. This form of conveying generally needs low superficial air velocities and high particle concentrations.

The dilute phase has been linked with high particle breakage due to the requirement of high superficial air velocities which results in high-energy impacts against the walls and bends (Kalman, 1999). Some research on IMF and WPI breakage in dilute phase pneumatic conveying found that the extent of breakage increased with increasing air velocities (Han et al., 2020; Hanley, 2011; Zhang et al., 2020). The same results were found in some studies on the breakage of general-purpose fertilizers in impact experiments or dilute phase pneumatic conveying (Salman et al., 2002, 2003). Salman et al. (2002) found that a threshold velocity existed in the single-particle impact studies, and below the threshold velocity, no breakage occurred. Another reason for the dilute phase resulting in high breakage is the low particle concentration in the pipeline. Based on some studies on particle breakage in dilute phase pneumatic conveying with different powder materials (such as IMF with large particle sizes between 710 μm and 850 μm, wood dust, Silica flour, Olivine sand, and sea salt), particle breakage decreases with increasing particle concentration (Han et al., 2003; Hanley, 2011; Macchini, Bradley, & Deng, 2013; McKee, Dyakowski, Williams, Bell, & Allen, 1995). This phenomenon is always explained by the shielding effect where high-velocity particle-pipeline impacts are partially mitigated by inter-particle contacts, thus only a fraction of the conveyed particles come into direct contact with the pipeline (Kotzur et al., 2018; Macchini et al., 2013).

5.2.2. Pipeline structure

Particle to particle interactions and impacts against pipeline walls and bends are thought to be the predominant causes of particle breakage in pneumatic conveying (Brosh, Kalman, & Levy, 2010; Kotzur et al., 2018). Among them, particles experience extensive impact loads mainly at the bends because the flow direction is changing. In addition, the mean inter-particle collision velocity is generally much lower than the normal impact velocity at the pipeline bends, thus, some researchers mainly considered the impact between particle and bends (Hanley, Byrne, & Cronin, 2013). Particle breakage due to impact at bends depends on the balance between the resulting impact force and is influenced by the bend radius and numbers.

Breakage occurs if the impact force between the particle and bend exceeds the intrinsic strength of the particle (Hanley et al., 2013). The collision velocity, angle, and elasticity of the collision significantly affect the impact force (Kalman, 2000). When particles collide with a wall at some slope, the impact can be divided into two components, normal and tangential (Kalman, 2000). The tangential component causes a slight slide and shear loads. The impact force is proportional to the normal impact velocity that causes the main breakage (Hanley et al., 2013). The normal component decreases with decreasing collision angle and at 90° when the particle collides with the wall perpendicular it becomes maximum. Single-particle impact research (Salman et al., 2003) showed that the breakage probability of a fertilizer particle at a given speed varied slowly with impact angles from 90° down to about 50°, but then decreased rapidly below 50°. At 10° only a limited amount of damage occurred. Similar results were found during the pneumatic conveying of feed pellets for livestock, showing that the fraction of broken particles was fairly similar for impact angles between 50° and 90° while for lower impact angles (<50°), the particle fracture decreased with the decreasing impact angle (Aarseth, 2004). Additional results in the literature that support the findings have been presented on the effect of impact angle by simulation, demonstrating that the energy dissipated in the collision remains relatively constant from 90 to about 50–60°, dropping significantly below that (Tavares et al., 2018). The radius of bends is an important factor affecting the impact angle, and the collision angle will decrease with increasing radius. At the same time, the radius also influences the elasticity of the collision, and particles are expected to be subjected to a few impacts in long radius bends (Kalman, 1999). Thus, short radius bends produce more breakage because of the high impact angle and the elasticity of the collision. In a study on the breakage of IMF in pneumatic conveying, it was found that the radius of bends significantly influenced the breakage, which then influenced the bulk density of powders (Hanley, 2011). Aarseth (2004) investigated the effects of bend radius on the breakage of commercial feeds during pneumatic conveying and found that a shorter bend radius resulted in more breakage for all conveying velocities (20–50 m/s) relative to bends of the longer radius.

Particles can also be broken due to lower impact loads than their strength when the collision occurs many times, which is known as fatigue (Goder, Kalman, & Ullmann, 2002; Kalman, 1999, 2000). In actual factories, powders are transported repeatedly through processes for receiving, storage, re-processing, and packing (Konami, Tanaka, & Matsumoto, 2002). Thus, the breakage that results from repetitive transport should be taken into account. The number of impacts is affected by the number of bends in the system and the elasticity of collision. The breakage is more sensitive to the number of impacts when the extent of breakage at the first impact is low (Samimi, Ghadiri, Boerefijn, Groot, & Kohlus, 2003). In the research on the relationship between the number of impacts and breakage of fertilizer particles, it was found that the number of impacts showed no effect on the breakage at three experimental impact velocities, while similar tests with polystyrene particles found a linear increase in the breakage with increasing impact number (Salman et al., 2002). Therefore, whether the breakage is affected by the number of impacts is dependent on the material of the particles.

5.3. Breakage during vibration

There is a long-distance for dairy powders from the production factories to customers, and once the product leaves the factory, breakage may still occur due to handling and transportation. **Surface** transportation by rail or road particularlysportation by rail or road **particularly** imposes multiple strains to the particulate material, and the vibration is inevitable. Breakage can be caused by the relative movement between particles induced by vibration in a bed of particles by using either a form of resonance or a simple mechanical motion transmitted from a container to the particles (Ortega-Rivas et al., 2006, chaps. 3, 6, 9, 12). When a container of powder is subject to vibration, in most cases, particles are rearranged and fine particles percolate through the coarse particles and fill the voids, so powder settles and the bulk density of powders increases (Ortega-Rivas et al., 2006, chaps. 3, 6, 9, 12).

Vibration tests in a container or on a sieve have been used to study the breakage tendency of particulate systems and determine agglomerated powders' friability which is defined as the tendency of particles to break down during storage and handling (Ortega-Rivas et al., 2006, chaps. 3, 6, 9, 12). The vibration intensity of the particles depends on particle size and density, vibration frequency and amplitude, and the depth of the bed of particles (Barletta, Kinight, & Barbosa-Cánovas, 1993; Bemrose & Bridgwater, 1987). A commercial tapping density tester was used to study the breakage tendency of instant coffee and milk powders (Barletta & Barbosa-Cánovas, 1993a, 1993b; Yan & Barbosa-Cánovas, 2001a). Remarkable bulk density changes were noticed for all tapping tests, especially at high tapping numbers. Gerhard et al. (2004) presented a vibration test that could be performed on any laboratory sieving machine to measure the breakage of agglomerated cocoa beverage powders and the particle size of powders significantly decreased. The breakage of ferric oxide granules during a tapping-test showed that the mechanism of breakage was mainly the interaction of granules themselves in the whole granule layer (Utsumi et al., 2001). The tapping of agglomerated instant coffee confined in a cylindrical container generated significant breakage where the particle size distribution shifted from a unimodal to a bimodal distribution and a lot of small-sized particles were produced (Barletta et al., 1993).

The process conditions (summarized in Table 2) play a fundamental role in the determination of dairy powders breakage and that, together with particle characteristics, dictates the response of a particle for a given loading condition (Antonyuk et al., 2005; Lu, Liu, Zhu, & Qu, 2014).

6. Influencing factors - particle characteristics

In addition to the applied stress, powder breakage depends on the powder strength, which is influenced by powder physical properties (particle size and PSD, powder porosity, and morphology) and composition (ingredients and moisture content). The powder properties

Table 2
Summary of the influence of processing conditions on the breakage of powders or particles.

Processing methods	Processing conditions	Trends or key points	Industries or powder materials	References
Dry-mixing	**Mixing mechanisms or rates**	• In convective mixing, large portions are moved at relatively high rates which causes a high extent of breakage. • The rate of mixing by diffusive is low compared with convective mixing so it could cause less breakage.	• Flour milling; • Manufacturing of drugs; • Preparing medical composites; • Blending pharmaceutical formulation;	(Bertrand et al., 2005; Duraccio et al., 2019; Niranjan et al., 1994; Ortega-Rivas et al., 2006, chaps. 3, 6, 9, 12; Portillo et al., 2008)
Transportation using bucket elevators	–	• Broken agglomerated powder.	• Dairy powders (IMP);	Boiarkina et al. (2016)
Pneumatic conveying	**Air velocity**	• Particle breakage increases with increasing air velocity which results in high-energy impacts against the walls and bends. • A threshold velocity existed in the single-particle impact studies, and below the threshold velocity, no breakage occurred.	• Dairy powders (IMF and WPI); • Fertilizer granules;	(Han et al., 2020; Hanley, 2011; Kalman, 1999; Salman et al., 2002, 2003; Zhang et al., 2020)
	Particle concentration	• Particle breakage decreases with increasing particle concentration, which may be caused by the shielding effect. • The increasing particle concentration increases inter-particle collisions leading to a wider distribution of impact velocities and impact angles.	• Dairy powders (IMF); • Wood dust; • Silica flour; • Olivine sand; • Sea salt;	(Han et al., 2003; Hanley, 2011; Macchini et al., 2013; McKee et al., 1995)
	Bend radius	• Particle breakage decreases with increasing pipe bend radius which decreases the collision angles and the number of collisions.	• Dairy powders (IMF); • Feed pellets for livestock; • Fertilizer granules;	(Aarseth, 2004; Hanley, 2011; Kalman, 1999; Salman et al., 2003; Tavares et al., 2018)
	Number of bends or collisions	• Particle breakage increases with increasing number of bends. • Particles can also be broken due to lower impact loads than their strength when the collision occurs many times (fatigue).	• Fertilizer granules; • Polystyrene particles; • Tungsten-carbide tablets;	(Goder et al., 2002; Kalman, 1999, 2000; Konami et al., 2002; Salman et al., 2002; Samimi et al., 2003)
Vibration	**Vibration frequency, amplitude, and numbers**	• Particles are rearranged and fine particles percolate through the coarse particles and fill the voids so powder settle and the bulk density of powders increases. • High tapping numbers causes a high extent of breakage.	• Instant coffee; • Ferric oxide granules; • Agglomerated cocoa beverage powders; • Dairy powders (IMP);	(Barletta & Barbosa-Cánovas, 1993a, 1993b; Barletta et al., 1993; Gerhards et al., 2004; Ortega-Rivas et al., 2006, chaps. 3, 6, 9, 12; Utsumi et al., 2001; Yan & Barbosa-Cánovas, 2001a)

1. - Not applicable. IMP: instant milk powder. IMF: infant milk formula. WPI: whey protein isolate powder.

(summarized in Table 3) influencing dairy powder breakage could be manipulated to control breakage.

6.1. Powder physical properties

6.1.1. Particle size and porosity

It has been repeatedly demonstrated that particle strength decreases with increasing particle size (Bonakdar et al., 2016; Gerhards, Kaell, & Schubert, 2004; Norazirah et al., 2016; Zhang & Ghadiri, 2002). This is attributed to the likelihood of a greater number of imperfections in larger particles, which in turn provides a greater number of cracks which may propagate as a result of an imposed load (Antonyuk et al., 2005; Norazirah et al., 2016). Large particle size and the porous structure can be obtained after agglomeration, which is necessary for sufficient rehydration properties and flowability. The porosity and its shape, orientation, and size distribution have a large effect on the breakage of the agglomerates. The pore can be regarded as a crack release zone (Antonyuk et al., 2005). The pores and the structural defects in agglomerates are analogous to imperfections, inhomogeneities, or microcracks in material science. The highest local tensile stress is generated at these defective zones in the agglomerates so that the fracture initiates from this zone. The number of contact points of a primary particle can be decreased with larger porosities, by which the strength of agglomerates decreases (Antonyuk et al., 2005). Besides the few flaws and low porosity, small particles are more difficult to break owing to the stronger interparticle forces that bind particles together including van der Waals forces, electrostatics, and liquid bonds (Reynolds et al., 2005). From an energy perspective, the probability of breakage is related to the amount of energy that is absorbed by the particle during the impact (if breakage is caused by the impact). The particle is able to absorb a certain amount of energy before it breaks during a collision. When a particle is subject to impact stress, it initially deforms elastically, absorbing impact energy as stored elastic strain. The internal stresses in the particle increase until a crack occurs at the most sensitive part. The stored elastic strain energy in the particle drives the growing crack and any remaining stored elastic energy is dissipated as the kinetic energy of the child particles. The energy that is absorbed and stored represents the minimum energy that is required to break the particle under the particular external loading and stress pattern that the particle experiences. This energy is called the particle fracture energy and it is a material property that is influenced by its particle size, shape, the orientation that the particle presents to the impact stress, and the presence of flaws in the particle. For particles of the same material, the smaller the particles, the higher the fracture energy, and hence the less likely the particle will break (King, 2012).

It was found that the breakage of IMF and WPI was very sensitive to the particle size of powders during the pneumatic conveying (Han et al., 2021; Zhang et al., 2020). The breakage of IMF increased with increasing particle size at the same processing conditions, and for WPI, there appeared to be a threshold size below which breakage was almost negligible. Three industrial spherical agglomerates, γ-Al_2O_3, synthetic zeolite, and sodium benzoate, were used as model materials in a single-particle compression test to study the mechanical behaviour of agglomerates from elastic to the plastic range during the breakage (Antonyuk et al., 2005). It was shown that more mass-related breakage energy was needed to break off smaller agglomerates than bigger ones. Compression tests were used to characterize the breakage of agglomerated skim milk powder, low-fat milk powder, and instant coffee powder (Yan & Barbosa-Cánovas, 1997). Particle size played a significant role in compression tests in that the greater the particle size, the greater the volume reduction. The same results were found in the compression test of crystalline α-lactose monohydrate (Fu et al., 2012). The big particle-sized sample was more compressible than the small-sized one. In tapping tests, the larger the agglomerates, the higher the breakage index which was defined as the ratio of the weight fraction of fines generated in the breakage test to that of the agglomerates retaining their original particle size (Yan & Barbosa-Cánovas, 2001a). Ghadiri et al. (1991) investigated the breakage of salt crystals using a single-particle impact test and micro-indentation. It was found that big-sized particles suffered more breakage than the smaller sized particles at all velocities, irrespective of which basis was used for breakage. During the breakage of lactose crystals, the particle size markedly affected breakage and the attrition index of the big-sized crystal (250–300 μm) was much higher than that of small-sized lactose (150–180 μm) (Agrawal et al., 2011).

6.1.2. Particle size distribution

It has been found that the PSD of the particulate material significantly influenced the breakage of particles. The extent of breakage is reduced with an increasing fine particle ratio (mass fraction). Presumably, that is because the particles enclose the coarse granules and thereby act as a cushioning medium that reduces the granule stress and levels of attrition, which is attributed to the cushioning action of fines (Konami et al., 2002). In the case of two types of cement clinkers and two types of coals, the breakage of all sizes slowed down significantly when the number of fines exceeded a certain limit in individual cases (Gupta, 2017). For IMF samples with the same median particle size (D_{50}, taken from the volume PSD), a narrowing of the PSD corresponded to a reduction of powder strength (Han et al., 2021).

6.1.3. Particle size and distribution of primary particles

It is generally assumed that high granule strength is associated with small primary particle size. It was found that the formulation parameters viscosity and primary particle size determined the eventual particle strength during the production of agglomerated lactose in a high shear mixer (van den Dries, de Vegt, Girard, & Vromans, 2003). A decreasing primary particle size increases the strength of agglomerates, which eventually leads to a clear reduction of the breakage. The large particle size results in a loose agglomerate structure and weak agglomerates that can easily be broken down (other agglomeration conditions are consistent) because smaller primary particles have a higher affinity for the layering agglomeration than coarser primary particles (Johansen & Schæfer, 2001; Keningley, Knight, & Marson, 1997; van den Dries et al., 2003). The layering mechanism is a way of agglomeration where small particles become layered on larger particles, combined with coalescence between the smallest particles. During the agglomeration of calcium carbonates, it was found that a narrowing of the PSD of primary particles corresponded to a reduction in the agglomerate strength because of the limitation of the layering mechanism (Johansen & Schæfer, 2001). The size of powder primary particles depends on the type of atomization and drying conditions (Moejes & van Boxtel, 2017).

6.1.4. Morphology

There is a heavy dependence upon the agglomerate shape and structure as to the type and extent of breakage (Golchert, Moreno, Ghadiri, & Litster, 2004; Norazirah et al., 2016). Different particle shapes have been the subject of different particles breakage studies, such as spherical particles, cubic crystalline particles, flaky particles, equidimensional shape, and irregular agglomerates (Golchert et al., 2004; Norazirah et al., 2016; Samimi et al., 2003). DEM simulation results show that the breakage behaviour of spherical, cuboidal, and cylindrical agglomerates differ from each other because for non-spherical agglomerates, the degree of breakage depends not only on the impact speed, impact angle, and interface energy but also on agglomerate orientation (Liu et al., 2010). The spherical particles follow classical tensile fracture behaviour by breaking along a fracture plane through the middle of the particle, with a limited number of contacts broken within the particle. In contrast, the load on the irregular particles until a sharp critical value causes the particle to shatter. The results of numerical compression studies on the breakage of spheres or irregular particles with DEM showed that spherical particles could break down at low impact energies along one or more fracture planes, producing a small number of large fragments and only 3% of contacts were broken (Golchert et al., 2004).

Table 3
Summary of the influence of particle characteristics on the breakage of powders or particles.

The characteristics of particles		Trends or key points	Industries or sample materials	References
Physical properties	**Particle size and porosity**	• Particle breakage increases with increasing particle size due to the likelihood of a greater number of imperfections in larger particles. • Particle breakage increases with increasing porosity because pores are analogous to imperfections and the number of contact points of primary particles decreases with increasing porosity. • The highest local tensile stress is generated at imperfections so that the fracture initiates from these zones. • Small particles are more difficult to break owing to the few flaws, the stronger interparticle forces, and the lowering of the collision energy.	• Dairy powders (IMF, WPI, SMP, LFMP, and lactose crystals); • Food powders (Instant coffee, salt crystals, and cocoa beverage powders); • Industrial agglomerates (γ-Al_2O_3, the synthetic zeolite, and sodium benzoate); • Pegmatite; • Burkeite particles; • Single crystals of MgO, NaCl, and KCl; • Detergent particles;	(Agrawal et al., 2011; Antonyuk et al., 2005; Bonakdar et al., 2016; Fu et al., 2012; Gerhards et al., 2004; Ghadiri et al., 1991; Han et al., 2021; Norazirah et al., 2016; Samimi et al., 2003; Yan & Barbosa-Cánovas, 1997; Yan & Barbosa-Cánovas, 2001a; Zhang et al., 2020; Zhang & Ghadiri, 2002)
	PSD	• Particle breakage decreases with increasing the fine particle ratio (mass fraction) due to the cushioning action of fines. • Particles enclose the coarse granules and thereby act as a cushioning medium.	• Dairy powders (IMF); • Cement clinkers; • Coals; • Tungsten-carbide tablets;	(Gupta, 2017; Han et al., 2021; Konami et al., 2002)
	Morphology	• The more alike to the sphere, the higher the particle strength. • For non-spherical agglomerates, breakage depends not only on the impact speed, impact angle, and interface energy but also on agglomerate orientation. • Spherical particles can break down along one or more fracture planes, producing a small number of large fragments, while irregular particles exhibit much more non-uniform loading, causing the forces to permeate through the particle, rather than along a particular plane or axis.	• Dairy powders (crystalline α-lactose monohydrate); • DEM model agglomerates (spherical, cuboidal, cylindrical, or different fractal dimensions); • Pegmatite;	(Deng & Davé, 2017; Fu et al., 2012; Golchert et al., 2004; Liu et al., 2010; Norazirah et al., 2016)
	Particle size and PSD of primary particles	• A decreasing primary particle size increases the agglomerates' strength and large primary particles result in a loose agglomerate structure and weak agglomerates. • A narrowing of the PSD of primary particles corresponds to a reduction in the agglomerate strength because of the limitation of the layering mechanism.	• Dairy powders (agglomerated lactose); • Agglomerated calcium carbonates;	(Johansen & Schæfer, 2001; Keningley et al., 1997; van den Dries et al., 2003)
Powder composition	**Protein**	• In some situations, the higher the protein content or protein to fat ratio, the higher the particle strength.	• Dairy powders (IMF);	(Hanley, 2011; Hanley, Cronin, et al., 2011)
	Fat	• Fat reduces the strength of dairy powders. • Fat liquefaction can soften the powder.	• Dairy powders (SMP, high-fat milk powder, WMP, and LFMP);	(Rennie et al., 1999; Yan & Barbosa-Cánovas, 1997)
	Lactose	• Increasing the percentage of carbohydrates increases the stiffness of infant milk formula. • When lactose is in solid-state, it can be in a crystalline state or an amorphous state: • Compared to tightly packed molecules in the crystalline state, lactose molecules in the amorphous state are disordered, forming a more open and porous structure, which makes powders more easily deformed and compacted. • Crystalline materials exhibit elasticity and brittleness upon exposure to external stress, while molecules in the amorphous state tend to exhibit varying degrees of viscoelasticity. • The mechanical strength of amorphous solids is brittle or fragile, while that of crystalline solids is strong.	• Dairy powders (IMF); • Food powders (lactose-sugars systems, including in glucose, maltose, sucrose, trehalose, and corn syrup solids);	(Hanley, 2011; Li et al., 2017, 2019)
	Binders	• The strength or particle size of agglomerates obtained using different kinds of binders is different. • Sucrose or glucose usually produces hard and brittle bridges while gelatin and acacia gum provide slow disintegration and high hardness to the agglomerates.	• Agglomerates of microcrystalline; • Dairy powders (agglomerated MPI, lactose monohydrate); • Cylindrical pellets (glass ballotini with a range of binders); • Agglomerated calcium carbonates;	(Eliasen et al., 1998; Ji et al., 2015; Johansen & Schæfer, 2001; Iveson & Litster, 1998; van den Dries et al., 2003; Zajic & Buckton, 1990)

(*continued on next page*)

Table 3 (*continued*)

The characteristics of particles	Trends or key points	Industries or sample materials	References
	• Using water as a binder creates more irregular agglomerated MPI than using lactose and sucrose and the larger agglomerate size fraction is produced with the lactose binder. • A high viscosity binder increases the strength of agglomerates. • The dynamic yield strength of agglomerates decreases with decreasing binder surface tension.	• Agglomerates (lactose and hydroxypropylcellulose);	
Moisture	• Drying strengthens the agglomerates presumably due to the solidification of bridges while humidifying the granules decreases their strength. • Increased moisture content can soften the powder material, resulting in the deformation of the powder. • There is lower yield stress and larger plastic deformation during the breakage of the humidified samples when compared to the dry samples. • The particle surface is altered by solubilization, liquid layer formation, or local plasticization, which influences the properties of binders thus influences the particle strength.	• Dairy powders (SMP and WMP); • Detergent granules;	(Rennie et al., 1999; Samimi et al., 2003; Yan & Barbosa-Cánovas, 2001a)

1. IMF: infant milk formula. WPI: whey protein isolate powder. SMP: skim milk powder. LFMP: low-fat (2%) milk powder. PSD: particle size distribution. WMP: whole milk powder. MPI: milk protein isolate powder.

The resistance to breakage at low compression distance could be due to the external spherical shape of the agglomerate. The irregular particles exhibited much more non-uniform loading than the spherical particles, causing the forces to permeate through the particle, rather than along a particular plane or axis and 14.2% of the total contacts were broken.

The more alike to the sphere, the higher the particle strength. DEM simulations were conducted to investigate the breakage of fractal agglomerates with fractal dimensions ranging from about 2.0 to 2.8 (Deng & Davé, 2017). The fractal dimension can vary from 1 to 3, corresponding respectively to a chain-like structure and spherical agglomerate. Simulation results showed that the damage ratio decreased with increasing fractal dimension in the range between 2.0 and 2.6. With the further increase of the fractal dimension, the damage ratio showed an asymptotic behaviour. Two crystalline α-lactose monohydrate samples with the same particle size but different shapes were used to analyse the effect of particle shape on the compressibility (Fu et al., 2012). It was found that the sample with irregular shape was more compressible than the sample that was more spherical. Samimi et al. (2003) studied the impact breakage of two types of detergent particles from different processes and exhibiting different structures. One type was denser and more spherical, and the other type had a more cauliflower-type structure and was more porous. It was found that the former exhibited less breakage than the latter. In terms of application, this means that the morphology of agglomerates may be an important part of controlling unwanted breakage.

Primary dairy powder particles are usually spherical whereas agglomerated particles are irregular (Kim, Chen, & Pearce, 2005). Three parameters were generally used to quantify and indicate the morphology of powders, circularity, convexity, and elongation (Ji, Cronin, Fitzpatrick, Fenelon, & Miao, 2015). The bigger circularity value means that the particles are more spherical. The maximum theoretical convexity is 1 that means the surface of the particle is very smooth. Elongation stands for aspect ratio of particles and a needle shape has a high value which is close to 1. The circularity, convexity, and elongation of un-agglomerated milk protein isolate were around 0.85, 0.95, and 0.2, respectively (Ji et al., 2015). After agglomeration using a laboratory fluidized bed, those three measures changed to 0.65, 0.75, and 0.28, respectively. However, there is currently no research on the influence of morphology on dairy powder breakage or strength.

6.2. *Powder composition*

6.2.1. *Protein*

In some situations, the higher the protein content or protein to fat ratio, the higher the particle strength. Four typical IMFs with different protein to fat ratios but the same particle size range (710–850 μm), were used to investigate the influence of protein and fat content on the breakage of IMF during the compression test and laboratory-scale dilute phase pneumatic conveying (Hanley, 2011; Hanley, Cronin, et al., 2011). As conveying velocity increased, the increases of the bulk density for those two samples containing the least protein were considerably greater than others, indicating that more breakage occurred for two IMFs with lower protein contents. The possible reason was as the percentage of protein increased, the bulk densities of samples increased accordingly before conveying, which increased powder strength. The results of the compression test showed that the force at breakage generally increased with increasing protein to fat ratio. As the description in 3.1, the maximum applied force can be taken as the particle strength in the single-particle compression test. Increasing the protein content caused an increase in the mean force and a decrease in the mean strain at breakage. This also explained why these samples showed the least variation in bulk density during pneumatic conveying. However, more research on the influence of protein content and different kinds of milk proteins on breakage is needed.

6.2.2. Fat

Current results suggest that fat reduces the strength of dairy powders. Compression characteristics of agglomerated instant non-fat milk and low-fat milk powder with the same particle size range were analysed using a texture analyser (Yan & Barbosa-Cánovas, 1997). The force-deformation data showed that compared with the non-fat milk powder, it was easier to compress low-fat milk powder, especially for samples with particle sizes of 212, 300, and 425 μm. This might be because fat liquefaction could soften powders, resulting in the easy deformation of powder particles during compression (Rennie, Chen, Hargreaves, & Mackereth, 1999).

6.2.3. Lactose

According to the research on the breakage of IMF, increasing the percentage of carbohydrates increased agglomerate stiffness (Hanley, 2011). Lactose is an important source of carbohydrate for infant milk formula. Hazlett et al. investigated the breakage of IMF (initial particle size: 252 μm; protein: 8.52% and fat: 25.6%; the decrease of particle size after breakage: 23%) and agglomerated WPC (initial particle size: 209 μm; protein: 80.0% and fat: 8.5%; the decrease of particle size after breakage: 26%) during a simulated pneumatic conveying (Hazlett et al., 2020). It was found that the particle size of IMF was bigger than that of WPC while the breakage of IMF was lower so the high concentration of lactose in IMF might increase its strength. But more studies are needed to analyse if the increase in lactose content is positively correlated with the increase in powder strength.

When lactose is in solid-state, it can be in a crystalline state or an amorphous state. Amorphous powders show good compressibility, low density, and high internal porosity, which makes powders more easily deformed and compacted. This is because compared to tightly packed molecules in the crystalline state, lactose molecules in the amorphous state are disordered, forming a more open and porous structure (Li, Roos, & Miao, 2017). The mechanical strength of amorphous solids is brittle or fragile, while that of crystalline solids is strong (Li et al., 2019). Typically, most crystalline materials tend to exhibit high levels of elasticity and brittleness upon exposure to external stress and may fracture along cleavage planes. By contrast, molecules in the amorphous state tend to exhibit varying degrees of viscoelasticity.

6.2.4. Binders

Fluidized bed agglomeration, as one of the most used agglomeration methods during dairy powder production, is a process by which agglomerated particles are obtained by spraying a binder as a solution, suspension, or melt onto a fluidized powder bed and then coalescing and agglomerating together by creating solid bridges between primary particles (Ji et al., 2015). Thus, binders are one of the important factors which influence particle properties including particle size, density, morphology, and strength (Iveson & Litster, 1998; Keningley et al., 1997). In food systems, aqueous solutions of lactose and sucrose are the most used binders in fluid bed agglomeration and a lot of other binders have been studied, such as dextrose, gelatin, and starch (Onwulata, 2005, pp. 39–142). Binders have different effects due to varied chemical compositions, mechanical properties, concentration, viscosity, and inter-particular interactions between the particles and the binders.

Firstly, the strength or particle size of agglomerates obtained using different kinds of binders is different. For example, sucrose or glucose usually produces hard and brittle bridges while gelatin and acacia gum provide slow disintegration and high hardness to the agglomerates (Ji et al., 2015). Agglomerates of microcrystalline cellulose were made using hydroxypropylmethylcellulose (HPMC), polyvinylpyrrolidone, and water as binding agents (Zajic & Buckton, 1990). Agglomerates made with HPMC were less friable and larger particle size than most of the other particles that were produced with the other two binders. Three different binders, water, lactose, and sucrose solution (15% *w/v*) were used to agglomerate milk protein isolate powder in a laboratory-scale fluidized bed (Ji et al., 2015). It was found that using water as a binder created more irregular particles than using the other two sugar binders while the larger agglomerate size fraction was produced with the lactose binder. In addition, it is also generally found that the strength of agglomerates shows strong viscosity effects and a high viscosity binder increases the strength of agglomerates (Iveson & Litster, 1998; Johansen & Schæfer, 2001; van den Dries et al., 2003). During the agglomeration of lactose monohydrate in a high shear mixer, a lower binder viscosity caused high porosity and decreased the strength of agglomerates (Eliasen, Schæfer, & Gjelstrup Kristensen, 1998). Increasing binder viscosity increases the agglomerates' dynamic yield stress, and for high viscosity binders, increasing binder content increases this yield stress (Iveson & Litster, 1998). During the agglomeration of calcium carbonates in a high shear mixer with a larger primary powder particle size, a high binder viscosity was necessary to achieve an agglomerate strength being sufficient to avoid breakage (Johansen & Schæfer, 2001). At the same time, to produce spherical agglomerates, a low viscosity binder had to be chosen when agglomerating a powder with small particle size, and a high viscosity binder must be applied for large particles. Furthermore, binder surface tension plays a role in determining granule strength by causing capillary force between primary particles (Iveson & Litster, 1998). Decreases in binder surface tension decrease the dynamic yield strength of agglomerates.

It should be noted that the mechanical characteristics of primary particles and bonding agents are randomly distributed within agglomerates. Even with the identical production process, the strength of the individual agglomerates differs in the microstructure because of the distribution and orientation of bonds, defects, and pore size distribution (Antonyuk et al., 2005).

6.2.5. Moisture content

Generally, the increase in moisture content within a certain range can reduce powder strength. All powders tend to absorb moisture from the air and then have two kinds of changes (Yan & Barbosa-Cánovas, 2001a). The first one is that the solid material softens and becomes plasticized. Increased moisture content can soften the powder material, especially the water-soluble constituents, which would result in the deformation of powders and the decrease of strength (Kim et al., 2005; Rennie et al., 1999). The second one is that the particle surface is altered by solubilization, liquid layer formation, or local plasticization, which influences the properties of binders and thus influences the particle strength. Solid bridge formation is the dominant agglomeration mechanism for materials in the agglomerated state and is mainly due to the crystallization of binders (lactose for example). Drying strengthens the agglomerates presumably due to the solidification of bridges while humidifying the granules decreases their strength (Samimi et al., 2003). There are lower yield stress and larger plastic deformation during the breakage of the humidified samples compared to the dry samples. For humidified agglomerates, a larger portion of the kinetic energy is dissipated during impact as plastic deformation or ductile failure (shown as stretching and the rupture of interparticle bonds) (Samimi et al., 2003). For agglomerated skim milk powder, the higher the water activity, the greater the breakage during the vibration test (Yan & Barbosa-Cánovas, 2001a).

7. Conclusion

Agglomerated dairy powder breakage usually occurs during production and transportation and may significantly impact dairy powder physical properties and functionalities. The influence of breakage on powder properties depends on the extent of breakage caused by different breakage mechanisms. The characteristics of particles and processing conditions are two main factors that influence breakage and can be considered to control dairy powder breakage. The processing conditions include the parameters during dry-mixing, vibration, and pneumatic conveying. The physical properties and the composition of powders can also dictate the response of powders for a given loading condition by

influencing the powder strength. Further research on the factors that control dairy powder breakage and their effectiveness is required. The methods suitable for investigating dairy powder breakage include single-particle or multi-particle tests. Both types of tests complement each other, single-particle tests providing fundamental information about particle breakage and multi-particle methods mimicking real industrial situations.

Acknowledgment

This work was supported financially by the Teagasc, Agriculture and Food Development Authority under the project MDDT 0153 entitled 'Powder breakage and functionality of dairy powders'.

References

Aarseth, K. A. (2004). Attrition of feed pellets during pneumatic conveying: The influence of velocity and bend radius. *Biosystems Engineering, 89*, 197–213.
Agrawal, S. G., Balandier, A., Paterson, A. H. J., & Jones, J. R. (2011). Study on lactose attrition inside the mixing cell of a laser diffraction particle sizer using a novel attrition index. *Powder Technology, 208*, 669–675.
Antonyuk, S., Tomas, J., Heinrich, S., & Mörl, L. (2005). Breakage behaviour of spherical granulates by compression. *Chemical Engineering Science, 60*, 4031–4044.
Barletta, B. J., & Barbosa-Cánovas, G. V. (1993a). An attrition index to assess fines formation and particle size reduction in tapped agglomerated food powders. *Powder Technology, 77*, 89–93.
Barletta, B. J., & Barbosa-Cánovas, G. V. (1993b). Fractal analysis to characterize ruggedness changes in tapped agglomerated food powders. *Journal of Food Science, 58*, 1030–1035.
Barletta, B. J., Kinight, K. M., & Barbosa-Cánovas, G. V. (1993). Compaction characteristics of agglomerated coffee during tapping. *Journal of Texture Studies, 24*, 253–268.
Bayham, S. C., Breault, R., & Monazam, E. (2016). Particulate solid attrition in CFB systems – an assessment for emerging technologies. *Powder Technology, 302*, 42–62.
Beekman, W. J., Meesters, G. M. H., Becker, T., Gaertner, A., Gebert, M., & Scarlett, B. (2003). Failure mechanism determination for industrial granules using a repeated compression test. *Powder Technology, 130*, 367–376.
Bemrose, C. R., & Bridgwater, J. (1987). A review of attrition and attrition test methods. *Powder Technology, 49*, 97–126.
Bertrand, F., Leclaire, L. A., & Levecque, G. (2005). DEM-based models for the mixing of granular materials. *Chemical Engineering Science, 60*, 2517–2531.
Bika, D. G., Gentzler, M., & Michaels, J. N. (2001). Mechanical properties of agglomerates. *Powder Technology, 117*, 98–112.
Bika, D., Tardos, G. I., Panmai, S., Farber, L., & Michaels, J. (2005). Strength and morphology of solid bridges in dry granules of pharmaceutical powders. *Powder Technology, 150*, 104–116.
Boiarkina, I., Sang, C., Depree, N., Prince-Pike, A., Yu, W., Wilson, D. I., et al. (2016). The significance of powder breakdown during conveying within industrial milk powder plants. *Advanced Powder Technology, 27*, 2363–2369.
Bonakdar, T., Ghadiri, M., Ahmadian, H., Martin de Juan, L., Xu, D., Tantawy, H., et al. (2016). Impact attrition of spray-dried burkeite particles. *Powder Technology, 304*, 2–7.
Bridgwater, J. (2010). Mixing of particles and powders: Where next? *Particuology, 8*, 563–567.
Bridgwater, J., Utsumi, R., Zhang, Z., & Tuladhar, T. (2003). Particle attrition due to shearing-the effects of stress, strain and particle shape. *Chemical Engineering Science, 58*, 4649–4665.
Brosh, T., Kalman, H., & Levy, A. (2010). DEM simulation of particle attrition in dilute-phase pneumatic conveying. *Granular Matter, 13*, 175–181.
Cleaver, J. A. S., Ghadiri, M., & Rolfe, N. (1993). Impact attrition of sodium carbonate monohydrate crystals. *Powder Technology, 76*, 15–22.
Deng, X., & Davé, R. N. (2017). Breakage of fractal agglomerates. *Chemical Engineering Science, 161*, 117–126.
van den Dries, K., de Vegt, O. M., Girard, V., & Vromans, H. (2003). Granule breakage phenomena in a high shear mixer; influence of process and formulation variables and consequences on granule homogeneity. *Powder Technology, 133*, 228–236.
Duraccio, D., Strongone, V., Faga, M. G., Auriemma, F., Mussano, F. D., Genova, T., et al. (2019). The role of different dry-mixing techniques on the mechanical and biological behavior of UHMWPE/alumina-zirconia composites for biomedical applications. *European Polymer Journal, 120*, Article 109274.
Einav, I. (2007). Breakage mechanics - Part I: Theory. *Journal of the Mechanics and Physics of Solids, 55*, 1274–1297.
Eliasen, H., Schæfer, T., & Gjelstrup Kristensen, H. (1998). Effects of binder rheology on melt agglomeration in a high shear mixer. *International Journal of Pharmaceutics, 176*, 73–83.
Forny, L., Marabi, A., & Palzer, S. (2011). Wetting, disintegration and dissolution of agglomerated water soluble powders. *Powder Technology, 206*, 72–78.
Fu, X., Huck, D., Makein, L., Armstrong, B., Willen, U., & Freeman, T. (2012). Effect of particle shape and size on flow properties of lactose powders. *Particuology, 10*, 203–208.
Gerhards, C., Kaell, C., & Schubert, H. (2004). Measurement of attrition of agglomerated cocoa beverage powders: A comparison of friabilator and vibration tests. *Journal of Food Engineering, 65*, 101–108.
Ghadiri, M., Yuregir, K. R., Pollock, H. M., Ross, J. D. J., & Rolfe, N. (1991). Influence of processing conditions on attrition of NaCl crystals. *Powder Technology, 65*, 311–320.
Ghadiri, M., & Zhang, Z. (2002). Impact attrition of particulate solids. Part 1: A theoretical model of chipping. *Chemical Engineering Science, 57*, 3659–3669.
Go Yanko, E. (2007). Hygienic engineering of transfer systems for dry particulate materials. *Trends in Food Science & Technology, 18*, 626–631.
Goalard, C., Samimi, A., Galet, L., Dodds, J. A., & Ghadiri, M. (2006). Characterization of the dispersion behavior of powders in liquids. *Particle & Particle Systems Characterization, 23*, 154–158.
Goder, D., Kalman, H., & Ullmann, A. (2002). Fatigue characteristics of granular materials. *Powder Technology, 122*, 19–25.
Golchert, D., Moreno, R., Ghadiri, M., & Litster, J. (2004). Effect of granule morphology on breakage behaviour during compression. *Powder Technology, 143–144*, 84–96.
Gupta, V. K. (2017). Effect of size distribution of the particulate material on the specific breakage rate of particles in dry ball milling. *Powder Technology, 305*, 714–722.
Gupta, V., Sun, X., Xu, W., Sarv, H., & Farzan, H. (2017). A discrete element method-based approach to predict the breakage of coal. *Advanced Powder Technology, 28*, 2665–2677.
Han, J., Fitzpatrick, J., Cronin, K., Maidannyk, V., & Miao, S. (2020). Breakage of infant milk formula through three different processing methods and its influence on powder properties. *Journal of Food Engineering, 282*, Article 109997.
Han, J., Fitzpatrick, J., Cronin, K., Maidannyk, V., & Miao, S. (2021). Particle size, powder properties and the breakage behaviour of infant milk formula. *Journal of Food Engineering, 292*, Article 110367.
Han, T., Levy, A., & Kalman, H. (2003). DEM simulation for attrition of salt during dilute-phase pneumatic conveying. *Powder Technology, 129*, 92–100.
Hanley, K. J. (2011). *Experimental quantification and modelling of attrition of infant formulae*. Cork, Ireland: Analytical Ph.D. thesis, University College Cork.
Hanley, K. J., Byrne, E. P., & Cronin, K. (2013). Probabilistic analysis of particle impact at a pipe bend in pneumatic conveying. *Powder Technology, 233*, 176–185.
Hanley, K. J., Byrne, E. P., Cronin, K., Oliveira, J. C., O'Mahony, J. A., & Fenelon, M. A. (2011). Effect of pneumatic conveying parameters on physical quality characteristics of infant formula. *Journal of Food Engineering, 106*, 236–244.
Hanley, K. J., Cronin, K., O'Sullivan, C., Fenelon, M. A., O'Mahony, J. A., & Byrne, E. P. (2011). Effect of composition on the mechanical response of agglomerates of infant formulae. *Journal of Food Engineering, 107*, 71–79.
Hazlett, R., Schmidmeier, C., & O'Mahony, J. A. (2020). Influence of mechanical integrity during pneumatic conveying on the bulk handling and rehydration properties of agglomerated dairy powders. *Journal of Food Engineering*, Article 110103.
Hogekamp, S., & Schubert, H. (2003). Rehydration of food powders. *Food Science and Technology International, 9*, 223–235.
Hu, X., Zhao, M., Li, L., Yang, B., Yang, X., Wang, H., et al. (2014). Emulsifying properties of cross-linking between proteins extracted from cold/hot pressed peanut meal and hydrolysed fish (Decapterus maruadsi) proteins. *International Journal of Food Properties, 17*, 1750–1762.
Iveson, S. M., & Litster, J. D. (1998). Liquid-bound granule impact deformation and coefficient of restitution. *Powder Technology, 99*, 234–242.
Jiang, Y. J., & Guo, M. (2014). 8 - processing technology for infant formula. In M. Guo (Ed.), *Human milk biochemistry and infant formula manufacturing technology* (pp. 211–229). Woodhead Publishing.
Ji, J., Cronin, K., Fitzpatrick, J., Fenelon, M., & Miao, S. (2015). Effects of fluid bed agglomeration on the structure modification and reconstitution behaviour of milk protein isolate powders. *Journal of Food Engineering, 167*, 175–182.
Ji, J., Cronin, K., Fitzpatrick, J., & Miao, S. (2017). Enhanced wetting behaviours of whey protein isolate powder: The different effects of lecithin addition by fluidised bed agglomeration and coating processes. *Food Hydrocolloids, 71*, 94–101.
Ji, J., Fitzpatrick, J., Cronin, K., Maguire, P., Zhang, H., & Miao, S. (2016). Rehydration behaviours of high protein dairy powders: The influence of agglomeration on wettability, dispersibility and solubility. *Food Hydrocolloids, 58*, 194–203.
Johansen, A., & Schæfer, T. (2001). Effects of interactions between powder particle size and binder viscosity on agglomerate growth mechanisms in a high shear mixer. *European Journal of Pharmaceutical Sciences, 12*, 297–309.
Kalman, H. (1999). Attrition control by pneumatic conveying. *Powder Technology, 104*, 214–220.
Kalman, H. (2000). Attrition of powders and granules at various bends during pneumatic conveying. *Powder Technology, 112*, 244–250.
Keningley, S. T., Knight, P. C., & Marson, A. D. (1997). An investigation into the effects of binder viscosity on agglomeration behaviour. *Powder Technology, 91*, 95–103.
Kent, R. M., Fitzgerald, G. F., Hill, C., Stanton, C., & Ross, R. P. (2015). Novel approaches to improve the intrinsic microbiological safety of powdered infant milk formula. *Nutrients, 7*, 1217–1244.
Kim, E. H. J., Chen, X. D., & Pearce, D. (2005). Effect of surface composition on the flowability of industrial spray-dried dairy powders. *Colloids and Surfaces B: Biointerfaces, 46*, 182–187.
King, R. P. (2012). Modeling and simulation of mineral processing systems. In *Society for mining, metallurgy, and exploration (SME)* (pp. 153–252).
Konami, M., Tanaka, S., & Matsumoto, K. (2002). Attrition of granules during repeated pneumatic transport. *Powder Technology, 125*, 82–88.
Kotzur, B. A., Berry, R. J., Zigan, S., García-Triñanes, P., & Bradley, M. S. A. (2018). Particle attrition mechanisms, their characterisation, and application to horizontal lean phase pneumatic conveying systems: A review. *Powder Technology, 334*, 76–105.

Kuakpetoon, D., Flores, R. A., & Milliken, G. A. (2001). Dry mixing of wheat fours: Effect of particle properties and blending ratio. *Lebensmittel-Wissenschaft und -Technologie-Food Science and Technology, 34*, 183–193.
Li, R., Lin, D., Roos, Y. H., & Miao, S. (2019). Glass transition, structural relaxation and stability of spray-dried amorphous food solids: A review. *Drying Technology, 37*, 287–300.
Lindley, J. A. (1991a). Mixing processes for agricultural and food materials: 1. Fundamentals of mixing. *Journal of Agricultural Engineering Research, 48*, 153–170.
Lindley, J. A. (1991b). Mixing processes for agricultural and food materials: 3. Powders and particulates. *Journal of Agricultural Engineering Research, 49*, 1–19.
Li, R., Roos, Y. H., & Miao, S. (2016). Roles of particle size on physical and mechanical properties of dairy model solids. *Journal of Food Engineering, 173*, 69–75.
Li, R., Roos, Y. H., & Miao, S. (2017). Characterization of physical and mechanical properties of miscible lactose-sugars systems. *Journal of Food Science, 82*, 2105–2112.
Little, L., Mainza, A. N., Becker, M., & Wiese, J. G. (2016). Using mineralogical and particle shape analysis to investigate enhanced mineral liberation through phase boundary fracture. *Powder Technology, 301*, 794–804.
Liu, L., Kafui, K. D., & Thornton, C. (2010). Impact breakage of spherical, cuboidal and cylindrical agglomerates. *Powder Technology, 199*, 189–196.
Lu, X., Liu, C., Zhu, L., & Qu, X. (2014). Influence of process parameters on the characteristics of TiAl alloyed powders by fluidized bed jet milling. *Powder Technology, 254*, 235–240.
Macchini, R., Bradley, M. S. A., & Deng, T. (2013). Influence of particle size, density, particle concentration on bend erosive wear in pneumatic conveyors. *Wear, 303*, 21–29.
Maidannyk, V., McSweeney, D. J., Hogan, S. A., Miao, S., Montgomery, S., Auty, M. A. E., et al. (2020). Water sorption and hydration in spray-dried milk protein powders: Selected physicochemical properties. *Food Chemistry, 304*, Article 125418.
Materic, V., Holt, R., Hyland, M., & Jones, M. I. (2014). An internally circulating fluid bed for attrition testing of Ca looping sorbents. *Fuel, 127*, 116–123.
McKee, S. L., Dyakowski, T., Williams, R. A., Bell, T. A., & Allen, T. (1995). Solids flow imaging and attrition studies in a pneumatic conveyor. *Powder Technology, 82*, 105–113.
Moejes, S. N., & van Boxtel, A. J. B. (2017). Energy saving potential of emerging technologies in milk powder production. *Trends in Food Science & Technology, 60*, 31–42.
Mun, S., McClements, D. J., & Surh, J. (2011). Influence of maltodextrin addition on the freeze-dry stability of β-lactoglobulin-based emulsions with controlled electrostatic and/or steric interactions. *Food Science and Biotechnology, 20*, 1143.
Murrieta-Pazos, I., Gaiani, C., Galet, L., & Scher, J. (2012). Composition gradient from surface to core in dairy powders: Agglomeration effect. *Food Hydrocolloids, 26*, 149–158.
Niranjan, K., Smith, D. L. O., Rielly, C. D., Lindley, J. A., & Phillips, V. R. (1994). Mixing processes for agricultural and food materials: Part 5, review of mixer types. *Journal of Agricultural Engineering Research, 59*, 145–161.
Norazirah, A., Fuad, S. H. S., & Hazizan, M. H. M. (2016). The effect of size and shape on breakage characteristic of mineral. *Procedia Chemistry, 19*, 702–708.
Onwulata, C. (2005). *Encapsulated and powdered foods*. Taylor & Francis Group.
Ortega-Rivas, E., Juliano, P., & Yan, H. (2006). *Food powders: Physical properties, processing, and functionality*. Springer US.
Paluszny, A., Tang, X., Nejati, M., & Zimmerman, R. W. (2016). A direct fragmentation method with Weibull function distribution of sizes based on finite- and discrete element simulations. *International Journal of Solids and Structures, 80*, 38–51.
Papadopoulos, D. G., & Ghadiri, M. (1996). Impact breakage of poly-methylmethacrylate (PMMA) extrudates: I. Chipping mechanism. *Advanced Powder Technology, 7*, 183–197.
Pernenkil, L., & Cooney, C. L. (2006). A review on the continuous blending of powders. *Chemical Engineering Science, 61*, 720–742.
Petukhov, Y., & Kalman, H. (2004). Empirical breakage ratio of particles due to impact. *Powder Technology, 143–144*, 160–169.
Portillo, P. M., Ierapetritou, M. G., & Muzzio, F. J. (2008). Characterization of continuous convective powder mixing processes. *Powder Technology, 182*, 368–378.
Pugliese, A., Cabassi, G., Chiavaro, E., Paciulli, M., Carini, E., & Mucchetti, G. (2017). Physical characterization of whole and skim dried milk powders. *Journal of Food Science & Technology, 54*, 3433–3442.
Rennie, P. R., Chen, X. D., Hargreaves, C., & Mackereth, A. R. (1999). A study of the cohesion of dairy powders. *Journal of Food Engineering, 39*, 277–284.
Reynolds, G. K., Fu, J. S., Cheong, Y. S., Hounslow, M. J., & Salman, A. D. (2005). Breakage in granulation: A review. *Chemical Engineering Science, 60*, 3969–3992.
Rhodes, M. (2008). Mixing and segregation. In M. Rhodes (Ed.), *Introduction to particle technology*- (2nd ed., pp. 293–310). John Wiley & Sons, Ltd.
Richard, B., Le Page, J. F., Schuck, P., Andre, C., Jeantet, R., & Delaplace, G. (2013). Towards a better control of dairy powder rehydration processes. *International Dairy Journal, 31*, 18–28.
Salman, A. D., Fu, J., Gorham, D. A., & Hounslow, M. J. (2003). Impact breakage of fertiliser granules. *Powder Technology, 130*, 359–366.
Salman, A. D., Ghadiri, M., & Hounslow, M. J. (2007a). *Handbook of powder technology-Volume 12-Particle breakage* (Vol. 12). Elsevier (Chapter 21), 25, 28.
Salman, A. D., Ghadiri, M., & Hounslow, M. J. (2007b). *Handbook of powder technology-Volume 12-Particle breakage* (Vol. 12, pp. 1–225). Elsevier.
Salman, A. D., Hounslow, M. J., & Verba, A. (2002). Particle fragmentation in dilute phase pneumatic conveying. *Powder Technology, 126*, 109–115.
Salman, Russell, A., Aman, S., & Tomas, J. (2015). Breakage probability of granules during repeated loading. *Powder Technology, 269*, 541–547.
Samimi, A., Ghadiri, M., Boerefijn, R., Groot, A., & Kohlus, R. (2003). Effect of structural characteristics on impact breakage of agglomerates. *Powder Technology, 130*, 428–435.
Scala, F., Chirone, R., & Salatino, P. (2013). 6 - attrition phenomena relevant to fluidized bed combustion and gasification systems. In F. Scala (Ed.), *Fluidized bed technologies for near-zero emission combustion and gasification* (pp. 254–315). Woodhead Publishing.
Scala, F., Montagnaro, F., & Salatino, P. (2007). Attrition of limestone by impact loading in fluidized beds. *Energy & Fuels, 21*, 2566–2572.
Schuck, P., Dolivet, A., & Jeantet, R. (2012). *Analytical methods for food and dairy powders*. Wiley-Blackwell.
Shan, J., Xu, S., Liu, Y., Zhou, L., & Wang, P. (2018). Dynamic breakage of glass sphere subjected to impact loading. *Powder Technology, 330*, 317–329.
Sharma, A., Jana, A. H., & Chavan, R. S. (2012). Functionality of milk powders and milk-based powders for end use applications - a review. *Comprehensive Reviews in Food Science and Food Safety, 11*, 518–528.
Subero, J., & Ghadiri, M. (2001). Breakage patterns of agglomerates. *Powder Technology, 120*, 232–243.
Swyngedau, S., Nussinovitch, A., Roy, I., Peleg, M., & Huang, V. (1991). Comparison of four models for the compressibility of breads and plastic foams. *Journal of Food Science, 56*, 756–759.
Tavares, L. M., Cavalcanti, P. P., de Carvalho, R. M., da Silveira, M. W., Bianchi, M., & Otaviano, M. (2018). Fracture probability and fragment size distribution of fired Iron ore pellets by impact. *Powder Technology, 336*, 546–554.
Tavares, L. M., & de Almeida, R. F. (2020). Breakage of green iron ore pellets. *Powder Technology, 366*, 497–507.
Thomas, M. E. C., Scher, J., Desobry-Banon, S., & Desobry, S. (2004). Milk powders ageing: Effect on physical and functional properties. *Critical Reviews in Food Science and Nutrition, 44*, 297–322.
Utsumi, R., Hata, T., Hirano, T., Mori, H., Tsubaki, J., & Maeda, T. (2001). Attrition testing of granules with a tapping sieve. *Powder Technology, 119*, 128–133.
Uzi, A., Kalman, H., & Levy, A. (2016). A novel particle attrition model for conveying systems. *Powder Technology, 298*, 30–41.
Van Laarhoven, B., Schaafsma, S. H., & Meesters, G. M. H. (2012). Toward a desktop attrition tester; validation with dilute phase pneumatic conveying. *Chemical Engineering Science, 73*, 321–328.
Walstra, P., Wouters, J. T., & Geurts, T. J. (2005). *Dairy science and technology*. CRC press.
Wu, F., & Wu, D. (2017). Attrition resistances and mechanisms of three types of FCC catalysts. *Powder Technology, 305*, 289–296.
Yan, H., & Barbosa-Cánovas, G. V. (1997). Compression characteristics of agglomerated food powders: Effect of agglomerate size and water activity Características de la compresión de alimentos en polvo: Efecto del tamaño del aglomerado y del contenido de humedad. *Food Science and Technology International, 3*, 351–359.
Yan, H., & Barbosa-Cánovas, G. V. (2001a). Attrition evaluation for selected agglomerated food powders: The effect of agglomerate size and water activity. *Journal of Food Process Engineering, 24*, 37–49.
Yan, H., & Barbosa-Cánovas, G. V. (2001b). The effect of padding foam on the compression characteristics of some agglomerated food powders. *Food Science and Technology International, 7*, 417–423.
Yildirim, N., & Genc, S. (2017). Energy and exergy analysis of a milk powder production system. *Energy Conversion and Management, 149*, 698–705.
Yuan, Y., & Lee, T. R. (2013). Contact angle and wetting properties. In *Surface science techniques* (pp. 3–34). Springer.
Zafar, U., Vivacqua, V., Calvert, G., Ghadiri, M., & Cleaver, J. A. S. (2017). A review of bulk powder caking. *Powder Technology, 313*, 389–401.
Zajic, L., & Buckton, G. (1990). The use of surface energy values to predict optimum binder selection for granulations. *International Journal of Pharmaceutics, 59*, 155–164.
Zhang, Z., & Ghadiri, M. (2002). Impact attrition of particulate solids. Part 2: Experimental work. *Chemical Engineering Science, 57*, 3671–3686.
Zhang, F., Olaleye, A. K., O'Mahony, J. A., Miao, S., & Cronin, K. (2020). Dilute phase pneumatic conveying of whey protein isolate powders: Particle breakage and its effects on bulk properties. *Advanced Powder Technology, 31*, 3342–3350.
Zhao, R., Goodwin, J. G., & Oukaci, R. (1999). Attrition assessment for slurry bubble column reactor catalysts. *Applied Catalysis A: General, 189*, 99–116.

Journal of Food Engineering 292 (2021) 110367

Contents lists available at ScienceDirect

Journal of Food Engineering

journal homepage: http://www.elsevier.com/locate/jfoodeng

Particle size, powder properties and the breakage behaviour of infant milk formula

Jie Han [a,b], John Fitzpatrick [b], Kevin Cronin [b], Valentyn Maidannyk [a], Song Miao [a,*]

[a] Teagasc Food Research Centre, Moorepark, Fermoy, Co. Cork, Ireland
[b] Process & Chemical Engineering, School of Engineering, University College Cork, Cork, Ireland

ARTICLE INFO

Keywords:
Infant milk formula
Breakage behaviour
Powder strength
Powder venturi feeder
Dilute phase pneumatic conveying
High-speed mixing

ABSTRACT

Dairy powder breakage occurs in many processes and causes deterioration in powder properties but there is currently no research presented in the literature on dairy powder breakage behaviour. The breakage behaviour and the effect of powder properties of an infant milk formula and its sieved size fractions were investigated during three processing methods (powder venturi feeder, lab-scale dilute phase pneumatic conveyor, and laboratory high-speed mixer) based on the changes of particle size distributions (PSD) before and after breakage. Particle size influenced other properties and the breakage behaviour of powders. Four breakage mechanisms were found, dispersion, chipping, disintegration, and splitting, corresponding to the increasing degree of breakage. More intense processing conditions were needed to cause the same breakage mechanism for smaller-sized particles because of their higher powder strength. The breakage of samples with wide PSD often displayed a combination of breakage mechanisms due to the influence of particle size on breakage behaviour.

1. Introduction

The production of dairy powders provides a good way to preserve and transport milk ingredients in a stable and convenient form. Currently, most of the commercial dairy powders are agglomerated powders as agglomeration results in the formation of large granules which improve some functional properties of powders. However, food agglomerates are normally less robust and have lower mechanical strength and aptitude for resisting loads than inorganic or polymeric particles, and they are also usually fragile, and brittle, thus unwanted particle breakage in agglomerated food powders easily happens when powders are exposed to mechanical impact or vibration during processing or transportation (Yan and Barbosa-Cánovas, 2001a, 2001b).

Breakage is one of the major and ubiquitous problems for some industries dealing with particulate solids, such as the pharmaceutical, agricultural, mineral, fertilizer, granulation and catalysts (Deng and Davé, 2017; Dosta et al., 2016; Gupta et al., 2017; Gupta, 2017; Norazirah et al., 2016; Salman et al., 2003; Shan et al., 2018). The most notable and serious consequences of unwanted particle breakage, include the dust generation, adverse effect on product properties and reduction of the product's functionalities (Kotzur et al., 2018; Salman et al., 2002; Wu and Wu, 2017). Based on limited published works on dairy powders breakage, particle attrition significantly decreased the particle size and increased the bulk density, reducing the rehydration properties and flowability of agglomerated dairy powders (Barleita and Barbosa-cáovas, 1993; Barletta and Barbosa-cánovas, 1993; Boiarkina et al., 2016; Han et al., 2020; Hanley et al., 2011; Hazlett et al., 2020; Yan and Barbosa-Cánovas, 2001b). Furthermore, for infant milk formula (IMF), breakage decreased the specific bulk volume, which influenced the size of product containers and the scoop volume requirement for the preparation of infant milk. Moreover, particle breakage takes place whenever there is relative movement between particles in contact with each other or against the container wall. In the context of particle attrition, it has been demonstrated that the collisions among agglomerates and against static container walls due to mechanical impact, shear, or compression provide the kinetic energy that causes the breakage of agglomerates (Kotzur et al., 2018). Unwanted dairy powder breakage occurs in many processes throughout production and transportation, such as in-plant transportation before packing (Boiarkina et al., 2016; Han et al., 2020; Hanley, 2011; Hazlett et al., 2020), dry mixing (Han et al., 2020), and vibration during transportation (Barleita and Barbosa-cáovas, 1993; Barletta and Barbosa-cánovas, 1993; Ortega-Rivas et al., 2006). Thus, the investigation of dairy powder breakage is very important for the quality control of dairy powders.

* Corresponding author.
E-mail address: Song.Miao@teagasc.ie (S. Miao).

https://doi.org/10.1016/j.jfoodeng.2020.110367
Received 24 June 2020; Received in revised form 25 August 2020; Accepted 4 October 2020
Available online 5 October 2020
0260-8774/© 2020 Elsevier Ltd. All rights reserved.

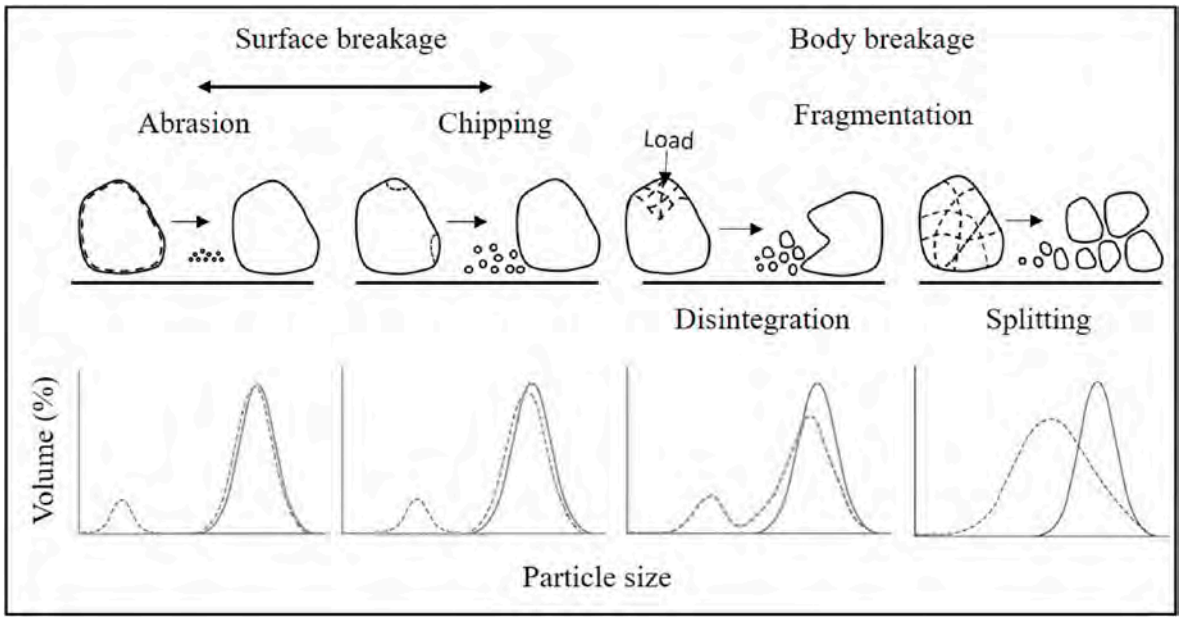


Fig. 1. Outline of particle breakage mechanisms and their typical particle size distribution curves before (solid line) and after (dotted line) breakage, recreated based on Scala et al. (Scala et al., 2013) and King (King, 2012).

Currently, two types of experimental tests have been designed to study the particle breakage of particulate systems: single-particle and multi-particle breakage tests (Bonakdar et al., 2016; Ortega-Rivas et al., 2006; Salman et al., 2007). Single-particle tests, including impact, crushing, and compression, have the advantage of applying a well-characterized load on the particle, providing fundamental information about particle properties, and enhancing the understanding of particle breakage. However, they are not fully representative of industrial conditions and results are difficult to compare with attrition observed in practice because of the variations among particles in a certain bulk. On the contrary, multi-particle tests, using shear cells, compression cells, and fluidized bed, are close to the real industrial situations. To study dairy powder breakage behaviour, the latter is more applicable because dairy powder particles are too small to use most of the single-particle methods.

Based on particle breakage research in other industries, agglomerated particle breakage can be classified into surface breakage and body breakage (Francioli, 2015; King, 2012). Surface breakage is generally associated with limited particle damage, while body breakage can change drastically the particle morphology. Of the various particulate materials, four breakage mechanisms have been reported to govern the breakage behaviour: abrasion (/erosion), chipping, disintegration, and splitting (Aarseth, 2004; Kotzur et al., 2018; Little et al., 2016; van Laarhoven et al., 2012; Zhang and Ghadiri, 2002). Disintegration and splitting are sometimes collectively termed fragmentation. Breakage patterns depend on the characteristics of the material and the applied stress (Petukhov and Kalman, 2004). Abrasion and chipping are associated with low load levels on the particle, and disintegration and splitting with higher levels. Associated with each breakage mechanism is a characteristic change to the particle size distribution (PSD) (Fig. 1) (Bayham et al., 2016; King, 2012; Materic et al., 2014; Scala et al., 2013). The changes of PSDs before and after breakage can indicate the breakage mechanisms and has been used and confirmed in some areas, such as lactose, limestone, calcium looping sorbents, and model porous powders (Agrawal et al., 2011; Bonakdar et al., 2016; Materic et al., 2014; Ortega-Rivas et al., 2006; Scala et al., 2007; Wu and Wu, 2017; Zhao et al., 1999). Abrasion and chipping result in the production of minuscule particles whilst still retaining the identity of the original particles. Hence the original PSD is still evident and moves a little to the smaller particle size with the appearance of the peak for the newly formed small particles and well separated from the original peak by a range of sizes that contains no particles (King, 2012). The difference between abrasion and chipping is where the small peak occurs. In principle, fragmentation of the large-scale breakage where the cracks are generated in the areas with high-level stresses, and then develop through the whole volume of the particle (Ghadiri and Zhang, 2002). Disintegration tends to produce one or a few relatively large fragments together with many smaller particles that originate at the points of application of the stress (Scala et al., 2013). The PSD of the product particles is relatively narrow but will often be bimodal or even multimodal (King, 2012). Splitting results in the generation of a small number of coarse fragments, all significantly smaller than the parent. The PSD moves to the smaller value but retaining its fundamental shape with a broad spectrum of particle sizes. Thus, different breakage behaviours have different influence on powders. However, there is currently no research on dairy powder breakage mechanisms as well as how the powder properties influence their breakage behaviour.

The objective of this study is to investigate dairy powder breakage and how powder properties, especially the particle size, affect breakage behaviour. A commercial agglomerated IMF was selected because of its larger particles, wide PSD range, and comprehensive composition. Three separate devices were employed, a powder venturi feeder, a lab-scale dilute phase pneumatic conveying pipeline and a laboratory high-speed mixer. These were selected to mimic the variety of processing conditions that powder experiences at the industrial scale, including the in-plant transportation in pneumatic conveying and dry mixing during the production of the IMF using the 'dry blending' process.

2. Materials and methods

2.1. Materials

A commercial agglomerated IMF, SMA PRO 'stage 2', was purchased from a local grocery store (Cork, Ireland). The IMF was sieved by a set of sieve screens to collect several fractions with narrow PSD. The opening sizes of the sieve screens used for size classification were 355, 250, and 180 μm, corresponding to four size fractions greater than 355 μm, from 355 to 250 μm, from 250 to 180 μm, and less than 180 μm, respectively (termed S > 355, S355–250, S250-180, and S < 180). The mass percentages of each component to the whole sample were 25.97%, 27.48%,

27.54%, and 19.01% respectively. Four fractions were mixed gently in equal proportions as the whole sample (termed WS) used for analyzing the breakage behaviour of samples with a wider PSD. The composition of samples is shown in Supplementary Table 1.

It should be noted that the commercial agglomerated IMF had most likely already undergone breakage during its handling from spray drying through to packing as a commercial product as well as the sieving process for preparing samples. Thus, samples were more resistant to breakage than the original spray-dried powder. Therefore, the processing conditions described below are relatively severe and were selected to ensure breakage could be expected.

2.2. Measurement of powder properties

2.2.1. Particle size and specific surface area

The Sauter mean particle size ($D_{3,2}$, the surface-weighted average of the PSD), median particle size (D_{50}, the size that splits the PSD with half above and half below this diameter) of the volume PSD, specific surface area (SSA), and PSD of powders were measured using a Malvern Mastersizer 3000 (Malvern Instruments Ltd., Worcestershire, UK) with a standard stainless steel venturi feeder. Samples were added to the disperser, and compressed air at 0 bar was used to transport powders to minimise damage to the powder during measurement. The background measurement time was 20 s and the sample measurement was 10 s. The laser obscuration level was at 1–4%. Measurements were performed in triplicate.

2.2.2. Powder density and porosity

Loose bulk density (ρ_b) and tapped (100 taps) bulk density (ρ_{tapped}) of samples were measured as per GEA Niro using a Gas Pycnometer (Accupyc II 1340 Gas Pycnometer, Micromeritics Instrument Corporation, USA) and Jolting volumeter (Funke Gerber, Berlin, Germany), respectively (Niro, 2006). The interparticle porosity (ε) was evaluated from Eq. (1).

$$\varepsilon = 1 - \frac{\rho_{tapped}}{\rho_p} \tag{1}$$

2.2.3. Surface free fat content

The surface free fat (SFF) content of samples was measured as per GEA Niro (2006), which is based on the extraction of the fat on the surface of particles. Approximately 50 ml of petroleum ether was added into around 10 g of sample then agitated 15 min. The solution was filtered then 25 ml of the filtrate was pipetted into the aluminium dish. Most of the petroleum ether was evaporated then it was dried in the oven for 1 h at 105 °C ± 1 °C. Samples were cooled in a desiccator until at room temperature then weighed. Measurements were carried out in duplicate. The SFF was calculated as Eq. (2):

$$SFF(\%) = \frac{a \times 50 \times 100}{\left(ml - \frac{a}{0.94}\right) \times b} \tag{2}$$

where *ml* (ml) is the volume of filtrate, *a* (g) is the evaporation residue, *b* (g) is the weight of the sample, and 0.94 is the estimated value of the density of free fat.

2.2.4. Cohesiveness

The cohesion of powders was assessed by measuring the flow function by the powder flow tester (PFT) (Brookfield Engineering Laboratories, Inc., Middleboro, MA, USA) using the standard flow function test. The axial and torsional speeds for the PFT were 1.0 mm/s and 1 rev/h, respectively. The involved uniaxial normal stresses were between 0.2 and 4.8 kPa. The cohesion of samples under major principal consolidating stress around 4.4 kPa was used to represent powder cohesiveness.

2.3. Sample breakage in a powder venturi feeder

There is a powder venturi feeder in the Malvern Mastersizer 3000, whose function is to disperse the cohesive powder into individual particles within an airflow before entering the particle size measuring zone. Three loading mechanisms are present and cannot be controlled: velocity gradients caused by shear stress, particle-to-particle collisions, and particle-to-wall collisions. The dispersion efficiency is controlled by air pressure, sample feed rate, and venturi feeder geometry. As the sample drops down into the funnel, it is entrained into the compressed air, which enters at right angles to the powder, and dispersed by the three mechanisms before entering into the measurement zone. The powder venturi feeder could break powder before measurement (Boiarkina et al., 2016). There are many similarities between this venturi feeder and the pneumatic conveying during dairy powder production (Hazlett et al., 2020). The feeder permits more conditions than pneumatic conveying, having a wide range of air pressure to control the different extents of breakage. Meanwhile, the particle size range measured by the Mastersizer 3000 is from 0.1 μm to 3500 μm which covers the agglomerated dairy powders and fragments. Therefore, a Malvern Mastersizer 3000 with a standard stainless steel venturi feeder (shown in Supplementary Figure S1A) was used to break samples.

Samples were fed to the powder venturi feeder, and the laser obscuration level was controlled at 1–4% by controlling the hopper gap and the feed speed. Low laser obscuration level ensured that most particles in the same fractions underwent similar conditions. For each sample, a series of air pressures (from 0 to 1.0 bar in 0.1 bar increments, and from 0.2 to 4.0 bar in 0.2 bar increments) were applied and the volume and number PSDs were measured. Measurements were performed in triplicate.

2.4. Sample breakage in the dilute phase pneumatic conveying

Samples were blown through the lab-scale pneumatic conveyor (presented in Supplementary Figure S1B which is adapted from Jie et al. (Han et al., 2020)) with an air velocity of 20, 30, and 40 m/s (termed PC20, PC30, and PC40) and a feeding rate of 3.0 g/s. Low feeding rate ensured that most particles in the same fractions underwent similar conditions. The dominant source of powder breakage during the dilute phase pneumatic conveying is caused by particle-wall impacts, particularly at the bends (Kotzur et al., 2018). The particle size and PSD of samples were measured using the method described in section 2.2.1 above.

2.5. Sample breakage in the high-speed mixing

Powders (50 g) were placed in the laboratory high-speed mixer (Waring, USA) (presented in Supplementary Figure S1C) operated at 22,000 rpm for four different durations of 10, 30, 60, and 180 s (termed HM10, HM30, HM60, and HM180). Samples just covered the blade of the mixer. Powder flow inside the mixer is that move from the bottom of the mixer, out towards the wall, up the wall and then cascades down towards the centre of the mixer (Tran, 2015). Momentum is transferred from the blade to the powder through a combination of impact, centrifugal, frictional, shear, gravity and inertial forces (Tran, 2015). The general perception in literature is that particles are more likely to break on impact during mixing (Iveson et al., 2001; van den Dries et al., 2003). The particle size and PSD of samples were measured using the method described in section 2.2.1 above.

2.6. Index of powder strength - breakage percentage

Particle strength can be defined as the minimum amount of stress that may be applied to a particle to cause macroscopic damage to the particle structure (Kotzur et al., 2018; Ortega-Rivas et al., 2006; Walton and Mumford, 1999). The physical strength of a single spray-dried dairy

Table 1
Properties of sieved infant milk formula samples.

Properties	WS	S > 355	S355-250	S250-180	S < 180
$D_{3,2}$ (μm)	214.7^{c}±2.5	443.7^{a}±4.1	295.3^{b} ± 0.5	207.0^{d}	107.0^{e}
D_{50} (μm)	284^{c}±5.1	473^{a}±4.9	308^{b} ± 0.8	216.7^{d} ± 0.5	123.0^{e}
Particle density (kg/L)	1.288^{b} ± 0.004	1.285^{c}±0.001	1.288^{b} ± 0.001	1.296^{a}±0.001	1.296^{a}±0.003
Bulk density (kg/L)	0.546^{b} ± 0.002	0.438^{d} ± 0.001	0.488^{c}±0.007	0.526^{b} ± 0.001	0.617^{a}±0.01
Porosity (%)	57.63^{c}±0.09	65.93^{a}±0.05	62.15^{b} ± 0.26	59.17^{bc}±0.01	52.41^{d} ± 0.55
Cohesion (kPa)	0.163^{b} ± 0.006	0.050^{d} ± 0.003	0.061^{c}±0.004	0.103^{bc}±0.003	0.311^{a}±0.005
SSA (m^2/kg)	26.6^{c}±0.3	12.9^{e}±0.1	20.3^{d} ± 0.1	29.0^{b} ± 0.1	56.1^{a}±0.1
SFF (%)	0.93^{c}±0.01	0.66^{d} ± 0.01	0.67^{d} ± 0.01	1.10^{b} ± 0.02	1.42^{a}±0.04

1. WS: whole sample. $D_{3,2}$: mean particle size. D_{50}: median particle size. SSA: specific surface area. SFF: surface free fat content.
2. Values are mean ± standard deviation (n = 3).
3. $^{a\text{-}e}$ different values within rows in each property are significantly different at $P < 0.05$.

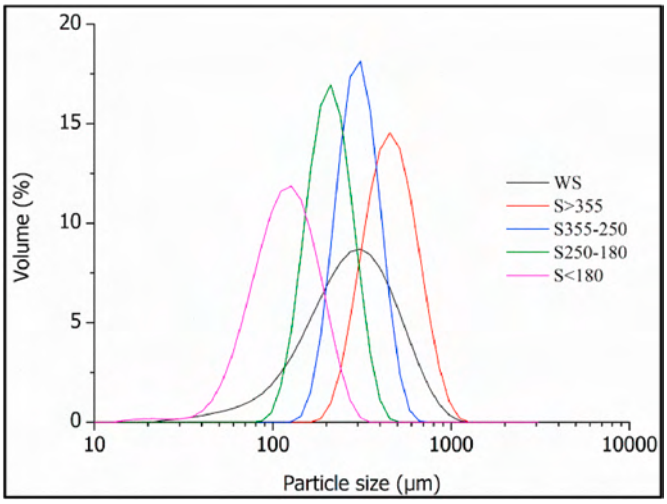


Fig. 2. The particle size volume distributions of samples. WS: whole sample.

powder particle is very difficult to determine because of its small physical size. Thus, indirect approaches were employed to measure powder strength. The breakage percentage (*BP*) was the percentage decrease in particle size under different processing conditions compared with the initial particle size (Agrawal et al., 2011; Hazlett et al., 2020). Dairy powder breakage results in the production of fine particles so the Sauter mean diameter ($D_{3,2}$) was used because it is more sensitive to the presence of fine particulates in the size distribution than the volume mean diameter ($D_{4,3}$) (Hu et al., 2014; Mun et al., 2011). It was calculated as Eq. (3), where $D3,2_b$ and $D3,2_i$ were the $D_{3,2}$ of broken samples and initial samples, respectively. The $D_{3,2}$ of powders before and after breakage was measured by a Malvern Mastersizer 3000 at 0 bar (the $D_{3,2}$ of broken samples in the powder venturi feeder was measured at their corresponding pressures, as described in section 2.3). The laser obscuration level was controlled at 1–4%, and measurements were performed in triplicate.

$$BP = \left(\frac{D3,2_i - D3,2_b}{D3,2_i}\right) \times 100 \quad (3)$$

2.7. Scanning electron microscopy (SEM) and light microscope

The SEM (Zeiss-Supra 40 VP/Gemini Column, Carl Zeiss, Germany) and the Light microscope with a build-in camera (Instruction BX51, Olympus, Tokyo, Japan) were employed to observe the morphology of some broken samples (S355-250). Samples were mounted on carbon adhesive discs attached to SEM specimen stubs and coated with gold ions in a sputter coater (K575X Sputter Coater, Quorum Technologies, UK). Samples were dropped on a microscope slide, covered with a glass coverslip, and observed using a 10× objective lens and 10× eyepiece of the optical microscopy.

2.8. Statistical analysis

Results were expressed as mean ± standard deviation (SD). One-way analysis of variance (ANOVA), followed by Tukey's test, was used to determine the significant differences (SPSS, IBM, USA). A significance level of $P < 0.05$ was used throughout the study.

3. Results and discussion

3.1. Powder physical properties

3.1.1. Particle size and distribution

The particle size and volume PSDs of samples are shown in Table 1 and Fig. 2, respectively. The $D_{3,2}$ of four fractions, S > 355, S355–250, S250-180, and S < 180 were 443, 295, 207, and 107 μm, respectively. Fig. 2 shows that the PSDs of all samples without S < 180 appeared as Log-normal distribution. There was a small peak in S < 180, from 14.5 μm to 30 μm which might be the fractions produced during handling or the sieving process. Almost 80% of sieved samples fell within the range of the opening sizes of the sieve screens. The $D_{3,2}$ of WS, 214 μm, was significantly different from other samples ($P < 0.05$) but closer to S250-180. The PSD of WS was wider than the four fractions, as expected, and the peak of the PSD plot was close to that of S355-250, which is consistent with the results of D_{50}.

3.1.2. Powder density and porosity

Particle density, bulk density, and porosity of samples are presented in Table 1. Particle density is the mass per unit volume of a particle, including the closed pores but excluding the open pores or cracks so it is also related to the particle structure properties. The particle density of all samples was around 1.29 or 1.30 kg/L and small particles had slightly higher particle density than large ones. This difference might be because big particles had more chance to have closed pores inside of the particle or the slight difference in composition. It was reported that, with the same parameters of spray drying, the composition of powders with different particle sizes was slightly different (O'Donoghue et al., 2019). The bulk density of powders depends on the PSD and particle shapes. The results show that the larger the particle size, the smaller the bulk density and the bigger the porosity as the larger particles are more agglomerated, and agglomerates tend to have more porous structures. The bulk density and porosity of WS were similar to those of S250-180 ($P > 0.05$).

3.1.3. Cohesiveness

Some of the dairy powders are cohesive and particles may exist as clusters held together by cohesive attractions. Small stresses could break the clusters and dispersed them into their original particles. SFF has a major influence on powder cohesiveness (Fitzpatrick et al., 2007). Cohesion increases with increased SFF, especially at higher

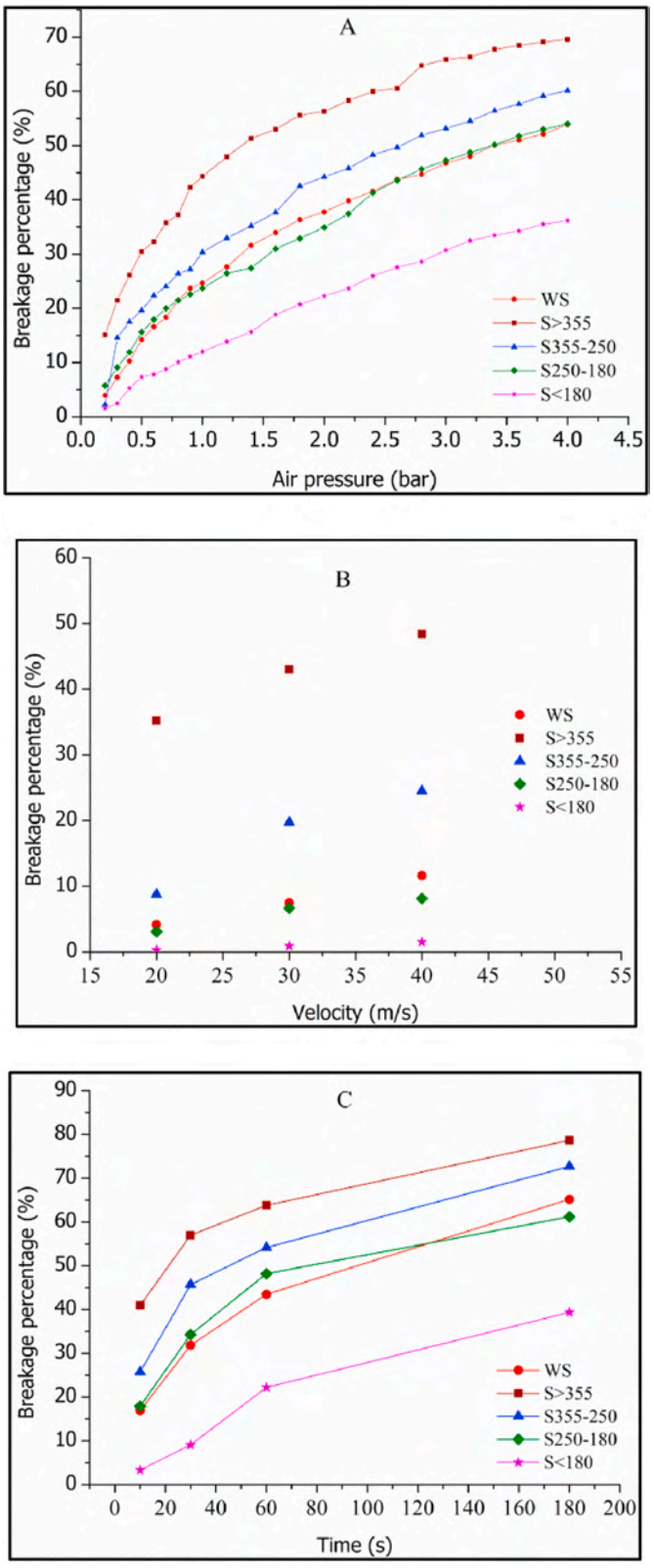


Fig. 3. The percentage decrease in particle size ($D_{3,2}$) of samples before and after breakage during three processing methods. A: Powder venturi feeder at different air pressures. B: Dilute phase pneumatic conveying under the air velocity of 20 m/s, 30 m/s, and 40 m/s. C: Laboratory high-speed mixing for 10 s, 30 s, 60 s, and 180 s. WS: whole sample.

temperatures with greater fat liquefaction and liquid bridge formation causing the particles to adhere to one another or agglomerate (Fitzpatrick et al., 2007). Meanwhile, the large SSA meant more surface area is available for cohesive forces, and SSA can also be correlated with the energy required to cause breakage (Bemrose and Bridgwater, 1987). The cohesion, SSA, and SFF of samples are presented in Table 1. The significant differences in SSA and SFF were found in most samples ($P < 0.05$), and both increased as particle size decreased. SSA and SFF of WS were similar to those of S250-180. The cohesiveness was increased with decreasing particle size and increasing SFF and SAA, which is consistent with other research (Fitzpatrick et al., 2004). There was no significant difference between the cohesion of WS and S250-180.

3.2. Index of powder strength – breakage percentage

BP was used as an index of powder strength that was applied to compare the strengths of the powder size fractions based on the changes of particle size before and after breakage at specific operating conditions. The lower the *BP*, the more resistant the powder is to breakage, thus the stronger the powder is. Fig. 3 displays the *BP* for each of the five IMF samples for each of the three processing methods as a function of process conditions. For any sample, the *BP* increased with increasing processing conditions in each method. Comparing different samples, results of the three processing methods show the same trends.

Firstly, for the four sieved fractions, under the same processing conditions, *BP* increased with increasing initial particle size, which shows that powder strength increased with decreasing initial particle size and porosity. This finding is in agreement with results of some research on the extent of breakage of agglomerated dairy powders (Boiarkina et al., 2016; Hazlett et al., 2020). It has been reported that particle size is one of the most important influencing factors for particle breakage and that particle strength decreases with increasing particle size (Fu et al., 2005; Ghadiri et al., 1991; Zhang and Ghadiri, 2002). It has been attributed to the likelihood of a greater number of imperfections in larger particles, which in turn provides a greater number of cracks. The highest local tensile stress is generated at these defective zones so that the fracture initiates from this zone and propagates (Antonyuk et al., 2005). This may also be the reason that porosity and density could influence particle strength because the pores and the structural defects in agglomerates are analogous to imperfections, inhomogeneities, or microcracks in material science (Antonyuk et al., 2005). In addition, the number of contact points of a primary particle can be decreased with larger porosities, by which the strength of agglomerates decreases. Besides the few flaws and low porosity, small particles are more difficult to break owing to the stronger interparticle forces that bind particles together including van der Waals forces, electrostatics, and liquid bonds (Reynolds et al., 2005). From an energy perspective, the more energy that can be absorbed, the lower the collision energy (if the breakage is caused by the impact), and the less likely the particle will break. Small particles can absorb a larger amount of energy than big particles (Agrawal et al., 2011; King, 2012), which results in the lowering of the breakage extent.

Moreover, WS and S355-250 have similar D_{50} values (Table 1), however, the strength of WS was higher than that of S355-250 and similar to S250-180, which means that the much broader PSD of WS corresponds to an increase in powder strength. This might be because the decrease of particle uniformity increased the cushioning action of fines. It has been found that the fine particles enclosed the coarse granules and thereby acted as a cushioning medium that reduced the granule stress and levels of attrition (Konami et al., 2002).

3.3. Breakage behaviour of four sieved fractions

The changes of PSDs were used to identify the breakage behaviour of four sieved fractions, S > 355, S355–250, S250-180, and S < 180, during three processing methods. It should be mentioned that in order to

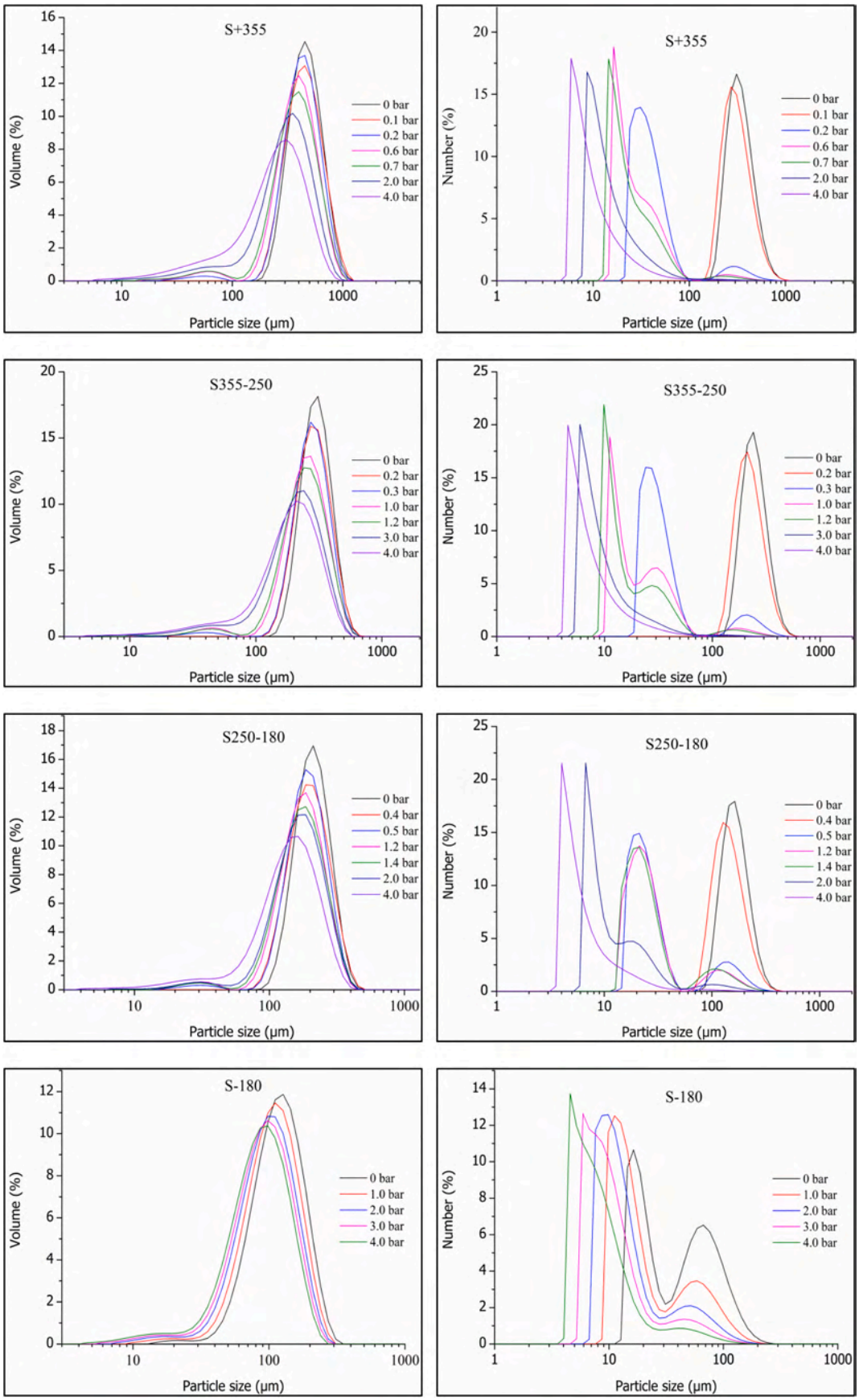


Fig. 4. The particle size volume and number distribution of samples broken by powder venturi feeder at different air pressures.

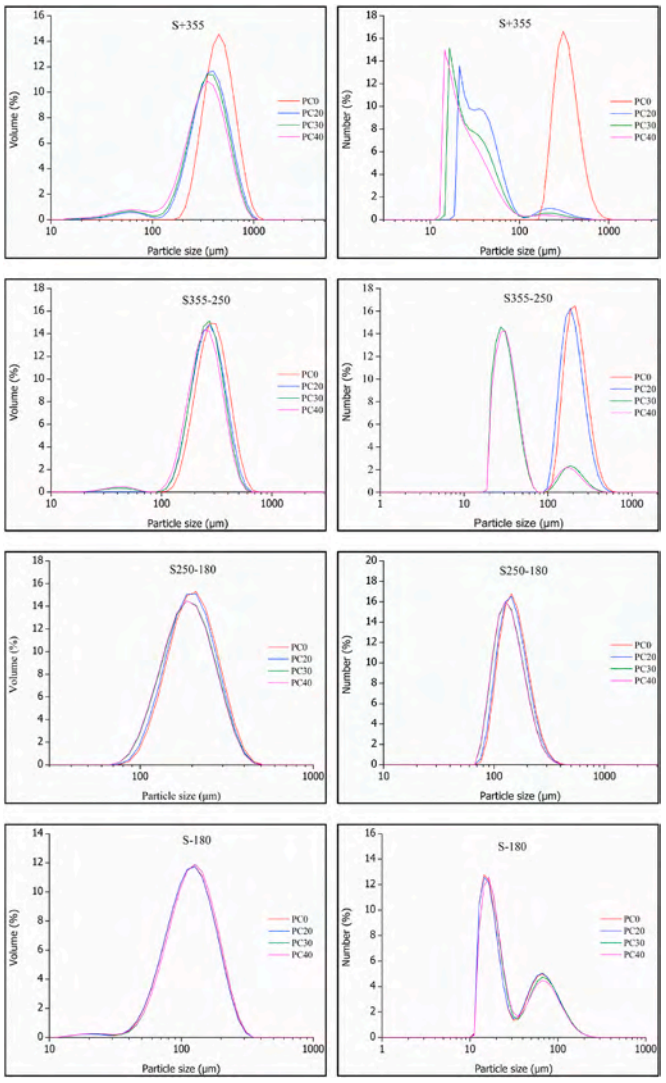


Fig. 5. The particle size volume and number distribution of samples broken by dilute phase pneumatic conveying under the air velocity of 20 m/s (PC20), 30 m/s (PC30), and 40 m/s (PC40).

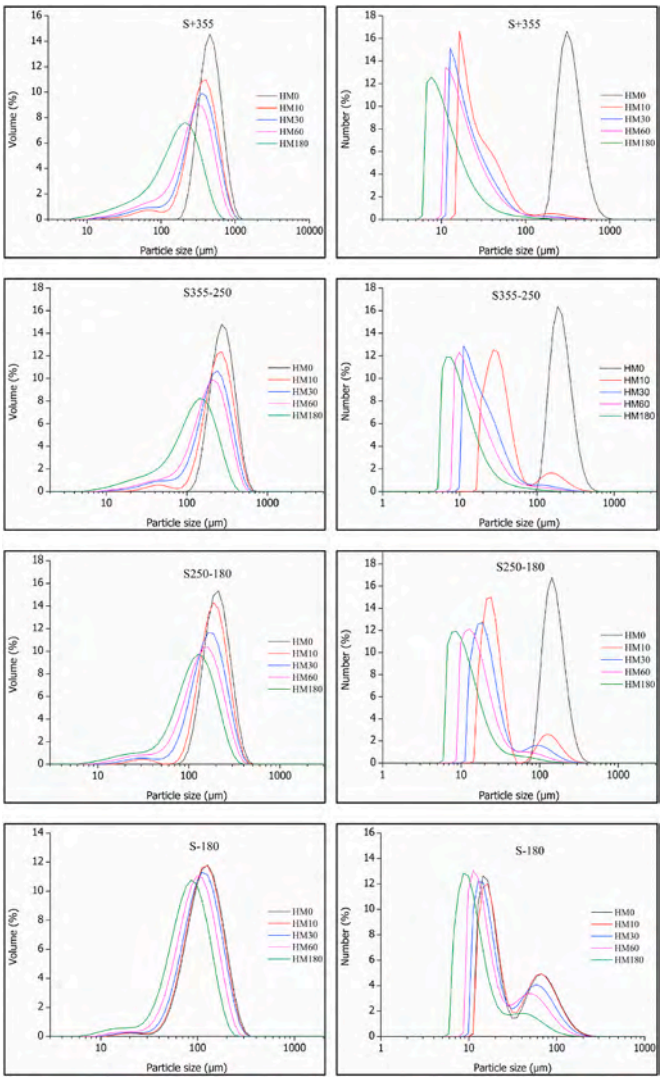


Fig. 6. The particle size volume and number distribution of samples broken by the laboratory high-speed mixing for 10 s (HM10), 30 s (HM30), 60 s (HM60), and 180 s (HM180).

facilitate analysis, different mechanisms were distinguished here according to their descriptions in the Introduction (Section 1) and particle size distributions (illustrated in Fig. 1). The mechanisms identified here were the primary mechanisms leading to breakage, not necessarily the sole mechanism. Moreover, the main breakage behaviour was not based on single impact or shear but compared the changes of particles before and after the entire processes where the stresses might act on the initial particles and their child particles.

3.3.1. *Powder venturi feeder*

The evolution of particle size volume (V-PSD) and number (N-PSD) distributions of four samples at different air pressures in the powder venturi feeder are shown in Fig. 4. The air pressures had a great impact on the PSD of all samples. Furthermore, the larger the particle size, the more sensitive the powder was to increasing air pressure, and the more breakage occurred, which is consistent with the data presented in Fig. 3.

In Fig. 4, the PSD of S > 355, S355-250, and S250-180 control samples (0 bar) were narrow and showed symmetric unimodal with the logarithm of particle size. The changes in the PSDs of these three samples at different air pressures were quite similar and there were four breakage patterns.

(1) For these three samples, the PSD plots gradually shifted left as the air pressure increased from 0 to 0.1, 0.2, and 0.4 bar, respectively. This implies that the particle size decreased but there were no small particles produced and all particles were still big (N-PSDs). Thus, the reason for this decrease in particle size was most likely due to the dispersion of clusters that were particles held together by cohesive attractions. The clusters existed in the larger sizes of the PSD and when they were broken, the particles were liberated causing the PSD shift to the left, with no occurrence of a fine's peak.

(2) With the further increase of air pressure, chipping most likely occurred according to the appearance of bimodal PSDs and the two peaks were well separated by a range of sizes that contained no particles. There were lots of small particles produced (N-PSDs) and showed up as a distinct peak at the small sizes in V-PSDs but the main volume of samples were big-sized particles (V-PSDs). The produced small particles for S > 355, S355-250, and S250-180 were around 50, 35, and 30 μm, respectively. They were big enough to decrease the particle size of mother particles implying that the main mechanism was not surface abrasion, that may have happened during the handling from spray drying through to packing or sieving process (the particle size of the

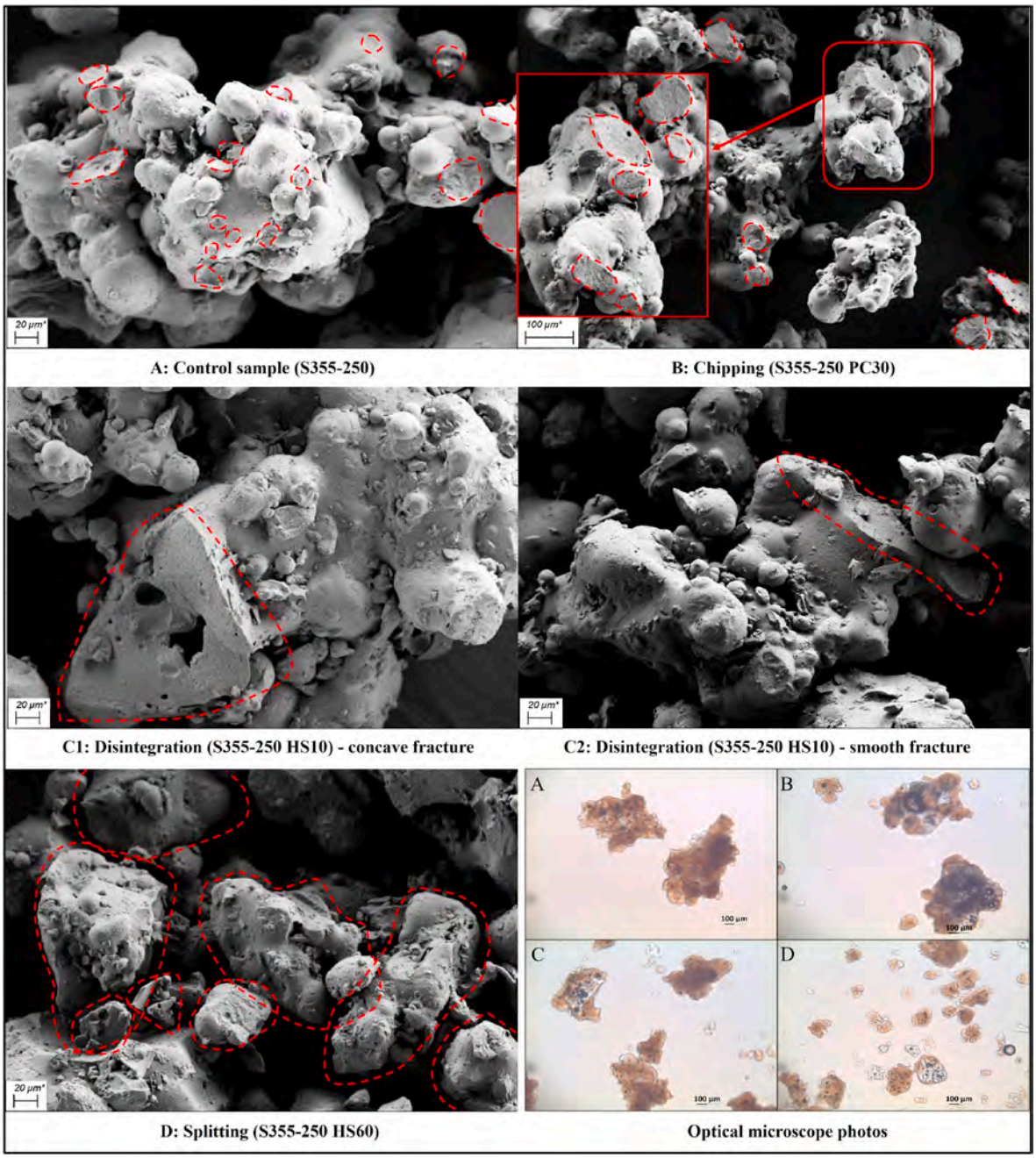


Fig. 7. The SEM and optical micrographs of some broken samples (S355-250). Control powder sample (A), and broken samples by chipping (B), disintegration (C) with a concave (C1) or a smooth fracture (C2), and splitting (D).

whole sample decreased 2.3% for $D_{3,2}$ and 2.8% for D_{50} after sieving, data not shown). There was a threshold air pressure for chipping (AP_c) where the small-sized peaks in V-PSDs or the middle peaks in N-PSDs appeared. The AP_c for S > 355, S355-250, and S250-180 were 0.2, 0.3 and 0.5 bar, respectively, which increased with decreasing particle size because smaller particles were more resistant to breakage, thus higher pressures were required to initiate chipping. Salman et al. also found that a threshold velocity existed in the single-particle impact studies, and below the threshold velocity, no breakage occurred (Salman et al., 2002). In this pattern, the proportion of small particles continued to increase and the V-PSDs shifted left and were always with two well-separated peaks which gradually got closer as air pressure increased.

(3) Disintegration most likely became the primary breakage mechanism with two V-PSDs' peaks merging when the threshold air pressures (AP_d) were reached. The AP_d for S > 355, S355-250, and S250-180 were 0.7, 1.2, and 1.4 bar, respectively, which increased with decreasing particle size. In this pattern, stress propagates through part of the particle from the point of application of the stress and causes a portion of it to fail as many small particles (Scala et al., 2013). The two peaks of V-PSD merged gradually, and the middle peaks of N-PSD lowered as air pressure increased.

(4) When the air pressure further increased, particles travel at higher speed and higher energy, which resulted in the breakage mainly by splitting with the disappearance of small-sized peaks in V-PSDs or the middle peaks in N-PSDs. Initial particles were broken into lots of fines (N-PSD) and mid-sized particles (V-PSD) with a



Fig. 8. Sieved infant milk formula breakage typical volume- (V-PSD) and number-particle size distribution (N-PSD) curves before (solid line) and after (dotted line) breakage.

broad spectrum of particle sizes. Same as AP_c and AP_d, for S > 355, S355-250, and S250-180, the threshold air pressures for splitting (AP_s) were 2.0, 3.0 and 3.6 bar, respectively.

Differing from the three samples above, the PSDs of S < 180 were bimodal and there were a lot of small particles in the control sample (N-PSD), which might be produced by abrasion during handling or sieving. Thus, the application of the analysis presented above for the other fractions could not be used as a basis for judgment. However, it was clear that the volume and population of fine particles continued to grow, and those of the big-sized particles were gradually lowered as air pressure increased, although there were still some big-sized particles even at high breakage intensities. Moreover, the above threshold air pressures increased with decreasing initial particle size, so the threshold air pressures of S < 180 should be higher than those of S250-180. Thus, it could be concluded that chipping and disintegration most likely played an important role in the breakage of S < 180. The mechanism at lower air pressure (at least lower than 0.5 bar which was the AP_c for S250-180) might be dispersion because the strength of S < 180 was higher than that of S250-180.

In summary, during powder venturi feeder at different air pressures, the breakage behaviour of four fractions with different particle sizes was different. Four breakage mechanisms were found, dispersion, chipping, disintegration, and splitting, corresponding to the increasing extent of breakage. For S < 180, chipping and disintegration might play leading roles at high air pressures. For the other three samples, the breakage was progressive with increasing air pressure: particle size decreased due to the dispersion when the air pressure was low, but when the air pressure was higher than AP_c, AP_d, and AP_s, the main mechanism was chipping, disintegration, and splitting, respectively. These threshold air pressures increased with decreasing particle size because of the increase of powder strength. The threshold air pressures were defined to facilitate analysis, however in reality, the mechanism around AP_d or AP_s might be a combination of disintegration and chipping or splitting, respectively.

3.3.2. Lab-scale dilute phase pneumatic conveying

The evolution of PSDs of samples during the dilute phase pneumatic conveying at different air velocities are shown in Fig. 5. The air velocity affected the PSD evolution of S > 355 and S355-250, especially for the former. For S > 355, disintegration most likely occurred at all air velocities and when the velocity increased, the breakage gradually increased. For S355-250, dispersion most likely occurred up to at least 20 m/s conveying and chipping mainly happened at the higher velocities. There was no significant breakage for S250-180 during conveying under 20 m/s. The decrease of particle size for S250-180 after 30 or 40 m/s conveying might be because of dispersion. There was no significant breakage for S < 180 at all speeds. These results indicate that disintegration and chipping in pneumatic conveying mainly occurred in S > 355 and S355-250 respectively while dispersion most likely occurred in S250-180 under high velocities.

3.3.3. Laboratory high-speed mixing

The changes of PSDs of samples during the high-speed mixing for different times are shown in Fig. 6. In some processes, the breakage evolves with repeated loads, such as with time spent in fluidized beds (Materic et al., 2014), ultrasonic systems (Raman and Abbas, 2008; Zhao et al., 1999), attrition tests (Wu and Wu, 2017), and mixing in this study. On the one hand, in some tests, breakage during the process can be analyzed and divided into primary and secondary breakage (Materic et al., 2014). The stress levels should not vary much over time during mixing because the mixing speed was constant. However, the stresses may act on the child particles rather than the initial particles due to the continuous formation of child particles over time. For example, disintegration appeared to be the main mechanism for S > 355 at 10 s mixing, and the small-sized peak grew over time and its distinctiveness disappeared that was likely to be due to a progressive breakage of child particles by either chipping or disintegration (assuming that only the initial particles were broken in the first 10 s). It was not applicable to analyse breakage during mixing in this way as it did not easily distinguish between primary and secondary breakage. On the other hand, the

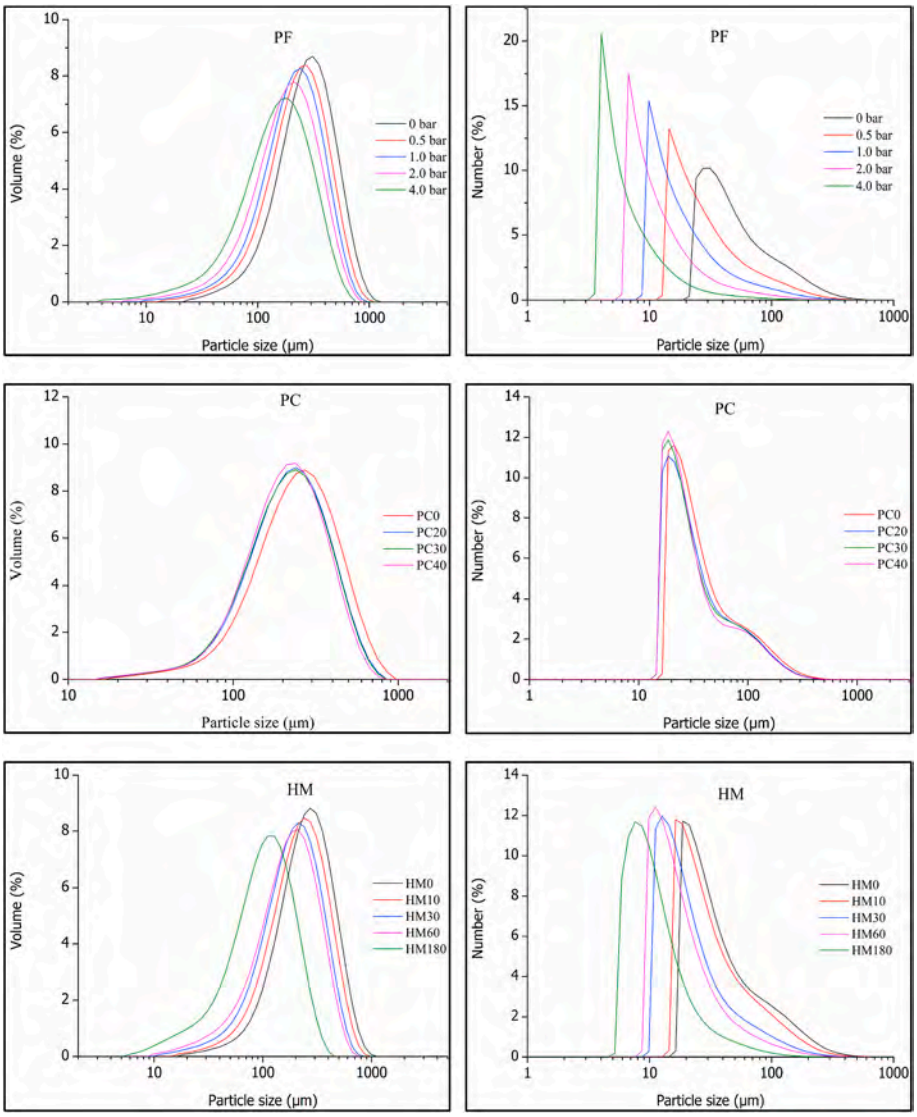


Fig. 9. The particle size volume and number distribution of whole samples (WS) broken by powder venturi feeder (PF) at different air pressures, by dilute phase pneumatic conveying (PC) under the air velocity of 20 m/s, 30 m/s, and 40 m/s, and by the laboratory high-speed mixing (HM) for 10 s, 30 s, 60 s, and 180 s.

Table 2
Summary of the properties and main breakage mechanisms [a] of infant milk formula.

Sample	Properties	Main breakage mechanisms		
		Powder venturi feeder	Dilute phase pneumatic conveying	High-speed mixing [b]
S > 355	**With PS**↓Particle density ↑Bulk density ↑Porosity ↓SSA ↑SFF ↑**These changes resulted in:**Cohesiveness ↑Powder strength ↓(BP↑)	Dispersion: 0.1 barChipping: 0.2–0.6 barDisintegration: 0.7–1.8 barSplitting: 2.0–4.0 bar	Disintegration for all speeds.	Disintegration: 10 s Splitting: 30 s, 60 s, 180 s
S355-250		Dispersion: 0.1–0.2 barChipping: 0.3–1.0 barDisintegration: 1.2–2.8 barSplitting: 3.0–4.0 bar	Dispersion: 20 m/s Chipping: 30 m/s, 40 m/s	Disintegration: 10 s Splitting: 30 s, 60 s, 180 s
S250-180		Dispersion: 0.1–0.4 barChipping: 0.5–1.2 barDisintegration: 1.4–3.4 barSplitting: 3.6–4.0 bar	No breakage: 20 m/s Dispersion: 30 m/s, 40 m/s	Chipping: 10 s Disintegration: 30 s Splitting: 60 s, 180 s
S < 180		Chipping and disintegration	No breakage	Chipping and disintegration
WS	Similar to S250-180	• Particles with different particle sizes underwent different breakage mechanisms at the same condition. • The breakage of WS displayed a combination of breakage mechanisms.		

1. [a]: Different mechanisms were distinguished according to their descriptions and particle size distributions. The mechanisms identified were the primary mechanisms leading to breakage, not necessarily the sole mechanism.
2. [b]: The main breakage mechanisms considered the effect of the whole process on the powders rather than the changes in the process.
3. WS: whole sample. PS: particle size ($D_{3,2}$). SSA: specific surface area. SFF: surface free fat content. BP: breakage percentage.

breakage of the whole process can be analyzed, such as the comparison of PSDs (Zhao et al., 1999) or attrition rates (Raman and Abbas, 2008) of catalysts before and after breakage in ultrasonic systems for certain times and energy outputs. This can obtain meaningful breakage information for the industrial processing conditions. From Fig. 6, fragmentation most likely occurred in all S > 355 and S355-250 samples, with disintegration occurring at 10 s mixing and splitting occurring at the other higher mixing times. The main breakage mechanisms for S250-180 were most likely chipping for 10 s, disintegration at 30 s, and splitting for the longer times. The changes of PSD in S < 180 during mixing was similar to that in the powder venturi feeder, so chipping and disintegration most likely played an important role in the breakage of S < 180. Consequently, during mixing for different times, the main breakage behaviour was chipping and two kinds of fragmentation.

According to the analysis of Figs. 4–6, the breakage behaviour of the four sieved IMF fractions during three processing methods was similar and there were four breakage mechanisms (dispersion, chipping, disintegration, and splitting) resulted in the increasing extent of breakage. The SEM and optical micrographs of some S355-250 samples, corresponding to the last three mechanisms, are shown in Fig. 7. Particles of the control sample (Fig. 7A) were irregular and there were some small defects (less than 20 μm) on the surface, which represents surface abrasion. Defects became bigger when chipping occurred (Fig. 7B) while the main particle body was not damaged. The body was partly broken when disintegration happened and left a concave (Fig. 7C1) or smooth (Fig. 7C2) fracture, and was completely crushed by splitting (Fig. 7D). Surface breakage likely occurred on the raised part of agglomerates, and this kind of structure was influenced by the spray drying and agglomerated parameters, and the composition of particles. The body breakage was influenced by the location of the applied stress and the structure of agglomerates. Dairy powder particles are heterogeneous in composition (Murrieta-Pazos et al., 2012), thus the location of a crack might also be affected by the composition. Fig. 8 outlines the typical V- and N-PSDs of these four patterns of breakage. The typical N-PSDs of chipping and disintegration was not unique and they depended on the initial particle size and the processing conditions. At the same condition, the breakage behaviour of different samples was different, depending on the powder strength. The combined results show that when the main breakage behaviour of S250-180 was dispersion, the bigger-sized sieved fractions mainly underwent chipping and disintegration. When the main breakage behaviour of S250-180 was disintegration, the bigger-sized sieved fractions were broken by splitting.

3.4. Breakage behaviour of whole samples (WS) during three processing methods

In order to easily observe the breakage behaviour, IMF was sieved into different fractions with narrow distributions, while the study of breakage behaviour of whole samples would provide more practical knowledge. The evolution of PSDs of WS during powder venturi feeder (PF), dilute phase pneumatic conveying (PC), and high-speed mixing (HM) are shown in Fig. 9. It was shown that varying extent of breakage occurred for WS during three processing methods with different conditions. Most breakages happened after HM for 180 s, and the least occurred during PC, which is consistent with the degree of breakage of four fractions during three processes.

For the breakage behaviour of WS during PF and HM, it was clear that V-PSDs of WS gradually became shorter and shifted left, and the population of fine particles continued to increase with increasing process conditions. There was not enough evidence to easily identify the main breakage mechanisms only based on the changes in PSDs because there was no bimodal PSDs or other features. This was due to the wide range of PSD of WS which was from tens to hundreds of microns, and the child particles were still in that range. Moreover, according to the analysis of four fractions, different sized particles had different breakage behaviours at the same process condition. Thus, the breakage of WS was a mixture of all particles' breakage and the breakage behaviour could be one or a combination of dispersion, chipping, and fragmentation. Splitting might be identified based on the changes of PSDs because almost all particles experienced splitting when the processing conditions were high enough, for example, the HM for 180 s or PF at 3.0–4.0 bar. Therefore, the breakage behaviour of WS was one or a combination of breakage mechanisms because particles with different particle size in WS underwent different breakage patterns at the same condition. Mechanisms without splitting could not be identified for WS based on the changes in PSDs because of the wide range of PSD.

4. Conclusion

A study was performed on the particle breakage behaviour and the effect of powder properties of sieved IMF samples during three different processing methods (powder venturi feeder, lab-scale pneumatic conveyor, and laboratory high-speed mixer) which mimic the industrial-scale processing conditions. Powder properties and breakage behaviours of samples were summarized in Table 2. Powder strength influenced the breakage behaviour, and it increased with the decrease of particle size and porosity, and the expansion of the PSD range. The main breakage mechanisms for IMF samples included dispersion, chipping, and fragmentation (disintegration and splitting), corresponding to the increasing extent of breakage and depending on the breakage process conditions and particle characteristics. The breakage behaviour of S > 355, S355-250, and S250-180 could be determined according to the changes of PSDs. Their main breakage mechanisms during powder venturi feeder changed gradually from dispersion until splitting with increasing air pressures. Smaller sized particles were more resistant to breakage and higher air pressures were needed to cause the same breakage mechanism for smaller sized particles. For dilute phase pneumatic conveying, disintegration, chipping, and dispersion occurred for three samples respectively. Mixing caused the greatest breakage and two kinds of fragmentations most likely happened during mixing. For S < 180, no breakage happened during dilute phase pneumatic conveying. Chipping and disintegration were the main mechanisms during the other two methods. The breakage behaviour of whole samples was one or a combination of breakage mechanisms because the breakage behaviour of samples with different particle size at the same process condition was different. Overall, a better understanding of the breakage behaviour of dairy powders and the impact of powder properties will assist efforts in trying to reduce powder breakage and the problems associated with it.

CRediT authorship contribution statement

Jie Han: Conceptualization, Formal analysis, Investigation, Methodology, Visualization, Writing - original draft, Data curation. **John Fitzpatrick:** Supervision, Writing - review & editing. **Kevin Cronin:** Supervision, Writing - review & editing. **Valentyn Maidannyk:** Investigation. **Song Miao:** Supervision, Conceptualization, Writing - review & editing, Funding acquisition, Project administration, Investigation.

Declaration of competing interests

The authors declare that they have no known competing financial interests or personal relationships that could have appeared to influence the work reported in this paper.

Acknowledgement

This work was supported financially by the Teagasc, Agriculture and Food Development Authority under the project MDDT 0153 entitled 'Powder breakage and functionality of dairy powders'. The authors would like to acknowledge Martina O'Brien, AnneMarie McAuliffe, Vijaya Lakshmi Chirumamilla, and Helen Slattery for the measurement of samples' composition.

Appendix A. Supplementary data

Supplementary data to this article can be found online at https://doi.org/10.1016/j.jfoodeng.2020.110367.

References

Aarseth, K.A., 2004. Attrition of feed pellets during pneumatic conveying: the influence of velocity and bend radius. Biosyst. Eng. 89 (2), 197–213.

Agrawal, S.G., Balandier, A., Paterson, A.H.J., Jones, J.R., 2011. Study on lactose attrition inside the mixing cell of a laser diffraction particle sizer using a novel attrition index. Powder Technol. 208 (3), 669–675.

Antonyuk, S., Tomas, J., Heinrich, S., Mörl, L., 2005. Breakage behaviour of spherical granulates by compression. Chem. Eng. Sci. 60 (14), 4031–4044.

Barleita, B.J., Barbosa-cáovas, G.V., 1993. Fractal analysis to characterize ruggedness changes in tapped agglomerated food powders. J. Food Sci. 58 (5), 1030–1035.

Barletta, B.J., Barbosa-cánovas, G.V., 1993. An attrition index to assess fines formation and particle size reduction in tapped agglomerated food powders. Powder Technol. 77 (1), 89–93.

Bayham, S.C., Breault, R., Monazam, E., 2016. Particulate solid attrition in CFB systems – an assessment for emerging technologies. Powder Technol. 302, 42–62.

Bemrose, C.R., Bridgwater, J., 1987. A review of attrition and attrition test methods. Powder Technol. 49 (2), 97–126.

Boiarkina, I., Sang, C., Depree, N., Prince-Pike, A., Yu, W., Wilson, D.I., Young, B.R., 2016. The significance of powder breakdown during conveying within industrial milk powder plants. Adv. Powder Technol. 27 (6), 2363–2369.

Bonakdar, T., Ghadiri, M., Ahmadian, H., Martin de Juan, L., Xu, D., Tantawy, H., Smith, D., 2016. Impact attrition of spray-dried burkeite particles. Powder Technol. 304, 2–7.

Deng, X., Davé, R.N., 2017. Breakage of fractal agglomerates. Chem. Eng. Sci. 161, 117–126.

Dosta, M., Dale, S., Antonyuk, S., Wassgren, C., Heinrich, S., Litster, J.D., 2016. Numerical and experimental analysis of influence of granule microstructure on its compression breakage. Powder Technol. 299, 87–97.

Fitzpatrick, J.J., Barry, K., Cerqueira, P.S.M., Iqbal, T., O'Neill, J., Roos, Y.H., 2007. Effect of composition and storage conditions on the flowability of dairy powders. Int. Dairy J. 17 (4), 383–392.

Fitzpatrick, J.J., Iqbal, T., Delaney, C., Twomey, T., Keogh, M.K., 2004. Effect of powder properties and storage conditions on the flowability of milk powders with different fat contents. J. Food Eng. 64 (4), 435–444.

Francioli, D.M., 2015. Effect of Operational Variables on Ball Milling. Universidade Federal do Rio de Janeiro, Brazil.

Fu, J., Reynolds, G.K., Adams, M.J., Hounslow, M.J., Salman, A.D., 2005. An experimental study of the impact breakage of wet granules. Chem. Eng. Sci. 60 (14), 4005–4018.

Ghadiri, M., Yuregir, K.R., Pollock, H.M., Ross, J.D.J., Rolfe, N., 1991. Influence of processing conditions on attrition of NaCl crystals. Powder Technol. 65 (1), 311–320.

Ghadiri, M., Zhang, Z., 2002. Impact attrition of particulate solids. Part 1: a theoretical model of chipping. Chem. Eng. Sci. 57 (17), 3659–3669.

Gupta, V., Sun, X., Xu, W., Sarv, H., Farzan, H., 2017. A discrete element method-based approach to predict the breakage of coal. Adv. Powder Technol. 28 (10), 2665–2677.

Gupta, V.K., 2017. Effect of size distribution of the particulate material on the specific breakage rate of particles in dry ball milling. Powder Technol. 305, 714–722.

Han, J., Fitzpatrick, J., Cronin, K., Maidannyk, V., Miao, S., 2020. Breakage of infant milk formula through three different processing methods and its influence on powder properties. J. Food Eng. 282, 109997.

Hanley, K.J., 2011. Experimental Quantification and Modelling of Attrition of Infant Formulae. Department of Process and Chemical Engineering. University College Cork, Cork, Ireland.

Hanley, K.J., Byrne, E.P., Cronin, K., Oliveira, J.C., O'Mahony, J.A., Fenelon, M.A., 2011. Effect of pneumatic conveying parameters on physical quality characteristics of infant formula. J. Food Eng. 106 (3), 236–244.

Hazlett, R., Schmidmeier, C., O'Mahony, J.A., 2020. Influence of mechanical integrity during pneumatic conveying on the bulk handling and rehydration properties of agglomerated dairy powders. J. Food Eng. 110103.

Hu, X., Zhao, M., Li, L., Yang, B., Yang, X., Wang, H., Ren, J., 2014. Emulsifying properties of cross-linking between proteins extracted from cold/hot pressed peanut meal and hydrolysed fish (Decapterus maruadsi) proteins. Int. J. Food Prop. 17 (8), 1750–1762.

Iveson, S.M., Litster, J.D., Hapgood, K., Ennis, B.J., 2001. Nucleation, growth and breakage phenomena in agitated wet granulation processes: a review. Powder Technol. 117 (1), 3–39.

King, R.P., 2012. Modeling and simulation of mineral processing systems. Soc. Mining Metall. Explor. 156–159 (SME).

Konami, M., Tanaka, S., Matsumoto, K., 2002. Attrition of granules during repeated pneumatic transport. Powder Technol. 125 (1), 82–88.

Kotzur, B.A., Berry, R.J., Zigan, S., García-Triñanes, P., Bradley, M.S.A., 2018. Particle attrition mechanisms, their characterisation, and application to horizontal lean phase pneumatic conveying systems: a review. Powder Technol. 334, 76–105.

Little, L., Mainza, A.N., Becker, M., Wiese, J.G., 2016. Using mineralogical and particle shape analysis to investigate enhanced mineral liberation through phase boundary fracture. Powder Technol. 301, 794–804.

Materic, V., Holt, R., Hyland, M., Jones, M.I., 2014. An internally circulating fluid bed for attrition testing of Ca looping sorbents. Fuel 127, 116–123.

Mun, S., McClements, D.J., Surh, J., 2011. Influence of maltodextrin addition on the freeze-dry stability of β-lactoglobulin-based emulsions with controlled electrostatic and/or steric interactions. Food Sci. Biotechnol. 20 (4), 1143.

Murrieta-Pazos, I., Gaiani, C., Galet, L., Scher, J., 2012. Composition gradient from surface to core in dairy powders: agglomeration effect. Food Hydrocolloids 26 (1), 149–158.

Niro, G., 2006. GEA Niro Analytical Methods Dry Products. GEA Process Engineering A/S, Gladsaxevej, Denmark.

Norazirah, A., Fuad, S.H.S., Hazizan, M.H.M., 2016. The effect of size and shape on breakage characteristic of mineral. Procedia Chem. 19, 702–708.

O'Donoghue, L.T., Haque, M.K., Kennedy, D., Laffir, F.R., Hogan, S.A., O'Mahony, J.A., Murphy, E.G., 2019. Influence of particle size on the physicochemical properties and stickiness of dairy powders. Int. Dairy J. 98, 54–63.

Ortega-Rivas, E., Juliano, P., Yan, H., 2006. Food Powders: Physical Properties, Processing, and Functionality. Springer US.

Petukhov, Y., Kalman, H., 2004. Empirical breakage ratio of particles due to impact. Powder Technol. 143–144, 160–169.

Raman, V., Abbas, A., 2008. Experimental investigations on ultrasound mediated particle breakage. Ultrason. Sonochem. 15 (1), 55–64.

Reynolds, G.K., Fu, J.S., Cheong, Y.S., Hounslow, M.J., Salman, A.D., 2005. Breakage in granulation: a review. Chem. Eng. Sci. 60 (14), 3969–3992.

Salman, A.D., Fu, J., Gorham, D.A., Hounslow, M.J., 2003. Impact breakage of fertiliser granules. Powder Technol. 130 (1), 359–366.

Salman, A.D., Ghadiri, M., Hounslow, M.J., 2007. Handbook of Technology-Pparticle Breakage.

Salman, A.D., Hounslow, M.J., Verba, A., 2002. Particle fragmentation in dilute phase pneumatic conveying. Powder Technol. 126 (2), 109–115.

Scala, F., Chirone, R., Salatino, P., 2013. 6 - attrition phenomena relevant to fluidized bed combustion and gasification systems. In: Scala, F. (Ed.), Fluidized Bed Technologies for Near-Zero Emission Combustion and Gasification. Woodhead Publishing, pp. 254–315.

Scala, F., Montagnaro, F., Salatino, P., 2007. Attrition of limestone by impact loading in fluidized beds. Energy Fuels 21 (5), 2566–2572.

Shan, J., Xu, S., Liu, Y., Zhou, L., Wang, P., 2018. Dynamic breakage of glass sphere subjected to impact loading. Powder Technol. 330, 317–329.

Tran, A.L.H., 2015. Powder Flow in Vertical High Shear Mixer Granulators. School of Chemical Engineering. The University of Queensland.

van den Dries, K., de Vegt, O.M., Girard, V., Vromans, H., 2003. Granule breakage phenomena in a high shear mixer; influence of process and formulation variables and consequences on granule homogeneity. Powder Technol. 133 (1), 228–236.

van Laarhoven, B., Schaafsma, S.H., Meesters, G.M.H., 2012. Toward a desktop attrition tester; validation with dilute phase pneumatic conveying. Chem. Eng. Sci. 73, 321–328.

Walton, D.E., Mumford, C.J., 1999. Spray dried products—characterization of particle morphology. Chem. Eng. Res. Des. 77 (1), 21–38.

Wu, F., Wu, D., 2017. Attrition resistances and mechanisms of three types of FCC catalysts. Powder Technol. 305, 289–296.

Yan, H., Barbosa-Cánovas, G.V., 2001a. Attrition evaluation for selected agglomerated food powders: the effect of agglomerate size and water activity. J. Food Process. Eng. 24 (1), 37–49.

Yan, H., Barbosa-Cánovas, G.V., 2001b. The effect of padding foam on the compression characteristics of some agglomerated food powders. Food Sci. Technol. Int. 7 (5), 417–423.

Zhang, Z., Ghadiri, M., 2002. Impact attrition of particulate solids. Part 2: experimental work. Chem. Eng. Sci. 57 (17), 3671–3686.

Zhao, R., Goodwin, J.G., Oukaci, R., 1999. Attrition assessment for slurry bubble column reactor catalysts. Appl. Catal. Gen. 189 (1), 99–116.

Journal of Food Engineering 321 (2022) 110939

Contents lists available at ScienceDirect

Journal of Food Engineering

journal homepage: www.elsevier.com/locate/jfoodeng

Effects of different breakage mechanisms on the physical, water sorption, and mechanical characteristics of infant milk formula

Jie Han [a,b], John Fitzpatrick [b], Kevin Cronin [b], Song Miao [a,*]

[a] Teagasc Food Research Centre, Moorepark, Fermoy, Co. Cork, Ireland
[b] Process & Chemical Engineering, School of Engineering, University College Cork, Cork, Ireland

ARTICLE INFO

Keywords:
Infant milk formula
Surface breakage
Body breakage
Physical properties
Water sorption behavior
Mechanical characteristics

ABSTRACT

Two main breakage mechanisms, surface breakage and body breakage, were both found during laboratory dilute-phase pneumatic conveying and high-speed mixing of infant milk formula, respectively. Body breakage had a greater influence on powder physical properties, particle shapes, and surface compositions than surface breakage. In particular, the particle size of samples decreased by only 10% after surface breakage but by 60% after body breakage. For samples where body breakage predominated, significant changes to both water sorption and mechanical properties of the powder were seen while surface breakage had very little effect on them. Body breakage significantly increased the water sorption rate of samples, at around 10%–126% higher than the other samples for the first 3 h, which accelerated the time-dependent crystallization. Moreover, at a_W 0.11 to 0.33, the final water contents of body breakage samples were 3.5%–22% higher than control samples. This decreased the crystallization temperature, by between 2 °C and 10 °C, and the overall molecular mobility of samples. These changes were due to the increase in the number of adsorbed monolayers, sorption surface area, and monolayer value of samples after body breakage.

1. Introduction

Dairy powder products are an important group of food powders and most commercial milk powders are agglomerates that improve the flowability and rehydration properties. However, breakage of agglomerates easily occurs in many processes throughout dairy powder production, transportation, and handling when particles are subjected to mechanical loads, such as impact, compression, and shear. These loads caused by collisions between particles and against equipment walls can provide the kinetic energy resulting in particle attrition (Kotzur et al., 2018).

In our previous study, three possible breakage mechanisms have been found for agglomerated infant milk formula (IMF), that are dispersion, surface breakage, and body breakage (Han et al., 2021a). Studies have shown that the changes in powder particle size distributions (PSD) indicate the breakage mechanisms (Han et al., 2021a; Materic et al., 2014; Scala et al., 2007; Wu and Wu, 2017). When the processing condition is very gentle, dispersion may occur on clusters that are particles attracted together by cohesiveness. The mechanical force can disperse clusters into their individual component particles, which shifts the PSD to the smaller value with no production of fines (Han et al., 2021a). When powders are exposed to low-level external mechanical stress, for example for IMF, the transportation by pneumatic conveying at 20–30 m/s or by powder venturi feeder at 0–1.2 bar, surface breakage produces tiny particles while the main body of the original particle still retains its integrity. Hence it occurs according to the birth of bimodal PSD where the original peak slightly shifts to the smaller value with the appearance of a newly produced peak of minuscule child particles and the two peaks are divided by a range of sizes containing no particles (King, 2012; Scala et al., 2013). Body breakage tends to produce a few coarse fragments or many smaller particles. After body breakage, the original PSD of powders clearly shifts to the smaller value with a broad PSD range maintaining its fundamental shape, or the PSD is bimodal PSD with peaks not separated (King, 2012; Scala et al., 2013). Different breakage mechanisms result in different PSDs and particle sizes of the final samples, which then can influence powder properties.

It has been reported that powder breakage significantly increased densities and reduced the particle size of several agglomerated milk powders (Boiarkina et al., 2016; Han et al., 2020; Hanley, 2011; Hazlett et al., 2020). The changes in powder density can cause errors in the dosage consumed of dairy powders, especially IMF. Furthermore, the changes in physical properties seriously led to a decline in the

* Corresponding author.
E-mail address: Song.Miao@teagasc.ie (S. Miao).

https://doi.org/10.1016/j.jfoodeng.2022.110939
Received 6 April 2021; Received in revised form 23 November 2021; Accepted 1 January 2022
Available online 4 January 2022
0260-8774/© 2022 Elsevier Ltd. All rights reserved.

flowability and rehydration properties of powders (Han et al., 2020; Hazlett et al., 2020). In addition to these properties, water sorption and plasticization behavior are also important for the physicochemical properties of dairy powders containing amorphous lactose. Spray-drying processes often produce amorphous lactose that is a nonequilibrium state with limited molecular mobility and high viscosity (Haque and Roos, 2006). The amorphous lactose tends to absorb moisture resulting in plasticization and is very sensitive to relative humidity and temperature (Saxena et al., 2019). When lactose is plasticized by moisture, or the environmental temperature higher than the glass transition temperature (T_g), the molecular mobility increases, which subsequently results in lactose rearranging into the highly ordered crystalline state (Saxena et al., 2019). This causes some further water liberation which enhances many deteriorative changes of dairy powders, such as stickiness, caking, non-enzymatic browning, and significantly decreases storage stability and quality (Haque and Roos, 2004). Besides, the mechanical properties of dairy powders, including the storage modulus, loss modulus, and α-relaxation are influenced by the molecular mobility which significantly changes at and above the T_g (Li et al., 2016c; Maidannyk et al., 2020). However, there is currently no published data on the influence of different breakage mechanisms on the water sorption behavior and mechanical characteristics (such as the glass transition, crystallization, α-relaxation, storage modulus, and loss modulus) of dairy powders. Such research is essential to increase the knowledge of dairy powder breakage and will assist efforts in the quality control of powders.

This study aims to fill this gap. Commercial agglomerated IMF was chosen due to its comprehensive composition and large particles. A laboratory dilute-phase pneumatic conveyor and high-speed mixer were used to mimic the industrial-scale processes that cause particle breakage, including in-plant pneumatic conveying transportation and dry mixing in the 'dry blending' process during IMF production. The main breakage mechanisms during different processing methods were determined, followed by the investigation of physical, water sorption, and mechanical properties of broken samples caused by different mechanisms.

2. Material and methods

2.1. Material

Two commercial agglomerated IMF, purchased from a local grocery store (Cork, Ireland), Aptamil Profutura (termed A, composition: 9.57% protein, 22.34% fat, and 47.23% lactose) and HIPP organic combiotic (termed B, composition: 8.57% protein, 17.76% fat, and 51.43% lactose) follow on milk 'stage 2', were selected because of their significant differences in physical properties, especially for the particle size and PSD. Fig. 1 shows their PSDs and light microscopy photos.

2.2. Sample preparation

Powders (50 g) were transported by the laboratory pneumatic conveyor (Han et al., 2021a) with a feeding rate of 3.0 g/s and an air velocity of 30 or 40 m/s (called pc30 and pc40, respectively). Most powder breakage during pneumatic conveying is a result of particle-wall collisions, specifically at the bends (Kotzur et al., 2018). Samples (50 g) were fed to the lab-scale high-speed mixer (Waring, USA) (Han et al., 2021a) operated for two different durations of 2 and 6 min (called hm2 and hm6, respectively). Similarly, the general perception is that impact during mixing is more likely leading to particle breakage (Iveson et al.,

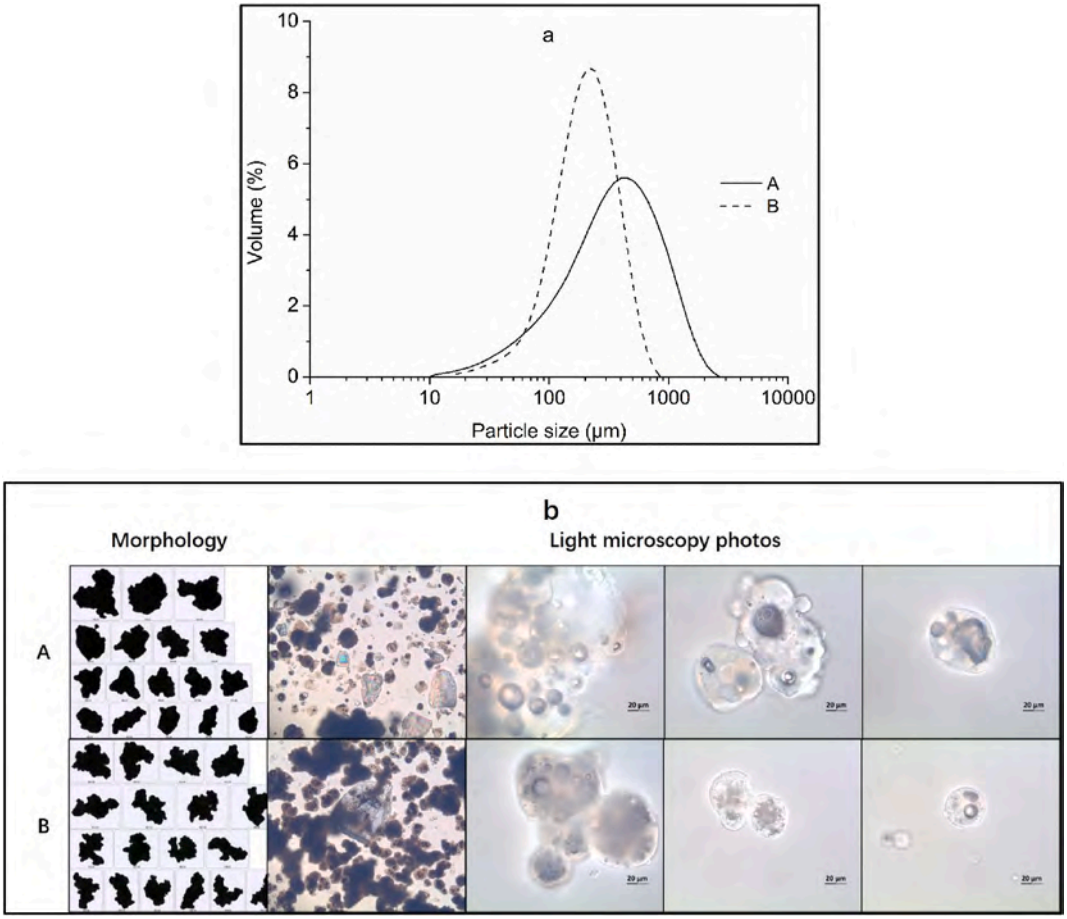


Fig. 1. Particle size distribution (a) and microscopy photos (b) of samples. A: Apt Pro stage 2 infant milk formula. B: Hipp stage 2 infant milk formula.

2001). For each process method, 250 g of each sample was broken and mixed for the following measurement. The particle size of each batch was compared before mixing and there were no significant differences between the batches (data not shown).

It should be mentioned that the processing conditions used above were selected based on our previous research (Han et al., 2021a) and the aim of this study. In the previous study, three different processing methods (powder venturi feeder transportation, lab-scale pneumatic conveying with an air velocity of 20, 30, and 40 m/s, and laboratory high-speed mixing for 10, 30, 60, and 180 s) were used to investigate the breakage behavior of IMF. It was found that the main breakage mechanism during high-speed mixing was body breakage and during pneumatic conveying was surface breakage. Pneumatic conveying and high-speed mixing were chosen for this study because samples after transportation by powder venturi feeder could not be collected and also this study aims to investigate the influence of different breakage mechanisms on powder properties. The main breakage mechanisms during these two treatments were different, which met the objectives of this study. In addition, in order to control the number of samples, two levels of flow velocity and treatment time were used to ensure different breakage mechanisms could be expected.

2.3. Breakage mechanisms determination

The dominant breakage mechanisms were determined according to the changes in PSD of samples before and after breakage, following the method described in previous research (Han et al., 2021a). A Malvern Mastersizer 3000 (Malvern Instruments Ltd., Worcestershire, UK) was used to measure the volume- and number-PSD of powders with the laser obscuration level at 1–4%. The sample and background measurement times were 10 and 20 s, respectively, with the transportation air pressure at 0 bar.

The main breakage mechanisms of samples broken in the higher-speed mixing were clear (and will be described in 3.1). In order to identify the primary breakage mechanisms of whole samples broken in the pneumatic conveying, samples were sieved into five size fractions, greater than 355 μm, from 355 to 250 μm, from 250 to 180 μm, from 180 to 125 μm, and less than 125 μm (called >355, 355-250, 250-180, 180-125, and <125, respectively). The mass percentages of each component (>355, 355-250, 250-180, 180-125, and <125) to the whole sample were 42.41%, 13.57%, 12.94%, 10.18%, and 20.90% for sample A, respectively, and were 9.88%, 16.58%, 27.43%, 24.73%, and 21.39% for sample B, respectively. Fractions were transported using the dilute-phase pneumatic conveyor, as described in 2.2, and then measured the PSD.

2.4. Determination of powder physical properties

2.4.1. Specific surface area and particle size

The specific surface area (SSA) and Sauter mean particle size ($D_{3,2}$) of the volume PSD of powders were measured using the Mastersizer 3000 with the transportation air pressure at 0.2 bar, as described in 2.3.

2.4.2. Friability

Friability refers to the ability of particles to break into smaller particles and can be used to represent powder strength. The bigger the friability index (*FI*), the easier it is for particles to be broken. The *FI* was deduced from the results of particle size measured by the Mastersizer 3000 with different compressed air pressures, as described in 2.3. *FI* can be calculated as Eq. (1) (Schuck et al., 2012)

$$FI = \left(\frac{D32_{0.5} - D32_{4.0}}{D32_{0.5}}\right) \times 100\% \quad (1)$$

where $D32_{0.5}$ and $D32_{4.0}$ were the $D_{3,2}$ measured with compressed air at 0.5 and 4.0 bar, respectively.

2.4.3. Densities and porosity

Bulk densities (tapped (100 taps) bulk density (ρ_{tapped}) and loose bulk density (ρ_b)) and particle density (ρ_p) of samples were measured using a Jolting volumeter (Funke Gerber, Berlin, Germany) and Gas Pycnometer (Accupyc II 1340, Micromeritics Instrument Corporation, USA), respectively, as per GEA Niro (2006). The porosity (ε) of powders was evaluated from Eq. (2).

$$\varepsilon = 1 - \rho_{tapped}/\rho_p \quad (2)$$

2.5. Powder surface composition

The relative amounts of C1s, N1s, and O1s at the surface of milk powder particles were determined by X-ray photoelectron spectroscopy measurements (XPS) using a Kratos AXIS Ultra spectrometer (Kratos Analytical Ltd., Manchester, UK). Any elements not detected may be absent or below the detection limit of the XPS (<0.1 atomic %). From C, N, and O percentages, the relative amount of fat, lactose, and protein (other components were neglected) of some dairy powders have been calculated with a matrix formula created from the elemental compositions of the pure milk components (Faldt et al., 1993; Murrieta-Pazos et al., 2012a). However, fat in IMF samples was mixed vegetable oil so the relative content of fat, lactose, and protein could not be calculated without the standard relative amount of C, N, and O of the mixed vegetable oil. Nevertheless, the N content can represent the relative protein content because only protein contains nitrogen.

2.6. Morphological characteristics

Three shape factors, convexity, elongation, and circularity, were used to indicate how similar the shape of a particle is to a perfect circle with values ranging from 0 to 1 (Ji et al., 2015). Convexity indicates particle surface roughness and the convexity of a smooth shape is 1. Elongation is calculated from [1-aspect ratio], where the value of shapes symmetrical in all axes, such as a circle or square, is 0. The circularity of a perfect circle is 1. The morphology of powders was determined via scanning and analyzing thousands of individual particles using a Malvern Morphologi G3 (Malvern Instruments Ltd.). Powders were dispersed into a single uniform layer and particles were well separated. Then all the particles were gradually scanned by the microscope and the average values were given.

2.7. Water sorption behavior

2.7.1. Water sorption and time-dependent lactose crystallization

The static gravimetric method was used to determine the water sorption behavior of IMF samples and the decrease in the sorbed water was a result of time-dependent lactose crystallization. Samples (1 g) were dried at 45 °C in a vacuum oven (OV-12, Lab Companion, Daejeon, Korea) for 48 h. Powders were then equilibrated at 25 °C for 168 h at different relative water vapor pressures (RVP) provided by different saturated salt solutions. They were NaCl, $NaNO_2$, $Mg(NO_3)_2$, K_2CO_3, $MgCl_2$, CH_3COOK, and LiCl which gave RVP of 76.1%, 65.6%, 54.5%, 44.1%, 33.2%, 23.1%, and 11.4%, respectively. Samples were weighed at 0, 3, 6, 9, 12, 24 h and then at 24 h intervals. The result was presented as the equilibrated water content of 100 g dry matter (based on non-fat solids as fat cannot absorb moisture (Kelly et al., 2015; Maidannyk et al., 2019)). The average was calculated from triplicate samples.

According to the water contents at different time points, the average water sorption rate of every 3 h in the first 48 h was calculated as Eq. (3) (Li et al., 2016b). It is hypothesized that the sorption rate during the calculated 3 h was constant.

$$Sorption\ rate = \frac{Absorbed\ water}{time}\left(\%h^{-1}\right) \quad (3)$$

The experimental sorption data at RVP ≤44.1% was analyzed and

correlated by the GAB (Guggenheim-Anderson de Boer) isotherm model that was given by Eq. (4). The constant α, β, and γ of its second-order polynomial (Eq. (5)) were calculated by plotting a_w/m against a_w where a_w was the water activity, and m (g/100 g non-fat dry solid) was the equilibrium water content. The monolayer moisture content m_m (g/100 g non-fat dry solid) and the constant K and C were calculated from Eqs. (6)–(8), respectively.

$$\frac{m}{m_m}=\frac{CKa_w}{(1-Ka_w)(1-Ka_w+CKa_w)} \tag{4}$$

$$\frac{a_w}{m}=\alpha a_w^2+\beta a_w+\gamma \tag{5}$$

$$m_m^2=-\frac{1}{4\alpha\gamma-\beta^2} \tag{6}$$

$$K=\frac{\beta-\frac{1}{m_m}}{-2\gamma} \tag{7}$$

$$C=\frac{1}{m_m\gamma K} \tag{8}$$

An indication of the fit of the GAB model, RMS (relative percentage Root Mean Square), was calculated from Eq. (9)

$$\%RMS=\sqrt{\frac{\sum_i^N\left[\frac{m_i-m_i^*}{m_i}\right]^2}{N}}\times 100 \tag{9}$$

where N was the number of experimental points, and m_i and m_i* were the experimental and the calculated moisture content, respectively.

2.7.2. Sorbed water properties

Some properties of sorbed water were analyzed using the linear form of Caurie's equation (Mazza and LeMaguer, 1978) (Eq. (10)), where c_d was the density of sorbed water (g/ml), and m and m_c were the equilibrium and monolayer moisture contents (g/100 g non-fat dry solid), respectively. The number of adsorbed monolayers (N_{am}) and the surface area of adsorbent (A, m^2/g) were calculated from Eqs. (11) and (12), respectively, where S was the slope of Eq. (10) (Červenka et al., 2015).

$$ln\left(\frac{1}{m}\right)=-ln(c_dm_c)+\frac{2c_d}{m_c}ln\frac{1-a_w}{a_w} \tag{10}$$

$$N_{am}=2/S \tag{11}$$

$$S=54.45/A \tag{12}$$

2.7.3. Spreading pressure

Spreading pressure (φ, J/m^2) is one of the thermodynamic properties which can be used to analyze the sorption phenomena. It is also known as surface potential, representing the excess free energy on the surface and has been used as the diffusion driving force in porous solids (Polatoğlu et al., 2011). φ is an indicator of the increase in surface tension in the free sorption sites because of the adsorption of molecules (Simón et al., 2016). High φ values indicate the high affinity of water molecules to active sites (Torres et al., 2012). φ was determined from Eq. (13)

$$\varphi=\frac{K_BT}{A_m}ln\left[\frac{1+CKa_w-Ka_w}{1-Ka_w}\right]_{0.05}^{a_w} \tag{13}$$

where the Boltzmann constant K_B was 1.380×10^{-23} J/K, T was the temperature (K), A_m was the surface area of a water molecule (1.06×10^{-19} m^2), and C and K were the constants in the GAB isotherm model (Lago et al., 2013). 0.05 was used as the lowest limit of Eq. (13) because the integral value of $a_w=0$ is indeterminate (Iglesias et al., 1976).

2.8. Glass transition, initial crystallization and α-relaxation

A differential scanning calorimeter (DSC Q2000, TA Instruments, Crawley, UK) was used to determine T_g (onset) and initial crystalized temperatures (T_{ic}) of samples equilibrated for 168 h at different RVP (11.4%, 23.1%, 33.2%, and 44.1%). Besides, a Dynamic Mechanical Analyzer (DMA Q800, TA Instruments) was used to measure the dynamic mechanical properties of those equilibrated samples, including storage modulus, loss modulus, and α-relaxation with multiple frequencies (0.5, 1, 2, 5, and 10 Hz). The temperatures of loss modulus peak values were taken as α-relaxation temperatures (T_α). Measurements followed the methods described by Li et al (2016a).

2.9. Experimental design and statistical analysis

Measurements of powder surface compositions, T_g, T_{ic}, T_α, and modulus changes were carried out in duplicate, and all other measurements were performed in triplicate. Results were shown as mean ± standard deviation (SD). One-way ANOVA with Tukey's test (IBM SPSS Statistics version 24, IBM, USA) was used to determine significant differences with a confidence level of $P<0.05$.

3. Result and discussion

3.1. Breakage mechanisms determination

The dominant breakage mechanisms (not necessarily the sole one) of IMF samples were determined according to the PSDs changes before and after breakage. The volume- and number-PSD of whole powders are given in Fig. 2. At the same processing conditions, the changes in PSD of the two whole samples were similar and compared with sample B (Fig. 2c&d), more breakage occurred for sample A (Fig. 2a&b) during mixing.

It was shown that after mixing for 2 or 6 min, the PSDs of the two samples significantly moved to the smaller value and most of the initial big-sized mother particles were broken into many small-sized child particles. This observation was supported by the movement of the number-PSD to the smaller value and most of the particles were small-sized particles. These results suggest that the main breakage mechanism after mixing for two IMF samples was body breakage.

Compared with mixing samples, there was not enough evidence to easily identify the main breakage mechanisms of the pneumatic conveying samples based only on the changes in PSDs of whole samples because there was no bimodal PSDs or other features. Thus, the volume PSD of sieved fractions of the two samples before and after transportation are given in Fig. 3. For sample A (Fig. 3a–c), transportation impacted the PSD of particles bigger than 250 μm. The larger the particles, the more sensitive they were to transportation, and the greater the PSD changed. It has been attributed to the likelihood of a greater number of imperfections in larger particles (Antonyuk et al., 2005; Norazirah et al., 2016). The highest local tensile stress is generated at these defective zones so that the fracture initiates from this zone and propagates. Besides the few flaws, small particles are more difficult to break owing to the stronger interparticle forces that bind particles together including van der Waals forces, electrostatics, and liquid bonds (Reynolds et al., 2005). From an energy perspective, the smaller the particles, the higher the fracture energy, and hence the less likely the particle will break (King, 2012). For samples A>355 and A355-250, the main particles were still big-sized particles but large numbers of small particles were produced and appeared as a well-separated peak on the left in PSDs. This means that surface breakage most likely occurred for these particles. For the other three small-sized fractions of sample A, the PSD slightly shifted to the smaller value for A250–180 and A180-125 without the production of small particles, and the PSD curves of A<125 were similar. This means that the slight decrease of particle size for A250–180 and A180-125 might be because of dispersion. These

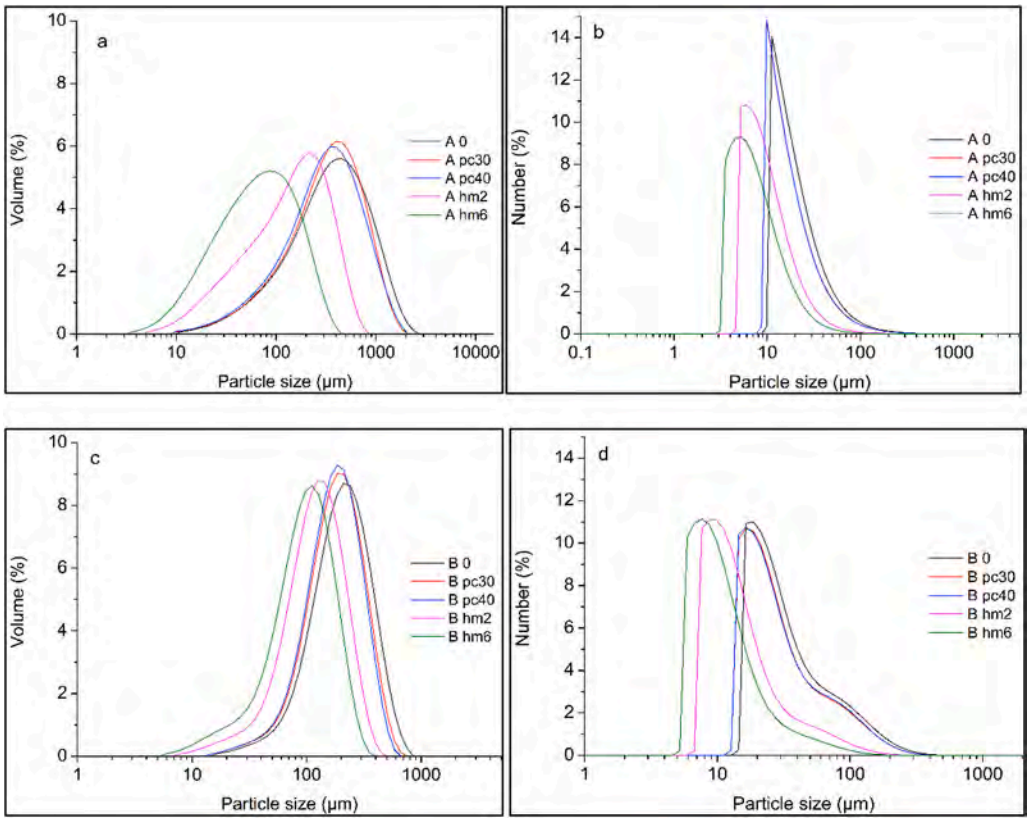


Fig. 2. Volume- (a and c) and number-particle size distributions (b and d) of whole infant milk samples. A: Apt Pro stage 2 infant milk formula. B: Hipp stage 2 infant milk formula. 0: control samples. pc: broken by pneumatic conveying under the air velocity of 30 m/s and 40 m/s hm: broken by the laboratory high-speed mixer for 2 min and 6 min.

results indicate that the breakage of sample A during pneumatic conveying mostly occurred on particles bigger than 250 μm. Besides, the mass percentage of A>355 and A355-250 to the whole sample was around 56%. Thus, it can be concluded that surface breakage occurred on around 56% of particles of sample A after pneumatic conveying. Similarly, for sample B (Fig. 3d–g), surface breakage most likely occurred at all air velocities transportation for B355-250 and 40 m/s conveying for B250-180 while dispersion was the main breakage mechanism for B180-125. Unlike A>355, low-degree body breakage most likely occurred for B > 355 after transportation but its mass percentage to the whole sample was only 10%. Thus, the breakage of sample B during pneumatic conveying mostly occurred on particles bigger than 180 μm and the dominant mechanism was surface breakage.

Overall, for the two samples, particle breakage after high-speed mixing was mainly due to body breakage, while breakage after the dilute-phase pneumatic conveying was mainly caused by surface breakage which occurred on big-sized particles. Different breakage mechanisms showed different effects on powder physical properties and subsequently on water sorption and mechanical properties, which will be discussed in the next few sections.

3.2. Powder characterization

3.2.1. Particle size and friability

The $D_{3,2}$ and its percentage change compared with control samples are shown in Table 1. The $D_{3,2}$ of broken powders was significantly lower ($P < 0.05$) than those of control powders and body breakage had a greater effect on the decrease of $D_{3,2}$ than surface breakage. This is consistent with the results of PSD changes. From Table 1, the $D_{3,2}$ decreased by around 10% after surface breakage but body breakage decreased it considerably more with reductions of 45–80%. Compared with sample A, the particle size of sample B decreased more after surface breakage while decreased less after body breakage. It has been reported that the strength of agglomerates decreased with increasing particle size (Fu et al., 2005; Han et al., 2021b). This is consistent with the results of *FI* that was decreased with decreasing particle size or the increasing breakage degree (Table 1). Thus, the reason for the higher $D_{3,2}$ decreases of sample A after body breakage might be because the initial particle size of sample A was bigger than that of sample B. This also explained why the *FI* of A samples were higher than those of B samples. However, this contradicted with the result that the $D_{3,2}$ of sample B decreased more after surface breakage. This might be because there were more big-sized crystalline particles in sample A (Fig. 1b). For crystalline particles, the breakage may occur at the interface of crystals instead of on the surface (Cleaver et al., 1993; Ghadiri et al., 1991). This means, at low processing conditions, compared with crystalline particles, the normal agglomerated dairy particles may be more sensitive to the mechanical force. This was supported by the analysis in 3.1 that at the same transportation condition, B > 355 suffered body breakage while surface breakage occurred for A>355.

3.2.2. Powder densities and porosity

The changes in densities and porosity may influence the water sorption behavior of samples through affecting the number of liquid bridges (Carpin et al., 2017). Besides, the bulk density of powders is used to calculate the volumetric capacity of packing materials. It is an important property for IMF as they are dispensed on a volume basis using a scoop. From Table 1, as expected, the particle density of sample B, around 1.2 kg/L, did not change a lot even after body breakage, which has been found in previous research (Han et al., 2020). However, the particle density of body breakage sample A significantly increased from 0.98 kg/L to around 1.2 kg/L. After breakage, particularly for body breakage, the bulk densities of sample B significantly increased and the porosity decreased. This corresponded with several studies on

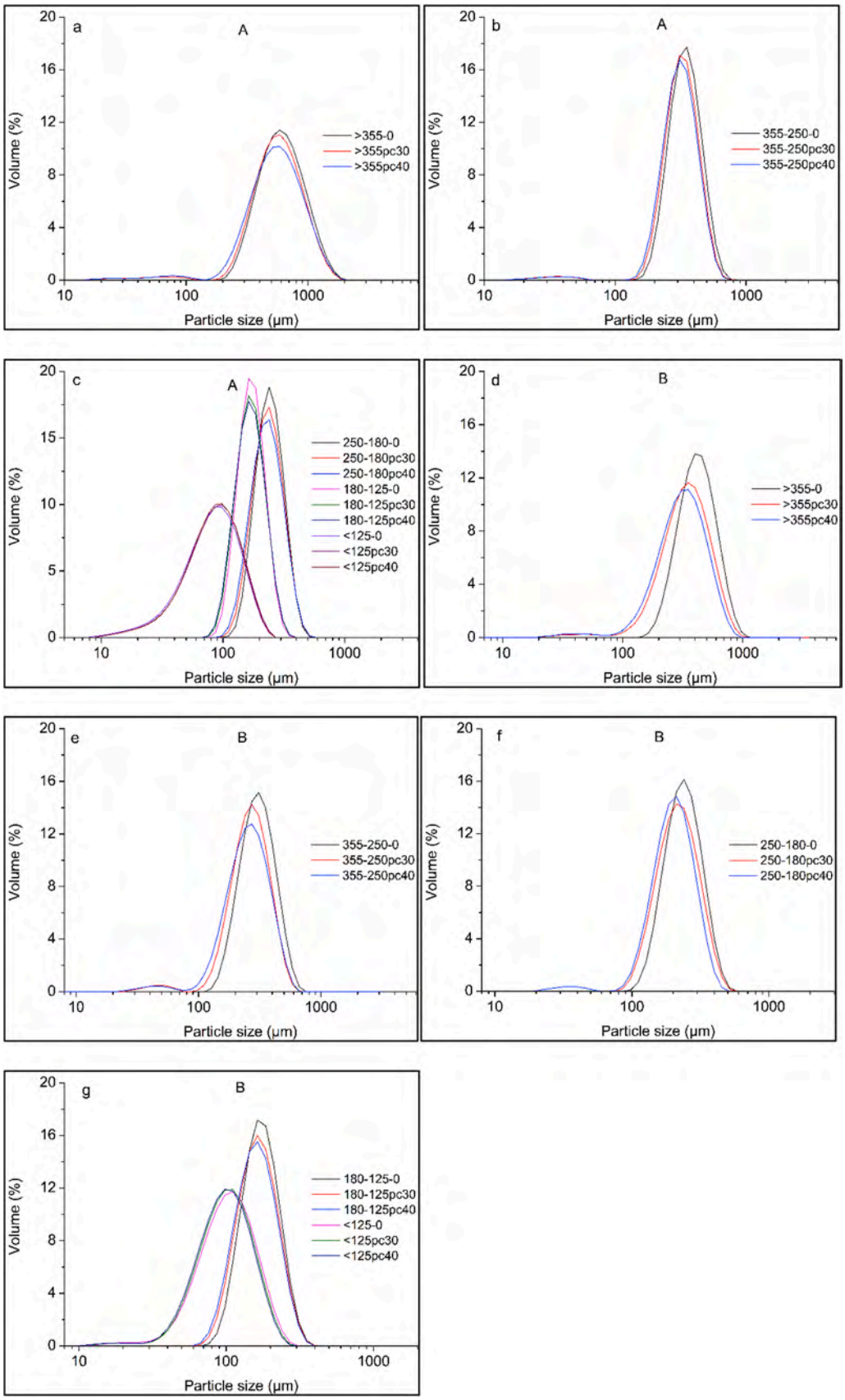


Fig. 3. Particle size distributions of sieved fractions of infant milk samples (a–c: sample A; d–g: sample B). A: Apt Pro stage 2 infant milk formula. B: Hipp stage 2 infant milk formula. 0: control samples. pc: broken by pneumatic conveying under the air velocity of 30 m/s and 40 m/s hm: broken by the laboratory high-speed mixer for 2 min and 6 min.

Table 1
Physical properties of infant milk formula samples.

Samples	Particle size $D_{3,2}$ (μm)	Percentage change in $D_{3,2}$ (%)	Friability index (%)	Particle density (Kg/L)	Loose bulk density (Kg/L)	Tapped bulk density (Kg/L)	Porosity (%)	SSA (m^2/kg)
IMF-A								
0	200.0^{a}±2.4	/	53.0^{b} ± 2.3	0.984^{e}±0.001	0.438^{a}±0.001	0.587^{e}±0.002	40.4^{e}±0.2	30.5^{e}±0.4
pc30	187.3^{b} ± 2.6	6.3^{d} ± 1.4	52.4^{b} ± 0.6	0.997^{d} ± 0.001	0.444^{a}±0.002	0.608^{d} ± 0.002	39.1^{d} ± 0.2	32.1^{d} ± 0.5
pc40	178.0^{c}±2.2	11.0^{c}±1.1	55.9^{a}±0.2	0.992^{c}±0.002	0.442^{a}±0.001	0.616^{c}±0.001	37.9^{c}±0.1	34.0^{c}±0.4
hm2	74.4^{d} ± 0.7	62.8^{b} ± 0.4	37.4^{c}±1.0	1.172^{b} ± 0.001	0.446^{a}±0.001	0.637^{b} ± 0.001	45.7^{b} ± 0.1	68.8^{b} ± 0.7
hm6	44.0^{e}±0.1	78.0^{a}	28.8^{b} ± 0.1	1.276^{a}±0.002	0.445^{a}±0.004	0.647^{a}±0.002	49.3^{a}±0.1	107.0^{a}±0.1
IMF-B								
0	165.0^{A}	/	45.7^{A} ± 0.6	1.214^{E}±0.001	0.465^{C} ± 0.002	0.571^{D}±0.001	52.9^{A} ± 0.1	30.0^{C} ± 0.1
pc30	148.0^{B} ± 0.8	10.3^{D}±1.3	41.5^{B}	1.217^{D}±0.001	0.491^{B} ± 0.003	0.593^{CD}±0.010	51.3^{AB}±0.8	33.4^{C} ± 0.3
pc40	143.3^{C} ± 1.2	13.1^{C} ± 1.1	40.6^{B} ± 1.1	1.219^{C} ± 0.001	0.499^{B} ± 0.013	0.611^{BC}±0.009	49.8^{BC}±0.7	34.4^{C} ± 0.3
hm2	91.4^{D}±0.6	44.6^{B} ± 0.4	31.3^{C} ± 0.4	1.234^{B} ± 0.001	0.527^{A} ± 0.003	0.640^{AB}±0.001	48.2^{CD}±0.1	56.1^{B} ± 4.2
hm6	68.5^{E}±0.2	58.5^{A}	26.3^{D}±0.2	1.251^{A} ± 0.001	0.543^{A} ± 0.003	0.663^{A} ± 0.007	47.0^{D}±0.6	70.1^{A} ± 0.3

1. IMF-A: Apt Pro stage 2 infant milk formula. IMF-B: Hipp stage 2 infant milk formula. 0: control samples. pc: broken by pneumatic conveying under the air velocity of 30 m/s and 40 m/s hm: broken by the laboratory high-speed mixer for 2 min and 6 min. SSA: specific surface area.
2. Values are mean ± standard deviation (n = 3).
3. $^{a-e}$ and $^{A-E}$ different values within columns in IMF-A and IMF-B groups are significantly different at $P < 0.05$, respectively.

agglomerated milk powder breakage (Han et al., 2020; Hanley, 2011; Hazlett et al., 2020). Similarly, the tapped bulk density of sample A significantly increased after breakage, while no significant difference was observed for its loose bulk density. Besides, the porosity of sample A was significantly increased after body breakage because its particle density substantially increased.

3.2.3. Powder surface properties

Dairy powder breakage may influence the surface area and the surface composition of particles because of the production of more particles and the uneven distribution of ingredients throughout the particles. The changes in the surface properties might affect their water sorption behavior (Li et al., 2016c). The SSA and the relative amounts of elements (C1s, O1s, N1s) on particles' surfaces are given in Table 1 and Fig. 4, respectively. The SSA of the two initial samples were similar, around 30 m^2/kg, and it slightly increased after surface breakage but significantly increased to 60–100 m^2/kg after body breakage because of the production of more particles.

From Fig. 4, the amount of N was increased after breakage, which means that powder breakage increased the protein proportion on the surface of particles. Besides, around 80% of the element on the surface of IMF particles was C. It has been reported that the standard relative amounts of C and O on the surface of lactose were very close, 52.2% and 47.8%, respectively, but for fat and protein, the relative content of C was much higher than O (milk fat: 89.1% C and 10.9% O; casein: 65% C, 19% O and 16% N) (Kim et al., 2002). This means that most of the particle surface was fat, consistent with previous research (O'Donoghue et al., 2019; O'Neill et al., 2019). In addition, after breakage, the relative amount of C and O slightly decreased and increased, respectively (Fig. 4). These results suggest that powder breakage slightly decreased the fat and increased the lactose proportions on the surface of particles, which could decrease particle hydrophobicity. This could be explained by the results of previous studies regarding the surface to core composition of agglomerated milk powder particles (Murrieta-Pazos et al., 2012b). For particles containing fat, the fat content significantly decreased from the surface to the core, and opposite behaviors were observed for proteins and lactose.

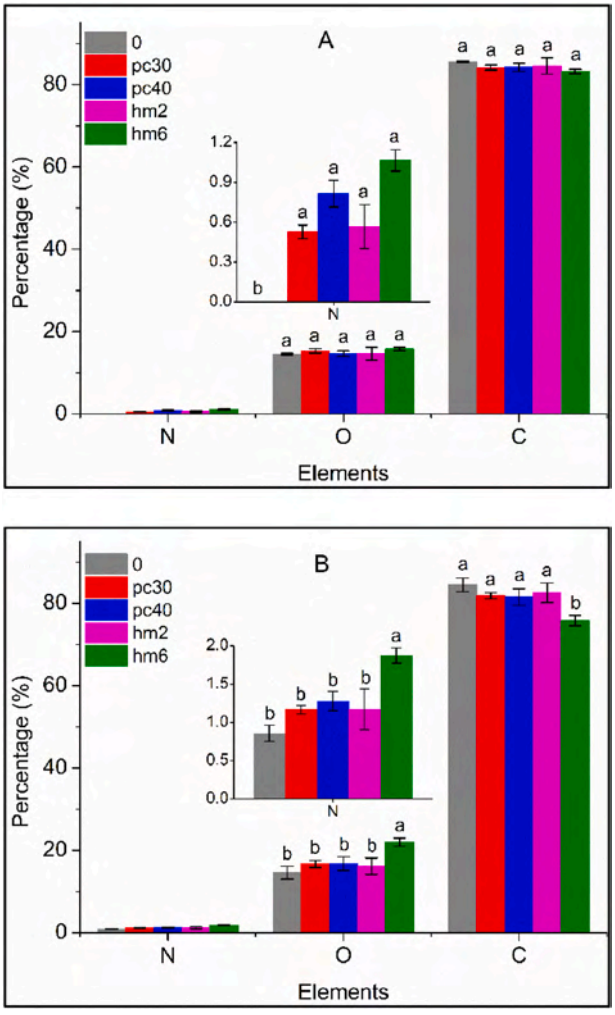


Fig. 4. Relative elements (C, O, and N) on the surface of particles. A: Apt Pro stage 2 infant milk formula. B: Hipp stage 2 infant milk formula. 0: control samples. pc: broken by pneumatic conveying under the air velocity of 30 m/s and 40 m/s hm: broken by the laboratory high-speed mixer for 2 min and 6 min. Different a-b values between samples in each group (A and B) within each element (C, O, and N) are significantly different at $P < 0.05$.

3.2.4. Morphological characteristics

The shape of particles can influence powder bulk density and porosity, which subsequently affects the water sorption property of powders. The morphological characteristics (circularity, convexity, and elongation) of samples are shown in Table 2. The elongation of samples largely remained unchanged before and after breakage, but the elongation of samples used in this study was higher than other non-agglomerated dairy powders (Li et al., 2017). This might be because

Table 2
Morphological characteristics of infant milk formula samples.

Samples	Elongation	Circularity	Convexity
IMF-A			
0	0.295^{a}±0.021	0.774^{b} ± 0.027	0.977^{b} ± 0.003
pc30	0.272^{ab} ± 0.007	0.804^{ab} ± 0.018	0.981^{b} ± 0.005
pc40	0.270^{b} ± 0.001	0.802^{ab} ± 0.010	0.979^{b} ± 0.005
hm2	0.284^{ab} ± 0.003	0.792^{ab} ± 0.012	0.980^{b} ± 0.004
hm6	0.276^{ab} ± 0.003	0.836^{a}±0.08	0.993^{a}±0.002
IMF-B			
0	0.240^{BC}±0.008	0.812^{D}±0.010	0.975^{D}±0.002
pc30	0.226^{CD}±0.002	0.836^{C} ± 0.004	0.981^{C} ± 0.001
pc40	0.225^{D}±0.004	0.838^{BC}±0.004	0.980^{C} ± 0.000
hm2	0.253^{AB}±0.001	0.855^{AB}±0.001	0.992^{B} ± 0.000
hm6	0.258^{A} ± 0.004	0.860^{A} ± 0.003	0.995^{A}

1. IMF-A: Apt Pro stage 2 infant milk formula. IMF-B: Hipp stage 2 infant milk formula. 0: control samples. pc: broken by pneumatic conveying under the air velocity of 30 m/s and 40 m/s hm: broken by the laboratory high-speed mixer for 2 min and 6 min.
2. Values are mean ± standard deviation (n = 3).
3. $^{a-b}$ and $^{A-D}$ different values within columns in IMF-A and IMF-B groups are significantly different at $P < 0.05$, respectively.

granulated particles were more irregular. Compared with surface breakage particles, the circularity and convexity of most body breakage particles were significantly higher than those of their control samples. These results indicate that body breakage particles had more rounded shapes and smoother surfaces and surface breakage did not significantly change particle shapes. This also can be observed from photos of some particles scanned by the Morphologi G3 (shown in Supplementary Figure S1).

3.3. Water sorption behavior

3.3.1. Water sorption and time-dependent lactose crystallization

The influence of breakage on the water sorption behavior of the two IMF samples was similar, thus the following discussion is mainly based on sample A. Water contents of A samples at several a_w (0.11–0.76) were plotted as a function of time and shown in Fig. 5 (the data of B samples are shown in Supplementary Figure S2). Table 3 shows the experimental water contents of samples equilibrated for 168 h at different a_w.

Surface breakage did not significantly influence the water sorption behavior of IMF samples at most of the corresponding RVP even though the particle size decreased around 10%. In contrast, body breakage samples sorbed 4–22% larger amount of water than those of control samples at RVP ≤33.2% and the difference decreased with increasing RVP. Besides, at the same RVP, the water content increased as the body breakage degree increased. The large SSA value and small particle size of body breakage samples might be reasons that they sorbed larger amounts of water. Water is mainly absorbed on the surface of particles, thus the larger SSA means more area for sorption of water molecules (Li et al., 2016c; McCarthy et al., 2013). Besides, hydrophilic groups bind moisture molecules via formatting hydrogen bonds, thus the amount of adsorbed water depends on the presence of compounds with hydrophilic groups (Červenka et al., 2015). Moreover, hydrogen bonds between molecules depend on the size of particles (Haque and Roos, 2004). Similar results were found where coarse powders sorbed less water than fine powders for lactose/different protein powder systems at PVR ≤33.2% (Haque and Roos, 2004). Li et al. and Carpin et al. also had similar findings for lactose/MPI samples at PVR ≤44.1% and lactose at PVR ≤95% (Carpin et al., 2017; Li et al., 2016c). It is also possible that the internal hydrophilic groups were exposed after body breakage, and samples had higher amounts of hydrogen bonding sites for sorption of moisture molecules. However, the same trend was not observed for skim milk powder, and the authors suggested that the difference in hygroscopicity between different size particles might be primarily due to the differences in composition (O'Donoghue et al., 2019). Thus, the changes in surface composition might be another reason for different water content between body breakage samples and other samples. After body breakage, the surface fat proportion slightly decreased and lactose proportion increased, which could decrease particle hydrophobicity.

These reasons also caused significantly higher water absorption rates of body breakage samples than other samples. The sorption rates of samples equilibrated at different a_w (0.11–0.76) in the first 3 h are shown in Fig. 6a&b. For all samples, the sorption rates increased with increasing a_w. Body breakage samples sorbed water significantly faster (at around 35%–126% higher for IMF-A and 10%–85% higher for IMF-B) than other samples at same storage conditions and this difference increased as a_w increased. Besides, the water sorption rate decreased with increasing equilibration time and it decreased faster for body breakage samples. The sorption rates of sample A equilibrated at 0.23 a_w at 3-h intervals in the first 48 h are shown in Fig. 6c, where the rates of body breakage samples were lower than those of other samples after equilibration around 10 h.

Due to time-dependent lactose crystallization, part of sorbed water bound by amorphous lactose was released within 24 or 48 h at RVP ≥54.5%. This is consistent with the result obtained by McCarthy et al. (2013) who found the discontinuity in the isotherm at 54.5% RVP for a model IMF sample. From Fig. 5, body breakage significantly influenced lactose crystallization during storage. Loss of sorbed water in body breakage samples appeared after 9 or 10, 9, and 12 h of storage and in other samples appeared after 11, 12, and 24 h of storage at 76.1%, 65.6%, and 54.5% of RVP, respectively. Besides, body breakage samples sorbed less water before crystallization. These results mean that body breakage accelerated the time-dependent lactose crystallization and samples crystallized at lower moisture contents. In addition, the water content of hm6 increased after the loss of sorbed water at 76.1% RVP, which might be because of the recrystallization of lactose. It has been reported that unstable anhydrous β-lactose could recrystallize into stable α-lactose monohydrate by further absorbing water during storage. Likewise, at the same storage considerations, loss of sorbed water levelled off at nearly the same time with similar water contents (Table 3) in body breakage samples and other samples. These results mean breakage might not affect final crystallization but might influence recrystallization during the crystal formation.

At 44.1% RVP, particle breakage did not influence the water content and there was no time-dependent lactose crystallization occurred. There was a rapid increase in the water content of samples in 33.2%–44.1% RVP (Table 3), indicative of water migrating into powders as it approached the glass transition region, before crystallization (Kelly et al., 2016).

3.3.2. Sorption isotherm

The GAB model was used to model the experimental water content of samples equilibrated at a_w ≤0.441 (Fig. 7) and the parameters are given in Table 4. From Fig. 7, equilibrium water content increased as a_w increased and moisture adsorption isotherms of all samples were sigmoid shape. Meanwhile, isotherms were similar for both control and surface breakage samples but different from body breakage samples. According to the low RMS values, the GAB model fitted well with the experimental water sorption data at a_w ≤0.441 where the water contents of body breakage samples were higher or similar to those of other samples. In contrast, the predicted water contents of body breakage samples were lower than those of other samples at higher a_w (>0.441). This is consistent with the results that body breakage samples sorbed less water before crystallization at a_w ≥0.545.

From Table 4, the m_m of body breakage powders were significantly higher than other powders, and it increased from around 3.4 to 4.5 g/100 g dry solids for sample A and from around 3 to 3.4 g/100 g dry solids for sample B. The m_m represents the moisture content when each polar group in a molecule binds with one moisture molecule (McCarthy et al., 2013). Thus, the higher m_m of body breakage samples corresponded to their higher water contents. Besides, after body breakage, K and C of

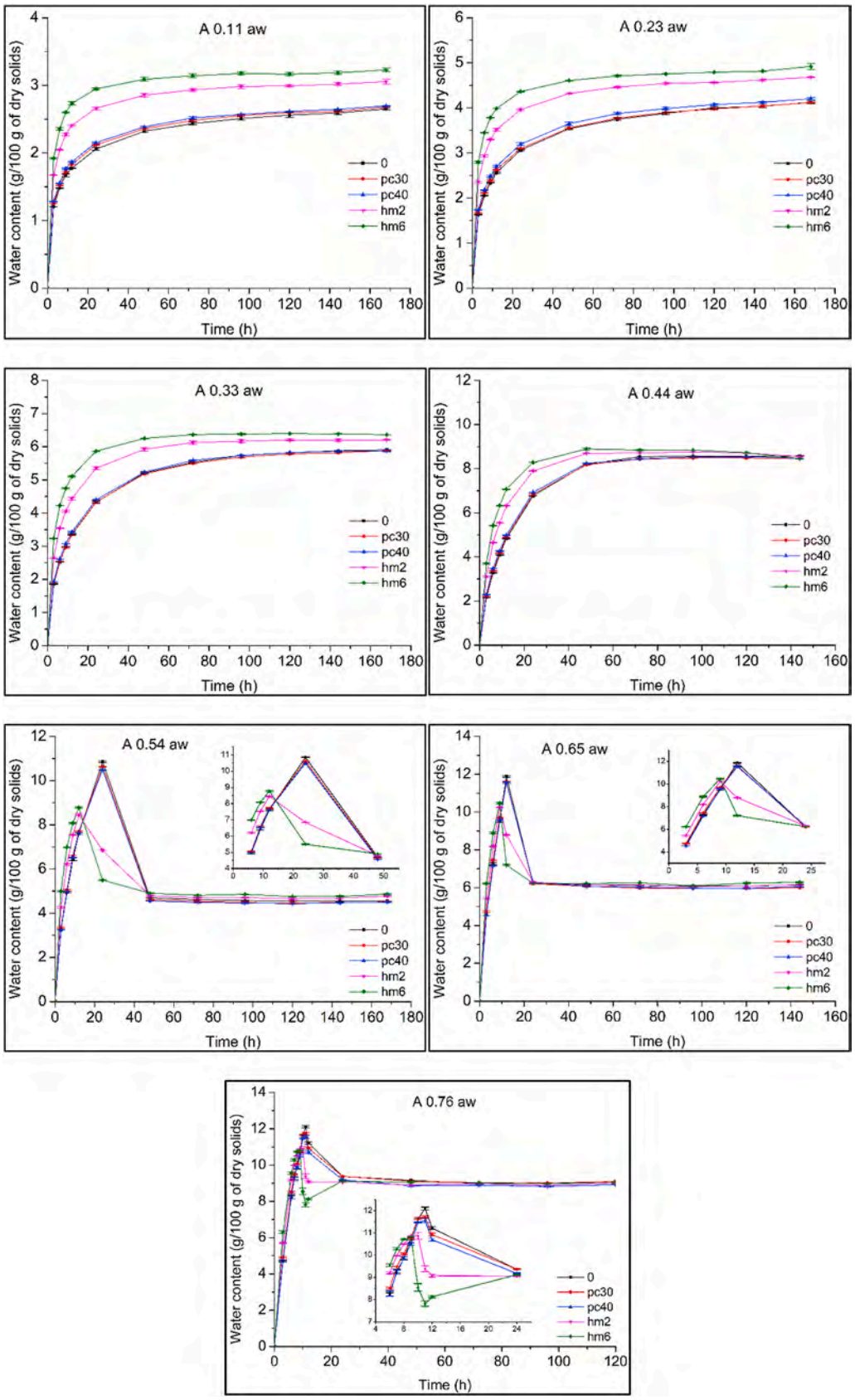


Fig. 5. Water sorption behavior of sample A equilibrated at various water activities (0.11–0.76) for 168 h at 25 °C. A: Apt Pro stage 2 infant milk formula. 0: control samples. pc: broken by pneumatic conveying under the air velocity of 30 m/s and 40 m/s hm: broken by the laboratory high-speed mixer for 2 min and 6 min.

Table 3
Water contents of samples equilibrated for 168 h at various water activities (0.11–0.76) at 25 °C.

Samples	Water activity						
	0.11	0.23	0.33	0.44	0.54	0.65	0.76
IMF-A							
0	$2.65^{c}\pm0.01$	$4.12^{c}\pm0.03$	$5.91^{c}\pm0.01$	$8.57^{a}\pm0.02$	$3.82^{a}\pm0.00$	$5.46^{a}\pm0.01$	$9.11^{a}\pm0.00$
pc30	$2.68^{c}\pm0.01$	$4.12^{c}\pm0.00$	$5.88^{c}\pm0.01$	$8.47^{b}\pm0.01$	$3.79^{ab}\pm0.03$	$5.54^{a}\pm0.00$	$9.10^{a}\pm0.01$
pc40	$2.70^{c}\pm0.00$	$4.20^{c}\pm0.02$	$5.88^{c}\pm0.03$	$8.47^{b}\pm0.01$	$3.68^{bc}\pm0.01$	$5.44^{a}\pm0.01$	$8.92^{b}\pm0.01$
hm2	$3.05^{b}\pm0.04$	$4.68^{b}\pm0.01$	$6.20^{b}\pm0.01$	$8.55^{a}\pm0.01$	$3.61^{c}\pm0.04$	$5.34^{b}\pm0.02$	$9.01^{ab}\pm0.03$
hm6	$3.23^{a}\pm0.02$	$4.92^{a}\pm0.06$	$6.36^{a}\pm0.00$	$8.45^{b}\pm0.00$	$3.78^{ab}\pm0.02$	$5.46^{a}\pm0.04$	$9.06^{a}\pm0.04$
IMF-B							
0	$2.70^{C}\pm0.00$	$3.82^{D}\pm0.03$	$5.90^{B}\pm0.03$	$8.53^{B}\pm0.02$	$4.44^{A}\pm0.00$	$6.74^{A}\pm0.05$	$9.79^{B}\pm0.01$
pc30	$2.73^{C}\pm0.00$	$3.92^{C}\pm0.01$	$6.00^{B}\pm0.01$	$8.62^{AB}\pm0.00$	$4.24^{BC}\pm0.03$	$6.52^{B}\pm0.05$	$9.82^{B}\pm0.03$
pc40	$2.76^{C}\pm0.05$	$3.95^{C}\pm0.03$	$5.96^{B}\pm0.05$	$8.60^{AB}\pm0.01$	$4.16^{BC}\pm0.03$	$6.52^{B}\pm0.00$	$9.80^{B}\pm0.03$
hm2	$2.94^{B}\pm0.02$	$4.06^{B}\pm0.02$	$6.10^{AB}\pm0.05$	$8.68^{A}\pm0.01$	$4.08^{C}\pm0.01$	$6.38^{C}\pm0.03$	$9.99^{A}\pm0.03$
hm6	$3.11^{A}\pm0.01$	$4.29^{A}\pm0.01$	$6.25^{A}\pm0.12$	$8.67^{A}\pm0.07$	$3.86^{D}\pm0.03$	$5.96^{D}\pm0.03$	$9.88^{B}\pm0.04$

1. IMF-A: Apt Pro stage 2 infant milk formula. IMF-B: Hipp stage 2 infant milk formula. 0: control samples. pc: broken by pneumatic conveying under the air velocity of 30 m/s and 40 m/s hm: broken by the laboratory high-speed mixer for 2 min and 6 min.
2. Values are mean ± standard deviation (n = 3).
3. $^{a-e}$ and $^{A-E}$ different values within columns in IMF-A and IMF-B groups are significantly different at $P < 0.05$, respectively.

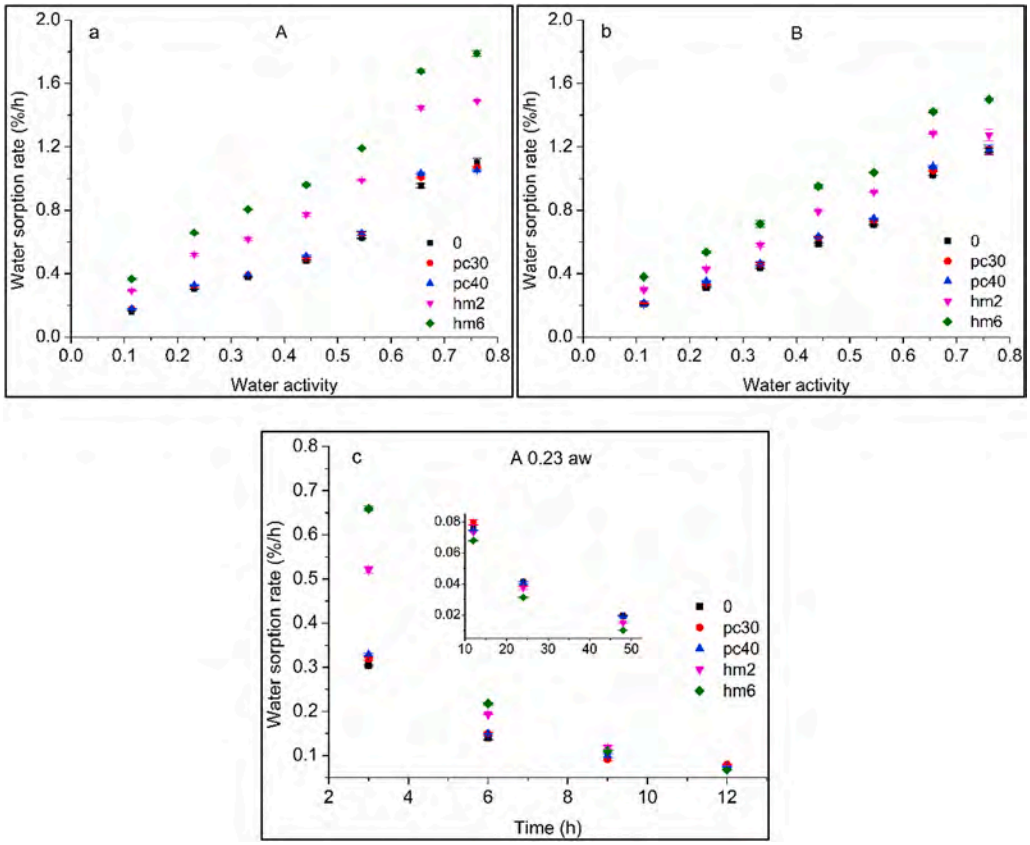


Fig. 6. Sorption rates of sample A (a) and B (b) equilibrated at various water activities (0.11–0.76) in the first 3 h and of sample A (c) equilibrated at 0.23 a_w at 3-h intervals in the first 48 h. A: Apt Pro stage 2 infant milk formula. B: Hipp stage 2 infant milk formula. 0: control samples. pc: broken by pneumatic conveying under the air velocity of 30 m/s and 40 m/s hm: broken by the laboratory high-speed mixer for 2 min and 6 min.

samples were decreased and increased, respectively. K was used to correct the properties of the multilayer molecules relative to the bulk liquid. C represents the strength of binding of water to the primary binding sites (Lazou and Krokida, 2011). Thus, water bounded stronger in the monolayer in body breakage samples than in other samples.

3.3.3. Sorbed water properties

Several properties of sorbed water derived from Caurie's equations are shown in Table 4. The monolayer values obtained from Caurie's equation (m_c) were higher than those derived from the GAB model (m_m). This is consistent with the previous reports that the monolayer values obtained using GAB and BET models were lower than those obtained using Caurie model (Dalgıç et al., 2012). Nevertheless, m_c showed the same trend as m_m, where the m_c significantly increased after the body breakage and surface breakage had no significant influence on it. Besides, body breakage samples had higher A compared with other samples, corresponding to the higher SSA, which confirmed that there were more effective areas for body breakage samples to adsorb water. This resulted in the higher N_{am}, corresponding to the higher final water contents.

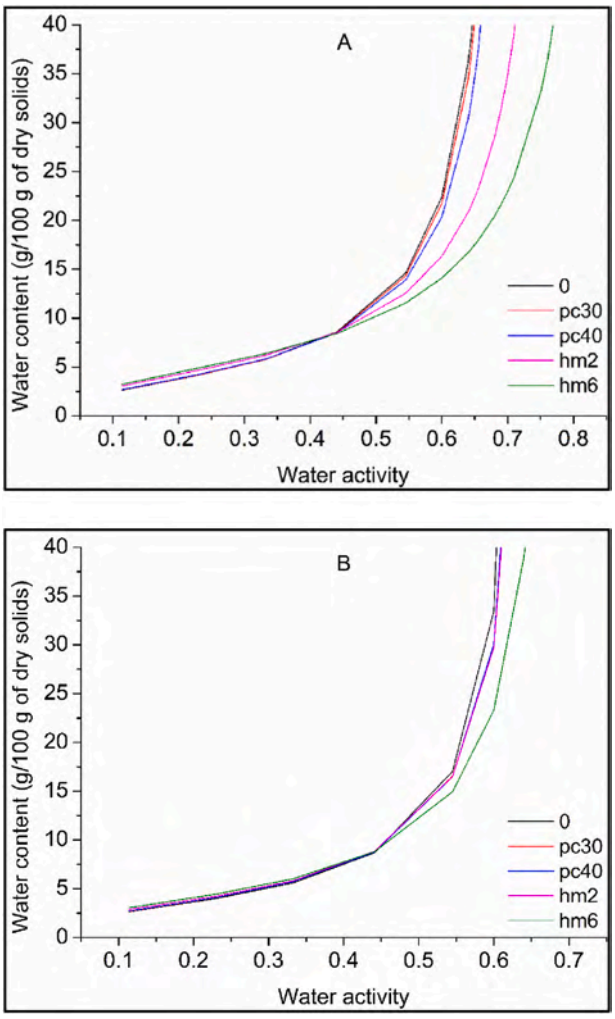


Fig. 7. Water sorption isotherms of samples stored for 168 h at 25 °C predicted with the GAB model using experimental data. A: Apt Pro stage 2 infant milk formula. B: Hipp stage 2 infant milk formula. 0: control samples. pc: broken by pneumatic conveying under the air velocity of 30 m/s and 40 m/s hm: broken by the laboratory high-speed mixer for 2 min and 6 min.

3.3.4. Spreading pressure

Fig. 8 illustrates the spreading pressures of samples at various a_w. As already shown for starch powders, the spreading pressure of samples

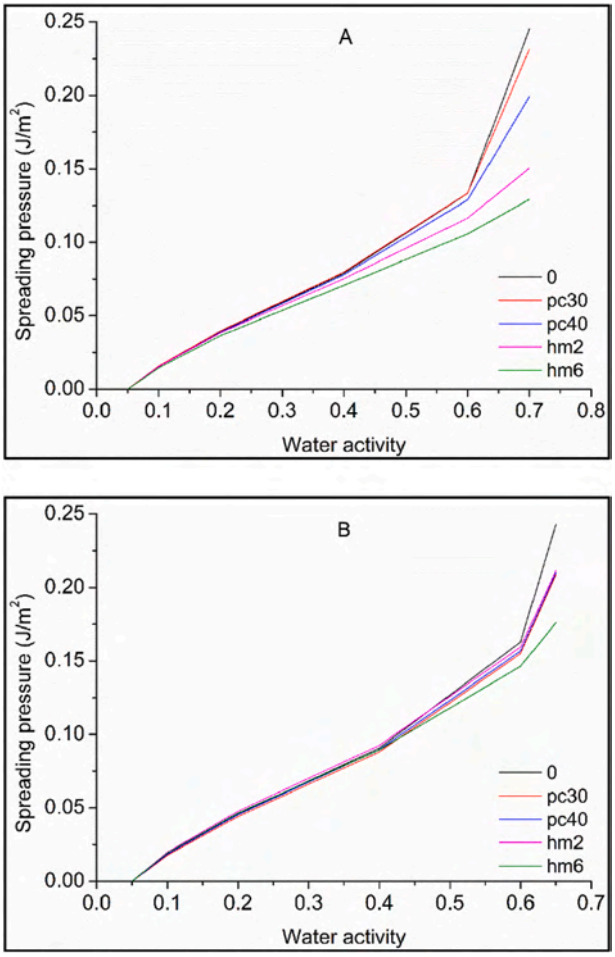


Fig. 8. Spreading pressure isotherms at different water activities of samples. A: Apt Pro stage 2 infant milk formula. B: Hipp stage 2 infant milk formula. 0: control samples. pc: broken by pneumatic conveying under the air velocity of 30 m/s and 40 m/s hm: broken by the laboratory high-speed mixer for 2 min and 6 min.

Table 4
Monolayer values (m_m, g/100 g dry solid), constants K and C for the GAB isotherms and monolayer values (m_c, g/100 g dry solid), number of adsorbed monolayers (N_{am}), surface area of adsorbent (A, m^2/g), and density of sorbed water (c_d, g/ml) of Caurie's equations.

Samples	GAB					Caurie's equations			
	m_m	K	C	R^2	%RMS	m_c	N_{am}	A	c_d
IMF-A									
0	$3.45^{c}\pm0.05$	$1.41^{a}\pm0.01$	$9.2^{a}\pm0.1$	0.9822	1.30	$5.44^{c}\pm0.01$	$3.12^{c}\pm0.02$	$84.8^{c}\pm0.6$	$1.75^{a}\pm0.01$
pc30	$3.43^{c}\pm0.03$	$1.41^{a}\pm0.01$	$9.7^{a}\pm0.2$	0.9813	1.39	$5.45^{c}\pm0.00$	$3.17^{c}\pm0.00$	$86.4^{c}\pm0.1$	$1.72^{a}\pm0.00$
pc40	$3.54^{c}\pm0.00$	$1.38^{a}\pm0.00$	$9.5^{a}\pm0.1$	0.9933	0.75	$5.48^{c}\pm0.00$	$3.20^{c}\pm0.01$	$87.1^{c}\pm0.4$	$1.71^{a}\pm0.01$
hm2	$4.07^{b}\pm0.12$	$1.26^{b}\pm0.02$	$10.8^{a}\pm0.9$	1.0000	0.02	$5.80^{b}\pm0.02$	$3.56^{b}\pm0.04$	$97.0^{b}\pm1.1$	$1.63^{b}\pm0.01$
hm6	$4.53^{a}\pm0.17$	$1.15^{c}\pm0.03$	$10.9^{a}\pm0.8$	0.9988	0.15	$5.97^{a}\pm0.00$	$3.80^{a}\pm0.02$	$103.5^{a}\pm0.6$	$1.57^{c}\pm0.01$
IMF-B									
0	$2.97^{B}\pm0.01$	$1.52^{A}\pm0.00$	$13.3^{A}\pm0.1$	0.8890	3.95	$5.41^{C}\pm0.00$	$3.15^{C}\pm0.00$	$85.8^{C}\pm0.0$	$1.72^{A}\pm0.00$
pc30	$3.11^{B}\pm0.01$	$1.50^{A}\pm0.00$	$12.2^{A}\pm0.1$	0.8963	3.70	$5.45^{C}\pm0.00$	$3.15^{C}\pm0.00$	$85.8^{C}\pm0.1$	$1.73^{A}\pm0.00$
pc40	$3.10^{B}\pm0.13$	$1.50^{A}\pm0.02$	$13.5^{A}\pm0.5$	0.9188	3.33	$5.47^{C}\pm0.02$	$3.20^{C}\pm0.05$	$87.0^{C}\pm1.4$	$1.71^{A}\pm0.02$
hm2	$3.11^{B}\pm0.03$	$1.50^{A}\pm0.01$	$16.2^{A}\pm0.1$	0.9178	3.68	$5.60^{B}\pm0.02$	$3.34^{B}\pm0.02$	$91.0^{B}\pm0.4$	$1.67^{AB}\pm0.00$
hm6	$3.37^{A}\pm0.06$	$1.43^{B}\pm0.00$	$16.1^{A}\pm0.4$	0.9430	3.11	$5.76^{A}\pm0.00$	$3.53^{A}\pm0.05$	$96.1^{A}\pm1.4$	$1.63^{B}\pm0.02$

1. IMF-A: Apt Pro stage 2 infant milk formula. IMF-B: Hipp stage 2 infant milk formula. 0: control samples. pc: broken by pneumatic conveying under the air velocity of 30 m/s and 40 m/s hm: broken by the laboratory high-speed mixer for 2 min and 6 min.
2. Values are mean ± standard deviation (n = 3).
3. $^{a-c}$ and $^{A-C}$ different values within columns in IMF-A and IMF-B groups are significantly different at $P < 0.05$, respectively.

increased as a_w increased (Al-Muhtaseb et al., 2004). Besides, breakage decreased the spreading pressure of powders especially for sample A whose spreading pressure decreased with increasing degree of breakage at a given a_w, and the effects of breakage increased with increasing a_w. These results mean, from the perspective of spreading pressure, breakage decreased the affinity of water molecules to active sites thus broken samples were easier to absorb water.

3.4. Glass transition and instant crystallization

The T_g (onset) and T_{ic} of samples over the a_w range of 0–0.441 are shown in Table 5. T_g represents the overall stability of powders to changes caused by moisture and temperature and lower T_g is indicative of problems more easily occurring during storage (Kelly et al., 2015). From Table 5, T_g decreased drastically with increasing a_w because of the water plasticization (Haque and Roos, 2004, 2006; Saxena et al., 2020; Zouari et al., 2020). Breakage did not influence the T_g of anhydrous samples, around 105 °C or 107 °C for A or B samples, respectively. This value was similar to the T_g of anhydrous freeze-dried lactose, around 105 °C (Haque and Roos, 2006). A significant difference in T_g was found between body breakage samples and other samples at a_w from 0.114 to 0.332, which was due to the higher water content of body breakage samples. It was shown that T_{ic} decreased as a_w and water content increased and surface breakage did not influence the T_{ic} while the T_{ic} of body breakage samples were significantly lower than those of other samples. This is similar to the effect of breakage on T_g but the influence on T_{ic} was greater. Thus, the temperature differences between glass transition and crystallization (T_{ic} - T_g) of body breakage samples were lower than those of other samples. All these results suggest that lower temperature or a_w is required for body breakage samples when stored.

3.5. Mechanical properties

For amorphous materials, the physical properties often change around T_g, which may result in an α-relaxation related to molecular mobility (Silalai and Roos, 2011a, b). The α-relaxation shows a peak in loss modulus and a decrease in storage modulus around T_g. T_α decreased with increasing frequency (data not shown) and a_w (Table 5), which agrees with previous research (Li et al., 2016b; Silalai and Roos, 2011b). From Table 5, breakage almost did not influence the T_α and only a few body breakage samples had significantly lower T_α than other samples. Nevertheless, it was found that body breakage significantly affected mechanical α-relaxation behavior that was the changes of storage modulus and loss modulus (Fig. 9). From Fig. 9a, compared with other samples, the storage modulus of body breakage samples showed smaller decreases and remained at higher levels for the rubbery plateau. For loss modulus (Fig. 9b), α-relaxation peaks of control and surface breakage samples were more pronounced, and the peak size of body breakage samples decreased with increasing breakage degree. The small magnitudes of modulus changes mean that body breakage decreased the overall molecular mobility of powders.

4. Conclusion

The influence of two different breakage mechanisms on the physical, water sorption, and mechanical properties of commercial agglomerated IMF was investigated. Two different processing methods (laboratory dilute-phase pneumatic conveying and high-speed mixing) were used to mimic the breakage of IMF samples during industrial-scale processing conditions. The dominant breakage mechanism during high-speed mixing was body breakage while surface breakage occurred on most particles during pneumatic conveying. Compared with surface breakage, body breakage had a greater impact on the properties of samples.

Breakage significantly increased the SSA and bulk densities, and decreased the particle size of samples. The effect of breakage on porosity and particle density was influenced by the particle size of initial samples.

Table 5
Glass transition temperature (T_g), initial crystallization temperature (T_{ic}), and α-relaxation temperature (T_α at 1 Hz) of infant formula samples stored for 168 h at various water activities (0–0.44) at 25 °C.

Samples		Water activity				
		0	0.11	0.23	0.33	0.44
IMF-A						
0	T_g	105.1 ± 0.2	66.3 ± 0.7	48.9 ± 0.3	32.0 ± 0.0	16.2 ± 0.1
	T_{ic}	/	120.9 ± 0.0	101.0 ± 0.7	83.7 ± 0.3	64.2 ± 0.0
	T_α	115.5 ± 0.6	87.3 ± 0.7	72.7 ± 1.1	54.7 ± 0.0	35.2 ± 0.2
pc30	T_g	104.4 ± 0.5	66.1 ± 0.4	48.4 ± 0.2	32.3 ± 0.1	15.9 ± 0.2
	T_{ic}	/	120.8 ± 0.8	100.4 ± 0.1	84.9 ± 0.5	64.0 ± 0.1
	T_α	114.0 ± 1.0	84.0 ± 0.8	69.7 ± 1.0	52.2 ± 0.2	33.8 ± 0.2
pc40	T_g	102.7	65.9 ± 0.0	48.7 ± 0.2	32.6 ± 0.1	16.1 ± 0.1
	T_{ic}	/	120.0 ± 0.4	100.5 ± 0.4	83.6 ± 0.1	63.9 ± 0.0
	T_α	115.6 ± 0.6	86.7 ± 0.9	70.6 ± 0.4	50.9 ± 0.0	35.0 ± 0.5
hm2	T_g	105.7 ± 0.0	64.8 ± 0.1	46.7 ± 0.1	31.7 ± 0.4	15.2 ± 0.3
	T_{ic}	/	114.2 ± 0.1	94.0 ± 0.1	78.8 ± 0.4	59.1 ± 0.6
	T_α	114.0 ± 0.1	83.9 ± 0.2	68.0 ± 0.6	51.1 ± 0.4	36.6 ± 0.4
hm6	T_g	105.9 ± 0.1	63.5 ± 0.5	46.0 ± 0.4	31.1 ± 0.1	14.84 ± 0.8
	T_{ic}	/	110.4 ± 0.8	91.6 ± 0.8	77.0 ± 0.0	58.4 ± 0.1
	T_α	115.7 ± 1.0	78.9 ± 0.2	67.0 ± 0.6	50.9 ± 0.2	34.8 ± 0.1
IMF-B						
0	T_g	107.5 ± 0.1	63.9 ± 0.4	49.0 ± 0.2	32.8 ± 0.1	15.9 ± 0.1
	T_{ic}	/	116.2 ± 0.3	98.9 ± 0.0	84.3 ± 0.2	64.3 ± 0.2
	T_α	117.6 ± 0.6	84.3 ± 0.1	70.9 ± 0.4	58.1 ± 0.0	36.5 ± 0.0
pc30	T_g	107.5 ± 0.1	63.2 ± 0.3	49.2 ± 0.1	32.8 ± 0.0	16.1 ± 0.1
	T_{ic}	/	115.3 ± 0.2	98.3 ± 0.0	83.5 ± 0.2	63.5 ± 0.0
	T_α	119.4 ± 1.6	87.8 ± 0.3	70.3 ± 0.6	55.6 ± 0.4	34.7 ± 0.1
pc40	T_g	107.3 ± 0.2	62.4 ± 0.5	48.7 ± 0.2	32.5 ± 0.1	15.7 ± 0.1
	T_{ic}	/	113.8 ± 0.4	98.5 ± 0.2	83.4 ± 0.1	63.2 ± 0.6
	T_α	119.6 ± 1.9	83.2 ± 1.2	71.2 ± 0.3	56.2 ± 0.0	34.6 ± 0.2
hm2	T_g	107.2 ± 0.2	62.5 ± 0.3	48.7 ± 0.1	32.5 ± 0.1	16.0 ± 0.5
	T_{ic}	/	112.3 ± 0.2	96.4 ± 0.4	81.1 ± 0.3	61.5 ± 0.8
	T_α	124.0 ± 1.9	85.0 ± 0.6	70.1 ± 0.4	57.9 ± 0.9	36.0 ± 1.1
hm6	T_g	107.7 ± 0.0	62.2 ± 0.4	48.1 ± 0.0	32.0 ± 0.1	15.1 ± 0.0
	T_{ic}	/	110.5 ± 0.6	99.9 ± 0.3	79.2 ± 0.0	59.3 ± 0.3
	T_α	121.2 ± 0.3	79.7 ± 1.0	67.6 ± 0.5	55.4 ± 0.1	36.7 ± 0.2

1. IMF-A: Apt Pro stage 2 infant milk formula. IMF-B: Hipp stage 2 infant milk formula. 0: control samples. pc: broken by pneumatic conveying under the air velocity of 30 m/s and 40 m/s hm: broken by the laboratory high-speed mixer for 2 min and 6 min.
2. Values are mean ± standard deviation (n = 2).

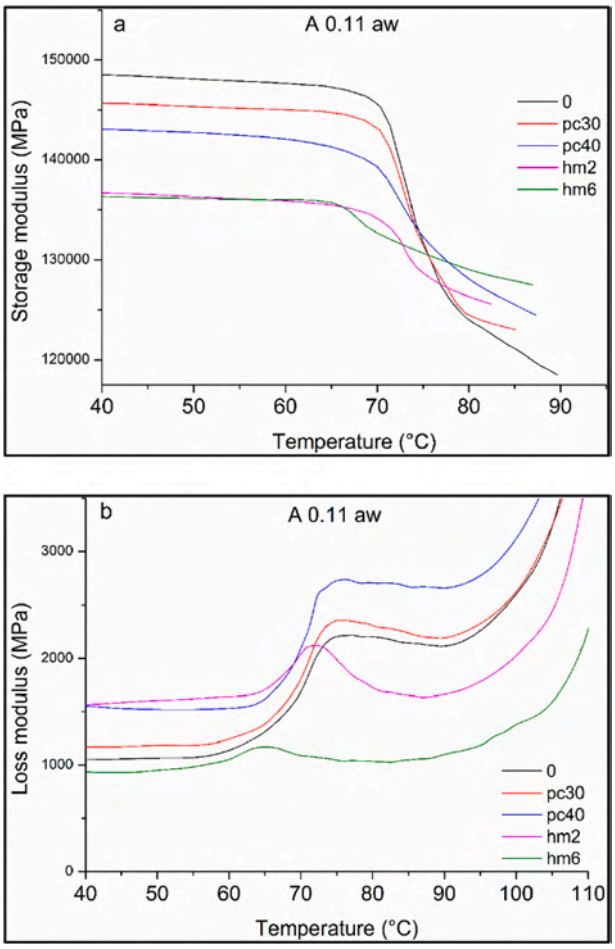


Fig. 9. Storage modulus (a) and loss modulus (b) of sample A equilibrated at 0.11 a_w for 168 h at 25 °C. A: Apt Pro stage 2 infant milk formula. 0: control samples. pc: broken by pneumatic conveying under the air velocity of 30 m/s and 40 m/s hm: broken by the laboratory high-speed mixer for 2 min and 6 min.

After breakage, the surface compositions slightly changed, protein and lactose proportions increased and fat decreased. In addition, body breakage particles had more rounded shapes and smoother surfaces while surface breakage did not significantly change particle morphology. Body breakage had a greater influence on powder physical properties, which subsequently affected the water sorption and mechanical properties. In contrast, surface breakage only slightly affected physical properties and not the other characteristics. Body breakage increased the water sorption rate and water content of samples and accelerated the time-dependent crystallization. The experimental water sorption data at $a_w \leq 0.441$ fitted well with the GAB model. The number of adsorbed monolayers, sorption surface area, and monolayer moisture content of body breakage powders were significantly higher than other powders and their spreading pressures were lower. Higher water contents of body breakage samples significantly decreased T_{ic} but slightly decreased T_g and T_α. Besides, body breakage decreased the overall molecular mobility of powders and resulted in smaller magnitudes of modulus changes than other samples.

Overall, surface breakage affected powder physical properties but not water sorption and mechanical properties, while body breakage significantly impacted those characteristics. This finding also has industrial importance. If powder breakage during production and transportation cannot be avoided, it should be limited to the surface breakage. However, this would still influence some functionalities such as bulk density that is important for IMF.

Credit author statement

Jie Han: Conceptualization, Methodology, Formal analysis, Investigation, Data curation, Writing – original draft, Visualization. John Fitzpatrick: Supervision, Writing – review & editing. Kevin Cronin: Supervision, Writing – review & editing. Song Miao: Supervision, Conceptualization, Writing – review & editing, Funding acquisition, Project administration.

Declaration of competing interest

The authors declare that they have no known competing financial interests or personal relationships that could have appeared to influence the work reported in this paper.

Acknowledgment

This work was supported by the Teagasc, Agriculture and Food Development Authority under the project MDDT 0153.

Appendix A. Supplementary data

Supplementary data to this article can be found online at https://doi.org/10.1016/j.jfoodeng.2022.110939.

References

Al-Muhtaseb, A.H., McMinn, W.A.M., Magee, T.R.A., 2004. Water sorption isotherms of starch powders. Part 2: thermodynamic characteristics. J. Food Eng. 62 (2), 135–142. https://doi.org/10.1016/S0260-8774(03)00202-4.

Antonyuk, S., Tomas, J., Heinrich, S., Mörl, L., 2005. Breakage behaviour of spherical granulates by compression. Chem. Eng. Sci. 60 (14), 4031–4044. https://doi.org/10.1016/j.ces.2005.02.038.

Boiarkina, I., Sang, C., Depree, N., Prince-Pike, A., Yu, W., Wilson, D.I., Young, B.R., 2016. The significance of powder breakdown during conveying within industrial milk powder plants. Adv. Powder Technol. 27 (6), 2363–2369. https://doi.org/10.1016/j.apt.2016.10.019.

Carpin, M., Bertelsen, H., Dalberg, A., Bech, J.K., Risbo, J., Schuck, P., Jeantet, R., 2017. How does particle size influence caking in lactose powder? J. Food Eng. 209, 61–67. https://doi.org/10.1016/j.jfoodeng.2017.04.006.

Červenka, L., Hloušková, L., Žabčíková, S., 2015. Moisture adsorption isotherms and thermodynamic properties of green and roasted Yerba mate (Ilex paraguariensis). Food Biosci. 12, 122–127. https://doi.org/10.1016/j.fbio.2015.10.001.

Cleaver, J.A.S., Ghadiri, M., Rolfe, N., 1993. Impact attrition of sodium carbonate monohydrate crystals. Powder Technol. 76 (1), 15–22. https://doi.org/10.1016/0032-5910(93)80036-A.

Dalgıç, A.C., Pekmez, H., Belibağlı, K.B., 2012. Effect of drying methods on the moisture sorption isotherms and thermodynamic properties of mint leaves. J. Food Sci. Technol. 49 (4), 439–449. https://doi.org/10.1007/s13197-011-0302-7.

Faldt, P., Bergenstahl, B., Carlsson, G., 1993. The surface coverage of fat on food powders analyzed by ESCA (electron spectroscopy for chemical analysis). Food Struct. 12 (2), 10.

Fu, J., Reynolds, G.K., Adams, M.J., Hounslow, M.J., Salman, A.D., 2005. An experimental study of the impact breakage of wet granules. Chem. Eng. Sci. 60 (14), 4005–4018. https://doi.org/10.1016/j.ces.2005.02.037.

Ghadiri, M., Yuregir, K.R., Pollock, H.M., Ross, J.D.J., Rolfe, N., 1991. Influence of processing conditions on attrition of NaCl crystals. Powder Technol. 65 (1), 311–320. https://doi.org/10.1016/0032-5910(91)80195-O.

Han, J., Fitzpatrick, J., Cronin, K., Maidannyk, V., Miao, S., 2020. Breakage of infant milk formula through three different processing methods and its influence on powder properties. J. Food Eng. 282, 109997. https://doi.org/10.1016/j.jfoodeng.2020.109997.

Han, J., Fitzpatrick, J., Cronin, K., Maidannyk, V., Miao, S., 2021a. Particle size, powder properties and the breakage behaviour of infant milk formula. J. Food Eng. 292, 110367. https://doi.org/10.1016/j.jfoodeng.2020.110367.

Han, J., Fitzpatrick, J., Cronin, K., Miao, S., 2021b. Dairy powder breakage: mechanisms, characterization methods, impacted properties and influencing factors. Trends Food Sci. Technol. 114, 608–624. https://doi.org/10.1016/j.tifs.2021.05.043.

Hanley, K.J., 2011. Experimental Quantification and Modelling of Attrition of Infant Formulae. Department of Process and Chemical Engineering. University College Cork, Cork, Ireland.

Haque, M.K., Roos, Y.H., 2004. Water sorption and plasticization behavior of spray-dried lactose/protein mixtures. J. Food Sci. 69 (8), E384–E391. https://doi.org/10.1111/j.1365-2621.2004.tb09900.x.

Haque, M.K., Roos, Y.H., 2006. Differences in the physical state and thermal behavior of spray-dried and freeze-dried lactose and lactose/protein mixtures. Innovat. Food Sci. Emerg. Technol. 7 (1), 62–73. https://doi.org/10.1016/j.ifset.2004.12.004.

Hazlett, R., Schmidmeier, C., O'Mahony, J.A., 2020. Influence of mechanical integrity during pneumatic conveying on the bulk handling and rehydration properties of agglomerated dairy powders. J. Food Eng. 110103. https://doi.org/10.1016/j.jfoodeng.2020.110103.

Iglesias, H.A., Chirife, J., Viollaz, P., 1976. Thermodynamics of water vapour sorption by sugar beet root. Int. J. Food Sci. Technol. 11 (1), 91–101. https://doi.org/10.1111/j.1365-2621.1976.tb00705.x.

Iveson, S.M., Litster, J.D., Hapgood, K., Ennis, B.J., 2001. Nucleation, growth and breakage phenomena in agitated wet granulation processes: a review. Powder Technol. 117 (1), 3–39. https://doi.org/10.1016/S0032-5910(01)00313-8.

Ji, J., Cronin, K., Fitzpatrick, J., Fenelon, M., Miao, S., 2015. Effects of fluid bed agglomeration on the structure modification and reconstitution behaviour of milk protein isolate powders. J. Food Eng. 167, 175–182. https://doi.org/10.1016/j.jfoodeng.2015.01.012.

Kelly, G.M., O'Mahony, J.A., Kelly, A.L., Huppertz, T., Kennedy, D., O'Callaghan, D.J., 2015. Influence of protein concentration on surface composition and physico-chemical properties of spray-dried milk protein concentrate powders. Int. Dairy J. 51, 34–40. https://doi.org/10.1016/j.idairyj.2015.07.001.

Kelly, G.M., O'Mahony, J.A., Kelly, A.L., O'Callaghan, D.J., 2016. Water sorption and diffusion properties of spray-dried dairy powders containing intact and hydrolysed whey protein. LWT - Food Sci. Technol. (Lebensmittel-Wissenschaft -Technol.) 68, 119–126. https://doi.org/10.1016/j.lwt.2015.11.056.

Kim, E.H.J., Chen, X.D., Pearce, D., 2002. Surface characterization of four industrial spray-dried dairy powders in relation to chemical composition, structure and wetting property. Colloids Surf. B Biointerfaces 26 (3), 197–212. https://doi.org/10.1016/S0927-7765(01)00334-4.

King, R.P., 2012. Modeling and Simulation of Mineral Processing Systems. Society for Mining, Metallurgy, and Exploration (SME), pp. 153–252.

Kotzur, B.A., Berry, R.J., Zigan, S., García-Triñanes, P., Bradley, M.S.A., 2018. Particle attrition mechanisms, their characterisation, and application to horizontal lean phase pneumatic conveying systems: a review. Powder Technol. 334, 76–105. https://doi.org/10.1016/j.powtec.2018.04.047.

Lago, C.C., Liendo-Cárdenas, M., Noreña, C.P.Z., 2013. Thermodynamic sorption properties of potato and sweet potato flakes. Food Bioprod. Process. 91 (4), 389–395. https://doi.org/10.1016/j.fbp.2013.02.005.

Lazou, A., Krokida, M., 2011. Thermal characterisation of corn–lentil extruded snacks. Food Chem. 127 (4), 1625–1633. https://doi.org/10.1016/j.foodchem.2011.02.029.

Li, R., Roos, Y.H., Miao, S., 2016a. Flavor release from spray-dried amorphous matrix: effect of lactose content and water plasticization. Food Res. Int. 86, 147–155. https://doi.org/10.1016/j.foodres.2016.06.003.

Li, R., Roos, Y.H., Miao, S., 2016b. Physical and mechanical properties of lactose/WPI mixtures: effect of pre-crystallisation. Int. Dairy J. 56, 55–63. https://doi.org/10.1016/j.idairyj.2015.12.014.

Li, R., Roos, Y.H., Miao, S., 2016c. Roles of particle size on physical and mechanical properties of dairy model solids. J. Food Eng. 173, 69–75. https://doi.org/10.1016/j.jfoodeng.2015.10.041.

Li, R., Roos, Y.H., Miao, S., 2017. Characterization of mechanical and encapsulation properties of lactose/maltodextrin/WPI matrix. Food Hydrocolloids 63, 149–159. https://doi.org/10.1016/j.foodhyd.2016.08.033.

Maidannyk, V., McSweeney, D.J., Hogan, S.A., Miao, S., Montgomery, S., Auty, M.A.E., McCarthy, N.A., 2020. Water sorption and hydration in spray-dried milk protein powders: selected physicochemical properties. Food Chem. 304, 125418. https://doi.org/10.1016/j.foodchem.2019.125418.

Maidannyk, V.A., Lim, A.S.L., Auty, M.A.E., Roos, Y.H., 2019. Effects of lipids on the water sorption, glass transition and structural strength of carbohydrate-protein systems. Food Res. Int. 116, 1212–1222. https://doi.org/10.1016/j.foodres.2018.10.008.

Materic, V., Holt, R., Hyland, M., Jones, M.I., 2014. An internally circulating fluid bed for attrition testing of Ca looping sorbents. Fuel 127, 116–123. https://doi.org/10.1016/j.fuel.2013.10.071.

Mazza, G., LeMaguer, M., 1978. Water sorption properties of yellow globe onion (Allium cepa L.). Can. Inst. Food Sci. Technol. J. 11 (4), 189–193. https://doi.org/10.1016/S0315-5463(78)73269-4.

McCarthy, N.A., Gee, V.L., Hickey, D.K., Kelly, A.L., O'Mahony, J.A., Fenelon, M.A., 2013. Effect of protein content on the physical stability and microstructure of a model infant formula. Int. Dairy J. 29 (1), 53–59. https://doi.org/10.1016/j.idairyj.2012.10.004.

Murrieta-Pazos, I., Gaiani, C., Galet, L., Calvet, R., Cuq, B., Scher, J., 2012a. Food powders: surface and form characterization revisited. J. Food Eng. 112 (1), 1–21. https://doi.org/10.1016/j.jfoodeng.2012.03.002.

Murrieta-Pazos, I., Gaiani, C., Galet, L., Scher, J., 2012b. Composition gradient from surface to core in dairy powders: agglomeration effect. Food Hydrocolloids 26 (1), 149–158. https://doi.org/10.1016/j.foodhyd.2011.05.003.

Niro, G., 2006. GEA Niro Analytical Methods Dry Products. GEA Process Engineering A/S, Gladsaxevej, Denmark.

Norazirah, A., Fuad, S.H.S., Hazizan, M.H.M., 2016. The effect of size and shape on breakage characteristic of mineral. Procedia Chem. 19, 702–708. https://doi.org/10.1016/j.proche.2016.03.073.

O'Donoghue, L.T., Haque, M.K., Kennedy, D., Laffir, F.R., Hogan, S.A., O'Mahony, J.A., Murphy, E.G., 2019. Influence of particle size on the physicochemical properties and stickiness of dairy powders. Int. Dairy J. 98, 54–63. https://doi.org/10.1016/j.idairyj.2019.07.002.

O'Neill, G.J., Hollingsworth, A., Harbourne, N., O'Riordan, E.D., 2019. Reducing stickiness in spray dried dairy emulsions. Food Hydrocolloids 90, 330–340. https://doi.org/10.1016/j.foodhyd.2018.12.033.

Polatoğlu, B., Beşe, A.V., Kaya, M., Aktaş, N., 2011. Moisture adsorption isotherms and thermodynamics properties of sucuk (Turkish dry-fermented sausage). Food Bioprod. Process. 89 (4), 449–456. https://doi.org/10.1016/j.fbp.2010.06.003.

Reynolds, G.K., Fu, J.S., Cheong, Y.S., Hounslow, M.J., Salman, A.D., 2005. Breakage in granulation: a review. Chem. Eng. Sci. 60 (14), 3969–3992. https://doi.org/10.1016/j.ces.2005.02.029.

Saxena, J., Adhikari, B., Brkljaca, R., Huppertz, T., Chandrapala, J., Zisu, B., 2019. Physicochemical properties and surface composition of infant formula powders. Food Chem. 297, 124967. https://doi.org/10.1016/j.foodchem.2019.124967.

Saxena, J., Adhikari, B., Brkljaca, R., Huppertz, T., Chandrapala, J., Zisu, B., 2020. Inter-relationship between lactose crystallization and surface free fat during storage of infant formula. Food Chem. 322, 126636. https://doi.org/10.1016/j.foodchem.2020.126636.

Scala, F., Chirone, R., Salatino, P., 2013. 6 - attrition phenomena relevant to fluidized bed combustion and gasification systems. In: Scala, F. (Ed.), Fluidized Bed Technologies for Near-Zero Emission Combustion and Gasification. Woodhead Publishing, pp. 254–315. https://doi.org/10.1533/9780857098801.1.254.

Scala, F., Montagnaro, F., Salatino, P., 2007. Attrition of limestone by impact loading in fluidized beds. Energy Fuels 21 (5), 2566–2572. https://doi.org/10.1021/ef0700580.

Schuck, P., Dolivet, A., Jeantet, R., 2012. Analytical Methods for Food and Dairy Powders.

Silalai, N., Roos, Y.H., 2011a. Coupling of dielectric and mechanical relaxations with glass transition and stickiness of milk solids. J. Food Eng. 104 (3), 445–454. https://doi.org/10.1016/j.jfoodeng.2011.01.009.

Silalai, N., Roos, Y.H., 2011b. Mechanical relaxation times as indicators of stickiness in skim milk–maltodextrin solids systems. J. Food Eng. 106 (4), 306–317. https://doi.org/10.1016/j.jfoodeng.2011.05.018.

Simón, C., Esteban, L.G., de Palacios, P., Fernández, F.G., García-Iruela, A., 2016. Thermodynamic properties of the water sorption isotherms of wood of limba (Terminalia superba Engl. & Diels), obeche (Triplochiton scleroxylon K. Schum.), radiata pine (Pinus radiata D. Don) and chestnut (Castanea sativa Mill.). Ind. Crop. Prod. 94, 122–131. https://doi.org/10.1016/j.indcrop.2016.08.008.

Torres, M.D., Moreira, R., Chenlo, F., Vázquez, M.J., 2012. Water adsorption isotherms of carboxymethyl cellulose, guar, locust bean, tragacanth and xanthan gums. Carbohydr. Polym. 89 (2), 592–598. https://doi.org/10.1016/j.carbpol.2012.03.055.

Wu, F., Wu, D., 2017. Attrition resistances and mechanisms of three types of FCC catalysts. Powder Technol. 305, 289–296. https://doi.org/10.1016/j.powtec.2016.09.077.

Zouari, A., Briard-Bion, V., Gaucheron, F., Schuck, P., Gaiani, C., Triki, M., Attia, H., Ali Ayadi, M., 2020. Effect of pH on the physicochemical characteristics and the surface chemical composition of camel and bovine whey protein's powders. Food Chem. 127514. https://doi.org/10.1016/j.foodchem.2020.127514.

Journal of Food Engineering 282 (2020) 109997

Contents lists available at ScienceDirect

Journal of Food Engineering

journal homepage: http://www.elsevier.com/locate/jfoodeng

Breakage of infant milk formula through three different processing methods and its influence on powder properties

Jie Han [a,b], John Fitzpatrick [b], Kevin Cronin [b], Valentyn Maidannyk [a], Song Miao [a,*]

[a] Teagasc Food Research Centre, Moorepark, Fermoy, Co. Cork, Ireland
[b] Process & Chemical Engineering, School of Engineering, University College Cork, Cork, Ireland

ARTICLE INFO

Keywords:
Dairy powder breakage
Physical characteristics
Rehydration properties
Flowability
Specific bulk volume
Powder compressibility

ABSTRACT

Dairy powder breakage has always occurred during production and transportation though few studies on it have been published. This paper examines the breakage of infant formula using three different processing methods (laboratory high-speed mixing, lab-scale pneumatic conveying, and factory-scale blending) and the effect of breakage on powder properties. In both mixing and high-velocity pneumatic conveying, particles were broken into smaller entities and the particle size of samples significantly decreased. Particle breakage was accompanied by a significant decrease in porosity and increase in density and surface free fat. This in-turn decreased the rehydration properties of samples, especially for high-speed mixing, while breakage had only a small influence on powder flowability. By contrast, some agglomeration occurred during blending for short time in the blender and the particle size did not decrease ($P > 0.05$) even for blending at longer time, thus, there were only minor impacts on physical and functional properties of powders.

1. Introduction

The production of dairy powders is growing rapidly worldwide. Several physical characteristics, including particle size, density, porosity, morphology, surface, and adsorption properties, are important to powder functionalities (Bronlund and Paterson, 2004; Fitzpatrick et al., 2004; Fu et al., 2012). There are many factors influencing these properties, from composition, production processes, transportation, to storage conditions (Finney et al., 2002; Ji et al., 2016b; Langrish et al., 2006; Sharma et al., 2012). Currently, most studies on factors influencing dairy powder characteristics have mainly focused on the ingredients, the parameters during homogenization and spray drying, but ignored powder changes caused by mechanical forces. Particle breakage will occur after spray drying due to mechanical forces acting on the powder during the post-drying and transportation processes. There are very few published works on the breakage of dairy powders. Boiarkina et al. investigated the breakage of instant whole milk powder in two different industrial plants with different transport systems, i.e. a pneumatic conveying system, and a bucket elevator (Boiarkina et al., 2016). Hanley investigated the disintegration of infant formula agglomerates with large particle sizes between 710 μm and 850 μm during pneumatic conveying (Hanley, 2011).

Particle breakage is the disintegration of powder particles caused by mechanical loads, such as impact, shear, and compression/crushing, which is the result of particle-particle and particle-equipment interactions (Aarseth, 2004; Zhao et al., 1999). Currently, research on particle breakage has mainly focused on the pharmaceutical industry, mining industry, catalysts chemical industry using numerical modeling combined with different types of single particle breakage tests (Deng and Davé, 2017; Dosta et al., 2016; Gupta et al., 2017; Gupta, 2017; Norazirah et al., 2016; Shan et al., 2018). There are three breakage mechanisms based on the resulting size distribution of child particles: fragmentation/damage, chipping/attrition, and fracture (Aarseth, 2004; Ghadiri and Zhang, 2002; Lawn and Swain, 1975). If the breakage is excessive, it can lead to a number of serious consequences including but not limited to an increase in dust generation (Kalman and Goder, 1998; Oveisi et al., 2013; Salman et al., 2002; Wu and Wu, 2017) and loss in functionality and product performance (Bemrose and Bridgwater, 1987; Boiarkina et al., 2016; Zumaeta et al., 2005). Specifically, fine dust produced may lead to air pollution and plugging of processing equipment, increased possibility of dust explosions, loss of product through the production of undersized particles. In addition, unwanted changes in bulk density may cause error in volumetric dosing processes, worsen wetting and dissolution properties, and influence the surface-sensitivity

* Corresponding author.
E-mail address: Song.Miao@teagasc.ie (S. Miao).

https://doi.org/10.1016/j.jfoodeng.2020.109997
Received 8 January 2020; Received in revised form 20 February 2020; Accepted 23 February 2020
Available online 27 February 2020
0260-8774/© 2020 Elsevier Ltd. All rights reserved.

of catalytic particles. Particle size is an essential and important property for dairy powders (Li et al., 2016b). Thus, particle breakage is a problem that cannot be ignored in dairy powder production. However, only a few studies about dairy powder breakage have been published and none have investigated the dairy powder breakage patterns.

The objective of this study is to investigate the breakage of commercial agglomerated infant formula using three processing methods, lab-scale pneumatic conveying, laboratory high-speed mixing and factory-scale blending. At the same time, the influences of breakage on physical properties and functional properties (rehydration, powder flowability, and specific storage volume) of infant formula were investigated. The aim is to build a better understanding of dairy powder breakage and its influence.

2. Material and methods

2.1. Materials

Two batches of Cow and Gate "follow on milk stage 2" infant milk formulas were purchased from a local pharmacy (Cork, Ireland) to complete all the experiments. The nominal composition was 56.4% lactose, 20.4% fat, and 9.5% protein in this infant formula.

2.2. Equipment and powder breakage sample preparation

An isometric view of the lab-scale pneumatic conveyor (Hanley, 2011) and photos of the inside of the laboratory high-speed mixer

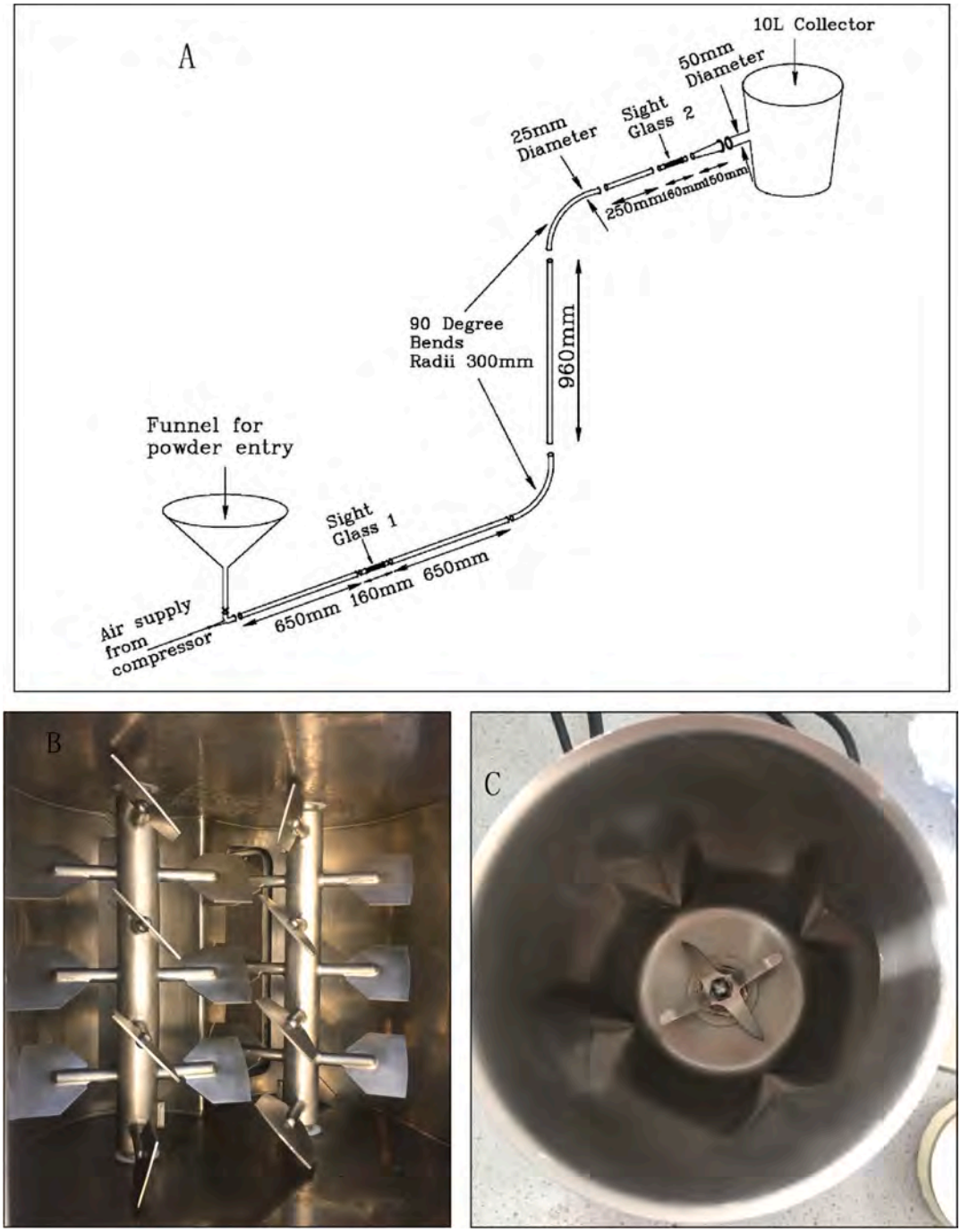


Fig. 1. An isometric view of the lab-scale pneumatic conveyor (A) and the inside of the Forberg blender (B) and laboratory high-speed mixer (C).

(Waring, USA) and the factory-scale blender (Forberg, F-20, Norway) are presented in Fig. 1. Samples were placed in the mixer operated at 22, 000 rpm for three different durations of 1 min, 2 min, and 7 min (termed HSM1, HSM2, and HSM7). Other samples were placed in the Forberg blender for the duration of 15 min, 30 min, and 70 min (termed FB15, FB30, and FB70). The processing capacities for mixer and blender were 100 g and 1600 g, respectively. Samples just covered the blade of the mixer and the level of the powder was in the middle of the blade in the blender.

The second batch of infant formula samples was blown through the pneumatic conveyor with an air velocity of 40 m/s and 50 m/s (termed PC40 and PC50) and feeding rate of 3.0 g/s. The diameter of the conveyor was constant at 25 mm, except for a 50 mm diameter terminal section (length was 150 mm). There were two horizontal sections linked to a vertical section (length was 960 mm) by two 90° bends (bend radii was 300 mm). The pressure of the compressed air was controlled to provide different air velocities which were measured with an airflow meter (Nixon NL/MIN AIR @ 7 bar'G 1.293kg/m3 20 °C) after the vertical section. Samples were poured into the air stream using a funnel and collected into a 10 L powder capture with a filter on the top of the capture in order to let the compressed air come out.

It should be noted that the samples used in this study were a packaged product that had most likely already undergone breakage during its handling from spray drying through to packing and thus this powder was more resistant to breakage than the original spray-dried powder. Therefore, the processing conditions described above are relatively severe and were selected to ensure breakage could be expected.

2.3. Particle size distribution and specific surface area

The particle size distribution (PSD) and specific surface area (SSA) were measured by laser light scattering using a Malvern Mastersizer 3000 (Malvern Instruments Ltd., Worcestershire, UK). Compressed air at 0.2 bar was used to transport and disperse powders through the optical cell. Measurements were performed in triplicate.

2.4. Bulk density, particle density, and porosity

Loose bulk density (ρ_b) and tapped (100 taps) bulk density (ρ_{tapped}) of all samples were measured using a Jolting volumeter (Funke Gerber, Berlin, Germany) as per analytical methods (Niro, 2006b) from GEA Niro (Gesellschaft für Entstaubungsanlagen, Germany). Particle density (ρ_p) was measured based on GEA Niro (2006d) using a Gas Pycnometer (Accupyc II 1340 Gas Pycnometer, Micromeritics Instrument Corporation, USA). The interparticle porosity (ε) is defined as the fraction of air or void space in the tapped bulk volume (Sharma et al., 2012) and was evaluated from Eq. (1).

$$\varepsilon = 1 - \frac{\rho_{tapped}}{\rho_p} \tag{1}$$

2.5. Scanning electron microscopy (SEM)

The SEM (Zeiss-Supra 40 VP/Gemini Column, Carl Zeiss, Germany) was employed to observe the morphology of the samples at 2.00 kV. Samples were mounted on carbon adhesive discs attached to SEM specimen stubs and coated with gold ions in a sputter coater (K575X Sputter Coater, Quorum Technologies, UK).

2.6. Surface free fat content

The surface free fat (SFF) content of milk powder was measured as per GEA Niro (2006c), which is based on the extraction of the fat on the surface of particles.

2.7. Rehydration properties

2.7.1. Wettability - contact angle

Dynamic contact angle was used to quantify the wetting process. This was monitored by an optical Tensiometer (Attention Theta, Biolin Scientific Ltd., Espoo, Finland) using the sessile drop spread wetting procedure (Ji et al., 2016a). A powder bed with a smooth surface was formed by passing a leveler across the surface. A set volume of 10 mL deionized water droplet was gently dropped onto the surface of the powder bed at room temperature. The contact angle was recorded as a function of penetrating time which had a total duration of 600 s. Measurements were repeated five times.

2.7.2. Dispersibility – dispersibility index

The dispersibility index (*DI*) of samples was measured as per GEA (Niro, 2006a). The use of *DI* is the traditional standard method to measure the percentage of dry matter that passes through a sieve (180 μm) after mixing for a short time. All the measurements were repeated three times. In this study, 25 g infant formula sample was added into a 600 mL beaker with 250 mL deionized water at 37 °C and then mixed vigorously with a spatula for exactly 20 s making 20 full strokes along the diameter of the beaker in both directions. The reconstituted samples were then poured onto the 180 μm sieve and the samples that passed through the sieve were collected for further measurement of dry matter content. The *DI* was calculated as Eq. (2):

$$DI = \frac{W_d \times (100 + W)}{w \times \frac{100 - W_m}{100}} \tag{2}$$

where w is the weight of the sample, W_d (%, w/w) is the dry matter, W_m (%, w/w) is the free moisture content of the powder. All the measurements were repeated three times.

2.8. Powder flowability - flow function test

The flowability of the powder samples was assessed by measuring their flow function. Powder flow functions were quantified and analyzed by the powder flow tester (PFT) (Brookfield Engineering Laboratories, Inc., Middleboro, MA, USA) using the standard flow function test. Samples were filled into the aluminum trough (with the internal diameter 15.2 cm) of the annular shear cell at room temperature. The axial and torsional speeds for the PFT were 1.0 mm/s and 1 rev/h, respectively. The uniaxial normal stresses applied were between 0.2 and 4.8 kPa.

2.9. Bulk density under consolidation

Bulk density and its variation under consolidation load is an important property of a powder. The PFT was used to measure the bulk density of the powders at the consolidation stresses used in section 2.8 above. The compressibility index (*CI*) indicates the extent to which the volume of a powder sample changes under a compressive load and it is used for analyzing the compressibility of powders during storage (Bhandari et al., 2013; Ji et al., 2017). The *CI* was calculated from Eq. (3):

$$CI(\%) = \frac{\rho_c - \rho_b}{\rho_c} \times 100 \tag{3}$$

where ρ_b is the loose bulk density without compressing; ρ_c is the compressed bulk density at 4.838 kPa major principle consolidation stress. All the measurements were repeated in triplicate.

2.10. Statistical analysis

Results were expressed as mean ± standard deviation (SD). One-way analysis of variance (ANOVA), followed by Turkey's test, was used to

determine the significant differences (SPSS, IBM, USA). A significance level of $P < 0.05$ was used throughout the study.

3. Results and discussion

Breakage directly affects powder particle size and other physical properties, and as a consequence, may influence its functional properties, such as the ability to rehydrate, flow properties and specific storage volume.

3.1. Powder physical properties

3.1.1. Particle size and specific surface area

The particle size and SSA of samples are shown in Fig. 2 and Table 1, respectively. After breakage, the particle size of PC and HSM samples was significantly smaller than that of control samples ($P < 0.05$). Meanwhile, with the increase of treatment time (in the HSM group) or air velocities (in the PC group), the particle size decreased gradually. For the pneumatic conveyor, particle size fell from 126 μm to 117.3 μm (at a conveying speed of 40 m/s) and to 109.3 μm for a speed of 50 m/s. For the high-speed mixer, breakage was significant too with particle size falling from 143 μm progressively to 65.4 μm for lengthening mixing times. The significant differences in SSA were also found in those two groups ($P < 0.05$) and SSA increased with the decrease of particle size. The SSA was doubled after breakage for 7 min by the high-speed mixer. By contrast, powder in the Forberg blender was relatively unaffected by breakage with marginal changes in mean size for different blending times ($P > 0.05$); particle size increased slightly for short blending times but then fell back at longer times.

In order to further investigate the breakage patterns of samples during the three processing methods, the percentage change in three different sizes, D_{10}, D_{50} and D_{90} for each system and condition and PSD plots were analyzed and shown in Figs. 3 and 4, respectively. The HSM and PC samples had much higher decreased ratios than FB samples, which illustrates that particles of HSM and PC group disintegrated much more than the FB group of particles. In pneumatic conveying, there was a similar decrease in all these sizes; a 5% decrease at 40 m/s and a 13% decrease at 50 m/s. This implies that all particles broke proportionally and the dispersion in size remained approximately the same. For the mixer, longer mixing times produced increasingly larger changes in these three size points ranging from 14% at the shortest time to over 45% at the longest time and their PSD plots shifted towards smaller values. Meanwhile, for this device, the D_{10} size always experienced a larger decrease than the D_{50} and D_{90} ($P < 0.05$), which means all particles were broken with the production of more fine particles. The breakage during mixing and pneumatic conveying is typically associated with high-magnitude loading conditions, where the stresses applied to the particle exceed the particle strength and generate free surface area (Kotzur et al., 2018). On the contrary for the Forberg blender, the D_{10}, D_{50} and D_{90} of FB15 and FB30 were slightly increased compared to their control sample. This result might be because some agglomeration occurred resulting in the decrease of fine particles and a slight increase of particle size.

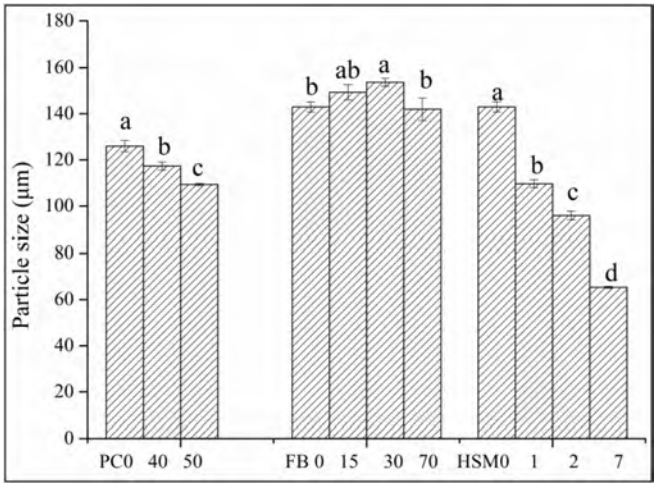


Fig. 2. The particle size ($[D_{3,2}]$) of powder samples. PC: broken by pneumatic conveying under the air velocity of 40 m/s and 50 m/s. FB: broken by the Forberg blender for 15 min, 30 min, and 70 min. HSM: broken by the laboratory high-speed mixer for 1 min, 2 min, and 7 min. Different a-d values within each group (PC, FB and HSM) are significantly different at $P < 0.05$.

Particle size is an important characteristic of dairy powder as it is closely related to many other characteristics, such as appearance, rehydration, flowability, and density (Fitzpatrick et al., 2004; Sharma et al., 2012). The SSA values might affect the water sorption behaviors as the large surface area of particles meant more area for water molecules to attach.

3.1.2. Bulk density, particle density, and porosity

The density and porosity values of samples are shown in Table 1. Powder bulk density is used for calculating the volumetric capacity of packing materials. It was shown that the bulk density of most broken samples significantly increased compared to control samples, and the porosity significantly decreased ($P < 0.05$). After breakage, small particles that were broken from the original particles possibly filled void spaces between large particles, which caused the increase of the bulk density and the decrease of the porosity. The bulk density and porosity of some FB samples also changed ($P < 0.05$), which suggests that blending did influence structure even though the particle size did not decrease.

Particle density is the mass per unit volume of a particle, excluding the open pores but including the closed pores (Sharma et al., 2012). After breakage, the particle density of PC and HSM samples increased ($P < 0.05$). The SEM micrographs of some samples are shown in Fig. 5. From micrographs, there were a lot of pores inside particles. Thus, the breakage did not only break solid bridges within agglomerated particles resulting in decreased particle size and increased bulk density, but also broke primary particles exposing internal stomata leading to the increase of the particle density.

3.1.3. Surface free fat

The surface free fat (SFF) content of samples is shown in Table 1. After breakage, the SFF of some samples were significantly increased ($P < 0.05$), especially for HSM samples, PC50 and FB70. Meanwhile, the SFF increased gradually with the increase of the processing time. HSM7 had the highest SFF, $1.88 \pm 0.04\%$, which was four times more than the control sample. Powder particles generally consist of a continuous mass of amorphous lactose and other components in which fat globules and proteins are embedded (Sharma et al., 2012). The unprotected fat on particles covers the outermost surface and, beneath it fat bound to protein or proteins is present (Kim et al., 2003; Nijdam and Langrish, 2006). Particle breakage produced more surface area and liberated more free fat, which resulted in an increase of the SFF. The increase in SFF of the Forberg blender samples might be because the inter-particle contact was sufficient to break fat globules on the surface. At the same time, it might explain the small increases in particle size as the fat acts as a binder inducing some agglomeration. The increase of the SFF might affect the rehydration properties, especially for the wettability, as the SFF influences the surface hydrophobicity of powders.

3.2. Rehydration properties

3.2.1. Wettability - contact angles

Wettability is the ability of particles to imbibe a liquid and overcome the surface tension between them based on the capillary force (Forny et al., 2011; Ji et al., 2015, 2016a; Richard et al., 2013). The contact

Table 1
Properties of infant formula samples.

Samples	SSA (m^2/kg)	Bulk density (kg/L)	Particle density (kg/L)	Porosity (%)	SFF(%)
PC0	47.6^{c}±0.8	0.492^{c}±0.003	1.2571^{b} ± 0.0008	55.80^{a}±0.08	1.183^{b} ± 0.012
PC40	51.2^{b} ± 0.8	0.506^{b} ± 0.001	1.2619^{a}±0.0008	53.47^{b} ± 0.03	1.238^{ab} ± 0.029
PC50	55.0^{a}±0.3	0.517^{a}±0.001	1.2627^{a}±0.0053	52.50^{c}±0.02	1.308^{a}±0.001
FB0	42.0^{a}±0.7	0.532^{b} ± 0.003	1.2119^{c}±0.0004	50.89^{a}±0.03	0.460^{d} ± 0.018
FB15	40.2^{ab} ± 0.9	0.532^{b} ± 0.005	1.2199^{a}±0.0007	50.30^{b} ± 0.03	0.503^{c}±0.001
FB30	39.0^{b} ± 0.4	0.541^{ab} ± 0.009	1.2125^{c}±0.0002	50.87^{a}±0.11	0.569^{b} ± 0.004
FB70	42.3^{a}±1.5	0.555^{a}±0.006	1.2185^{b} ± 0.0005	48.81^{c}±0.12	0.645^{a}±0.003
HSM0	42.0^{d} ± 0.7	0.532^{c}±0.003	1.2119^{d} ± 0.0004	50.89^{a}±0.03	0.460^{d} ± 0.018
HSM1	54.8^{c}±0.8	0.580^{b} ± 0.007	1.2203^{c}±0.0003	45.64^{b} ± 0.15	0.947^{c}±0.019
HSM2	62.6^{b} ± 1.3	0.586^{b} ± 0.006	1.2285^{b} ± 0.0005	45.15^{c}±0.06	1.233^{b} ± 0.039
HSM7	91.8^{a}±0.6	0.600^{a}±0.005	1.2311^{a}±0.0004	44.88^{c}±0.14	1.884^{a}±0.041

1. PC: broken by pneumatic conveying under the air velocity of 40 m/s and 50 m/s. FB: broken by the Forberg blender for 15 min, 30 min, and 70 min. HSM: broken by the laboratory high-speed mixer for 1 min, 2 min, and 7 min.
2. Values are mean ± standard deviation (n = 3).
3. $^{a\text{-}d}$ different values within columns in each group (PC, FB and HSM) are significantly different at $P < 0.05$.

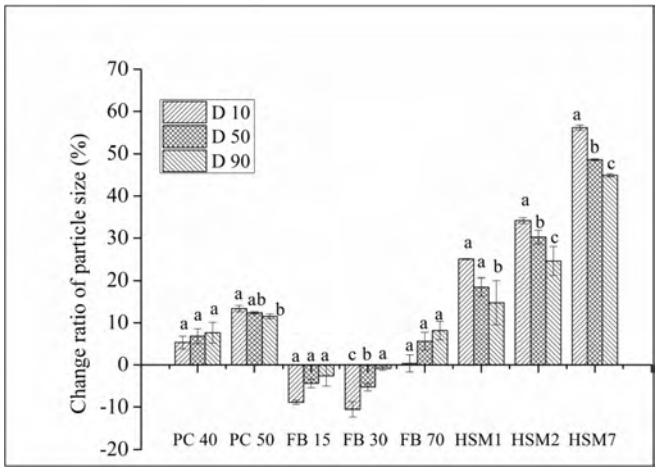


Fig. 3. Percent decreases in different kinds of particle sizes (D_{10}, D_{50}, and D_{90}) of samples. D_{10}, D_{50}, and D_{90} mean 10%, 50%, and 90% of the sample are below this diameter, separately. PC: broken by pneumatic conveying under the air velocity of 40 m/s and 50 m/s. FB: broken by the Forberg blender for 15 min, 30 min, and 70 min. HSM: broken by the laboratory high-speed mixer for 1 min, 2 min, and 7 min. Different a-c values within each group (PC, FB and HSM) are significantly different at $P < 0.05$.

angle is usually used as a primary parameter to indicate the degree of the wetting process with a small contact angle ($\theta < 90°$) representing good wettability and a large angle ($\theta > 90°$) corresponding to poor wettability (Yuan and Lee, 2013). It is important to monitor the change of contact angle until reaching an equilibrium angle to quantify the wettability of powders as wetting behavior is a dynamic procedure (Crowley et al., 2015). The penetrating time for water droplets to disappear and curves of contact angle as a function of penetrating time are shown in Fig. 6. There was no significant difference in the penetrating time between FB samples, and water droplets were absorbed in 0.75 s. For PC40 and PC50 samples, droplets took 1.94 and 2.95 s to disappear, respectively; while the PC0 sample took around 0.94 s. These significant differences ($P < 0.05$) mean when the air velocity is high enough, pneumatic conveying samples have poorer wettability compared to the control sample. The HSM samples exhibited extremely poor wetting behaviors with penetration times of 4 s, 35 s, and 5 min for HSM1, HSM2, and HSM7, respectively. Fig. 6B also showed that the changes in contact angles of PC and HSM samples were significantly slower than that of control samples. Thus, broken samples had poor wettability compared to control samples and as the degree of breakage increased, the wettability became worse.

There are two steps for the wetting process of powders. The first step is the replacement of gas by water so the interface of powder-gas is replaced by the interface of powder-water. Secondly, inward diffusion of the liquid occurs through the capillary structures of the porous powder particle (Yuan and Lee, 2013). It is usually believed that wettability improves with larger particle size with higher bed porosity (Hogekamp and Schubert, 2003). The significant decrease of the particle size and porosity, as well as the increase of the SFF, especially for the HSM samples, is most likely the main reason for the poor wettability. Lower porosity with a small capillary radius between particles and greater surface hydrophobicity due to higher SFF inhibited water penetration into the powders, thus slowing down the wetting process.

3.2.2. *Dispersibility - dispersibility index*

Dispersibility is also an important step in the rehydration process, as it is necessary for particles to be dispersed into the liquid before dissolving (Galet et al., 2004; Goalard et al., 2006). Fig. 7 illustrates the influence of breakage on the *DI* of samples. For PC and HSM samples, the *DI* significantly decreased compared to control samples and decreased gradually with the increase of treatment time. While, for FB samples, there was no significant difference between the *DI*. The substantial decrease of particle size and porosity, and increased SFF might be the reason for the deterioration of the dispersibility of broken samples by slowing down the penetration of water into the powder.

3.3. *Flow properties*

For spray-dried dairy powder, the flow properties are very important in handling and processing operations (Kim et al., 2005; Peleg, 1977). The measured powder flow functions are presented in Fig. 8. The flow functions show that all powder samples were essentially easy-flowing. It also shows that breakage had only a small influence on the flow functions. For the PC and HSM samples, it shows that breakage resulted in a small reduction in powder flowability. However, the FB powders displayed the poorest flowability relative to the others, even though there was little or no breakage.

Flow properties of dairy powders depend on their composition, in particular surface composition and physical characteristics, such as particle size distribution, porosity, particle shape, surface properties, and water content (Crowley et al., 2014; Janjatović et al., 2012; Kim et al., 2005). The SFF of powders increased after breakage, which could be one of the reasons for the small decrease in powder flowability. SFF influences powder stickiness and liquid fat can form liquid bridges

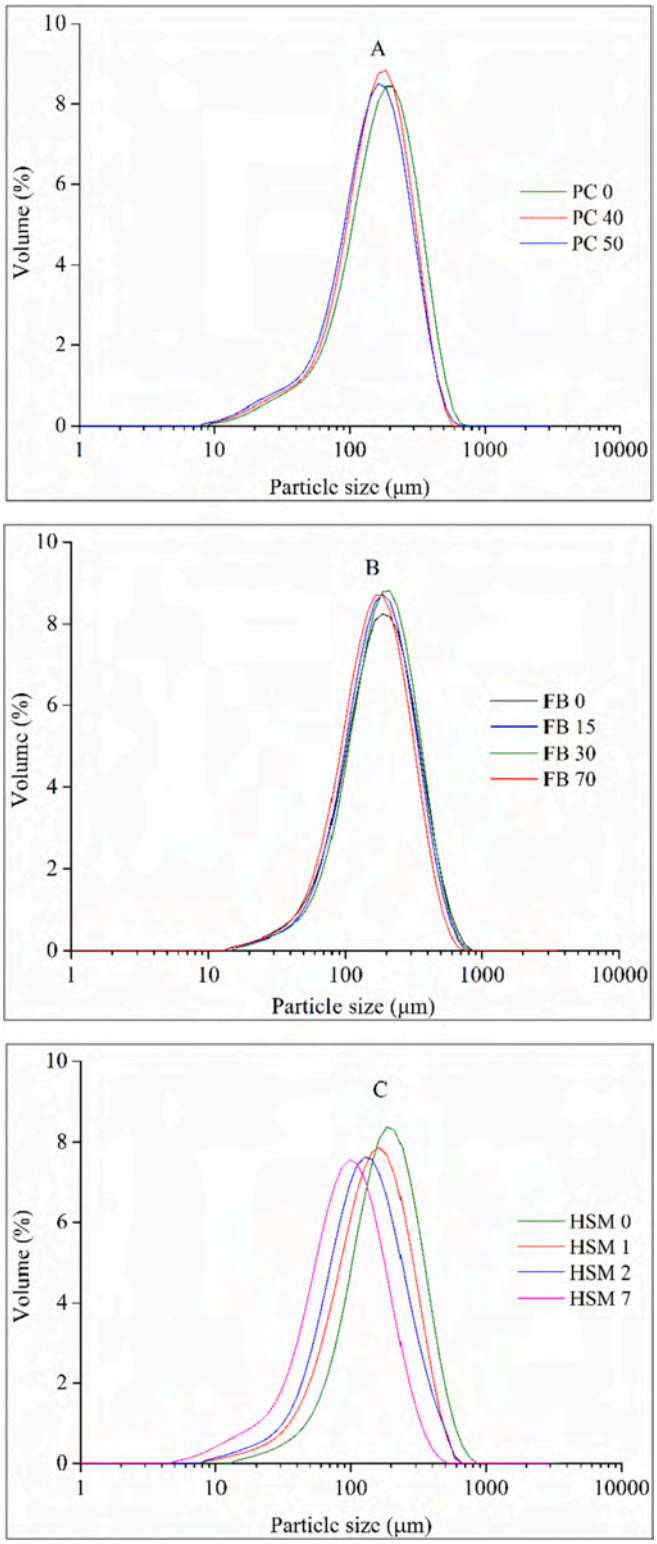


Fig. 4. The particle size distribution plots of samples. PC: broken by pneumatic conveying under the air velocity of 40 m/s and 50 m/s; FB: broken by the Forberg blender for 15 min, 30 min, and 70 min. HSM: broken by the laboratory high-speed mixer for 1 min, 2 min, and 7 min.

between individual particles reducing flowability (Kim et al., 2005; Peleg, 1977; Sharma et al., 2012). Furthermore, particle size decreased and bulk density increased after breakage, which meant more particle surface area was available for cohesive and frictional forces to resist flow. Thus powder flowability was reduced. However, overall, the

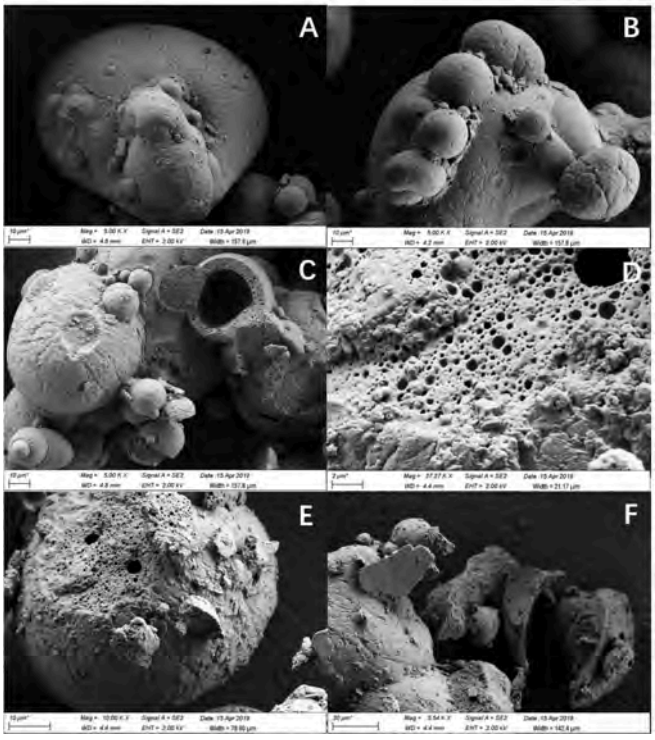


Fig. 5. The SEM micrographs of control powder sample (A–B) and broken samples by the laboratory high-speed mixer for 7 min (C–F).

powder flow functions showed that the powder breakage observed did not have a major impact on powder flowability.

3.4. Specific bulk volume and powder compressibility

The specific bulk volume and how it is influenced by consolidation is an important powder functionality, as it influences the storage volume required to store a given mass of powder. Furthermore, for infant formula, the specific bulk volume influences the size of product containers and the scoop volume requirement for the preparation of infant milk (Hanley, 2011; Li et al., 2016a). The loose specific bulk volume is presented in Table 2 (This is the inverse of loose bulk density). It shows that the breakage occurring during pneumatic conveying and high-speed mixing significantly reduced the specific bulk volume requirement by about 3–11%. It also shows little or no reduction in specific bulk volume for the Forberg blender, as there was little or no breakage.

Fig. 9 shows how bulk density varies for the different powder samples under consolidation. As expected, consolidation resulted in higher bulk densities for all the samples. Like the loose powder case, Fig. 9 shows that breakage resulted in higher bulk densities for all consolidations. This shows that breakage resulted in reduced specific bulk volume requirements under consolidations tested.

The compressibility index (*CI*) was calculated using the bulk density data (at 4.838 kPa major principle consolidation stress). A high *CI* indicates the potential for high compressibility of powders during storage or transportation (Crowley et al., 2014). Table 2 presents the *CI* of the different powder samples, which shows values mainly in the range of 26–29%, due to increases in bulk density during consolidation. Table 2 also shows that there was no significant relationship between breakage and the *CI* of the samples, which means that breakage had no influence on the compressibility of samples, even with the significant decrease in particle size and porosity. This is in-part due to the definition of *CI* in Eq. (3). Even though the compressed bulk density (ρ_c) is higher with greater breakage, the loose bulk density (ρ_b) is also higher, resulting in no clear relationship between breakage and *CI*.

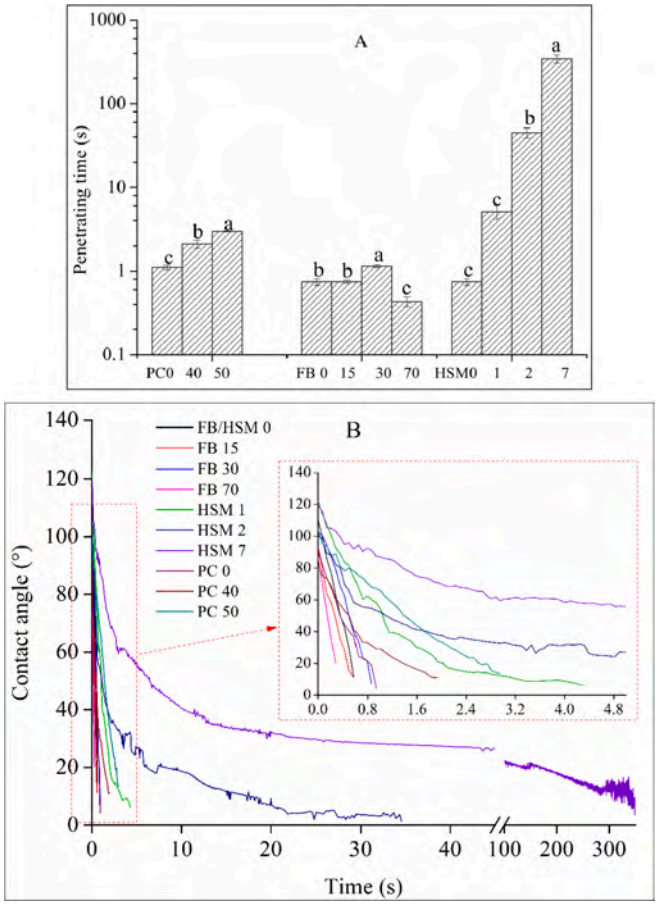


Fig. 6. A: The penetrating time takes for water droplets to be absorbed. B: The change of contact angle as a function of penetrating time in approx. 20 °C temperature. PC: broken by pneumatic conveying under the air velocity of 40 m/s and 50 m/s. FB: broken by the Forberg blender for 15 min, 30 min, and 70 min. HSM: broken by the laboratory high-speed mixer for 1 min, 2 min, and 7 min. Different a-c values within each group (PC, FB and HSM) are significantly different at $P < 0.05$.

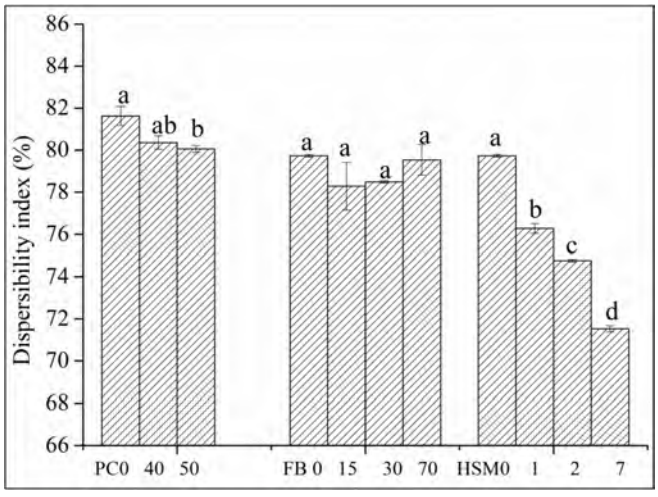


Fig. 7. Dispersibility index for samples. PC: broken by pneumatic conveying under the air velocity of 40 m/s and 50 m/s. FB: broken by the Forberg blender for 15 min, 30 min, and 70 min. HSM: broken by the laboratory high-speed mixer for 1 min, 2 min, and 7 min. Different a-d values within each group (PC, FB and HSM) are significantly different at $P < 0.05$.

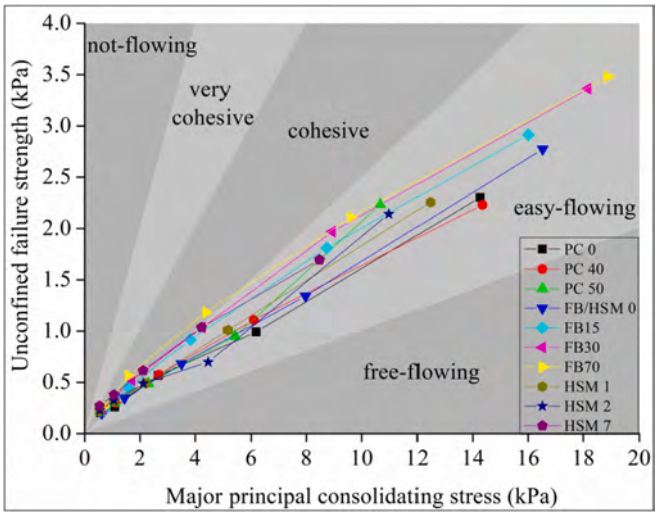


Fig. 8. Unconfined strength as a function of major principal consolidating stress for infant formula samples. PC: broken by pneumatic conveying under the air velocity of 40 m/s and 50 m/s. FB: broken by the Forberg blender for 15 min, 30 min, and 70 min. HSM: broken by the laboratory high-speed mixer for 1 min, 2 min, and 7 min.

Table 2
Loose specific bulk volume and compressibility index of infant formula samples.

Samples	Loose specific bulk volume (L/kg)	*CI* (%)
PC0	$2.031^{a}\pm0.001$	$25.8^{a}\pm0.7$
PC40	$1.976^{b}\pm0.003$	$27.6^{a}\pm0.4$
PC50	$1.934^{c}\pm0.005$	$26.5^{a}\pm0.1$
FB0	$1.88^{a}\pm0.01$	$26.5^{a}\pm0.8$
FB15	$1.88^{a}\pm0.02$	$28.3^{a}\pm2.9$
FB30	$1.85^{a}\pm0.03$	$28.4^{a}\pm2.1$
FB70	$1.80^{b}\pm0.02$	$28.9^{a}\pm0.3$
HSM0	$1.88^{a}\pm0.01$	$26.5^{a}\pm0.8$
HSM1	$1.72^{b}\pm0.02$	$25.6^{a}\pm0.1$
HSM2	$1.71^{bc}\pm0.02$	$29.3^{a}\pm0.2$
HSM7	$1.67^{c}\pm0.01$	$24.7^{a}\pm0.3$

1. PC: broken by pneumatic conveying under the air velocity of 40 m/s and 50 m/s. FB: broken by the Forberg blender for 15 min, 30 min, and 70 min. HSM: broken by the laboratory high-speed mixer for 1 min, 2 min, and 7 min.
2. Values are mean ± standard deviation (n = 3).
3. $^{a\text{-}c}$ different values within columns in each group (PC, FB and HSM) are significantly different at $P < 0.05$.

4. Conclusion

A study was performed on the particle breakage of commercial infant formula during three different processing methods (lab-scale pneumatic conveyor, laboratory high-speed mixer and Forberg blender), and how the breakage influenced the powder physical properties and functional properties (rehydration, flowability, and storage volume). The Forberg blender had a relatively small effect on particle size, even for very long blending times, but it did cause a gradual increase in SFF content, which may explain the small increases in average particle size observed. There were only minor impacts on the physical and functional properties of powder blended in the Forberg blender due to the minor changes in particle size.

Significant particle breakage occurred in the pneumatic conveyor and the high-speed laboratory mixer, and the longer or the more intense the processing, the greater was the breakage. Particle breakage was accompanied by an increase in SFF content and bulk density. This in-turn impacted on powder rehydration in particular. Particle breakage

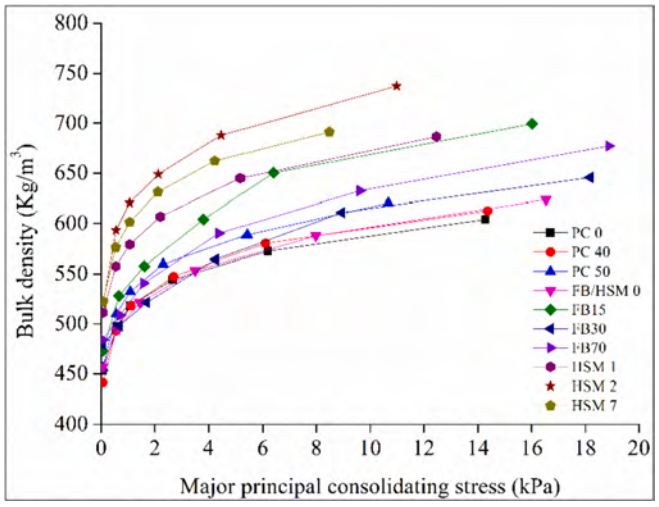


Fig. 9. Bulk density as a function of major principal consolidating stress for infant formula samples. PC: broken by pneumatic conveying under the air velocity of 40 m/s and 50 m/s. FB: broken by the Forberg blender for 15 min, 30 min, and 70 min. HSM: broken by the laboratory high-speed mixer for 1 min, 2 min, and 7 min.

caused a major reduction in powder wettability, especially for the high-speed mixer at longer times where much breakage occurred. This was most likely due to the combined effect of increased SFF and smaller particle size. These results emphasize the importance of controlling breakage levels in processing to maintain rehydration properties. Particle breakage increased bulk density, which in-turn reduced specific bulk storage volume by about 3–11%. Breakage in the high-speed mixer and pneumatic conveyor did not have a major impact on powder flowability, where there was only a minor negative impact observed.

Declaration of competing interests

The authors declare that they have no known competing financial interests or personal relationships that could have appeared to influence the work reported in this paper.

CRediT authorship contribution statement

Jie Han: Conceptualization, Methodology, Writing - original draft, Data curation. **John Fitzpatrick:** Supervision, Writing - review & editing. **Kevin Cronin:** Supervision, Writing - review & editing. **Valentyn Maidannyk:** Investigation. **Song Miao:** Supervision, Conceptualization, Writing - review & editing, Funding acquisition, Project administration, Investigation.

Acknowledgment

This work was supported financially by the Teagasc, Agriculture and Food Development Authority under the project MDDT 0153 entitled ‘Powder breakage and functionality of dairy powders’. Ms. Han was funded under the Teagasc Walsh Fellowship Scheme.

References

Aarseth, K.A., 2004. Attrition of feed pellets during pneumatic conveying: the influence of velocity and bend radius. Biosyst. Eng. 89 (2), 197–213.
Bemrose, C.R., Bridgwater, J., 1987. A review of attrition and attrition test methods. Powder Technol. 49 (2), 97–126.
Bhandari, B.R., Bansal, N., Zhang, M., Schuck, P., 2013. Handbook of Food Powders: Processes and Properties. Elsevier.
Boiarkina, I., Sang, C., Depree, N., Prince-Pike, A., Yu, W., Wilson, D.I., Young, B.R., 2016. The significance of powder breakdown during conveying within industrial milk powder plants. Adv. Powder Technol. 27 (6), 2363–2369.
Bronlund, J., Paterson, T., 2004. Moisture sorption isotherms for crystalline, amorphous and predominantly crystalline lactose powders. Int. Dairy J. 14 (3), 247–254.
Crowley, S.V., Desautel, B., Gazi, I., Kelly, A.L., Huppertz, T., O’Mahony, J.A., 2015. Rehydration characteristics of milk protein concentrate powders. J. Food Eng. 149, 105–113.
Crowley, S.V., Gazi, I., Kelly, A.L., Huppertz, T., O’Mahony, J.A., 2014. Influence of protein concentration on the physical characteristics and flow properties of milk protein concentrate powders. J. Food Eng. 135, 31–38.
Deng, X., Davé, R.N., 2017. Breakage of fractal agglomerates. Chem. Eng. Sci. 161, 117–126.
Dosta, M., Dale, S., Antonyuk, S., Wassgren, C., Heinrich, S., Litster, J.D., 2016. Numerical and experimental analysis of influence of granule microstructure on its compression breakage. Powder Technol. 299, 87–97.
Finney, J., Buffo, R., Reineccius, G.A., 2002. Effects of type of atomization and processing temperatures on the physical properties and stability of spray-dried flavors. J. Food Sci. 67 (3), 1108–1114.
Fitzpatrick, J.J., Iqbal, T., Delaney, C., Twomey, T., Keogh, M.K., 2004. Effect of powder properties and storage conditions on the flowability of milk powders with different fat contents. J. Food Eng. 64 (4), 435–444.
Forny, L., Marabi, A., Palzer, S., 2011. Wetting, disintegration and dissolution of agglomerated water soluble powders. Powder Technol. 206 (1), 72–78.
Fu, X., Huck, D., Makein, L., Armstrong, B., Willen, U., Freeman, T., 2012. Effect of particle shape and size on flow properties of lactose powders. Particuology 10 (2), 203–208.
Galet, L., Vu, T.O., Oulahna, D., Fages, J., 2004. The wetting behaviour and dispersion rate of cocoa powder in water. Food Bioprod. Process. 82 (4), 298–303.
Ghadiri, M., Zhang, Z., 2002. Impact attrition of particulate solids. Part 1: a theoretical model of chipping. Chem. Eng. Sci. 57 (17), 3659–3669.
Goalard, C., Samimi, A., Galet, L., Dodds, J.A., Ghadiri, M., 2006. Characterization of the dispersion behavior of powders in liquids. Part. Part. Syst. Char. 23 (2), 154–158.
Gupta, V., Sun, X., Xu, W., Sarv, H., Farzan, H., 2017. A discrete element method-based approach to predict the breakage of coal. Adv. Powder Technol. 28 (10), 2665–2677.
Gupta, V.K., 2017. Effect of size distribution of the particulate material on the specific breakage rate of particles in dry ball milling. Powder Technol. 305, 714–722.
Hanley, K.J., 2011. Experimental Quantification and Modelling of Attrition of Infant Formulae, Department of Process and Chemical Engineering. University College Cork, Cork, Ireland.
Hogekamp, S., Schubert, H., 2003. Rehydration of Food powders. Food Sci. Technol. Int. 9 (3), 223–235.
Janjatović, D., Benković, M., Srečec, S., Ježek, D., Špoljarić, I., Bauman, I., 2012. Assessment of powder flow characteristics in incoherent soup concentrates. Adv. Powder Technol. 23 (5), 620–631.
Ji, J., Cronin, K., Fitzpatrick, J., Fenelon, M., Miao, S., 2015. Effects of fluid bed agglomeration on the structure modification and reconstitution behaviour of milk protein isolate powders. J. Food Eng. 167, 175–182.
Ji, J., Fitzpatrick, J., Cronin, K., Crean, A., Miao, S., 2016a. Assessment of measurement characteristics for rehydration of milk protein based powders. Food Hydrocolloids 54, 151–161.
Ji, J., Fitzpatrick, J., Cronin, K., Fenelon, M.A., Miao, S., 2017. The effects of fluidised bed and high shear mixer granulation processes on water adsorption and flow properties of milk protein isolate powder. J. Food Eng. 192, 19–27.
Ji, J., Fitzpatrick, J., Cronin, K., Maguire, P., Zhang, H., Miao, S., 2016b. Rehydration behaviours of high protein dairy powders: the influence of agglomeration on wettability, dispersibility and solubility. Food Hydrocolloids 58, 194–203.
Kalman, H., Goder, D., 1998. Design criteria for particle attrition. Adv. Powder Technol. 9 (2), 153–167.
Kim, E.H.J., Chen, X.D., Pearce, D., 2005. Effect of surface composition on the flowability of industrial spray-dried dairy powders. Colloids Surf. B Biointerfaces 46 (3), 182–187.
Kim, E.H.J., Dong Chen, X., Pearce, D., 2003. On the mechanisms of surface formation and the surface compositions of industrial milk powders. Dry. Technol. 21 (2), 265–278.
Kotzur, B.A., Berry, R.J., Zigan, S., García-Triñanes, P., Bradley, M.S.A., 2018. Particle attrition mechanisms, their characterisation, and application to horizontal lean phase pneumatic conveying systems: a review. Powder Technol. 334, 76–105.
Langrish, T.A.G., Marquez, N., Kota, K., 2006. An investigation and quantitative assessment of particle shape in milk powders from a laboratory-scale spray dryer. Dry. Technol. 24 (12), 1619–1630.
Lawn, B.R., Swain, M.V., 1975. Microfracture beneath point indentations in brittle solids. J. Mater. Sci. 10 (1), 113–122.
Li, R., Roos, Y.H., Miao, S., 2016a. Influence of pre-crystallisation and water plasticization on flow properties of lactose/WPI solids systems. Powder Technol. 294, 365–372.
Li, R., Roos, Y.H., Miao, S., 2016b. Roles of particle size on physical and mechanical properties of dairy model solids. J. Food Eng. 173, 69–75.
Nijdam, J.J., Langrish, T.A.G., 2006. The effect of surface composition on the functional properties of milk powders. J. Food Eng. 77 (4), 919–925.
Niro, G., 2006a. A 6 a - Powder Dispersibility. GEA Process Engineering A/S, Gladsaxevej, Denmark.
Niro, G., 2006b. A2a - Powder Bulk Density. GEA Process Engineering A/S, Gladsaxevej, Denmark.
Niro, G., 2006c. A10a - Surface Free Fat of Powder. GEA Process Engineering A/S, Gladsaxevej, Denmark.
Niro, G., 2006d. A11c - Particle Density, Occluded Air and Interstitial Air by Air Pycnometer. GEA Process Engineering A/S, Gladsaxevej, Denmark.

Norazirah, A., Fuad, S.H.S., Hazizan, M.H.M., 2016. The effect of size and shape on breakage characteristic of mineral. Procedia Chem. 19, 702–708.
Oveisi, E., Lau, A., Sokhansanj, S., Lim, C.J., Bi, X., Larsson, S.H., Melin, S., 2013. Breakage behavior of wood pellets due to free fall. Powder Technol. 235, 493–499.
Peleg, M., 1977. Flowability OF food powders and methods for its evaluation — a review. J. Food Process. Eng. 1 (4), 303–328.
Richard, B., Le Page, J.F., Schuck, P., Andre, C., Jeantet, R., Delaplace, G., 2013. Towards a better control of dairy powder rehydration processes. Int. Dairy J. 31 (1), 18–28.
Salman, A.D., Hounslow, M.J., Verba, A., 2002. Particle fragmentation in dilute phase pneumatic conveying. Powder Technol. 126 (2), 109–115.
Shan, J., Xu, S., Liu, Y., Zhou, L., Wang, P., 2018. Dynamic breakage of glass sphere subjected to impact loading. Powder Technol. 330, 317–329.
Sharma, A., Jana, A.H., Chavan, R.S., 2012. Functionality of milk powders and milk-based powders for end use applications—a review. Compr. Rev. Food Sci. Food Saf. 11 (5), 518–528.
Wu, F., Wu, D., 2017. Attrition resistances and mechanisms of three types of FCC catalysts. Powder Technol. 305, 289–296.
Yuan, Y., Lee, T.R., 2013. Contact Angle and Wetting Properties, *Surface Science Techniques*. Springer, pp. 3–34.
Zhao, R., Goodwin, J.G., Oukaci, R., 1999. Attrition assessment for slurry bubble column reactor catalysts. Appl. Catal. Gen. 189 (1), 99–116.
Zumaeta, N., Cartland-Glover, G.M., Heffernan, S.P., Byrne, E.P., Fitzpatrick, J.J., 2005. Breakage model development and application with CFD for predicting breakage of whey protein precipitate particles. Chem. Eng. Sci. 60 (13), 3443–3452.

Food Research International 150 (2021) 110775

Contents lists available at ScienceDirect

Food Research International

journal homepage: www.elsevier.com/locate/foodres

Investigation of the influence of powder characteristics on the breakage of dairy powders

Jie Han [a,b], John Fitzpatrick [b], Kevin Cronin [b], Song Miao [a,*]

[a] Teagasc Food Research Centre, Moorepark, Fermoy, Co. Cork, Ireland
[b] Process & Chemical Engineering, School of Engineering, University College Cork, Cork, Ireland

ARTICLE INFO

Keywords:
Dairy powder breakage
Powder venturi feeder
Powder dispersion and conveying process
Breakage proportion
Particle size
Particle structure

ABSTRACT

Dairy powder breakage occurs in many processes and deteriorates powder properties and functionalities. This study investigated the influence of powder and particle characteristics on the dynamic breakage of dairy powders during the dispersion and conveying in a powder venturi feeder to provide information on assessing and reducing powder breakage during production and transportation. Four kinds of dairy powders (fifteen samples) were analysed: lactose crystals, agglomerates, commercial and lab-scale non-agglomerates. During the dispersion and conveying, breakage degree increased with increasing particle size and decreasing particle structural strength. Considering particle structure, the strength of crystals was the highest, followed by the continuum solids, followed by particles with numerous small holes throughout the particle, followed by particles with a small number of randomly distributed internal holes, followed by the hollow sphere particle with a very thin shell. The breakage behaviour of crystals during conveying was different from the other powders due to the difference in particle structures. Besides, the fat in particles might decrease the breakage of powders.

1. Introduction

Dairy powders provide a good means to transport and preserve milk ingredients in a convenient and stable form. Some properties are important for the use and storage of dairy powders, including flowability, rehydration properties, water sorption properties, mechanical properties, and so on. In order to improve these functionalities, many studies have focused on the influence of powder ingredients and the parameters during production. However, recent researches showed that dairy powder breakage happened after spray drying and significantly deteriorated powders properties (Han, Fitzpatrick, Cronin, Maidannyk, & Miao, 2020; Hazlett, Schmidmeier, & O'Mahony, 2020).

It has been reported that there were two kinds of dairy powder breakage mechanisms, surface breakage and body breakage. Body breakage had a greater influence on powder physical properties and functionalities than surface breakage. Powder breakage significantly increased densities and surface free fat contents and reduced the particle size and porosities of agglomerated dairy powders, including infant milk formula (IMF), instant whole milk powder, fat-filled milk powder, and whey protein concentrate powder (Boiarkina et al., 2016; Han et al., 2020; Hazlett et al., 2020). Besides, powder breakage changed the surface area and surface composition of dairy powders, as well as the particle shapes. The changes in these physical properties of dairy powders led to a decline in the flowability and rehydration properties (Han et al., 2020; Hazlett et al., 2020). Among these, the rehydration properties were more affected, especially for the wetting and dispersing stages of reconstitution. In addition, body breakage increased the water sorption rate and final water content of IMF with the increase in the monolayer value and the surface area of sorption. It also accelerated the time-dependent crystallization of powders, consistent with the decrease of the instant crystallization temperature. As the higher water contents of body breakage samples, their glass transition and α-relaxation temperatures slightly decreased. This indicates that broken samples have more strict requirements on the storage environment, such as lower storage temperature and water activity.

On the other hand, breakage of agglomerates easily occurs in many processes throughout dairy powder production, transportation, storage, and handling when powders are subjected to mechanical loads. These mechanical loads, such as impact, shear, or compression, can cause collisions between particles and against equipment walls, which provide the kinetic energy resulting in the breakage of agglomerates (Kotzur, Berry, Zigan, García-Triñanes, & Bradley, 2018). Dairy powder breakage

* Corresponding author.
E-mail address: Song.Miao@teagasc.ie (S. Miao).

https://doi.org/10.1016/j.foodres.2021.110775
Received 25 May 2021; Received in revised form 8 October 2021; Accepted 18 October 2021
Available online 21 October 2021
0963-9969/© 2021 Elsevier Ltd. All rights reserved.

has been found during the in-plant transportation by pneumatic conveying or a bucket elevator at the industrial scale (Boiarkina et al., 2016), during the mimic industrial situations including dry mixing and pneumatic conveying transportation (Han et al., 2020; Han, Fitzpatrick, Cronin, Maidannyk, & Miao, 2021; Hazlett et al., 2020; Zhang, Olaleye, O'Mahony, Miao, & Cronin, 2020), and during vibration tests in a container or on a sieve (Barletta & Barbosa-Cánovas, 1993a, 1993b; Yan & Barbosa-Cánovas, 2001).

In order to keep the functionalities of dairy powders, it is necessary to control the unwanted breakage during the production, storage, and transportation of powders. Based on the particle breakage studies of other materials, the applied stress from processing conditions and the characteristics of particles are two main effects that influence particle breakage (Petukhov & Kalman, 2004). The process conditions (including the parameters during dry-mixing, vibration, and pneumatic conveying) play a fundamental role in the determination of particle breakage and that, together with particle characteristics, dictates the response of particles for given loading conditions (Kotzur et al., 2018; Lu, Liu, Zhu, & Qu, 2014; Petukhov & Kalman, 2004; Yan & Barbosa-Cánovas, 2001). Thus, the control of dairy powder breakage can be considered from these two aspects. For the former, Hanley (2011) investigated the breakage of agglomerated IMF during the pneumatic conveying. It was found that, compared with dense-phase pneumatic conveying, dilute-phase pneumatic conveying resulted in high breakage and the extent of breakage increased with increasing air velocities. Besides, the number and the radius of bends in the pneumatic conveyor also influenced the breakage of IMF. During the tapping test of instant non-fat milk powders, it was found that powder breakage increased with increasing tapping number (Yan & Barbosa-Cánovas, 2001). However, there is currently not enough research on the influence of particle characteristics on dairy powder breakage when particles are subjected to mechanical loads.

This study mainly considered the influence of powder and particle characteristics on dairy powder breakability during the dispersion and conveying in a powder venturi feeder (the Aero S disperser of Malvern Mastersizer 3000). The powder venturi feeder is commonly used to disperse fine and cohesive but it also could break particles during the dispersion and conveying. There are many similarities in the conditions that dairy powder experiences in this device and during the pneumatic conveying at the industrial scale for in-plant transportation or packaging (Han, Fitzpatrick, Cronin, Maidannyk, et al., 2021; Hazlett et al., 2020). Fifteen commercial or lab-scale dairy powders with different physical properties and ingredients were studied to provide as comprehensive situations as possible. The aim is to provide information on reducing or controlling dairy powder breakage from the aspect of powder characteristics rather than the process parameters.

2. Material and methods

2.1. Material

Fifteen different dairy powders were studied including ten commercial samples, α-Lactose Monohydrate (LAC, Arla Food Ingredients, Sønderhøj 10–12 8260 DK-Viby J, Denmark), nutritional whey protein (NWP, Volac International Limited, Hertfordshire, UK), sodium caseinate (SC, protein content around 90%, Kerry Ingredients, County Kerry, Ireland), micellar casein concentrate (MCC, Molkereigesellschaft Lauingen mbH, Lauingen, Germany), IMF (IMF1 and IMF2 were Aptamil Profutura follow on milk 'stage 1′ and 'stage 2′, respectively), skim milk powder (SMP1: Kerry Ingredients, County Kerry, Ireland; SMP2: Glanbia plc, Kilkenny, Ireland), enriched milk powder (EMP, Glanbia plc, Kilkenny, Ireland), and full-fat milk powder (FFMP, Lakelands dairies, Bailieborough, Cavan, Ireland), and five lab-scale model samples with different percentages of whey protein isolate (WPI) and lactose (WPI: LAC were around 1:1, 2:1, 4:1, 1:2, and 1:4) produced with the same process by a single-stage spray dryer, termed as WL11, WL21, WL41, WL12, and WL14, respectively.

As the particle size distributions of LAC, IMF, SMP, FFMP, and EMP were wide, samples were also sieved into four size fractions, from 125 to 75 μm, from 180 to 125 μm, from 250 to 180 μm, from 355 to 250 μm (termed 125–75, 180–125, 250–180, and 355–250, respectively) to investigate the influence of particle size on breakage. Due to the high cohesiveness of powders, FFMP and EMP were only sieved into the first two size fractions and the other particles were not separated.

2.2. The main bulk and surface composition of samples

The lactose content of samples was determined using the HPLC method. Total protein content was measured using the LECO FP628 (LECO Corporation, St. Joseph, Michigan, USA) to measure total nitrogen and calculated using a nitrogen-to-protein conversion factor of 6.38. Total fat contents of samples were determined using the CEM SMART Trac 2 (CEM Corporation, Matthews, USA).

From the C, O, and N percentages, the relative surface contents in protein, fat, and lactose (other components like minerals were neglected) of samples were calculated with a matrix formula created from the elemental composition of the pure milk components (Gaiani et al., 2010; O'Donoghue et al., 2019). The relative amounts of C, O and N at the surface of model powder particles were determined by X-ray photoelectron spectroscopy (XPS) measurements using a Kratos AXIS Ultra spectrometer (Kratos Analytical Ltd., Manchester, UK). It should be mentioned that the surface fat content in IMF1 and IMF2 was calculated based on the elemental composition of milk fat because the fat in infant milk formula was mixed vegetable fat.

2.3. Sauter mean particle size of samples

The Sauter mean particle size is the surface-weighted average of the particle size distribution ($D_{3,2}$) of samples. $D_{3,2}$ of dairy powder samples was measured by a Malvern Mastersizer 3000 (Malvern Instruments Ltd., Worcestershire, UK), following the method as described by Han et al (2021).

2.4. Particle apparent density, bulk density, and interparticle porosity

Particle apparent density (ρ_p) and bulk density (tapped (100 taps) bulk density (ρ_{tapped}) and loose bulk density (ρ_b)) of samples were measured as per GEA Niro using a Gas Pycnometer (Accupyc II 1340 Gas Pycnometer, Micromeritics Instrument Corporation, USA) and Jolting volumeter (Funke Gerber, Berlin, Germany), respectively (Niro, 2006). The interparticle porosity (ε) was calculated from Eq. (1).

$$\epsilon = 1 - \frac{\rho_{\text{tapped}}}{\rho_{\text{p}}} \tag{1}$$

2.5. Friability

Friability assesses the susceptibility to the loss of component particles due to abrasion, friction, or mechanical shock. In food powders, friability refers to the tendency of particulates to break down in size during handling or storage under the influence of physical forces (Ortega-Rivas, Juliano, & Yan, 2006), shown as friability indices, which can be used to represent particle strength. Friability can be commonly determined using the shear, impact, compression, and vibration tests either on a bulk of particles or on a single particle, and different methods used different friability indices, such as the production of fragments and the changes in particle size. In this study, the friability index (*FI*) of powders was deduced from the results of particle size which was measured by the Mastersizer 3000 with different compressed air pressures, as described in 2.2. *FI* can be calculated as Eq. (2) (Schuck, Dolivet, & Jeantet, 2012) and the bigger the *FI*, the easier it is for particles to be broken

$$FI = \left(\frac{D32_{0.5} - D32_{4.0}}{D32_{0.5}}\right) \times 100\% \quad (2)$$

where $D32_{0.5}$ and $D32_{4.0}$ were the particle size $D_{3,2}$ measured with compressed air at 0.5 and 4.0 bar, respectively.

2.6. Powder structural properties

A polarised light microscope (Instruction BX51, Olympus Optical Co. Ltd., Tokyo, Japan) with a ProgRes® camera system (JENOPTIK I Optical Systems, Jena, Germany) was employed to observe the samples. Powders were spread on slides and one drop of sunflower oil was used to blend with the samples. Coverslips were then placed on the sample, which was observed with a 10 × objective or a 60 × oil objective.

2.7. Powder breakage in the powder venturi feeder

2.7.1. Powder venturi feeder

The powder venturi feeder or dispersion unit (diagram is shown in Fig. 1) in the Malvern Mastersizer 3000 has been developed for particle size analysis and is used to disperse powders into individual particles within an airflow by the three mechanisms (velocity gradients caused by particle-to-particle impacts, shear stress, and particle-to-wall impacts) before entering the particle size measuring zone.

The compressed air (0 to 4.0 bar), coming out from the nozzle (Fig. 1), produces slight vacuum and a high-velocity airflow, which entrains particles into the airflow. Based on the modelling results, the maximum velocity of airflow inside the venturi feeder is at the tip of the nozzle and the velocity reduces as it moves downstream (Bonakdar, Ali, & Ghadiri, 2021). The trajectories of particles inside the venturi feeder were predicted based on the numerical analysis of the fluid flow field by Computational Fluid Dynamic modelling and Lagrangian particle tracking (Bonakdar et al., 2021). Particles at low impact velocity collide with the surrounding walls at an oblique angle in the entrance and then accelerate along the pipe by the compressed air while also having impact or attrition with the wall or other particles, potentially causing breakage. Compared to larger particles, smaller particles accelerate to higher velocities because of lower inertia. For example, at 2.5 bar, the velocities of particles before entrance into the airflow are around 5 m/s or 15 m/s for 250 μm or 50 μm particles, respectively. The velocities of these particles can be accelerated inside the entrance region until 20–35 m/s or 35–70 m/s, respectively. The speeds of particles conveying in the horizontal pipe before entering the measuring zone are around 30 m/s or 60 m/s, respectively. The slight decrease of the velocity is because of the decrease in kinetic energy during the mechanical impacts or attritions. The particle initially deforms elastically when it is subject to impact or attrition, absorbing impact energy as stored elastic strain (King, 2012). The internal stresses in the particle increase until a crack occurs at the most sensitive part. The stored elastic strain energy in the particle drives the growing crack and the remaining stored elastic energy is converted into the kinetic energy of the child particles. Then these child particles (or damaged particles) are conveyed immediately by the airflow to the laser diffraction zone for particle size analysis.

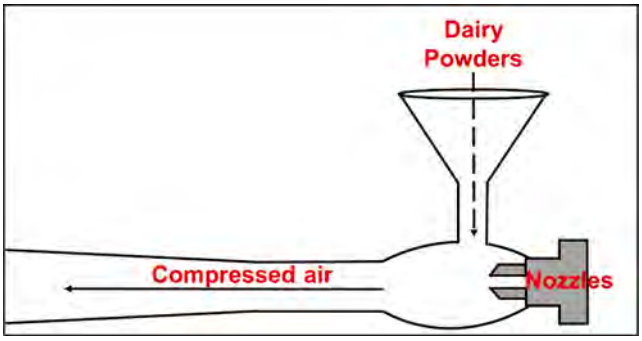


Fig. 1. The diagram of the powder venturi feeder.

There are many similarities in the trajectories and the collisions of particles during the dispersion and conveying by this venturi feeder and during the transportation by the pneumatic conveying that dairy powder experiences at the industrial scale for in-plant transportation or packaging. Also, particle velocities during the dispersion and conveying in the venturi feeder are close to the speed used during the pneumatic conveying in the industrial scale. Therefore, the powder venturi feeder or dispersion unit in the Malvern Mastersizer 3000 was used to apply loading on powders and assess their breakability.

2.7.2. Sample breakage

Powders were fed to the powder venturi feeder of the Mastersizer 3000, and the $D_{3,2}$ of samples was measured at a series of air pressures (from 0 to 4.0 bar in 0.5 bar increments). During the measurements, a low laser obscuration level (1–4 %) to ensure that most particles underwent similar conditions – breakage occurring at the individual level. Other parameters were the same as described in 2.2. The degree of breakage was shown as the breakage proportion (*BP*) that was the difference of $D_{3,2}$ compared with the initial sample. *BP* of samples under certain air pressures was evaluated as Eq. (3)

$$BP = \left(\frac{D3,2_0 - D3,2_b}{D3,2_0}\right) \times 100 \quad (3)$$

where $D3,2_0$ and $D3,2_b$ were the $D_{3,2}$ of powders measured at the atmospheric pressure (0 bar) and b bar, respectively. The *BP* under a series of air pressures represents the breakage of powders under different loads, which is different from the *FI*, although the calculation of *BP* under 4 bar (difference between $D3,2_0$ and $D3,2_{4.0}$) is similar to the *FI* (difference between of $D3,2_{0.5}$ and $D3,2_{4.0}$).

2.8. Experimental design and statistical analysis

The experimental design was completely randomized. Measurements of bulk density and porosity were carried out in duplicate, and all other measurements were performed in triplicate. Results were expressed as mean ± standard deviation (SD). Student's *t*-test with a 95% confidence interval was used to determine the significant differences in particle size and friability between two size fractions (355–250 and 250–180) in each sample (EMP and FFMP). One-way ANOVA with Tukey's test (IBM SPSS Statistics version 24, IBM, USA) was used to determine significant differences in other results with a confidence level of $P < 0.05$.

3. Result and discussion

The physical and structural characteristics of samples were firstly determined and then samples were divided into several groups for breakage discussion based on the differences in characteristics.

3.1. Composition and physical properties of powders

3.1.1. The bulk and surface composition

The main bulk and surface composition (fat, protein, and lactose) of fifteen samples are shown in Table 1. As expected, the purity of commercial ingredients (LAC, MCC, SC, and NWP) were relatively high where the bulk lactose content of LAC was higher than 99%, and the bulk protein contents of MCC, SC, and NWP were around 85%. For other commercial powders (SMP, IMF, EMP, and FFMP), SMP had the highest bulk protein contents, around 35%, and the lowest bulk fat contents, around 1%. The bulk fat contents of the other four samples were around 20% or 30%, and those of EMP and FFMP were higher than those of IMF who had the highest bulk lactose content. The ratio of bulk protein to lactose of lab-scale non-agglomerated WPI/lactose model powders met the expectation where the bulk protein content ranged from 18 to 71%,

Table 1
The main bulk and surface composition of different dairy powders.

Group	Sample	Bulk composition (%)			Surface composition (%)		
		Fat	Protein	Lactose	Fat	Protein	Lactose
A	LAC	0^{i}	$0.15^{j} \pm 0.02$	$99.57^{a} \pm 0.12$	0^{e}	$4.6^{d} \pm 2.7$	$95.4^{a} \pm 2.7$
	IMF1	$26.02^{c} \pm 0.01$	$11.05^{h} \pm 0.01$	$62.08^{c} \pm 0.05$	$87.2^{a} \pm 2.4$	$4.2^{d} \pm 0.5$	$8.6^{de} \pm 1.8$
	IMF2	$20.98^{d} \pm 0.14$	$9.91^{i} \pm 0.03$	$67.85^{b} \pm 0.04$	$88.5^{a} \pm 2.3$	$4.1^{d} \pm 0.8$	$7.4^{def} \pm 1.5$
	EMP	$33.33^{a} \pm 0.01$	$26.75^{g} \pm 0.21$	$39.37^{f} \pm 0.04$	$78.6^{b} \pm 0.6$	$7.0^{d} \pm 0.3$	$13.5^{d} \pm 0.3$
	FFMP	$28.14^{b} \pm 0.07$	$44.93^{d} \pm 0.01$	$40.02^{f} \pm 0.05$	$84.9^{a} \pm 1.0$	$5.5^{d} \pm 2.5$	$9.0^{de} \pm 1.5$
	SMP1	$0.82^{g} \pm 0.01$	$37.59^{e} \pm 0.05$	$51.92^{e} \pm 0.04$	$15.3^{d} \pm 1.0$	$44.9^{c} \pm 0.4$	$38.0^{c} \pm 0.8$
	SMP2	1.05^{f}	$34.71^{f} \pm 0.09$	$55.64^{d} \pm 0.06$	$26.7^{c} \pm 0.6$	$11.5^{d} \pm 1.1$	$60.5^{b} \pm 0.3$
	NWP	$0.59^{h} \pm 0.01$	$86.00^{b} \pm 0.01$	$2.45^{gh} \pm 0.26$	$3.1^{e} \pm 0.7$	$91.8^{a} \pm 1.0$	$3.9^{ef} \pm 0.3$
	MCC	$1.27^{f} \pm 0.02$	$87.24^{a} \pm 0.01$	$3.07^{g} \pm 0.05$	$20.1^{d} \pm 4.4$	$76.9^{b} \pm 5.0$	0^{f}
	SC	$1.53^{e} \pm 0.02$	$82.48^{c} \pm 0.05$	$2.65^{g} \pm 0.14$	$18.6^{d} \pm 0.8$	$76.9^{b} \pm 3.9$	$3.4^{ef} \pm 2.9$
B	WL11	$0.58^{A} \pm 0.01$	$44.93^{C} \pm 0.09$	$40.02^{C} \pm 0.05$	$12.2^{A} \pm 2.5$	$59.2^{C} \pm 2.5$	$28.2^{B} \pm 0.1$
	WL21	$0.55^{A} \pm 0.01$	$58.73^{B} \pm 0.19$	$23.06^{D} \pm 0.02$	$9.7^{A} \pm 2.6$	$69.4^{B} \pm 4.2$	$20.3^{C} \pm 1.8$
	WL41	0.55^{A}	$70.23^{A} \pm 0.12$	$18.03^{E} \pm 0.06$	$6.3^{A} \pm 1.5$	$81.3^{A} \pm 1.2$	$11.4^{D} \pm 0.1$
	WL12	$0.57^{A} \pm 0.01$	$30.34^{D} \pm 0.01$	$58.60^{B} \pm 0.06$	$8.1^{A} \pm 1.7$	$53.2^{CD} \pm 0.5$	$38.2^{A} \pm 2.1$
	WL14	$0.57^{A} \pm 0.01$	$18.86^{E} \pm 0.06$	$71.24^{A} \pm 0.06$	$8.4^{A} \pm 2.5$	$49.3^{D} \pm 1.0$	$41.8^{A} \pm 1.7$

LAC: α-Lactose Monohydrate; IMF: infant milk formula; EMP: enriched milk powder; FFMP: full-fat milk powder; SMP: skim milk powder; NWP: nutritional whey protein; MCC: micellar casein concentrate; SC: sodium casein; WL: model samples with different percentage of whey protein and lactose.
Values are mean ± standard deviation (n = 2).
[a-j] and [A-E] different values within columns in each group, A and B, respectively, are significantly different at $P < 0.05$.

and lactose contents were from 19 to 70% with around 0.5% fat. From Table 1, the most component on the surface of particles from LAC and commercial protein ingredients (NWP, MCC, and SC) are lactose and protein, respectively. For other commercial agglomerated powders, the composition on the surfaces of sample particles was very different from their bulk composition and the fat contents on the surface of particles were remarkably higher than their bulk fat contents. This was not surprising and similar results were found in some commercial milk particles, such as milk protein concentrate, low-fat milk powder, and whole milk powder (Foerster, Gengenbach, Woo, & Selomulya, 2016; Kim, Chen, & Pearce, 2009). This might be because of the different migration properties of components toward the interior or surface of the particle during the drying. For lab-scale non-agglomerated WPI/lactose model powders, the highest content on particle surfaces was whey protein, from 49.3% to 81.3%, even for WL12 and WL14 whose bulk whey protein content was lower than 50%. The distribution of components on the surface of particles is driven by the bulk composition of powders and also the drying approach and parameters.

From the perspective of powder characteristics, breakage is influenced by powder composition and powder physical properties, such as particle size, shape, density, and particle structure (Han, Fitzpatrick, Cronin, & Miao, 2021). The fifteen samples used in this study covered a whole variety of composition (Table 1). Also, the physical properties of powders, such as particle size and structure of particles, are determined by several factors with the composition and drying conditions being the most prominent. Therefore, powder composition and drying conditions influence the breakage properties of powders through affecting powder physical properties. However, the drying conditions of 10 commercial powders were not known and different dairy companies may use different drying conditions for different products. Thus, there was a limitation to establish a clear relationship between powder composition and physical properties without drying information. Nevertheless, the composition and the drying parameters determine the physical properties of powders. Therefore, the discussion of the influence of powder characteristics on the breakage in this study was mainly focused on the physical properties of the dairy powders.

3.1.2. Particle size

The particle sizes of initial whole samples and sieved fractions are given in Table 2 and Table 3, respectively. As expected, the particle sizes of sieved fractions significantly increased as the sieve aperture size increased. For initial whole samples, the particle sizes of WPI/lactose model powders were the smallest, at around 6 or 7 μm. The particle sizes of WL11, WL21, and WL41 were significantly bigger than those of WL12

Table 2
Physical properties of different dairy powders.

Group	Sample	Particle size $D_{3,2}$ (μm)	Particle apparent density (kg/L)	Loose bulk density (kg/L)	Tapped bulk density (kg/L)	Porosity (%)	Friability Index (%)
A	LAC	$160.3^{e} \pm 1.2$	$1.543^{a} \pm 0.029$	$0.743^{a} \pm 0.003$	$0.917^{a} \pm 0.008$	$50.5^{f} \pm 0.4$	$23.6^{h} \pm 0.5$
	IMF1	$203.7^{b} \pm 1.9$	$1.053^{g} \pm 0.002$	$0.446^{c} \pm 0.003$	$0.577^{e} \pm 0.001$	$45.2^{g} \pm 0.1$	$48.9^{b} \pm 1.1$
	IMF2	$224^{a} \pm 3.6$	$1.023^{h} \pm 0.001$	$0.441^{cd} \pm 0.006$	$0.602^{d} \pm 0.002$	$41.1^{h} \pm 0.2$	$53.8^{a} \pm 1.8$
	EMP	184^{d}	$1.197^{f} \pm 0.001$	$0.364^{f} \pm 0.001$	$0.507^{g} \pm 0.002$	$57.6^{c} \pm 0.1$	$39.3^{e} \pm 0.4$
	FFMP	$191^{c} \pm 2.4$	$1.244^{d} \pm 0.001$	$0.384^{e} \pm 0.001$	$0.547^{f} \pm 0.001$	$56.0^{d} \pm 0.1$	$36.3^{f} \pm 0.2$
	SMP1	$117.3^{g} \pm 0.5$	$1.219^{e} \pm 0.001$	$0.460^{b} \pm 0.002$	$0.576^{e} \pm 0.001$	$52.7^{e} \pm 0.1$	$31.2^{g} \pm 0.8$
	SMP2	130^{f}	$1.402^{b} \pm 0.001$	$0.433^{d} \pm 0.001$	$0.617^{c} \pm 0.001$	$56.0^{d} \pm 0.1$	$41.2^{d} \pm 0.4$
	NWP	$87.9^{h} \pm 1.2$	$1.195^{f} \pm 0.001$	$0.376^{e} \pm 0.002$	$0.485^{h} \pm 0.002$	$59.4^{b} \pm 0.1$	$44.7^{c} \pm 0.6$
	MCC	$33.9^{j} \pm 0.1$	$1.230^{de} \pm 0.002$	$0.295^{g} \pm 0.004$	$0.373^{i} \pm 0.001$	$69.6^{a} \pm 0.1$	$16.2^{i} \pm 0.4$
	SC	$60.1^{i} \pm 1.0$	$1.312^{c} \pm 0.001$	$0.436^{d} \pm 0.002$	$0.627^{b} \pm 0.001$	$52.2^{e} \pm 0.1$	$10.1^{j} \pm 0.1$
B	WL11	$7.0^{A} \pm 0.1$	$1.315^{D} \pm 0.001$	$0.229^{C} \pm 0.003$	$0.289^{B} \pm 0.003$	$78.0^{A} \pm 0.2$	$32.3^{D} \pm 0.2$
	WL21	$6.7^{B} \pm 0.1$	$1.320^{C} \pm 0.002$	$0.273^{A} \pm 0.002$	$0.316^{A} \pm 0.001$	$76.1^{B} \pm 0.1$	$42.9^{B} \pm 0.4$
	WL41	$6.6^{B} \pm 0.1$	$1.300^{E} \pm 0.001$	$0.267^{A} \pm 0.002$	$0.314^{A} \pm 0.005$	$75.9^{C} \pm 0.4$	$46.4^{A} \pm 0.1$
	WL12	$6.3^{C} \pm 0.1$	$1.343^{A} \pm 0.002$	0.257^{B}	0.292^{B}	78.3^{A}	$35.8^{C} \pm 0.2$
	WL14	$6.1^{D} \pm 0.1$	$1.333^{B} \pm 0.002$	$0.272^{A} \pm 0.004$	$0.309^{A} \pm 0.001$	$76.9^{BC} \pm 0.1$	$30.4^{E} \pm 0.2$

LAC: α-Lactose Monohydrate; IMF: infant milk formula; EMP: enriched milk powder; FFMP: full-fat milk powder; SMP: skim milk powder; NWP: nutritional whey protein; MCC: micellar casein concentrate; SC: sodium casein; WL: model samples with different percentage of whey protein and lactose.
Values are mean ± standard deviation (n ≥ 2).
[a-j] and [A-E] different values within columns in each group, A and B, respectively, are significantly different at $P < 0.05$.

Table 3
Particle size and friability index of sieved fractions of several agglomerated dairy powders.

Sample	Size range	Particle size $D_{3,2}$ (μm)	Friability Index (%)	Sample	Size range	Particle size $D_{3,2}$ (μm)	Friability Index (%)
LAC	355–250	$334.7^{a} \pm 1.2$	$30.1^{a} \pm 0.2$	IMF1	355–250	$329.3^{a} \pm 1.9$	$53.9^{a} \pm 0.2$
	250–180	$247.0^{b} \pm 1.4$	$20.1^{b} \pm 0.2$		250–180	$244.5^{b} \pm 0.5$	51.3^{c}
	180–125	$182.3^{c} \pm 0.5$	$15.9^{d} \pm 0.1$		180–125	$174.5^{c} \pm 0.5$	$53.0^{b} \pm 0.1$
	125–75	$117.7^{d} \pm 0.5$	$17.1^{c} \pm 0.3$		125–75	$113.0^{d} \pm 1.0$	46.8^{d}
IMF2	355–250	$344.3^{a} \pm 0.5$	$57.5^{a} \pm 0.1$	SMP1	355–250	$302.0^{a} \pm 1.4$	$47.8^{a} \pm 1.0$
	250–180	$249.7^{b} \pm 0.5$	$56.3^{b} \pm 0.1$		250–180	229.0^{b}	$44.2^{b} \pm 0.2$
	180–125	177.0^{c}	$52.2^{c} \pm 0.2$		180–125	158.0^{c}	$34.2^{c} \pm 0.2$
	125–75	109.0^{d}	$49.3^{d} \pm 0.1$		125–75	$107.3^{d} \pm 0.5$	$30.3^{d} \pm 0.1$
EMP	355–250	$309.5^{a} \pm 0.5$	$51.3^{a} \pm 0.2$	FFMP	355–250	$332.0^{a} \pm 0.8$	$49.8^{a} \pm 0.2$
	250–180	235.0^{b}	46.7^{b}		250–180	$240.5^{b} \pm 0.5$	$39.2^{b} \pm 0.5$

LAC: α-Lactose Monohydrate; IMF: infant milk formula; EMP: enriched milk powder; FFMP: full-fat milk powder; SMP: skim milk powder; NWP: nutritional whey protein.
Values are mean ± standard deviation (n = 3).
a-d different values within columns in each powder (LAC, IMF1, IMF2, SMP1, EMP and FFMP) are significantly different at $P < 0.05$.

and WL14. This means WPI/lactose model samples with high protein content have slightly larger particles when the parameters of production processes with the single-stage spray dryer are the same. The same trend was observed for milk protein isolate and lactose mixtures, where the particle size of powders with 60% or 80% protein was around 50 μm while that of powders with 20% and 40% of proteins was around 40 μm (Li, Roos, & Miao, 2016a). Different from the WPI/lactose model samples, the particle size of commercial ingredients - NWP, SC, MCC, and LAC were around 88, 60, 34, and 160 μm, respectively. In addition, as commercial dairy powders, the particle size of EMP, FFMP, and IMF was the biggest, at around 200 μm, because of the agglomeration to increase the flowability and rehydration properties of powders. The particle size of SMP was smaller than them, at around 120 or 130 μm because its fat content was low (Table 1) and the smaller particles could meet the requirements for flow and rehydration.

It has been demonstrated that particle size is one of the most important factors affecting particle breakage and particle strength decreases as the particle size increases (Bonakdar et al., 2016; Gerhards, Kaell, & Schubert, 2004; Norazirah, Fuad, & Hazizan, 2016; Z. Zhang & Ghadiri, 2002). This is attributed to the likelihood of a greater number of imperfections in larger particles. The structural defects in particles are analogous to microcracks, imperfections, or inhomogeneities in material science. The highest local tensile stress is generated at these defective zones in the agglomerates so that the fracture initiates from this zone. Besides lesser flaws, small particles are more difficult to break because of the stronger interparticle forces (including van der Waals forces, electrostatics, and liquid bonds) that bind particles together (Reynolds, Fu, Cheong, Hounslow, & Salman, 2005). From an energy perspective, the probability of breakage is related to the amount of energy that is absorbed by the particle during the breakage. The particle can absorb a certain amount of energy as stored elastic strain before it breaks. The energy that is absorbed and stored represents the minimum energy that is required to break the particle under the particular external loading and stress pattern that the particle experiences. This energy is called the particle fracture energy and it is a material property that is influenced by its particle size, shape, the orientation that the particle presents to the impact stress, and the presence of flaws in the particle. For particles of the same material, the smaller the particles, the higher the fracture energy, and hence the less likely particles will break (King, 2012).

3.1.3. Powder densities and interparticle porosities

The particle densities, bulk densities, and porosities of the initial whole samples are shown in Table 2. Particle apparent density is the mass per unit volume of particles, including the closed pores but excluding the cracks or open pores so it is related to particle structure characteristics that may affect the breakage behaviour of particles. From Table 2, the particle apparent density of IMF was the smallest, at around 1.0 kg/L, and LAC had the highest particle apparent density that was around 1.9 kg/L. Besides, SC and WPI/lactose model samples had a similar particle apparent density, around 1.3 kg/L, which was slightly lower than that of SMP2 but higher than those of other samples. The bulk density of powders is also influenced by particle structure and shapes. Similar to the particle apparent density, LAC had the highest tapped bulk density and loose bulk density and they were significantly higher than those of other samples. However, instead of the IMF, the bulk densities of WPI/lactose model samples were the smallest. This is because these small particles were much lighter and had much higher specific surface areas and thus trapped air much more easily in a bed of powder, which reduced the bulk density and increased the porosity. The bulk densities of other samples were in between those of LAC and model samples, where those of IMF, SMP, and SC were higher than those of NWP, FFMP, EMP, and MCC. By definition, interparticle porosity is affected by the particle apparent density and tapped bulk density of powders and it may influence the multi-particles behaviour of dairy powders. From Table 2, the porosity of IMF was the smallest, at around 40% or 45%, while WPI/lactose model samples had the highest porosities, at around 75% to 78%. The porosities of other samples were in between of them, where those of LAC, SMP1, and SC were around 50%, those of EMP, FFMP, SMP2, and NWP were around 60%, and that of MCC was around 70%.

3.1.4. Friability

Friability is the most used index to indicate the strength of food powders or the sensitivity of particles to the breakage when particles are subjected to mechanical loads. The *FI* of the initial whole samples and sieved fractions are given in Table 2 and Table3, respectively. For the initial whole sample, it was shown that the *FI* of samples was different, ranging from 10% to 54%. IMF, NWP, and WL41 particles were the easiest to break while SC and MCC particles were the most difficult to break. For sieved fractions of most samples, the *FI* increased with increasing particle size, except for the sieved fractions of LAC 125–75 and IMF1 180–125. This means the bigger the particles, the easier it is for them to be broken, which is consistent with previous studies (Han, Fitzpatrick, Cronin, Maidannyk, et al., 2021). However, this trend was not suitable for comparing some powders with different composition or production conditions. For example, for the same sieved size fraction of 250–180, the particle size of SMP1, FFMP, and LAC were 229, 240.5, and 247.0 μm, respectively while their *FI* were 44%, 39%, and 20%, respectively. Besides, the particle size of model samples was much smaller than those of other samples while their *FI* was not the smallest, especially for WL21 and WL41. These results show that although particle size has a major influence on powder breakage, there are other powder characteristics that influence breakage, including composition and the structure of the particles and the powder.

3.2. Structural properties of powders

Light microscopy photos from initial whole powders are presented in Fig. 2 and it shows a few different microstructures of powders. Particle microstructure is influenced by the parameters of the powder drying process and powder compositions.

3.2.1. Crystal and irregular continuum solid structure

From Fig. 2, the characteristic tomahawk-like shape for α-lactose monohydrate crystal was observed (LAC). The α-lactose crystals are monoclinic sphenoidal and have only 1 axis of symmetry. They have trapezoidal side faces, rhombic tops and bottoms, and bevelled faces at the base and apex, giving the crystal a distinct tomahawk appearance (Hunziker & Nissen, 1927). The shapes of lactose crystals depend on the types and conditions of crystallization (Wong & Hartel, 2014). Compared with amorphous lactose, lactose crystals are very hard and brittle (Li, Roos, & Miao, 2016b). This may result in different breakage behaviour of lactose crystals and other samples. Compared with other samples, the microstructure of SC particles was most similar to that of LAC. From Fig. 2, the particles of SC were irregular continuum solid without internal holes and their surface was unsmooth.

3.2.2. Hollow sphere structure

The structure of particles in WPI/lactose model samples was similar so only two samples' microscopy photos are shown in Fig. 2 (WL14 and WL41). These particles separated from each other and had spherical shapes with large internal holes and thin outer covering. Besides, some fragments were observed, which means some particles were broken. This could also be used to explain why particle apparent densities of WPI/lactose model samples were much higher than most of the other samples even though their particles were hollow. For some of the particles, there were multiple bubbles inside before the droplets were dried. From Fig. 2, particles from NWP and MCC were also non-agglomerated and they had hollow sphere structures similar to WPI/lactose model sample particles. Compared with MCC particles, NWP particles were more spherical and their outer walls were thinner. A similar structure was observed in previous researches on milk protein concentrate particles (Bouvier, Collado, Gardiner, Scott, & Schuck, 2013). This structure is generated during the final stage of spray drying when there is no more wet area on the particle surface. The air that is trapped inside the particle expands as the particle temperature increased, which leads to particles with a hollow interior. This structure might be the reason that the particle densities of NWP and MCC were significantly smaller than that of SC. Besides, the internal holes may reduce the strength of particles because the pores inside particles can be regarded as imperfections and crack release zones (Antonyuk, Tomas, Heinrich, & Mörl, 2005).

3.2.3. Irregular agglomerated particle structure with internal holes

From Fig. 2, the particle shapes of FFMP, EMP, and SMP2 particles were similar and they were irregular agglomerated particles with a small number of randomly distributed small internal holes. SMP1 particles were agglomerated and irregular, similar to the other agglomerated particles but had highly porous matrices with numerous small holes distributed throughout the particle. Besides, the diameters of most internal holes in SMP1 particles (around 2.5 μm) were much smaller than those in other agglomerated samples (≥8 μm). This might result in a stronger structure of SMP1 particles than other agglomerated particles as the particle was more homogenous. The structure of SMP1 and SMP2 were different but their composition (fat, protein, and lactose) were similar, which might be because of the different drying parameters. For IMF, samples were mixtures of lactose crystals and agglomerated particles (Fig. 2 IMF1 and IMF2). Some of the lactose crystals were tomahawk shape and some were irregular fragments. The shapes of agglomerated particles were similar to those of FFMP, EMP, and SMP2 but the internal holes were more and larger.

3.3. Powder breakage in the venturi feeder

The dynamic breakage of dairy powders under different loads during the dispersion and conveying in the venturi feeder was represented by a series of *BP*. The *BP* of all initial whole samples and the sieved size fractions at different air pressures are given in Fig. 3 and Fig. 4, respectively. The *BP* increased with increasing air pressures, which was because increasing the air pressure increased the airspeed which in turn increased the particle speed. Hence higher air pressures mean more severe particle collisions and higher kinetic energy and this caused more breakage. It was clear that the changes in *BP* of LAC and other dairy powders were different, where the *BP* of LAC increased linearly with increasing air pressure while those of other samples increased logarithmically (Fig. 3). Besides, based on the analyses in the physical and structural properties, other dairy powders could be divided into three groups: agglomerated powders (A group, including IMF, SMP, FFMP, and EMP), non-agglomerated powders (B group, including NWP, MCC, and SC), and model samples (C group, including WL11, WL21, WL41,

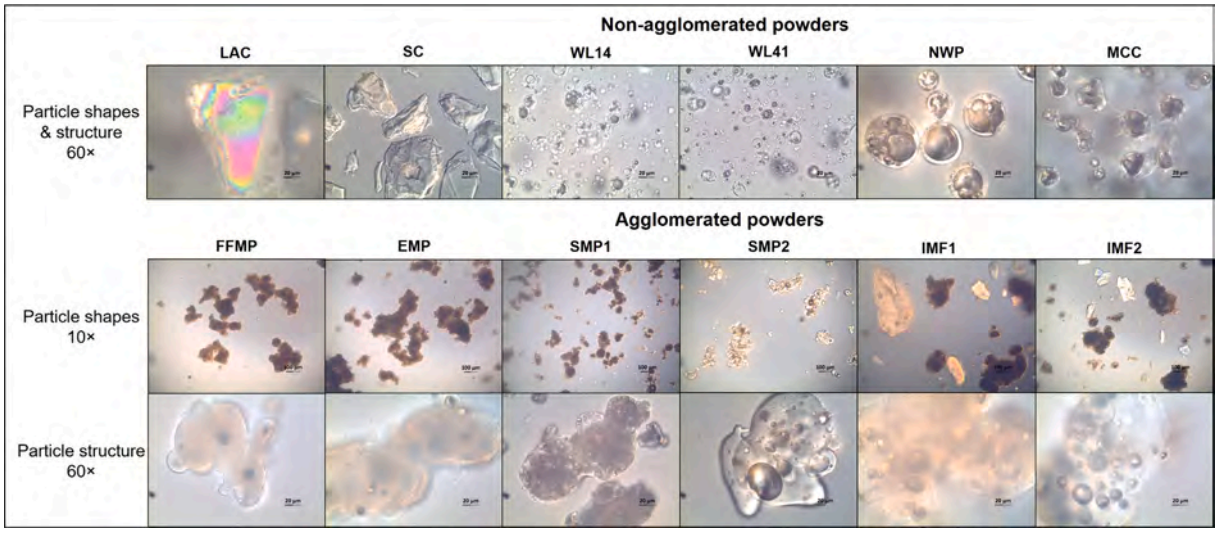


Fig. 2. Microscopy photos of dairy powders with different scales (60 × oil objective: 20 μm; 10 × objective: 100 μm) for showing particle shapes and structures. LAC: α-Lactose Monohydrate; SC: sodium casein; WL: whey protein and lactose model samples (WL14: WPI: lactose was 1:4; WL41: WPI: lactose is 4:1); NWP: nutritional whey protein; MCC: micellar casein concentrate; FFMP: full-fat milk powder; EMP: enriched milk powder; SMP: skim milk powder; IMF: infant milk formula.

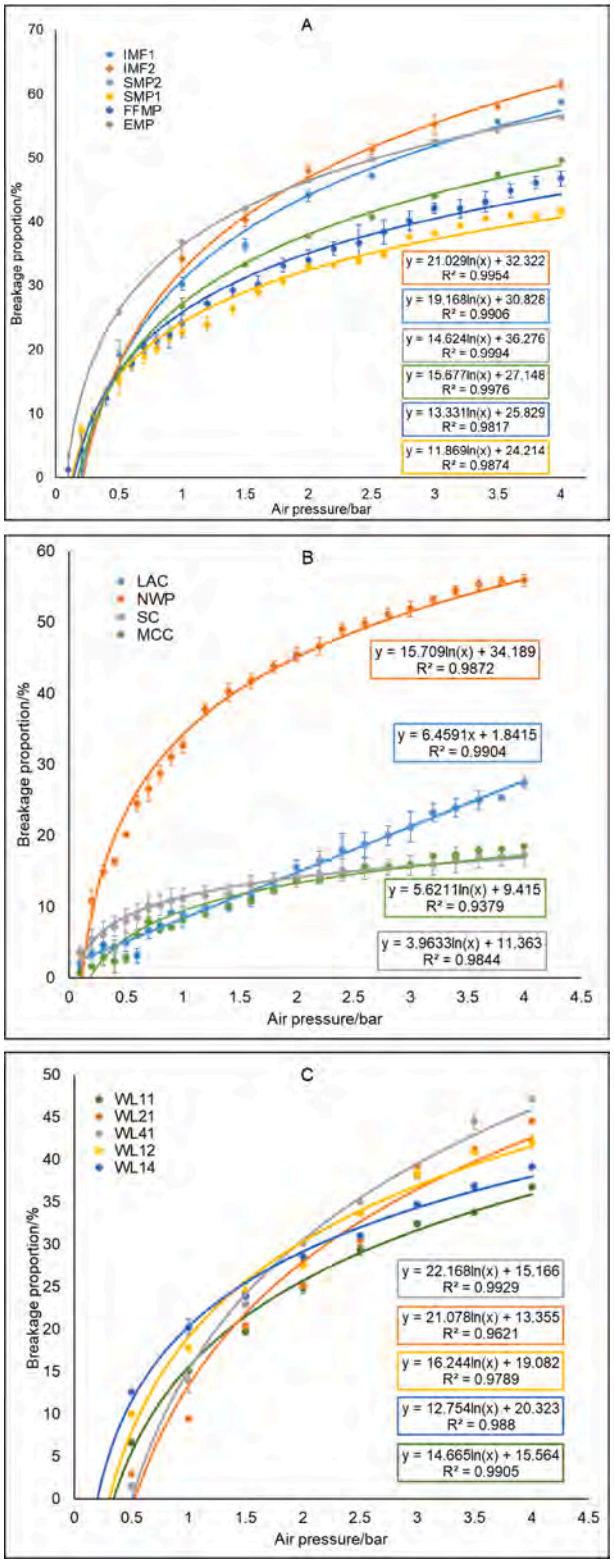


Fig. 3. Breakage proportions of dairy powders during the transportation by the powder venturi feeder at different air pressures. Its trendlines and the corresponding mathematical functions are presented in the boxes by colour. A: commercial agglomerated powders (IMF: infant milk formula; SMP: skim milk powder; FFMP: full-fat milk powder; EMP: enriched milk powder). B: commercial non-agglomerated powders and α-Lactose Monohydrate (LAC: α-Lactose Monohydrate; NWP: nutritional whey protein; SC: sodium casein; MCC: micellar casein concentrate). C: lab-scale model samples (WL: model samples with different percentages of whey protein and lactose).

WL12, and WL14). The breakage behaviour of different group powders and the influence of powder characteristics on the breakage was discussed in the following parts.

3.3.1. *Breakage of agglomerated powders*

From Fig. 3A, as expected, the *BP* of IMF were higher than those of most other samples because their particle sizes were the biggest. Besides, the particle sizes of FFMP and EMP were similar to that of IMF but their *BP* was smaller than those of IMF. This might be because IMF had lower particle apparent density and there were more internal holes in IMF particles, resulting in the relatively weaker particle structure. In addition, the *BP* of SMP1 were much smaller than those of SMP2, which might be because the particle size of SMP2 was slightly bigger but this was more likely due to the difference in the particle structure. The more homogeneous porous structure with numerous smaller holes (SMP1) was stronger than the structure with several randomly distributed bigger internal holes (SMP2).

On the other hand, if the impact of particle size on breakage was considered, the *BP* of SMP should be much smaller than those of other agglomerated powders. However, the *BP* of SMP were similar or higher than those of other agglomerates. Besides, for 355–250 and 250–180 sieved fractions, the particle size of FFMP was bigger than those of the corresponding SMP1 while the particle structure of SMP1 was stronger than that of FFMP. Thus, the breakage degree of FFMP should be higher than that of the corresponding SMP1. In contrast, the *BP* of SMP1 fractions were higher than those of corresponding FFMP (Fig. 4A&B). This might be because the fat in FFMP and other agglomerated powders (Table 1) could soften powders, resulting in the easy plastic deformation of particles during the dispersion and conveying instead of brittle fracture. Also, the *FI* of LAC 125–75 was bigger than that of LAC 180–125 but their *BP* at different air pressures were similar and smaller than those of the other two bigger-sized fractions. The *FI* of IMF1 180–125 was bigger than that of IMF1 250–180 but its *BP* were always smaller than those of IMF1 250–180. This indicates that sometimes it is inaccurate to predict the strength of different powders only by their *FI* because the *FI* only compared the size of particles under two specific mechanical stresses (0.5 bar and 4.0 bar) instead of comparing with the initial particle.

3.3.2. *Breakage of commercial non-agglomerated powders*

From microscopy photos, particles in NWP, SC, and MCC were non-agglomerated particles. From Fig. 3, the *BP* of NWP were similar or higher than those of agglomerated powders but the particle sizes of most agglomerates were around 200 μm and that of NWP was only 88 μm. This might be because the particle structure of NWP, like a hollow ball, was weaker than the normal agglomerated particle structure. It was shown in Fig. 3B that the *BP* of NWP were much higher than those of SC and MCC, which is consistent with the result of friability. This means that the particles of NWP were weaker than the other two samples, which might be because of its bigger particle size and weaker particle structure. This also caused the particles from NWP to be more sensitive to the increase in force compared to particles from SC and MCC. Therefore, the *BP* of SC and MCC were more stable with increasing air pressures compared with that of NWP.

Besides, MCC had a similar particle structure to NWP while the structure of SC particles was continuum solids and the particle size of SC was nearly twice that of MCC. From Fig. 3B, compared with MCC, SC broke more when the air pressure was lower than 2.8 bar but broke slightly less at higher air pressures. The bigger particle size of SC might be the reason for the higher degree of breakage at low air pressures. When particles were subjected to higher-level external mechanical stress, compared with continuum solid structure, the weaker particle structure of MCC might result in more breakage. This means that the particle structural strength of continuum solid particles might be higher than spherical particles with a hollow interior surrounded by a highly compacted shell. On the other hand, it could be considered that for some

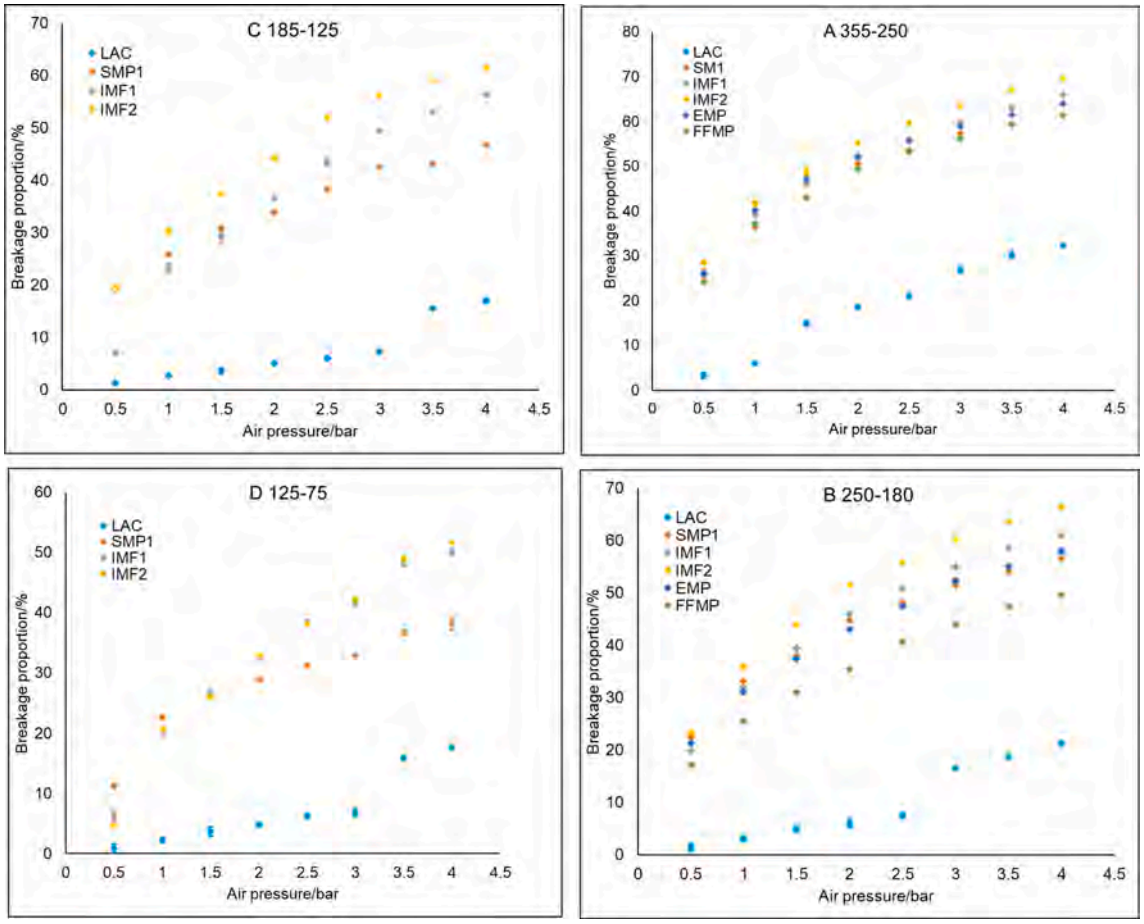


Fig. 4. Breakage proportions of sieved sized fractions of several agglomerated samples during the transportation by the powder venturi feeder at different air pressures. A, B, C and D: particle size from 355 to 250 μm, from 250 to 180 μm, from 180 to 125 μm, from 125 to 75 μm, respectively. IMF: infant milk formula; SMP: skim milk powder; FFMP: full-fat milk powder; EMP: enriched milk powder; LAC: α-Lactose Monohydrate.

dairy powders, the breakage might be mainly affected by the particle size when particles subjected to low-level external mechanical stress while the particle structure mainly affected the breakage when the stress was high. This also resulted in the inconsistent friability and *BP* of SC and MCC. The friability of SC was significantly lower than that of MCC while the changes in *BP* of SC were not always lower than those of MCC. This indicates that sometimes it is inaccurate to predict the breakage degree of different powders only by their friability. The accuracy will depend on the difference between the actual force exerted during the production and the force during the transportation in the venturi feeder at 4.0 bar.

3.3.3. *Breakage of non-agglomerated lab-scale WPI/lactose model solids*

From Fig. 3, the *BP* of model samples were between those of agglomerated and non-agglomerated powders. This implies the degree of breakage was very high even though the particle size of the model powders was very small, which might be because the particle structure, hollow sphere with a very thin shell, was weak. From Fig. 3C, at low air pressures, the *BP* increased with increasing lactose content but not much difference. At high air pressures, WL11 had the lowest degree of breakage, and the *BP* of other model samples increased as the protein content increased, which is consistent with the result of particle size. From Fig. 2, particle structures of model samples were similar. These results confirm that, with the same production conditions, the composition of powder affects the particle size of samples, which then influences the breakage during transportation.

3.3.4. *Breakage of lactose crystals*

The particle size of whole LAC (160 μm) was closer to those of group A samples while its *BP* at different air pressures were much lower than these samples even though for SMP whose particle size (120 or 130 μm) were smaller than that of LAC (Fig. 3). From Fig. 4, the *BP* of lactose fractions were lower than other samples. Besides, the *BP* of whole LAC were similar to those of MCC and SC while their particle sizes were 34 and 60 μm, respectively, much smaller than LAC particles. These results mean that the strength of the crystalline structure is much higher than those of other dairy powder particle structures thus lactose crystals had less breakage than other samples even if its particles were larger.

On the other hand, the changes in *BP* at different air pressures of LAC sieved fractions were different from those of other samples (Fig. 4). The *BP* of other fractions increased logarithmically with increasing air pressure while those of LAC fractions increased steadily then sharply when the air pressure reached a particular threshold. This might be because the breakage behaviour of normal particles and crystals was different. It has been established that different from continuum solids or agglomerates, the breakage mechanism of crystalline particles is due to the distribution of loading forces across the topography of the particle. It will typically break via the surface breakage mechanism if crystalline material is semi-brittle. When particles are subject to low-level external mechanical stress, the main mechanism of breakage is the surface breakage, leading to the production of minuscule particles whilst still retaining the identity of the original particles. These minuscule child particles originate at the points of the surface of the initial particle where the stress is applied. If crystalline material breaks via a pure brittle mechanism, rupture along preferred fracture planes is expected. When a

particle is composed of two or more crystals, cleavage may occur at the interface, and child particles are relatively undamaged (Cleaver, Ghadiri, & Rolfe, 1993; Ghadiri, Yuregir, Pollock, Ross, & Rolfe, 1991). Thus, the slight increase of the *BP* might be because of the surface breakage while the sharp increase was caused by the cleavage that happened at the interface. Besides, the threshold air pressures increased as the particle size decreased (Fig. 4, 1.5 bar for LAC355-250, 2.5 bar LAC 250–180, and 3 bar for LAC185-75), which also documented that the larger the particles, the easier it is for them to be broken.

4. Conclusion

A study was performed on the influence of particle characteristics on dairy powder breakage during the dispersion and conveying in a powder venturi feeder. The physical and structural characteristics and the breakage behaviour of dairy powders were analysed. Four kinds of dairy powders (fifteen samples) were considered: lactose crystals, agglomerated powders (including IMF, SMP, FFMP, and EMP), commercial non-agglomerated powders (NWP, SC, and MCC), and lab-scale non-agglomerated powders (model samples with different percentages of WPI and lactose).

During the dispersion and conveying, the breakage of powders was mainly influenced by the particle size and structures. The degree of breakage increased with increasing particle size and decreasing particle structural strength. For particle structure response, the strength of crystals was the highest, followed by continuums solids, followed by the highly porous matrices with numerous small holes distributed throughout the particle, followed by the particles with a small number of randomly distributed internal holes, followed by the hollow sphere particle with a very thin shell. Sometimes the breakage degree of small particles (model samples with a particle size around 7 μm) was higher than that of big particles (SC with particle size 60 μm) because of the weaker particle structure. Also, due to the difference in particle structures, the breakage behaviour of lactose crystals was different from other dairy powder particles. Besides, the fat in particles might decrease the breakage degree of powders. Overall, this study provides a better understanding of the influence of powder characteristics on dairy powder breakage and this can be used to assess and reduce powder breakage and related problems during the production and transportation of dairy powders.

CRediT authorship contribution statement

Jie Han: Conceptualization, Methodology, Formal analysis, Investigation, Data curation, Writing – original draft, Visualization. **John Fitzpatrick:** Supervision, Writing – review & editing. **Kevin Cronin:** Supervision, Writing – review & editing. **Song Miao:** Supervision, Conceptualization, Writing – review & editing, Funding acquisition, Project administration.

Declaration of Competing Interest

The authors declare that they have no known competing financial interests or personal relationships that could have appeared to influence the work reported in this paper.

Acknowledgment

This work was supported financially by the Teagasc, Agriculture and Food Development Authority under the project MDDT 0153 entitled ‘Powder breakage and functionality of dairy powders’.

References

Antonyuk, S., Tomas, J., Heinrich, S., & Mörl, L. (2005). Breakage behaviour of spherical granulates by compression. *Chemical Engineering Science, 60*(14), 4031–4044. https://doi.org/10.1016/j.ces.2005.02.038

Barletta, B. J., & Barbosa-Cánovas, G. V. (1993). An attrition index to assess fines formation and particle size reduction in tapped agglomerated food powders. *Powder Technology, 77*(1), 89–93. https://doi.org/10.1016/0032-5910(93)85011-W

BARLEITA, BLAS. J., & BARBOSA-CÁOVAS, GUSTAVO. V. (1993). Fractal analysis to characterize ruggedness changes in tapped agglomerated food powders. *Journal of Food Science, 58*(5), 1030–1035. https://doi.org/10.1111/jfds.1993.58.issue-510.1111/j.1365-2621.1993.tb06105.x

Boiarkina, I., Sang, C., Depree, N., Prince-Pike, A., Yu, W., Wilson, D. I., & Young, B. R. (2016). The significance of powder breakdown during conveying within industrial milk powder plants. *Advanced Powder Technology, 27*(6), 2363–2369. https://doi.org/10.1016/j.apt.2016.10.019

Bonakdar, T., Ali, M., & Ghadiri, M. (2021). Particle breakability assessment using an Aero S disperser. *International Journal of Pharmaceutics, 597*, 120365. https://doi.org/10.1016/j.ijpharm.2021.120365

Bonakdar, T., Ghadiri, M., Ahmadian, H., Martin de Juan, L., Xu, D., Tantawy, H., & Smith, D. (2016). Impact attrition of spray-dried burkeite particles. *Powder Technology, 304*, 2–7. https://doi.org/10.1016/j.powtec.2016.08.024

Bouvier, J.-M., Collado, M., Gardiner, D., Scott, M., & Schuck, P. (2013). Physical and rehydration properties of milk protein concentrates: Comparison of spray-dried and extrusion-porosified powders. *Dairy Science & Technology, 93*(4), 387–399. https://doi.org/10.1007/s13594-012-0100-7

Cleaver, J. A. S., Ghadiri, M., & Rolfe, N. (1993). Impact attrition of sodium carbonate monohydrate crystals. *Powder Technology, 76*(1), 15–22. https://doi.org/10.1016/0032-5910(93)80036-A

Foerster, M., Gengenbach, T., Woo, M. W., & Selomulya, C. (2016). The impact of atomization on the surface composition of spray-dried milk droplets. *Colloids and Surfaces B: Biointerfaces, 140*, 460–471. https://doi.org/10.1016/j.colsurfb.2016.01.012

Gaiani, C., Morand, M., Sanchez, C., Tehrany, E. A., Jacquot, M., Schuck, P., … Scher, J. (2010). How surface composition of high milk proteins powders is influenced by spray-drying temperature. *Colloids and Surfaces B: Biointerfaces, 75*(1), 377–384. https://doi.org/10.1016/j.colsurfb.2009.09.016

Gerhards, C., Kaell, C., & Schubert, H. (2004). Measurement of attrition of agglomerated cocoa beverage powders: A comparison of Friabilator and vibration tests. *Journal of Food Engineering, 65*(1), 101–108. https://doi.org/10.1016/j.jfoodeng.2004.01.002

Ghadiri, M., Yuregir, K. R., Pollock, H. M., Ross, J. D. J., & Rolfe, N. (1991). Influence of processing conditions on attrition of NaCl crystals. *Powder Technology, 65*(1), 311–320. https://doi.org/10.1016/0032-5910(91)80195-O

Han, J., Fitzpatrick, J., Cronin, K., Maidannyk, V., & Miao, S. (2020). Breakage of infant milk formula through three different processing methods and its influence on powder properties. *Journal of Food Engineering, 282*, 109997. https://doi.org/10.1016/j.jfoodeng.2020.109997

Han, J., Fitzpatrick, J., Cronin, K., Maidannyk, V., & Miao, S. (2021). Particle size, powder properties and the breakage behaviour of infant milk formula. *Journal of Food Engineering, 292*, 110367. https://doi.org/10.1016/j.jfoodeng.2020.110367

Han, J., Fitzpatrick, J., Cronin, K., & Miao, S. (2021). Dairy powder breakage: Mechanisms, characterization methods, impacted properties and influencing factors. *Trends in Food Science & Technology, 114*, 608–624. https://doi.org/10.1016/j.tifs.2021.05.043

Hanley, K. J. (2011). *Experimental quantification and modelling of attrition of infant formulae*. Cork, Ireland: University College Cork.

Hazlett, R., Schmidmeier, C., & O'Mahony, J. A. (2020). Influence of mechanical integrity during pneumatic conveying on the bulk handling and rehydration properties of agglomerated dairy powders. *Journal of Food Engineering, 110103*. https://doi.org/10.1016/j.jfoodeng.2020.110103

Hunziker, O. F., & Nissen, B. H. (1927). Lactose Solubility and Lactose Crystal Formation: II. Lactose Crystal Formation. *Journal of Dairy Science, 10*(2), 139–154. https://doi.org/10.3168/jds.S0022-0302(27)93825-9

Kim, E. H. J., Chen, X. D., & Pearce, D. (2009). Surface composition of industrial spray-dried milk powders. 2. Effects of spray drying conditions on the surface composition. *Journal of Food Engineering, 94*(2), 169–181. https://doi.org/10.1016/j.jfoodeng.2008.10.020

King, R. P. (2012). Modeling and simulation of mineral processing systems. In (pp. 153-252): Society for Mining, Metallurgy, and Exploration (SME).

Kotzur, B. A., Berry, R. J., Zigan, S., García-Triñanes, P., & Bradley, M. S. A. (2018). Particle attrition mechanisms, their characterisation, and application to horizontal lean phase pneumatic conveying systems: A review. *Powder Technology, 334*, 76–105. https://doi.org/10.1016/j.powtec.2018.04.047

Li, R., Roos, Y. H., & Miao, S. (2016a). The effect of water plasticization and lactose content on flow properties of dairy model solids. *Journal of Food Engineering, 170*, 50–57. https://doi.org/10.1016/j.jfoodeng.2015.09.014

Li, R., Roos, Y. H., & Miao, S. (2016b). Physical and mechanical properties of lactose/WPI mixtures: Effect of pre-crystallisation. *International Dairy Journal, 56*, 55–63. https://doi.org/10.1016/j.idairyj.2015.12.014

Lu, X., Liu, C., Zhu, L., & Qu, X. (2014). Influence of process parameters on the characteristics of TiAl alloyed powders by fluidized bed jet milling. *Powder Technology, 254*, 235–240. https://doi.org/10.1016/j.powtec.2013.11.013

Niro, G. (2006). *GEA Niro analytical methods dry products*. Gladsaxevej, Denmark: GEA Process Engineering A/S.

Norazirah, A., Fuad, S. H. S., & Hazizan, M. H. M. (2016). The effect of size and shape on breakage characteristic of mineral. *Procedia Chemistry, 19*, 702–708. https://doi.org/10.1016/j.proche.2016.03.073

O'Donoghue, L. T., Haque, M. K., Kennedy, D., Laffir, F. R., Hogan, S. A., O'Mahony, J. A., & Murphy, E. G. (2019). Influence of particle size on the physicochemical properties and stickiness of dairy powders. *International Dairy Journal, 98*, 54–63. https://doi.org/10.1016/j.idairyj.2019.07.002

Ortega-Rivas, E., Juliano, P., & Yan, H. (2006). *Food powders: Physical properties, processing, and functionality*. US: Springer.

Petukhov, Y., & Kalman, H. (2004). Empirical breakage ratio of particles due to impact. *Powder Technology, 143–144*, 160–169. https://doi.org/10.1016/j.powtec.2004.04.009

Reynolds, G. K., Fu, J. S., Cheong, Y. S., Hounslow, M. J., & Salman, A. D. (2005). Breakage in granulation: A review. *Chemical Engineering Science, 60*(14), 3969–3992. https://doi.org/10.1016/j.ces.2005.02.029

Schuck, P., Dolivet, A., & Jeantet, R. (2012). *Analytical methods for food and dairy powders*.

Wong, S. Y., & Hartel, R. W. (2014). Crystallization in Lactose Refining—A Review. *Journal of Food Science, 79*(3), R257–R272. https://doi.org/10.1111/jfds.2014.79.issue-310.1111/1750-3841.12349

YAN, HONG, & BARBOSA-CÁNOVAS, G. V. (2001). Attrition evaluation for selected agglomerated food powders: The effect of agglomerate size and water activity. *Journal of Food Process Engineering, 24*(1), 37–49. https://doi.org/10.1111/jfpe.2001.24.issue-110.1111/j.1745-4530.2001.tb00530.x

Zhang, F., Olaleye, A. K., O'Mahony, J. A., Miao, S., & Cronin, K. (2020). Dilute phase pneumatic conveying of whey protein isolate powders: Particle breakage and its effects on bulk properties. *Advanced Powder Technology, 31*(8), 3342–3350. https://doi.org/10.1016/j.apt.2020.06.019

Zhang, Z., & Ghadiri, M. (2002). Impact attrition of particulate solids. Part 2: Experimental work. *Chemical Engineering Science, 57*(17), 3671–3686. https://doi.org/10.1016/S0009-2509(02)00241-5